Dynamics of the Liquid State

UMBERTO BALUCANI and MARCO ZOPPI

OXFORD SERIES ON NEUTRON SCATTERING IN
CONDENSED MATTER

General Editors
S. W. Lovesey and E. W. J. Mitchell

OXFORD SERIES ON NEUTRON SCATTERING IN
CONDENSED MATTER

Dynamics of the Liquid State

Umberto Balucani and **Marco Zoppi**

Istituto di Elettronica Quantistica CNR, Firenze, Italy

Preface

When compared with the conventional pictures of gases and crystals, the physical representation of a liquid does not seem particularly attractive. For this intermediate state of matter it is indeed rather easy to compile a list of 'unpleasant' features, comprising the absence both of long-range structural order and ideal disorder, the need to consider particle interactions far from harmonic, the lack of an immediately evident 'small parameter' in the microscopic dynamics of the system, and so on. In this respect, the characterization of a liquid appears to be dominated by just those complicated aspects which are rather marginal in the other two states of matter.

A well-known consequence of this perverse attitude is the ultimate failure of the attempts to describe the features of the liquid state by extrapolating the behaviour of either gases (density expansions) or solids (cell theories). Even if in a historical perspective the heuristic value of these approaches should not be undervalued, the appearance of divergences in some predictions signals that liquids are much too complicated for the success of these 'natural' perturbative schemes.

In view of all this, the only sensible choice is to take the bull by the horns by focusing on those properties which appear to characterize the liquid state as unambiguously as possible. This strategy can be followed at a purely macroscopic level, in a voyage which moves from the gentle waves of linearized hydrodynamics to explore more turbulent waters or whirling maelstroms. Alternatively, one may adopt a microscopic point of view, in which the emphasis is put on the spatial arrangement and on the motion of the atomic constituents. In the latter case, a comparison with the behaviour typical of the other two phases of matter may shed some extra light on the problem, or even suggest useful approximation schemes. To give just one example, the microscopic structure of monatomic liquids appears to be dominated by close-packing effects, rather than by the details of the interatomic potential as in moderately dense gases. Although this recognition is far from being the full story, it is certainly one of the cornerstones of the structural theories of the liquid state.

The purpose of the book is to present a comprehensive discussion of the physical concepts and theoretical approaches developed for the study of the *dynamical properties* of liquids (or, more generally, of high-density fluids) at a microscopic level. To keep in touch with real life, a rather detailed

account of the experimental techniques in common use in this field is also included. As we shall see, in most cases the inherent complexity of these systems does not mean that we require abstract mathematical treatments or, say, exotic concepts for a satisfactory account of their properties. Even if occasionally the appearance of some kinetic-theory expressions may be rather discouraging for the average reader, that reader's patience will be rewarded, we hope, by the successful application of the framework to some specific property of physical interest. To mitigate any residual formal complication, attention will be focused mostly on the so-called 'simple fluids', namely classical monatomic fluids or those equivalent to the latter as far as the property under consideration is concerned. Even if nowadays the study of much more 'complex' systems (ranging from glass-forming liquids to polymers, colloids, and microemulsions) is in rapid evolution, most of the basic concepts and results discussed in this book turn out to provide useful guidelines even in these challenging cases.

Coming back to the specific field of our concern, the progress achieved in the last decade permits a theoretical description from a unified point of view. For example, this inherent conceptual unity is useful in order to stress many common aspects of single-particle vs. collective atomic dynamics. Nevertheless, this traditional distinction will be kept even here, mostly because it is convenient when making contact with experiments. In this context, it is well known that thermal neutrons inelastically scattered by the fluid are quite efficient probes of its dynamics at an atomic level. As we shall see, a good deal of information is also provided by light scattering, not only in its conventional use in Rayleigh–Brillouin spectroscopy but also in more unusual (and 'microscopic') applications, like interaction-induced light scattering. Finally, it is worth mentioning the extremely important role of 'simulation experiments' in the development of the whole field over the years. As a consequence, we shall frequently refer to computer simulation data, particularly in situations where they are useful to clarify concepts or to illustrate phenomena whose practical observation is difficult. Trying never to forget that, after all, nature is supposed to be real, and that the correctness of any theoretical model, including the mimic-system investigated in the simulations, should ultimately be tested against experiment.

The book begins with a rather extensive introduction to the quantities of physical interest in the microscopic dynamics of liquids. Each of these has a specific behaviour, conveniently described by a suitable correlation function in the time domain or by the corresponding spectrum in the frequency domain. A preliminary contact with experimental data indicates that there is a large variety of phenomena for which a comprehensive theory must be able to account. This immersion in reality is continued in Chapter 2, a sort of 'experimentalists' corner' where several possible ways to probe the atomic dynamics in fluids are discussed in detail. Chapter 3

then establishes the theoretical framework needed to interpret the observed features. After a rather general description of favourite theoretical tools such as projection operators and memory functions, there are some of the first rewarding applications to the field of interest, including a microscopic deduction of the results of ordinary Navier–Stokes hydrodynamics. In Chapter 4, the framework is shown to provide a sound basis for the buildup of a modern version of kinetic theory. This turns out to be quite successful, even in the liquid state, as shown by the subsequent applications both to single-particle properties (Chapter 5) and to collective quantities (Chapter 6).

One of the most important results of the general theory is the natural emergence in dense fluids of two basic dynamical mechanisms governing the time decay of the correlation functions of interest. The first decay channel, well known from the traditional kinetic theory of gases, is provided by fast and largely uncorrelated collisional events. The second mechanism is much less localized both in space and in time, and in very dense fluids is basically associated with the sluggishness of any structural relaxation process. The importance of this long-lasting mechanism rapidly increases as we move toward the liquid range, and under suitable conditions the decay time becomes eventually so long as to give rise to a structural arrest, heralding the birth of a 'frozen' amorphous system. Hence, even at a dynamical level the awkward 'intermediate character' of the liquid phase is seen to have far-reaching consequences.

It is customary at this point to acknowledge all those who have contributed to some extent to the authors' efforts. In our case, this support ranged from active collaborations to profitable discussions and contacts, including a few embarassing question marks. Given these premises, a comprehensive list of these colleagues would be too long; we express our gratitude to all of them, as well as to the Oxford University Press reader for his valuable comments and suggestions. One of us (U. B.) takes this opportunity to remember Tom Gaskell, who until his premature death has been to him both a valued companion of intellectual adventures in this field and a sincere friend. Both of us have of course benefited from cooperation with several colleagues in the familiar atmosphere of our Institute in Florence. In our homes not far from there, the encouragement and tolerance of Adriana and Brunella have made much smoother any asperity met in the course of our work.

Florence U. B.
March 1994 M. Z.

Contents

xii   *Contents*

Symbols

Throughout this book, vectors $\mathbf{v}$ are denoted with boldface characters. Tensors $\mathbf{T}$ and matrices are instead written with sans-serif boldface characters.

$a, a^\dagger$	annihilation and creation operators
$A(t)$	general dynamical variable
$\mathbf{A}(t)$	a column vector of dynamical variables
$A_v(t)$	general set of dynamical variables ($v = 1, 2, \ldots$)
$\mathbf{A}(\mathbf{r})$	vector potential
$\mathbf{A}_i, \mathbf{A}(i)$	general polarizability tensor of the ith particle
b_i	neutron scattering length of the ith nucleus
c	speed of light
c_P	specific heat at constant pressure
c_V	specific heat at constant volume
$\mathbf{C}(t)$	correlation matrix
$c(k)$	direct correlation function
$c_\mathrm{L}(k)$	wavevector-dependent longitudinal sound velocity (instantaneous)
$c_\mathrm{T}(k)$	wavevector-dependent transverse sound velocity (instantaneous)
$C(\mathbf{r}\,\mathbf{p}, \mathbf{r}'\,\mathbf{p}'; t)$	collective phase-space time correlation function
$C_s(\mathbf{r}\,\mathbf{p}, \mathbf{r}'\,\mathbf{p}'; t)$	self phase-space time correlation function
$C(\mathbf{k}, \mathbf{p}\mathbf{p}'; t)$	wavevector-dependent phase-space time correlation function (collective)
$C_s(\mathbf{k}, \mathbf{p}\mathbf{p}'; t)$	wavevector-dependent phase-space time correlation function (self)
$C_\mathrm{L}(k, t)$	longitudinal current time correlation function
$C_\mathrm{T}(k, t)$	transverse current time correlation function
D	diffusion coefficient
e	electron charge (absolute value)
$\mathbf{e}$	polarization unit vector
$e(\mathbf{k}, t)$	wavevector-dependent energy density at time t
E	total internal energy
$\mathbf{f}(t)$	general fluctuating force at time t
$f(\mathbf{r}\,\mathbf{p}, t)$	phase-space density at time t
$f_s(\mathbf{r}\,\mathbf{p}, t)$	self phase-space density at time t

$\mathbf{f}_{ij}(t)$	pair force on the ith particle at time t (due to the jth particle)
$f_0(p)$	normalized Maxwellian momenta distribution function
$F(k, t)$	intermediate scattering function
$\mathfrak{F}(\mathbf{k}, t)$	general intermediate scattering function (quantum-mechanical)
$F_s(k, t)$	self intermediate scattering function
$F_0(k, t)$	free-particle intermediate scattering function
$\mathbf{F}_i(t)$	total force on the ith particle at time t
$g(r)$	pair distribution function
$g^{(3)}(\mathbf{r}, \mathbf{r}')$	triplet distribution function
G	rigidity modulus
$G(\mathbf{r}, t)$	van Hove correlation function (collective)
$\mathcal{G}(\mathbf{r}, t)$	general van Hove correlation function (quantum-mechanical)
$G_s(\mathbf{r}, t)$	van Hove correlation function (single-particle)
$G_2(\mathbf{r}\,0; \mathbf{r}'\,t)$	time-dependent pair distribution function
$\mathcal{G}(\mathbf{r}\,0; \mathbf{r}'\,t)$	time-dependent many-particle distribution function
$H_\lambda(\mathbf{p})$	three-dimensional Hermite polynomial of order λ
$\mathfrak{IC}$	Hamiltonian
$\mathbf{I}$	unit tensor
i, j, l, m	(as subscripts) particle labels
i	imaginary unit (i $= \sqrt{-1}$)
$I_L(\mathbf{k}, t)$	experimental intermediate scattering function (light scattering)
$I_n(\mathbf{k}, t)$	experimental intermediate scattering function (neutron scattering)
$j_n(x)$	spherical Bessel function of order n
$\mathbf{j}(\mathbf{k}, t)$	wavevector-dependent current at time t (j_L longitudinal current, j_T transverse current)
$\mathbf{k}$	wavevector (of magnitude k)
k_m	position of the main peak of the static structure factor
$K(t)$	memory function of the velocity autocorrelation function
$\mathbf{K}(t)$	general memory matrix
l	mean free path
L	Liouville operator
m	mass of an atom
m_e	mass of the electron
m_n	mass of the neutron
M	mass of a Brownian particle
$M(\mathbf{k}, t)$	general memory function
n	number density at equilibrium ($n = N/V$)

$n(\mathbf{k}, t)$	wavevector-dependent number density at time t
$n_{s,i}(\mathbf{k}, t)$	wavevector-dependent self density for the ith particle at time t
N	number of particles in the system
$\mathbf{p}$	general momentum vector
$\mathbf{p}_i(t)$	momentum of the ith particle at time t
P	pressure
$P_n(x)$	Legendre polynomial of order n
$\mathcal{P}$	general projection operator
$\mathbf{q}$	wavevector variable
$\mathbf{q}(\mathbf{k}, t)$	wavevector-dependent microscopic energy current at time t
Q_N	canonical partition function (configuration)
$\mathbf{r}$	general position vector (with cartesian components x, y, z)
r_e	classical radius of the electron ($r_e = e^2/m_e c^2$)
r_0	position of the minimum of the pair potential
$\mathbf{r}_i(t)$	position of the ith particle at time t
$\mathbf{r}_{ij}(t)$	separation between the ith and the jth particle at time t ($\mathbf{r}_{ij}(t) = \mathbf{r}_i(t) - \mathbf{r}_j(t)$)
$S(k)$	static structure factor
$S(k, \omega)$	dynamic structure factor
$\mathcal{S}(\mathbf{k}, \omega)$	general dynamic structure factor (quantum-mechanical)
$S_s(k, \omega)$	self part of $S(k, \omega)$
t	time
T	temperature
$\mathbf{v}_i(t)$	velocity of the ith particle at time t
v_s	adiabatic sound velocity
v_T	isothermal sound velocity
V	volume of the system
V_N	total potential energy
z	Laplace transform variable (not to be confused with the cartesian component of $\mathbf{r}$)
Z	atomic number
Z_N	canonical partition function (total)
a	polarization index
a, β, γ, δ	indexes denoting the cartesian components of a vector or of a tensor
$\mathbf{a}_n$	n-particle component of the polarizability tensor
β	inverse temperature in energy scale ($\beta = 1/k_B T$)
$\beta(r)$	scalar pair polarizability anisotropy
γ	ratio of the specific heats ($\gamma = c_P/c_V$)
$\delta_{i,j}$	Kronecker delta

$\delta(x)$	Dirac delta-function
$\delta r^2(t)$	mean square displacement of a particle
ε	well depth of the pair potential
η	shear viscosity coefficient
η_{L}	longitudinal viscosity coefficient $(\eta_{\mathrm{L}} = (4/3)\eta + \eta_V)$
η_V	volume (bulk) viscosity coefficient
$\eta(t)$	(shear) stress autocorrelation function
κ	thermal conductivity coefficient
λ	wavelength
σ	scattering cross section; also, a characteristic length associated with the pair potential (typically, the first zero of $\phi(r)$)
σ_{c}	coherent neutron scattering cross section
σ_{i}	incoherent neutron scattering cross section
$\sigma(\mathbf{k}, t)$	wavevector-dependent microscopic stress tensor at time t
$\sigma^{\alpha\beta}$	element of the microscopic stress tensor
τ	time variable
$\phi(r)$	interparticle pair potential
χ_T	isothermal compressibility
$\psi(t)$	velocity autocorrelation function (normalized to its initial value)
ω	angular frequency
$\overline{\omega^n}$	general nth frequency moment
$\langle \omega^n \rangle$	general normalized nth frequency moment $(\langle \omega^n \rangle = \overline{\omega^n}/\overline{\omega^0})$
$\omega_{\mathrm{L}}(k)$	wavevector-dependent longitudinal frequency
$\omega_{\mathrm{T}}(k)$	wavevector-dependent transverse frequency
Ω	solid angle
Ω	general proper frequency matrix in the memory function formalism
Ω_0	Einstein frequency

In this book the physical quantities have been expressed in cgs units, except in a few cases (such as Å or eV) where we have followed a long-established tradition. Some fundamental constants of common use are: $k_{\mathrm{B}} = 1.38 \times 10^{-16}\,\mathrm{erg\,K^{-1}}$ (Boltzmann constant): $\hbar = 1.054 \times 10^{-27}\,\mathrm{erg\,s}$ (Planck constant h divided by 2π); $e = 4.8 \times 10^{-10}\,\mathrm{esu}$ of electric charge (the charge of an electron being $-e$); $m_{\mathrm{e}} = 0.911\,10^{-27}\,\mathrm{g}$ (electron mass); $m_{\mathrm{n}} = 1.67\,10^{-24}\,\mathrm{g}$ (neutron mass). An useful conversion relation among the various 'energy units' used in spectroscopic studies of condensed system is

$$1\,\mathrm{meV} = 10^{-3}\,\mathrm{eV} = 1.6 \times 10^{-9}\,\mathrm{erg} = 8.07\,\mathrm{cm^{-1}} = 11.61\,\mathrm{K} = 0.24 \times 10^{12}\,\mathrm{Hz}.$$

1

The basic dynamical quantities

1.1 MICROSCOPIC CHARACTERIZATION OF A LIQUID SYSTEM

On the gross scale of everyday experience, a liquid can be described by a relatively small number of quantities. As in any other physical system, the criteria of choice of these macroscopic variables are established by thermodynamics. For example, the equilibrium state of a one-component fluid[*] is specified by the volume V of the system, its pressure P, and its absolute temperature T. The actual independence of these equilibrium thermodynamic variables is limited by 'constitutive relations' (in the example, the equation of state), whose specific form is taken phenomenologically from some experimental evidence. The well-established 'principia' of thermodynamics are subsequently exploited to yield the best possible description of the equilibrium properties of the system from a macroscopic point of view.

Similar steps can be found in the logical structure of irreversible thermodynamics, which explicitly deals with non-equilibrium processes (de Groot and Mazur 1962). If the deviation from equilibrium is not too large, semiphenomenological results such as, for example, Fick's law for diffusion or the Navier–Stokes hydrodynamic equations may be exploited. Irreversible thermodynamics then predicts several formal results for the coefficients in these equations, including those symmetry requirements known as Onsager relations. However, the explicit expressions of these dissipative (or 'transport') coefficients cannot be deduced, and their values for a given system have ultimately to be taken from experiment.

This frequent recourse to phenomenology appears rather natural in a macroscopic framework. In contrast, one of the purposes of a microscopic description at an atomic level is to try to avoid any resort to experiment in the development of the theory. In our specific subject of concern, this ambitious strategy is of course made possible by a framework based on statistical mechanics. Besides any methodological merit or aesthetic appeal,

---

[*]Henceforth we shall adhere to the common use of denoting as 'fluid' a system macroscopically characterized by the absence of a definite shape. For a given substance, this definition clearly encompasses both its ordinary gaseous and liquid phases.

the microscopic approach has the practical advantage of dealing even with phenomena which are rather far from 'everyday experience', and yet are directly observable. In particular, rather sophisticated experimental probes may yield invaluable pieces of information on several physical events occurring in the system over different length and time scales. In this respect, an obvious example is provided by the experiments in which a beam of thermal neutrons is scattered by the system: at least in principle, a proper choice of the scattering conditions and of the isotopic species provides an almost complete description of the structural and dynamical properties of the system, both in their single-particle aspects and in the collective features.

Needless to say, in the microscopic framework a more complicated formalism is the price to pay for all these advantages. Also, the toll is particularly expensive in a strongly interacting system such as a 'liquid' in its conventional meaning. In such a situation, it is wiser to take a moderate attitude, confining our attention to the so-called 'simple liquids'. In the literature there is no consensus about the precise definition of a simple liquid, but there is at least the widespread agreement that this model should encompass most of the basic features of real liquids without the unnecessary complications which may be present in a particular system.

In this respect, a *classical monatomic system* in a limited range of densities and temperatures is a convenient physical model for a simple liquid. Denoting by $\mathbf{r}_i$ and $\mathbf{p}_i$ the position and the momentum of the ith particle in a laboratory frame, the Hamiltonian $\mathcal{H}$ of our model system is written as a sum of kinetic and potential energy contributions:

$$\mathcal{H} = (1/2m) \sum_i p_i^2 + V_N(\mathbf{r}_1, \ldots, \mathbf{r}_N) \qquad (1.1)$$

where the summation runs over the N particles of the system, each of mass m. The potential energy V_N is assumed to depend only on the interatomic interactions, which in the simplest scheme are written as a sum of pairwise central contributions

$$V_N(\mathbf{r}_1, \ldots, \mathbf{r}_N) = \frac{1}{2} \sum_{i \neq j} \phi(r_{ij}) \qquad (1.2)$$

where the pair potential ϕ depends on the interatomic separation $r_{ij} = |\mathbf{r}_i - \mathbf{r}_j|$ between the ith and the jth atoms. Combining eqns (1.1) and (1.2), the resulting Hamiltonian is the simplest which we may envisage for a classical interacting system made of identical particles. The system is implicitly assumed to be homogeneous and isotropic, that is $\mathcal{H}$ is not affected by a translation or a rotation of the reference frame.

In general, the pair potential $\phi(r)$ comprises both attractive ($\phi(r) < 0$) and repulsive ($\phi(r) > 0$) portions, with the latter dominant for sufficiently small separations. Broadly speaking, the pairwise approximation (1.2) with a more or less phenomenological form of $\phi(r)$ is fairly successful in the description of real fluids, although the presence of non-negligible triplet contributions has been detected in moderately dense gases (Egelstaff 1990). In liquids the situation is still far from being defined, and for simplicity we shall adopt the pairwise model, which proves indeed sufficient to account for most of the complicated features of the dynamics of the liquid state.

Before exploring the consequences of the above-mentioned classical model, it is worth ascertaining the possible presence of *quantum effects* in real monatomic liquids. Generally speaking, these effects fall into the following three classes:

(i) *Quantum diffraction*. Physically, the wave-like character of a particle begins to be relevant when its de Broglie wavelength $\lambda = h/p$ is comparable with a suitable 'size' of the particle. Denoting this size by σ, a classical framework is expected to be appropriate only if $h/p \ll \sigma$. If quantum effects are not severe, the particle momentum p can be replaced by its classical average at thermal equilibrium, of the order of $(mk_BT)^{1/2}$. In practice, quantum diffraction effects turn out to be small in almost all cases, an exception being the systems made of light particles at very low temperatures, such as liquid helium.

(ii) *Quantum statistics*. Systems of identical particles are known to require an appropriate treatment of the inherent indistinguishability of their constituents. This task involves the consideration of the symmetric or antisymmetric character of the system wavefunction under a permutation of two particles, and ultimately leads to the nonclassical Bose–Einstein and Fermi–Dirac statistics. On the other hand, the relevance of such effects is expected to be pronounced only if there is a significant overlap between the single-particle wavefunctions. A convenient measure of the spatial extent of the latter is again provided by the previous 'thermal' de Broglie wavelength. Taking the average interparticle separation as $(V/N)^{1/3}$, the overlap will be negligible if

$$h/(2\pi mk_BT)^{1/2} \ll (V/N)^{1/3}. \qquad (1.3)$$

Since in the liquid range the particles are almost in mutual contact, $(V/N)^{1/3} \approx \sigma$ and the criterion (1.3) becomes essentially equivalent to the neglect of the aforementioned quantum diffraction effects.

(iii) *Detailed balance factors*. The quantized character of the energy transfers at a microscopic level leads to a natural unbalance of the spectral properties of a system, depending whether energy gains or losses are considered (see Section 2.3). Here we limit ourselves to state that a classical treatment of these features is approximately valid only for frequencies ω such that

$$\hbar\omega \ll k_BT. \qquad (1.4)$$

1.2 THE STRUCTURAL BACKGROUND

1.2.1 The basic structural properties

Before embarking on the study of the dynamical features of simple liquids, it is essential to recall a few concepts about their time-independent properties. The latter comprise all the equilibrium quantities familiar from ordinary thermodynamics, such as the internal energy, the pressure, the specific heats and so on. For a given system, all these quantities depend on 'state parameters' such as the temperature T and the volume V. In addition to these thermodynamic properties, in a microscopic framework it is convenient to consider other 'static' quantities which are directly related to the atomic nature of the system. Typical examples of such properties are the various 'n-particle distribution functions' which describe the average spatial arrangements of clusters of n atoms. Besides the dependence on the state parameters of the system, these quantities are also functions of additional 'field' variables, usually vectorial distances or separations. Because of their more microscopic nature, this second class of equilibrium properties is more fundamental than the thermodynamical quantities, which in most cases can be written as simple integrals involving these functional probes of structure.

In any case, both kinds of properties can be expressed as statistical averages ot suitable microscopic quantities involving the positions and the momenta of the constituent particles. In the following, we shall almost exclusively deal with systems with a fixed number of particles and at thermal equilibrium at the temperature T; in such a situation the appropriate statistical average is the *canonical ensemble average*

$$\langle \ldots \rangle = (1/Z_N) \int d\mathbf{r}^N d\mathbf{p}^N (\ldots) \exp(-\beta \mathcal{H}) \qquad (1.5)$$

where $\beta \equiv (k_B T)^{-1}$ and the $6N$-dimensional integral runs over the set of coordinates $\mathbf{r}^N \equiv \{\mathbf{r}_1, \ldots, \mathbf{r}_N\}$ and conjugate momenta $\mathbf{p}^N \equiv \{\mathbf{p}_1, \ldots, \mathbf{p}_N\}$. Moreover,

$$Z_N = \int d\mathbf{r}^N d\mathbf{p}^N \exp(-\beta \mathcal{H}) \qquad (1.6)$$

is the canonical partition function. In our classical model, Z_N factors in the product of a kinetic contribution

$$(Z_N)_{\text{kin}} \equiv \int d\mathbf{p}^N \exp\left(-\beta \sum_i p_i^2/2m\right)$$
$$= \left[4\pi \int_0^\infty dp\, p^2 \exp(-\beta p^2/2m)\right]^N = (2\pi m k_B T)^{3N/2} \qquad (1.7)$$

and a potential contribution

$$(Z_N)_{\text{pot}} \equiv \int d\mathbf{r}^N \exp[-\beta V_N(\mathbf{r}^N)] \equiv Q_N(V, T). \qquad (1.8)$$

In contrast with $(Z_N)_{\text{kin}}$, in general the potential part of Z_N (also referred to as the 'configurational partition function' $Q_N(V, T)$) cannot be evaluated exactly; a trivial exception is the 'ideal gas' situation where $V_N(\mathbf{r}_N) \equiv 0$ and $Q_N(V, T) = V^N$. In a dilute gas, the first deviations from nonideality can also be treated exactly by means of a 'virial' expansion in the small parameter $n\sigma^3$, where $n = N/V$ is the number density and σ is a microscopic length of the order of the range of the interatomic potential. As already remarked, such expansions are bound to fail at high densities (in particular, in the liquid range where $n\sigma^3 \approx 1$).

As an example of evaluation of a thermodynamic property by eqn (1.5), consider the internal energy of the system. In the pairwise approximation (1.2) this is simply given by

$$E = \langle \mathcal{H} \rangle = (1/2m) \sum_i \langle p_i^2 \rangle + \langle V_N(\mathbf{r}^N) \rangle$$

$$= \frac{3}{2} N k_B T + \frac{1}{2} \left\langle \sum_{i \neq j} \phi(r_{ij}) \right\rangle$$

$$= \frac{3}{2} N k_B T + \frac{1}{2} N n \int d\mathbf{r}\, \phi(r) g(\mathbf{r}) \qquad (1.9)$$

where we have exploited the fundamental property of a classical system

$$\langle p_i^2 \rangle = m^2 \langle v_i^2 \rangle = 3m k_B T \qquad (1.10)$$

and defined

$$n g(\mathbf{r}) \equiv (1/N) \sum_{i \neq j} \langle \delta(\mathbf{r} - \mathbf{r}_{ij}) \rangle. \qquad (1.11)$$

The quantity $g(\mathbf{r})$, referred to as the *pair distribution function* of the system, is the simplest example of the microscopic structural properties mentioned earlier. After eqns (1.5)–(1.8), an alternative expression of $g(\mathbf{r})$ is given by

$$n g(\mathbf{r}) = [(N-1)/Q_N(V, T)] \int d\mathbf{r}_1 \int d\mathbf{r}_2 \delta(\mathbf{r} - \mathbf{r}_{12}) \int d\mathbf{r}_3 \ldots d\mathbf{r}_N \exp(-\beta V_N)$$

$$= [(N-1)/Q_N(V, T)] V \int d\mathbf{r}_{13} \ldots d\mathbf{r}_{1N} \exp[-\beta V_N(\mathbf{r}, \mathbf{r}_{13}, \ldots \mathbf{r}_{1N})] \qquad (1.12)$$

where in the last part we have introduced relative coordinates and exploited the homogeneity of the system. Since the fluid is also isotropic, $g(\mathbf{r})$ turns out to depend only on $r = |\mathbf{r}|$, and in the following it is denoted by
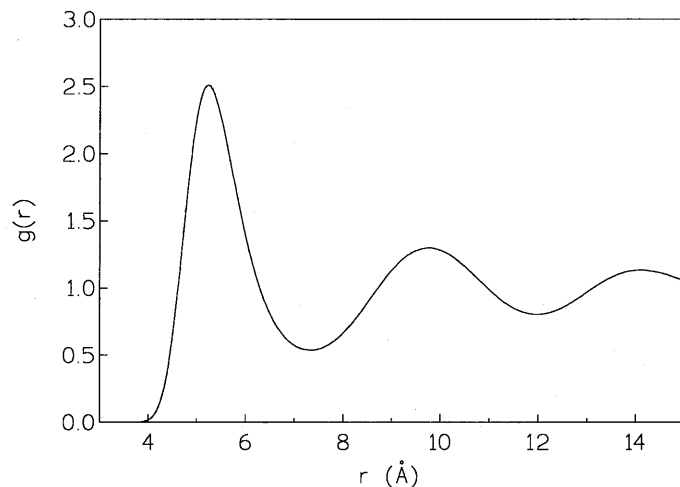
Fig. 1.1 Pair distribution function in liquid Cs as obtained in a computer simulation experiment at a temperature $T = 308$ K and a number density $n = 0.0083$ Å^{-3} (after Balucani *et al.* 1992).

Fig. 1.2 Experimental static structure factor of liquid Cs at the same state point as in Fig. 1.1. The data have been obtained by X-ray diffraction (open circles; Huijben and van der Lust 1979) and by neutron scattering (asterisks; Bodensteiner *et al.* 1992). The full line is the result obtained from eqn (1.14) using for $g(r)$ the simulation data reported in Fig. 1.1.

$g(r)$. Its functional form is exactly known only at low densities, where $g(r) = \exp[-\beta\phi(r)]$.

From its definition (1.11), $g(r)$ is seen to measure the probability density that a particle is separated by a distance r from another one. In particular, the average number of neighbours of a given atom up to a distance R is:

$$\mathfrak{N}(R) = 4\pi n \int_0^R dr\, r^2 g(r) \qquad (1.13)$$

The typical features of $g(r)$ in the liquid range are illustrated in Fig. 1.1, which refers to liquid Cs near its melting point. In particular, the vanishingly small value of $g(r)$ below $r \approx 4$ Å reflects the strong interparticle repulsion occurring for such small separations. Beyond this region, the presence of several oscillations indicates that the average arrangement of particles around an arbitrary atom proceeds through 'clusters' resembling the shells of neighbours occurring in a crystal. The analogy is however incomplete, both because of the inherent isotropy of the liquid and for the ill-defined character of the shells, which are considerably broader than those of a crystal at finite temperatures. From eqn (1.13) the number of 'nearest neighbours' up to the position of the first minimum of $g(r)$ turns out to be $\mathfrak{N}(R \approx 7$ Å$) \approx 12$, a value consistent with a nearly close-packed arrangement. For very large separations, $g(r)$ eventually approaches unity and the system effectively behaves as a structureless continuum.

An experimentally accessible quantity which is closely related to $g(r)$ is the *static structure factor* defined by

$$S(\mathbf{k}) \equiv 1 + n \int d\mathbf{r}[g(\mathbf{r}) - 1]\exp(i\mathbf{k}\cdot\mathbf{r})$$
$$= 1 + 4\pi n \int_0^\infty dr\, r^2 [g(r) - 1]\frac{\sin kr}{kr} \qquad (1.14)$$

which can be measured either by X-ray or neutron diffraction. Note that in the last step of (1.14) the angular integrations have been performed by exploiting the independence of the pair distribution function on the direction of $\mathbf{r}$. Thus, as a consequence of the isotropy of the system, the static structure factor of a fluid is seen to depend only on the magnitude of the 'wave vector' $\mathbf{k}$.

Broadly speaking, the shapes of $S(k)$ and $g(r)$ in typical simple liquids are remarkably similar (see Fig. 1.2), although of course the physical meaning to be attributed to the various features is completely different in the wave vector domain. Thus, the first sharp peak of $S(k)$ reflects the existence of a dominant nearly regular arrangement of the particles in real space; in the specific example of Fig. 1.2 the position of the main peak of $S(k)$ is at

$k_m \approx 1.43$ Å^{-1}, corresponding to a 'lattice spacing' $2\pi/k_m \approx 4.4$ Å in fair agreement with the period of the oscillations of $g(r)$ from Fig. 1.1. The sharp decrease of $g(r)$ at small separations ($r < 5$ Å) is responsible for the subsequent maxima and minima of $S(k)$, which become more and more damped as k increases. Eventually, at large wave vectors, $S(k)$ probes the 'hard core' region where $g(r)$ is vanishingly small: here the contribution of the integral in eqn (1.14) becomes negligible, and $S(k) \rightarrow 1$. In the opposite extreme, $S(k \rightarrow 0)$ reflects in an average sense the features of $g(r)$, including its asymptotic approach to unity at very large separations. As a consequence, $S(0)$ can be expected to be associated with some macroscopic property of the system. It can indeed be shown that (Hansen and McDonald 1986)

$$S(0) = nk_B T \cdot \chi_T \qquad (1.15)$$

where χ_T is the isothermal compressibility. The very low values of $S(k \rightarrow 0)$ apparent from Fig. 1.2 are typical for all liquids near melting, and reflect our very limited ability to compress such systems. This situation is to be contrasted with those met in an ideal gas (where $g(r) \equiv 1$ for all r, making $S(k) = 1$ at any k) and in a fluid near the liquid–gas critical point (where the onset of huge density fluctuations over macroscopic distances causes $S(0)$ to diverge).

Given a particular pair potential $\phi(r)$, the main objective of the *structural theories* of dense fluids and liquids is to deduce the appropriate form of $g(r)$ and $S(k)$ in a specified state point. For simple liquids, this task was essentially accomplished in the early 1970s by the so-called 'reference-system' approaches. These approximate methods are based on the physical recognition that the structure of a dense fluid is mostly determined by the interatomic repulsive forces, which give rise to the so-called 'excluded volume' effects. As a consequence, for a fluid specified by a given $\phi(r)$ a convenient starting point is the determination of the 'underlying' repulsive system. For the latter, one is ultimately led to the consideration of a system of *hard spheres* with infinitely strong repulsive forces, whose structural properties can approximately be worked out (Percus and Yevick 1958). Having established the appropriate reference system, the actual fluid under consideration is investigated by variational methods by determining the specific form of the remaining nonrepulsive interactions, as well as their effect in modifiying the structure of the reference fluid (Weeks *et al.* 1971).

1.2.2   More complicated structural quantities

Although very important, the knowledge of $g(r)$ alone is not sufficient to give a full account of the structural properties of a dense fluid. In principle, such a complete description is provided by the consideration of *n-particle*

distribution functions (with $n > 2$), which are proportional to the probability of occurrence of clusters of n particles with specified mutual separations. These higher-order distribution functions are mutually linked by complicated hierarchical equations (Hansen and McDonald 1986). Fortunately, in most applications of interest a reasonably accurate description of structural effects can be obtained by considering only the first few distribution functions. In particular, besides $g(r)$ we shall often deal with the *triplet distribution function* $g^{(3)}(\mathbf{r}, \mathbf{r}')$ defined by

$$n^2 g^{(3)}(\mathbf{r}, \mathbf{r}') \equiv (1/N) \sum_{j \neq i, l \neq i, j} \langle \delta(\mathbf{r} - \mathbf{r}_{ij}) \delta(\mathbf{r}' - \mathbf{r}_{il}) \rangle. \qquad (1.16)$$

As in the case of $g(r)$, the isotropy of the fluid simplifies somewhat the functional dependence of $g^{(3)}$ on $\mathbf{r}$ and $\mathbf{r}'$. Using simple symmetry arguments, there turn out to be only three really independent variables, namely $r = |\mathbf{r}|$, $r' = |\mathbf{r}'|$ and $|\mathbf{r} - \mathbf{r}'|$ (or, alternatively, r, r' and the angle $\theta_{rr'}$ between $\mathbf{r}$ and $\mathbf{r}'$). Even after this reduction, the functional dependence of $g^{(3)}$ is rather complicated and very scarce information on it is generally available for dense systems. Computer simulation studies have partially dealt with this problem by restricting the attention on special configurations (equilateral, isosceles) of the 'triangle' formed by $\mathbf{r}$, $\mathbf{r}'$, and $\mathbf{r} - \mathbf{r}'$ (Tanaka and Fukui 1975, Haymet *et al.* 1981*a, b*). These data indicate that a fairly good account of the quantitative features of $g^{(3)}$ is provided by the so-called *superposition approximation* (Kirkwood 1935):

$$g^{(3)}(\mathbf{r}, \mathbf{r}') \approx g(r) g(r') g(|\mathbf{r} - \mathbf{r}'|). \qquad (1.17)$$

Equation (1.17) is exact for all separations in the limiting case of a low density fluid, and is found to be rather accurate even for liquids at intermediate and large separations. The largest discrepancies occur for clusters of three particles close to each other, with deviations which are typically of the order of 20%.

In contrast with $g(r)$, which in a fluid probes atomic distances only in a scalar sense, the triplet distribution function yields additional information on *local orientational order*. Suppose, for example, that we are looking for the probability distribution of the angle θ between the 'bonds' joining a central atom with two neighbouring particles. In a fluid these neighbours may be defined as in eqn (1.13), namely by considering all the particles separated by a distance up to R from the central atom. In terms of the cosine of θ the required probability distribution can be written as

$$P(R, \cos\theta) = An^2 \int d\mathbf{r} \int d\mathbf{r}' \, g^{(3)}(\mathbf{r}, \mathbf{r}') \delta(\cos\theta - \cos\theta_{rr'}) \qquad (1.18)$$

where A is a normalization constant, and the integrals over $\mathbf{r}$ and $\mathbf{r}'$ comprise separations up to R. In an isotropic system eqn (1.18) becomes
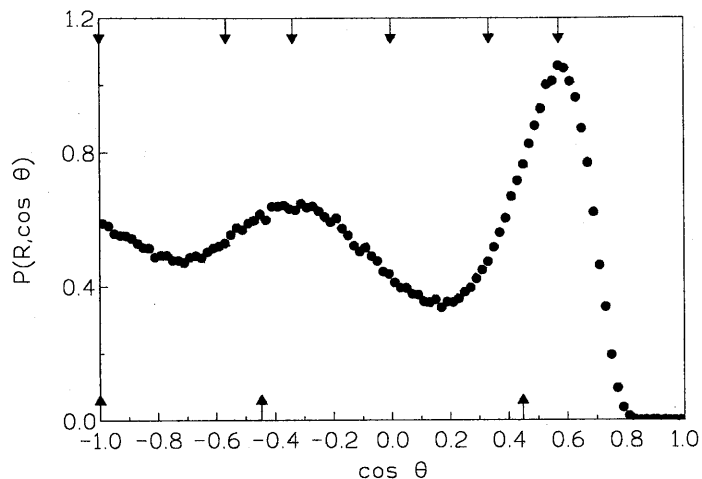
Fig. 1.3 Bond angle distribution $P(R, \cos \theta)$ in liquid Rb at $T \approx 320$ K and $n = 0.010$ Å^{-3}. The filled circles represent the simulation data of Balucani and Vallauri (1990) obtained with a cutoff distance $R = 6.61$ Å. The arrows in the upper part of the figure indicate the cosines of the bond angles for the first two shells of neighbours in a body-centred cubic (bcc) lattice. The arrows at the bottom refer to a similar evaluation for the neighbours of a local icosahedral environment. The total number of involved neighbours is ≈ 12.4 in the liquid, 14 for the bcc lattice and 12 in the icosahedral arrangement.

$$P(R, \cos \theta) = 8\pi^2 A n^2 \int\limits_0^R \mathrm{d}r\, r^2 \int\limits_0^R \mathrm{d}r'\, r'^2 g^{(3)}(r, r', |\mathbf{r} - \mathbf{r}'|) \quad (1.19)$$

where $|\mathbf{r} - \mathbf{r}'|^2 = r^2 + r'^2 - 2rr' \cos \theta$. The quantity $P(R, \cos \theta)$ has been 'measured' in several model systems by computer simulation techniques, choosing in most cases R as the position of the first minimum of $g(r)$. The typical features of $P(R, \cos \theta)$ for simple liquids near the melting point are ilustrated in Fig. 1.3, which refers to liquid rubidium. It is apparent that P vanishes for small angles (up to $\theta \approx 36°$, namely for $\cos \theta \geqslant 0.8$) because of the repulsive core in $\phi(r)$, which prevents any interpenetration of the neighbours. The subsequent peak near $\cos \theta = 0.5$ (i.e. for $\theta \approx 60°$) indicates the presence of local arrangements with the three particles in nearly close contact near the vertices of an equilateral triangle. As $\cos \theta$ decreases larger bond angles and 'open' arrangements are eventually probed, with two broad peaks appearing for $\theta \approx 110°$ ($\cos \theta \approx -0.35$) and $\theta = 180°$ ($\cos \theta = -1$). Liquid Rb is known to crystallize in a body-centred cubic (bcc) structure, but comparing the features of $P(R, \cos \theta)$ in the liquid with those expected for an ideal bcc lattice one hardly notes any

resemblance. Rather, the peak positions of P in the liquid agree closely with those expected for a local *icosahedral* arrangement.

These noteworthy features are only an example of the kind of information deducible from triplet correlations. In addition to $P(R, \cos \theta)$, other more refined probes of local orientational order have been devised (Steinhardt *et al.* 1981) and exploited to investigate, for example, the transition toward a 'glassy' phase as the liquid is supercooled and/or the onset of nucleation events (Hsu and Rahman 1979*a, b*; Mountain 1982; Mountain and Basu 1983; Haymet 1984).

Whether positional or orientational, the microscopic structural properties discussed above yield a sort of 'equilibrium background' against which several quantities of physical interest may fluctuate. These fluctuations are both space and time dependent, and the rest of this chapter will be devoted to their analysis.

1.3 AN INTRODUCTION TO LIQUID-STATE DYNAMICS

The dynamical properties of liquids at the microscopic level are conveniently expressed in terms of time-dependent correlations of the form $\langle B(0)A(t) \rangle$, where the quantities A, B are functions of the $6N$ phase-space variables $(\mathbf{r}^N, \mathbf{p}^N)$ and $A(t) \equiv A(\mathbf{r}^N(t), \mathbf{p}^N(t))$. Leaving aside for the moment any statistical aspect, the basic problem in the dynamics is the solution of the $6N$ classical equations of motion

$$\frac{\mathrm{d}\mathbf{r}_i(t)}{\mathrm{d}t} = \frac{\mathbf{p}_i(t)}{m} \quad (1.20a)$$

$$\frac{\mathrm{d}\mathbf{p}_i(t)}{\mathrm{d}t} = -\frac{\partial V_N(\mathbf{r}^N(t))}{\partial \mathbf{r}_i(t)} \quad (1.20b)$$

where $i = 1, \ldots, N$. In principle, the availability of the $6N$ solutions of eqns (1.20) determines the time evolution of any other phase-space variable such as $A(\mathbf{r}^N(t), \mathbf{p}^N(t))$. Such a program is obviously hopeless for a real macroscopic system where $N \approx 10^{23}$; however, under well-defined conditions this kind of strategy has been successfully adopted in the *molecular-dynamics simulations*, which deal with much smaller systems ($N \approx 10^2$–10^3) so that eqns (1.20) are amenable to a numerical solution by high-speed computers. The widespread use of such simulation techniques in liquid state physics has indeed been of considerable help to the genuine theoretical developments. However, for the time being, we shall ignore these mutual relationships and, having dismissed as unpractical the direct approach of eqns (1.20), we look for an alternative starting point.

Rather than dealing with $6N$ nonlinear differential equations for $\mathbf{r}^N(t)$

and $\mathbf{p}^N(t)$, we may choose to consider the *infinite* set of dynamical equations in a functional space comprising all the phase-space variables like $A(t)$. At first sight the merits of such a new formulation seem questionable, and can really be appreciated only after the introduction of additional tools, like the projection operators discussed in Chapter 3. A first advantage which is, however, immediately apparent in this framework is that the new equations of motion turn out to have a formal structure which is *linear* in the infinite set of phase-space functions. This result is obtained by introducing the *Liouville operator* associated with the Hamiltonian of the system. According to classical mechanics, the equation of motion of a dynamical variable such as $A(t)$ can be written in the form

$$\frac{dA(t)}{dt} = \{A(t), \mathcal{H}\} \equiv iLA(t) \tag{1.21}$$

where the symbol $\{\ ,\ \}$ denotes a classical Poisson bracket (Goldstein 1980) and the Liouville operator of the system is defined by

$$L \equiv i\{\mathcal{H}, \ldots\} \equiv i\sum_i \left[\left(\frac{\partial \mathcal{H}}{\partial \mathbf{r}_i}\right) \cdot \left(\frac{\partial}{\partial \mathbf{p}_i}\right) - \left(\frac{\partial \mathcal{H}}{\partial \mathbf{p}_i}\right) \cdot \left(\frac{\partial}{\partial \mathbf{r}_i}\right) \right]. \tag{1.22}$$

For the Hamiltonian specified by eqns (1.1), (1.2) we deduce that

$$iL = \sum_i \mathbf{v}_i \cdot \left(\frac{\partial}{\partial \mathbf{r}_i}\right) - \frac{1}{m} \sum_{i,j \neq i} \left[\frac{\partial \phi(r_{ij})}{\partial \mathbf{r}_i}\right] \cdot \left(\frac{\partial}{\partial \mathbf{v}_i}\right) \tag{1.23}$$

where $\mathbf{v}_i = \mathbf{p}_i/m$ is the velocity of the ith particle. The linear equation (1.21) can be formally integrated to yield

$$A(t) = \exp(iLt)A \tag{1.24}$$

where $A = A(0)$. The results (1.21) and (1.24) bear a close resemblance with those for the time evolution of quantum-mechanical operators in the Heisenberg picture. This similarity is not fortuitous, since the Poisson bracket of two variables A, B is known to be the limiting form of the commutator $(1/i\hbar)[A_{op}, B_{op}]$ of the corresponding operators in the 'classical case' $\hbar \to 0$.

In the cases of interest the formal solution (1.24) is of little practical use because of the complicated structure of L. Nevertheless, we shall see in Chapter 3 that eqns (1.21) and (1.24) turn out to be quite useful as a starting point of formalisms from which we can develop powerful approximation schemes.

As is customary in the mathematical treatment of functional spaces, it is convenient to associate with any pair A, B of phase-space functions a complex number, denoted by (A, B) and referred as the 'inner' (or 'scalar') products of the two elements A, B. For our purposes, a convenient and

mathematically sound choice for (A, B) is provided by the statistical average $\langle A^*B \rangle$, where A^* denotes the complex conjugate of A. In this functional space the Liouville operator is found to be Hermitian, in the sense that

$$(A, LB) = (B, LA)^* \tag{1.25}$$

(see Appendix A) . A first consequence of this property is that the operator $\exp(iLt)$ appearing in eqn (1.24) is unitary: as a result, the 'length' (A, A) is constant and the time evolution of $A(t)$ can be viewed as a rotation in the functional space.

A second consequence has even more interesting implications. Choosing a well defined form of the scalar product in the functional space, the Liouvillian can in principle be 'diagonalized' with respect to this choice. Since the Hermitian character of L guarantees that its eigenvalues are real, eqn (1.24) yields a simple oscillatory time-dependence for the mutually orthogonal eigenvectors of L. Pursuing the argument even further, we may expect that the time evolution of any dynamical variable can be expressed as a combination of these oscillatory eigenmodes ('normal modes').

If this were the case, we would of course have solved the full dynamical problem. However, the actual situation is different as is clear from the frequent recourse made previously to terms like 'formally' and 'in principle'. Indeed, only a very limited number of eigenmodes of L can be known and exploited in the analysis. Typically, these eigenmodes correspond to dynamical variables having a zero eigenvalue, namely such that $A(t) = A(0)$ at all times. As a matter of fact, some of these 'conserved variables' can immediately be recognized on a purely physical basis, such as the total number of particles, the total momentum and the total energy of the system. Usually, these conserved quantities have a collective character and can be written as $A(0) = A(t) = \sum_j a_j(t)$, where the summation runs over all the particles of the system. We may consider a simple generalization of these special dynamical variables by defining the new quantities

$$A(\mathbf{k}, t) \equiv \sum_j a_j(t) \exp(i\mathbf{k} \cdot \mathbf{r}_j(t)). \tag{1.26}$$

Except in the case $k = 0$, in general the variables $A(\mathbf{k}, t)$ are neither conserved quantities nor exact eigenmodes of the Liouvillian. Even so, it is reasonable to expect that if k is sufficiently small with respect to the inverse of some microscopic length, the time evolution of $A(\mathbf{k}, t)$ is slow enough that this variable can be considered as 'quasi' conserved. In liquids, this small k behaviour is typical of the so-called *hydrodynamic variables*, which probe the dynamics over length scales distinctly larger than the interatomic distances and over time-scales which are much longer than the proper microscopic interaction times (typically, mean collision times). If we focus our attention on this limited set of *quasi-conserved variables*, we may expect

to obtain some important information on the dynamics of the fluid over a 'gross' quasi-macroscopic scale. As we shall see in detail in the following, the fact that these few slow variables are only approximate eigenmodes of L is reflected in their 'eigenvalues', which now have a small imaginary part. In turn, the latter provides for the quasi-conserved modes a damping mechanism, which is physically due to the coupling to the multitude of the other microscopic modes which have been ignored in the analysis.

The previous considerations indicate that the discussion of quasi-conserved modes is a convenient starting point for the study of the dynamics of the liquid state. A further advantage is that quantities like $A(\mathbf{k}, t)$ in eqn (1.26) happen to play an important role even in experimental situations where the 'wave vector' k is not vanishing and the dynamics is not 'slow'. As a result, our analysis will eventually provide a comprehensive account of most time-dependent quantities which are experimentally accessible, ranging from the gross hydrodynamic features down to the genuine microscopic dynamics. In this context, we shall now begin our study by adopting the traditional distinction between single-particle and collective dynamical variables.

1.4 SINGLE-PARTICLE PROPERTIES

1.4.1 The self-intermediate scattering function

The simplest time-dependent quantity we may envisage is associated with the probability that at time t a tagged particle has moved a specified distance from its initial position. (The latter may be chosen arbitrarily, for example in the origin of the reference frame, because of the homogeneity of the system.) To this end, for the ith particle we introduce the dynamical variable

$$n_{s,i}(\mathbf{R}, t) = \delta(\mathbf{R} - \mathbf{r}_i(t)) \qquad (1.27)$$

usually referred as the ith *single-particle* (or *self-*) *density* at the point $\mathbf{R}$ and time t. As it stands, eqn (1.27) is merely the definition of a scalar field; the interpretation of $n_{s,i}(\mathbf{R}, t)$ as a 'density' follows by integrating eqn (1.27) over the full range of $\mathbf{R}$ (typically chosen as the volume V of the system). The resulting normalization condition $\int d\mathbf{R}\, n_{s,i}(\mathbf{R}, t) = 1$ simply means that at any time the tagged particle is 'counted' as being certainly somewhere in the volume V. As is clear from its definition, $n_{s,i}(\mathbf{R}, t)$ is expected to change very rapidly with both $\mathbf{R}$ and t. A convenient 'gross' measure of this variable is provided by its statistical average, which after eqns (1.5)–(1.8) reads

$$\langle n_{s,i}(\mathbf{R}, t) \rangle = \langle n_{s,i}(\mathbf{R}, 0) \rangle$$

$$= [Q_N(V, T)]^{-1} \int d\mathbf{r}^N \delta(\mathbf{R} - \mathbf{r}_i) \exp[-\beta V_N(\mathbf{r}^N)] = 1/V \qquad (1.28)$$

where the first line follows from the invariance of the average with respect to the choice of the time origin. In turn, this 'stationarity' property is a general consequence of the absence of an explicit time-dependence in the Hamiltonian (1.1) of the system. The final result of eqn (1.28) is consistent with the previous interpretation of $n_{s,i}$ as a number density for one particle.

Rather than dealing directly with $n_{s,i}(\mathbf{R}, t)$, in the following we shall find it convenient to consider its space Fourier transform

$$n_{s,i}(\mathbf{k}, t) = \int d\mathbf{R} \exp(i\mathbf{k} \cdot \mathbf{R}) n_{s,i}(\mathbf{R}, t) = \exp[i\mathbf{k} \cdot \mathbf{r}_i(t)]. \qquad (1.29)$$

The equation of motion for this new variable reads

$$dn_{s,i}(\mathbf{k}, t)/dt = i\mathbf{k} \cdot \mathbf{v}_i(t) n_{s,i}(\mathbf{k}, t). \qquad (1.30)$$

For $k = 0$, we clearly deal with a 'conserved' variable, a consequence of the fact that the tagged particle cannot be annihilated. From the discussion in the previous section, the time evolution of $n_{s,i}(\mathbf{k}, t)$ can be expected to be 'slow' if k is small enough.

The time correlation associated with $n_{s,i}(\mathbf{k}, t)$ is usually referred as the *self-intermediate scattering function*:

$$F_s(k, t) \equiv \langle n_{s,i}^*(\mathbf{k}, 0) n_{s,i}(\mathbf{k}, t) \rangle = \langle \exp[i\mathbf{k} \cdot (\mathbf{r}_i(t) - \mathbf{r}_i(0))] \rangle \qquad (1.31)$$

and is one of the basic quantities in any theory of the dynamics of liquids. Coming back to the space domain, from $F_s(k, t)$ we obtain the so-called *self-correlation function* (van Hove 1954):

$$G_s(r, t) = (2\pi)^{-3} \int d\mathbf{k} \exp(-i\mathbf{k} \cdot \mathbf{r}) F_s(k, t)$$

$$= \langle \delta(\mathbf{r} - (\mathbf{r}_i(t) - \mathbf{r}_i(0))) \rangle. \qquad (1.32)$$

This time-dependent quantity probes the dynamics of a single particle in terms of its displacement from an initial position, namely just in the way mentioned at the beginning of this section. In particular, $G_s(r, 0) = \delta(\mathbf{r})$ and $\int dr\, G_s(r, t) = 1$.

Alternatively, one may transform $F_s(k, t)$ with respect to the time variable to obtain its frequency spectrum

$$S_s(k, \omega) = (1/2\pi) \int_{-\infty}^{\infty} dt \exp(-i\omega t) F_s(k, t), \qquad (1.33)$$

which has a direct experimental relevance because of its connection to the incoherent part of the inelastic neutron scattering cross-section (see Chapter 2).

Besides providing a justification for the 'intermediate' character attributed to $F_s(k, t)$, the previous considerations do not throw much light on the behaviour expected for this time correlation function. Some of these features can straightforwardly be deduced from the general properties of any time-dependent average in a classical system (see Appendix B). In particular, by this kind of argument we may establish that in a fluid $F_s(k, t)$ is real (real-valued), and even both in k and t (such that $F_s(k, t) = F_s(-k, t)$ and $F_s(k, t) = F_s(k, -t)$). Moreover, at sufficiently short times $F_s(k, t)$ may be expanded as

$$F_s(k, t) = F_s(k, 0)\left[1 - \langle \omega_k^2 \rangle_s (t^2/2) + \langle \omega_k^4 \rangle_s (t^4/4!) + \cdots\right]$$

(1.34)

where the initial value $F_s(k, 0) = 1$ after eqn (1.30). The quantities $\langle \omega_k^n \rangle_s$ are clearly related to the derivatives of $F_s(k, t)$ evaluated at $t = 0$. Alternatively, $\langle \omega_k^n \rangle_s$ can be identified with the nth *frequency moment* of the spectrum $S_s(k, \omega)$:

$$\langle \omega_k^n \rangle_s = \int\limits_{-\infty}^{\infty} d\omega \, \omega^n S_s(k, \omega).$$

(1.35)

As is implicit in eqn (1.34), all the frequency moments with odd n vanish because of the even character of $F_s(k, t)$, which implies that in eqn (1.33) $S_s(k, \omega)$ is an even function of ω.

By definition, the frequency moments convey information on the *short-time dynamics* of the system, as probed by the correlation function under consideration. In practice, only the first few moments are amenable to a direct evaluation; such a task is made easier by a repeated use of the result (B.17), by which a single time derivative in a correlation function can be 'shifted' from one variable to the other one, the net result being only a change of sign. Thus, denoting a time derivative with a dot we write

$$\langle \omega_k^2 \rangle_s = - \langle n_{s,i}^*(\mathbf{k}, 0) \ddot{n}_{s,i}(\mathbf{k}, 0) \rangle = \langle \dot{n}_{s,i}^*(\mathbf{k}, 0) \dot{n}_{s,i}(\mathbf{k}, 0) \rangle \quad (1.36a)$$

$$\langle \omega_k^4 \rangle_s = \langle n_{s,i}^*(\mathbf{k}, 0) \ddddot{n}_{s,i}(\mathbf{k}, 0) \rangle = \langle \ddot{n}_{s,i}^*(\mathbf{k}, 0) \ddot{n}_{s,i}(\mathbf{k}, 0) \rangle. \quad (1.36b)$$

The evaluation of the second moment $\langle \omega_k^2 \rangle_s$ from eqn (1.36a) is straightforward. Indeed, using eqn (1.30) we immediately obtain ($a, \beta \equiv x, y, z$):

$$\langle \omega_k^2 \rangle_s = \langle (\mathbf{k} \cdot \mathbf{v}_i)^2 \rangle = \sum_{a, \beta} k_a k_\beta \langle v_{i,a} v_{i,\beta} \rangle$$

$$= \left(\sum_a k_a^2\right) \langle (v_{i,x})^2 \rangle = \frac{1}{3} k^2 \langle v_i^2 \rangle \quad (1.37)$$

where in the last line we have exploited well-known properties of the Maxwellian velocity distribution, such as the statistical independence of different cartesian components and their inherent isotropy. Finally, using eqn (1.10) we find

$$\langle \omega_k^2 \rangle_s = (k_B T/m)k^2. \quad (1.38)$$

Because of its kinetic origin, the result (1.38) is valid for all classical systems, irrespective of their interatomic potential.

Although comparatively more involved, the evaluation of $\langle \omega_k^4 \rangle_s$ from (1.36b) is typical of several liquid-state calculations and we shall report it in some detail. Noting that $\ddot{n}_{s,i}(\mathbf{k}, 0) = [-(\mathbf{k} \cdot \mathbf{v}_i)^2 + i(\mathbf{k} \cdot \dot{\mathbf{v}}_i)]\exp(i\mathbf{k} \cdot \mathbf{r}_i)$, we have to evaluate

$$\langle \omega_k^4 \rangle_s = \langle (\mathbf{k} \cdot \mathbf{v}_i)^4 \rangle + \langle (\mathbf{k} \cdot \dot{\mathbf{v}}_i)^2 \rangle \quad (1.39)$$

since the mixed contributions cancel each other. The first term at the right-hand side of (1.39) is purely kinetic and can be expressed as

$$\langle (\mathbf{k} \cdot \mathbf{v}_i)^4 \rangle = \sum_{a\beta\gamma\delta} k_a k_\beta k_\gamma k_\delta \langle v_{i,a} v_{i,\beta} v_{i,\gamma} v_{i,\delta} \rangle$$

$$= \sum_a k_a^4 \langle v_{i,a}^4 \rangle + \sum_{a, \beta \neq a} k_a^2 k_\beta^2 \langle v_{i,a}^2 v_{i,\beta}^2 \rangle \quad (1.40)$$

where the summations over the cartesian components have been split in all the possible ways yielding nonvanishing averages in the velocity space. Since $\langle v_{i,a}^4 \rangle = 3(k_B T/m)^2$ and $\langle v_{i,a}^2 v_{i,\beta}^2 \rangle = \langle v_{i,a}^2 \rangle \langle v_{i,\beta}^2 \rangle = (k_B T/m)^2$ for $a \neq \beta$, we finally obtain

$$\langle (\mathbf{k} \cdot \mathbf{v}_i)^4 \rangle = 3(k_B T/m)^2 \sum_{a\beta} k_a^2 k_\beta^2 = 3(k_B T/m)^2 k^4. \quad (1.41)$$

The second contribution in eqn (1.39) involves the acceleration $\dot{\mathbf{v}}_i = (1/m)\mathbf{F}_i$, where $\mathbf{F}_i = -(\partial V_N/\partial \mathbf{r}_i)$ is the total force acting on the ith particle. The resulting statistical average in the configurational space can be written as

$$\langle (\mathbf{k} \cdot \dot{\mathbf{v}}_i)^2 \rangle = \frac{1}{m^2} \sum_{a\beta} k_a k_\beta \left\langle \frac{\partial V_N}{\partial r_{i,a}} \frac{\partial V_N}{\partial r_{i,\beta}} \right\rangle$$

$$= \frac{1}{m^2 Q_N(V, T)} \sum_{a\beta} k_a k_\beta \int d\mathbf{r}^N \frac{\partial V_N}{\partial r_{i,a}} \frac{\partial V_N}{\partial r_{i,\beta}} \exp(-\beta V_N)$$

$$= \frac{k_B T}{m^2 Q_N(V, T)} \sum_{a\beta} k_a k_\beta \int d\mathbf{r}^N \frac{\partial^2 V_N}{\partial r_{i,a} \partial r_{i,\beta}} \exp(-\beta V_N) \quad (1.42)$$

where the last step follows from a partial integration. We now write the total potential energy V_N in terms of pairwise contributions (eqn (1.2)),

and exploit the independence of the average on the labelling of the particles. As a result,

$$\langle (\mathbf{k} \cdot \dot{\mathbf{v}}_i)^2 \rangle = \frac{k_B T (N-1)}{m^2 Q_N(V,T)} \sum_{\alpha\beta} k_\alpha k_\beta \int d\mathbf{r}_1 d\mathbf{r}_2 \frac{\partial V_N}{\partial r_{i,\alpha} \partial r_{i,\beta}} \int d\mathbf{r}_3 \cdots d\mathbf{r}_N \exp(-\beta V_N)$$

$$= \frac{n^2 k_B T}{m^2 N} \sum_{\alpha\beta} k_\alpha k_\beta \int d\mathbf{r}_1 d\mathbf{r}_2 \frac{\partial \phi(r_{12})}{\partial r_{12,\alpha} \partial r_{12,\beta}} g(\mathbf{r}_{12})$$

$$= \frac{n k_B T}{m^2} \sum_{\alpha\beta} k_\alpha k_\beta \int d\mathbf{r}_{12} \frac{\partial \phi(r_{12})}{\partial r_{12,\alpha} \partial r_{12,\beta}} g(\mathbf{r}_{12}) \tag{1.43}$$

where we have used the definition (1.12) of $g(\mathbf{r})$, introduced relative coordinates $\mathbf{r}_{12} = \mathbf{r}_1 - \mathbf{r}_2$ and finally exploited the homogeneity of the system. Since in an isotropic fluid $g(\mathbf{r}_{12})$ only depends on the magnitude of $\mathbf{r}_{12}$, the angular integrations implicit in the last step of (1.43) can be performed immediately, with the result that only the terms with $\alpha = \beta$ yield a non-zero contribution. Consequently, we may write

$$\langle (\mathbf{k} \cdot \dot{\mathbf{v}}_i)^2 \rangle = \frac{n k_B T}{m^2} \sum_\alpha k_\alpha^2 \int d\mathbf{r} \frac{\partial^2 \phi(r)}{\partial r_\alpha^2} g(r)$$

$$= \frac{n k_B T}{3 m^2} k^2 \int d\mathbf{r} \, \nabla^2 \phi(r) g(r) \tag{1.44}$$

where we have again made use of the isotropy of the system and finally introduced

$$\nabla^2 \phi(r) \equiv \sum_\alpha \frac{\partial^2 \phi(r)}{\partial r_\alpha^2} = \phi''(r) + \frac{2\phi'(r)}{r}. \tag{1.45}$$

Summing the results found for both contributions on the right-hand side eqn (1.39), we finally obtain

$$\langle \omega_k^4 \rangle_s = \frac{k_B T}{m} k^2 \left[\left(\frac{3 k_B T}{m} \right) k^2 + \Omega_0^2 \right] \tag{1.46}$$

where Ω_0 is the so-called *Einstein frequency* defined by

$$\Omega_0^2 \equiv (n/3m) \int d\mathbf{r} \, \nabla^2 \phi(r) g(r). \tag{1.47}$$

A first consequence of these results is that, in contrast to $\langle \omega_k^2 \rangle_s$, the fourth moment $\langle \omega_k^4 \rangle_s$ depends on the interatomic potential $\phi(r)$. Besides the explicit appearance of $\nabla^2 \phi(r)$ in eqn (1.47), this dependence is due to the presence of $g(r)$, which is itself a function of $\phi(r)$.

In the limiting case of *free particles* ($\phi(r) \equiv 0$) we obtain

$$\langle \omega_k^4 \rangle_s = 3(k_B T/m)^2 k^4. \tag{1.48}$$

In such a case we find that $\langle \omega_k^4 \rangle_s = 3\langle \omega_k^2 \rangle_s^2$. This relation between the second and the fourth moments is exactly satisfied for a Gaussian spectrum $S_s(k, \omega)$ centred at $\omega = 0$. To confirm that this is actually the correct shape, we insert in eqn (1.32) for $G_s(r, t)$ the free particle dynamics $\mathbf{r}_i(t) = \mathbf{r}_i(0) + \mathbf{v}_i t$. Performing the statistical average in the velocity space, we find

$$G_s(r, t) = \left[\frac{\beta m}{2 \pi t^2} \right]^{3/2} \exp\left(\frac{-\beta m r^2}{2 t^2} \right). \tag{1.49}$$

To obtain the intermediate scattering function we use a Fourier transform in the space domain, giving

$$F_s(k, t) = \exp\left(\frac{-k^2 t^2}{2 m \beta} \right), \tag{1.50}$$

namely a Gaussian both in the wavevector and in time. Finally, a second Fourier transform in the time domain yields the spectrum

$$S_s(k, \omega) = \left[\frac{m \beta}{2 \pi k^2} \right]^{1/2} \exp\left(\frac{-\beta m \omega^2}{2 k^2} \right), \tag{1.51}$$

which is indeed a Gaussian function of the frequency ω.

Summarizing all these simple results, life with free particles is found to be easy, but rather trivial. Much more interesting is to see under which conditions real interacting systems can approach this limiting behaviour. In the present single-particle case such a trend is always present at sufficiently short times, where $\mathbf{r}_i(t) = \mathbf{r}_i(0) + \mathbf{v}_i t + O(t^2)$. The initial time decay of $F_s(k, t)$ is indeed ruled by $\langle \omega_k^2 \rangle$, which is not affected by the interactions among the particles. In addition, the exact fourth moment (1.46) reduces to the free-particle one for wave vectors such that

$$k \gg \Omega_0 (3 k_B T/m)^{-1/2}. \tag{1.52}$$

At these large k, $F_s(k, t)$ is thus expected to probe a dynamics of essentially noninteracting particles. The condition (1.52) can be written as $kl \gg 1$, where the length

$$l = (3 k_B T/m)^{1/2} \Omega_0^{-1}. \tag{1.53}$$

The factor $(3 k_B T/m)^{1/2}$ on the right-hand side is the average thermal speed of a particle. From eqn (1.47) the time Ω_0^{-1} is seen to depend on the pair potential, and to become very large for dilute systems. As a consequence, it is reasonable to interpret Ω_0 as the average interaction (or 'collision') frequency for the tagged particle (see Section 1.4.2 for a more detailed discussion). Then the length l plays the role of an effective *mean free path*,

and the condition $kl \gg 1$ simply means that the particles appear to behave as free when probed over a spatial range ($\approx 2\pi/k$) much shorter than l.

It is also instructive to discuss the opposite case, $kl \ll 1$. Such a condition is verified when the dynamics of the tagged particle is probed over a length scale involving many collisional events. Although initially the particle again appears as free, at finite times a new situation emerges. In particular, at times much longer than Ω_0^{-1} we approach a quasi-macroscopic description of the dynamics, in which the number of collisions experienced by the particle is so large that the microscopic details of each of them effectively become irrelevant. An indication of the kind of dynamics probed in this low k regime is provided by the exact result

$$\lim_{k \to 0} \left\{ -\frac{1}{k^2} \left[\frac{d^2 F_s(k,t)}{dt^2} \right] \right\} = \tfrac{1}{3} \langle \mathbf{v}_i(0) \cdot \mathbf{v}_i(t) \rangle \qquad (1.54)$$

where we have exploited the isotropy of the system. The time correlation on the right-hand side is referred to as the *velocity autocorrelation function* for the tagged particle. In view of its relevance in liquid state dynamics, this time-dependent quantity deserves a separate discussion, which is the subject of the following subsection.

1.4.2 Mean square displacement and velocity autocorrelation function

The best way to appreciate the physics underlying $\langle \mathbf{v}_i(0) \cdot \mathbf{v}_i(t) \rangle$ is to introduce a closely related dynamical quantity, the *mean square displacement* of a particle. This is defined as

$$\delta r^2(t) \equiv \langle [\mathbf{r}_i(0) - \mathbf{r}_i(t)]^2 \rangle = \int d\mathbf{r} \, r^2 G_s(r,t). \qquad (1.55)$$

The relation between $\delta r^2(t)$ and $\langle \mathbf{v}_i(0) \cdot \mathbf{v}_i(t) \rangle$ is readily obtained noting that $\mathbf{r}_i(t) = \mathbf{r}_i(0) + \int_0^t dt' \, \mathbf{v}_i(t')$, so that

$$\delta r^2(t) = \int_0^t dt' \int_0^t dt'' \, \langle \mathbf{v}_i(t') \cdot \mathbf{v}_i(t'') \rangle. \qquad (1.56)$$

The double integration appearing on the right-hand side may be reduced to a single one by exploiting the stationarity of the average in (1.56) and by performing a partial integration in the variable $t'' - t'$. After some algebra we eventually obtain

$$\delta r^2(t) = 2 \int_0^t d\tau (t - \tau) \langle \mathbf{v}_i(0) \cdot \mathbf{v}_i(\tau) \rangle. \qquad (1.57)$$

Alternatively, we may verify that

$$\langle \mathbf{v}_i(0) \cdot \mathbf{v}_i(t) \rangle = \tfrac{1}{2} \frac{d^2 [\delta r^2(t)]}{dt^2}. \qquad (1.58)$$

At short times, the decay of the velocity autocorrelation function from its initial value $\langle \mathbf{v}_i^2(0) \rangle = 3k_B T/m$ can be expressed as

$$\langle \mathbf{v}_i(0) \cdot \mathbf{v}_i(t) \rangle = \langle \mathbf{v}_i^2(0) \rangle - \langle \dot{\mathbf{v}}_i^2(0) \rangle (t^2/2) + \cdots. \qquad (1.59)$$

The evaluation of $\langle \dot{\mathbf{v}}_i^2(0) \rangle$ involves the same steps previously seen for the potential part of $\langle \omega_k^4 \rangle_s$, and leads to $\langle \dot{\mathbf{v}}_i^2 \rangle = (3k_B T/m) \Omega_0^2$. The normalized correlation function $\psi(t) \equiv \langle \mathbf{v}_i(0) \cdot \mathbf{v}_i(t) \rangle / \langle \mathbf{v}_i^2(0) \rangle$ consequently reads

$$\psi(t) = 1 - \Omega_0^2(t^2/2) + \cdots. \qquad (1.60)$$

The insertion of these short-time results into eqn (1.57) leads to

$$\delta r^2(t) = (3k_B T/m)t^2 - (k_B T/4m) \Omega_0^2 t^4. \qquad (1.61)$$

Equation (1.61) shows that initially the mean square displacement increases quadratically with time, as if the particle were free. However, after a time of the order of Ω_0^{-1} the particle experiences a collision and its motion is drastically modified, leading to a considerably smaller value of $\delta r^2(t)$.

From eqn (1.54) it is straightforward to verify that the results (1.60), (1.61) follow from those previously obtained for the short-time dynamics of $F_s(k, t)$. In the particular case of the velocity autocorrelation function, eqn (1.60) shows that the initial decrease of $\psi(t)$ is ruled by the Einstein frequency. The collisional nature of this decay mechanism has been anticipated in the last subsection, and can be further clarified by a simple analysis of the definition (1.47) of Ω_0^2. To this purpose, we shall assume that the pair interaction $\phi(r)$ can approximately be written as a *generalized Lennard–Jones potential*

$$\phi(r) = \left[\frac{\varepsilon}{(q-p)} \right] \left[p \left(\frac{r_0}{r} \right)^q - q \left(\frac{r_0}{r} \right)^p \right] \qquad (1.62)$$

where p and q ($>p$) are the exponents pertinent to the attractive and repulsive portions of $\phi(r)$, respectively. With this representation, $\phi(r)$ is characterized by a negative potential well of depth ε located at $r = r_0$. The usual Lennard–Jones parameter σ is defined by $\phi(r = \sigma) = 0$, and follows from $(\sigma/r_0)^{q-p} = p/q$. In several cases of interest, both p and q are distinctly larger than 1; for example, the choice $p = 6$, $q = 12$ is known to give a fairly good approximation for the pair potential in inert gas fluids.

Inserting (1.62) in the definition (1.47) we obtain

$$\Omega_0^2 = \frac{4\pi n\varepsilon r_0}{3m} \frac{pq}{q-p} \int_0^\infty dr^* \, [(q-1)(r^*)^{-q} - (p-1)(r^*)^{-p}] g(r^*)$$

$$\qquad (1.63)$$

Table 1.1 Values of several quantities of interest for single-particle motion in two monatomic liquids slightly above the melting point. Liquid Ar is considered at a temperature $T = 86.5\,\text{K}$ and a number density $n = 0.0213\,\text{Å}^{-3}$; the potential parameters are $\varepsilon/k_B \approx 120\,\text{K}$ and $r_0 \approx 3.82\,\text{Å}$. For liquid Rb at 318 K, $n = 0.01\,\text{Å}^{-3}$, $\varepsilon/k_B \approx 402\,\text{K}$, and $r_0 \approx 5.16\,\text{Å}$. The quoted values of Ω_0^2 are deduced from the simulation data of Levesque *et al.* (1973) for Ar and of Rahman (1974) for Rb. The quantities l (eqn (1.53)) and Ω_0^{-1} provide 'natural' length scales and timescales for the microscopic dynamics. Note that $l \ll r_0$.

	nr_0^3	ε/mr_0^2 (ps^{-2})	$n\varepsilon r_0/m$ (ps^{-2})	Ω_0^2 (ps^{-2})	l (Å)	Ω_0^{-1} (ps)
Argon	1.19	0.170	0.202	59.3	0.301	0.130
Rubidium	1.43	0.147	0.210	37.2	0.498	0.164

where $r^* = r/r_0$. Since at liquid density $g(r)$ has a first sharp peak at $r \approx r_0$, the leading contribution to the integral is provided by values $r^* \approx 1$. Thus Ω_0^2 can approximately be written as

$$\Omega_0^2 \approx Cnr_0^3(\varepsilon/mr_0^2)pq \tag{1.64}$$

where typically the dimensionless constant $C \approx 4$ in all liquids characterized by close-packed arrangements of atoms.

The result (1.64) expresses Ω_0 in terms of the natural frequency unit $(\varepsilon/mr_0)^{1/2}$ and shows that, other things being equal, Ω_0 is larger in systems where $\phi(r)$ has a harsh repulsive portion. In Table 1.1 we report the values of the relevant quantities for two typical systems, liquid argon and liquid rubidium. As already mentioned, in Ar the actual $\phi(r)$ is satisfactorily modelled by eqn (1.62) with $p = 6$ and $q = 12$. On the other hand, effective pair potentials in alkali metals are characterized by a considerably softer repulsive portion, as well as by small damped oscillations at large separations (Rahman 1974). Whereas the latter are relatively unimportant in the present context, in the relevant r range $\phi(r)$ can be satisfactorily modelled by eqn (1.62) with $p = 6$ and $q = 7$. As a result, eqn (1.64) predicts that $(\Omega_0^2)_{Ar}/(\Omega_0^2)_{Rb} = 1.65$, in satisfactory agreement with the actual ratio ≈ 1.59 deduced from Table 1.1.

Another consequence of (1.64) is that Ω_0^2 is predicted to be proportional to the curvature of $\phi(r)$ at its minimum, namely to $\phi''(r_0) = (\varepsilon/r_0^2)pq$. This circumstance is intuitively expected in a solid-like picture in which the tagged particle performs a localized *oscillatory motion* as a result of the interactions with its near neighbours. Such a picture is in fact analogous to the model initially proposed by Einstein to account for the lattice

vibrations in a crystal, a circumstance which justifies the name traditionally used for Ω_0.

In a liquid, this simple representation of single-particle dynamics turns out to be valid only at short times. Indeed, a tagged particle initially experiences the local disorder inherent to the liquid state only in an average sense, and its motion is not basically different from the one that would be performed in a crystal lattice. However, at longer times the neighbours are themselves affected by a continuous dynamic rearrangement, which ultimately leads to a disruption of the original shell of atoms and to the actual 'escape' of the test particle from the 'cage' of its initial neighbours. In such a physical situation, the solid-like analogy is clearly untenable, and after its initial 'attempts' to oscillate the particle is expected to move in a way which rapidly becomes uncorrelated with any short-time feature. Ultimately, the particle is indeed found to perform a *diffusive motion*.

To see how this new kind of dynamics emerges from the previous equations, we go back to the result (1.57) for the mean square displacement. If we now consider times t so long that the velocity $\mathbf{v}_i(t)$ of the particle is totally uncorrelated with the initial value $\mathbf{v}_i(0)$, eqn (1.57) can be approximately expressed as

$$\delta r^2(t) = 2\int_0^t d\tau \langle \mathbf{v}_i(0) \cdot \mathbf{v}_i(\tau) \rangle t \tag{1.65}$$

where the upper integration limit can safely be extended to infinity since at such long times the velocity autocorrelation function is negligibly small. Equation (1.65) is usually written in the form

$$\delta r^2(t) = 6Dt \qquad (t \to \infty) \tag{1.66}$$

where we have introduced the *diffusion coefficient*

$$D = \tfrac{1}{3}\int_0^\infty d\tau \langle \mathbf{v}_i(0) \cdot \mathbf{v}_i(\tau) \rangle. \tag{1.67}$$

Equation (1.67) is the simplest example of a *Green–Kubo relation* expressing the transport coefficients of a fluid in terms of time integrals of suitable microscopic correlation functions (Green 1954, Kubo 1957; Helfland 1960). The establishment of this connection is one of the most important successes of statistical mechanics. Also, by this link we may better appreciate the physical factors ultimately relevant to the variation of transport coefficients in different systems, as well as their dependence on the state parameters.

The typical time dependence of the mean square displacement $\delta r^2(t)$ in a liquid is illustrated in Fig. 1.4. It is apparent that the parabolic increase associated with free-particle behaviour is valid only for very short times;
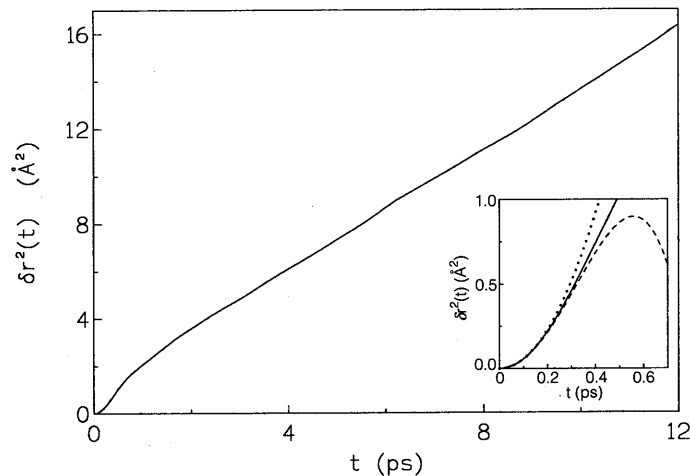
Fig. 1.4 Typical time dependence of the mean square displacement $\delta r^2(t)$ of a particle in a monatomic fluid near melting. The full line is the result of a simulation study of liquid Cs at 308 K (unpublished data by A. Torcini, 1992). The insert shows the short-time portion of these data, along with the behaviour expected for free particles (dotted line) and the predictions of eqn (1.61) (dashed line).

even the inclusion of the additional t^4 term (cf.(1.61)) leads to a rather modest extension of the time region which is possible to account for. The bulk of the results are instead seen to be consistent with the linear time dependence typical of the diffusive regime (1.66).

After eqn (1.54), all these dynamical features are expected to have important consequences on the time dependence of $F_s(k, t)$ at sufficiently small wave vectors. In the present context, we shall limit ourselves to a simplified discussion; a more rigorous derivation of the final result is reported in Section 3.4. At the lowest order in k we may use eqn (1.54), which can be integrated to give

$$\frac{1}{k^2} \dot{F}_s(k, t) = -\tfrac{1}{3} \int_0^t d\tau \langle \mathbf{v}_i(0) \cdot \mathbf{v}_i(\tau) \rangle. \tag{1.68}$$

This result is valid at all times provided that $k \to 0$. As t increases, the right-hand side of (1.68) approaches $-D$, and a second integration yields

$$F_s(k, t) \approx 1 - k^2 D t \tag{1.69}$$

which is valid provided that $k \to 0$, $t \to \infty$ (with the k limit taken first, in such a way that $k^2 D t \ll 1$). Equation (1.69) is the limiting form of the correct result for $F_s(k, t)$ in the diffusive regime

$$F_s(k, t) = \exp(-D k^2 |t|). \tag{1.70}$$

While the presence of $|t|$ in (1.70) ensures the correct even character of $F_s(k, t)$, it is immediately apparent that the results (1.69) and (1.70) violate the exact short-time behaviour as given by eqn (1.34). This is hardly surprising, as in the derivation we have explicitly assumed that the time t is long enough to encompass all the microscopic dynamics probed by the velocity autocorrelation function. Otherwise stated, we effectively deal with two *distinctly different time-scales*. The first one concerns short times, and is truly microscopic in the sense that the underlying dynamics can be accounted for by simple averages, directly related to the microscopic Hamiltonian. In contrast, the second time-scale probes dynamical processes (diffusive behaviour in the present case) which comprise such a large number of microscopic events (free motion, collisions, etc.) to prevent a detailed description of each one of them. Other examples of this separation of time-scales will frequently be met in the following. Once that the underlying physics is clear, this feature can be exploited to yield a comprehensive account of a complicated dynamical problem.

1.4.3   A closer contact with typical single-particle data

To conclude this section, we report the results of several tests of single-particle dynamics in monatomic liquids. Part of these results (as well as of those reported in the following for collective dynamics) are actual experimental data, obtained, for example, by inelastic neutron scattering. The reader is referred to Chapter 2 for a detailed account of this and other experimental techniques of common use in this field.

In some cases, however, it is difficult or impossible to perform a direct measurement of the property of interest. In such a circumstance, the traditional remedy is to resort to computer simulation techniques, with the implicit assumption that for the property under consideration the simulated system is sufficiently 'realistic' to mimic with a good approximation the behaviour of the actual liquid. These 'numerical experiments' will be briefly discussed in Section 2.7.

Typical neutron-scattering results for the spectrum $S_s(k, \omega)$ are reported in Fig. 1.5, which refers to liquid argon (Sköld *et al.* 1972). It is apparent that at all wave vectors $S_s(k, \omega)$ exhibits a monotonous decay with frequency. As a result, the relevant physical information is provided by the spectral width $\Gamma_s(k)$, which is found to increase with k. This trend can be qualitatively understood starting from the low wave vectors typical of the diffusive regime. Here, a Fourier transform of eqn (1.70) yields

$$S_s(k, \omega) = (1/\pi) \frac{D k^2}{\omega^2 + (D k^2)^2}, \tag{1.71}$$
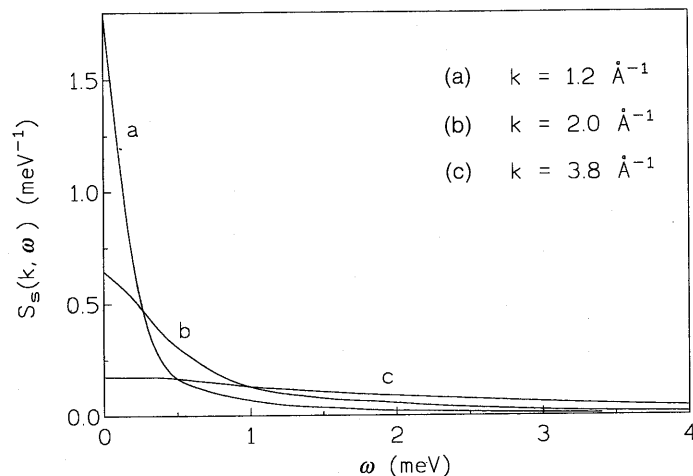
Fig. 1.5 Spectral shapes of $S_s(k, \omega)$ at several wave vectors as obtained by inelastic neutron scattering in liquid Ar at 85 K (after Sköld *et al.* 1972).

namely a Lorentzian spectrum with a halfwidth at half maximum $\Gamma_s(k) = Dk^2$. At least in this low wave vector domain, the spectra are thus expected to become considerably broader as k increases. Although with a weaker k dependence, a similar broadening effect can be predicted in the opposite limit of large wave vectors, namely for $kl \gg 1$ (cf. eqn (1.52)). Here $S_s(k, \omega)$ should eventually approach the free-particle spectrum (1.51), with a corresponding halfwidth given by $\Gamma_s(k) = (2 \ln 2 \, k_B T/m)^{1/2}k$. No exact result for $\Gamma_s(k)$ is instead available in the (rather large!) 'transition region', roughly specified by $kl \approx 1$.

The experimental width $\Gamma_s(k)$ is usually reported as 'normalized' with respect to its small-k value Dk^2. The typical features of this wave vector dependence are illustrated in Fig. 1.6, which again refers to liquid argon. Along with the neutron data of Sköld *et al.* (1972), we also report the results obtained in a previous simulation study in 'Lennard–Jones' argon (Levesque and Verlet 1970). At the lowest wave vectors accessible, both sets of data indicate for $\Gamma_s(k)$ a k dependence somewhat weaker than the one implied by a k^2 law. This tendency increases with the wave vector up to $k \approx 2$ Å^{-1}, a value near the position of the main peak of $S(k)$ in this system. After a maximum decrease of $\approx 10\%$ with respect to the diffusive prediction, $\Gamma_s(k)$ rapidly becomes larger than Dk^2 by as much as 20% in the real liquid. Only for $k > 6$ Å^{-1} does the ratio $\Gamma_s(k)/Dk^2$ begin to approach the limiting $1/k$ behaviour appropriate for the free-particle regime. The oscillations of $\Gamma_s(k)/Dk^2$ are a clear indication that at increas-
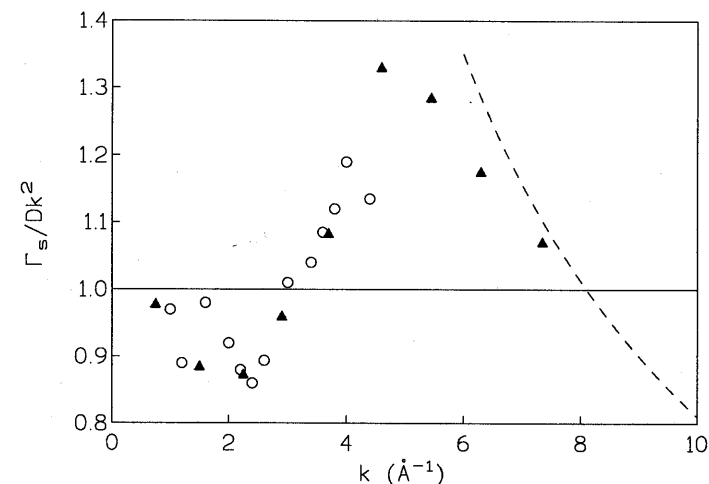
Fig. 1.6 Wavevector dependence of the 'normalized halfwidth' $\Gamma_s(k)/Dk^2$ in liquid argon. The open circles are the neutron data of Sköld *et al.* (1972), and the triangles denote the simulation results of Levesque and Verlet (1970). The dashed line is the limiting free-particle behaviour.

ing wave vectors a variety of dynamical processes are effectively probed. As anticipated, an important role in this respect is played by the 'mean free path' l: for liquid argon, the value of $l^{-1} \approx 3.3$ Å^{-1} gives an approximate measure of the extent of the initial k range where $\Gamma_s(k) < Dk^2$.

Coming back to the self-intermediate scattering function, the results (1.69) and (1.50) show that $F_s(k, t)$ is a Gaussian function of k both in the diffusive regime ($kl \ll 1$) and in the free-particle limit ($kl \gg 1$). This circumstance suggests that we look to determine whether such a simple k dependence is valid even for intermediate wave vectors. If this Gaussian ansatz (assumption) were correct, $F_s(k, t)$ could be written as $\exp[-k^2 a(t)]$, where the quantity $a(t)$ can be inferred from the exact results found in the two limiting situations. Proceeding in such a way, it is straightforward to deduce that

$$F_s(k, t) = \exp\left[-\tfrac{1}{6} k^2 \delta r^2(t)\right]. \tag{1.72}$$

This 'Gaussian approximation' has been tested against computer simulation data for Lennard–Jones fluids at different densities (Nijboer and Rahman 1966). In the liquid range, the discrepancies are found to be rather small, and mainly occur in the intermediate range of wave vectors and times, as expected. The same features are apparent from Fig. 1.7, which reports a similar comparison for a liquid alkali metal near melting. The overall
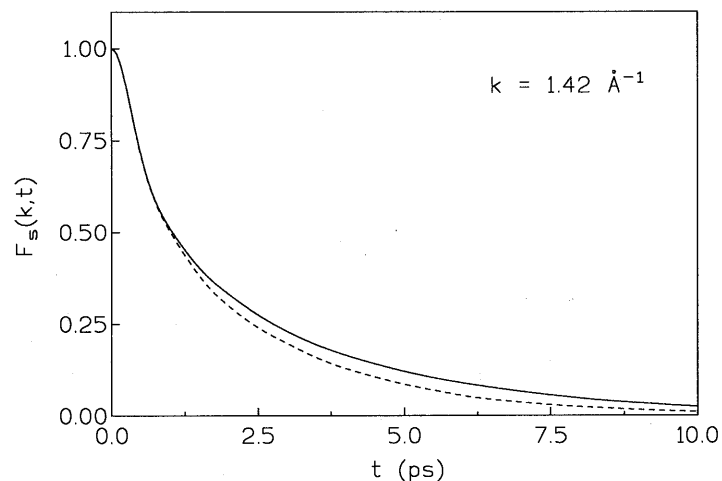
Fig. 1.7 Comparison between the predictions of the Gaussian approximation (1.72) for $F_s(k, t)$ (dashed line) and the computer simulation data (full line) for liquid Cs at the wavevector $k = 1.42$ Å^{-1} where $S(k)$ has its main peak (Balucani et al. 1992). To make the test more crucial, the mean square displacement $\delta r^2(t)$ to be inserted in eqn (1.72) has separately been evaluated in the same simulation runs (cf. Fig. 1.4).

fair agreement with the data has made the use of eqn (1.72) attractive in several physical situations, some of which will be discussed in Chapter 5. In early works, the Gaussian approximation has been complemented by choosing a simple 'ad-hoc' form of $\delta r^2(t)$, and used to obtain a convenient analytical expression for the shapes observed in the experimental spectra of $S_s(k, \omega)$ (Egelstaff and Schofield 1962).

The other important probe of single-particle dynamics is provided by the velocity autocorrelation function. Its frequency spectrum $Z(\omega)$ can in principle be deduced from measurements of $S_s(k, \omega)$ at sufficiently small wave vectors, since

$$Z(\omega) \equiv (2\pi)^{-1} \int_{-\infty}^{\infty} dt \exp(-i\omega t) \langle v_i(0) \cdot v_i(t) \rangle$$

$$= 3 \lim_{k \to 0} \omega^2 S_s(k, \omega)/k^2, \qquad (1.73)$$

where in the last step eqn (1.54) has been used. In practice, however, the accuracy of the procedure is intrinsically limited by the finite wave vectors accessible in conventional neutron spectrometers. Although much smaller wave vectors are instead involved in light scattering, this technique typically

probes collective properties, rather than single-particle ones (see Chapter 2). As a result, we are in a situation where only computer simulations may provide accurate information on this basic time correlation function.

Figure 1.8 reports the results of such simulations for the two typical classes of monatomic liquids, the 'Lennard–Jones' rare-gas liquids (Levesque and Verlet 1970) and the liquid alkali metals Na, K, Rb, and Cs (Balucani et al. 1992). In the latter case, satisfactory pair potentials $\phi(r)$ are density dependent, and only available in a numerical form; the simulations of Fig. 1.8(b) were performed with the potentials implemented by Price et al. (1970), which turn out to be both simple and sufficiently 'realistic'. To emphasize the analogies and the differences between the two classes of liquids, in Fig. 1.8 all the data are reported in dimensionless units. In particular, the normalized velocity autocorrelation function $\psi(t) = \langle v_i(0) \cdot v_i(t) \rangle / \langle v_i^2 \rangle$ is plotted in terms of the time unit $\tau = (m\sigma^2/\varepsilon)^{1/2}$, where ε and σ denote, respectively, the well depth and the first zero of the pair potential appropriate to each system. Note that, in these units, all the data for the liquid metals coincide to an excellent approximation, even if, in contrast with the Lennard–Jones case, this sort of 'scaling' is not a priori evident from the expressions of the different $\phi(r)$.

The most noteworthy feature in Fig. 1.8 is in both cases the appearance of a negative correlation region. This is pictorially interpreted as being due to the 'rebound' of the tagged particle against the 'cage' formed by its nearest neighbours. In this respect, the feature appears to be consonant with a solid-like picture of the dynamics, and indeed this *cage effect* is found to be present only in very dense fluids and at low temperatures. A comparison between the actual findings for the two classes of systems shows that the magnitude of the negative correlation in the Lennard–Jones case is smaller than the one found for the liquid metals; also, in the latter systems even a few secondary oscillations are discernible at longer times. These features indicate that the liquid alkalis appear to be more 'solid-like' than, say, liquid argon. In turn, this peculiar behaviour of liquid metals stems from the softer repulsive portion of $\phi(r)$ (cf. Section 1.4.2), which eventually leads to a more symmetric potential well and to smaller 'anharmonicities' (Lewis and Lovesey 1977).

On the other hand, from the discussion in the previous section we expect that even for liquid metals such a solid-state picture is realistic only for rather short times, and that ultimately a diffusive behaviour should prevail. This is already clear if we compare the features of the mean square displacement $\delta r^2(t)$ as reported in Fig. 1.4 with those expected for a harmonic crystal. In the latter case, the displacement of an atom from its equilibrium position R_i in a Bravais lattice is conveniently expressed in terms of phonon creation and annihilation operators $a^\dagger$, a according to

$$\mathbf{r}_i(t) - = \sum_{ka} (\hbar/2mN\omega_{ka})^{1/2} \exp(i\mathbf{k}\cdot\mathbf{R}_i) [a_{ka}(t) + a^{\dagger}_{-ka}(t)] \mathbf{e}_{ka}$$

$$(1.74)$$

(e.g Bruesch 1982) Here $a_{ka}(t) = a_{ka}(0) \exp(-i\omega_{ka}t)$, where ω_{ka} is the frequency of the phonon with wave vector $\mathbf{k}$ and polarization index a, and $\mathbf{e}_{ka}$ the corresponding dimensionless polarization vector. In such a system, the mean square displacement can be expressed as

$$\langle [\mathbf{r}_i(t) - \mathbf{r}_i(0)]^2 \rangle = \langle [\mathbf{r}_i(t) - \mathbf{R}_i]^2 \rangle + \langle [\mathbf{r}_i(0) - \mathbf{R}_i]^2 \rangle$$
$$- \langle [\mathbf{r}_i(t) - \mathbf{R}_i] \cdot [\mathbf{r}_i(0) - \mathbf{R}_i] \rangle$$
$$- \langle [\mathbf{r}_i(0) - \mathbf{R}_i] \cdot [\mathbf{r}_i(t) - \mathbf{R}_i] \rangle \qquad (1.75)$$

where the first two terms on the right-hand side are actually identical because of stationarity. At sufficiently long times and finite temperatures, the presence of small anharmonic effects ensures that the remaining two terms in (1.75) decay to zero. As a result, for long times we find that

$$\langle [\mathbf{r}_i(t) - \mathbf{r}_i(0)]^2 \rangle \to 2\langle [\mathbf{r}_i(0) - \mathbf{R}_i]^2 \rangle$$

$$= \frac{2}{N} \sum_{ka} \frac{\hbar}{2m\omega_{ka}} [2\langle a^{\dagger}_{ka}a_{ka} \rangle + 1]$$

$$\approx \frac{2}{N} \sum_{ka} \frac{k_B T}{m\omega_{ka}^2} \qquad (1.76)$$

where the last step follows from the consideration of the 'classical limit' $\langle a^{\dagger}_{ka}a_{ka} \rangle \approx k_B T/\hbar\omega_{ka} \gg 1$. As a consequence, in a crystal the mean square displacement approaches a constant value. This is in marked contrast with the situation reported in Fig. 1.4 for the liquid, and implies a vanishing diffusion coefficient for the crystal, in accord with physical intuition.

Similar conclusions can be drawn by considering the spectrum $Z(\omega)$ of the velocity autocorrelation function (eqn (1.73)). In the crystal, from the time derivative of (1.74) we obtain

$$\langle \mathbf{v}_i(0) \cdot \mathbf{v}_i(t) \rangle = \frac{1}{N} \sum_{ka} \frac{\hbar\omega_{ka}}{2m} [2\langle a^{\dagger}_{ka}a_{ka} \rangle + 1] \exp(i\omega_{ka}t)$$

$$\approx \frac{k_B T}{m} \cdot \frac{1}{N} \sum_{ka} \exp(i\omega_{ka}t) \qquad (1.77)$$

where we have exploited the equation of motion $\dot{a}_{ka}(t) = -i\omega_{ka}a_{ka}(t)$, and finally performed the classical limit. As a consequence

$$Z(\omega) = \frac{k_B T}{m} \frac{1}{N} \sum_{ka} \delta(\omega - \omega_{ka}), \qquad (1.78)$$

Fig. 1.8 Computer simulation results for the normalized velocity autocorrelation function $\psi(t)$ in two typical classes of monatomic liquids near the melting point: (a) 'Lennard–Jones' rare-gas liquids in the state specified by the reduced units $n\sigma^3 = 0.85$ and $k_B T/\varepsilon \approx 0.76$ (redrawn from Levesque and Verlet 1970); (b) liquid sodium at $n\sigma^3 = 0.895$ and $k_B T/\varepsilon \approx 0.80$ (Balucani *et al.* 1992). In both cases, the time unit $\tau = (m\sigma^2/\varepsilon)^{1/2}$.

a result which shows that the spectrum of $\langle \mathbf{v}_i(0) \cdot \mathbf{v}_i(t) \rangle$ is proportional to the phonon density of states. For our present purposes, the latter quantity can be approximated by a simple Debye model, with the result that

$$Z(\omega) = \begin{cases} (3k_B T/m) \cdot (2\pi^2 n c_s^3)^{-1} \omega^2 & \omega < \omega_D \\ 0 & \omega > \omega_D \end{cases} \quad (1.79)$$

Here, c_s is an average sound velocity, and the cutoff frequency ω_D is related to the Debye temperature θ_D by $\hbar \omega_D = k_B \theta_D$. The quantity $Z(\omega)$ is reported in Fig. 1.9 with a choice of parameters appropriate for sodium. The comparison with the Fourier transform of the corresponding $\psi(t)$ in the liquid (cf. Fig. 1.8) shows clear differences, which are particularly noteworthy in the low-frequency region ($\omega \to 0$) where the Debye model is more reliable. Since $Z(\omega = 0) = (3/\pi)D$ (eqns (1.73) and (1.67)), the discrepancies in this range are again associated with the absence of diffusive processes in the crystal.

All these results reinforce our previous statements about the limited validity of a solid-state picture to understand the features of single-particle dynamics in liquids. This state of affairs occurs particularly when features are explored over long times (or low frequencies), namely when the tagged atom has already suffered a significant number of collisions with the other particles. It is then worthwhile to consider an alternative picture in whith these long-time, collision-dominated features are emphasized. In this respect, the simplest situation is provided by a model in which the only effect of the collisions is to yield an exponential decay of the velocity autocorrelation function:

$$\langle \mathbf{v}_i(0) \cdot \mathbf{v}_i(t) \rangle = (3k_B T/m) \exp(-\gamma_c |t|), \quad (1.80)$$

where the decay constant γ_c is expected to be connected with the collision rate. Equation (1.80) is found to describe rather well the situation occurring in a fluid at moderate densities. As a matter of fact, the result (1.80) turns out to be correct in two limiting cases.

(i) A dilute system of 'hard spheres', where the collisions can be regarded as binary and mutually uncorrelated. This is the celebrated *Enskog model*, which will be discussed in some detail in Chapter 3. Note that for this artificial system the apparent violation of the short-time expansion (1.59) is due to the pathological form of the pair potential, $\phi(r < d) = \infty$ and $\phi(r > d) = 0$, where d is the hard sphere diameter (e.g. McQuarrie 1976). (ii) A particle immersed in a 'bath' made of much lighter molecules. Due to the collisions with the latter, the massive particles undergoes a zigzag motion, with a mean square displacement increasing linearly with time according the diffusive law (1.66). The physics behind this *Brownian motion* is actually a typical example of a situation frequently met in the dynamics of interacting systems (see Chapter 3).
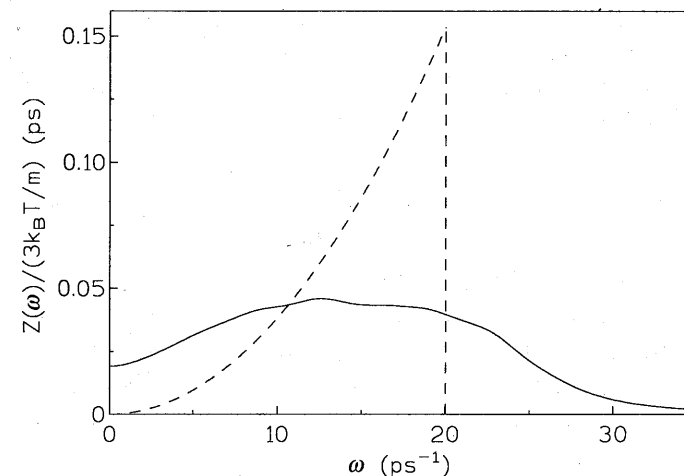
Fig. 1.9 Spectrum $Z(\omega)$ of the velocity autocorrelation function in liquid Na as obtained by a Fourier transform of the data reported in Fig. 1.8. The dashed line is the result deduced from eqn (1.79) taking $c_s = 2300 \text{ m s}^{-1}$ and $\theta_D = 150 \text{ K}$.

The result (1.80) implies a simple relation between the collisional decay rate γ_c and the diffusion coefficient, which after eqn (1.67) reads

$$D = k_B T/m\gamma_c. \quad (1.81)$$

In addition, the spectrum $Z(\omega)$ of the velocity autocorrelation function (1.80) can be written as

$$Z(\omega) = \frac{3k_B T}{\pi m} \frac{\gamma_c}{\omega^2 + \gamma_c^2}. \quad (1.82)$$

The comparison with the actual $Z(\omega)$ of the liquid shows at low frequencies the expected improvement with respect to the result for the crystal (see Fig. 1.9). Even in this region, however, there are evident shortcomings, which are mostly due to the failure of eqn (1.80) to reproduce the long-lasting negative correlations in $\psi(t)$. More subtle discrepancies are found to occur even at lower densities, where the absence of 'cage effects', yielding a $\psi(t) > 0$ at all times, should a priori make reasonable the use of (1.80). In this case, at long times $\psi(t)$ appears to exhibit a slow $t^{-3/2}$ decay rather than an exponential one (Alder and Wainwright 1970; Levesque and Ashurst 1974).

Summing up, the previous results provide a first indication of the features which a comprehensive theory of single-particle dynamics should be able to explain on a quantitative basis. As is clear from the above, this task is

made nontrivial by the variety of phenomena likely to occur over a wide range of distances and times. Similar problems are expected to arise if we consider dynamical variables having an explicit collective character; this will be the subject of the remaining sections of this Chapter.

1.5 THE RELATIVE MOTIONS OF ATOMIC PAIRS

1.5.1 The time-dependent pair distribution function

When viewed in the ordinary space-and-time domain, all the previous single-particle properties can be derived from the knowledge of the self-correlation function $G_s(r, t)$ as given by (1.32). In a classical and homogeneous system, one may equivalently consider the quantity

$$G_1(\mathbf{R}\, 0; \mathbf{R}'\, t) \equiv \langle \delta(\mathbf{R} - \mathbf{r}_i(0)) \delta(\mathbf{R}' - \mathbf{r}_i(t)) \rangle \qquad (1.83)$$

which measures the joint probability that *i*th particle is in the position $\mathbf{R}$ at $t = 0$ and in the position $\mathbf{R}'$ at time t. With this definition, $G_s(|\mathbf{R} - \mathbf{R}'|, t) = \int d\mathbf{R}\, G_1(\mathbf{R}\, 0; \mathbf{R}'\, t)$.

A first step in the direction of probing the liquid on a more collective scale is provided by the quantity (Bloom and Oppenheim 1967)

$$G_2(\mathbf{r}\, 0; \mathbf{r}'\, t) \equiv (1/N) \sum_{i,j(\neq i)} \langle \delta(\mathbf{r} - \mathbf{r}_{ij}(0)) \delta(\mathbf{r}' - \mathbf{r}_{ij}(t)) \rangle$$

$$= \sum_{j(\neq 1)} \langle \delta(\mathbf{r} - \mathbf{r}_{1j}(0)) \delta(\mathbf{r}' - \mathbf{r}_{1j}(t)) \rangle$$

$$= (N - 1) \langle \delta(\mathbf{r} - \mathbf{r}_{12}(0)) \delta(\mathbf{r}' - \mathbf{r}_{12}(t)) \rangle. \qquad (1.84)$$

According to this definition, $G_2(\mathbf{r}\, 0; \mathbf{r}'\, t)$ is proportional to the joint probability that two different particles are separated by $\mathbf{r}$ at $t = 0$ and by $\mathbf{r}'$ at time t. Initially one has that

$$G_2(\mathbf{r}\, 0; \mathbf{r}'\, 0) = ng(r)\delta(\mathbf{r} - \mathbf{r}'), \qquad (1.85)$$

a result which accounts for the name *time-dependent pair distribution function* often given to $G_2(\mathbf{r}\, 0; \mathbf{r}'\, t)$. In the opposite limit of long times, the averages in (1.84) may approximately be factorized, yielding (cf. (1.11))

$$G_2(\mathbf{r}\, 0; \mathbf{r}'\, t \to \infty) = (N - 1)^{-1} ng(r)ng(r'). \qquad (1.86)$$

For future purposes, it is convenient to introduce a quantity $g_2(\mathbf{r}\, 0; \mathbf{r}'\, t)$ which may be interpreted as a conditional (rather than joint) probability. This is defined according to

$$G_2(\mathbf{r}\, 0; \mathbf{r}'\, t) = \sum_{j(\neq 1)} \langle \delta(\mathbf{r} - \mathbf{r}_{1j}(0)) \rangle g_2(\mathbf{r}\, 0; \mathbf{r}'\, t)$$

$$= ng(r)g_2(\mathbf{r}\, 0; \mathbf{r}'\, t). \qquad (1.87)$$

Clearly, $g_2(\mathbf{r}\, 0; \mathbf{r}'\, 0) = \delta(\mathbf{r} - \mathbf{r}')$ and $g_2(\mathbf{r}\, 0; \mathbf{r}'\, t \to \infty) = (N - 1)^{-1} ng(r')$.

The merits of G_2 as a basic dynamical quantity are immediately apparent if we note that its knowledge makes accessible an important class of time correlation functions, namely those explicitly associated with the relative dynamics of a pair of particles. As a matter of fact, denoting by $\langle A(\mathbf{r}_{ij}(0)) A(\mathbf{r}_{ij}(t)) \rangle$ an arbitrary member of this class, it is immediately found that

$$\frac{1}{N} \sum_{i,j \neq i} \langle A(\mathbf{r}_{ij}(0)) A(\mathbf{r}_{ij}(t)) \rangle = \int d\mathbf{r} \int d\mathbf{r}'\, A(\mathbf{r}) A(\mathbf{r}') G_2(\mathbf{r}\, 0; \mathbf{r}'\, t). \qquad (1.88)$$

Several examples of such dynamical correlations – some having direct experimental relevance – will be met in the following; for the time being, we shall limit ourselves to a discussion of the general properties of $G_2(\mathbf{r}\, 0; \mathbf{r}'\, t)$. Introducing a suitable δ-function into the statistical average, G_2 can readily be written as

$$G_2(\mathbf{r}\, 0; \mathbf{r}'\, t) = \sum_{j \neq 1} \int d\mathbf{R} \langle \delta(\mathbf{r} - \mathbf{r}_{1j}(0)) \delta(\mathbf{R} - (\mathbf{r}_1(t) - \mathbf{r}_1(0))$$

$$\delta(\mathbf{R} - \mathbf{r}' + \mathbf{r} - (\mathbf{r}_j(t) - \mathbf{r}_j(0))) \rangle. \qquad (1.89)$$

This formal result shows that G_2 actually probes the dynamics of each particle in the pair with a weight associated with their initial separation. Since this occurs inside the average, possible fluctuations and correlation effects are automatically taken into account. It is interesting, nevertheless, to discuss the implications of (1.89) in the case when all fluctuations are ignored. Then, the statistical average can be factorized yielding

$$G_2(\mathbf{r}\, 0; \mathbf{r}'\, t) \approx ng(r) \int d\mathbf{R}\, G_s(R, t) G_s(|\mathbf{R} - \mathbf{r}' + \mathbf{r}|, t). \qquad (1.90)$$

In such a case, the motions of the two particles would be essentially uncorrelated, with the factor $ng(r)$ only providing a time-independent initial probability distribution. Whereas the approximation (1.90) reproduces the correct initial value (1.85), at short times it predicts that each particle propagates as though it were free. As a result, in this domain we obtain

$$G_2(r\, 0; r'\, t) \approx ng(r) \left(\frac{\beta \mu_r}{2\pi t^2} \right)^{3/2} \exp \frac{-\beta \mu_r (\mathbf{r}' - \mathbf{r})^2}{2t^2} \qquad (1.91)$$

where the presence of the reduced mass $\mu_r = m/2$ appears natural in the context of relative motions. Similarly, exploiting the long-time result (cf. eqns (1.32) and (1.70))

$$G_s(R, t) = (4\pi D|t|)^{-3/2}\exp(-R^2/4Dt),\qquad(1.92)$$

eqn (1.90) predicts that in the diffusive regime $(t \to \infty)$

$$G_2(\mathbf{r}\,0;\mathbf{r}'\,t) \approx ng(r)(4\pi D_r|t|)^{-3/2}\exp[-(\mathbf{r}'-\mathbf{r})^2/4D_r t]\quad(1.93)$$

where the *relative diffusion coefficient* $D_r = 2D$.

Generally speaking, all these results derived from the convolution approximation (1.90) are expected to be accurate if the separations r, r' are large enough that mutual correlations may be neglected. For example, in the liquid range eqn (1.90) is likely to be valid for separations beyond the first few peaks of $g(r)$. On the other hand, when both r and r' lie in the nearest neighbour range new dynamical features are expected. This situation is of considerable interest, both by itself and in connection with eqn (1.88), especially in those cases where the 'weight' $A(\mathbf{r})$ is short ranged in space.

These aspects of the dynamics of the time-dependent pair distribution function have been addressed in several simulations studies (Haan 1979, Balucani and Vallauri 1980a, b). The analysis is simplified by considering suitable 'projections' of the full $G_2(\mathbf{r}\,0;\mathbf{r}'\,t)$. By symmetry, G_2 depends on $\mathbf{r}$ and $\mathbf{r}'$ only through the magnitudes r, r' and the angle θ between $\mathbf{r}$ and $\mathbf{r}'$; as a result, it is convenient to introduce 'radial' and 'angular' portions defined as

$$G_{2,\text{rad}}(r'\,t) = \int_{(a,b)}\mathbf{dr}\int_{-1}^{1}\mathrm{d}(\cos\theta)G_2(\mathbf{r}\,0;\mathbf{r}'\,t)\qquad(1.94)$$

and

$$G_{2,\text{ang}}(\cos\theta, t) = \int_{(a,b)}\mathbf{dr}\int_{0}^{\infty}\mathrm{d}r'\,r'^2 G_2(\mathbf{r}\,0;\mathbf{r}'\,t)\qquad(1.95)$$

where in both cases the initial separations have been selected to lie within a suitable range (a, b). As expected, the simulation data indicate that the approximation (1.90) yields satisfactory results if (a, b) is chosen outside the range of r with important structural effects. At increasing times, the angular distribution $G_{2,\text{ang}}$ is found in any case to spread from its initial sharp peak at $\theta = 0$ (cf.(1.85)) and eventually to approach an uniform distribution of angles. On the other hand, for small separations the dynamics of $G_{2,\text{rad}}$ turns out to be strongly affected by the choice of the range (a, b). For Lennard–Jones liquids this situation is illustrated in Fig. 1.10, which refers to two narrow ranges of initial separations. For the

(a)

(b)
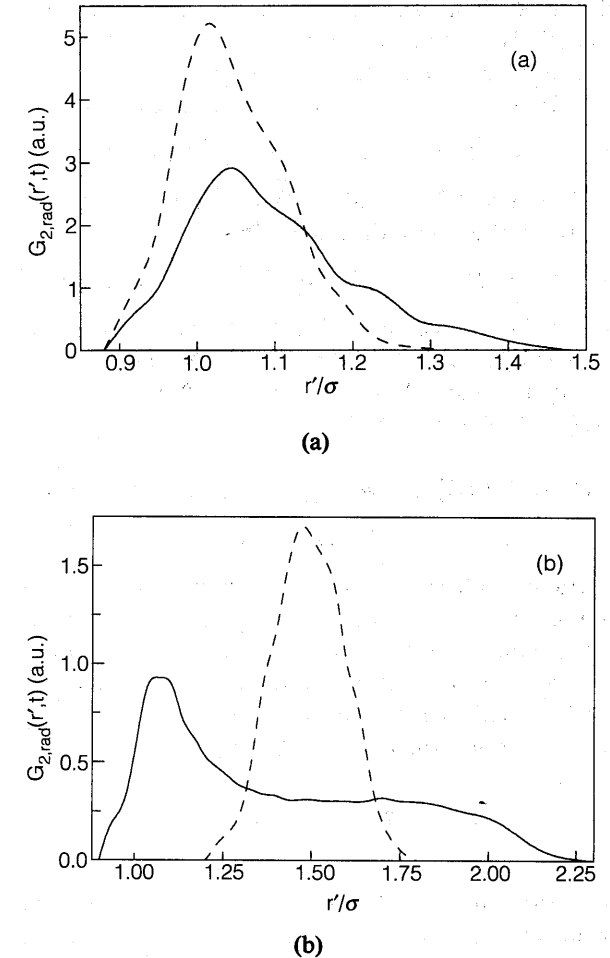
Fig. 1.10 Time evolution of the radial distribution function (1.94) in a Lennard–Jones fluid with $n^* = n\sigma^3 = 0.95$ and $T^* = k_B T/\varepsilon = 1.32$. (a) An initial separation range centered at $r = 1.04\sigma$, while in (b) $r = 1.5\sigma$. In both cases, the dashed and the full curves, in the case of argon, refer respectively to $t = 0.145\,\text{ps}$ and $1.44\,\text{ps}$. Redrawn from Haan (1979).

first one (centred on the position of the main peak of $g(r)$), $G_{2,\text{rad}}$ appears to be relatively stable even for rather long times. On the other hand, the second range (a, b) comprises 'unfavoured' separations around the first minimum of $g(r)$; as a result, the initial structure of $G_{2,\text{rad}}$ is rapidly washed out, and eventually the spread becomes so large that the shape of $G_{2,\text{rad}}$ resembles the one appropriate for the equilibrium pair distribution $g(r')$. This trend is in qualitative agreement with the asymptotic result (1.86), but cannot be accounted for by the simple approximation (1.93).

It is therefore evident that the structural effects have a dynamical counterpart which is relevant both at short and long times. In the first case, the correct expansion turns out to be $G_2(\mathbf{r}\,0; \mathbf{r}'\,t) = G_2(\mathbf{r}\,0; \mathbf{r}'\,0) + \ddot{G}_2(\mathbf{r}\,0; \mathbf{r}'\,0)(t^2/2) + \cdots$, where the first term follows from eqn (1.85) and

$$\ddot{G}_2(\mathbf{r}\,0; \mathbf{r}'\,0) = - (2/m\beta)\,n\nabla_r \cdot \nabla_{r'}[g(r)\delta(\mathbf{r} - \mathbf{r}')] \qquad (1.96)$$

(Balucani and Vallauri 1980*a*). The result (1.96) is to be compared with the one predicted from the approximation (1.90):

$$\ddot{G}_2(\mathbf{r}\,0; \mathbf{r}'\,0) \approx - (2/m\beta)\,ng(r)\nabla_r \cdot \nabla_{r'}[\delta(\mathbf{r} - \mathbf{r}')] \qquad (1.97)$$

which is seen to be correct only for large separations where $g(r) \approx 1$. Starting from eqns (1.85) and (1.96) and performing two partial integrations, it is straightforward to deduce that at short times the correlation function $\langle A(\mathbf{r}(0))A(\mathbf{r}(t))\rangle$ decays as

$$\langle A(\mathbf{r}(0))A(\mathbf{r}(t))\rangle = \langle A^2(\mathbf{r})\rangle - (n/\beta\mu_r)\int d\mathbf{r}\,[\nabla_r(A(\mathbf{r}))]^2$$
$$g(r)(t^2/2) + \cdots \qquad (1.98)$$

a result important in all interaction-induced phenomena, where it establishes the short-time dynamics of atomic pairs (see Appendix J).

With some recourse to intuitive arguments, even the discrepancies occurring at long times between the data and the results of eqn (1.93) can be partially eliminated. As is verified from (1.92), in the convolution approximation the conditional probability $g_2(\mathbf{r}\,0; \mathbf{r}'\,t)$ satisfies a standard diffusive equation

$$\frac{\partial g_2}{\partial t} = 2D\nabla_{r'}^2 g_2 \qquad (1.99)$$

with the initial condition $g_2(\mathbf{r}\,0; \mathbf{r}'\,0) = \delta(\mathbf{r} - \mathbf{r}')$. The neglect of correlations has the unwanted effect of yielding a uniform spread of g_2 at long times. To account for the structural features gradually emerging in the time evolution (cf. Fig. 1.10b), the leading correlation effects are approximately taken into account by introducing an effective interaction potential $\Phi(r)$ between the two particles of the pair. Physically, $\Phi(r)$ is expected to coincide with the true pair potential $\phi(r)$ only in dilute systems; at higher densities the presence of structural effects yields a sort of 'renormalization', which can be accounted for by the choice (e.g. Haan 1979)

$$\Phi(r) = - (1/\beta) \ln g(r). \qquad (1.100)$$

The consequence of the introduction of this *potential of mean force* is that eqn (1.99) for free diffusion is replaced by the one appropriate for diffusion in a force-field ('Smoluchowski equation'), with the latter being given by $-\nabla\Phi$. As a result, the new diffusive equation reads

$$\partial g_2/\partial t = 2D\nabla_{r'} \cdot [\nabla_{r'}g_2 - g_2\beta\nabla_{r'}\Phi(r')]. \qquad (1.101)$$

In contrast with (1.99), eqn (1.101) has the merit of providing a stationary solution proportional to $g(r')$, consistently with the asymptotic result (1.86). Moreover, the numerical solution of (1.101) is found to reproduce satisfactory the gradual approach to the stationary solution apparent from the data of Fig. 1.10. Various attempts to merge these long-time features with the correct short-time behaviour (1.96) have also been proposed (Haan 1979; Balucani and Vallauri 1980*b*).

1.5.2   Transfer of momentum among the particles

Denoting by $\mathbf{v}_{ij} = \mathbf{v}_i - \mathbf{v}_j$ ($j \neq i$) the relative velocity of two arbitrary particles, the corresponding velocity autocorrelation function reads

$$\langle \mathbf{v}_{ij}(0) \cdot \mathbf{v}_{ij}(t)\rangle = 2\langle \mathbf{v}_i(0) \cdot \mathbf{v}_i(t)\rangle - 2\langle \mathbf{v}_i(0) \cdot \mathbf{v}_j(t)\rangle \qquad (1.102)$$

where the cross correlation on the right-hand side describes the transfer of velocity (or momentum) between the ith and the jth particle of the system. This quantity can be written as

$$\begin{aligned}
\langle \mathbf{v}_i(0) \cdot \mathbf{v}_j(t)\rangle &= (N - 1)^{-1}\Big\langle \mathbf{v}_i(0) \cdot \sum_{j \neq i} \mathbf{v}_j(t)\Big\rangle \\
&= (N - 1)^{-1}\Big\langle \mathbf{v}_i(0) \cdot \Big[\sum_j \mathbf{v}_j(t) - \mathbf{v}_i(t)\Big]\Big\rangle \\
&= (N - 1)^{-1}\Big[\Big\langle \mathbf{v}_i(0) \cdot \sum_j \mathbf{v}_j(0)\Big\rangle - \langle \mathbf{v}_i(0) \cdot \mathbf{v}_i(t)\rangle\Big] \\
&= (N - 1)^{-1}[\langle \mathbf{v}_i^2(0)\rangle - \langle \mathbf{v}_i(0) \cdot \mathbf{v}_i(t)\rangle] \qquad (1.103)
\end{aligned}$$

where the condition $\sum_j \mathbf{v}_j(t) = \sum_j \mathbf{v}_j(0)$ expresses the conservation of the total momentum of the system. As a result, the effects of the cross correlation are of the order $1/N$, making virtually negligible in the present case any difference between the relative dynamics and the single-particle one.

The situation becomes more interesting if, rather then considering two arbitrary particles, we focus our attention on pairs having a specified range of initial separations, $a \leqslant r_{ij}(0) \leqslant b$ (for example, we may be interested in knowing how momentum is transferred between a 'central' particle and its immediate neighbours). Such a specification clearly requires the introduction of a *restricted statistical average*. If two particles have an initial separation in the range (a, b), the appropriate relative velocity autocorrelation function can be written as

$$\langle \mathbf{v}_{ij}(0) \cdot \mathbf{v}_{ij}(t)\rangle_{ab} = \frac{\langle \mathbf{v}_{ij}(0) \cdot \mathbf{v}_{ij}(t)\theta(r_{ij}(0) - a)\theta(b - r_{ij}(0))\rangle}{\langle \theta(r_{ij}(0) - a)\theta(b - r_{ij}(0))\rangle} \qquad (1.104)$$

the cross correlation as the central particle 'loses' its initial momentum to the immediate neighbours and $\langle \mathbf{v}_i(0) \cdot \mathbf{v}_i(t) \rangle$ decays. If this transfer of momentum were complete before any further spread to outer shells, at times where the initial decay has made $\langle \mathbf{v}_i(0) \cdot \mathbf{v}_i(t) \rangle \approx 0$ we would expect a peak of the cross correlation with an amplitude

$$\langle \mathbf{v}_i(0) \cdot \mathbf{v}_j(t) \rangle_{ab} \approx [\mathfrak{N}(a, b)]^{-1} \langle \mathbf{v}_i^2(0) \rangle \qquad (1.107)$$

indicating a uniform spread over the atoms of the first shell. The results of Fig. 1.11 almost support this simple picture on a quantitative basis (more than 80% of the initial kinetic energy is transferred to the first shell). At longer times $\langle \mathbf{v}_i(0) \cdot \mathbf{v}_j(t) \rangle_{ab}$ decreases, mostly because of further spread of momentum over more distant shells. The subsequent oscillations of the cross correlation have a clear phase relationship with those of $\langle \mathbf{v}_i(0) \cdot \mathbf{v}_i(t) \rangle$, and indicate that in this liquid a non-negligible portion of the initial momentum is 'given back' to the central particle, bouncing back and forth for some time before the eventual spread over the system. Similar overall results have been reported for Lennard–Jones liquids (Balucani *et al.* 1983), with a more marked spread of momentum outwards and no evident 'bouncing' oscillations.

1.5.3 Pairs, triplets, and quadruplets

In liquid state dynamics one meets several time correlation functions which probe relative motions involving clusters of particles, rather than a simple atomic pair. Typically, these quantities involve a collective variable of the form $\sum_{i, j \neq i} A(\mathbf{r}_{ij})$, with $\langle A(\mathbf{r}_{ij}) \rangle = 0$. As a result, the time correlation can be split into three different contributions of increasing complexity:

$$\left\langle \sum_{i, j \neq i} A(\mathbf{r}_{ij}(0)) \sum_{l, m \neq 1} A(\mathbf{r}_{lm}(t)) \right\rangle = 2 \sum_i \sum_{j \neq i} \langle A(\mathbf{r}_{ij}(0)) A(\mathbf{r}_{ij}(t)) \rangle$$

$$+ 4 \sum_i \sum_{j \neq i} \sum_{l \neq i,j} \langle A(\mathbf{r}_{ij}(0)) A(\mathbf{r}_{il}(t)) \rangle$$

$$+ \sum_i \sum_{j \neq i} \sum_{l \neq i,j} \sum_{m \neq i,j,l} \langle A(\mathbf{r}_{ij}(0)) A(\mathbf{r}_{lm}(t)) \rangle$$

$$(1.108)$$

where the terms on the right-hand side involve respectively atomic pairs, triplets, and quadruplets. If the system is dilute, the correlations involving three or four different particles are expected to be much less important than the pair term because the presence of triplets and quadruplets of particles sufficiently close together is unlikely. This is clearly not the case at liquid
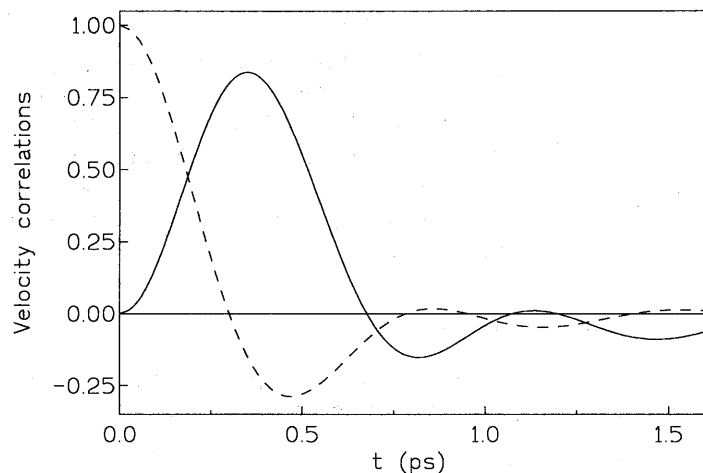
Fig. 1.11 The cross correlation function $\mathfrak{N}(a, b)\langle \mathbf{v}_i(0) \cdot \mathbf{v}_j(t) \rangle_{ab} / \langle v_i^2 \rangle$ (full line) as obtained by computer simulation in liquid rubidium (Balucani *et al.* 1984). The range (a, b) of initial separations comprises the first shell of neighbours. The dashed line is the normalized velocity autocorrelation function $\psi(t) = \langle \mathbf{v}_i(0) \cdot \mathbf{v}_i(t) \rangle / \langle v_i^2 \rangle$.

where the step function $\theta(x)$ is 1 for $x > 0$ and 0 for $x < 0$. The restricted average can be split as in eqn (1.102), yielding

$$\langle \mathbf{v}_{ij}(0) \cdot \mathbf{v}_{ij}(t) \rangle_{ab} = 2 \langle \mathbf{v}_i(0) \cdot \mathbf{v}_i(t) \rangle_{ab} - 2 \langle \mathbf{v}_i(0) \cdot \mathbf{v}_j(t) \rangle_{ab}. \qquad (1.105)$$

Here the single-particle velocity autocorrelation $\langle \mathbf{v}_i(0) \cdot \mathbf{v}_i(t) \rangle_{ab}$ differs from the ordinary one because the contributions from each particle are weighted by the number of neighbours actually found in the range (a, b), which in principle may vary from one particle to another. In monatomic liquids, however, the arrangement of particles is sufficiently close packed that we may safely neglect any fluctuation in the number of neighbours around the average value

$$\mathfrak{N}(a, b) = \langle \theta(r_{ij}(0) - a) \theta(b - r_{ij}(0)) \rangle = 4\pi n \int_a^b \mathrm{d}r \, r^2 g(r). \qquad (1.106)$$

In such a case, $\langle \mathbf{v}_i(0) \cdot \mathbf{v}_i(t) \rangle_{ab} = \langle \mathbf{v}_i(0) \cdot \mathbf{v}_i(t) \rangle$, and the difference between relative and single-particle dynamics is entirely due to the cross correlation $\langle \mathbf{v}_i(0) \cdot \mathbf{v}_j(t) \rangle_{ab}$. The latter quantity has been evaluated in several simple liquids by computer simulation techniques; Fig. 1.11 reports the results found for liquid rubidium for a range (a, b) which comprises the first 'shell' of neighbours (Balucani *et al.* 1984). The data show an increase of

densities, where typically the three contributions turn out to be of the same order of magnitude. Moreover, it is often found that their signs are such that a considerable cancellation occurs. This circumstance magnifies any errors due to an approximate treatment of each term, and eventually makes a reliable evaluation of the total correlation function very difficult.

As a consequence, even if it is possible to introduce time-dependent distribution functions for triplets and quadruplets as in the pair case, the advantages of such a procedure appear to be rather limited, and often it is more convenient to deal directly with the full correlation function on the left-hand side of eqn (1.108). In this case we face a typical collective problem, and it is worthwhile at this stage to discuss the basic dynamical quantities appropriate for such an analysis. This will be the subject of the last section of this Chapter.

1.6   COLLECTIVE PROPERTIES

1.6.1   Density fluctuations and longitudinal and transverse currents

In close analogy with the approach followed for single-particle properties, even in the collective case it is convenient to introduce a scalar density field $n(\mathbf{R}, t)$ as the leading dynamical variable. An extension of eqn (1.27) leads to the definition

$$n(\mathbf{R}, t) = \sum_i \delta(\mathbf{R} - \mathbf{r}_i(t)).$$
(1.109)

Noting that

$$\langle n(\mathbf{R}, t) \rangle = \langle n(\mathbf{R}, 0) \rangle = \sum_i \frac{1}{V} = \frac{N}{V} = n,$$
(1.110)

it is natural to interpret $n(\mathbf{R}, t)$ as the *number density variable* at point $\mathbf{R}$ and time t. For our purposes, it is also useful to consider *density fluctuations* defined as

$$\hat{n}(\mathbf{R}, t) = n(\mathbf{R}, t) - \langle n(\mathbf{R}, t) \rangle = n(\mathbf{R}, t) - n.$$
(1.111)

The space Fourier transforms of the variables (1.109) and (1.111) read

$$n(\mathbf{k}, t) = \sum_i \exp(i\mathbf{k} \cdot \mathbf{r}_i(t))$$
(1.112)

and

$$\hat{n}(\mathbf{k}, t) = \sum_i \exp(i\mathbf{k} \cdot \mathbf{r}_i(t)) - (2\pi)^3 n\delta(\mathbf{k}).$$
(1.113)

The equation of motion of $n(\mathbf{k}, t)$ is readily written as

$$\frac{\mathrm{d}n(\mathbf{k}, t)}{\mathrm{d}t} = i\mathbf{k} \cdot \sum_i \mathbf{v}_i(t) \exp(i\mathbf{k} \cdot \mathbf{r}_i(t))$$
(1.114)

where the vectorial variable

$$\mathbf{j}(\mathbf{k}, t) \equiv \sum_i \mathbf{v}_i(t) \exp(i\mathbf{k} \cdot \mathbf{r}_i(t))$$
(1.115)

is known as the *current* associated with the overall motion of the particles. A first noteworthy feature apparent from eqn (1.114) is that for small enough wavevectors $\dot{n}(\mathbf{k}, t) \to 0$; as a consequence, $n(\mathbf{k} \to 0, t)$ may be considered as a 'slow' variable in the sense discussed in Section 1.3. This result (which parallels a similar one found for the single-particle density $n_{s,i}(\mathbf{k}, t)$) follows from the conservation of the total number of particles $n(\mathbf{k} = 0, t) = N$, and gives to (1.114) the typical structure of a 'continuity' equation.

Rather than the full current, eqn (1.114) only involves the component of $\mathbf{j}(\mathbf{k}, t)$ parallel to the wavevector $\mathbf{k}$. In more formal terms, the current can be split according to

$$\mathbf{j}(\mathbf{k}, t) = \hat{k}\hat{k} \cdot \mathbf{j}(\mathbf{k}, t) + (\mathbf{1} - \hat{k}\hat{k}) \cdot \mathbf{j}(\mathbf{k}, t)$$
$$\equiv \mathbf{j}_{\mathrm{L}}(\mathbf{k}, t) + \mathbf{j}_{\mathrm{T}}(\mathbf{k}, t)$$
(1.116)

where $\hat{k} \equiv \mathbf{k}/k$, $\mathbf{1}$ is the unit tensor, and the last step defines the *longitudinal* ($\mathbf{j}_{\mathrm{L}}$) and *transverse* ($\mathbf{j}_{\mathrm{T}}$) components of $\mathbf{j}(\mathbf{k}, t)$ with respect to $\mathbf{k}$. Then, eqn (1.114) may be simply written as $\dot{n}(\mathbf{k}, t) = ikj_{\mathrm{L}}(\mathbf{k}, t)$, where $\mathbf{j}_{\mathrm{L}}(\mathbf{k}, t) = j_{\mathrm{L}}(\mathbf{k}, t)\hat{k}$.

The equation of motion of the full current $\mathbf{j}(\mathbf{k}, t)$ reads

$$\frac{\mathrm{d}\mathbf{j}(\mathbf{k}, t)}{\mathrm{d}t} = \sum_i [i\mathbf{k} \cdot \mathbf{v}_i(t)\mathbf{v}_i(t) + \dot{\mathbf{v}}_i(t)] \exp(i\mathbf{k} \cdot \mathbf{r}_i(t)).$$
(1.117)

For sufficiently small wavevectors, both terms in square brackets give a vanishing contribution (the second being proportional to the total force acting on the system, which is zero by Newton's third law). As a result, even the variable $\mathbf{j}(\mathbf{k}, t)$ becomes 'slow' in the limit $k \to 0$. Since $\mathbf{k}$ is fixed, the same is also true for the separate longitudinal and transverse components of the current. Thus, in the collective case we a priori deal with several quasi-conserved variables (another one, the energy density fluctuation, will be met in Section 1.6.4), some of which being mutually connected. Such a situation should be contrasted with the one found for single-particle properties, where $n_{s,i}(\mathbf{k}, t)$ is the only natural quasi-conserved variable. As $k \to 0$ the collective correlation functions may consequently be expected

to provide much more information than $F_s(k, t)$. Before discussing the physical implication in this low-k 'hydrodynamic' regime, in the two next subsections the collective dynamics will be studies on a more general basis. As in the single-particle case, a convenient starting point is the analysis of the short-time behaviour of the correlation functions at arbitrary wavevectors.

1.6.2   The intermediate scattering function

The time correlation function associated with the dynamics of k-dependent density fluctuations is defined by

$$F(k, t) \equiv (1/N)\langle \hat{n}^*(\mathbf{k}, 0)\hat{n}(\mathbf{k}, t)\rangle$$

$$= (1/N)\sum_{ij}\langle \exp[\mathrm{i}\mathbf{k} \cdot (\mathbf{r}_j(t) - \mathbf{r}_i(0))]\rangle - (2\pi)^3 n\delta(\mathbf{k}).$$

$$(1.118)$$

In close analogy with the analysis seen in Section 1.4.1, we may Fourier-transform $F(k, t)$ back to the space domain to obtain the *van Hove correlation function*

$$G(r, t) = (1/N)\sum_{ij}\langle \delta(\mathbf{r} + \mathbf{r}_i(0) - \mathbf{r}_j(t))\rangle - n. \qquad (1.119)$$

The summation over j in eqn (1.118) or (1.119) can be split into a 'self'-contribution with $j = i$ which accounts for the single-particle properties, and a 'distinct' part with $j \neq i$ responsible for collective properties. In particular, for the initial values $F(k, 0)$ this splitting yields

$$F(k, 0) = 1 + (1/N)\sum_{i,j \neq i}\langle \exp(-\mathrm{i}\mathbf{k} \cdot \mathbf{r}_{ij})\rangle - (2\pi)^3 n\delta(\mathbf{k})$$

$$= 1 + \int \mathrm{d}\mathbf{r}\exp(-\mathrm{i}\mathbf{k} \cdot \mathbf{r})[g(r) - 1] = 1 + [S(k) - 1]$$

$$(1.120)$$

where we have exploited the definition (1.14) of the static structure factor. As a result

$$F(k, 0) = S(k) \qquad (1.121)$$

Alternatively, from $F(k, t)$ we may proceed with a time Fourier transform to obtain the spectrum

$$S(k, \omega) = (1/2\pi)\int_{-\infty}^{\infty} \mathrm{d}t\exp(-\mathrm{i}\omega t)F(k, t) \qquad (1.122)$$

usually called the *dynamic structure factor* (or the 'coherent scattering law' because of its connection with neutron scattering experiments; cf. Chapter 2). In turn, because of its 'mixed' character with respect to $G(r, t)$ and $S(k, \omega)$, $F(k, t)$ is referred to as the *intermediate scattering function*.

The short-time properties of $F(k, t)$ follow from the expansion

$$F(k, t) = F(k, 0) + \ddot{F}(k, 0)(t^2/2) + \ddddot{F}(k, 0)(t^4/4!) + \cdots$$

$$= S(k) - \overline{\omega_k^2}(t^2/2) + \overline{\omega_k^4}(t^4/4!) + \cdots$$

$$= S(k)[1 - \langle \omega_k^2\rangle(t^2/2) + \langle \omega_k^4\rangle(t^4/4!) + \cdots] \qquad (1.123)$$

where only even powers of time appear, because of the even character of $F(k, t)$ (cf. Appendix B). The quantities $\overline{\omega_k^n}$ are given by

$$\overline{\omega_k^n} \equiv (-1)^{n/2}\left[\frac{\mathrm{d}^n F(k, t)}{\mathrm{d}t^n}\right]_{t=0} = \int_{-\infty}^{\infty} \mathrm{d}\omega\,\omega^n S(k, \omega) \qquad (1.124)$$

and called the nth *frequency moments* of $S(k, \omega)$. In the last step of (1.123) we have introduced 'normalized' frequency moments defined as

$$\langle \omega_k^n\rangle \equiv \overline{\omega_k^n}/S(k). \qquad (1.125)$$

As in the single-particle case, the evaluation of the first few frequency moments is expected to provide some useful information on the collective dynamics actually probed at the various wavevectors (i.e. over different length scales). Again, the calculation is accomplished via the use of the stationarity of the statistical averages and the consequent possibility of shifting the time derivatives inside the average from one variable to the other. Thus

$$\overline{\omega_k^2} = -(1/N)\langle \hat{n}^*(\mathbf{k}, 0)\ddot{\hat{n}}(\mathbf{k}, 0)\rangle$$

$$= (1/N)\langle \dot{\hat{n}}^*(\mathbf{k}, 0)\dot{\hat{n}}^*(\mathbf{k}, 0)\rangle$$

$$= (1/N)\sum_{ij}\langle (\mathbf{k} \cdot \mathbf{v}_i)(\mathbf{k} \cdot \mathbf{v}_j)\exp(-\mathrm{i}\mathbf{k} \cdot \mathbf{r}_{ij})\rangle. \qquad (1.126)$$

Since the average over the velocities vanishes unless $i = j$, we obtain

$$\overline{\omega_k^2} = \frac{1}{N}\sum_i\langle (\mathbf{k} \cdot \mathbf{v}_i)^2\rangle = \frac{k_B T}{m}k^2. \qquad (1.127)$$

As only single-particle contributions are relevant in the result (1.127), clearly $\overline{\omega_k^2}$ coincides with the corresponding self quantity $\langle \omega_k^2\rangle_s$. However, in the collective case the last member of eqn (1.123) shows that the short-time decay of $F(k, t)$ from its initial value is ruled by the normalized second moment

$$\langle \omega_k^2 \rangle = \frac{k_{\rm B} T}{m S(k)} k^2, \tag{1.128}$$

rather than simply by $\overline{\omega_k^2}$. The presence of $S(k)$ at the denominator of (1.128) has important consequence on the qualitative features expected for the collective dynamics. In particular, the differences between the dynamic structure factor $S(k, \omega)$ and its self counterpart $S_s(k, \omega)$ are anticipated as being large in the low wave vector region, where in the liquid range $S(k) \approx S(0) \ll 1$. Indeed, we shall see that in this hydrodynamic regime $S(k, \omega)$ exhibits well-defined inelastic peaks associated with the propagation of sound-like excitations.

Even beyond the low-k range, the short-time dynamics of density fluctuations is affected by the oscillatory behaviour of the static structure factor. As k increases and the length scale $2\pi/k$ becomes more and more microscopic, the liquid is not able to support any collective excitation, and both $F(k, t)$ and $S(k, \omega)$ should decay monotonically. In such a case, the quantity $\langle \omega_k^2 \rangle^{1/2}$ gives an approximate measure of the spectral width of $S(k, \omega)$. The more interesting situation occurs for wave vectors near the position $k_{\rm m}$ of the main peak of $S(k)$, where the marked decrease of $\langle \omega_k^2 \rangle$ implies a considerable narrowing of $S(k, \omega)$ and a slowing down of $F(k, t)$ (de Gennes 1959). Physically, the long decay time of $F(k, t)$ for $k \approx k_{\rm m}$ can be understood by arguing that the sharp peak of $S(k)$ at $k_{\rm m}$ reflects a high probability of occurrence of density fluctuations with k in this range; as a result, the latter cannot easily be destroyed by collisional mechanisms and their lifetime is very long. At even larger wave vectors, correlation effects lose their importance, until eventually $S(k) \approx 1$. Here any distinction between collective and single-particle dynamics is expected to disappear, with both $F_s(k, t)$ and $F(k, t)$ approaching the limiting result (1.50) appropriate for free particles.

In close analogy with the analysis of Section 1.4.1, the dynamics of density fluctuations can be explored at a more detailed level by evaluating the fourth moment

$$\overline{\omega_k^4} = \frac{1}{N} \langle \hat{n}^*(\mathbf{k}, 0) \, \ddddot{\hat{n}}(\mathbf{k}, 0) \rangle = \frac{1}{N} \langle \ddot{\hat{n}}^*(\mathbf{k}, 0) \ddot{\hat{n}}(\mathbf{k}, 0) \rangle \tag{1.129}$$

The calculation of $\overline{\omega_k^4}$ proceeds along lines similar to those previously reported for $\langle \omega_k^4 \rangle_s$, starting from $\hat{n}(\mathbf{k}, 0) = \sum_i [-(\mathbf{k} \cdot \mathbf{v}_i)^2 + i(\mathbf{k} \cdot \dot{\mathbf{v}}_i)] \exp(i\mathbf{k} \cdot \mathbf{r}_i)$. Then

$$\overline{\omega_k^4} = \frac{1}{N} \sum_{ij} \langle \{ (\mathbf{k} \cdot \mathbf{v}_i)^2 (\mathbf{k} \cdot \mathbf{v}_j)^2 + i[(\mathbf{k} \cdot \dot{\mathbf{v}}_i)(\mathbf{k} \cdot \mathbf{v}_j)^2 - (\mathbf{k} \cdot \mathbf{v}_i)^2(\mathbf{k} \cdot \dot{\mathbf{v}}_j)]$$
$$+ (\mathbf{k} \cdot \dot{\mathbf{v}}_i)(\mathbf{k} \cdot \dot{\mathbf{v}}_j) \} \exp(-i\mathbf{k} \cdot \mathbf{r}_{ij}) \rangle \tag{1.130}$$

In the summation over j, the 'self'-contribution with $j = i$ reproduces the single-particle result $\langle \omega_k^4 \rangle_s$ (cf. eqn (1.39)). The 'distinct' part of $\overline{\omega_k^4}$ with $\sum_{i,j \neq i}$ comprises three kinds of contributions. In the first one, all the averages can be factorized yielding

$$\frac{1}{N} \sum_{i,j \neq i} \langle (\mathbf{k} \cdot \mathbf{v}_i)^2 (\mathbf{k} \cdot \mathbf{v}_j)^2 \exp(-i\mathbf{k} \cdot \mathbf{r}_{ij}) \rangle = \langle (\mathbf{k} \cdot \mathbf{v}_i)^2 \rangle^2 \frac{1}{N} \sum_{i,j \neq i} \langle \exp(-i\mathbf{k} \cdot \mathbf{r}_{ij}) \rangle$$
$$= (k_{\rm B} T/m)^2 k^4 [S(k) - 1] \tag{1.131}$$

where in the last line we have used (cf. (1.118), (1.121))

$$\frac{1}{N} \sum_{i,j \neq i} \langle \exp(-i\mathbf{k} \cdot \mathbf{r}_{ij}) \rangle = S(k) - 1 + (2\pi)^3 n\delta(\mathbf{k}) \tag{1.132}$$

with the last term giving a zero contribution to (1.131). The other two contributions to eqn (1.130) are evaluated by expressing the accelerations $\dot{\mathbf{v}}_i$ and $\dot{\mathbf{v}}_j$ in terms of derivatives of the total potential energy V_N, and by exploiting the result

$$\left\langle f(\mathbf{r}^N) \frac{\partial V_N}{\partial r_{i,a}} \right\rangle = k_{\rm B} T \left\langle \frac{\partial f(\mathbf{r}^N)}{\partial r_{i,a}} \right\rangle. \tag{1.133}$$

Equation (1.133) is valid for any variable f which is a regular function of the atomic coordinates, and is readily verified by performing a partial integration (cf. (1.42)). As a result, the distinct part of the two terms in square brackets in (1.130) reads

$$\frac{1}{N} \sum_{i,j \neq i} \langle i[(\mathbf{k} \cdot \dot{\mathbf{v}}_i)(\mathbf{k} \cdot \mathbf{v}_j)^2 - (\mathbf{k} \cdot \mathbf{v}_i)^2(\mathbf{k} \cdot \dot{\mathbf{v}}_j)] \exp(-i\mathbf{k} \cdot \mathbf{r}_{ij}) \rangle$$
$$= \frac{k_{\rm B} T}{m} k^2 \cdot \frac{1}{N} \sum_{i,j \neq i} \langle i[(\mathbf{k} \cdot \dot{\mathbf{v}}_i) - (\mathbf{k} \cdot \dot{\mathbf{v}}_j)] \exp(-i\mathbf{k} \cdot \mathbf{r}_{ij}) \rangle$$
$$= -\frac{2}{N} \left(\frac{k_{\rm B} T}{m} \right)^2 k^4 \sum_{i,j \neq i} \langle \exp(-i\mathbf{k} \cdot \mathbf{r}_{ij}) \rangle$$
$$= -2 \left(\frac{k_{\rm B} T}{m} \right)^2 k^4 [S(k) - 1]. \tag{1.134}$$

Finally, using (1.133) the last term in eqn (1.130) with $i \neq j$ can be written as

$$\frac{1}{N} \sum_{i,j \neq i} \langle (\mathbf{k} \cdot \dot{\mathbf{v}}_i)(\mathbf{k} \cdot \dot{\mathbf{v}}_j) \exp(-i\mathbf{k} \cdot \mathbf{r}_{ij}) \rangle$$
$$= \frac{k_{\rm B} T}{m^2} \cdot \frac{1}{N} \sum_{i,j \neq i} \sum_{\alpha\beta} k_\alpha k_\beta \left\langle \left[\frac{\partial^2 V_N}{\partial r_{i,a} \partial r_{j,\beta}} + ik_\beta \frac{\partial V_N}{\partial r_{i,a}} \right] \exp(-i\mathbf{k} \cdot \mathbf{r}_{ij}) \right\rangle$$

$$= \frac{k_B T}{m^2} \cdot \frac{1}{N} \sum_{i,j \neq i} \sum_{\alpha\beta} k_\alpha k_\beta \left\langle \left[-\frac{\partial^2 \phi(r_{ij})}{\partial r_{ij,\alpha} \partial r_{ij,\beta}} + k_B T k_\alpha k_\beta \right] \exp(-i\mathbf{k} \cdot \mathbf{r}_{ij}) \right\rangle \tag{1.135}$$

where in the first term in square brackets V_N has been expressed in pairwise contributions, and in the second we have again exploited (1.133). Then, introducing the pair distribution function (1.11) and using (1.132), we obtain

$$\frac{1}{N} \sum_{i,j \neq i} \langle (\mathbf{k} \cdot \dot{\mathbf{v}}_i)(\mathbf{k} \cdot \dot{\mathbf{v}}_j) \exp(-i\mathbf{k} \cdot \mathbf{r}_{ij}) \rangle$$

$$= -\frac{n k_B T}{m^2} \sum_{\alpha\beta} k_\alpha k_\beta \int d\mathbf{r} \frac{\partial^2 \phi(r)}{\partial r_\alpha \partial r_\beta} \exp(-i\mathbf{k} \cdot \mathbf{r}) g(r)$$

$$+ \left(\frac{k_B T}{m}\right)^2 k^4 [S(k) - 1]. \tag{1.136}$$

Summing up all the contributions with $j \neq i$, all the terms with the factor $[S(k) - 1]$ are seen to cancel. Adding now the 'self' part with $j = i$ we eventually find that

$$\overline{\omega_k^4} = \frac{k_B T}{m} k^2 \left[3\frac{k_B T}{m} k^2 + \Omega_0^2 - \Omega_k^2 \right] \tag{1.137}$$

with the definition

$$\Omega_k^2 \equiv \frac{n}{m} \sum_{\alpha\beta} \frac{k_\alpha k_\beta}{k^2} \int d\mathbf{r} \frac{\partial^2 \phi(r)}{\partial r_\alpha \partial r_\beta} \exp(-i\mathbf{k} \cdot \mathbf{r}) g(r)$$

$$= \frac{n}{m} \int d\mathbf{r} \frac{\partial^2 \phi(r)}{\partial z^2} \exp(-ikz) g(r) \tag{1.138}$$

where in the last step we have exploited the isotropy of the system and chosen $\mathbf{k}$ along the z-axis of the laboratory frame. The angular integrations in (1.138) are readily performed by using

$$\frac{\partial^2 \phi(r)}{\partial r_\alpha \partial r_\beta} = \phi''(r) \frac{r_\alpha r_\beta}{r^2} + \frac{\phi'(r)}{r} \left[\delta_{\alpha,\beta} - (r_\alpha r_\beta / r^2) \right] \tag{1.139}$$

and we eventually obtain

$$\Omega_k^2 = \frac{4\pi n}{3m} \int_0^\infty dr\, r^2 \{ \phi''(r) [j_0(kr) - 2j_2(kr)]$$

$$+ (2/r)\, \phi'(r) [j_0(kr) + j_2(kr)] \} g(r) \tag{1.140}$$

where $j_0(x) = \sin x / x$ and $j_2(x) = (3/x^2)[(\sin x / x) - \cos x] - \sin x / x$

are the spherical Bessel functions of order 0 and 2, respectively. Since $j_n(x \to 0) \approx x^n / (2n + 1)!!$, for small wavevectors the quantity Ω_k approaches the Einstein frequency Ω_0.

Equation (1.140) can be further simplified if, as in Section 1.4.2, we exploit the fact that in most simple liquids the integral is dominated by separations r near the position r_0 of the main peak of $g(r)$. Moreover, adopting the representation (1.62) of the pair potential with $p, q \gg 1$, the leading contribution to the integral is provided by the term with $\phi''(r)$ and we eventually obtain

$$\Omega_k^2 \approx \Omega_0^2 [j_0(kr_0) - 2j_2(kr_0)]. \tag{1.141}$$

For future use, it is convenient to introduce the quantity

$$\omega_L^2(k) \equiv \frac{\overline{\omega_k^4}}{\overline{\omega_k^2}} = \frac{\langle \omega_k^4 \rangle}{\langle \omega_k^2 \rangle} \tag{1.142}$$

which has the dimensions of a squared frequency. In view of the results (1.127) and (1.137), we find that

$$\omega_L^2(k) = \frac{3k_B T}{m} k^2 + \frac{n}{m} \int d\mathbf{r} \frac{\partial^2 \phi(r)}{\partial z^2} [1 - \exp(-ikz)] g(r)$$

$$= \frac{3k_B T}{m} k^2 + \Omega_0^2 - \Omega_k^2$$

$$\approx \frac{3k_B T}{m} k^2 + \Omega_0^2 [1 - j_0(kr_0) + 2j_2(kr_0)] \tag{1.143}$$

where the last step follows from the approximation (1.141).

As in the single-particle case, it is interesting to explore the behaviour of $\overline{\omega_k^4}$ in the two limiting cases of very small and very large wavevectors. For large k, the phase factor $\exp(-ikz)$ in (1.138) oscillates so rapidly that the integral vanishes, making $\overline{\omega_k^4}$ approach the self value $\langle \omega_k^4 \rangle_s$. For $k \to \infty$ both $\overline{\omega_k^4}$ and $\langle \omega_k^4 \rangle_s$ eventually yield the free-particle result $3(k_B T/m)^2 k^4$; in this limit, $S(k) \to 1$ and $\langle \omega_k^4 \rangle = 3\langle \omega_k^2 \rangle^2$, as expected for a Gaussian spectrum centred at $\omega = 0$.

In the opposite limit of small wavevectors, expanding Ω_k^2 up to the order k^2 it is readily found that

$$\omega_L^2(k) = \frac{3k_B T}{m} k^2 + \frac{n}{2m} \int d\mathbf{r} \frac{\partial^2 \phi(r)}{\partial z^2} z^2 g(r) \cdot k^2$$

$$\equiv c_L^2 k^2 \tag{1.144}$$

where the quantity c_L has the dimension of a velocity. Since $\overline{\omega_k^2} = (k_B T/m) k^2$, for small k $\overline{\omega_k^4}$ is found to vanish as k^4. This result is to be

contrasted with the $k \to 0$ behaviour of $\langle \omega_k^4 \rangle_s$, which vanishes as k^2. The ultimate origin of this difference is the quasi-conserved character in the collective case of both the variables $\hat{n}(\mathbf{k} \to 0, t)$ and $j_L(\mathbf{k} \to 0, t)$ (cf. Section 1.6.1).

1.6.3   The correlation functions of the currents

The partitioning (1.116) of the current $\mathbf{j}(\mathbf{k}, t)$ naturally suggests the introduction of two distinct autocorrelation functions, respectively associated with flows of particles parallel and perpendicular to the external wavevector $\mathbf{k}$. Taking again the latter along the z-axis, 'longitudinal' and 'transverse' current correlation functions are defined as

$$C_L(\mathbf{k}, t) \equiv (1/N) \langle j_L^*(\mathbf{k}, 0) j_L(\mathbf{k}, t) \rangle$$

$$= (1/N) \langle j_z^*(\mathbf{k}, 0) j_z(\mathbf{k}, t) \rangle \qquad (1.145)$$

and

$$C_T(\mathbf{k}, t) \equiv (1/2N) \langle j_T^*(\mathbf{k}, 0) \cdot j_T(\mathbf{k}, t) \rangle$$

$$= (1/N) \langle j_x^*(\mathbf{k}, 0) j_x(\mathbf{k}, t) \rangle$$

$$= (1/N) \langle j_y^*(\mathbf{k}, 0) j_y(\mathbf{k}, t) \rangle \qquad (1.146)$$

where the last steps follow from the isotropy of the fluid.

There is a considerable difference between the physical phenomena probed by these two dynamic correlations. Since $\dot{\hat{n}}(\mathbf{k}, t) = ik j_L(\mathbf{k}, t)$, the *longitudinal current correlation function* can be written as

$$C_L(k, t) = - (1/k^2) \ddot{F}(k, t) \qquad (1.147)$$

As a result, no really new information on collective dynamics is provided by $C_L(k, t)$. For example, the longitudinal current spectrum is simply given by

$$C_L(k, \omega) = (1/2\pi) \int_{-\infty}^{\infty} dt \, C_L(k, t) \exp(-i\omega t)$$

$$= (\omega^2/k^2) S(k, \omega). \qquad (1.148)$$

Thus, at any wavevector, $C_L(k, \omega)$ starts from zero and has at least one peak at finite frequencies. Similarly, the short-time behaviour of $C_L(k, t)$ can easily be deduced from that of $F(k, t)$. In particular, $C_L(k, 0) = (1/k^2)\overline{\omega_k^2} = k_B T/m$, and $\ddot{C}_L(k, 0) = - (1/k^2)\overline{\omega_k^4}$. Hence, the normalized second frequency moment of $C_L(k, \omega)$ reads

$$-[\ddot{C}_L(k, 0)/C_L(k, 0)] = \omega_L^2(k), \qquad (1.149)$$

a result which justifies the notation chosen in the definition (1.142). Even if the physics behind the longitudinal correlations is not new, in some cases their explicit consideration turns out to be particularly useful. An example in this respect is provided by those physical situations in which $S(k, \omega)$ has hardly discernible peaks (or 'shoulders') at finite frequencies. In view of eqn (1.148), these features are naturally emphasized in the longitudinal current spectrum, thus permitting a more reliable extraction of any associated physical information.

In contrast with $\mathbf{j}_L(\mathbf{k}, t)$, the transverse current $\mathbf{j}_T(\mathbf{k}, t)$ is not directly coupled with the density fluctuations. Thus, the *transverse current correlation function* $C_T(k, t)$ is expected to provide information on new dynamical events occuring in the fluid. Broadly speaking, the transverse character of the flow of particles indicates that $C_T(k, t)$ probes any 'shear mode' possibly propagating in the fluid at the given wavevector. Performing even in this case the usual analysis of short-time features, we find that $C_T(k, 0) = k_B T/m$, whereas

$$\ddot{C}_T(k, 0) = - \frac{1}{N} \langle \dot{j}_x^*(\mathbf{k}, 0) \dot{j}_x(\mathbf{k}, 0) \rangle \equiv - \frac{k_B T}{m} \omega_T^2(k), \qquad (1.150)$$

where $\omega_T^2(k)$ is the normalized second frequency moment of the transverse current spectrum $C_T(k, \omega)$. The quantity $\omega_T^2(k)$ can be evaluated in a way similar to that previously seen for $\overline{\omega_k^4}$ and $\omega_L^2(k)$. The final result is

$$\omega_T^2(k) = \frac{k_B T}{m} k^2 + (n/m) \int d\mathbf{r} \frac{\partial^2 \phi(r)}{\partial x^2} [1 - \exp(-ikz)] g(r)$$

$$= \frac{k_B T}{m} k^2 + \Omega_0^2 - (\Omega_k')^2. \qquad (1.151)$$

Here

$$(\Omega_k')^2 \equiv \frac{4\pi n}{3m} \int_0^{\infty} dr \, r^2 \{\phi''(r) [j_0(kr) + j_2(kr)]$$

$$+ \frac{\phi'(r)}{r} [2j_0(kr) - j_2(kr)]\} g(r)$$

$$\approx \Omega_0^2 [j_0(kr_0) + j_2(kr_0)] \qquad (1.152)$$

where the last step is valid within the same approximations as in eqn (1.141).

In the limit of very large wavevectors, where both Ω_k^2 and $(\Omega_k')^2$ vanish, $C_L(k, t)$ and $C_T(k, t)$ are expected to approach their free-particle expressions, respectively given by

$$C_L(k, t) = \frac{k_B T}{m}\left[1 - \frac{k_B T}{m}k^2 t^2\right]\exp\left[-\frac{k_B T}{2m}k^2 t^2\right], \qquad (1.153)$$

$$C_T(k, t) = \frac{k_B T}{m}\exp\left[-\frac{k_B T}{2m}k^2 t^2\right]. \qquad (1.154)$$

The corresponding spectra read

$$C_L(k, \omega) = \left(\frac{m}{2\pi k_B T}\right)^{1/2}\frac{\omega^2}{k^3}\exp\left(\frac{-m\omega^2}{2k_B T k^2}\right), \qquad (1.155)$$

$$C_T(k, \omega) = \left(\frac{k_B T}{2\pi m k^2}\right)^{1/2}\exp\left(\frac{-m\omega^2}{2k_B T k^2}\right). \qquad (1.156)$$

Thus, whereas in this limit $C_T(k, \omega)$ has a Gaussian shape as $S(k, \omega) \equiv S_s(k, \omega)$, $C_L(k, \omega)$ is peaked at frequencies $\omega = \pm (2k_B T/m)^{1/2}k$, of the same order as the halfwidth $\Gamma_s(k \to \infty)$ (cf. Section 1.4.3).

Like $\omega_L^2(k)$, the quantity $\omega_T^2(k)$ is found to vanish as k^2 for small wavevectors, as a result of the quasi-conserved character of $j_T(k, t)$. Equation (1.151) gives

$$\omega_T^2(k) = \frac{k_B T}{m}k^2 + \frac{n}{2m}\int dr \frac{\partial^2 \phi(r)}{\partial x^2} z^2 g(r) \cdot k^2$$

$$\equiv c_T^2 k^2. \qquad (1.157)$$

Comparing the two velocities c_L and c_T as deduced by eqns (1.144) and (1.157)

$$c_L^2 = \frac{3k_B T}{m} + \frac{2\pi n}{15m}\int_0^\infty dr\, r^4\left[3\phi''(r) + \frac{2\phi'(r)}{r}\right]g(r), \qquad (1.158)$$

$$c_T^2 = \frac{k_B T}{m} + \frac{2\pi n}{15m}\int_0^\infty dr\, r^4\left[\phi''(r) + \frac{4\phi'(r)}{r}\right]g(r) \qquad (1.159)$$

and noting that the term with $\phi'(r)/r$ usually gives a small negative contribution, we find that $c_L^2 \geqslant 3c_T^2$. Even if it is tempting to interpret c_L and c_T as the longitudinal and transverse velocities of some 'sound-like' collective excitation, the fact that these results were obtained by a short-time analysis indicates that such an interpretation is only appropriate for the instantaneous response of the liquid. As in the case of single-particle properties, this short-time (or high-frequency) description over-emphasizes the solid-like features of the liquid. In particular, for small k this picture is certainly bound to fail if $C_L(k, t)$ or $C_T(k, t)$ are probed over timescales comparable or longer than the typical collisional times. Eventually, one approaches the genuine hydrodynamic regime, explicitly discussed in the next subsection.

1.6.4 The dynamical variables relevant in the hydrodynamic regime

When probed over sufficiently large distances and long times, both the single-particle and the collective dynamics of a fluid can be discussed in terms of a quasi-macroscopic framework in which the relevant variables are treated as though the system were a continuum. To illustrate the procedure, consider, for example, the microscopic number density $n(\mathbf{R}, t)$ as defined in eqn (1.109). The presence of the δ-function clearly implies a highly discontinuous character of this variable, depending on whether $\mathbf{R}$ coincides or not with the instantaneous position of an atom. If, however, the dynamical phenomenon under consideration is known to be associated with slow enough variations both in space and in time, we may not bother with any violent dependence on $\mathbf{R}$ and t, and replace $n(\mathbf{R}, t)$ with a suitable average over all the microscopic spatial and temporal 'details'. Albeit a priori a precise assessment of this 'coarse-graining' procedure is far from trivial, it is intuitively clear that we eventually approach a quasi-macroscopic dynamical variable $n_{av}(\mathbf{R}, t)$, which can be considered as a continuous and slowly varying function of both $\mathbf{R}$ and t.

As a result, the dynamical behaviour of the system is ultimately phrased in terms of several variables $A_{av}(\mathbf{R}, t)$, or $A_{av}(\mathbf{k}, t)$, fluctuating around their equilibrium values. In several cases of interest, the departures from static equilibrium conditions are comparatively small, justifying a perturbative treatment in the magnitude of the corresponding fluctuations. In fluids, such a linearized framework is conventionally referred to as *ordinary hydrodynamics*. Rather than providing an extensive account of these macroscopic approaches (which can be found in several excellent textbooks, e.g. Landau and Lifshitz (1959)), we shall simply report the final output for the relevant time correlation functions, denoted with the suffix 'hyd' to remember that they involve the appropriate coarse-grained variables rather than the microscopic ones. The detailed results can be summarized as follows:

$$[F_s(k, t)]_{hyd} = \exp(-k^2 D|t|), \qquad (1.160)$$

$$[F(k, t)]_{hyd} = [F(k, 0)]_{hyd}\{[1 - (1/\gamma)]\exp[-k^2(\kappa/nc_p)|t|]$$
$$+ (1/\gamma)\exp(-k^2\Gamma|t|)[\cos(v_s kt) + bk\sin(v_s k|t|)]\}, \qquad (1.161)$$

$$[C_L(k, t)]_{hyd} = -(1/k^2)[\ddot{F}(k, t)]_{hyd}, \qquad (1.162)$$

$$[C_T(k, t)]_{hyd} = [C_T(k, 0)]_{hyd}\exp[-k^2(\eta/nm)|t|]. \qquad (1.163)$$

The quantities appearing on the right-hand side of eqns (1.160)–(1.163) fall into two distinct categories. Specifically, we deal with:

(i) *equilibrium* (or *thermodynamic*) *quantities*, such as the initial values of F and C_T, the ratio $\gamma = c_P/c_V$ between the specific heats at constant pressure and at constant volume and the adiabatic sound velocity v_s;

(ii) *transport properties*, such as the diffusion coefficient D, the thermal conductivity κ, the shear viscosity coefficient η and the bulk viscosity coefficient η_v. In the equations above, these quantities appear either explicitly or through

$$\Gamma \equiv \tfrac{1}{2}\left[(\gamma - 1)(\kappa/nc_P) + (\eta_L/nm)\right] \tag{1.164}$$

and

$$b \equiv (1/\gamma v_s)\left[3\Gamma - (\eta_L/nm)\right] \tag{1.165}$$

where

$$\eta_L \equiv \tfrac{4}{3}\eta + \eta_v \tag{1.166}$$

is the so-called 'longitudinal viscosity' coefficient.

Far from being a mere matter of terminology, this distinction contains important physical implications. Indeed, all the equilibrium quantities in eqns (1.160)–(1.163) can in principle be expressed by ordinary thermodynamic approaches. For example, using thermodynamic fluctuation theory one readily establishes that (Landau and Lifshitz 1959)

$$[F(k, 0)]_{\text{hyd}} = nk_B T\chi_T \tag{1.167}$$

where χ_T is the isothermal compressibility. Also, the adiabatic sound velocity can be expressed as

$$v_s = (\gamma/nm\chi_T)^{1/2}. \tag{1.168}$$

On the other hand, similar simple results for the transport coefficients cannot be established within a purely macroscopic approach. Rather, one relies on the fact that the hydrodynamic equations provide a highly successful description of most phenomena observed in conventional fluid dynamics. As a result, the transport coefficients are simply regarded as 'parameters' which can reliably be determined by matching the predictions of the equations with the actual experimental findings. Since the latter are typically in the frequency domain, the above procedure is accomplished by considering the Fourier transforms of eqns (1.160)–(1.163), namely

$$[S_s(k, \omega)]_{\text{hyd}} = \frac{1}{\pi} \frac{Dk^2}{\omega^2 + (Dk^2)^2} \tag{1.169}$$

$$[S(k, \omega)]_{\text{hyd}} = \frac{nk_B T\chi_T}{\pi} \left\{ \frac{1}{\gamma}\left[\frac{\Gamma k^2 + bk(\omega - v_s k)}{(\omega - v_s k)^2 + (\Gamma k^2)^2} + \frac{\Gamma k^2 + bk(\omega + v_s k)}{(\omega + v_s k)^2 + (\Gamma k^2)^2}\right] \right.$$
$$\left. + \left(1 - \frac{1}{\gamma}\right) \frac{(\kappa/nc_V)k^2}{\omega^2 + [(\kappa/nc_V)k^2]^2} \right\}, \tag{1.170}$$

$$[C_L(k, \omega)]_{\text{hyd}} = \frac{\omega^2}{k^2}[S(k, \omega)]_{\text{hyd}}, \tag{1.171}$$

$$[C_T(k, \omega)]_{\text{hyd}} = \frac{k_B T}{m\pi} \frac{(\eta/nm)k^2}{\omega^2 + [(\eta/nm)k^2]^2}. \tag{1.172}$$

Summarizing all these results, eqns (1.160) and (1.169) are the continuum version of single-particle motion (often referred to as the *Fick's law*), and appear to be identical with the 'microscopic' equations reported in Sections 1.4.2 and 1.4.3 for the diffusive regime. At the collective level, the time correlations (1.161)–(1.163), along with the corresponding spectra (1.170)–(1.172), are the final results of *Navier–Stokes hydrodynamics*. In particular, the density fluctuation spectrum (1.170) is characterized by the presence of a Lorentzian component centred at $\omega = 0$ (the so-called 'Rayleigh spectrum') which turns out to be associated with slowly varying temperature fluctuations, and of two inelastic 'Brillouin' contributions. In the domain of applicability of hydrodynamics, the wavevector k is sufficiently small that the three components are well separated, with spectral widths of the order of k^2. As a result, the inelastic components are sharply peaked at frequencies $\omega \approx \pm v_s k$, and the terms with b can be neglected, yielding for the Brillouin portion two Lorentzians centred at $\omega = \pm v_s k$ with a halfwidth Γk^2. The inelastic peaks account for the presence in the fluid of longitudinal sound waves propagating with the ordinary adiabatic velocity v_s. In contrast, eqn (1.172) shows that, according to hydrodynamics, the fluid does not support the propagation of transverse sound waves. At a macroscopic level, this result reflects the well-known inability of fluids to resist shear forces.

As stated in Section 1.1, the ideal goal of a microscopic theory for the time-dependent properties of liquids is to use statistical mechanics to account for dynamical phenomena occurring over arbitrary length and time scales. In particular, the framework should be able to yield an independent derivation of all the previous results of ordinary hydrodynamics, to provide physical criteria for the validity of such a description, and finally to suggest possible extensions (if any) of the hydrodynamic equations beyond their strict limits of application. As a by-product, the general statistical framework should also provide microscopic expressions for the transport properties, thus making an important step in the direction of their theoretical prediction. A first result in this respect has already been seen in Section 1.4.2 with the 'Green–Kubo relation' (1.67) for the diffusion coefficient. In the same context, it was also argued that a reasonable criterion for the validity of a quasi-macroscopic description is provided by the large-distances and long-times conditions $k \ll l^{-1}$ and $t \gg \Omega_0^{-1}$.

In Chapter 3 we shall arm ourselves with the theoretical equipment (the 'memory functions') appropriate for providing a definite answer to the

previous points. In particular, all the results of ordinary hydrodynamics will be deduced in Section 3.4. The discussion about a possible extension of such a framework (referred to as *generalized hydrodynamics*) is postponed until the beginning of Chapter 6. For the time being, it is convenient to introduce some additional dynamical quantities which will be relevant in the subsequent developments of the theory. Since in hydrodynamics one is concerned with slowly varying phenomena, a basic role is naturally played by the variables $n_{s,i}(\mathbf{k}, t)$, $\hat{n}(\mathbf{k}, t)$ and $\mathbf{j}(\mathbf{k}, t)$ which are quasi-conserved as $k \rightarrow 0$. Also, since the total energy of the system is conserved, it is appropriate to introduce in the same respect an *energy-density* variable. In the wavevector space, this is defined by

$$e(\mathbf{k}, t) \equiv \tfrac{1}{2} \sum_i \left[mv_i^2(t) + \sum_{j(\neq i)} \phi(r_{ij}(t)) \right] \exp(i\mathbf{k} \cdot \mathbf{r}_i(t)). \quad (1.173)$$

Noting that $\langle e(\mathbf{k}, t) \rangle = \langle e(\mathbf{k}, 0) \rangle = [(2\pi)^3/V] \langle \mathcal{H} \rangle \delta(\mathbf{k})$, we may introduce energy density fluctuations defined as $\hat{e}(\mathbf{k}, t) = e(\mathbf{k}, t) - \langle e(\mathbf{k}, 0) \rangle$. Because of their quasi-conserved character, the equations of motion of the variables $n_{s,i}(\mathbf{k}, t)$, $\hat{n}(\mathbf{k}, t)$, $\mathbf{j}(\mathbf{k}, t)$ and $\hat{e}(\mathbf{k}, t)$ have the general form of a 'continuity equation', i.e.

$$\dot{n}_{s,i}(\mathbf{k}, t) = i\mathbf{k} \cdot \{ \mathbf{v}_i(t) \exp[i\mathbf{k} \cdot \mathbf{r}_i(t)] \}, \quad (1.174)$$

$$\dot{\hat{n}}(\mathbf{k}, t) = i\mathbf{k} \cdot \mathbf{j}(k, t), \quad (1.175)$$

$$\dot{j}(\mathbf{k}, t) = (i/m)\mathbf{k} \cdot \sigma(\mathbf{k}, t), \quad (1.176)$$

$$\dot{\hat{e}}(\mathbf{k}, t) = i\mathbf{k} \cdot \mathbf{q}(\mathbf{k}, t). \quad (1.177)$$

Here $\sigma(\mathbf{k}, t) = \exp(iLt)\sigma(\mathbf{k})$ is the k-dependent *microscopic stress tensor* at time t. Writing the total potential energy as a sum of pairwise contributions, it is easily found that the cartesian components of $\sigma(\mathbf{k})$ read

$$\sigma_{\alpha,\beta}(\mathbf{k}) = \sum_i \left\{ mv_{i,\alpha}v_{i,\beta} - \tfrac{1}{2} \sum_{j \neq i} [r_{ij,\alpha}r_{ij,\beta}/r_{ij}^2] P_k(r_{ij}) \right\} \exp(i\mathbf{k} \cdot \mathbf{r}_i) \quad (1.178)$$

where

$$P_k(r) \equiv r\phi'(r) \frac{1 - \exp(-i\mathbf{k} \cdot \mathbf{r})}{i\mathbf{k} \cdot \mathbf{r}}. \quad (1.179)$$

Note that

$$\langle \sigma_{\alpha,\beta}(\mathbf{k}) \rangle = (2\pi)^3 n\delta(\mathbf{k}) \left[k_B T \delta_{\alpha,\beta} - \tfrac{1}{2} n \int d\mathbf{r} (r_\alpha r_\beta/r)\phi'(r)g(r) \right]$$

$$= (2\pi)^3 \delta(\mathbf{k}) \left[nk_B T - \tfrac{1}{2} n^2 \int d\mathbf{r} (r_\alpha^2/r)\phi'(r)g(r) \right] \delta_{\alpha,\beta}. \quad (1.180)$$

Exploiting again the isotropy of the system, the quantity in square brackets can be written as

$$P = nk_B T - \tfrac{1}{6} n^2 \int d\mathbf{r}\, r\phi'(r)g(r), \quad (1.181)$$

which is the well-known *virial theorem* for the pressure P of the fluid (Hansen and McDonald 1986). Thus the averaged diagonal components of the microscopic stress tensor are proportional to the pressure.

On the other hand, eqn (1.177) involves the *microscopic energy current* $\mathbf{q}(\mathbf{k}, t) = \exp(iLt)\mathbf{q}(\mathbf{k})$. The cartesian components of $\mathbf{q}(\mathbf{k})$ read

$$q_\alpha(\mathbf{k}) = \tfrac{1}{2} \sum_i \left\{ \left[mv_i^2 + \sum_{j \neq i} \phi(r_{ij}) \right] v_{i,\alpha} \right.$$
$$\left. - \tfrac{1}{2} \sum_{j \neq i} \sum_\beta (v_{i,\beta} + v_{j,\beta}) [r_{ij,\alpha}r_{ij,\beta}/r_{ij}^2] P_k(r_{ij}) \right\} \exp(i\mathbf{k} \cdot \mathbf{r}_i).$$
$$(1.182)$$

In contrast with $n_{s,i}(\mathbf{k}, t)$, $\hat{n}(\mathbf{k}, t)$, $\mathbf{j}(\mathbf{k}, t)$ and $\hat{e}(\mathbf{k}, t)$, the variables $\mathbf{j}_i(\mathbf{k}, t) \equiv \mathbf{v}_i(t)\exp[i\mathbf{k} \cdot \mathbf{r}_i(t)]$, $\sigma(\mathbf{k}, t)$ and $\mathbf{q}(\mathbf{k}, t)$ are not conserved in the limit $k \rightarrow 0$. Therefore the corresponding time correlation functions are not expected to exhibit any slow character even for vanishing wavevectors. As we shall see in Chapter 3, the time integrals of these correlation functions are closely connected to the transport coefficients of the fluid.

1.6.5 Collective dynamics: experimental and simulation data

In the last two decades, the dynamic structure factor $S(k, \omega)$ has been measured in several monatomic liquids by inelastic scattering either of electromagnetic radiation or of thermal neutrons. As we shall discuss in Chapter 2, the portion of the (k, ω) domain which is in practice accessible in these measurements depends strongly on the nature of the experimental probe. For example, the shortest wavelengths $\lambda = 2\pi/k$ explorable by conventional light scattering turn out to be some 10^3 Å, much larger than both the interatomic distances and the values of l typical of the liquid range (cf. Table 1.1). Consequently, light scattering usually probes the dynamics of density fluctuations under quasi-macroscopic conditions, making an interpretation of the data in terms of ordinary hydrodynamics reasonable. In contrast, coherent inelastic neutron scattering turns out to be best suited to investigate the genuine microscopic regime, where the quantities kl and ω/Ω_0 are comparable with (or even larger than) 1. As a result, the two techniques may be thought as being almost complementary with a possible gap in between, depending both on the experimental setup and on the particular fluid. The 'closure of the gap' (i.e. the study of the transition
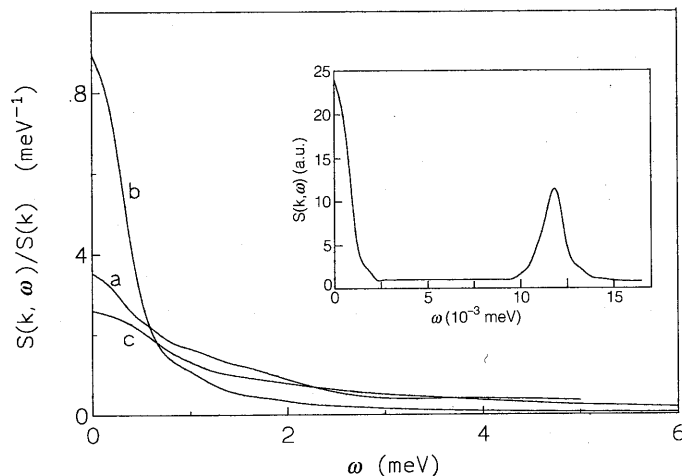
Fig. 1.12   The dynamic structure factor $S(k, \omega)/S(k)$ in liquid Ar as measured by inelastic neutron scattering (Sköld *et al*. 1972). Curves a, b, and c refer respectively to $k = 1, 2$, and 3 Å^{-1}. At these wavevectors the values of $S(k)$ are 0.07, 2.70 (the main peak), and 0.69. In the insert, we report the corresponding light scattering spectrum at $k \approx 0.002$ Å^{-1} (Fleury and Boon 1969).

between the two regimes) is a very active field of research, particularly from the neutron side ('Brillouin neutron scattering', e.g. Bafile *et al*. 1990).

As for single-particle dynamics, important pieces of information have been provided even in the collective case by computer simulation 'experiments', performed both in simple model fluids (e.g. made of hard spheres) and in systems where a more realistic form of the interatomic potential is available. As far as $S(k, \omega)$ is concerned, the (k, ω) domain usually investigated in the simulations overlaps substantially with the one explorable by the neutron experiments. In some cases, the use of large-size systems and the performance of long simulation runs have improved considerably our understanding of the dynamical features occurring in the above-mentioned transition region.

Figure 1.12 reports the results obtained for the density fluctuation spectra $S(k, \omega)$ in liquid argon at different wavevectors. The insert shows the data with the smallest k value, obtained by light scattering (Fleury and Boon 1969). A typical Rayleigh–Brillouin structure is clearly visible, and the analysis of the various spectral features gives results which are consistent with the hydrodynamic predictions. The other data in Fig. 1.12 were instead obtained by Sköld *et al*. (1972) by inelastic neutron scattering, and do not show any trace of inelastic peaks even at the smallest wavevector explored in the measurements, $k = 1$ Å^{-1}. Simulation data in
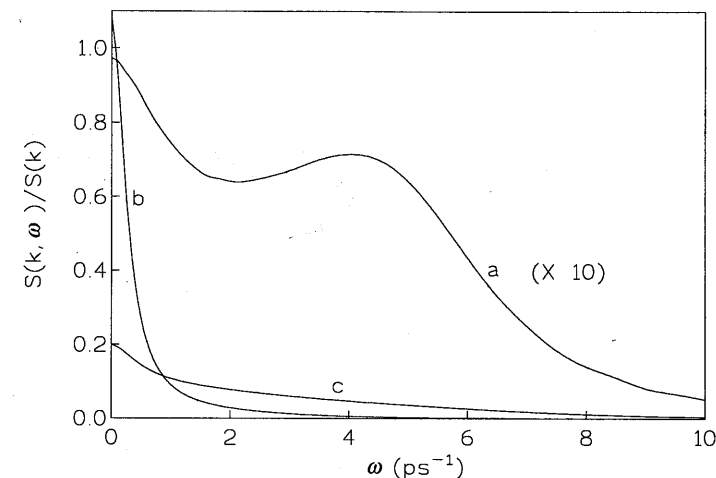
Fig. 1.13   The dynamic structure factor $S(k, \omega)/S(k)$ at different wavevectors as measured by inelastic neutron scattering in liquid Cs at 308 K (Bodensteiner *et al*. 1992). The curves a, b, and c refer respectively to $k = 1, 1.4$, and 2 Å^{-1}. At these wavevectors the values of $S(k)$ are 0.136, 2.814 (the main peak), and 0.598.

Lennard–Jones liquids (Levesque *et al*. 1973) have indeed indicated that in argon a broad inelastic peak is discernible only for $k < 0.26$ Å^{-1}, i.e. up to about 1/8 of the wavevector $k_m \approx 2$ Å^{-1} where $S(k)$ has its main peak. For larger wavevectors, $S(k, \omega)$ continues to exhibit a monotonous decay, the only noteworthy feature being the expected 'de Gennes narrowing' as $k \approx k_m$ (cf. Section 1.6.2). Eventually, at the largest values of k where $S(k) \approx 1$, $S(k, \omega)$ approaches the 'self' spectrum $S_s(k, \omega)$.

These argon results are to be compared with the neutron scattering data recently reported by Bodensteiner *et al*. (1992) for liquid cesium (Fig. 1.13), and with similar findings previously obtained in liquid rubidium (Copley and Rowe 1974). In marked contrast with argon, clear inelastic peaks have been detected up to $k \approx \frac{2}{3} k_m$ for both alkali metals, implying that some well-defined longitudinal excitation is supported in these liquids even over truly microscopic distances. A consistent theory should of course account for this different behaviour, as well as provide an understanding for the nature of the excitation and give a quantitative interpretation of the wavevector dependence of its frequency $\omega_{peak}(k)$, i.e. of its 'dispersion'. In this respect, the data indicate that the corresponding 'velocity' $\omega_{peak}(k)/k$ is somewhat higher than the ordinary hydrodynamic sound speed. The presence of this *positive dispersion* at finite wavevectors contrasts with what we would naively expect from solids, where in the same k range the phonon dispersion curves bend downwards. Thus the effect should clearly be
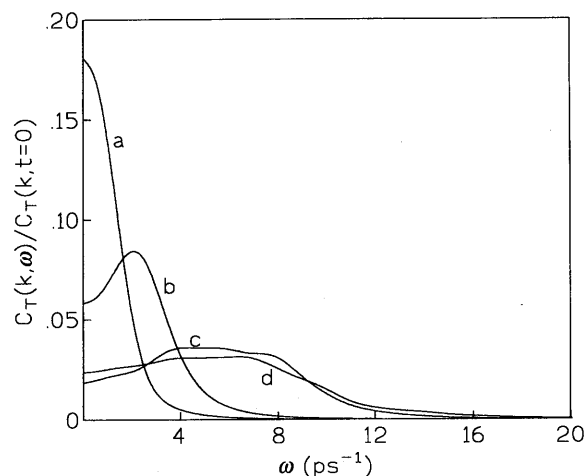
Fig. 1.14 The transverse current spectrum $C_T(k, \omega)/C_T(k, t = 0)$ at different wavevectors as obtained by simulation data in liquid Rb at 332 K (Balucani *et al.* 1987). The curves a–d refer respectively to reduced wavevectors $k\sigma = 0.766, 1.53, 4.594$, and 7.66 ($\sigma = 4.405$ Å).

associated with some important dynamical process typical of the liquid state.

Finally, we shall discuss the data available at different wavevectors for the dynamical correlations of the transverse current. In contrast with F or C_L, $C_T(k, t)$ is not accessible by inelastic neutron scattering experiments, and computer simulation data are the only direct source of information. Broadly speaking, all the liquids are found to share the same qualitative behaviour, illustrated in Fig. 1.14 for liquid rubidium. At the lowest wavevectors the transverse current spectra appear to decay monotonically, in substantial agreement with the hydrodynamic prediction (1.172). As k increases, however, $C_T(k, \omega)$ begins to exhibit a more and more defined inelastic peak, which persists up to wavevectors even larger than k_m. The associated peak frequency initially increases with k, and only for large wavevectors does its dispersion relation flatten as the peak begins to become broader. This feature can tentatively be associated with a transverse sound-like wave, but of course we would like to understand the physics behind the onset of this excitation not predicted by ordinary hydrodynamics. The situation becomes clearer only at very large wavevectors, where $C_T(k, \omega)$ approaches the free-particle form (1.154).

REFERENCES

Alder, B. and Wainwright, T. E. (1970). *Phys. Rev. A*, **1**, 18.
Bafile, U., Verkerk, P., Barocchi, F., de Graaf, L. A., Suck, J.-B., and Mutka, H. (1990). *Phys. Rev. Lett.*, **65**, 2394 and 3458.
Balucani, U. and Vallauri, R. (1980*a*). *Phys. Lett.*, **76A**, 223.
Balucani, U. and Vallauri, R. (1980*b*). *Physica*, **102A**, 70.
Balucani, U., Vallauri, R., Murthy, C. S., Gaskell, T., and Woolfson, M. S. (1983). *J. Phys. C*, **16**, 5605.
Balucani, U. and Vallauri, R. (1990). *Chem. Phys. Lett.*, **166**, 77.
Balucani, U., Vallauri, R., Gaskell, T., and Gori, M. (1984). *Physics Lett.*, **102A**, 109.
Balucani, U., Vallauri, R., and Gaskell, T. (1987). *Phys. Rev. A*, **35**, 4263.
Balucani, U., Torcini, A., and Vallauri, R. (1992). *Phys. Rev. A*, **46**, 2159.
Bloom, M. and Oppenheim, I. (1967). *Adv. Chem. Phys.*, **12**, 549.
Bodensteiner, T., Morkel, C., Gläser, W., and Dorner, B. (1992). *Phys. Rev. A*, **45**, 5709.
Bruesch, P. (1982). *Phonons: theory and experiments I*, Springer Series on Solid-State Sciences, Vol. 34. Springer, Berlin.
Copley, J. R. D. and Rowe, J. M. (1974). *Phys. Rev. A*, **9**, 1656.
de Gennes, P. G. (1959). *Physica*, **25**, 825.
de Groot, S. R. and Mazur, P. (1962). *Non-equilibrium thermodynamics*. North Holland, Amsterdam.
Egelstaff, P. A. (1990). *Nuovo Cimento*, **12D**, 403.
Egelstaff, P. A. and Schofield, P. (1962). *Nucl. Sci. and Engng.*, **12**, 260.
Fleury, P. A. and Boon, J. P. (1969). *Phys. Rev. A*, **4**, 1616.
Goldstein, H. (1980). *Classical mechanics*, 2nd edn. Addison-Wesley, Cambridge, MA.
Green, M. S. (1954). *J. Chem. Phys.*, **22**, 398.
Haan, S. W. (1979). *Phys. Rev. A*, **20**, 2516.
Hansen, J. P. and McDonald, I. R. (1986). *Theory of simple liquids*, 2nd edn. Academic Press, London.
Haymet, A. D. J. (1984). *Chem. Phys. Lett.*, **107**, 77.
Haymet, A. D. J., Rice, S. A., and Madden, W. G. (1981*a*). *J. Chem. Phys.*, **74**, 3033.
Haymet, A. D. J., Rice, S. A., and Madden, W. G. (1981*b*). *J. Chem. Phys.*, **75**, 4696.
Helfland, E. (1960). *Phys. Rev.*, **119**, 1.
Hsu, C. S. and Rahman, A. (1979*a*). *J. Chem. Phys.*, **70**, 5234.
Hsu, C. S. and Rahman, A. (1979*b*). *J. Chem. Phys.*, **71**, 4974.
Huijben, M. J. and van der Lugt, W. (1979). *Acta Cryst. A*, **35**, 431.
Kirkwood, J. G. (1935). *J. Chem. Phys.*, **3**, 300.
Kubo, R. (1957). *J. Phys. Soc. Japan*, **12**, 570.
Landau, L. D. and Lifshitz, E. M. (1959). *Fluid mechanics*. Pergamon Press, London.
Levesque, D. and Ashurst, W. T. (1974). *Phys. Rev. Lett.*, **33**, 277.

Levesque, D. and Verlet, L. (1970). *Phys. Rev. A*, **2**, 2514.

Levesque, D., Verlet, L., and Kürkijarvi, J. (1973). *Phys. Rev. A*, **7**, 1690.

Lewis, J. W. E. and Lovesey, S. W. (1977). *J. Phys. C*, **10**, 3221.

McQuarrie, D. A. (1976). *Statistical mechanics*. Harper and Row, New York.

Mountain, R. D. (1982). *Phys. Rev. A*, **26**, 2859.

Mountain, R. D. and Basu, P. K. (1983). *J. Chem. Phys.*, **78**, 7318.

Nijboer, B. R. A. and Rahman, A. (1966). *Physica*, **32**, 415.

Percus, J. K. and Yevick, G. J. (1958). *Phys. Rev.*, **110**, 1.

Price, D. L., Singwi, K. S., and Tosi, M. P. (1970). *Phys. Rev. B*, **2**, 2983.

Rahman, A. (1974). *Phys. Rev. A*, **4**, 1667.

Sköld, K., Rowe, J. M., Ostrowski, G., and Randolph, P. D. (1972). *Phys. Rev. A*, **6**, 1107.

Steinhardt, P. J., Nelson, D. R., and Ronchetti, M. (1981). *Phys. Rev. Lett.*, **47**, 1297.

Tanaka, M. and Fukui, Y. (1975). *Progr. Theor. Phys.*, **53**, 1547.

van Hove, L. (1954). *Phys. Rev.*, **95**, 249.

Weeks, J. D., Chandler, D. and Andersen, H. C. (1971). *J. Chem. Phys.*, **54**, 5237.

2

The experimental side

2.1 THE REAL 'SIMPLE' LIQUIDS

In Chapter 1 we have provided some intuitive arguments for restricting our attention to a limited class of liquids, namely those approximately described by the Hamiltonian (1.1), (1.2). Such a picture of 'simple' liquids deserves a more detailed discussion if we wish to make contact with the real liquids which can be investigated experimentally. In principle, a liquid can be described as a state of matter occurring in a limited range of pressures and densities, where it exhibits peculiar macroscopic properties (absence of a definite shape, very low compressibility, fluidity, etc.) well known from everyday experience. Microscopically, we deal with a system of interacting particles (henceforth referred to as the 'molecules'). In a first idealization, we may assume that the molecules are individually characterized by a well-defined set of properties, independent of the overall state of the system. This assumption has important consequences even from an experimental point of view, since it implies that collective properties can be studied by assuming that the relevant 'single-molecule' parameters (such as the dipole moment or the polarizability) can be used as a basic set, independent of the thermodynamic conditions such as temperature and pressure.

A similar simplifying assumption can be made for the interactions among the different molecules. Besides being mathematically simple, the intermolecular potential should ideally be state-independent and its essential features should easily be obtained from low-density experiments in the gas phase. If this is the case, the same interactions can be assumed to determine the behaviour of the system even in its condensed phases.

In practice, the assumption that the interaction potential is not dependent upon the state of the system (e.g. its density) is rather well established for several liquids of interest, at least in the normal conditions of existence of the liquid phase (namely, the region of the PV plane between the saturation line, the melting line, and the critical isotherm). By itself, the possibility of establishing from dilute gas data a potential valid for the liquid phase is consistent with the pairwise approximation (1.2). As already mentioned, the observed density-dependence effects are rather small, and if necessary can be accounted for by adding phenomenologically a slight, irreducible, three-body contribution.

Even within this framework of simple 'molecular' liquids, one has to deal with manifold degrees of freedom. In fact, any molecule may translate with the molecular centre of mass, may rotate rigidly around any of the three principal axes of inertia, and may vibrate according to any one of its internal normal vibrational modes. Moreover, some molecules may even change their internal structure and experience the so called 'frame distortion' by which some of the chemical bonds lose their angular rigidity. Of course, in investigating the dynamical properties of the liquid state, one is willing to separate the features of the collective motion from the internal molecular structure. This is easily done by the theory, where model systems can be invented which obey some very peculiar Hamiltonian. From the experimental point of view, however, the choice is much more restricted. Since the liquid should be simple, its molecular constituents should be as simple as possible. Monatomic liquids are then selected as a first choice.

Traditionally, *liquid noble gases* represent the favorite selection for a simple real liquid that can be studied experimentally. Even with these systems, however, not all the difficulties are overcome. In some special case, a particular combination of the atomic mass and the parameters of the potential may yield for the actual liquid state a range of temperatures where *quantum effects* become sizeable, and new complications arise. This is the case of helium which is a good example of a quantum liquid. In this case the quantum effects are so large that they prevent the system from becoming solid under normal conditions: crystalline helium is only obtained by a slight pressurization. Neon too shows non-negligible quantum effects: these are, however, considerably smaller than for helium, and may be treated as a perturbation of a substantially classical behaviour. Quantum corrections can be instead safely neglected in the other noble gas elements: for example liquid argon, since the old days, has been considered as the prototype of a simple classical liquid. Moreover, this liquid has the unique peculiarity that the pairwise approximation (1.2) appears to be valid to the best accuracy of present measurements, so that on a strict experimental basis one can paradoxically state that the conventional approaches developed for simple liquids are really theories of liquid argon. As a matter of fact, even if liquid krypton and xenon can be considered as good examples of simple classical liquids in many respects, most of the experimental work has been devoted to argon for the simple reason that this is the most abundant of the three and may be easily obtained, to a very high degree of purity, without too many efforts.

Within these limitations, the previous considerations support the basic characterization of a simple liquid made in Section 1.1. However, taken literally, they would exclude from the present study the class of *liquid metals*. In particular, liquid alkali metals are found experimentally to exhibit several features of considerable interest for the dynamics of the

liquid state. In fact, although all these monatomic systems are simple in many respects, their liquid phase is characterized by the presence of nearly free electrons. Besides being directly responsible for the electrical conductivity of the system, these electrons affect the interaction between the ions by introducing screening and polarization effects. A discussion of these features is beyond the scope of this book (see March (1990) for a comprehensive account), but the net result is that most structural and dynamical properties of these liquids can be described in terms of an effective, *density dependent* pair potential between screened 'pseudo-ions'. Clearly, this potential has nothing in common with the interactions occurring in the gas phase, where we deal with an assembly of essentially neutral atoms. On the other hand, the effective potential in the liquid metal is expected to share many features with the one in the corresponding crystal phase, making possible a satifactory determination of the potential parameters by suitable fitting procedures, for example to phonon dispersion curves. Having this in mind, we shall adopt a less conservative point of view by including liquid metals in our study of the dynamics of simple monatomic liquids, the latter being characterized by an interparticle pair potential which it is possible to access experimentally from independent measurements.

2.2   THE AVAILABLE EXPERIMENTAL PROBES

In planning an experiment to investigate the microscopic dynamics of a liquid, one has to face the two-fold problem of which are the space and time ranges of interest. An ordinary liquid has a number density n which is three orders of magnitude larger than that of the gas in standard conditions. For example, the density of liquid argon at the triple point (83.8 K) is 35.41 mol litre^{-1} corresponding to $n = 0.021$ atoms Å^{-3} (to be compared with the density of the gas in normal conditions $\approx 4.46 \times 10^{-2}$ mol litre^{-1}). The average interatomic distance $n^{-1/3}$ is therefore 3.6 Å, slightly larger than the hard core diameter $\sigma \approx 3.4$ Å. These figures give an order of magnitude of the spatial resolution which is necessary to resolve any microscopic structural feature.

As far as the timescale is concerned, the important parameter is the duration of a collision. At liquid density the usual distinction between the two timescales, namely the *collision time* and the *time between collisions*, is not very meaningful, since the intermolecular distance is practically the same as the size of a single molecule. This subject has been discussed in Section 1.4 and a 'natural' timescale has been defined which is of the order of a fraction of a picosecond. Also, Table 1.1 shows that in typical simple liquids the natural length scale for collisions is some 10^{-1} Å.

The particle mean free path and the collision time give an order of

magnitude for the lower limit of the space and time range of a possible experimental probe. In contrast, the definition of an upper limit is more difficult. As discussed in Chapter 1, depending on the particular phenomenon we wish to explore, space or time correlations may be limited to a few molecular diameters (and to a few collision times), or they may extend to long distances and times, as for example in hydrodynamics. Therefore, the ideal probe should cover a range of times which extends from fractions of a picosecond (to resolve the collision process in the time domain) up to, say, the relaxation times (around several nanoseconds) associated with the damping of a hypersonic wave. In space, the corresponding length scales should range from a few tenths of an angstrom up to almost macroscopic distances of the order of the hypersound attenuation lengths ($\sim 10^{-3}$ cm). No single experimental probe can cover such a large space–time interval.

Since we are particularly interested in the dynamical processes occurring at a microscopic level, we shall not discuss those experimental techniques which probe liquids *uniquely* as they were effectively continuous media. Ultrasonic experiments are typical examples of such a kind of measurements (see Litovitz and Davis 1965). On the other hand, light scattering techniques deserve a detailed discussion because, as we shall see, they can in principle provide information on dynamical events occurring both at a quasi-macroscopic level and in the typical collisional domain. Summing up, for our main purposes the upper limit in time and space may be fixed in the range where the continuum description starts to break down and the molecular characteristics start to emerge. Broadly speaking, this occurs when the hypersonic frequency becomes comparable to the damping, that is for wavelengths $\lambda \sim 10^2$ Å and frequencies $\nu \sim 10^{10}$ Hz.

To cover the wavelength and frequency ranges useful to probe the dynamic properties of liquids, either particles or radiation can in principle be used. Since we are interested in the bulk properties of the system, the penetration of the probe should be long enough to minimize surface problems. This eliminates from the possible choices the use of charged particles (e.g. electrons). Moreover, the experimental probe should be characterized by the minimum possible interference with the system so that the equilibrium properties of the liquid can be studied without being substantially changed by the interaction with the probe. Therefore, among particles, the choice reduces to low-energy neutrons. For the same reasons, the energy of the electromagnetic radiation that can be used should be limited to a range such that no electronic transition is excited.

Finally, it is worthwhile to make a few remarks about the *intensity* of the probe. Depending on the strength of the interaction between the probe and the system, there exists a limit in the intensity of the flux of the incident particles (neutrons or photons) below which only the linear term in the amplitude of the perturbation is important. This is the regime in which the
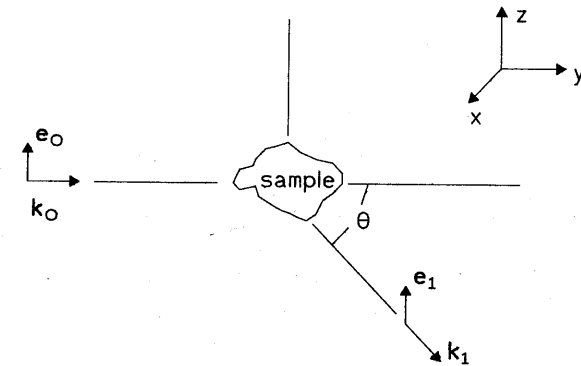
Fig. 2.1 A typical scattering configuration. The z-axis is the vertical direction of the laboratory reference frame. The incident particles, either neutrons or photons, are characterized by their energy E_0, momentum $\hbar k_0$, and polarization vector e_0. The same quantities for the scattered particles are denoted by E_1, $\hbar k_1$, and e_1. The scattering angle is denoted by θ.

linear response theory applies (Kubo 1957). Within this limit, the scattering cross section does not depend on the intensity of the incident flux and the intrinsic properties of the system are probed as if it were unperturbed. Nowadays, no neutron sources exist such that corrections to the linear response theory have to be taken into account. However, when using the intense light beam generated by a laser, some care should be used in order to make sure that the experiment is performed within the limits of applicability of the linear response theory. This point is particularly important when using pulsed lasers as photon sources.

2.3 A TYPICAL SCATTERING EXPERIMENT

When probing the properties of a sample by means of a scattering experiment, the typical experimental setup is the one depicted in Fig. 2.1. The incident particles (either neutrons or photons) are characterized by their initial energy E_0, momentum $\hbar k_0$ and polarization e_0. The sample is placed in a small volume around the origin of the laboratory reference system; the scattered particles with selected final energy E_1, momentum $\hbar k_1$, and polarization e_1 are finally collected relatively far from the sample by a suitable detector.

Within the limits of the linear response theory, the scattering cross section yields information on the dynamics of the unperturbed sample as a function of the momentum transfer $\hbar k$ and the energy transfer $\hbar \omega$. The quantities k and ω are defined by the conservation relations:

$$\mathbf{k} = \mathbf{k}_0 - \mathbf{k}_1, \tag{2.1}$$

$$\hbar\omega = E_0 - E_1. \tag{2.2}$$

Squaring eqn (2.1) we obtain

$$k^2 = k_0^2 + k_1^2 - 2k_0 k_1 \cos\theta \tag{2.3}$$

where θ is the scattering angle (cf. Fig. 2.1). The kinematically allowed region in the plane (k, ω) is not the same for neutrons and photons. For *neutrons*, the relation which connects energy and momentum is

$$E_j = \hbar^2 k_j^2 / 2m_n \tag{2.4}$$

where $j = 0, 1$ and m_n is mass of the neutron. Hence eqn (2.3) becomes

$$(k/k_0)^2 = 1 + [1 - (\hbar\omega/E_0)] - 2\cos\theta [1 - (\hbar\omega/E_0)]^{1/2}. \tag{2.5}$$

As a result, for a fixed incident neutron energy not all the plane (k, ω) is accessible. In particular, due to the square root, $\hbar\omega$ can never exceed E_0, which consequently is the maximum energy which the neutron can transfer to the system. This imposes an experimental limit to the extension of the scattering spectrum for positive energy transfers (the 'Stokes' side). Figure 2.2(a) illustrates the allowed kinematic region in reduced units for a neutron scattering experiment at several scattering angles.

If scattering of *photons* is instead considered, we deal with the energy–momentum relation

$$E_j = \hbar c k_j \tag{2.6}$$

where c is the speed of light. Equation (2.3) consequently reads

$$(k/k_0)^2 = 1 + [1 - (\hbar\omega/E_0)]^2 - 2\cos\theta [1 - (\hbar\omega/E_0)] \tag{2.7}$$

and no mathematical limitation appears on the magnitude of $\hbar\omega$, even though the physical limitation still holds. The allowed kinematic region for a photon scattering experiment is depicted in Fig. 2.2(b) for the same scattering angles as in (a).

A comparison between neutron scattering and photon scattering, however, should be performed with care. In fact, even if the two plots of Fig. 2.2 show a very similar behaviour for the kinematically allowed region in units of k_0 and E_0, the picture is drastically changed on an absolute scale. For example, neutrons thermalized at 300 K have an average energy $E_0 = 25.8\,\text{meV}$ and a characteristic wavevector $k_0 = 3.5\,\text{Å}^{-1}$, while photons in the green region of the optical spectrum (wavelength $\lambda_0 \approx 5000\,\text{Å}$) have $E_0 = 2.48\,\text{eV}$ and $k_0 = 1.26 \times 10^{-3}\,\text{Å}^{-1}$. As a result, totally different regions in the (k, ω) plane are actually sampled. This situation is illustrated for the two probes in Fig. 2.3, where absolute values are reported for the energy and wavevector scales. In the figure, the scattering
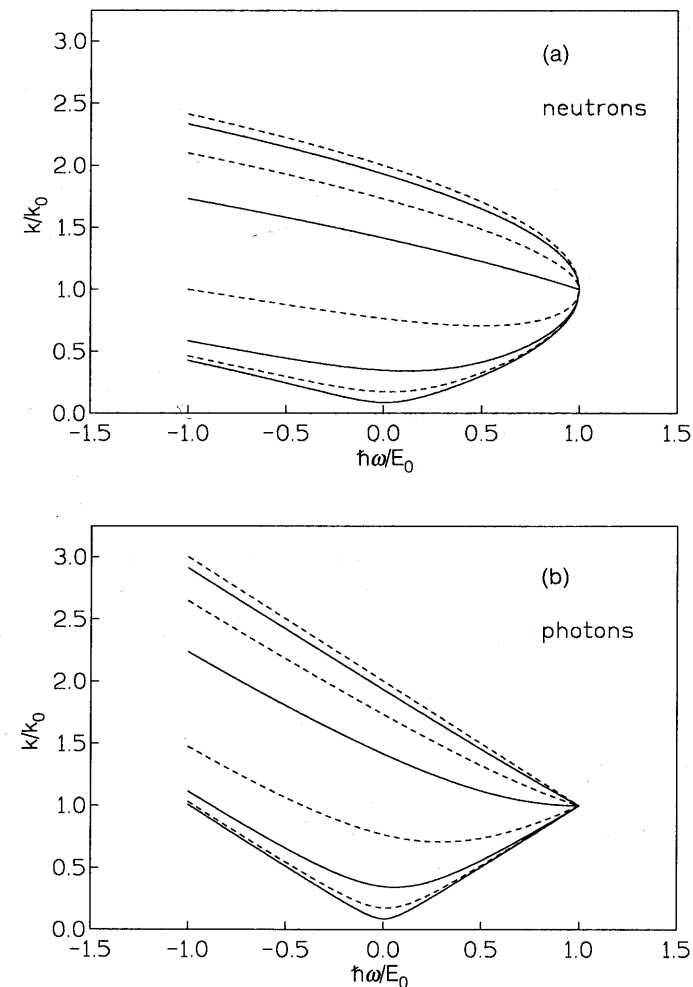
Fig. 2.2 (a) The allowed kinematic region, in reduced units, for an experiment of neutron scattering according to eqn (2.5); (b) the same region for an experiment of light scattering (eqn (2.7)). The scattering angles are (from bottom to top) $\theta = 5°$, $10°$, $20°$, $45°$, $90°$, $120°$, $150°$, and $180°$.

angles are the same as in Fig. 2.2, and again the portions (a) and (b) refer to scattering experiments performed with neutrons and with light, respectively. Whereas energies are expressed in the units usually employed in these two techniques, namely meV for neutrons and cm^{-1} for photons, the reported range of $\hbar\omega$ is the same in both cases. It appears that, while for neutron scattering one has to convert, with a considerable effort, constant

scattering-angle data to constant momentum ones, this procedure is not necessary for photons, where the exchanged momentum is constant for a fixed scattering angle. This is a direct consequence of the much smaller range of k probed by the light scattering experiment which, as already mentioned, is three orders of magnitude smaller than for neutron scattering.

From Fig. 2.3(b) it is also apparent that, in practice, for light scattering the physical limitation on frequency never becomes effective, the frequency shift ω always being much smaller than the frequency $E_0/\hbar$ of the incoming photons. In other words, for light scattering, $\hbar\omega \ll E_0$. As a consequence, eqn (2.7) reduces to

$$k^2 = 2k_0^2(1 - \cos\theta) = 4k_0^2 \sin^2(\theta/2) \qquad (2.8)$$

which is valid, for all practical purposes, for a photon scattering experiment which involves frequencies higher than those of the near infrared region.

Before closing this subsection, it is important to spend a few words on the so-called *detailed-balance principle*. This is effective on any energy-dependent cross section $\sigma(\omega)$ and states that

$$\sigma(-\omega) = \sigma(\omega)\exp(-\hbar\omega/k_B T) \qquad (2.9)$$

Equation (2.9) can be rigorously derived from a quantum-mechanical calculation of the cross section and originates from the difference in the initial population of the energy levels of the sample. For any energy-dependent process, $\sigma(\omega)$ is in fact proportional to the product between the population of the initial state of the system (given by the Boltzmann factor) and the actual transition probability of the process. The latter quantity is proportional to the square matrix element $|\langle 0|\mathcal{H}'|1\rangle|^2$ of the effective scattering Hamiltonian $\mathcal{H}'$ between the initial ($|0\rangle$) and the final ($|1\rangle$) states of the combined system (sample + probe). Due to its symmetry, the transition probability is unchanged if the sample gains or loses energy. However, depending on the actual initial state of the sample, the ratio between the weight of the two processes is given by the factor

$$\exp\frac{(\varepsilon_0 - \varepsilon_1)}{k_B T} = \exp\frac{-(E_0 - E_1)}{k_B T} = \exp\frac{-\hbar\omega}{k_B T} \qquad (2.10)$$

where ε_0 and ε_1 denote the initial and final energies of the sample, and we have made use both of the energy conservation relation $\varepsilon_0 + E_0 = \varepsilon_1 + E_1$ and of eqn (2.2).

The presence in eqn (2.9) of the *detailed balance factor* (or 'Stokes factor') $\exp(-\hbar\omega/k_B T)$ has important consequences from the experimental point of view. First, the relation (2.9) must always be verified, and its fulfilment gives a first check on the reliability of any measured energy-dependent cross section. Second, it is apparent that, especially at low temperatures, the cross section for negative energy shifts (the 'anti-Stokes'

Fig. 2.3 The allowed kinematic region, in absolute units, for an experiment of (a) neutron scattering and (b) light scattering. In both cases, the scattering angles θ are (from bottom to top) 5°, 10°, 20°, 45°, 90°, 120°, 150°, and 180°. The incident neutrons have an energy corresponding to $T = 300\,\mathrm{K}$ ($\lambda = 1.78$ Å), while the photons have a wavelength of 5000 Å (green light). In (a) and (b) the actual values of $\hbar\omega$ are the same, even if the units are different.

Table 2.1 Detailed balance 'Stokes factor' for different energy shifts (in various units) as a function of temperature.

ω			T(K)					
(cm^{-1})	(meV)	(GHz)	10	20	50	100	300	1000
0.1	0.01	3.0	0.986	0.993	0.997	0.999	0.999	1.000
0.2	0.02	6.0	0.972	0.986	0.994	0.997	0.999	1.000
0.5	0.06	15.0	0.931	0.965	0.986	0.993	0.998	0.999
1	0.12	30.0	0.866	0.931	0.972	0.986	0.995	0.999
2	0.25	60.0	0.750	0.866	0.944	0.972	0.990	0.997
5	0.62	150.0	0.487	0.698	0.866	0.931	0.976	0.993
10	1.24	299.8	0.237	0.487	0.750	0.866	0.953	0.986
20	2.48	599.6	0.056	0.237	0.562	0.750	0.908	0.972
50	6.20	1499.0	0.001	0.027	0.237	0.487	0.788	0.931
100	12.40	2997.9	0.000	0.001	0.056	0.237	0.619	0.866
200	24.80	5995.9	0.000	0.000	0.003	0.056	0.383	0.750
500	62.00	14989.6	0.000	0.000	0.000	0.001	0.091	0.487

spectrum) decreases much faster than for the positive side (the 'Stokes' spectrum). Moreover, the ratio between the intensities of the two spectra is independent both of the sample and the experimental probe.

A closer look at the Stokes factor (see Table 2.1) in several cases of interest is quite instructive. For example, in liquid argon ($T \approx 100$ K) the anti-Stokes spectrum at $\hbar\omega \approx 6$ meV is seen to be reduced by a factor of two with respect to the Stokes counterpart. In liquid neon ($T \approx 20$ K) the same situation occurs already for shifts $\hbar\omega \approx 1.5$–2 meV. Therefore in simple rare-gas liquids it is immediately seen that one cannot rely too much on the anti-Stokes side of the spectrum, despite the absence of boundaries in Figs 2.2 and 2.3. In these liquids, the dynamic range of thermal neutrons is consequently limited even for negative energy shifts because of the strong decrease of the cross section. On the other hand, photons do not suffer any limitation on the Stokes side, and their use would in principle be of great help. This situation is to be contrasted with the one occurring in liquid metals, where the probed temperature range is so high (room temperature and above) that the Stokes factor becomes ineffective and neutrons can be used to their maximum efficiency. Moreover, in these metallic systems one may also take advantage of the good transparency to neutrons, a property which is unfortunately not shared by photons.

2.3.1 Probing liquids with thermal neutron scattering

The interaction between neutrons and ordinary matter is, in general, very weak. A neutron of thermal energy may penetrate very deeply before being

scattered or absorbed in its path. For example, neutrons may travel as long as 24 cm in liquid argon before their number is reduced to one half the initial value by absorption or scattering processes. Except for a few known cases, the variation of the neutron cross section with the nuclear species is not dramatic, and the previous figure can be considered as providing a typical order of magnitude.

The de Broglie wavelength of neutron of energy E is given by

$$\lambda = h/(2m_n E)^{1/2} \tag{2.11}$$

which means that a thermal neutron, with an energy corresponding to 300 K, is associated with a wavelength of 1.8 Å. This is the typical order of magnitude of the intermolecular spacings occurring in condensed systems. Moreover, from Planck's law

$$\nu = E/h, \tag{2.12}$$

the frequency associated with the same neutron is found to be $\nu = 6.25$ THz. The corresponding period of 0.16 ps compares well with the collision times given above. However, from Fig. 2.3 it is apparent that any extension of the accessible frequency range is limited, on the Stokes side, by the low energy of the incident neutrons and on the anti-Stokes side by the detailed balance condition, which is particularly restrictive at low temperatures.

2.3.2 Neutron-scattering cross section

For a neutron scattering experiment, the nuclear cross section can be easily evaluated in terms of the Born approximation (van Hove 1954). If $|s_0\rangle$ and $|s_1\rangle$ are the initial and final states of the system, then for the differential scattering cross section per unit solid angle and per unit energy change of the scattered neutron we obtain

$$\frac{\mathrm{d}^2\sigma}{\mathrm{d}\Omega\,\mathrm{d}E_1} = A\,N\mathcal{S}(\mathbf{k}, \omega) \tag{2.13}$$

where

$$A = \frac{(2\pi)^3 m_n^2}{\hbar^5}\frac{k_1}{k_0}\,W(\mathbf{k}), \tag{2.14}$$

$$\mathcal{S}(\mathbf{k}, \omega) = N^{-1}\sum_{s_0}p(s_0)\sum_{s_1}\left|\left\langle s_0\left|\sum_j\exp(\mathrm{i}\mathbf{k}\cdot\mathbf{r}_j)\right|s_1\right\rangle\right|^2\delta\left(\omega + \frac{E_0 - E_1}{\hbar}\right), \tag{2.15}$$

and

$$W(\mathbf{k}) = \left[\int\mathrm{d}\mathbf{r}\,V(\mathbf{r})\exp(\mathrm{i}\mathbf{k}\cdot\mathbf{r})\right]^2. \tag{2.16}$$

In eqns (2.15)-(2.16) the operators r_j represent the position vectors of the N particles in the scattering volume, $p(s_0)$ is the probability of finding the system in the initial state $|s_0\rangle$ and $V(\mathbf{r})$ is the interaction potential between the neutron and the nucleus. If the true interaction, which is not known, is replaced by the corresponding 'Fermi pseudopotential' (e.g. Lovesey 1987)

$$V(\mathbf{r}) = (h^2/2\pi m_n)b\delta(\mathbf{r}) \tag{2.17}$$

where b is the so-called *scattering length* of the nucleus, then eqn (2.14) becomes

$$A = \frac{b^2}{\hbar}\frac{k_1}{k_0} \tag{2.18}$$

and therefore

$$\frac{d^2\sigma}{d\Omega\,dE_1} = \frac{b^2}{\hbar}\frac{k_1}{k_0}N\mathcal{S}(\mathbf{k},\omega). \tag{2.19}$$

As shown by van Hove, the 'dynamic structure factor' $\mathcal{S}(\mathbf{k},\omega)$ (also referred to as the 'scattering law') can be written as

$$\mathcal{S}(\mathbf{k},\omega) = (1/2\pi)\int_{-\infty}^{\infty} dt \int d\mathbf{r}\exp\{i(\mathbf{k}\cdot\mathbf{r}-\omega t)\}\mathcal{G}(\mathbf{r},t), \tag{2.20}$$

namely as the double Fourier transform of the space-time pair correlation function

$$\mathcal{G}(\mathbf{r},t) = (2\pi)^{-3}(1/N)\sum_{i,j}\int d\mathbf{k}\exp(i\mathbf{k}\cdot\mathbf{r})\langle\exp[-i\mathbf{k}\cdot\mathbf{r}_i(0)]\exp[i\mathbf{k}\cdot\mathbf{r}_j(t)]\rangle \tag{2.21}$$

which contains the Heisenberg position-operator of the ith atom at time $t=0$, $\mathbf{r}_i(0)$, and that of the jth atom at time t, $\mathbf{r}_j(t)$. The angled brackets in eqn (2.21) stand for a quantum-statistical average. Finally, it is useful to introduce the 'intermediate scattering function' $\mathcal{F}(\mathbf{k},t)$ as the space Fourier transform of the correlation function $\mathcal{G}(\mathbf{r},t)$:

$$\mathcal{F}(\mathbf{k},t) = (1/N)\sum_{i,j}\langle\exp[-i\mathbf{k}\cdot\mathbf{r}_i(0)]\exp[i\mathbf{k}\cdot\mathbf{r}_j(t)]\rangle. \tag{2.22}$$

To make contact between the definitions (2.15), (2.20), and (2.22) and the quantities $S(k,\omega)$, $G(r,t)$, and $F(k,t)$ introduced in Section 1.6.2, it is sufficient to note that for a classical system the quantum-statistical averages are replaced by their classical counterparts, and that in a isotropic system such as a fluid all these quantities depend only on the magnitude of the vectors $\mathbf{k}$ and $\mathbf{r}$. Consequently, apart from constant terms which ultimately

give rise to trivial contributions $\propto\delta(\omega)$ in the spectra, in a classical fluid one may establish the direct correspondence $\mathcal{S}(\mathbf{k},\omega) \to S(k,\omega)$, $\mathcal{G}(\mathbf{r},t) \to G(r,t)$, and $\mathcal{F}(\mathbf{k},t) \to F(k,t)$.

In the above formulation, for simplicity we have considered the sample as composed of identical spinless nuclei. This assumption has allowed us to extract the nuclear scattering amplitude b from the quantum-statistical average in eqn (2.19). However, in general, the sample is made of a mixture of different isotopes; in this case, we actually deal with a different 'intermediate scattering function', namely

$$I_n(\mathbf{k},t) = (1/N)\sum_{i,j}\langle b_i^* b_j\exp[-i\mathbf{k}\cdot\mathbf{r}_i(0)]\exp[i\mathbf{k}\cdot\mathbf{r}_j(t)]\rangle \tag{2.23}$$

where the subscript n stands for 'neutrons', b_i represents the scattering amplitude for the ith nucleus, and the angled brackets now mean a composite average both on the nuclear internal states and on the configurational degrees of freedom.

For practical purposes, it is finally convenient to write the differential cross section (2.19) in a slightly different way. Under conditions of 'quasi-elastic' scattering one has that $k_1 \approx k_0$, and eqn (2.19) can easily be integrated over E_1 to yield

$$\frac{d\sigma}{d\Omega} = Nb^2\int_{-\infty}^{\infty} d\omega\,\mathcal{S}(\mathbf{k},\omega) \tag{2.24}$$

where

$$\int_{-\infty}^{\infty} d\omega\,\mathcal{S}(\mathbf{k},\omega) = (1/2\pi)\int_{-\infty}^{\infty} dt\,\mathcal{F}(\mathbf{k},t)\int_{-\infty}^{\infty} d\omega\exp(-i\omega t) = \mathcal{F}(\mathbf{k},0). \tag{2.25}$$

In a classical fluid one has $\mathcal{F}(\mathbf{k},0) = F(k,0) = S(k)$, and the differential cross section can be expressed as

$$\frac{d^2\sigma}{d\Omega\,dE_1} \approx N\frac{b^2}{\hbar}\frac{k_1}{k_0}S(k)\cdot\left[\frac{S(k,\omega)}{S(k)}\right] \tag{2.26}$$

where the term in square brackets represents the scattering spectral shape normalized to unit area, and the static structure factor $S(k)$ gives a measure of the overall intensity of the spectrum at different wavevectors.

2.3.3 The coherent and incoherent neutron-scattering cross section

The intermediate scattering function for neutrons (2.23) involves the scattering length of the ith nucleus, which is independent both of its

position $\mathbf{r}_i$ and of time. As a result, the average in eqn (2.23) can be split into a 'nuclear' part, which involves variables as the isotopic composition and the nuclear spin orientation, and into a proper statistical average involving the phase-space variables. On the other hand, the presence of the double summation in (2.23) affects both these averages, and leads to a natural separation between 'self' and 'distinct' contributions to the total correlation function.

In the case of a one-component system, with only one isotopic species, the involved nuclear averages can be written as $\langle b_i^* b_j \rangle$, where the indexes i and j may label either the same or two different atoms. Then, according to whether $i = j$ or $i \neq j$ we have

$$\langle b_i^* b_i \rangle = \langle |b_i|^2 \rangle = \langle |b|^2 \rangle, \qquad (2.27)$$

$$\langle b_i^* b_j \rangle = \langle b_i^* \rangle \langle b_j \rangle = \langle b \rangle^* \langle b \rangle = |\langle b \rangle|^2. \qquad (2.28)$$

The latter result is valid only if there is a negligible quantum correlation between the different nuclei, as is the case for monatomic systems in ordinary conditions. On the other hand, if the de Broglie wavelength becomes comparable with the atomic size (as in superfluid helium), quantum exchange effects are non-negligible and the above assumption should be critically revised.

Equations (2.27) and (2.28) can be merged together to give

$$\langle b_i^* b_j \rangle = |\langle b \rangle|^2 + \delta_{i,j} [\langle |b|^2 \rangle - |\langle b \rangle|^2]$$

$$\equiv (1/4\pi) [\sigma_c + \delta_{ij} \sigma_i] \qquad (2.29)$$

where the quantities σ_c and σ_i are respectively referred to as the 'coherent' and 'incoherent' scattering cross sections for the nucleus under consideration (Lovesey 1987). Inserting (2.29) into the expression (2.21) of $I_n(\mathbf{k}, t)$, we find

$$I_n(\mathbf{k}, t) = I_{n,c}(\mathbf{k}, t) + I_{n,i}(\mathbf{k}, t). \qquad (2.30)$$

Here

$$I_{n,c}(\mathbf{k}, t) = \frac{\sigma_c}{4\pi} \mathcal{F}(\mathbf{k}, t), \qquad (2.31)$$

$$I_{n,i}(\mathbf{k}, t) = \frac{\sigma_i}{4\pi} \frac{1}{N} \left\langle \sum_i \exp[-i\mathbf{k} \cdot \mathbf{r}_i(0)] \exp[i\mathbf{k} \cdot \mathbf{r}_i(t)] \right\rangle$$

$$= \frac{\sigma_i}{4\pi} \left\langle \exp[-i\mathbf{k} \cdot \mathbf{r}_1(0)] \exp[i\mathbf{k} \cdot \mathbf{r}_1(t)] \right\rangle \qquad (2.32)$$

where the index 1 labels any one of the atoms of the system. Thus in a classical fluid we simply have that

$$I_{n,i}(\mathbf{k}, t) = \frac{\sigma_i}{4\pi} F_s(k, t) \qquad (2.33)$$

where $F_s(k, t)$ is the self intermediate scattering function introduced in Section 1.4.1.

Owing to the variation of the scattering length with both the isotope and the nuclear spin, the splitting (2.30) occurs even in a monatomic system with a single isotope, provided that this has a non-zero spin (Lovesey 1984). The first contribution $I_{n,c}(\mathbf{k}, t)$ (referred to as the *coherent* component) stems from the correlation between atom i, at time t, and atom j, at time 0. In contrast, the *incoherent* component $I_{n,i}(\mathbf{k}, t)$ only involves single particle dynamic correlations. In a classical fluid, these two components are respectively proportional to $F(k, t)$ and $F_s(k, t)$, with amplitude factors determined by the appropriate coherent and incoherent scattering cross sections, σ_c and σ_i. Typically, a single neutron scattering experiment on a monatomic system produces a well defined combination of the two contributions, which are weighted by the scattering cross sections pertinent to the natural isotopic composition of the system. However, if a second experiment is performed, only changing the isotopic composition of the sample, it is in principle possible to extract both contributions, thus allowing a separate determination of both $F(k, t)$ and $F_s(k, t)$ (see Section 2.2.4). For a proper experimental design, standard textbooks (e.g. Lovesey 1987) report the values of the quantities σ_c and σ_i (as well as those of the neutron absorption cross section) for the different isotopes.

2.3.4 Deep inelastic neutron scattering

With the recent availability of pulsed neutron sources, very energetic neutrons can be used for spectroscopic purposes. In this case, the amount of the transferred energy and momentum is so high that the effect of the neighbours of the target nucleus can be neglected. The sample may then be considered as being composed of a collection of isolated atoms and only the free particle motion modulates the scattering cross section. The effect is the neutron equivalent of the Compton scattering of very energetic X-rays on electrons. Since there is no correlation between the different nuclei, eqn (2.23) simplifies to:

$$I_n(\mathbf{k}, t) = (1/N) \left\langle \sum_i |b_i|^2 \exp[-i\mathbf{k} \cdot \mathbf{r}_i(0)] \exp[i\mathbf{k} \cdot \mathbf{r}_i(t)] \right\rangle \qquad (2.34)$$

and, for a monoisotopic sample, this further reduces to

$$I_n(\mathbf{k}, t) = b^2 \langle \exp(-it\mathbf{k} \cdot \mathbf{p}_i/m) \rangle \qquad (2.35)$$

where due to the high energy of the incoming nucleus, the system is

approximated by an ideal gas, in which $\mathbf{p}_i$ is the initial momentum of the ith nucleus, and b its scattering length. The energy dependence of the scattering law can be written as

$$S(\mathbf{k}, E) = \int d\mathbf{p}\, n(\mathbf{p}) \delta(E - E_r - \hbar \mathbf{k} \cdot \mathbf{p}/m) \qquad (2.36)$$

where $n(\mathbf{p})$ is the momentum distribution of the scattering centres and $E_r = \hbar^2 k^2/2m$ is the recoil energy. If, as in a classical liquid, we deal with a Gaussian momentum density of the form

$$n(\mathbf{p}) = C \exp(-p^2/\sigma_p^2) \qquad (2.37)$$

then $S(\mathbf{k}, E)$ reads

$$S(\mathbf{k}, E) = C \exp[-m(E - E_r)^2/2E_r\sigma_p^2]. \qquad (2.38)$$

As a result, the scattering cross section has a simple Gaussian shape whose width, as a function of the energy, is directly related to the width of the momentum distribution of the atoms of the sample, namely to the average kinetic energy.

Clearly, the application of this experimental technique to simple monatomic classical liquids (where the momentum distribution is well known and the average kinetic energy is simply $\frac{3}{2}k_B T$) is trivial. In contrast, when applied to quantum liquids, the technique provides direct information on typical quantum features, such as the amplitude of the zero-point motion, or the condensation fraction in a Bose liquid. At these low temperatures where the average kinetic energy turns out to be virtually independent of T, the technique has been exploited to investigate its density dependence (Herwig *et al.* 1990; Sosnick *et al.* 1990).

2.3.5 Probing liquids with radiation

Electromagnetic radiation can be used to probe the bulk properties of non-conducting liquids, provided that the energy lost by the photons is not sufficient to excite the first electronic state. For the atoms of rare gases, the energies E_1 of the first electronic level are reported in Table 2.2 along with the corresponding wavelengths λ_1. It appears that, in order to avoid absorption of the electromagnetic radiation, wavelengths longer than the so called vacuum ultraviolet (VUV) are necessary. In this respect, optical wavelengths, lying in the range 4000–7000 Å, can be safely used, along with the corresponding available laser radiation.

An obvious drawback is that, in any case, these wavelengths are too large with respect to the scale characteristic of the intermolecular distances. This difficulty can be circumvented by using photons of higher energy, with a correspondingly shorter wavelength. The typical range of intermolecular

Table 2.2 Energies E_1 of the first electronic level in the atoms of rare gases. The corresponding wavelengths $\lambda_1 = hc/E_1$ are also reported.

	E_1 (eV)	λ_1 (Å)
Helium	19.8	620
Neon	16.1	770
Argon	11.8	1050
Krypton	9.9	1250
Xenon	8.7	1430

distances is then reached in the X-ray domain, and indeed *X-ray diffraction* is a standard tool to probe the structure of condensed matter at the microscopic level. On the other hand, for X-rays the previous requirement of a negligible excitation of electronic states is obviously not met. As a matter of fact, the energy of photons is so high that the binding energy of the electrons can be considered negligible. Therefore, even if X-rays, being scattered from the local distribution of electrons around the nuclei, carry information upon the instantaneous local atomic distribution, their use to probe dynamic properties of condensed matter may appear doubtful for the simple fact that they would destroy the electronic equilibrium of the sample. However, in a scattering experiment the important parameters, rather than being the absolute values of the energy and momentum of the probe, are the fraction of these quantities which is exchanged with the molecular system under study. Therefore, for a given choice of the energy–momentum relation of the probe, it is possible to find a scattering angle small enough that the energy and momentum transfer is below any preselected limit. If this condition is fulfilled, even X-ray scattering can be used to probe the dynamic behaviour of a liquid. In fact, the recent development of synchrotron machines for the production of high-energy radiation has provided very intense X-ray sources that can be used for this purpose. Even if many technical problems are still to be solved, preliminary results show the feasibility of X-ray inelastic scattering experiments to probe the dynamics of the liquid state (Burkel 1991). For the time being, however, short-wavelength photons are essentially used only for structural studies; in practice, any information on dynamic properties is obtained using photons of much longer wavelength (i.e. in the optical region).

It is common opinion that ordinary light scattering, whose range of λ is ~5000 Å, could be used only to probe very long wavelength correlations, such as those associated with hydrodynamic modes. However, this is not completely true. In fact, in the following we shall see that in

well-specified experimental conditions ordinary light scattering can actually probe intermolecular correlations occurring on length ranges much shorter than λ, namely those associated with collisional events.

2.3.6 Photon-scattering cross section

The cross section for a photon-scattering experiment by a many-body system is obtained by a generalization of the well-known Kramers–Heisenberg result for a one-electron atom, which reads (Louisell 1973):

$$\frac{d\sigma}{d\Omega} = \left(\frac{e^2}{m_e c^2}\right)^2 \left[\left(\frac{\omega_1}{\omega_0}\right) |M_{ab}|^2\right] (n_1 + 1). \tag{2.39}$$

Here m_e and $-e$ are the mass and the charge of the electron, ω_0 and ω_1 are the respective frequencies of the incident and the scattered photon, n_1 is the photon population of the final state (accounting for stimulated scattering effects), and M_{ab} is a matrix element for the electronic transition from an initial eigenstate $|a\rangle$ to a final one $|b\rangle$. Denoting respectively by e_0 and e_1 the polarization unit vectors of the incoming and scattered photon, and by $|I\rangle$ a general intermediate electron eigenstate, it turns out that M_{ab} can be expressed in terms of the matrix elements of the electron momentum operator p_{bI} and p_{Ia} as follows:

$$M_{ab} = (e_0 \cdot e_1)\delta_{a,b} - \frac{1}{m_e} \sum_I \left[\frac{(e_0 \cdot p_{bI})(e_1 \cdot p_{Ia})}{E_I - E_a + \hbar\omega_1} + \frac{(e_1 \cdot p_{bI})(e_0 \cdot p_{Ia})}{E_I - E_a - \hbar\omega_0}\right]. \tag{2.40}$$

The square-bracketed factor in eqn (2.39) has to be evaluated taking into account the energy conservation of the total system (atom + electromagnetic field), that is

$$\omega_1 = \omega_0 - (E_b - E_a)/\hbar. \tag{2.41}$$

Equation (2.39) explicitly involves only the electronic term of the Coulomb interaction with the electromagnetic field; the nuclear contribution is smaller by more than three orders of magnitude, and can safely be neglected. Denoting by d the 'size' of the atom, the disappearance of the electron coordinates in (2.39) is a direct consequence of the 'electric dipole approximation' $\lambda \gg d$, which is well satisfied for optical wavelengths. On the other hand, the nuclear position would appear in a phase factor which is contained in $|M|^2$ and results from averaging the electron coordinates in the electromagnetic field. In a single-atom problem, this phase factor is actually irrelevant, and in eqn (2.39) has been ignored by assuming that the nucleus is in the origin of the reference frame.

If the atom has more than one electron, only the matrix element expression (2.40) changes, and a definition of 'atomic polarizability' is

introduced. However, the structure of eqn (2.39) remains unchanged and, in the expression for $|M|^2$ only the centre of the electronic distribution (for a monatomic system, the nuclear position) appears in the phase term.

When a system of interacting atoms (or molecules) is considered, the problem can be made manageable by exploiting the 'Born–Oppenheimer approximation', which assumes that the electronic eigenstates depend only parametrically upon the nuclear positions. As a result, the nuclear and the electronic eigenstates can be factorized. A derivation of the cross section for light scattering from a system of interacting atoms is given in Appendix C, where explicit results are derived for a monatomic system.

The approach can be easily generalized to a molecular system, provided that the basic approximations remain valid. In particular, for a system of simple molecules (i.e. molecules composed of a few atoms), the light scattering cross section can be written in a form analogous to (2.39) (cf. eqn (C.43) in Appendix C). However, now the phase factor appears explicitly in the expression of the matrix element:

$$|M_{ab}|^2 = \omega_0^4 (m_e^2/e^4) \left\langle \sum_{i,j} [e_0 \cdot A_i \cdot e_1][e_0 \cdot A_j \cdot e_1] \exp\{-ik \cdot (r_i - r_j)\}\right\rangle. \tag{2.42}$$

Here A_i is a second-order tensor which represents the *polarizability* of the ith molecule, while r_i is the position of the 'centre of polarizability' which can be roughly assumed as coincident with the molecular centre of mass. In eqn (2.42) the vector k is the momentum transfer defined by (2.1), and again the angular brackets indicate a statistical average over the initial configurations of the molecules.

In deriving eqn (2.42) the scattering has been approximately considered as being quasi-elastic. This approximation holds quite well for light (and for photons in general), provided that the scattering process probes the genuine collective properties of the system. In fact, the dynamics of a dense medium is ruled either by short-range collisions, which typically last some fraction of a picosecond, or by collective modes of hydrodynamic or phonon origin. When translated into a wavenumber domain, this gives a range which extends up to a few hundreds cm^{-1} from the exciting wavelength. As an optical photon in the green region of the spectrum ($\lambda \approx 5000$ Å) has a frequency of $20\,000\,cm^{-1}$, the scattering can indeed be considered as quasi-elastic. However, this approximation would eventually fail if large frequency shifts were detected, as for example in molecular Raman scattering of very light systems.

In analogy with the neutron scattering case, we may define an intermediate scattering function for light scattering as

$$I_L(\mathbf{k}, t) = \frac{1}{N} \sum_{i,j} \langle (\mathbf{e}_0 \cdot \mathbf{A}_i(0) \cdot \mathbf{e}_1)^* (\mathbf{e}_0 \cdot \mathbf{A}_j(t) \cdot \mathbf{e}_1)$$

$$\exp\{-i\mathbf{k} \cdot [\mathbf{r}_i(0) - \mathbf{r}_j(t)]\} \rangle, \tag{2.43}$$

whose time Fourier transform is proportional to the spectral distribution of the scattered intensity. The comparison of eqn (2.43) with the corresponding quantity (2.23) for neutrons shows the similar structure of the two results. However, there are several important differences:

(i) In contrast with the scattering amplitudes for neutrons, the corresponding quantities for light scattering are position-dependent. As a matter of fact, whereas in neutron scattering we deal with the Fermi pseudopotential (2.17), in light scattering the same role is effectively played by the molecular polarizability tensor **A**, which in general depends on the coordinates of all molecules of the system (cf. Appendix C).

(ii) The magnitude k of the momentum transfer is very different in the two cases, being of the order of a few Å^{-1} for neutrons and about three orders of magnitude smaller for light scattering.

(iii) The two functions are not even dimensionally consistent. In fact, while the neutron function $I_n(\mathbf{k}, t)$ has the dimensions of the square of a length, the corresponding function for light scattering $I_L(\mathbf{k}, t)$ has the dimensions of the square of a polarizability (cm^6, cgs units).

2.3.7 An analysis of light scattering

In the case of light scattering, eqn (2.43) involves the polarizability tensor $\mathbf{A}_i \equiv \mathbf{A}(i)$ of the ith molecule. This is a second-order tensor with nine linearly independent components which, in general, can be decomposed into three parts associated with different symmetry properties:

$$\mathbf{A}(i) = \mathbf{A}^{(0)}(i) + \mathbf{A}^{(1)}(i) + \mathbf{A}^{(2)}(i). \tag{2.44}$$

More precisely, the tensor **A** is split into a scalar part $\mathbf{A}^{(0)}$ (one component), an antisymmetric term $\mathbf{A}^{(1)}$ (three components), and a symmetric, traceless, term $\mathbf{A}^{(2)}$ (five components). In practice, the antisymmetric term turns out to be important only in rather specific systems (for example, in the case of solutions of sugar molecules in water). Dealing with simple molecular systems, we may consequently restrict our attention only on the first and the third contributions on the right-hand side of eqn (2.44).

As already discussed, rather than being a single-molecule observable, the polarizability tensor $\mathbf{A}(i)$ depends also on the positions of neighbouring molecules. In particular, we may express this dependence in terms of 'cluster' contributions as

$$\mathbf{A}(i) = \mathbf{\alpha}_1 + \sum_{j(\neq i)} \mathbf{\alpha}_2(\mathbf{r}_i, \mathbf{r}_j) + \sum_{j(\neq i), l(\neq i, j)} \mathbf{\alpha}_3(\mathbf{r}_i; \mathbf{r}_j, \mathbf{r}_l) + \cdots. \tag{2.45}$$

Here, $\mathbf{\alpha}_1$ is the polarizability of the isolated molecule, which is independent of its position. The *irreducible pair polarizability* $\mathbf{\alpha}_2(\mathbf{r}_i, \mathbf{r}_j)$ is the extra polarizability of the ith molecule induced by the presence of a neighbouring molecule j, and depends on both the positions $\mathbf{r}_i$ and $\mathbf{r}_j$. Finally, the *irreducible triplet polarizability* $\mathbf{\alpha}_3(\mathbf{r}_i; \mathbf{r}_j, \mathbf{r}_l)$ is the extra polarizability arising from the presence of a pair of molecules in the vicinity of the ith molecule; the summation is extended to all possible pairs (j, l), with $j \neq i$ and $l \neq i$, and with $j \neq l$.

Equations (2.44) and (2.45) can be combined to give, for the scalar part:

$$\mathbf{A}^{(0)}(i) = \alpha_0 \mathbf{I} + \sum_{j(\neq i)} \mathbf{\alpha}_2^{(0)}(\mathbf{r}_i, \mathbf{r}_j) + \sum_{j(\neq i), l(\neq i, j)} \mathbf{\alpha}_3^{(0)}(\mathbf{r}_i; \mathbf{r}_j, \mathbf{r}_l) + \cdots. \tag{2.46}$$

Here $\alpha_0 = (1/3)\,\text{Tr}\{\mathbf{\alpha}_1\}$ is the scalar polarizability of the isolated molecule, whereas $\mathbf{\alpha}_2^{(0)}$ and $\mathbf{\alpha}_3^{(0)}$ are the scalar components of the irreducible pair and triplet polarizability, respectively. The corresponding result for the traceless symmetric tensor $\mathbf{A}^{(2)}(i)$ is

$$\mathbf{A}^{(2)}(i) = \mathbf{\alpha}_1^{(2)} + \sum_{j(\neq i)} \mathbf{\alpha}_2^{(2)}(\mathbf{r}_i, \mathbf{r}_j) + \sum_{j(\neq i), l(\neq i, j)} \mathbf{\alpha}_2^{(2)}(\mathbf{r}_i; \mathbf{r}_j, \mathbf{r}_l) + \cdots \tag{2.47}$$

where we remind the reader that the lower index labels the 'order' of the cluster, while the upper one (in brackets) labels the spherical rank of the tensor.

We shall now focus our attention on a system of monatomic molecules (e.g. the liquefied rare gases); at a price of some additional complications, most of the results which we shall find are valid even for polyatomic molecules. For a monatomic system, however, some simplifying relations make more straightforward both the theoretical treatment and the actual setup of experiments. In this case, the isolated molecule polarizability is a scalar quantity, which in the absence of electronic transitions is simply a molecular constant. As a result, $\mathbf{\alpha}_1^{(2)} \equiv 0$ and eqn (2.47) becomes

$$\mathbf{A}^{(2)}(i) = \sum_{j(\neq i)} \mathbf{\alpha}_2^{(2)}(\mathbf{r}_i, \mathbf{r}_j) + \sum_{j(\neq i), l(\neq i, j)} \mathbf{\alpha}_3^{(2)}(\mathbf{r}_i; \mathbf{r}_j, \mathbf{r}_l) + \cdots. \tag{2.48}$$

Finally, we make some remarks on the magnitudes of the induced polarizability terms which appear in eqns (2.46) and (2.48). As a matter of fact, both from the experiments and from theory it turns out that in eqn (2.46) the induced terms, with $\mathbf{\alpha}_2$, $\mathbf{\alpha}_3$, etc., give a much smaller contribution to the scattering cross section than the single-molecule term. Also, we may expect (and the experimental observations confirm) that in any case

the triplet terms contribute much less than the pair ones. As a result, the leading contribution to (2.46) is provided by the single-molecule polarizability, while in (2.47) this role is played by the pair term.

2.4 THERMAL NEUTRON SCATTERING

Neutron-scattering experiments can be classified into two broad categories, namely diffraction and inelastic experiments. In the first case, no energy selection is performed on the scattered particles and energy-integrated information is collected. In the second class of experiments, information on the microscopic dynamics can instead be obtained. Being mostly concerned with dynamic problems, in the following we shall focus our attention on the second class.

An inelastic scattering experiment on a liquid may give information on a number of energy transfer processes. Broadly speaking, these can be classified either as characteristic of the particular molecular species (intra-molecular processes such as internal vibrations in a polyatomic molecule) or affected by the interactions among the different molecules. We are mostly interested in this second class of processes which are directly related to the many-body dynamics. In turn, the latter can be probed either by focusing on single-particle aspects ($S_s(k, \omega)$) or by looking at genuine collective properties ($S(k, \omega)$). For a liquid, the region where $S_s(k, \omega)$ and $S(k, \omega)$ show the most interesting features is at relatively small ω; that is, quite close to the energy of the excitation probe ('quasi-elastic scattering'). Due to the intrinsic isotropy of the system, both $S_s(k, \omega)$ and $S(k, \omega)$ depend only on $k = |\mathbf{k}|$; also, the collective features embodied in $S(k, \omega)$ which can be probed by a scattering experiment are directly associated only with a specific part of the dynamical response ('longitudinal collective modes').

In Chapter 1 we have seen that a measure of the quantities $S_s(k, \omega)$ and $S(k, \omega)$ at increasing wavevectors provides information on a variety of dynamical situations occurring in the liquid. In particular, in the limit $k \rightarrow 0$ the liquid effectively behaves as a continuum, in which the basic dynamical features that are observed are diffusive processes (in S_s) and propagation of longitudinal sound waves (in S). In this regime, the molecular structure influences the dynamics only through a few macroscopic quantities, which are related both to thermodynamic and to transport properties (cf. Section 1.6.4). At increasing wavevectors, the dynamics of the liquid is effectively investigated on a shrinking length scale, and genuine micro-scopic effects become more and more important. Eventually, at very large values of k the system behaves as a collection of essentially free particles, and any distinction between $S_s(k, \omega)$ and $S(k, \omega)$ tends to disappear.

As seen in Section 2.3, the wavevector range that is accessible to a thermal neutron scattering experiment cannot be much smaller than a fraction of 1 Å^{-1}, which corresponds to a wavelength in the range 10–50 Å (cf. Fig. 2.3(a)). This is a range of distances where the micro-scopic aspects are already fully effective. In contrast, a light-scattering experiment probes a k range which is three orders of magnitude smaller and therefore well within a hydrodynamic description of the liquid (see Fig. 2.3(b)).

2.4.1 A typical experiment: inelastic neutron scattering in liquid argon

The previous considerations can be illustrated in some more detail by reporting the results obtained by inelastic neutron scattering in the prototype simple liquid, namely liquid argon. This offers the possibility of discussing some typical procedures used by experimentalists to analyze data.

Quasi-elastic neutron scattering experiments on liquid argon at the triple point (85.2 K) have been carried out by Sköld *et al.* (1972) in the range of $k = 1$–4.4 Å^{-1} and $\omega = 0$–10.6 meV. A separate determination of $S_s(k, \omega)$ and $S(k, \omega)$ was made possible by performing two independent experiments with samples of different isotopic composition (cf. Section 2.3.3). At all wavevectors both the scattering functions show a monotonic decrease with ω; the corresponding widths are of the order of a few meV, and show an overall increase with k (see Figs 1.5 and 1.12). Sköld *et al.* analysed their spectra by fitting the low-frequency part to a Lorentzian shape, and looking at the deviations of the experimental data from the predictions of such an idealized model. As far as the single particle spec-trum is concerned, the overall spectral shape of $S_s(k, \omega)$ appears to be dominated by simple diffusive motion (Fig. 2.4(a)). The spectrum is in fact very close to a Lorentzian (particularly at low frequencies, $\omega < 2 \text{ meV}$), the only signature of a deviation being an excess intensity in the wings ($2 < \omega < 7 \text{ meV}$). On other hand, the collective spectrum $S(k, \omega)$ shows a more marked wavevector-dependence (Fig. 2.4(b)). Again the low-frequency region may be approximated by a Lorentzian, but the behaviour in the wings is less regular, showing a much larger excess scattering for almost all values of k. An exception is the data at the position $k_m = 2 \text{ Å}^{-1}$ of the main peak of $S(k)$ where some intensity appears to be missing with respect to the Lorentzian prediction.

More recently, the dynamic structure factor $S(k, \omega)$ of liquid argon has been measured by van Well *et al.* (1985) at a higher temperature, $T = 120 \text{ K}$, covering a range of $k = 0.42$–3.90 Å^{-1} and $\omega = 0$–20 ps^{-1} (i.e. up to 13.16 meV). The new data, which are in substantial agreement with the old, give more extensive information on the features of liquid argon. In particular, the determination of the width of $S(k, \omega)$ as a function of k is
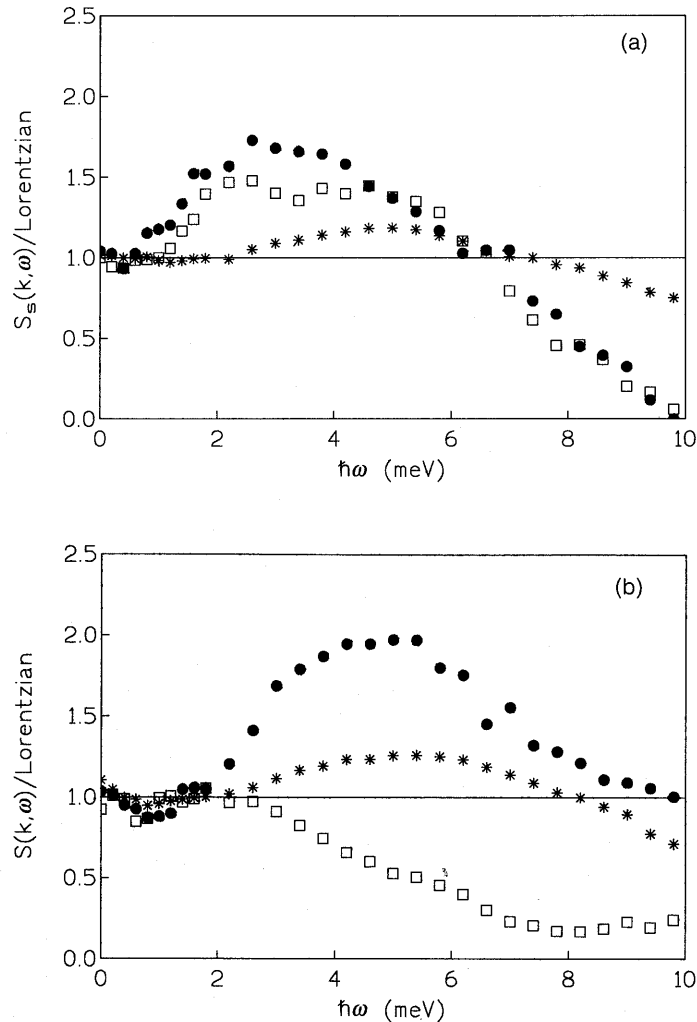
Fig. 2.5 Full width at half maximum of $S(k, \omega)$ (in ps^{-1}) in liquid argon at $T = 120\,K$ and $n = 0.0176\,\text{Å}^{-3}$. The dashed line is the hydrodynamic result $(\kappa/nc_v)k^2$ for the Rayleigh part of the spectrum (cf. Section 1.6.4). The chain and the solid lines denote the results $2Dk^2$ and $2Dk^2/S(k)$, which are appropriate within a simple and modified 'Vineyard approximation' in the diffusional limit (see text). The dots are the experimental data by van Well *et al.* (1985).

Fig. 2.4 (a) Deviation of the self spectrum $S_s(k, \omega)$ from a Lorentzian of the same width at different wavevectors: $k = 1.4\,\text{Å}^{-1}$ (dots), $2\,\text{Å}^{-1}$ (open squares) and $4.4\,\text{Å}^{-1}$ (asterisks). A similar trend is observed even at the other wavevectors. (b) The same for the collective spectrum $S(k, \omega)$. Both graphs are deduced from the neutron scattering data of Sköld *et al.* (1972) in liquid Ar. The behaviour at other wavevectors is similar to that of the $k = 1.4$ and $4.4\,\text{Å}^{-1}$ data.

much more accurate. These data are reported in Fig. 2.5, along with the results of various simple theoretical models:

(i) the hydrodynamic prediction $(\kappa/nc_V)k^2$ for the width of the Rayleigh peak (cf. Section 1.6.4). Even if no trace of inelastic peaks is found in the observed $S(k, \omega)$, the poor results of this model indicate a clear breakdown of the ordinary hydrodynamic expressions.

(ii) the results of the *Vineyard approximation*, $S(k, \omega) \approx S(k) \cdot S_s(k, \omega)$. This rather crude model for the collective dynamics has the only merit of incorporating the correct zeroth moment of $S(k, \omega)$ (namely, the initial value $S(k)$ of $F(k, t)$). In the diffusional limit for $S_s(k, \omega)$, the model predicts for $S(k, \omega)$ a full width $2Dk^2$, where D is the diffusion coefficient (cf. eqn (1.71)). Figure 2.5 indicates that the overall results of this approximation are unsatisfactory.

(iii) the results of the so-called *modified Vineyard approximation* $S_s(k, \omega) \approx S(k) \cdot S_s(k/\sqrt{S(k)}, \omega)$. This ad-hoc model accounts even for the correct second frequency moment $\langle \omega_k^2 \rangle$ of $S(k, \omega)$ (cf. (1.128)). In the diffusional limit for S_s, the full width of $S(k, \omega)$ is now predicted to be $2Dk^2/S(k)$. The results of this approximation are seen to reproduce several features of the experimental data (in particular, they account rather well

for the 'de Gennes narrowing' near 2 Å^{-1}), even if on the whole the quantitative agreement is still rather poor.

As in the previous experiment, at not too high wavevectors the intensity in the wings of the spectra was found to be larger than that of a Lorentzian shape centred at $\omega = 0$. This excess intensity was interpreted as a remnant of an inelastic peak which should become resolved for lower values of k (de Schepper *et al.* 1983, 1984). Accordingly, $S(k, \omega)$ was fitted by the sum of three Lorentzians, which represent the high-k limit of the (overdamped) Rayleigh–Brillouin triplet characteristic of the hydrodynamic regime (cf. Section 1.6.4). A plot of the fitted position of the peak of the Brillouin doublet as a function of k ('extended sound dispersion') reveals several unexpected features (Fig. 2.6(a)). To begin with, in the k-interval between 0.4 and 1.3 Å^{-1} the peak position is found to be *higher* than the extrapolated sound frequency $v_s k$, where v_s is the hydrodynamic sound velocity. This behaviour is in the opposite direction with respect to the one usually found in phonon dispersion curves (which bend *downwards* at increasing k), and will be discussed in detail in Section 6.2.3. At even larger wavevectors the 'extended sound' frequency passes through a maximum, and then rapidly decreases. At $k = 1.7$ Å^{-1} the fitting procedure yields a vanishing value for the peak position, a feature which persists even beyond 2 Å^{-1} (the approximate position of the main peak of $S(k)$). Finally, at larger k the 'extendend sound' frequency is again found to increase. This striking behaviour opened a debate about the actual existence of this 'propagation gap' (cf. Section 6.1). In Fig. 2.6(b) we report a similar 'extended sound' dispersion as obtained in liquid argon at the same temperature as in Fig. 2.6(a), but at a much higher pressure (Verkerk 1985; Bruin *et al.* 1985). Here the density corresponds to that of the liquid at the triple point, and no sound 'propagation gap' appears. Again, there is a marked decrease of the effective sound velocity in the k-region around 1.3 Å^{-1}, but now this is followed by a broad minimum in correspondence to the peak of $S(k)$. Aside from these controversial aspects, the three-Lorentzian fit can be regarded as a convenient tool of data analysis in a wavevector region where the conventional hydrodynamic expressions start to break down.

2.4.2 Neutron Brillouin scattering

In inelastic neutron scattering there have been several attempts to extend the wavevector range to smaller values, in order to resolve the Rayleigh–Brillouin triplet and possibly to fill the gap between neutron- and light-scattering techniques. With the exception of quantum liquids such as superfluid helium (Henshaw and Woods 1961) and liquid para-hydrogen
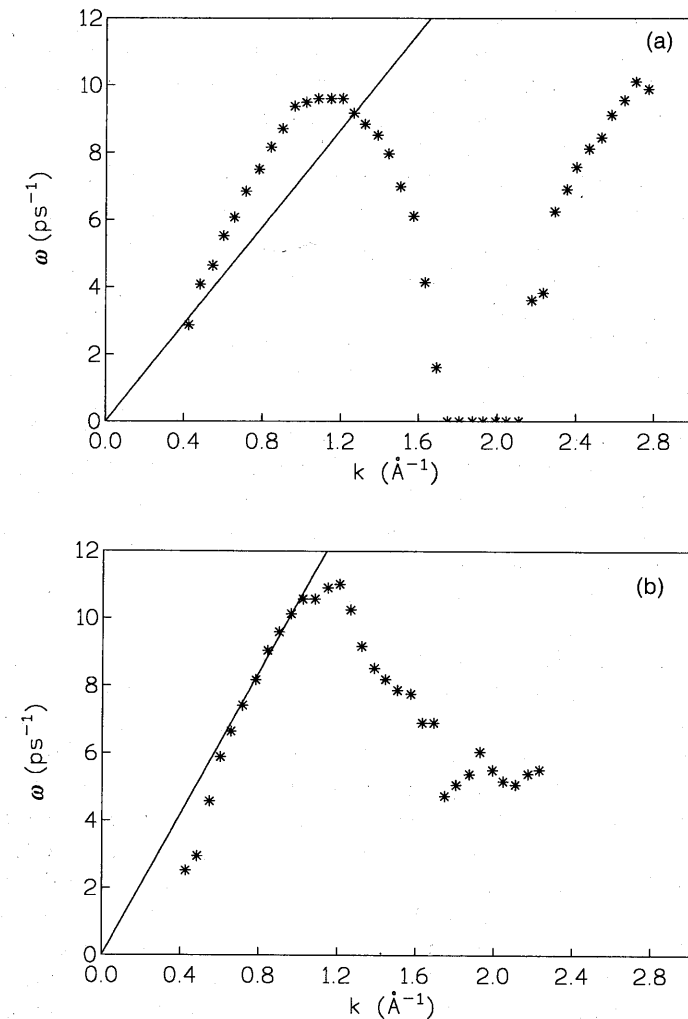
Fig. 2.6 The extended sound dispersion of liquid Ar. In (a) where ($T = 120$ K and $n = 0.0185$ Å^{-3} a propagation gap is visible in the region 1.7–2.2 Å^{-1}. In (b) where $T = 120$ K and $n = 0.0216$ Å^{-3}, the density being very similar to that of the liquid at the triple point, no propagation gap appears, but only a slowing down of the effective sound velocity. The lines represent the hydrodynamic dispersion relation $\omega = v_s k$ (van Well *et al.* 1985).

(Carneiro *et al.* 1973), well-defined excitations propagating at finite k accessible by neutron scattering have been detected only in some liquid metals. In particular, in the case of molten alkali metals clear inelastic peaks were detected in liquid rubidium (Copley and Rowe 1974) and more recently in liquid caesium (Bodensteiner *et al.* 1992).

In contrast, in the liquified rare gases the detection of sound-like peaks is a difficult task to achieve by neutrons. For example, in liquid neon Bell *et al.* (1973) were able to observe broad Brillouin peaks only at very small wavevectors ($0.06 \text{ Å}^{-1} \leqslant k \leqslant 0.14 \text{ Å}^{-1}$), where the difficulty of working at small scattering angles was augmented by the weakness of the signal related to the small values of $S(k)$ in this range (cf. eqn (2.26)). Experiments in liquid argon, on the other hand, have never been extended to sufficiently low wavevectors to detect clear Brillouin peaks in $S(k, \omega)$. Well-defined collective modes were instead observed at room temperature in compressed gaseous argon (pressure $P = 462$ bar) by Postol and Pellizzari (1978) and more recently by Bafile *et al.* (1990) at $P = 200$ bar. Also, well-defined inelastic peaks were detected in compressed gaseous neon at a density of about one-third that of the liquid (Bell *et al.* 1975), as well as in a more recent experiment on gaseous nitrogen (Egelstaff *et al.* 1989, Youden *et al.* 1992).

It appears, therefore, that in insulating fluids the transition from the microscopic to the hydrodynamic regime can be more easily observed by neutron scattering if one works at densities smaller than those typical of the liquid range. Experimentally, there are in fact two advantages of dealing with gases. First of all, due to the higher compressibility of gases, at small wavevectors the static structure factor $S(k)$ (i.e. the cross section for coherent neutron scattering) is considerably larger than at liquid density. Moreover, as n decreases the sound velocity decreases as well, and the Brillouin peak is pushed toward lower energy shifts. As a result, once the experimental scattering angle has been set to a minimum value, in a gas it is easier to fulfil the requirements of eqn (2.5) by using 'cold' neutrons with the lowest possible value of E_0. In contrast, in a liquid, due to the higher sound velocity the only possibility of obtaining values of $\hbar\omega$ in the Brillouin range is to decrease the wavevector k. This would be feasible only by further reducing both E_0 and θ beyond the previous 'minimum' values. As a consequence, the detection by inelastic neutron scattering of the Brillouin portion of the spectrum is by no means an easy task in the liquid range.

2.5 POLARIZED LIGHT SCATTERING

2.5.1 Probing the hydrodynamic regime

Both the scalar and the symmetric components of the polarizability (namely

$\mathbf{A}^{(0)}$ and $\mathbf{A}^{(2)}$ in eqn (2.44)) give rise to polarized light scattering. However, as discussed in Section 2.3.7, the contribution coming from $\mathbf{A}^{(2)}$ is of the same order of magnitude as the first induced term which was neglected in eqn (2.46). Therefore, for polarized light scattering the leading contribution comes from the first term in eqn (2.46), namely from the polarizability of an isolated molecule. For a spherically symmetric molecule, this reduces to

$$\mathbf{A}^{(0)}(i) = \alpha_0 \mathbf{I} \qquad (2.49)$$

where $\mathbf{I}$ is the unit tensor of the second order and α_0 is the scalar polarizability of the molecule. If we assume that both the incoming and scattered photons are polarized along the z direction, the intermediate scattering function (2.43) becomes

$$I_{\mathrm{L}}^{(zz)}(\mathbf{k}, t) = \alpha_0^2 F(k, t) \qquad (2.50)$$

which is formally identical to eqn (2.31) for coherent neutron scattering. This correspondence should not, however, be taken too literally. In fact, as has been thoroughly discussed in Section 2.3, two completely different regions of the plane (k, ω) are explored by these two techniques.

In order to understand better the sort of information provided by polarized light scattering in a classical fluid, it is essential to realize the implications set by the allowed kinematic region (Fig. 2.3(b)) on the quantities $F(k, t)$ and $G(r, t)$. In a typical light-scattering experiment with photon wavelengths $\lambda_0 \approx 5000 \text{ Å}$, the value of the momentum transfer k may range in the interval between 0.0002 and 0.0026 Å^{-1} (cf. eqn (2.8)), with a corresponding spatial interval $(2\pi/k)$ which ranges between 2500 and 30 000 Å. According to the definition (1.32), the van Hove correlation function $G(r, t)$ is bound to vanish unless the difference $|\mathbf{r}_i(0) - \mathbf{r}_j(t)|$ becomes close to this value. Since no single-particle correlation may survive up to these large distances in a dense medium, a first consequence of the kinematic restrictions is that only the distinct part of $G(r, t)$ with $i \neq j$ is effective. Secondly, we see immediately that a huge number of molecules lies between the two correlated scattering points. Since the wavelength of the optical photon, is of the same order as $2\pi/k$ and all molecular dipoles oscillate with the same phase as the electromagnetic field (i.e. the scattering is coherent), we are justified in moving from a microscopic picture to an hydrodynamic description where the fluid can be considered as a continuum.

The hydrodynamic limit of the intermediate scattering function, as well as its time Fourier transform, the dynamic structure factor, have already been given in Section 1.6.4 (cf. eqns (1.161) and (1.170)). A typical polarized-light-scattering spectrum is reported in Fig. 2.7, which refers to liquid argon at $T = 84.97 \text{ K}$ (Fleury and Boon 1969). In this experiment the magnitude of the wavevector transfer is $k = 0.00173 \text{ Å}^{-1}$, and therefore the Brillouin doublet appears as completely resolved.
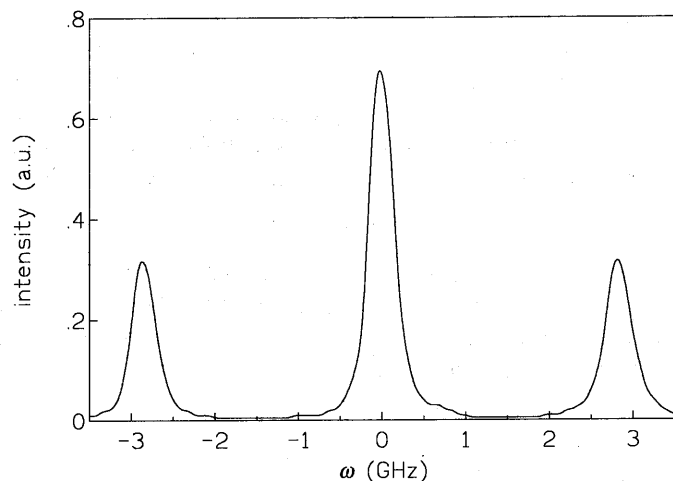
Fig. 2.7 Polarized light scattering in liquid Ar at $T = 84.9\,\mathrm{K}$. (Redrawn from Fleury and Boon 1969) The radiation probe is provided by the beam of an argon-ion laser operating in a single $\mathrm{TEM_{00}}$ mode with an average power of 100 mW. The radiation scattered at $\theta = 90°$ is analysed by a Fabry–Perot interferometer and detected by a cooled photomultiplier. The central elastic peak is related to non-propagating temperature fluctuations (Rayleigh component) while the two inelastic side peaks are associated with propagating density fluctuations (Brillouin components) which are shifted in frequency of the amount $\pm v_s k$, and are characterized by a halfwidth Γk^2 (cf. Section 1.6.4).

2.5.2 The transition between the hydrodynamic and the microscopic regime in light scattering

As we have seen in Section 2.4, the standard condition for a neutron-scattering experiment is to probe the microscopic regime of the liquid, owing to the similarity between the transferred wavevector k and the reciprocal of the average intermolecular distance. There are, at present, attempts to extend the applicability of thermal neutron scattering toward the hydrodynamic region by designing new neutron spectrometers which would allow us to explore liquids in the low-k region. However, for the time being, a contact with hydrodynamics has only been obtained by decreasing the density and carrying out experiments on compressed gases (cf. Section 2.4.2).

In parallel, for a long while, there have been similar attempts, on the side of light scattering, to close the gap between the 'natural' hydrodynamic regime and the microscopic one, again by decreasing the density of the fluid. More precisely, if the mean free path becomes comparable with the

wavelengths typical of light scattering, one should be able to go from one regime to the other. In this case, the fluid is clearly more similar to an ideal gas than to a strongly interacting system such as a liquid. However, for the sake of completeness, we briefly discuss the features of this crossover as observed by light-scattering experiments.

The first systematic study of this transition in a monatomic system dates back to Clark (1975). In this experiment, the large polarizability of xenon was exploited to perform accurate measurements of the Rayleigh–Brillouin spectrum of this system in the very dilute gas phase. Specifically, the experiment was carried out at room temperature and at pressures between 0.02 and 0.6 atmospheres. The observed spectra show very clearly the crossover between the hydrodynamic regime and the microscopic one. In particular, a well defined Rayleigh–Brillouin triplet was detected at the highest pressure, whereas only a Gaussian-like spectrum is observed at the lowest densities. In these dilute gas conditions, the natural theoretical tool to study the dynamics of the fluid is provided by conventional kinetic theory (e.g. Huang 1987). In the whole density region explored by Clark, the kinetic model solution of the Boltzmann equation was indeed found to account for the evolution of the spectrum, including the Rayleigh–Brillouin structure observed at high densities, where the kinetic and the hydro-dynamic results nearly coincide. As the density decreases, one notices devia-tions between the spectra predicted by kinetic theory and those obtained by the Navier–Stokes equations; however, these discrepancies can be readily accounted for by a simple 'generalization' of the hydrodynamic framework (Selwyn and Oppenheim 1971).

The crossover between the kinetic and the hydrodynamic regimes has subsequently been detected in helium, neon, and argon gases (Ghaem-Maghami and May 1980). A specific aim of this work was to study the validity of an approximate 'scaled version' of the Boltzmann equation (Sugawara *et al.* 1968). In particular, the scaling assumption is equivalent to saying that the spectral shape $S(k, \omega)$ can be expressed in terms of two reduced variables, namely the 'reduced frequency'

$$x = \omega/\sqrt{2}kv_0 \qquad (2.51)$$

and the 'uniformity parameter'

$$y = \sqrt{2}nmv_0/3\eta k \qquad (2.52)$$

where $v_0 = (k_B T/m)^{1/2}$ and η is the shear viscosity coefficient. Strictly speaking, the scaling relations (2.51) and (2.52) do not follow from a rigorous solution of the Boltzmann equation; however, the expected discrepancies are so small that they are commonly accepted as a convenient scheme when dealing with the Brillouin spectroscopy of gases. In any case, their validity has been tested by Ghaem-Maghami and May by comparing

the experimental data for the three gases helium, neon, and argon in a wide range of densities. The experiment was carried out at room temperature and in a range of pressures such that a wide common range of y (from 1 to 20) can be covered for the three gases. Again, a strong density-dependence of the Rayleigh–Brillouin triplet structure was observed, with a narrowing of all the features at increasing density. The covered wavevector range was wider than in previous work on xenon, both for the choice of larger scattering angle ($\theta = 90°$ rather than 10°) and for the use of a higher incident frequency ($\lambda_0 = 5145$ Å rather than 6328 Å). In contrast with Clark's experiment (where y ranged from 0.1 to 6), the limiting case of a Gaussian spectrum was not reached. As far as the validity of the scaled model is concerned, the main conclusion of the work by Ghaem-Maghami and May is that a perfect scaling of the spectra is never observed, even in the low-density region. This failure of the model is rather unexpected. Indeed, the effects of the different potentials in the collisional term of the Boltzmann equation should tend to decrease with density; moreover, it is a well-recognized fact that the best pair interaction potentials for the rare gases scale to within a few per cent (Scoles 1980). The origin of the discrepancy is likely to be connected to a different relevance of quantum effects in the three gases, owing to the large difference of their atomic mass (Barocchi *et al*. 1987).

2.6 DEPOLARIZED LIGHT SCATTERING

When the polarization vectors of the incoming and scattered radiation are set perpendicular, only the symmetric component of the polarizability (namely $\mathbf{A}^{(2)}$) contributes to the scattering. Again, if only the leading term in eqn (2.48) is retained, this component appears to be governed by the excess polarizability which is produced by the interactions of pairs of particles. In this case, the intermediate scattering function (2.43) becomes

$$I_{\text{L},xy}(\mathbf{k}, t) = (1/N) \sum_{i \neq j} \sum_{l \neq m} \langle a_{xy}^{(2)}[\mathbf{r}_i(0), \mathbf{r}_j(0)]$$

$$a_{xy}^{(2)}[\mathbf{r}_l(t), \mathbf{r}_m(t)] \exp\{-i\mathbf{k} \cdot [\mathbf{r}_i(0) - \mathbf{r}_l(t)]\}\rangle \quad (2.53)$$

where, as indicated by the superscript (2), only the symmetric traceless component (i.e. the spherical component of rank 2) of the polarizability tensor is to be considered. In eqn (2.53), the labels 'xy' denote any two perpendicular components of the laboratory frame, and we have dropped the subscript 2 from the alphas since, for the time being, interactions of order higher than *pairs* shall be neglected.

It is worthwhile focusing our attention on the k-dependence of eqn (2.53).

As already discussed in Section 2.3.7, in a typical light-scattering experiment the transferred wavevector has a magnitude $k \approx 10^5 \text{cm}^{-1}$, which corresponds to a length scale of some 10^3 Å. In addition to the k-dependent factor, the statistical average in eqn (2.53) involves the correlation between two independent pairs of molecules, such as (i, j) and (l, m). Noting that the field scattered by the ith particle at time $t = 0$, modulated by the presence of its neighbours (j), has to be correlated with the field scattered by the lth particle at time t, which in turn is modulated by its neighbours (m), we conclude that, due to the molecular interactions, the coherence of the fields is lost if particles i and l are more than a few molecular diameters apart. This means that the distance $|\mathbf{r}_i(0) - \mathbf{r}_l(t)|$ which appears in eqn (2.53) cannot exceed a few molecular diameters; in view of the magnitude of k, the exponential factor can consequently be set equal, to unity. The validity of this approximation at a quantitative level can be assessed by using the Rayleigh expansion of the exponential factor in spherical harmonics (cf. eqn (J.11) in Appendix J). It turns out that to within an overall accuracy of a few parts in 10 000, eqn (2.53) can simply be written as:

$$I_{\text{L},xy}(\mathbf{k}, t) = (1/N) \sum_{i,j \neq i} \sum_{l,m \neq l} \langle a_{xy}^{(2)}[\mathbf{r}_i(0), \mathbf{r}_j(0)] a_{xy}^{(2)}[\mathbf{r}_l(t), \mathbf{r}_m(t)] \rangle$$

$$(2.54)$$

where any $\mathbf{k}$-dependence has disappeared. Hence, in this case the restriction over k, which stems from momentum conservation and is so relevant in polarized light scattering, is seen to play a different role because of the specific character of the dynamical variables in the statistical average. Since the ultimate origin of the effect is the interaction among the molecules, the phenomenon is traditionally referred to as *interaction-induced* (or, somewhat less properly, *collision-induced*) depolarized light scattering. As we shall see later in more detail, the correlation function (2.54) involves clusters of particles of increasing complexity steming from different combinations of the labels (i, j) and (l, m) (cf. eqn (1.108) in Section 1.5.3).

From the previous considerations it emerges clearly that the depolarized scattering of light can effectively be used to test the dynamic properties of simple liquids at a microscopic level. In fact, only interactions among neighbouring molecules rule the time behaviour of the correlation function for this phenomenon, and therefore the spectral shape of depolarized light scattering directly probes the dynamics of molecules at a microscopic level. To see in more detail which kind of dynamic correlations are involved and how the result is related to the well-known van Hove time-dependent pair correlation function, it is convenient to write eqn (2.54) in a more manageable form.

We start by considering an isolated pair of atoms and writing the total polarizability of the pair as

$$\mathbf{\alpha}(\mathbf{r}_i, \mathbf{r}_j) = [a_0(i) + a_0(j)]\mathbf{I} + \mathbf{\alpha}_2(\mathbf{r}_i, \mathbf{r}_j) \qquad (2.55)$$

where a_0 is the single-atom scalar polarizability, and $\mathbf{\alpha}_2(\mathbf{r}_i, \mathbf{r}_j)$ represents the excess pair polarizability which is induced by the interactions within the pair. The determination of models for $\mathbf{\alpha}_2(\mathbf{r}_i, \mathbf{r}_j)$ has been the subject of several investigations, dealing with both first-principles calculations and with empirical expressions based on depolarized light scattering (DLS) on low-density rare gases (e.g. Gelbart 1974; Tabisz 1979; Frommhold 1980; Birnbaum 1982, and 1985; Meinander *et al.* 1986). In a first approximation, the excess pair polarizability can be considered as originating from the so called 'dipole-induced-dipole' (DID) interaction; that is, from the same phenomenon which produces the long range r^{-6} portion of the interaction pair potential in Lennard–Jones systems. The excess contribution (usually referred to as the *irreducible pair polarizability*) can conveniently be expressed by choosing as the z-axis the line joining the centres of mass. In this 'principal axis' reference frame, $\mathbf{\alpha}_2(\mathbf{r}_i, \mathbf{r}_j)$ takes the diagonal form

$$\mathbf{\alpha}_2(\mathbf{r}_i, \mathbf{r}_j) = \begin{pmatrix} a_{xx}(r_{ij}) & 0 & 0 \\ 0 & a_{yy}(r_{ij}) & 0 \\ 0 & 0 & a_{zz}(r_{ij}) \end{pmatrix} \qquad (2.56)$$

where the dependence of each matrix element on the (scalar) distance between the atoms has been explicitly written out. For obvious symmetry reasons, the (xx) and (yy) matrix elements turn out to be equal; consequently, only two components of the matrix are relevant, namely $a_\perp = a_{xx} = a_{yy}$ and $a_\parallel = a_{zz}$. These can in turn be expressed in terms of the 'trace' and the 'anisotropy' of the matrix; that is, $a_\parallel + 2a_\perp$ and $a_\parallel - a_\perp$. Whereas for polarized light scattering the pair irreducible anisotropy is nearly negligible with respect to the single particle term, it yields the dominant contribution in the case of depolarized scattering (cf. Section 2.3.7).

For notational simplicity, we define the anisotropy of the pair in its own reference frame as

$$\beta(r_{ij}) = a_{zz}(r_{ij}) - a_{xx}(r_{ij}) \qquad (2.57)$$

After some straightforward manipulations, the DLS intermediate scattering function (2.54) becomes:

$$I_{\mathrm{L,DEP}}(t) = \frac{1}{15N} \sum_{i,j(\neq i)} \sum_{l,m(\neq l)} \langle \beta[r_{ij}(0)] \beta[r_{lm}(t)] P_2[\cos\theta(ij, 0; lm, t)] \rangle.$$

$$(2.58)$$

Here $P_2(x) = \frac{1}{2}(3x^2 - 1)$ is the second-order Legendre polynomial, with an argument which is the scalar product between the unit vectors $\hat{r}_{ij}$ (time $t = 0$) and $\hat{r}_{lm}$ (time t).

An equivalent way of writing eqn (2.58) is

$$I_{\mathrm{L,DEP}}(t) = \frac{1}{15} \int d\mathbf{r} \int d\mathbf{r}' \beta(r)\beta(r') P_2[(\mathbf{r}\cdot\mathbf{r}')/rr'] \, \mathcal{G}(\mathbf{r}\,0; \mathbf{r}'\,t) \quad (2.59)$$

where we have introduced the time-dependent correlation function $\mathcal{G}(\mathbf{r}\,0; \mathbf{r}'\,t)$ defined as:

$$\mathcal{G}(\mathbf{r}\,0; \mathbf{r}'\,t) = (1/N) \sum_{i,j(\neq i)} \sum_{l,m(\neq l)} \langle \delta[\mathbf{r}_{ij}(0) - \mathbf{r}] \delta[\mathbf{r}_{lm}(t) - \mathbf{r}'] \rangle.$$

$$(2.60)$$

As a consequence, depolarized light scattering is ruled by a four-point correlation function which represents the joint probability that two particles of the liquid are separated by a distance $\mathbf{r}$ at time $t = 0$, and two independent particles are separated by a distance $\mathbf{r}'$ at time t.

If the particles referred to at the later time t are the same as the two original particles, the dynamics of a single pair is described. If only one particle of the second pair is identical to either one of the two original particles, then we are concerned with the dynamics of a triplet. Finally, if all the four particles are different, we are dealing with the dynamics of a quadruplet.

These three cases have an experimental counterpart. The broad depolarized wing which appears on either side of the quasi-elastic Rayleigh spectrum is determined by eqn (2.58); that is, by the sum of contributions from pairs, triplets, and quadruplets of particles (cf. Section 1.5.3). This is the typical interaction-induced depolarized spectrum observed in rare-gas fluids (e.g. McTague and Birnbaum 1971). On the other hand, the depolarized wing observed near an allowed molecular Raman line is another interaction-induced effect, determined only by the sum of pair and triplet contributions. In fact, owing to the phase independence of the Raman transitions, for a non-vanishing scattering at least one particle should be common to the sets (i, j) and (l, m) (Le Duff and Gharbi 1978). Finally, there is the possibility of detecting even interaction-induced phenomena due only to the same particle pair. This situation is clearly the dominant one at low densities, where the occurrence of correlated triplet and quadruplet contributions becomes negligible. At higher densities, a purely pair-interaction-induced spectrum can only be observed in rather unusual cases, such as a simultaneous Raman transition of two molecules. Despite the difficulties in its detection, this situation would provide direct information on the dynamic correlations of pairs in a dense fluid, thereby making
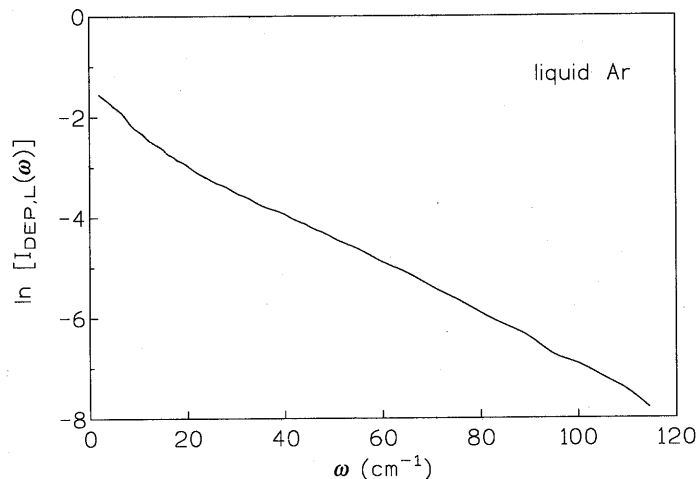
Fig. 2.8 Depolarized light scattering spectrum in liquid Ar at $T = 89$ K (Redrawn from An *et al.* 1976). Note the logarithmic scale on the ordinate axis.

experimentally accessible the time-dependent pair distribution function $G_2(r\,0; r'\,t)$ discussed in Section 1.5.1.

Aside from these limiting cases, the depolarized light scattering spectrum as observed in simple liquids (Fig. 2.8) is proportional to the Fourier transform of eqns (2.58). As is clear from the alternative representation (2.59), in DLS one effectively probes some averaged dynamical features of $\mathcal{G}(r\,0; r'\,t)$, with suitable weight factors being provided by the scalar polarizability anisotropies $\beta(r)$, $\beta(r')$ and by a purely orientational term (the Legendre polynomial P_2). The problem is clearly much more complicated than those met in connection with neutron-scattering experiments, and can only be dealt with by an approximate analysis of the many-particle contributions embodied in $\mathcal{G}(r\,0; r'\,t)$. Some of these approaches are discussed in detail in Appendix J.

2.7   THE TWOFOLD ROLE OF COMPUTER SIMULATIONS

Since their invention in the 1950s, computer simulation studies have had an increasing impact on our understanding of the physics of liquids (Ciccotti *et al.* (1987) give a collection of the pioneering works in this area). Presently, the subject has developed to a such an extent that *computer simulation experiments* can be regarded as a widely used tool to investigate

several aspects of the physics of disordered systems, ranging from the simplest one (a collection of 'hard spheres' in a specified thermodynamic state) to more and more complex molecular systems of physico-chemical interest. In the following we shall limit ourselves to an extremely short account of these techniques, trying to stress their 'intermediate' character with respect to both theory and 'real' experiments rather than attempting a discussion of the basic technical details behind the actual 'setup' of a computer simulation study. For the latter aspects, we refer the reader to the comprehensive book by Allen and Tildesley (1987).

Broadly speaking, we deal with two classes of computer simulations. The first, referred to as the *Monte Carlo method*, dates back to the work by Metropolis *et al.* (1953) and is uniquely devoted to the study of time-independent properties. Typically, equilibrium averages are evaluated by starting from an arbitrary set of space coordinates of the interacting particles, and performing random 'moves' to generate new configurations. The latter can be either accepted or rejected, according to well-defined criteria which depend on the statistical ensemble of interest. Eventually, one obtains a more or less accurate 'sampling' of this ensemble in the configuration space, permitting the evaluation of statistical averages. Since time does not enter explicitly, the technique is intrinsically restricted to the calculation of static equilibrium quantities. Usually, one wishes to sample a canonical ensemble in which a fixed number of particles interact with a specified potential, and the system is assumed to be in thermal equilibrium (constant temperature).

For our purposes, the really important simulation data are, however, provided by a second technique which deals with both structural and dynamical quantities of a classical systems. The approach was originally developed by Alder and Wainwright (1957) for a hard sphere fluid, and subsequently extended by Rahman (1964) to encompass systems with a continuous interparticle potential. The core of this technique (traditionally referred to as *molecular dynamics* (MD) simulation) is the numerical solution of Newton's equations of motion for a system with a limited number of particles ($N = 100$–$10\,000$). The particles are usually enclosed in a cubic box, whose edge L is chosen in such a way that N/L^3 reproduces the actual number density of the real system which one wishes to simulate. Unwanted surface effects arising from the finite size of the box can be, to some extent, minimized by the use of periodic boundary conditions. Initially the particles are assumed to be in well-specified positions (e.g. in a periodic arrangement inside the box) and with a velocity distribution such that (i) there is no net total momentum of the system, and (ii) the average kinetic energy per particle, $(1/N)\sum_i \frac{1}{2}mv_i^2$, is $\frac{3}{2}k_B T$, where T is the temperature of the real system of interest. The particles are then allowed to interact through a specified potential, and their equations of motion

solved by appropriate numerical algorithms (see Allen and Tildesley 1987). After a certain number of time integration steps δt (in which possibly the kinetic energy of the system needs to be scaled in order to keep its effective temperature as close as possible to T), the simulated system can be considered to be in an equilibrium state. Then a repeated stepwise integration of the equations of motion generates a whole set of 'phase-space configurations' of the system at different times for the entire duration τ_{MD} of the simulation run. Typically, $\delta t \approx 1\text{--}10\,\text{fs}$ and $\tau_{MD} \approx 10^4\text{--}10^5\,\delta t$.

The static and dynamical correlations of interest can now be evaluated by replacing the corresponding ensemble averages by time averages (*ergodic assumption*). In the notation of Section 1.3, if $A(t) \equiv A(\mathbf{r}^N(t), \mathbf{p}^N(t))$ and $B(t) \equiv B(\mathbf{r}^N(t), \mathbf{p}^N(t))$ are two dynamical variables of the system, this is equivalent to assuming that

$$\langle A(0) B(t) \rangle = \langle A(\tau) B(t + \tau) \rangle$$
$$= \lim_{T \to \infty} (1/T) \int_0^T d\tau\, A(\tau) B(t + \tau) \qquad (2.61)$$

where we have exploited the stationarity of the ensemble average. The second line of eqn (2.61) defines the time average, which in the MD simulation is approximately replaced by

$$\frac{1}{\tau_{MD}} \int_0^{\tau_{MD}} d\tau\, A(\tau) B(t + \tau) = \frac{1}{n_{MD}} \sum_{n=0}^{n_{MD}-1} A(n\delta\tau) B(t + n\delta\tau) \qquad (2.62)$$

where $n_{MD} = \tau_{MD}/\delta\tau$ is the total number of integration steps of the simulation run in equilibrium conditions.

In the above representation, the statistical ensemble naturally sampled in the simulation is a constant-energy microcanonical ensemble. More sophisticated algorithms have been developed to deal directly with other ensembles, such as constant-temperature (canonical) or constant-pressure (isobaric) ensembles. Strictly speaking, the averages evaluated with different ensembles coincide only in the thermodynamic limit ($N \to \infty$), where the effects of fluctuations become negligible. Consequently, in some cases reliable results can be obtained only after a careful analysis of the MD data in systems with different number of particles (Allen and Tildesley 1987).

Since the early 1960s computer simulation techniques have played a very important role in liquid state physics, and their relevance can be expected to increase in the future. Indeed, simulation data have often been the only link between the oversimplifications of the theoretical models and the experimental findings. From one side, one can in fact use computer simulations as a powerful experimental technique to provide 'data' on

model systems against which the theoretical predictions on the same models can be tested with no ambiguity. On the other hand, once a model of the microscopic interactions of a real system has been assumed, computer simulations can be used as a theoretical method to evaluate the quantities actually measured in a real experiment, and ultimately to test the validity of the original assumptions on the interparticle potential.

In Chapter 1 we have seen some examples of MD computer simulations used as an 'experimental' tool to obtain data which need to be accounted for by a theory of liquid state dynamics. This first application of simulation techniques is of widespread use, and becomes particularly important when the property under consideration is of very difficult experimental access (as in the case of the velocity autocorrelation function), or even cannot be directly obtained by real experiments (as in the case of the transverse current autocorrelation function).

A second application of computer simulation techniques is more directly connected with experimental work. In this case, the role of a simulation becomes similar to that of a 'theory', in the sense that the MD results can be compared with the findings of real experiments. While a satisfactory comparison between the two sets of data means that the simulation is sufficiently 'realistic', the presence of discrepancies indicates that the model system needs to be improved. Clearly, this second use of the simulation techniques is particularly interesting in all the cases where the quantity under consideration cannot be evaluated, within the requested accuracy, by a genuine theoretical approach. As already mentioned, the typical example of such an application is the study of all those properties closely related to a specific intermolecular potential (which is often too complicated to be amenable to *ab initio* calculations). A repeated comparison between the MD findings obtained by a well-defined empirical potential model (which is possible to improve) and the experimental data is quite helpful to establish a reliable connection between the simulated system and the real one. A second example is the MD evaluation of quite complex many-particle correlation functions, such as those involved in depolarized light scattering (cf. Section 2.6). Some important results in this respect are discussed in Appendix J.

REFERENCES

Alder, B. J. and Wainwright, T. E. (1957). *J. Chem. Phys.*, **27**, 1208.

Allen, M. P. and Tildesley, D. J. (1987). *Computer simulation of liquids*. Oxford University Press.

An, S. C., Montrose, C. J., and Litovitz, T. A. (1976). *J. Chem. Phys.*, **64**, 3717.

Bafile, U., Verkerk, P., Barocchi, F., de Graaf, I. A., Suck, J. -B., and Mutka, H. (1990). *Phys. Rev. Lett.*, **65**, 2394 and 3458.

Barocchi, F., Neumann, M., and Zoppi, M. (1987). *Phys. Rev. A*, **36**, 2440.

Bell, H. G., Kollmar, A., Alefeld, B., and Springer, T. (1973). *Phys. Lett. A*, **45**, 479.

Bell, H. G., Moeller-Wenghoffer, H., Kollmar, A., Stockmayer, R., Springer, T., and Stiller, H. (1975). *Phys. Rev. A*, **11**, 316.

Birnbaum, G. (1982). *Adv. Chem. Phys.*, **51**, 49.

Birnbaum, G. (ed.) (1985). *Phenomena induced by intermolecular interactions*. Plenum, New York.

Bodensteiner, T., Morkel, C., Gläser, W., and Dorner, B. (1992). *Phys. Rev. A*, **46**, 2159.

Bruin, C., Michels, J. P. J., van Rijs, J. C., de Graaf, L. A., and de Schepper, I. M. (1985). *Phys. Lett.*, **110A**, 40.

Burkel, E. (1991). *Inelastic scattering of X-rays with very high energy resolution*. Springer Tracts in Modern Physics. Springer, Berlin.

Carneiro, K., Nielson, M., and McTague, J. P. (1973). *Phys. Rev. Lett.*, **30**, 481.

Ciccotti, G., Frenkel, D., and McDonald, I. R. (1987). *Simulation of liquids and solids: molecular dynamics and Monte Carlo methods in statistical mechanics* (a collection of reprints). North Holland, Amsterdam.

Clark, N. A. (1975). *Phys. Rev. A*, **12**, 232.

Copley, J. R. D. and Rowe, J. M. (1974). *Phys. Rev. A*, **9**, 1656.

de Schepper, I. M., Verkerk, P., van Well, A. A., and de Graaf, L. A. (1983). *Phys. Rev. Lett.*, **50**, 974.

de Schepper, I. M., Verkerk, P., van Well, A. A., and de Graaf, L. A. (1984). *Phys. Lett. A*, **104**, 29.

Egelstaff, P. A., Kearley, G., Suck, J. B., and Youden, J. P. A. (1989). *Europhys. Lett.*, **10**, 37.

Fleury, P. A. and Boon, J. P. (1969). *Phys. Rev.*, **186**, 244.

Frommhold, L. (1980). *Adv. Chem. Phys.*, **46**, 1.

Gelbart, W. M. (1974). *Adv. Chem. Phys.*, **26**, 1.

Ghaem-Maghami, V. and May, A. D. (1980). *Phys. Rev. A*, **22**, 692.

Huang, K. (1987). *Statistical mechanics*, 2nd edn. Wiley, New York.

Henshaw, D. G. and Woods, A. D. B. (1961). *Phys. Rev.*, **121**, 1266.

Herwig, K. W., Sokol, P. E., Sosnick, T. R., Snow, W. M., and Blasdell, R. C. (1990). *Phys. Rev. B*, **41**, 103.

Kubo, R. (1957). *J. Phys. Soc. Japan*, **12**, 570.

Le Duff, Y. and Gharbi, A. (1978). *Phys. Rev. A*, **17**, 1729.

Litovitz, T. A. and Davis, C. M. (1965). In *Physical acoustics* (ed. W. P. Mason), Vol. IIA. Academic Press, New York.

Louisell, W. H. (1973). *Quantum statistical properties of radiation*. Wiley, New York.

Lovesey, S. W. (1987). *Theory of neutron scattering from condensed matter*, 3rd edition, Vol. 1. Clarendon Press, Oxford.

McTague, J. P. and Birnbaum, G. (1971). *Phys. Rev. A*, **3**, 1376.

March, N. H. (1990). *Liquid metals*. Cambridge University Press.

Meinander, N., Tabisz, G. C., and Zoppi, M. (1986). *J. Chem. Phys.*, **84**, 3005.

Metropolis, N., Rosenbluth, A. W., Rosenbluth, M. N., Teller, A. H., and Teller, E. (1953). *J. Chem. Phys.*, **21**, 1087.

Postol, T. A. and Pellizzari, C. A. (1978). *Phys. Rev. A*, **18**, 2321.

Rahman, A. (1964). *Phys. Rev.*, **136**, A405.

Scoles, G. (1980). *Ann. Rev. Phys. Chem.*, **31**, 81.

Selwyn, P. A. and Oppenheim, I. (1971). *Physica*, **54**, 161 and 195.

Sköld, K., Rowe, J. M., Ostrowski, G. and Randolph, P. D. (1972). *Phys. Rev. A*, **6**, 1107.

Sosnick, T. R., Snow, W. M., and Sokol, P. E. (1990). *Phys. Rev. B*, **41**, 11–185.

Sugawara A., Yip, S., and Sirovich, L. (1968). *Phys. Fluids*, **11**, 925.

Tabisz, G. C. (1979). In *Molecular spectroscopy*, Vol. 6 (ed. G. Barrow and D. Long). Chemical Society, London.

van Hove, L. (1954). *Phys. Rev.*, **95**, 249.

van Well, A. A., Verkerk, P., de Graaf, L. A., Suck, J. B., and Copley, J. R. D. (1985). *Phys. Rev. A*, **31**, 3391.

Verkerk, P. (1985). Ph.D. Thesis, University of Delft.

Youden, J., Egelstaff, P. A., Mutka, J., and Suck, J. -B. (1992). *J. Phys. Condens. Matter*, **4**, 8945.

3

The general theoretical framework

Since their introduction in the 1960s (Zwanzig 1961; Mori 1965a), projection operators and memory functions pervade many theoretical approaches dealing with the dynamics of strongly interacting systems. In particular, their presence is nearly ubiquitous in the microscopic treatments of liquid state dynamics. Indeed, the idea of describing a many-body system by a limited number of 'relevant' variables characterized by a relatively simple dynamics appears to be extremely appealing. Moreover, an analysis of the formally exact expressions of the memory functions can shed light on the nature of the physical processes involved and their relative importance.

Physical intuition plays a very important role at several stages of these approaches. In a correct physical framework, the results of the formalism are particularly rewarding because of their simple mathematical form, which may encompass several ranges of dynamical situations. Unfortunately, the latter aspect has sometimes led to a misuse of the formalism, which has been exploited as a tool in the art of 'lineshape engineering'. As we shall see, in a few cases even this improper use may be of some heuristic value, while in other situations the results may be entirely misleading. In any case, these kinds of results cannot be claimed to be the output of a real theory firmly rooted on physical intuition and reasoning.

In this chapter we shall discuss the general aspects of the memory function approach, which follow merely from a formal rephrasing of the dynamical equations. The actual interest of the framework can only be appreciated by restricting it to some physical situations; in this respect, several simple examples relevant for liquid state dynamics will be discussed. The overall formalism will be used in Chapter 4 as the backbone of a general theory of classical fluids, encompassing both single-particle and collective features.

3.1 THE MEMORY FUNCTION APPROACH

Let us consider a classical system of N interacting particles, each with mass m. The Hamiltonian $\mathcal{H}$ of the system depends on the coordinates $(\mathbf{r}_1, \ldots, \mathbf{r}_N)$ and momenta $(\mathbf{p}_1, \ldots, \mathbf{p}_N)$ of all the particles, but is assumed to have no explicit time dependence. Suppose that we consider a set of

$n < N$ dynamical variables denoted by $A_1, A_2, \ldots, A_n$, or synthetically by an n-dimensional column vector A. The time evolution of each A_ν ($\nu = 1, \ldots, n$) is ruled by the equation of motion (cf. eqn (1.21))

$$\frac{\mathrm{d}A_\nu(t)}{\mathrm{d}t} = \{A_\nu(t), \mathcal{H}\} = \{A_\nu, \mathcal{H}\}(t) \equiv \mathrm{i}LA_\nu(t) \qquad (3.1)$$

where the Liouvillian L is formally defined as in eqn (1.22). We recall the expression (1.23) of L, valid in the case that the potential part of $\mathcal{H}$ can be written as a sum of pairwise central contributions $\phi(r_{ij})$:

$$\mathrm{i}L = (1/m) \sum_i \mathbf{p}_i \cdot \frac{\partial}{\partial \mathbf{r}_i} - \sum_{i,j \neq i} \frac{\partial \phi(r_{ij})}{\partial \mathbf{r}_i} \cdot \frac{\partial}{\partial \mathbf{p}_i}. \qquad (3.2)$$

Equation (3.1) is formally integrated to yield

$$A_\nu(t) = \exp(\mathrm{i}Lt)A_\nu \qquad (3.3)$$

where $A_\nu = A_\nu(0)$. The operator $\exp(\mathrm{i}Lt)$ is referred to as the *time propagator* associated with the dynamical variables of the system.

As already remarked in Section 1.3, for an interacting system the formal solution (3.3) is in general too complicated to be useful in practice. An exception is the case in which the system can naturally be characterized by some 'small parameter' whose presence would suggest some kind of perturbative treatment of the part of $\mathcal{H}$ or L which is effectively small. For example, in a dilute fluid the deviations from the ideal gas behaviour can be found by a 'virial expansion' in the number density n, a quantity which is effectively present in eqn (3.2) through the double summations of the potential term. Unfortunately, this convenient framework does not work in a dense (i.e. strongly interacting) system such as a liquid, where no perturbation scheme is a priori evident (for example, from Table 1.1 it is apparent that in typical simple liquids the dimensionless density parameter $nr_0^3 \approx 1$).

In such a situation, a frequently adopted strategy is to rephrase the problem in a different way, still avoiding any approximations. Strictly speaking, this new description is again formal and no real progress has apparently been made. However, in practice the establishment of the alternative framework is strongly biased by a number of physical arguments, with the ultimate expectation that practicable approximation schemes may now be much more apparent. A well-known example of this logical procedure is the theory of lattice vibrations in a crystalline solid, where the original awkward description in terms of atomic sites is abandoned in favour of a new one with lattice waves as the central variables. Mathematically, this formal rephrasing is nothing more than a space Fourier transform; physically, the choice of this new description is guided by the recognition of the role of translational symmetry and by the

non-localized character of the vibrations. On this basis, it is relatively straightforward to arrive at the final picture of nearly independent harmonic oscillators, slightly perturbed by comparatively small anharmonic interactions.

From a purely formal point of view, a convenient starting point for the memory function approach is the introduction of the *scalar product* (A, B) between two dynamical variables A, B of the system, a quantity which has already been mentioned in Section 1.3. Mathematically, (A, B) is a c-number which is required to have all the formal properties of the ordinary scalar product in a (possibly complex) vector space. In particular, we demand that

$$(A, A) \geqslant 0 \tag{3.4a}$$

$$(A, B) = (B, A)^* \tag{3.4b}$$

$$\left(A, \sum_v c_v B_v\right) = \sum_v c_v (A, B_v) \tag{3.4c}$$

$$\left(\sum_v c_v A_v, B\right) = \sum_v (c_v)^* (A_v, B) \tag{3.4d}$$

where the c_v are arbitrary constants. As is easily verified, all these properties are satisfied by identifying the scalar product with the ordinary statistical average; that is, by letting

$$(A, B) \equiv \langle A^* B \rangle. \tag{3.5}$$

A physical justification of (3.5) is based on linear response theory applied to a classical system, with the final result that $(A, B) \equiv \langle A^* B \rangle - \langle A^* \rangle \langle B \rangle$ (Mori 1965*a*). In the following we shall assume to deal with dynamical variables with zero average; if this is not the case, a variable A is implicitly replaced by its fluctuation $A - \langle A \rangle$ around the average.

Let us now come back to our physical system, and focus our attention on the n dynamical variables $A_1, \ldots, A_n$. These variables are assumed to be independent, in the sense that a given A_v cannot be expressed as a linear combination of the other $n - 1$ variables of the set. As an extreme case of this independence, the (A_v) may be mutually orthogonal, a situation expressed by $(A_\lambda, A_v) = 0$ for any $\lambda \neq v$, with a clear analogy with the meaning of the scalar product in ordinary vector spaces. Pursuing this analogy, we may think of the set (A_v) as spanning an n-dimensional subspace comprising all the dynamical variables which can be expressed as linear combinations of $A_1, \ldots, A_n$. The correspondence can be pushed even further if we deal with an orthonormal set in which $(A_\lambda, A_v) = \delta_{\lambda, v}$, so that each A_v can be interpreted as a 'unit vector'. Starting from a given set of independent variables, by well-known procedures it is always possible

to obtain the associated orthonormal set; this construction, although not strictly necessary for the development of the approach, leads to simpler expressions in the applications to specific cases.

After these formal definitions, the central point of all the framework is the introduction of a *projection operator* $\mathcal{P}$. When applied to an arbitrary dynamical variable, $\mathcal{P}$ has the property of extracting the 'portion' lying in the subspace spanned by the set (A_v). A more explicit definition of $\mathcal{P}$ is conveniently given in terms of the n-dimensional column vector A:

$$\mathcal{P} \equiv (A, \ldots)(A, A)^{-1} A \tag{3.6}$$

where $(A, A)^{-1}$ is the inverse of the $n \times n$ matrix (A, A). Clearly $\mathcal{P}A = A$, and $\mathcal{P}^2 A = \mathcal{P}A = A$, the latter relation being a particular example of the 'idempotent' property $\mathcal{P}^m = \mathcal{P}$ $(m = 1, 2, \ldots)$ typical of all projection operators. The scalar version of eqn (3.6) reads

$$\mathcal{P} \equiv \sum_{\lambda, v} (A_\lambda, \ldots)[(A, A)^{-1}]_{\lambda v} A_v. \tag{3.7}$$

In particular, if we deal with an orthogonal set we have $[(\mathbf{A}, \mathbf{A})^{-1}]_{\lambda v} = \delta_{\lambda, v}/(A_\lambda, A_\lambda)$ and eqn (3.7) becomes

$$\mathcal{P} \equiv \sum_{\lambda} (A_\lambda, \ldots)/(A_\lambda, A_\lambda) A_\lambda. \tag{3.8}$$

Let us now consider the equation of motion of $A(t) = \exp(\mathrm{i}Lt)A$ and insert the identity operator $\mathcal{P} + (1 - \mathcal{P})$ after the propagator $\exp(\mathrm{i}Lt)$ on the right-hand side. We obtain

$$\mathrm{d}A(t)/\mathrm{d}t = \exp(\mathrm{i}Lt)[\mathcal{P} + (1 - \mathcal{P})]\mathrm{i}LA$$
$$= \mathrm{i}\mathbf{\Omega} \cdot A(t) + \exp(\mathrm{i}Lt)(1 - \mathcal{P})\mathrm{i}LA \tag{3.9}$$

where we have introduced the $n \times n$ *proper frequency* matrix $\mathrm{i}\mathbf{\Omega} \equiv (A, \mathrm{i}LA) \cdot (A, A)^{-1}$ whose matrix elements are given by

$$\mathrm{i}\Omega_{\lambda v} = \sum_{\lambda'} (A_{\lambda'}, \mathrm{i}LA_\lambda)[(A, A)^{-1}]_{\lambda' v}. \tag{3.10}$$

Here $\mathrm{i}LA_\lambda = [\mathrm{d}A_\lambda(t)/\mathrm{d}t]_{t=0}$. In the case of an orthogonal set

$$\mathrm{i}\Omega_{\lambda v} = (A_v, \mathrm{i}LA_\lambda)/(A_\lambda, A_\lambda). \tag{3.11}$$

The stationarity of the system (cf. Appendices A, B) implies that $(A_v, \mathrm{i}LA_\lambda) = \langle (A_v)^* \mathrm{i}LA_\lambda \rangle = -\langle (\mathrm{i}LA_v)^* A_\lambda \rangle = -(\mathrm{i}LA_v, A_\lambda)$. In particular, $(A_\lambda, \mathrm{i}LA_\lambda) = 0$. Thus all the diagonal elements of the frequency matrix (3.11) vanish; in particular, if the set (A_v) comprises only one variable, there is no proper frequency term in the last member of eqn (3.9). The other term in eqn (3.9) can be rearranged by writing

$$\exp(\mathrm{i}Lt) = \exp(\mathrm{i}Lt)S(t) + \exp[\mathrm{i}(1 - \mathcal{P})Lt] \qquad (3.12)$$

where $S(t)$ is determined by solving the equation $\mathrm{d}S(t)/\mathrm{d}t = \exp(-\mathrm{i}Lt)$ $\mathrm{i}\mathcal{P}L\exp[\mathrm{i}(1 - \mathcal{P})Lt]$ with the initial condition $S(0) = 0$:

$$S(t) = \int_0^t \mathrm{d}\tau \exp(-\mathrm{i}L\tau)\mathrm{i}\mathcal{P}L\exp[\mathrm{i}(1 - \mathcal{P})L\tau]. \qquad (3.13)$$

As a result of these manipulations, the last term of eqn (3.9) splits into two contributions

$$\exp(\mathrm{i}Lt)\mathrm{i}(1 - \mathcal{P})LA = \int_0^t \mathrm{d}\tau \exp[\mathrm{i}L(t - \tau)]\mathrm{i}\mathcal{P}Lf(\tau) + f(t) \qquad (3.14)$$

where the quantity

$$f(t) = \exp[\mathrm{i}(1 - \mathcal{P})Lt]\mathrm{i}(1 - \mathcal{P})LA \qquad (3.15)$$

is referred as the *fluctuating force*. By construction, the time evolution of $f(t)$ from its initial value $(1 - \mathcal{P})\mathrm{i}LA$ is ruled by the anomalous propagator $\exp[\mathrm{i}(1 - \mathcal{P})Lt]$ rather than by the usual one $\exp(\mathrm{i}Lt)$. The presence of $(1 - \mathcal{P})$ has the important consequence that

$$(A, f(t)) = 0 \qquad (3.16)$$

or $(A_\lambda, f_\nu(t)) = 0$ in a scalar notation. In other words, the fluctuating force is orthogonal to A at all times; that is, it evolves in a subspace intrinsically different from the one spanned by the set (A_ν).

The first term on the right-hand side of eqn (3.14) can be written in a more convenient form by exploiting for two arbitrary dynamical variables A, B the relation $(A, LB) = (LA, B)$ which follows from eqns (1.25) and (3.4b). Since $\mathcal{P}Lf(\tau) = (A, Lf(\tau)) \cdot (A, A)^{-1}A$, we have that

$$\mathrm{i}(A, Lf(\tau)) = \mathrm{i}(LA, f(\tau)) = \mathrm{i}((1 - \mathcal{P})LA, f(\tau))$$
$$= -(f(0), f(\tau)). \qquad (3.17)$$

As a result, the equation of motion (3.9) can be written as

$$\frac{\mathrm{d}A(t)}{\mathrm{d}t} = \mathrm{i}\Omega \cdot A(t) - \int_0^t \mathrm{d}\tau K(\tau) \cdot A(t - \tau) + f(t) \qquad (3.18)$$

where we have introduced the quantity

$$K(t) \equiv (f, f(t)) \cdot (A, A)^{-1} \qquad (3.19)$$

referred as the *memory matrix* (or the *memory function* in the case in which the set (A_ν) reduces to a single variable, i.e. for $n = 1$).

From eqn (3.18) it is straightforward to obtain the corresponding

equation of motion for the 'correlation matrix' $C(t) \equiv \langle A^*(0)A(t) \rangle = (A, A(t))$. Exploiting the orthogonality of $f(t)$ to A we obtain

$$\mathrm{d}C(t)/\mathrm{d}t = \mathrm{i}\Omega \cdot C(t) - \int_0^t \mathrm{d}\tau K(\tau) \cdot C(t - \tau) \qquad (3.20a)$$

or, in scalar notation,

$$\mathrm{d}C_{\lambda\nu}(t)/\mathrm{d}t = \mathrm{i}\sum_{\lambda'}\Omega_{\lambda\lambda'}C_{\lambda'\nu}(t) - \sum_{\lambda'}\int_0^t \mathrm{d}\tau K_{\lambda\lambda'}(\tau)C_{\lambda'\nu}(t - \tau) \qquad (3.20b)$$

where $C_{\lambda\nu}(t) = (A, A(t))_{\lambda\nu} = (A_\nu, A_\lambda(t))$. Equations (3.18) and (3.20) are respectively referred as the *generalized Langevin equation* and the *memory equation*. No approximation has been made in their derivation, so both equations are still equivalent to the original formulation in terms of eqn (3.1). In particular, the formal structure of (3.18) is still linear in the variables of interest $A(t)$, and the same is true of the eqns (3.20) for the corresponding time correlation matrix $C(t)$.

The linear integro-differential equation (3.20a) is solved by introducing the Laplace transforms

$$\tilde{C}(z) \equiv \int_0^\infty \mathrm{d}t \exp(-zt)C(t) \qquad (3.21a)$$

$$\tilde{K}(z) \equiv \int_0^\infty \mathrm{d}t \exp(-zt)K(t) \qquad (3.21b)$$

yielding

$$\tilde{C}(z) = [z\mathsf{I} - \mathrm{i}\Omega + \tilde{K}(z)]^{-1} \cdot C(0) \qquad (3.22)$$

where I is the unit matrix. Since the elements (3.10) of the proper frequency matrix Ω are in principle evaluable in terms of equilibrium statistical averages, the solution of the dynamical problem has ultimately been shifted from $C(t)$ to $K(t)$. On the other hand, from its definition (3.19) the memory matrix $K(t)$ appears to have a time dependence ruled by the anomalous propagator $\exp[\mathrm{i}(1 - \mathcal{P})Lt]$, even more complicated than that of $C(t)$, so that at this stage the merits of the new formulation seem rather academic.

Suppose, however, that we have been so 'clever' to include in the set $\{A_\nu\}$ all the dynamical variables with a time dependence much slower than any microscopic timescale predictable from the Hamiltonian $\mathcal{H}$. Since the previous formalism gives no particular hint for the selection of the variables of the set, the choice of which variables are actually 'slow' is largely guided by our physical intuition. For example, if we are dealing with wavevector-dependent dynamical variables, we should certainly include in

the slow set $\{A_\nu\}$ all those variables which become conserved as $k \to 0$. In any case, assuming that a careful selection has been made, the orthogonality (3.16) of the fluctuating forces to all the variables of the set A now means that the random forces $f(t)$ evolve instead in a 'fast' portion of the full functional space of dynamical variables. As a consequence, all the elements of the memory matrix $\mathbf{K}(t)$ are likely to be characterized by decay times considerably shorter than those associated with the elements of the correlation matrix $\mathbf{C}(t)$. Pursuing the argument to its extreme, we may assume that over the timescale of $\mathbf{C}(t)$ the decay time of the memory matrix is so short that $\mathbf{K}(t)$ may be approximately written as proportional to a δ-function in time:

$$\mathbf{K}(t) \approx 2\mathbf{\Gamma}\delta(t) \qquad (3.23)$$

where

$$\mathbf{\Gamma} = \int_0^\infty \mathrm{d}t\, \mathbf{K}(t) = \tilde{\mathbf{K}}(z=0) \qquad (3.24)$$

As a result of the 'ansatz' (3.23) (often referred to as the *Markov approximation*), eqns (3.18) and (3.20a) can respectively be written as

$$\mathrm{d}A(t)/\mathrm{d}t = \mathrm{i}\mathbf{\Omega} \cdot A(t) - \mathbf{\Gamma} \cdot A(t) + f(t) \qquad (3.25)$$

$$\mathrm{d}\mathbf{C}(t)/\mathrm{d}t = (\mathrm{i}\mathbf{\Omega} - \mathbf{\Gamma}) \cdot \mathbf{C}(t) \qquad (3.26)$$

In both cases, it is seen that the extreme separation of timescales implicit in the Markov approximation yields a complete loss of 'memory effects' in the dynamical equations, in which only the instantaneous values of $A(t)$ and $\mathbf{C}(t)$ now appear. Equation (3.26) is easily integrated to give

$$\mathbf{C}(t) = \exp[(\mathrm{i}\mathbf{\Omega} - \mathbf{\Gamma})|t|] \cdot \mathbf{C}(0). \qquad (3.27)$$

This result shows that the ultimate effect of the rapidly varying fluctuating forces is to provide a damping mechanism for the slow oscillations of $\mathbf{C}(t)$ at the proper frequency $\mathbf{\Omega}$. At this stage, the actual evaluation of the relaxation matrix $\mathbf{\Gamma}$ from eqn (3.24) is still an open problem, but at least the framework provides a simple answer for the time-dependence expected for the correlation matrix $\mathbf{C}(t)$. By itself, the Markovian result (3.27) does not require any perturbative assumption about the magnitude of the elements of $\mathbf{\Gamma}$ with respect to those of $\mathbf{\Omega}$; in particular, eqn (3.27) still retains its validity if $\mathbf{\Omega}$ vanishes, as is indeed the case if we deal with a physical situation in which only one 'slow' variable is effectively relevant. In such a circumstance, eqn (3.27) reduces to

$$\mathbf{C}(t) = \mathbf{C}(0) \exp(-\mathbf{\Gamma}|t|) \qquad (3.28)$$

showing that the correlation of the slow variable decays exponentially. As a result, the corresponding frequency spectrum is a Lorentzian with

halfwidth $\mathbf{\Gamma}$. In fact, the ubiquity of exponential time decays and Lorentzian spectral shapes in many areas of physics reflects in most cases our ability to probe the dynamics of a system only through variables which relax slowly with respect to the appropriate microscopic times. For the liquid state, some examples of this typical situation will be discussed in the next subsections.

Needless to say, nature is not always so gentle (or our understanding of the problem so deep) that clear criteria of selection between slow and fast variables are available. Also, the distinction becomes meaningless in the cases where we are really probing the microscopic dynamics of the system. Since the memory function framework remains valid even in these cases, it is worthwhile to discuss possible strategies and remedies in such 'unpleasant' situations.

The first recipe is, of course, to learn as much as possible about the general properties of the memory functions. For example, in Appendix D we report the information deducible for the elements $K_{\lambda\nu}(t)$ on the basis of several symmetry requirements. In addition, even in this case it is useful to ascertain the short-time behaviour of $\mathbf{K}(t)$. The initial value $\mathbf{K}(0)$ is readily obtained either from (3.19) or by performing a time derivative of the memory equation (3.20a) and evaluating the result at $t = 0$. Exploiting the relation $\mathrm{i}\mathbf{\Omega} = \dot{\mathbf{C}}(0) \cdot [\mathbf{C}(0)]^{-1}$ we find that

$$\mathbf{K}(0) = -\ddot{\mathbf{C}}(0) \cdot [\mathbf{C}(0)]^{-1} - \mathbf{\Omega} \cdot \mathbf{\Omega}. \qquad (3.29)$$

Further differentiating (3.20a) with respect to time, we may relate the initial behaviour of $\mathbf{K}(t)$ with the higher derivatives of $\mathbf{C}(t)$ at $t = 0$. Introducing the frequency moments of the corresponding spectrum $\mathbf{C}(\omega)$

$$\overline{\omega^n} \equiv \int_{-\infty}^\infty \mathrm{d}\omega\, \omega^n \mathbf{C}(\omega) = \frac{1}{\mathrm{i}^n} \left[\frac{\mathrm{d}^n \mathbf{C}(t)}{\mathrm{d}t^n} \right]_{t=0} \qquad (3.30)$$

along with their 'normalized' counterparts $\langle \omega^n \rangle \equiv \overline{\omega^n} \cdot [\mathbf{C}(0)]^{-1}$, it is easily found that $\mathbf{\Omega} = \bar{\omega} \cdot [\mathbf{C}(0)]^{-1} = \langle \omega \rangle$, and

$$\mathbf{K}(0) = \langle \omega^2 \rangle - \langle \omega \rangle \cdot \langle \omega \rangle \qquad (3.31a)$$

$$\dot{\mathbf{K}}(0) = \mathrm{i}[\langle \omega^3 \rangle - 2\langle \omega^2 \rangle \cdot \langle \omega \rangle + \langle \omega \rangle \cdot \langle \omega \rangle \cdot \langle \omega \rangle] \qquad (3.31b)$$

$$\ddot{\mathbf{K}}(0) = -\langle \omega^4 \rangle + 2\langle \omega^3 \rangle \cdot \langle \omega \rangle - 3\langle \omega^2 \rangle \cdot \langle \omega \rangle \cdot \langle \omega \rangle$$

$$+ \langle \omega^2 \rangle \cdot \langle \omega^2 \rangle + \langle \omega \rangle \cdot \langle \omega \rangle \cdot \langle \omega \rangle \cdot \langle \omega \rangle \qquad (3.31c)$$

and so on. In all these equations, the appearance of odd frequency moments is due to the presence of non-diagonal elements in the matrices $\mathbf{C}(t)$ and $\mathbf{K}(t)$. The expressions are, of course, simplified in the single-variable case, where $\mathbf{C}(t) = \langle A^* A(t) \rangle$ is an even function of time and all odd frequency moments vanish. In such a case, the initial behaviour of the memory function is found to be

$$K(t) = K(0) + \ddot{K}(0)(t^2/2) + \cdots = K(0)[1 - (t/\tau_0)^2 + \cdots] \,. \tag{3.32}$$

Here $K(0) = \langle \omega^2 \rangle$, $\ddot{K}(0) = -\langle \omega^4 \rangle + \langle \omega^2 \rangle^2$, and we have introduced the initial decay time

$$\tau_0 = \left[\frac{-\ddot{K}(0)}{2K(0)} \right]^{-1/2} = \left[\frac{(\langle \omega^4 \rangle - \langle \omega^2 \rangle^2)}{2\langle \omega^2 \rangle} \right]^{-1/2} . \tag{3.33}$$

Thus, the short-time dependence of the memory matrix can be expressed in terms of the lowest frequency moments of $\mathbf{C}(\omega)$; that is, of equilibrium averages which are usually amenable to a direct evaluation. Using eqn (3.21b), the knowledge of $\mathbf{K}(t)$ as $t \to 0$ is seen to be equivalent to that of the Laplace transform $\mathbf{K}(z)$ for large z. When inserted into eqn (3.22), these results provide some exact 'constraints' for $\tilde{\mathbf{C}}(z)$ which should be fulfilled in any further development. Yet, up to now we are still at the level of a short-time expansion of $\mathbf{C}(t)$, which is in general not sufficient to obtain a reliable account of the dynamics. On the other hand, we may include even long-time information by demanding that the memory functions should vanish as $t \to \infty$, like any other time-dependent correlation. In practice, this paves the way for attempting a solution of the problem by simple 'guesses' of the functional form of $K_{\lambda\nu}(t)$, chosen in such a way that the short- and long-time requirements are both satisfied. In the single-variable case, a simple example of this ad-hoc procedure for the memory function is provided by the Gaussian 'ansatz'

$$K(t) = K(0) \exp[-(t/\tau_0)^2] \tag{3.34}$$

which is clearly consistent both with the short-time expansion (3.32) and with the requirement that $K(t) \to 0$ for long times. Equation (3.34) is readily Laplace-transformed to obtain $\tilde{K}(z)$, and the latter is inserted into eqn (3.22) for $\tilde{C}(z)$. The spectrum $C(\omega)$ is finally found from

$$C(\omega) = (1/\pi) \operatorname{Re} \tilde{C}(z = i\omega) \tag{3.35}$$

where Re denotes the real part.

In the absence of any additional information, these (or other equivalent) procedures are of course respectable, once it is clear that they are adopted for heuristic purposes, rather than for providing a 'theory'. In other cases, we may instead have some partial physical insight into the phenomenon. For illustrative purposes, consider again the case of a single variable, and assume that only one physical mechanism is suspected to be relevant as a decay channel for the memory function. If the decay rate is large enough, the decrease of $K(t)$ can reasonably be described in terms of the single time τ_0 of eqn (3.34), and some arbitrariness in the functional form of $K(t)$ providing the fast decay can be tolerated. An extreme case of this situation

occurs when we approach the Markovian limit (3.24), in which the detailed shape of $K(t)$ becomes ultimately irrelevant, and the only important quantity is the area $\tilde{K}(z = 0)$ under the memory function.

As an alternative, we may instead explore the dynamics of $\mathbf{K}(t)$ at a more refined level by looking at higher-order terms in its short-time expansion. This can be done systematically by exploiting results similar to (3.31), even if the calculation of higher-order moments $\langle \omega^n \rangle$ rapidly becomes very cumbersome. The advantages brought from the additional information are, however, limited if we remain at the level of a series expansion. Some help is provided by looking at the mathematical structure of eqn (3.22), in which $\tilde{K}(z)$ appears at the 'denominator'. Intuitively, this indicates that the limited short-time (or large z) information can be exploited in a way which is more rapidly convergent than a series expansion. Thus, it appears worthwhile to see whether it is possible to make use of this feature even at a higher level. The problem has been solved on a rigorous basis in a second paper by Mori (1965b). One starts by noting that the equation of motion of the fluctuating force (3.15) can be written as

$$\frac{df(t)}{dt} = i(1 - \mathcal{P})Lf(t) \tag{3.36}$$

Formally, eqn (3.37) is analogous to the original equation of motion for the components of the set A, with the ordinary Liouvillian L being replaced by the 'anomalous' one $L_1 \equiv (1 - \mathcal{P})L$. We may then introduce a new projection operator $\mathcal{P}_1$ which projects on the subspace spanned by the set (f_ν) of the random forces, and formally repeat all the previous manipulations. Eventually, we arrive at a result which can be interpreted as a generalized Langevin equation for $f(t)$

$$\frac{df(t)}{dt} = i\Omega_1 \cdot f(t) - \int_0^t d\tau\, \mathbf{K}_1(\tau) \cdot f(t - \tau) + f_1(t) \tag{3.37}$$

where

$$i\Omega_1 \equiv (f, iL_1 f) \cdot (f, f)^{-1}, \tag{3.38a}$$

$$f_1(t) \equiv \exp[i(1 - \mathcal{P}_1)L_1 t]i(1 - \mathcal{P}_1)L_1 f(0), \tag{3.38b}$$

$$\mathbf{K}_1(t) \equiv (f_1(0), f_1(t)) \cdot (f, f)^{-1}. \tag{3.38c}$$

Note that since $\mathcal{P}_0\mathcal{P}_1 = \mathcal{P}_1\mathcal{P}_0 = 0$, the new random force $f_1(t)$ is orthogonal both to f and to A. From eqn (3.38) we eventually arrive at a formally exact equation for the memory matrix $\mathbf{K}(t) = (f, f(t)) \cdot (A, A)^{-1}$:

$$\frac{d\mathbf{K}(t)}{dt} = i\Omega_1 \cdot \mathbf{K}(t) - \int_0^t d\tau\, \mathbf{K}_1(\tau) \cdot \mathbf{K}(t - \tau). \tag{3.39}$$

This can be Laplace-transformed to give

$$\tilde{\mathbf{K}}(z) = [z\mathbf{l} - i\Omega_1 + \tilde{\mathbf{K}}_1(z)]^{-1} \cdot \mathbf{K}(0). \qquad (3.40)$$

Inserting this result into eqn (3.22), it is readily seen that the previous mathematical structure is shifted to a higher level. Repeating the entire procedure for the fluctuating force $f_1(t)$ and iterating, we ultimately arrive at an expression for $\tilde{C}(z)$ in terms of a *continued fraction*. This representation is frequently adopted in the single-variable case, where all the quanties $\Omega, \Omega_1, \ldots$ vanish because of time-reversal symmetry (cf. Appendix B). In this case $\tilde{C}(z)$ can be written as

$$\frac{\tilde{C}(z)}{C(0)} = \left[z + \frac{\Delta_1}{z + \Delta_2/(z + \cdots)} \right]^{-1} \qquad (3.41)$$

where the coefficients $\Delta_1, \Delta_2, \ldots$ can be expressed in terms of the normalized frequency moments of the spectrum $C(\omega)$. In particular,

$$\Delta_1 \equiv K(0) = \langle \omega^2 \rangle, \qquad (3.42a)$$

$$\Delta_2 \equiv K_1(0) = -\frac{\ddot{K}(0)}{K(0)} = \frac{\langle \omega^4 \rangle}{\langle \omega^2 \rangle} - \langle \omega^2 \rangle, \qquad (3.42b)$$

$$\Delta_3 \equiv K_2(0) = -\frac{\ddot{K}_1(0)}{K_1(0)} = \frac{1}{\Delta_2} \left[\left(\frac{\langle \omega^6 \rangle}{\langle \omega^2 \rangle} \right) - \left(\frac{\langle \omega^4 \rangle}{\langle \omega^2 \rangle} \right)^2 \right]. \qquad (3.42c)$$

In view of the self-reproducing structure of the right-hand side of (3.41), all the considerations previously made for the first memory function $K(t)$ can in principle be repeated at any 'level' of the continued fraction. In liquid dynamics, this procedure has indeed been followed (e.g. Machida and Murase (1973)). As the level increases, the main problems usually met in these approaches are the difficulties of a reliable evaluation of moments such as $\langle \omega^6 \rangle, \ldots$, as well as the progressively more obscure physical meaning of the higher-order memory functions $K_n(t)$.

Because of its general character (including a straightforward extension to quantum systems), the Mori framework since 1965 has been applied to an impressive number of physical situations. In the next sections we shall discuss three applications of increasing complexity which are particularly relevant for the dynamics of liquids.

3.2 A SIMPLE APPLICATION: BROWNIAN MOTION

Let us consider a 'heavy' particle of mass M immersed in a fluid (the 'bath') made of N classical particles of mass $m \ll M$. Denoting by $\mathbf{R}$ and $\mathbf{P}$ the position and the momentum of the heavy particle, the Hamiltonian of the composed system can be written as

$$\mathcal{H}_{\text{tot}} = \sum_i \left[(p_i^2/2m) + \sum_{(j \neq i)} \phi(r_{ij}) \right] + (P^2/2M) + \sum_i v(|\mathbf{R} - \mathbf{r}_i|) \qquad (3.43)$$

where the last term at rhs accounts for the interactions (assumed as pairwise) between the heavy particle and light ones. The corresponding total Liouvillian reads

$$L_{\text{tot}} = L_0 + L_1 \qquad (3.44)$$

where

$$L_0 = (-i) \sum_i \left[\frac{1}{m} \mathbf{p}_i \cdot \frac{\partial}{\partial \mathbf{r}_i} - \sum_{j \neq i} \frac{\partial \phi(r_{ij})}{\partial \mathbf{r}_i} \cdot \frac{\partial}{\partial \mathbf{p}_i} \right] + i \sum_i \frac{\partial v}{\partial \mathbf{r}_i} \cdot \frac{\partial}{\partial \mathbf{p}_i} \qquad (3.45)$$

is the Liouvillian of the fluid (including the action exerted on it by the heavy particle), and

$$L_1 = (-i) \left(\frac{1}{M} \mathbf{P} \cdot \frac{\partial}{\partial \mathbf{R}} + \mathbf{F} \cdot \frac{\partial}{\partial \mathbf{P}} \right) \qquad (3.46)$$

is the Liouvillian of the heavy particle. Here the quantity

$$\mathbf{F} = - \sum_i \frac{\partial v(|\mathbf{R} - \mathbf{r}_i|)}{\partial \mathbf{R}} \qquad (3.47)$$

is the total force acting on the particle as a result of its interaction with the fluid.

Historically, the interest in the dynamics of such a composed system dates back to 1829, when the botanist Robert Brown observed by a microscope the irregular motion of a pollen particle suspended in a fluid. The phenomenon (referred to as *Brownian motion*) has much more general implications, investigated theoretically by Einstein and by Langevin at the beginning of this century. Equations (3.43)–(3.47) provide a convenient basis for a microscopic theory of Brownian motion as well as for a simple application of the Mori framework. For this purpose, let us take as a basic set of variables the three components (P_x, P_y, P_z) of the momentum of the heavy particle. Since $(P_\alpha, P_\beta) = \langle P_\alpha P_\beta \rangle = Mk_B T \delta_{\alpha,\beta}$, the set is orthogonal and the projection operator (3.6) over $\mathbf{P}$ can be expressed as

$$\mathcal{P} = (Mk_B T)^{-1} \sum_\alpha (P_\alpha, \ldots) P_\alpha. \qquad (3.48)$$

We shall now apply the formalism of Section 3.1 to write a generalized Langevin equation for the variable $\mathbf{P}(t)$. Since $\mathbf{P}$ and $\dot{\mathbf{P}}$ have opposite time-reversal symmetries, all the elements of the proper frequency matrix $\Omega_{\alpha,\beta} = (iMk_B T)^{-1}(P_\beta, \dot{P}_\alpha)$ vanish and the above equation can be written as

$$\dot{\mathbf{P}}(t) = -\int_0^t d\tau \, \mathbf{K}(\tau) \cdot \mathbf{P}(t-\tau) + \mathbf{f}(t) \qquad (3.49)$$

with the random force

$$\mathbf{f}(t) = \exp[i(1 - \mathcal{P})L_{\text{tot}} t]\mathbf{f}(0). \qquad (3.50)$$

Here $\mathbf{f}(0) = i(1 - \mathcal{P})L_{\text{tot}}\mathbf{P} = iL_{\text{tot}}\mathbf{P} = iL_1\mathbf{P} = \mathbf{F}$. The elements of the memory matrix are given by

$$K_{\alpha\beta}(t) = (f_\beta, f_\alpha(t))(P_\alpha, P_\alpha)^{-1} = (Mk_BT)^{-1}\langle f_\beta f_\alpha(t)\rangle. \qquad (3.51)$$

We shall now exploit the identity

$$\exp[i(1 - \mathcal{P})L_{\text{tot}} t] = \exp[iL_0 t] + i\int_0^t d\tau \exp[i(1 - \mathcal{P})L_{\text{tot}}(t-\tau)]$$

$$\times [(1 - \mathcal{P})L_{\text{tot}} - L_0]\exp(iL_0\tau) \qquad (3.52)$$

where

$$(1 - \mathcal{P})L_{\text{tot}} - L_0 = (1 - \mathcal{P})L_1 - \mathcal{P}L_0. \qquad (3.53)$$

As a result, the random force (3.50) can be written as

$$\mathbf{f}(t) = \mathbf{F}(t) + i\int_0^t d\tau \exp[i(1 - \mathcal{P})L_{\text{tot}}(t-\tau)][(1 - \mathcal{P})L_1 - \mathcal{P}L_0]\mathbf{F}(\tau) \qquad (3.54)$$

where $\mathbf{F}(t) = \exp(iL_0 t)\mathbf{F}$ is the force acting on the Brownian particle with a time evolution associated with the dynamics of the particles of the bath. In practice, the latter is sufficiently 'large' that its dynamics is virtually unaffected by the the presence of the particle, and L_0 can be assumed to describe the 'unperturbed' dynamics of the fluid.

Equations (3.49)–(3.54) are still exact. Now we take advantage of the fact that the mass m of the bath particles is much smaller than M. As a consequence, the Brownian particle has an average thermal velocity $\approx (k_BT/M)^{1/2}$ which is a factor $(m/M)^{1/2}$ smaller than that of the molecules of the fluid. This means that the position $\mathbf{R}(t)$ of the heavy particle is slowly varying over the typical bath timescales. Also, after a 'collision' the heavy particle suffers an average momentum change $\approx (mk_BT)^{1/2}$, smaller than its average momentum $\approx (Mk_BT)^{1/2}$ by the same factor $(m/M)^{1/2}$. Thus, even $\mathbf{P}(t)$ can be considered as a slowly varying variable in the same sense as $\mathbf{R}(t)$. These intuitive results can be formalized in the Liouvillians L_0 and L_1 by scaling the momenta $\mathbf{p}_i$ and $\mathbf{P}$ respectively according to $(mk_BT)^{1/2}$ and $(Mk_BT)^{1/2}$, and by adopting units k_BT for the pair potentials ϕ and v. Denoting L_0' and L_1' the scaled Liouvillians, it is readily seen that $L_0 = (k_BT/m)^{1/2}L_0'$ and $L_1 = (k_BT/M)^{1/2}L_1'$. As a consequence, we obtain

$$L_{\text{tot}} = \left(\frac{k_BT}{m}\right)^{1/2}\left[L_0' + \left(\frac{m}{M}\right)^{1/2}L_1'\right] \qquad (3.55)$$

which shows that the effects of L_1 are a factor $(m/M)^{1/2}$ smaller than those of L_0. This confirms that the time variation of $\mathbf{R}(t)$ and $\mathbf{P}(t)$ is much slower than that of the corresponding quantities $\mathbf{r}_i(t)$ and $\mathbf{p}_i(t)$ for the bath particles. Thus, in the limit $m/M \ll 1$ we expect the occurrence of distinctly different timescales.

To see the formal consequences of these results, we go back to eqn (3.54). Since the slowness of the Brownian dynamics implies that the force $\mathbf{F}(t)$ is already a $(m/M)^{1/2}$ effect, in the second term on the right-hand side of (3.54) we may neglect any higher-order contribution in this perturbative parameter. At leading order we find that

$$(1 - \mathcal{P})L_1 \approx O[(m/M)^{1/2}] \qquad (3.56)$$

and

$$i\mathcal{P}L_0\mathbf{F}(\tau) = (Mk_BT)^{-1}\sum_\alpha \langle P_\alpha iL_0\mathbf{F}(\tau)\rangle P_\alpha$$

$$= (Mk_BT)^{-1}\sum_\alpha [\langle P_\alpha iL_0\mathbf{F}(\tau)\rangle_0 P_\alpha + O(m/M)] \qquad (3.57)$$

where the symbol $\langle\cdots\rangle_0$ denotes a statistical average performed with respect to the dynamical variables of the fluid. Now, $\langle P_\alpha L_0\mathbf{F}(\tau)\rangle_0 = \langle L_0 P_\alpha\mathbf{F}(\tau)\rangle_0 = 0$ since L_0 acts only on the bath variables. As a result, in (3.54) the entire contribution of the term with the integral is of higher order in m/M, and we may write that

$$\mathbf{f}(t) = \mathbf{F}(t)\{1 + O[(m/M)^{1/2}]\} \approx \mathbf{F}(t) \qquad (3.58)$$

Inserting this results into eqn (3.51) for the memory matrix, and consistently replacing the exact statistical average with the one taken with respect to the bath variables, we find that

$$K_{\alpha\beta}(t) \approx (Mk_BT)^{-1}\langle F_\beta(0)F_\alpha(t)\rangle_0$$

$$= (Mk_BT)^{-1}\langle F_\alpha(0)F_\alpha(t)\rangle_0 \delta_{\alpha,\beta} \qquad (3.59)$$

where in the last step we have exploited the isotropy of the fluid. Note that, as a result of the perturbative treatment, the elements $K_{\alpha\beta}(t)$ are expressed in terms of ordinary time correlation functions associated with the 'fast' dynamics of the bath. Since $\mathbf{P}(t - \tau) = \mathbf{P}(t) + O[(m/M)^{1/2}]$, in the limit $m/M \to 0$ any memory effect in eqn (3.49) disappears and the Markovian approximation (3.23) becomes exact. Then eqn (3.49) can be written as

$$\dot{\mathbf{P}}(t) = -\Gamma\mathbf{P}(t) + \mathbf{F}(t) \qquad (3.60)$$

where

$$\Gamma \equiv (3Mk_B T)^{-1} \int_0^\infty d\tau \langle \mathbf{F}(0) \cdot \mathbf{F}(t) \rangle_0 \tag{3.61}$$

with the upper integration limit extended to infinity because of the rapid decay of $\mathbf{K}(t)$ over the timescale of the heavy particle. After its proposer, eqn (3.60) is referred to as the 'ordinary' *Langevin equation* for Brownian motion. The presence of the bath is seen to be 'felt' by the Brownian particle both directly through the rapidly varying fluctuating force $\mathbf{F}(t)$ and by the 'viscous' term $-\Gamma \mathbf{P}(t)$ which damps the motion. Equation (3.61) shows that the two effects have ultimately the same microscopic origin (a result usually referred to as the *fluctuation-dissipation theorem*). As a matter of fact, a more general statement of the same interrelation has already been met in Section 3.1 for non-Markovian situations (cf. eqns (3.18) and (3.19)).

Coming back to the Langevin eqn (3.60), as in Section 3.1 we may now exploit the orthogonality of $\mathbf{f}(t) \approx \mathbf{F}(t)$ to the momentum $\mathbf{P}$ to obtain a differential equation for the dynamic correlations of interest. In particular, the time correlation function of the velocity $\mathbf{V} = \mathbf{P}/M$ of the Brownian particle is readily found to be

$$\langle \mathbf{V}(0) \cdot \mathbf{V}(t) \rangle = (3k_B T/M) \exp(-\Gamma|t|). \tag{3.62}$$

Recalling eqn (1.57), this result can be used to obtain the mean square displacement $\delta R^2(t)$ of the Brownian particle:

$$\delta R^2(t) = 2 \int_0^t d\tau (t - \tau) \langle \mathbf{V}(0) \cdot \mathbf{V}(\tau) \rangle$$

$$= (6k_B T/M\Gamma^2)\{\Gamma t - [1 - \exp(-\Gamma t)]\}. \tag{3.63}$$

At short times $t \ll 1/\Gamma$, eqn (3.63) yields the result appropriate for free particles, $\delta R^2(t) = (3k_B T/M)t^2$. In the opposite limit $t \gg 1/\Gamma$, the mean square displacement is seen to increase linearly with time (cf. eqn (1.66)):

$$\delta R^2(t) \to 6Dt \tag{3.64}$$

with a 'diffusion coefficient'

$$D = \tfrac{1}{3} \int_0^\infty d\tau \langle \mathbf{V}(0) \cdot \mathbf{V}(\tau) \rangle = k_B T/M\Gamma. \tag{3.65}$$

These long-time results were established in 1905 by Einstein using a different approach. The irregular motion of the pollen particle observed by Brown are in fact associated with this diffusive regime: as a result of the innumerable 'collisions' with the molecules of the fluid (accounted for by $\mathbf{F}(t)$), the pollen particle performs a 'random walk' with a mean square displacement given by eqn (3.64).

3.3 MEMORY FUNCTIONS AT WORK: THE VELOCITY AUTOCORRELATION FUNCTION

The previous microscopic theory for Brownian motion relies heavily on a clearcut separation of timescales brought about by the smallness of the ratio m/M. It is therefore expected that such a perturbative framework falls into ruins when we deal with a monatomic fluid in which all the particles have the same mass. Indeed, the data reported in Figure 1.8 for the velocity autocorrelation function in two typical simple liquids show evident discrepancies with respect to the exponential decay predicted by eqn (3.62), which clearly cannot account for the 'cage effect' discussed in Section 1.4.3.

In reality, for a fluid made of particles with the same mass the situation is better than one would expect from the breakdown of the previous perturbative criterion. After all, the Markovian approximation (3.23) only implies the existence of two distinctly different timescales, with the shorter one associated with the decay of the memory function. The separation in timescales may actually occur for several physical reasons, the Brownian criterion $m/M \ll 1$ being only a particularly simple example. In this section we shall discuss a 'heuristic' model which qualitatively accounts for the main features of the velocity autocorrelation function of a monatomic fluid at any density. In particular, the model is useful to establish the physical conditions of possible validity of the Markovian approximation even in this 'non-Brownian' case.

Let us start from the memory equation appropriate for the normalized velocity autocorrelation $\psi(t) = \langle \mathbf{v}_i(0) \cdot \mathbf{v}_i(t) \rangle / \langle v_i^2 \rangle$ of an arbitrary particle of the fluid. Because of the isotropy of the system, in such a case we effectively deal with a single-variable set, and no proper frequency term is present in the memory equation. Thus the latter is simply written as

$$\dot{\psi}(t) = -\int_0^t dt'\, K(t')\psi(t - t') = -\int_0^t dt'\, K(t - t')\psi(t'). \tag{3.66}$$

The simplest way to explore the consequences of a non-Markovian memory function is to assume that the decay of $K(t)$ from its initial value occurs through a single relaxation time τ. For mathematical convenience, Berne *et al.* (1966) assumed that the decay was exponential:

$$K(t) = K(0)\exp(-t/\tau). \tag{3.67}$$

Substituting into eqn (3.66) and introducing the auxiliary function $\psi_1(t) \equiv \psi(t) \exp(t/\tau)$, one arrives at an ordinary second-order differential equation

$$\ddot{\psi}_1(t) - (1/\tau)\,\dot{\psi}_1(t) + K(0)\psi_1(t) = 0 \tag{3.68}$$

which is easily solved for $\psi_1(t)$. The corresponding solution for $\psi(t)$ is obtained by exploiting the initial conditions $\psi(0) = 1$ and $\dot{\psi}(0) = 0$. Letting $A^2 = 1 - 4K(0)\tau^2$, we eventually obtain

$$\psi(t) = \exp\left(\frac{-t}{2\tau}\right)\left[\cosh\frac{At}{2\tau} - \frac{1}{A}\sinh\frac{At}{2\tau}\right]. \qquad (3.69)$$

The dynamical features predicted by this simple model for $\psi(t)$ are controlled by the sign of A^2. In this quantity, the initial value of the memory function is given by the normalized second moment of the velocity autocorrelation function (cf. eqn (3.42a)). Hence, after eqn (1.60) we obtain

$$K(0) = \Omega_0^2. \qquad (3.70)$$

Then we have the following cases:

(i) $A^2 > 0$, that is $(1/\tau) > 2\Omega_0$. In such a case, the memory function $K(t)$ decays faster than $\psi(t)$, whose initial decay rate is $\approx \Omega_0/\sqrt{2}$. According to eqn (3.69), this situation yields a monotonic decay of $\psi(t)$. In the extreme case that $(1/\tau) \gg 2\Omega_0$, eqn (3.69) predicts that

$$\psi(t) \approx \exp[-(\Omega_0^2\tau)t]. \qquad (3.71)$$

Since this limiting condition corresponds to an essentially Markovian situation, the result (3.71) is expected.

(ii) $A^2 < 0$, that is $(1/\tau) < 2\Omega_0$. Now the decay rate of $K(t)$ may be comparable with the one appropriate to $\psi(t)$ at short times. In this case the quantity A is imaginary, $A = i[(2\Omega_0\tau)^2 - 1]^{1/2} \equiv ia$, and the result (3.69) can be written as

$$\psi(t) = \exp\left(\frac{-t}{2\tau}\right)\left[\cos\frac{at}{2\tau} + \frac{1}{a}\sin\frac{at}{2\tau}\right] \qquad (3.72)$$

which indicates a damped oscillatory behaviour. In the extreme situation $2\Omega_0\tau \gg 1$ (which corresponds to a memory function nearly constant over the initial timescale of $\psi(t)$), eqn (3.72) predicts for $\psi(t)$ long-lived oscillations at a frequency which essentially coincides with the Einstein frequency Ω_0.

The physics behind the predictions of the model in these two regimes becomes clearer once we realize the meaning of the time τ which rules the decay of the memory function according the ansatz (3.67). The processes affecting the dynamics of $K(t)$ are more transparent at short times, where the comparison between Newton's second law $\dot{\mathbf{v}}(t) = (1/m)\mathbf{F}_i(t)$ and the generalized Langevin equation

$$\dot{\mathbf{v}}_i(t) = \mathbf{f}_i(t) - \int_0^t dt' \, K(t')\mathbf{v}_i(t - t') \qquad (3.73)$$
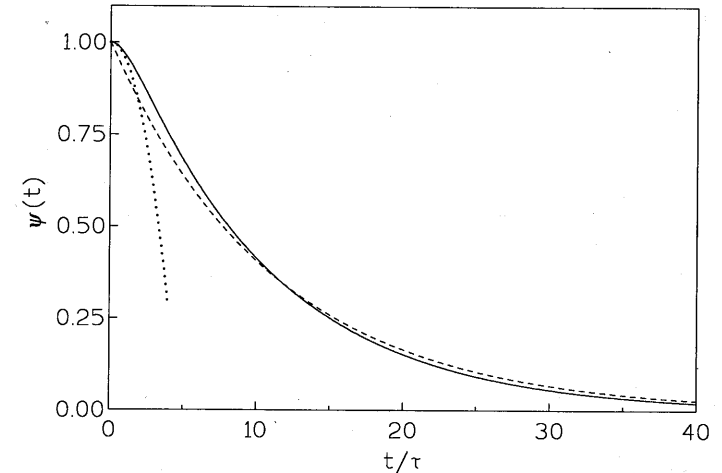
Fig. 3.1 Schematic illustration of the situation occurring for $\psi(t)$ in a low-density fluid ($\Omega_0\tau = 0.3$) according to the model (3.67). The full line denotes the result predicted by eqn (3.69), and the dashed line is the Markovian approximation (3.71). The dotted line refers to the parabolic law (3.74).

shows that the basic information over the initial dynamics of $K(t)$ is provided by the force autocorrelation function $\Xi(t) = \langle \mathbf{F}_i(0) \cdot \mathbf{F}_i(t)\rangle$. On the other hand, the main short-time effects in $\Xi(t)$ are felt during a collisional event, where the interatomic forces are likely to undergo rapid variations. In view of this, it appears natural to interpret τ as the *duration of a 'binary' collision*. Intuitively, we expect that the magnitude of τ depends strongly on the details of the pair potential, and is instead much less affected by macroscopic quantities such as the density of the fluid. This behaviour is to be compared with the one expected for the quantity Ω_0, which gives an approximate measure of the frequency of the collisional events. Even Ω_0 depends on the 'shape' of $\phi(r)$ (cf. (1.63)); however, in contrast with τ, it increases strongly with the density as the occurrence of collisions becomes more and more likely.

As a result, for a relatively *dilute fluid* we expect that Ω_0 is small enough that the condition $1/\tau > 2\Omega_0$ is satisfied. In such a case, initially the velocity autocorrelation function exhibits the usual parabolic decrease

$$\psi(t) = 1 - \tfrac{1}{2}\Omega_0^2 t^2 \qquad (3.74)$$

which is common to all densities (cf. Section 1.4.2). This situation lasts only for a very short time $\approx \tau$, being rapidly taken over by a regime ruled by the exponential decay (3.71), which according to the model should account for virtually all the dynamical features of $\psi(t)$ (see Figure 3.1). Hence, for

not too dense fluids it appears natural to characterize the overall decay of $\psi(t)$ as being ruled by a time constant $(\Omega_0^2\tau)^{-1}$ rather than by the initial decay time $\approx \Omega_0^{-1}$. In this respect, a limiting case is provided by those systems in which the pair potential is approximately modelled as harshly repulsive (e.g. as $\phi(r) \approx r^{-q}$ with $q \gg 1$). In such a case, the spatial range over which the interaction ('collision') takes place becomes smaller and smaller as q increases, and the same occurs for the effective duration τ of the collision. Consequently, the time domain over which the parabolic behaviour (3.74) is observed shrinks more and more as q becomes larger. In the limiting case $q \to \infty$, we deal with a 'hard spheres' system where the binary collisions are instantaneous ($\tau = 0$), and the initial decrease (3.74) is not observed. On the other hand, the quantity Ω_0^2 tends to increase with the exponent q, so that the decay rate $\Omega_0^2\tau$ predicted for $\psi(t)$ is expected to be much less affected by the hardness of the repulsive potential. These intuitive considerations are confirmed by a detailed calculation by Schofield (1974), which shows that as q increases τ vanishes as q^{-1}, whereas Ω_0^2 is dominated by a binary contribution which diverges as q. As a result, the quantity $\Omega_0^2\tau$ remains finite even for hard spheres ($q \to \infty$). In this limiting case, because of the instantaneous character of the collisions the simple model (3.67) predicts that the Markovian result (3.71) is exact at all times. The exponential decay of $\psi(t)$ is in fact consistent with the results of a kinetic approach firstly developed by Enskog for hard sphere fluids (Chapman and Cowling 1970). More precisely, in this theory the decay rate $\Omega_0^2\tau$ is usually written as $\frac{2}{3}\gamma_E$, where the quantity

$$\gamma_E \equiv 4(\pi k_B T/m)^{1/2} n d^2 g(d) \tag{3.75}$$

is referred to as the 'Enskog collision rate'. In eqn (3.75), d is the hard sphere diameter and $g(d)$ represents the pair distribution function at contact, which in terms of $\eta_d \equiv \pi n d^3/6$ is approximately expressed as $g(d) = (1 - \frac{1}{2}\eta_d)/(1 - \eta_d)^3$.

In practice, for low-density fluids the predictions of the Markovian theory are found to be satisfactory. The Enskog results, supplemented by some reasonable choice for the diameter d, have in particular extensively been used by experimentalists to test and/or predict the state dependence of several dynamic properties. In the present context, the relevant quantity is the diffusion coefficient

$$D = \frac{k_B T}{m} \int_0^\infty d\tau\, \psi(\tau) = \frac{k_B T}{m} \left[\int_0^\infty d\tau\, K(\tau) \right]^{-1} \tag{3.76}$$

which following eqn (3.67) is predicted to be

$$D = \frac{K_B T}{m\Omega_0^2\tau}. \tag{3.77}$$

For hard spheres, the corresponding result of Enskog theory reads

$$D_E = \frac{k_B T}{m} \int_0^\infty d\tau \exp\left(-\tfrac{2}{3}\gamma_E t\right) = \frac{3k_B T}{2m\gamma_E}$$

$$= \frac{3}{8\sqrt{\pi}} \left(\frac{k_B T}{m}\right)^{1/2} \frac{1}{nd^2 g(d)}. \tag{3.78}$$

Some defects of the Markovian predictions are already beginning to appear at intermediate number densities (roughly, one half of those typical for liquids near the melting point). As anticipated in Section 1.4.3, the discrepancies are associated with the appearance in $\psi(t)$ of a non-exponential 'tail' $\propto t^{-3/2}$, which occurs at rather long times. Since in this range the decay of $\psi(t)$ has already been quite substantial, the quantitative relevance of the discrepancies is not dramatic and is mostly felt on the diffusion coefficient, which is found to be larger because of the slower decay implied by the $t^{-3/2}$ law. Nevertheless, the occurrence of these flaws is disturbing, and cannot be eliminated even using the more 'refined' model (3.67) rather than the Markovian scheme. Even more embarassing is the fact that the discrepancies are observed even in the hard sphere case (Alder and Wainwright 1970); that is, just where the Markovian results should in principle be 'exact'. These findings provide a first indication that as the density is increased the memory function $K(t)$ is affected by additional dynamical processes, presumably of much longer duration than the fast decay channel associated with 'binary' collisions.

This suspicion is reinforced as we enter the density range appropriate for typical simple liquids. Here, the previous discussion leads us to conclude that the collision rate ($\approx \Omega_0$) has increased so much with n to become eventually comparable with $1/\tau$. In such a situation typical of the liquid state, a particle appears to be always 'colliding' and any physical distinction between the duration of a collision and the interval between two consecutive collisions tends to disappear. Clearly, for such a regime the appropriate prediction of the model is provided by (3.72). Since the Einstein frequency is readily evaluated from eqn (1.47) in terms of $\phi(r)$ and purely structural data, to arrive at quantitative results we need some procedure to estimate the time constant τ. A phenomenological recipe proposed by Berne *et al.* (1966) exploited the result (3.77) of the model and determined τ from the value of D actually observed for the liquid under consideration. With this choice, the theoretical $\psi(t)$ (eqn (3.72)) is obviously forced to have the same area as the 'true' $\psi(t)$ obtained by suitable simulation experiments.

The results of such a procedure for liquid caesium are reported in Fig. 3.2. It is apparent that the short-time features of $\psi(t)$ are well reproduced by the model, which is even able to account qualitatively for the subsequent negative region (cf. Section 1.4.3). However, the model
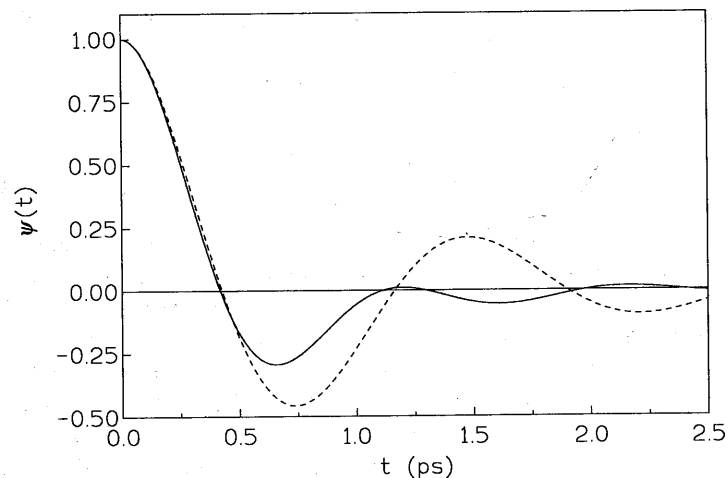
Fig. 3.2 Test of the prediction (3.72) (dashed line) against the simulation data for $\psi(t)$ in liquid Cs at 308 K (full line; cf. Fig. 1.8b). The Einstein frequency $\Omega_0 = 4.384\,ps^{-1}$ has been evaluated according to its definition (1.47). Following the original prescription by Berne *et al.* (1966), the time constant τ has been estimated from the actual diffusion coefficient of the liquid (cf. eqn (3.77)). In the present case, from $D = 2.11 \times 10^{-5}\,cm^2\,s^{-1}$ we find $\tau = 0.472\,ps$.

tends to grossly overestimate both the actual magnitude of this 'cage effect' and the oscillations present in $\psi(t)$ at longer times. The same remarks apply to the 'Lennard–Jones' liquids, where the quality of the comparison is even worse (the model again yields damped oscillations, whereas the actual $\psi(t)$ only shows a long-lasting negative region; cf. Fig. 1.8a). It is of course possible to assume for $K(t)$ another functional shape, at the price of obtaining results for $\psi(t)$ not expressible in simple analytical terms. Several attempts in this sense have been made (see Boon and Yip (1980) for a detailed discussion), but there is no significant improvement as long as the decay of $K(t)$ is assumed to be ruled by a single process with a rate fixed in order to reproduce the correct D.

Still within the simple model (3.67), we may finally decide to evaluate the decay time of $K(t)$ theoretically, by assuming that τ can be deduced from the initial dynamics of the memory function. Strictly speaking, the ansatz (3.67) violates the short-time expansion (3.33), but we may provisionally consider these shortcomings as minor ones, and simply evaluate the decay time τ according to eqn (3.33). The details of such a calculation are reported in Appendix E. For liquid caesium, the resulting $\psi(t)$ is shown in Fig. 3.3 along with the previous simulation data. Although now the comparison appears more favourable as far as the amplitudes are concerned, on the whole the results are still unsatisfactory. The theoretical values of
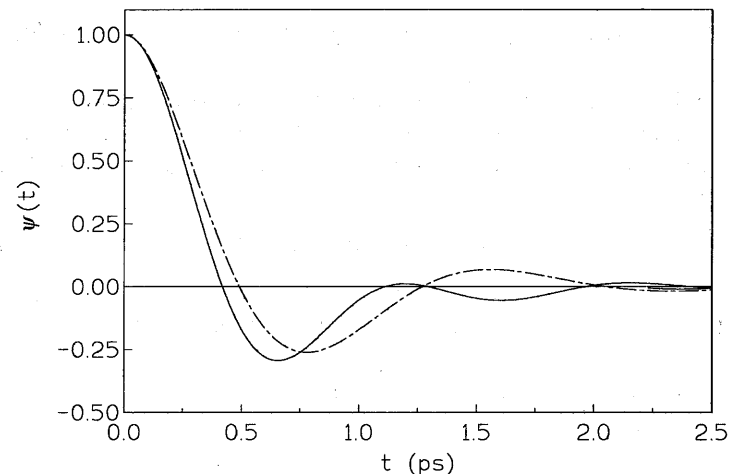
Fig. 3.3 The same comparison as in Fig. 3.2, except that the chain line is the result (3.72) with the time constant $\tau \approx 0.29\,ps$, as deduced from the initial decay of the memory function $K(t)$. The predicted diffusion coefficient $\approx 3.4 \times 10^{-5}\,cm^2\,s^{-1}$.

τ (which now really represents a collision duration) are always found to be considerably shorter than those obtained by the previous phenomenological procedure. As a result, the predicted diffusion coefficients are much larger than their actual values. According to eqn (3.76), this means that the model (3.67) underestimates the area under the memory function. Since now the short-time dynamics of $K(t)$ is essentially correct, we again infer that some long-lasting decay channel has not been taken into account.

On a purely empirical basis, these conclusions are supported by the fact that the simulation data for $\psi(t)$ in Lennard–Jones systems are well reproduced by using the three-parameter memory function (Levesque and Verlet 1970)

$$K(t) = \Omega_0^2 \exp(-a^2 t^2) + \beta t^4 \exp(-\gamma t). \qquad (3.79)$$

The form of (3.79) reproduces the correct initial value $K(0) = \Omega_0^2$ and is chosen in such a way that at short times the leading contribution is provided by the first term on the right-hand tide. As the parameter a is related to the quantity $1/\tau$ ruling the initial decay of $K(t)$, this first term can be interpreted as the previous collisional decay channel. On the other hand, the physical meaning of the second contribution on the right-hand ride of (3.89) cannot be ascertained at the present stage of our analysis. This task will be accomplished in Chapter 5, after the development of a theoretical framework much more general (and elaborate) than the simple model discussed in this section.

3.4 HYDRODYNAMICS AND TRANSPORT PROPERTIES

Let us apply the memory function formalism to an orthogonal set $\{A_\lambda(\mathbf{k})\}$ of dynamical variables which become 'quasi-conserved' in the limit of small wavevectors. As a result, the ordinary equation of motion of $A_\lambda(\mathbf{k}, t)$ can be written as

$$\dot{A}_\lambda(\mathbf{k}, t) = i\mathbf{k} \cdot \mathbf{j}_\lambda(\mathbf{k}, t) \tag{3.80}$$

where $\mathbf{j}_\lambda(\mathbf{k}, t)$ is the 'current' variable appropriate to $A_\lambda(\mathbf{k}, t)$. On the other hand, for $A_\lambda(\mathbf{k}, t)$ we may also write the generalized Langevin equation

$$\dot{A}_\lambda(\mathbf{k}, t) = \sum_\nu \left\{ i\Omega_{\lambda\nu}(k)A_\nu(\mathbf{k}, t) - \int_0^t d\tau\, K_{\lambda\nu}(k, t)A_\nu(\mathbf{k}, t - \tau) \right\} + f_\lambda(\mathbf{k}, t). \tag{3.81}$$

Provided that the elements $(A_\nu(\mathbf{k}), A_\nu(\mathbf{k}))$ are finite as $k \to 0$, the proper frequency matrix elements

$$i\Omega_{\lambda\nu}(k) = (A_\nu(\mathbf{k}), \dot{A}_\lambda(\mathbf{k}))/(A_\nu(\mathbf{k}), A_\nu(\mathbf{k})) \tag{3.82}$$

are seen to vanish as k in the limit $k \to 0$. Then the components of the fluctuating force

$$f_\lambda(\mathbf{k}, t) = \exp[i(1 - \mathcal{P})Lt] \left\{ \dot{A}_\lambda(\mathbf{k}) - \sum_\nu i\Omega_{\lambda\nu}(k)A_\nu(\mathbf{k}) \right\} \tag{3.83}$$

are also proportional to k for small wavevectors. As a result, all the elements of the memory matrix

$$K_{\lambda\nu}(t) = (f_\nu(\mathbf{k}), f_\lambda(\mathbf{k}, t))/(A_\nu(\mathbf{k}), A_\nu(\mathbf{k})) \tag{3.84}$$

vanish as k^2 as $k \to 0$. Noting that (cf. eqns (3.12), (3.13))

$$\exp[i(1 - \mathcal{P})Lt] = \exp(iLt) - \int_0^t d\tau \exp[iLt(t - \tau)]i\mathcal{P}L \exp[i(1 - \mathcal{P})L\tau] \tag{3.85}$$

it is found that

$$f_\lambda(\mathbf{k}, t) = \exp[i(1 - \mathcal{P})Lt]f_\lambda(\mathbf{k})$$

$$= \exp(iLt)f_\lambda(\mathbf{k}) - \sum_\nu \int_0^t d\tau \frac{(A_\nu(\mathbf{k}), iLf_\lambda(\mathbf{k}, t))}{(A_\nu(\mathbf{k}), A_\nu(\mathbf{k}))} A_\nu(\mathbf{k}, t - \tau)$$

$$= \exp(iLt)f_\lambda(\mathbf{k}) - \sum_\nu \int_0^t d\tau \frac{(\dot{A}_\nu(\mathbf{k}), f_\lambda(\mathbf{k}, \tau))}{(A_\nu(\mathbf{k}), A_\nu(\mathbf{k}))} A_\nu(\mathbf{k}, t - \tau) \tag{3.86}$$

where in the last step we have exploited the hermiticity of the Liouvillian. As $k \to 0$, the second contribution on the right-hand side is of the order k^2 and can safely be neglected in comparison with the first one (which is $O(k)$). Therefore for sufficiently small wavevectors the anomalous time propagator ruling the dynamics of $f_\lambda(\mathbf{k}, t)$ may be replaced by the conventional one. It follows immediately that in the limit $k \to 0$ the elements (3.84) of the memory matrix become ordinary time correlation functions. Since all these elements are proportional to k^2, it is convenient to introduce the quantities

$$I_{\lambda\nu}(t) = \lim_{k \to 0} \frac{K_{\lambda\nu}(k, t)}{k^2}. \tag{3.88}$$

In the following subsections we shall make explicit use of all these results to derive by a microscopic framework all the equations of hydrodynamics in its linearized version (cf. Section 1.6.4). In particular, we shall find that the conventional transport coefficients can naturally be expressed as simple time integrals of the quantities $I_{\lambda\nu}(t)$.

3.4.1 Single-particle motion

As already remarked in Chapter 1, in the single-particle case we deal with only one quasi-conserved variable, the self density of a tagged particle density $n_{s,i}(\mathbf{k}) = \exp(i\mathbf{k} \cdot \mathbf{r}_i)$. The dynamics of this variable is ruled by the equation of motion

$$\dot{n}_{s,i}(\mathbf{k}, t) = i\mathbf{k} \cdot \mathbf{j}_{s,i}(\mathbf{k}, t) \tag{3.88}$$

where $\mathbf{j}_{s,i}(\mathbf{k}, t) \equiv \mathbf{v}_i(t) \exp[i\mathbf{k} \cdot \mathbf{r}_i(t)]$ is the 'current' associated with the ith particle at the wavevector $\mathbf{k}$. We are ultimately interested in writing a memory equation for the self intermediate scattering function $F_s(k, t) = \langle n_{s,i}^*(\mathbf{k}, 0)\, n_{s,i}(\mathbf{k}, t) \rangle$. This is easily done by introducing a projection operator over $n_{s,i}(\mathbf{k}, 0) = n_{s,i}(\mathbf{k})$,

$$\mathcal{P} = (n_{s,i}(\mathbf{k}), \ldots)(n_{s,i}(\mathbf{k}), n_{s,i}(\mathbf{k}))^{-1}n_{s,i}(\mathbf{k}) = \langle n_{s,i}^*(\mathbf{k}) \ldots \rangle n_{s,i}(\mathbf{k}) \tag{3.89}$$

and repeating all the steps seen in the general treatment of Section 3.1. Since there is no proper frequency case in the single-variable case, the memory equation for $F_s(k, t)$ is simply written as

$$\dot{F}_s(k, t) = -\int_0^t d\tau\, K_s(k, \tau)F_s(k, t - \tau). \tag{3.90}$$

Here the memory function $K_s(k, t)$ reads ($\hat{\mathbf{k}} \equiv \mathbf{k}/k$):

$$K_s(k,t) = \langle [\dot{n}_{s,i}(\mathbf{k})]^* \exp[i(1-\mathcal{P})Lt] \dot{n}_{s,i}(\mathbf{k}) \rangle$$

$$= k^2 \langle [\hat{\mathbf{k}} \cdot \mathbf{j}_{s,i}(\mathbf{k})]^* \exp[i(1-\mathcal{P})Lt] \hat{\mathbf{k}} \cdot \mathbf{j}_{s,i}(\mathbf{k}) \rangle$$

$$\equiv k^2 D(k,t). \tag{3.91}$$

The Laplace-transformed version of eqn (3.90) is

$$\tilde{F}_s(k,z) = [z + \tilde{K}_s(k,z)]^{-1} = [z + k^2 \tilde{D}(k,z)]^{-1}. \tag{3.92}$$

All these results are valid for arbitrary wavevectors. Consider now the case $k \to 0$, in which the dynamics of the fluid is probed over an essentially macroscopic length scale. The quasi-conserved character of $n_{s,i}(\mathbf{k},t)$ in this limit has two important consequences:

(i) The memory function $K_s(k,t)$ can be evaluated at the lowest non-vanishing order; that is, up to terms $O(k^2)$. This implies that the quantity $D(k,t)$ can be evaluated by setting $k=0$ everywhere. For consistency, we must also replace $\exp[i(1-\mathcal{P})Lt]$ with $\exp(iLt)$, since we have seen that the difference between the two propagators is of higher order in k. As a result

$$K_{s,i}(k,t) = k^2 \langle (\hat{k} \cdot \mathbf{v}_i) \exp(iLt) (\hat{k} \cdot \mathbf{v}_i) \rangle$$

$$= k^2 \langle v_{i,z}(0) v_{i,z}(t) \rangle \tag{3.93}$$

where, without any loss in generality, the direction of the wavevector $\mathbf{k}$ has been chosen along the z-axis. Thus, as $k \to 0$ the quantity $D(k,t)$ approaches the ordinary velocity autocorrelation function.

(ii) Whereas $F_s(k,t)$ becomes a slowly varying function of time as $k \to 0$, the decay rate of $K_s(k,t)$ remains finite even in this limit at a value $\langle \dot{v}_{i,z}^2 \rangle / \langle v_{i,z}^2 \rangle = \Omega_0^2$. Ultimately, we approach a typical Markovian situation where

$$\dot{F}_s(k \to 0, t) = -k^2 \int_0^\infty d\tau\, D(k \to 0, \tau)\, F_s(k \to 0, t). \tag{3.94}$$

Here

$$D = \int_0^\infty d\tau\, D(k \to 0, \tau) = \int_0^\infty d\tau\, \langle v_{i,z}(0) v_{i,z}(\tau) \rangle \tag{3.95}$$

is the *diffusion coefficient*. In the Laplace domain, the Markovian limit corresponds to approximate in (3.92) the 'generalized diffusion coefficient' $\tilde{D}(k,z)$ with the constant $\tilde{D}(k \to 0, z = 0) = D$.

As a result, in the case of small wavevectors and long times from eqn (3.95) we obtain

$$F_s(k,t) = \exp(-Dk^2 |t|) \tag{3.96}$$

which coincides with the previously quoted result (1.160) obtained from ordinary continuum hydrodynamics. As is clear from the derivation, the $k \to 0$ limit should be taken first. Besides having the merit of providing a microscopic 'Green-Kubo' expression for the diffusion coefficient, the present framework is able to establish the conditions $k \ll \Omega_0 (k_B T/m)^{-1/2}$ and $t \gg 1/\Omega_0$ as broad criteria for the validity of the result (3.96), both in the wavevector and in the time domain.

3.4.2 Transverse current

Turning our attention to the quasi-conserved collective variables, we must in principle consider a five-component set comprising the density fluctuations $\hat{n}(\mathbf{k})$, the vector current $\mathbf{j}(\mathbf{k})$ (three components) and the energy fluctuations $\hat{e}(\mathbf{k})$. However, from the microscopic equations of motion (1.175)–(1.179) it is immediately seen that the variable $\hat{n}(\mathbf{k},t)$ is directly coupled only with the component of $\mathbf{j}(\mathbf{k},t)$ directed along $\mathbf{k}$ (longitudinal current). For isotropy arguments, the same is true even for the variable $\hat{e}(\mathbf{k},t)$ at sufficiently small wavevectors (cf. the expression (1.182) of the microscopic energy current). As a result, a convenient 'choice' of variables for dealing with the hydrodynamic regime is made by splitting the original five-component set into two separate subsets, the first of which comprises the three variables $\hat{n}(\mathbf{k})$, $j_L(\mathbf{k})$ and $\hat{e}(\mathbf{k})$ and the second the two components of the current perpendicular to $\mathbf{k}$ (transverse currents). As far as the latter are concerned, because of the isotropy of the system the final results should be the same for the two components. Again choosing $\mathbf{k}$ along the z-axis, in this subsection we shall consider the transverse current component

$$j_x(\mathbf{k},t) = \sum_i v_{i,x}(t) \exp[i\mathbf{k} \cdot \mathbf{r}_i(t)] \tag{3.97}$$

whose equation of motion can be written as (cf. eqn (1.176))

$$\frac{dj_x(\mathbf{k},t)}{dt} = i\frac{k}{m} \sigma^{zx}(\mathbf{k},t) \tag{3.98}$$

where

$$\sigma^{zx}(\mathbf{k}) = \sum_i \left\{ m v_{i,z} v_{i,x} - \tfrac{1}{2} \sum_{j(\neq i)} [z_{ij} x_{ij}/r_{ij}^2] P_k(r_{ij}) \right\} \exp(ikz_i) \tag{3.99}$$

is the zx-component of the microscopic stress tensor (1.178). Now we introduce the projection operator over the single variable $j_x(\mathbf{k})$:

$$\mathcal{P} = (j_x(\mathbf{k}), \dots)(j_x(\mathbf{k}), j_x(\mathbf{k}))^{-1} j_x(\mathbf{k}) = (m/Nk_B T)\langle j_x^*(\mathbf{k}) \dots \rangle j_x(\mathbf{k}) \tag{3.100}$$

and write down in the usual way a memory equation for the transverse current correlation function $C_T(k, t) = (1/N)\langle j_x^*(\mathbf{k}, 0) j_x(\mathbf{k}, t)\rangle$. We finally obtain

$$\dot{C}_T(k, t) = -\int_0^t d\tau K_T(k, \tau) C_T(k, t - \tau). \tag{3.101}$$

Here the memory function $K_T(k, t)$ reads

$$K_T(k, t) = \langle [\dot{j}_x(\mathbf{k})]^* \exp[i(1 - \mathscr{P})Lt] \dot{j}_x(\mathbf{k})\rangle \langle [j_x(\mathbf{k})]^* j_x(\mathbf{k})\rangle^{-1}$$

$$= \frac{k^2}{Nmk_BT} \langle [\sigma^{zx}(\mathbf{k})]^* \exp[i(1 - \mathscr{P})Lt] \sigma^{zx}(\mathbf{k})\rangle$$

$$\equiv \frac{k^2}{nm} \eta(k, t) \tag{3.102}$$

where the last step is a mere definition of the quantity $\eta(k, t)$. Note that, similarly to the previous quantity $D(k, t)$, $\eta(k, t)$ is not an ordinary time correlation function because of the presence of the anomalous propagator. This implies, for example, that in general $D(k, t)$ and $\eta(k, t)$ cannot be *directly* determined by suitable computer simulation techniques.

The situation changes when we limit ourselves to wavevectors $k \to 0$. Since eqns (3.101) and (3.102) have a formal structure entirely analogous to the previous results (3.90),(3.91), for $k \to 0$ we may repeat all the simplifying arguments seen in the single-particle case. In particular, for sufficiently small wavevectors the memory function $K_T(k, t)$ can be expressed as

$$K_T(k, t) = \frac{k^2}{Nmk_BT} \langle \sigma^{zx} \exp(iLt) \sigma^{zx}\rangle$$

$$= \frac{k^2}{mk_BT} \frac{1}{N} \langle \sigma^{zx}(0) \sigma^{zx}(t)\rangle \tag{3.103}$$

where

$$\sigma^{zx} \equiv \sigma^{zx}(\mathbf{k} = 0) = \sum_i \left[m v_{i,z} v_{i,x} - \frac{1}{2} \sum_{j(\neq i)} (z_{ij} x_{ij}/r_{ij}) \phi'(r_{ij}) \right]. \tag{3.104}$$

Clearly $\sigma^{zx} = \sigma^{xz}$. Moreover, because of the inherent isotropy of the fluid, the (now ordinary) time autocorrelation function $S_{zx}(t) \equiv (1/N) \langle \sigma^{zx}(0) \sigma^{zx}(t)\rangle$ is independent of the particular combination (zx) of the Cartesian indexes, which can equivalently be replaced by (xy) or (yz). Then the quantity

$$S_T(t) \equiv S_{zx}(t) = S_{xy}(t) = S_{yz}(t) = (k_BT/n)\eta(k \to 0, t) \tag{3.105}$$

is *tout court* referred to as the *transverse* (or *shear*) *stress autocorrelation function*. Since they only differ by a factor (k_BT/n), the same name is frequently used even for the quantity

$$\eta(t) \equiv \eta(k \to 0, t) = (k_BTV)^{-1}\langle \sigma^{zx}(0)\sigma^{zx}(t)\rangle. \tag{3.106}$$

Even in this case, the marked slowing down of $C_T(k, t)$ as $k \to 0$ implies that in this limit we eventually reach a Markovian situation. Consequently, eqn (3.101) simplifies to

$$\dot{C}_T(k \to 0, t) = -(k^2/nm)\left[\int_0^\infty d\tau \eta(k \to 0, \tau)\right] C_T(k \to 0, t) \tag{3.107}$$

where the square-bracketed factor has the typical Green–Kubo form of a transport property. Indeed, comparing the solution of (3.107) with the hydrodynamic result (1.163), this quantity is identified with the ordinary *shear viscosity coefficient* η. Thus we have

$$C_T(k \to 0, t) = \frac{k_BT}{m} \exp\left(-k^2 \frac{\eta}{nm} |t|\right) \tag{3.108}$$

where

$$\eta = \int_0^\infty d\tau \eta(\tau) = \frac{1}{k_BTV} \int_0^\infty d\tau \langle \sigma^{zx}(0)\sigma^{zx}(\tau)\rangle. \tag{3.109}$$

From eqn (3.108) we deduce that for $k \to 0$

$$\tilde{C}_T(k, z) = \frac{k_BT}{m} \left[z + \frac{\eta}{nm} k^2\right]^{-1} \tag{3.110}$$

whereas the corresponding transverse current spectrum $C_T(k, \omega) = (1/\pi) \text{Re}[\tilde{C}_T(k, z = i\omega)]$ is a Lorentzian:

$$C_T(k, \omega) = \frac{k_BT}{m\pi} \frac{(\eta/nm)k^2}{\omega^2 + [(\eta/nm)k^2]^2}. \tag{3.111}$$

Note that at arbitrary wavevectors the Laplace transform of (3.101) can be written in the form

$$\frac{\tilde{C}_T(k, z)}{k_BT/m} = \frac{1}{z + \tilde{K}_T(k, z)} = \frac{1}{z + (k^2/nm)\tilde{\eta}(k, z)}. \tag{3.112}$$

From this result we see that the features of the spectrum $C_T(k, \omega)$ outside the $k \to 0$ Lorentzian regime are controlled by the (generally complex) quantity $\tilde{\eta}(k, z = i\omega)$, which can formally be interpreted as a wavevector-

and frequency-dependent shear viscosity coefficient. These kinds of arguments, which even at finite wavevectors insist on expressions formally similar to those valid for $k \to 0$, are at the basis of the so-called 'generalized hydrodynamics' approaches (see Chapter 6).

3.4.3 Density fluctuations

As remarked in the previous subsection, the three collective variables $\hat{n}(\mathbf{k})$, $j_L(\mathbf{k})$ and $\hat{e}(\mathbf{k})$ are to be considered together in a separate subset of quasi-conserved variables. The algebraic manipulations are consequently expected to be more involved than in the previous single-variable examples. It is therefore convenient to deal with an orthogonal set $\{A_1(\mathbf{k}), A_2(\mathbf{k}), A_3(\mathbf{k})\}$, where the scalar product $(A_\lambda(\mathbf{k}), A_\nu(\mathbf{k}))$ vanishes unless $\lambda = \nu$. It is readily seen that $j_L(\mathbf{k})$ is orthogonal to both $\hat{n}(\mathbf{k})$ and $\hat{e}(\mathbf{k})$ because of its different symmetry under time reversal. On the other hand, $\hat{n}(\mathbf{k})$ and $\hat{e}(\mathbf{k})$ are not orthogonal, and it is advantageous to replace $\hat{e}(\mathbf{k})$ with the new variable

$$\hat{\varepsilon}(\mathbf{k}) \equiv \hat{e}(\mathbf{k}) - \frac{(\hat{n}(\mathbf{k}), \hat{e}(\mathbf{k}))}{(\hat{n}(\mathbf{k}), \hat{n}(\mathbf{k}))} \hat{n}(\mathbf{k}). \tag{3.113}$$

By this definition, $(\hat{n}(\mathbf{k}), \hat{\varepsilon}(\mathbf{k})) = 0$. Hence, a convenient orthogonal set is built with the following quasi-conserved variables

$$A_1(\mathbf{k}) = \hat{n}(\mathbf{k}) \qquad A_2(\mathbf{k}) = j_L(\mathbf{k}) \qquad A_3(\mathbf{k}) = \hat{\varepsilon}(\mathbf{k}) \tag{3.114}$$

With this choice, we introduce a projection operator over the variables of the set (cf. eqn (3.8)):

$$\mathcal{P} = \sum_\nu \frac{(A_\nu(\mathbf{k}), \ldots)}{(A_\nu(\mathbf{k}), A_\nu(\mathbf{k}))} A_\nu(\mathbf{k}). \tag{3.115}$$

Here

$$(A_1(\mathbf{k}), A_1(\mathbf{k})) = \langle \hat{n}^*(\mathbf{k}) \hat{n}(\mathbf{k}) \rangle = NS(k), \tag{3.116}$$

$$(A_2(\mathbf{k}), A_2(\mathbf{k})) = \langle j_L^*(\mathbf{k}) j_L(\mathbf{k}) \rangle = Nk_BT/m, \tag{3.117}$$

$$(A_3(\mathbf{k}), A_3(\mathbf{k})) = \langle \hat{\varepsilon}^*(\mathbf{k}) \hat{\varepsilon}(\mathbf{k}) \rangle$$

$$= \langle \hat{e}^*(\mathbf{k}) \hat{e}(\mathbf{k}) \rangle - \langle \hat{n}^*(\mathbf{k}) \hat{e}(\mathbf{k}) \rangle / NS(k). \tag{3.118}$$

Recalling (1.175)–(1.177) and choosing $\mathbf{k}$ along the z-axis, the microscopic equations of motion of the three variables read

$$\frac{d\hat{n}(\mathbf{k}, t)}{dt} = ikj_L(\mathbf{k}, t), \tag{3.119}$$

$$\frac{dj_L(\mathbf{k}, t)}{dt} = \frac{ik}{m} \sigma^{zz}(\mathbf{k}, t), \tag{3.120}$$

$$\frac{d\hat{e}(\mathbf{k}, t)}{dt} = ik \left\{ q_z(\mathbf{k}, t) - \left[\frac{\langle \hat{n}^*(\mathbf{k}) \hat{e}(\mathbf{k}) \rangle}{NS(k)} \right] j_L(\mathbf{k}, t) \right\}. \tag{3.121}$$

With all these ingredients, for each component $A_\lambda(\mathbf{k})$ of the set it is now possible to write down a generalized Langevin equation of the form (3.81). Here all the diagonal elements of the proper frequency matrix (3.82) vanish because $A_\lambda(\mathbf{k})$ and $\dot{A}_\lambda(\mathbf{k})$ have opposite parities under time reversal. On the other hand, the non-diagonal elements $\Omega_{\lambda\nu}(\mathbf{k})$ are at least proportional to k in view of the quasi-conserved character of the variables. In particular, after some straightforward calculations we obtain

$$i\Omega_{12}(k) = \frac{\langle j_L^*(\mathbf{k}) \hat{n}(\mathbf{k}) \rangle}{\langle j_L^*(\mathbf{k}) j_L(\mathbf{k}) \rangle} = ik, \tag{3.122}$$

$$i\Omega_{21}(k) = \frac{\langle \hat{n}^*(\mathbf{k}) \dot{j}_L(\mathbf{k}) \rangle}{\langle \hat{n}^*(\mathbf{k}) \hat{n}(\mathbf{k}) \rangle} = \frac{-\langle \dot{\hat{n}}^*(\mathbf{k}) j_L(\mathbf{k}) \rangle}{NS(k)} = \frac{ikk_BT}{mS(k)}, \tag{3.123}$$

$$i\Omega_{13}(k) = i\Omega_{31}(k) = 0, \tag{3.124}$$

$$i\Omega_{23}(k) = \frac{\langle \hat{\varepsilon}^*(\mathbf{k}) \dot{j}_L(\mathbf{k}) \rangle}{\langle \hat{\varepsilon}^*(\mathbf{k}) \hat{\varepsilon}(\mathbf{k}) \rangle} = ik \frac{a(k)}{m\langle \hat{\varepsilon}^*(\mathbf{k}) \hat{\varepsilon}(\mathbf{k}) \rangle}, \tag{3.125}$$

$$i\Omega_{32}(k) = \frac{\langle j_L^*(\mathbf{k}) \dot{\hat{\varepsilon}}(\mathbf{k}) \rangle}{\langle j_L^*(\mathbf{k}) j_L(\mathbf{k}) \rangle} = \frac{-\langle \dot{j}_L^*(\mathbf{k}) \hat{\varepsilon}(\mathbf{k}) \rangle}{Nk_BT/m} = \frac{ika^*(k)}{Nk_BT}, \tag{3.126}$$

where

$$a(k) \equiv \langle \hat{e}^*(\mathbf{k}) \sigma^{zz}(\mathbf{k}) \rangle - [k_BT/S(k)] \langle \hat{e}^*(\mathbf{k}) \hat{n}(\mathbf{k}) \rangle. \tag{3.127}$$

The components $f_\lambda(\mathbf{k})$ of the random force at $t = 0$ follow from eqn (3.83). Exploiting eqns (3.129)–(3.126) we find

$$f_1(\mathbf{k}) = 0, \tag{3.128}$$

$$f_2(\mathbf{k}) = i(k/m) \left\{ \sigma^{zz}(\mathbf{k}) - \frac{k_BT}{S(k)} \hat{n}(\mathbf{k}) - \frac{a(k)}{\langle \hat{\varepsilon}^*(\mathbf{k}) \hat{\varepsilon}(\mathbf{k}) \rangle} \hat{\varepsilon}(\mathbf{k}) \right\}$$

$$\equiv i(k/m)(\sigma')^{zz}(\mathbf{k}), \tag{3.129}$$

$$f_3(\mathbf{k}) = ik[q_z(\mathbf{k}) - (Nk_BT)^{-1}\langle \hat{e}^*(\mathbf{k}) \sigma^{zz}(\mathbf{k}) \rangle^* j_L(\mathbf{k})]$$

$$\equiv ik(q')_z(\mathbf{k}). \tag{3.130}$$

As a result, the non-vanishing elements of the memory matrix (3.84) read

$$K_{22}(k, t) = (m/Nk_BT)\langle f_2^*(\mathbf{k}) \exp[i(1 - \mathcal{P})Lt]f_2(\mathbf{k}) \rangle, \tag{3.131}$$

$$K_{23}(k, t) = \langle \hat{\varepsilon}^*(\mathbf{k})\hat{\varepsilon}(\mathbf{k}) \rangle^{-1}\langle f_3^*(\mathbf{k}) \exp[i(1 - \mathcal{P})Lt]f_2(\mathbf{k}) \rangle, \tag{3.132}$$

$$K_{32}(k, t) = (m/Nk_BT)\langle f_2^*(\mathbf{k}) \exp[i(1 - \mathcal{P})Lt]f_3(\mathbf{k}) \rangle, \tag{3.133}$$

$$K_{33}(k, t) = \langle \hat{\varepsilon}^*(\mathbf{k})\hat{\varepsilon}(\mathbf{k}) \rangle^{-1}\langle f_3^*(\mathbf{k}) \exp[i(1 - \mathcal{P})Lt]f_3(\mathbf{k}) \rangle. \tag{3.134}$$

In view of its experimental relevance, we are interested in the intermediate scattering function $F(k, t) = (1/N)\langle \hat{n}^*(k)\,\hat{n}(\mathbf{k}, t)\rangle = (1/N)\langle A_1^*(\mathbf{k})\,A_1(\mathbf{k}, t)\rangle$. To obtain its Laplace transform $\tilde{F}(k, z)$, we multiply by $A_1^*(\mathbf{k})$ the three generalized Langevin equations for $A_1(\mathbf{k}, t)$, $A_2(\mathbf{k}, t)$ and $A_3(\mathbf{k}, t)$, take the average, and perform a Laplace transform. In such a way we arrive at a linear system of three equations which can be readily solved for $\langle A_1^*(\mathbf{k})\,\tilde{A}_1(\mathbf{k}, z)\rangle = N\tilde{F}(k, z)$. Eventually it is found that (Mountain 1976; Lovesey 1987):

$$\frac{\tilde{F}(k, z)}{S(k)} = \left[z + \frac{k^2[k_B T/mS(k)]}{z + \tilde{K}_{22}(k, z) - \dfrac{[i\Omega_{23}(k) - \tilde{K}_{23}(k, z)][i\Omega_{32}(k) - \tilde{K}_{32}(k, z)]}{z + \tilde{K}_{33}(k, z)}} \right]^{-1}.$$

(3.135)

Even though this result is valid for arbitrary wavevectors, the emphasis put on the choice of variables which become quasi-conserved as $k \to 0$ qualifies eqn (3.135) as a typical result of 'generalized hydrodynamics'. In particular, if the wavevector is sufficiently small we may exploit all the limiting results discussed at the beginning of this section. Namely, in the memory functions (3.131)–(3.134) the anomalous propagator is replaced by an ordinary one, and at the same time the results are evaluated at leading order in k^2 (which implies that the fluctuating forces (3.129), (3.130) are taken at the order k). In this respect we may neglect $K_{23}(k, t)$ and $K_{32}(k, t)$, which turn out to be of higher order than k^2 because of the different symmetry of $f_2(\mathbf{k})$ and $f_3(\mathbf{k})$ under time reversal. Finally, as $k \to 0$ the Markovian approximation for the memory functions $K_{22}(k, t)$ and $K_{33}(k, t)$ becomes exact, and in eqn (3.135) the Laplace transforms $\tilde{K}_{22}(k, z)$ and $\tilde{K}_{33}(k, z)$ may be replaced by their values at $z = 0$. Thus the limiting form of eqn (3.135) in the $k = 0$ regime can be written as

$$\frac{\tilde{F}(k \to 0, z)}{S(k \to 0)} = \left[z + \frac{k^2[k_B T/mS(k \to 0)]}{z + k^2 I_{22} + \dfrac{k^2 B}{z + k^2 I_{33}}} \right]^{-1}.$$

(3.136)

Here

$$k^2 B \equiv \Omega_{23}(k \to 0)\Omega_{21}(k \to 0) = k^2 \frac{|a(k = 0)|^2}{Nmk_B T\langle \hat{\varepsilon}^*(k = 0)\,\hat{\varepsilon}(k = 0)\rangle},$$

(3.137)

$$k^2 I_{22} \equiv \tilde{K}_{22}(k \to 0, z = 0)$$
$$= k^2(Nmk_B T)^{-1} \int_0^\infty dt \langle [(\sigma')^{zz}(k = 0)]\exp(iLt)[(\sigma')^{zz}(k = 0)]\rangle,$$

(3.138)

$$k^2 I_{33} \equiv \tilde{K}_{33}(k \to 0, z = 0)$$
$$= k^2[\langle \hat{\varepsilon}^*(\mathbf{k} = 0)\,\hat{\varepsilon}(\mathbf{k} = 0)\rangle]^{-1} \int_0^\infty dt \langle q_z'(\mathbf{k} = 0)\exp(iLt)q_z'(\mathbf{k} = 0)\rangle.$$

(3.139)

Splitting eqn (1.136) into simple fractions, we find that the behaviour of $\tilde{F}(k, z)$ as $k \to 0$ is dominated by three simple poles at

$$z_0 = -\frac{v_T^2}{v_T^2 + B} I_{33} k^2,$$

(3.140)

$$z_\pm = \pm i(v_T^2 + B)^{1/2} - \frac{1}{2}\left[I_{22} + \frac{B}{v_T^2 + B} I_{33} \right] k^2,$$

(3.141)

where we have let

$$v_T^2 = k_B T/mS(0).$$

(3.142)

Since $S(k, \omega) = (1/\pi)\,\mathrm{Re}\,\tilde{F}(k, z = i\omega)$, in the frequency spectrum the imaginary part of a pole corresponds to the position of a peak, whereas the real part determines the halfwidth. Also, since a simple pole is equivalent to a Lorentzian spectrum, we find that as $k \to 0$ $S(k, \omega)$ consists of three Lorentzians, peaked respectively at $\omega = 0$ and $\omega = \pm (v_T^2 + B)^{1/2}$ and with halfwidths $\propto k^2$ whose magnitude is determined by the integrals I_{22} and I_{33}.

This structure is clearly reminiscent of the Rayleigh-Brillouin spectrum (1.170) as obtained in ordinary hydrodynamics. To explore this analogy in detail, we evaluate the quantity B which enters into the predicted position of the inelastic peak. Noting that $\hat{e}(\mathbf{k} \to 0) = \hat{\mathcal{H}} = \mathcal{H} - \langle \mathcal{H} \rangle$, a simple calculation of statistical averages in a canonical ensemble shows that for a variable $A = \sum_i A(\mathbf{r}_i, \mathbf{v}_i)$

$$\langle \hat{e}^*(\mathbf{k} = 0)A \rangle = \langle \hat{\mathcal{H}}A \rangle = -\frac{\partial \langle A \rangle}{\partial \beta} = k_B T^2\left(\frac{\partial \langle A \rangle}{\partial T} \right)_V$$

(3.143)

where the 'constant volume' suffix has been added to make contact with the usual thermodynamic notations. As a consequence,

$$a(k = 0) = k_B T^2\left(\frac{\partial \langle \sigma^{zz}(\mathbf{k} = 0)\rangle}{\partial T} \right)_V = k_B T^2 V\left(\frac{\partial P}{\partial T} \right)_V$$

$$= -k_B T^2 V\left(\frac{\partial P}{\partial V} \right)_T\left(\frac{\partial V}{\partial T} \right)_P$$

(3.144)

where for the pressure P we have used the result $\langle \sigma^{zz}(\mathbf{k} = 0)\rangle = PV$ (cf. eqn (1.180)). Moreover,

$$\langle \hat{\varepsilon}^*(\mathbf{k}=0)\,\hat{\varepsilon}(\mathbf{k}=0)\rangle = \langle \hat{e}^*(\mathbf{k}=0)\mathfrak{K}\rangle = k_B T^2 \left(\frac{\partial\langle\mathfrak{K}\rangle}{\partial T}\right)_V = k_B T^2 N c_V$$
(3.145)

where c_V is the specific heat per particle at constant volume. Introducing the isothermal compressibility χ_T and the isobaric thermal expansion coefficient β_P

$$\chi_T = -\frac{1}{V}\left(\frac{\partial V}{\partial P}\right)_T \qquad \beta_P \equiv \frac{1}{V}\left(\frac{\partial V}{\partial T}\right)_P ,$$
(3.146)

after some algebra we obtain

$$B = \frac{1}{nm\chi_T c_V}\frac{T\beta_P^2}{n\chi_T} = \frac{\gamma-1}{nm\chi_T}$$
(3.147)

where we have exploited the well-known thermodynamic relation

$$\frac{T\beta_P^2}{n\chi_T} = c_P - c_V$$
(3.148)

and introduced the ratio $\gamma = c_P/c_V$ between the specific heats at constant pressure and at constant volume. Recalling the relation (1.15) between $S(0)$ and χ_T, we see that the inelastic peaks in $S(k,\omega)$ are predicted to be at the frequencies

$$\omega(k) = \pm (nm\chi_T)^{-1/2}[1 + (\gamma-1)]^{1/2}k = \pm (\gamma/nm\chi_T)^{1/2}k.$$
(3.149)

The corresponding collective excitation is a longitudinal sound wave, propagating with a velocity

$$v_s = (\gamma/nm\chi_T)^{1/2} = [\gamma k_B T/mS(0)]^{1/2}$$
(3.150)

whose value coincides with the one found by ordinary hydrodynamics (eqn (1.168)). Looking back at eqns (3.136)–(3.137), it is seen that the 'renormalization' of the sound velocity from the isothermal value v_T to the actual adiabatic value v_s is ultimately due to the coupling to energy fluctuations. At the small wavevectors of interest in the present context, these effects are simply proportional to the quantity $(\gamma - 1)$.

3.4.4 Collective transport properties

Although the microscopic derivation of (3.150) is quite instructive, it would not be worthwhile building up a new framework only to derive results already obtainable from ordinary hydrodynamics. In the small-k region, the real advantages of the microscopic approach lie in the ability to provide

detailed Green–Kubo expressions for the transport coefficients, which in the hydrodynamic treatments appear as purely phenomenological parameters. The identification of these coefficients is readily obtained if we compare the results (3.140), (3.141) for the poles

$$z_0 = - (1/\gamma)I_{33}k^2,$$
(3.151)

$$z_\pm = \pm i v_s k - \tfrac{1}{2}\{I_{22} + [(\gamma-1)/\gamma]I_{33}\}k^2,$$
(3.152)

with those obtained at the same order in k by Laplace transforming the hydrodynamic result (1.161), namely

$$(z_0)_{\text{hyd}} = - (\kappa/nc_P)k^2,$$
(3.153)

$$(z_\pm)_{\text{hyd}} = + i v_s k - \tfrac{1}{2}[(\eta_L/nm) + (\gamma-1)(\kappa/nc_P)]k^2.$$
(3.154)

It follows immediately that the thermal conductivity κ and the longitudinal viscosity coefficient η_L are, respectively:

$$\kappa = nc_V I_{33} = (k_B T^2 V)^{-1}\int_0^\infty dt\langle q_z'(\mathbf{k}=0)\exp(iLt)\,q_z'(\mathbf{k}=0)\rangle,$$
(3.155)

$$\eta_L = \tfrac{4}{3}\eta + \eta_V = nmI_{22}$$
$$= (k_B TV)^{-1}\int_0^\infty dt\langle (\sigma')^{zz}(\mathbf{k}=0)\exp(iLt)(\sigma')^{zz}(\mathbf{k}=0)\rangle$$
(3.156)

These results can be further simplified by looking at the detailed microscopic expressions (3.129), (3.130) of the variables $(\sigma')^{zz}(\mathbf{k})$ and $q_z'(\mathbf{k})$. In the latter case, eqn (3.130) shows that $q_z'(\mathbf{k}=0)$ differs from $q_z(\mathbf{k}=0)$ by a term with $j_L(\mathbf{k}=0) = \sum_i v_{i,z}(0)$. This contribution is proportional to the overall momentum of the system in the z-direction, which can always be made to vanish by a suitable choice of the reference frame. As a result, letting $q_z(t) = \exp(iLt)q_z(\mathbf{k}=0)$, the thermal conductivity may also be expressed as

$$\kappa = (k_B T^2 V)^{-1}\int_0^\infty dt\langle q_z(0)q_z(t)\rangle$$
(3.157)

where from eqn (1.182)

$$q_z = \tfrac{1}{2}\sum_i [mv_i^2 + \sum_{j\neq i}\phi(r_{ij})]v_{i,z} - \tfrac{1}{2}\sum_{i,j\neq i}\mathbf{v}_i\cdot\mathbf{r}_{ij}(z_{ij}/r_{ij})\phi'(r_{ij}).$$
(3.158)

The case of the longitudinal viscosity η_L is slightly more delicate. According to (3.129), for $\mathbf{k}=0$ the variable $(\sigma')^{zz}(\mathbf{k})$ has a non-zero average

$\langle(\sigma')^{zz}(\mathbf{k}=0)\rangle = \langle\sigma^{zz}(\mathbf{k}=0)\rangle = PV$. This would lead to the undesirable feature that the Green–Kubo integrand in (3.156) tends to a plateau, with dramatic consequences on η_L. The difficulty stems from the fact that, as it stands, the expression (3.131) of $K_{22}(k,t)$ is not correct. According to the Mori framework, the appropriate expression of this memory function is written as

$$K_{22}(k,t) = (A_2(\mathbf{k}), A_2(\mathbf{k}))^{-1}(f_2(\mathbf{k}), \exp[i(1-\mathcal{P})Lt]f_2(\mathbf{k})).$$
(3.159)

As remarked in Section 3.1, the identification of the scalar product (A, B) with the correlation function $\langle A^*B \rangle$ is correct only if at least one of the variables A, B has a zero average. Otherwise, on the basis of linear response theory the appropriate correspondence is (Mori 1965a)

$$(A, B) = \langle A^*B \rangle - \langle A^* \rangle \langle B \rangle = \langle[A^* - \langle A^* \rangle][B - \langle B \rangle]\rangle \equiv \langle \hat{A}^* \hat{B} \rangle$$
(3.160)

Since it is readily shown that $\langle\exp[i(1-\mathcal{P})Lt]f_2(\mathbf{k})\rangle = \langle f_2(\mathbf{k})\rangle$, the correct expression of $K_{22}(k,t)$ in terms of correlation functions reads

$$K_{22}(k,t) = \langle A_2^*(\mathbf{k})A_2(\mathbf{k})\rangle^{-1} \langle \hat{f}_2^*(\mathbf{k}) \exp[i(1-\mathcal{P})Lt] \hat{f}_2(\mathbf{k})\rangle$$
$$= k^2(Nmk_BT)^{-1} \langle[(\hat{\sigma}')^{zz}(\mathbf{k})]^* \exp[i(1-\mathcal{P})Lt] (\hat{\sigma}')^{zz}(\mathbf{k})\rangle$$
(3.162)

where $(\hat{\sigma}')^{zz}(\mathbf{k}) \equiv (\sigma')^{zz}(\mathbf{k}) - PV\delta_{\mathbf{k},0}$. As a consequence, the correct result for the *longitudinal viscosity coefficient* can be written as

$$\eta_L = (k_BTV)^{-1} \int_0^\infty dt \langle[(\sigma')^{zz}(\mathbf{k}=0) - PV] \exp(iLt)$$
$$[(\sigma')^{zz}(\mathbf{k}=0) - PV]\rangle.$$
(3.162)

Recalling the definition (3.129) of $(\sigma')^{zz}(\mathbf{k})$, it is interesting to note that the *explicit expression* of the Green–Kubo integrand in eqn (3.162) depends in general on the statistical ensemble adopted to evaluate the average. In the simplest case of the microcanonical ensemble normally used in the simulation work, there is no fluctuation both in the number of particles and in the energy; as a result,

$$(\sigma')^{zz}(\mathbf{k}=0) = \sigma^{zz}(\mathbf{k}=0) = \sum_i \left[m(v_{i,z})^2 - \frac{1}{2}\sum_{j\neq i} (z_{ij}^2/r_{ij})\phi'(r_{ij}) \right]$$
(3.163)

(cf. eqn (1.178)). In the case of a canonical ensemble, we must instead keep the term in (3.129) with $\hat{\varepsilon}(\mathbf{k}=0)$, whereas both the contributions with $\hat{n}(\mathbf{k}=0)$ and $\hat{\varepsilon}(\mathbf{k}=0)$ should be retained for a grand-canonical ensemble

(Zwanzig 1965). The final outcome for η should of course be the same in any case.

From eqn (3.162) and the previous result (3.109) for η, it is of course possible to deduce the value of the bulk viscosity coefficient $\eta_V = \eta_L - \frac{4}{3}\eta$. It is, however, instructive to discuss an independent derivation, which starts from the consideration of the general correlation function of the stress tensor

$$S_{\alpha\beta,\gamma\delta}(t) = (1/N)\langle\sigma^{\alpha\beta}(0)\sigma^{\gamma\delta}(t)\rangle$$
(3.164)

where $\sigma^{\alpha\beta} = \sigma^{\alpha\beta}(\mathbf{k}=0)$. According to all the possible combinations of the indexes $\alpha, \beta, \gamma, \delta \equiv (x,y,z)$, we have in principle $3^4 = 81$ correlation functions. Exploiting the symmetric character of the stress tensor ($\sigma^{\alpha\beta} = \sigma^{\beta\alpha}$), the actual number of different functions is reduced to 36. An aid for the visualization of the latter is provided by the so-called 'Voigt convention' of indexes:

$$\begin{array}{cccccc} xx \to 1 & & yy \to 2 & & zz \to 3 \\ zx \to 4 & & xy \to 5 & & yz \to 6 \end{array}$$
(3.165)

As a result, the 36 functions $S_{\lambda\nu}(t)$ where $\lambda, \nu = 1, \ldots, 6$ can be arranged in a 6×6 square matrix. Because of the stationarity and its even character in time, the matrix $(S_{\lambda\nu}(t))$ is symmetric, and the number of independent functions is decreased to 21. Further reductions are possible only if the Hamiltonian of the system exhibits additional local symmetries. This is always the case in crystals having unit cells with symmetry higher than triclinic. In particular, choosing the axes x, y, z along the cell edges, for cubic lattices it is readily seen that

$$S_{11}(t) = S_{22}(t) = S_{33}(t),$$
(3.166a)

$$S_{12}(t) = S_{13}(t) = S_{23}(t),$$
(3.166b)

$$S_{44}(t) = S_{55}(t) = S_{66}(t),$$
(3.166c)

$$S_{\lambda\nu}(t) = S_{\lambda\lambda}(t)\delta_{\lambda,\nu} \quad (\lambda = 4, 5, 6).$$
(3.166d)

In such a case, the independent quantities are reduced to three, namely $S_{11}(t)$, $S_{12}(t)$, and $S_{44}(t)$. In an isotropic system such as a liquid, a further constraint comes from the fact that the invariance is not restricted to the particular angles of the cubic point group. Requiring that, for example, $S_{11}(t) = S_{xx,xx}(t)$ is unchanged under a rotation by an arbitrary angle around the z-axis, we eventually find that

$$S_{11}(t) = S_{12}(t) + 2S_{44}(t).$$
(3.167)

In the standard theory of elasticity, the initial values $S_{\lambda\nu}(t=0)$ are

actually referred to as the *elastic constants* of the medium, and eqn (3.167) at $t = 0$ is known as the 'Cauchy isotropy condition'.

All the previous symmetry arguments remain unchanged by replacing the tensor components $\sigma^{\alpha\beta}$ with $(\hat{\sigma}')^{\alpha\beta}$, where $(\hat{\sigma}')^{\alpha\alpha} = (\sigma')^{\alpha\alpha} - PV$ and $(\hat{\sigma}')^{\alpha\beta} = \sigma^{\alpha\beta}$ for $\alpha \neq \beta$. Letting $S'_{\alpha\beta,\gamma\delta} \equiv (1/N) \langle (\hat{\sigma}')^{\alpha\beta}(0) (\hat{\sigma}')^{\gamma\delta}(t) \rangle$, consider in an isotropic system the quantity

$$S'(t) \equiv \tfrac{1}{9} \sum_{\alpha\beta} S'_{\alpha\alpha,\beta\beta}(t) = \tfrac{1}{9} \left[\sum_{\alpha} S'_{\alpha\alpha,\alpha\alpha}(t) + 2 \sum_{\alpha,\beta > \alpha} S'_{\alpha\alpha,\beta\beta}(t) \right]$$
$$= \tfrac{1}{3} S'_{11}(t) + \tfrac{2}{3} S'_{12}(t) = S'_{11}(t) - \tfrac{4}{3} S'_{44}(t) \tag{3.168}$$

where in the last step $S'_{12}(t)$ has been eliminated by using the primed version of eqn (3.167). Since from eqns (3.162) and (3.106)

$$\frac{N}{k_B T V} \int_0^\infty dt\, S'_{11}(t) = \eta_L, \tag{3.169}$$

$$\frac{N}{k_B T V} \int_0^\infty dt\, S'_{44}(t) = \eta, \tag{3.170}$$

we deduce that a convenient Green–Kubo representation for the *bulk viscosity coefficient* $\eta_V = \eta_L - \tfrac{4}{3}\eta$ can be written as

$$\eta_V = \frac{N}{k_B T V} \int_0^\infty dt\, S'(t)$$

$$= \frac{N}{k_B T V} \int_0^\infty dt\, \langle [\tfrac{1}{3} \mathrm{Tr}\, \boldsymbol{\sigma}'(0)] [\tfrac{1}{3} \mathrm{Tr}\, \boldsymbol{\sigma}'(t)] \rangle \tag{3.171}$$

where $\mathrm{Tr}\, \boldsymbol{\sigma}' = \sum_\alpha (\sigma')^{\alpha\alpha}$.

Summing up, the Green–Kubo expressions of the transport properties show that a large amount of microscopic information is actually hidden in these few coefficients. The integral character of the relationships seems to indicate that a relatively simple account of the dynamics behind the integrands may be sufficent. However, in several cases both short- and long-time features turn out to be equally important. To be more specific, the presence of a long-lasting 'tail' in a Green–Kubo integrand may have a substantial relevance on the value of the corresponding transport coefficient, even if by itself the tail has a relatively small amplitude. In dense fluids, the simultaneous occurrence of fast and slow decay channels is so frequent to justify an extension of the conventional kinetic approaches to encompass both these dynamical features. This will be the subject of the forthcoming Chapter.

REFERENCES

Alder, B. J. and Wainwright, T. E. (1970). *Phys. Rev. A*, **1**, 18.

Alley, W. B., Alder, B. J., and Yip, S. (1983). *Phys. Rev. A*, **27**, 3174.

Berne, B. J., Boon, J. P., and Rice, S. A. (1966). *J. Chem. Phys.*, **45**, 1086.

Boon, J. P. and Yip, S. (1980). *Molecular hydrodynamics*. McGraw-Hill, New York.

Chapman, S. and Cowling, T. G. (1970). *The mathematical theory of nonuniform gases*. Cambridge University Press, London.

Levesque, D. and Verlet, L. (1970). *Phys. Rev. A*, **2**, 2514.

Lovesey, S. W. (1987). *Theory of neutron scattering from condensed matter*, 3rd edition, Vol. 1. Clarendon Press, Oxford.

Machida, M. and Murase, C. (1973). *Progr. Theor. Phys.*, **50**, 1.

Mori, H. (1965a). *Progr. Theor. Phys.*, **33**, 423.

Mori, H. (1965b). *Progr. Theor. Phys.*, **34**, 399.

Mountain, R. D. (1976). *Adv. Molec. Relaxation Processes*, **9**, 225.

Schofield, P. (1974). In *Molecular motions in liquids* (ed. J. Lascombe), p. 15. D. Reidel, Dordrecht.

Zwanzig, R. (1961). In *Boulder Lectures in Theoretical Physics* (ed. W. E. Brittin, B. W. Downs, and J. Downs), Vol. III, p. 106. Wiley-Interscience, New York.

Zwanzig, R. (1965). *Ann. Rev. Phys. Chem.*, **16**, 67.

4

Generalized kinetic theory

4.1 THE MICROSCOPIC DYNAMICS OF PHASE-SPACE DENSITIES

4.1.1 Phase-space densities and their correlation functions

Up to the early 1970s, a 'kinetic approach' to the time-dependent properties of fluids was synonymous with a framework based on statistical mechanics in which a central role is played by those dynamical events referred to as *uncorrelated binary collisions*. Although the details of these collisional events depend on the specific form of the interatomic potential, in most cases the relevant effects are due to the harsh repulsion prevailing at small separations, often modelled as a 'hard sphere' interaction. As a consequence, a collision may usually be considered as an event strongly localized both in space and time. Because of this character, it seems reasonable to assume that two subsequent collisions are mutually uncorrelated. This assumption is actually one of the cornerstones of the traditional kinetic frameworks since their invention by Boltzmann more than a century ago. If we explore at a deeper qualitative level the physical content of the uncorrelated-collisions assumption, we arrive at the conclusion that this ansatz is indeed justified for dilute fluids, where the collisional events are comparatively rare so that, in a sense, a particle has available an amount of space and time sufficient to 'forget' a collision before the occurrence of another one.

On the other hand, the assumption is expected to be on shaky grounds for dense fluids or liquids, where the collisions are so frequent that they are likely to interfere with each other. The uncorrelation ansatz is clearly equivalent to a loss of memory, or to a 'Markov approximation' in the language of Section 3.1. As a result, for dense fluids the conventional kinetic approach should be critically revisited to allow for the presence of non-Markovian effects. Since the revised framework should ideally encompass all the successful low-density results of the old one, its formal structure is initially phrased in a quite similar way.

The bases for such a *generalized kinetic theory* were set during the 1970s and the early 1980s by several independent workers, who arrived at essentially similar conclusions despite some minor differences and/or

emphasis on particular aspects. For example, the explicit form of many results depends upon the individual choice of dealing with hard-sphere fluids (whose treatment is more rigorous) or with systems characterized by continuous potentials (which are certainly more realistic, but require additional approximations).

In any case, the basic ingredients of any kinetic framework are the dynamical variables known as 'phase-space densities'. If we consider a specified particle at a position $r_i(t)$ and with momentum $p_i(t)$, the *self-phase-space density* is defined as

$$f_{s,i}(\mathbf{rp}; t) \equiv \delta(\mathbf{r} - \mathbf{r}_i(t))\delta(\mathbf{p} - \mathbf{p}_i(t)). \tag{4.1}$$

Its equilibrium average reads

$$\langle f_{s,i}(\mathbf{rp}; t)\rangle = \langle f_{s,i}(\mathbf{rp}; 0)\rangle = (1/V)f_0(p) \tag{4.2}$$

where $\langle \delta(\mathbf{r} - \mathbf{r}_i)\rangle = 1/V$ and

$$\langle \delta(\mathbf{p} - \mathbf{p}_i)\rangle \equiv f_0(p) = (\beta/2\pi m)^{3/2}\exp(-\beta p^2/2m) \tag{4.3}$$

is the normalized Maxwell distribution of momenta. Note that in the thermodynamic limit ($N \to \infty$, $V \to \infty$, with $N/V = n$ finite) $\langle f_{s,i}(\mathbf{rp}; t)\rangle \to 0$. The single-particle density $n_{s,i}(\mathbf{r}, t)$ (cf. eqn (1.27)) is simply the integral of (4.1) over the field momentum $\mathbf{p}$. We shall now introduce the time correlation funtion of $f_{s,i}(\mathbf{rp}; t)$, defined as

$$C_s(\mathbf{rp}, \mathbf{r'p'}; t) = \langle f_{s,i}(\mathbf{r'p'}; t)f_{s,i}(\mathbf{rp}; t)\rangle. \tag{4.4}$$

The homogeneity of the system requires that $C_s(\mathbf{rp}, \mathbf{r'p'}; t)$ depends on the difference $\mathbf{r} - \mathbf{r'}$. In particular, the initial value of (4.4) is

$$C_s(\mathbf{rp}, \mathbf{r'p'}; 0) = (1/V)f_0(p)\delta(\mathbf{r} - \mathbf{r'})\delta(\mathbf{p} - \mathbf{p'}). \tag{4.5}$$

For future purposes, it is also convenient to introduce the space Fourier transform

$$f_{s,i}(\mathbf{k}, \mathbf{p}; t) \equiv \int d\mathbf{r} f_{s,i}(\mathbf{rp}; t)\exp(i\mathbf{k} \cdot \mathbf{r})$$

$$= \exp[i\mathbf{k} \cdot \mathbf{r}_i(t)]\delta(\mathbf{p} - \mathbf{p}_i(t)) \tag{4.6}$$

as well as the correlation function

$$C_s(\mathbf{k}, \mathbf{pp'}; t) \equiv \int d(\mathbf{r} - \mathbf{r'})C_s(\mathbf{rp}, \mathbf{r'p'}; t)\exp[i\mathbf{k} \cdot (\mathbf{r} - \mathbf{r'})]$$

$$= (1/V)\langle f_{s,i}^*(\mathbf{k}, \mathbf{p'}; 0)f_{s,i}(\mathbf{k}, \mathbf{p}; t)\rangle \tag{4.7}$$

where in the last step we have exploited the $\mathbf{k}$-space version of the homogeneity requirement

$$\langle f_{s,i}^*(\mathbf{k}'\,\mathbf{p}';0)f_{s,i}(\mathbf{k},\mathbf{p};t)\rangle = \langle f_{s,i}^*(\mathbf{k},\mathbf{p}';0)f_{s,i}(\mathbf{k},\mathbf{p};t)\rangle \delta_{\mathbf{k},\mathbf{k}'}$$

$$= (8\pi^3/V)\langle f_{s,i}^*(\mathbf{k},\mathbf{p}';0)f_{s,i}(\mathbf{k},\mathbf{p};t)\rangle \delta(\mathbf{k}-\mathbf{k}').$$

(4.8)

Clearly,

$$C_s(\mathbf{k},\mathbf{pp}';0) = (1/V)f_0(p)\delta(\mathbf{p}-\mathbf{p}').$$

(4.9)

Quite similar quantities can be introduced for collective dynamics. Here we define a *phase-space density*

$$f(\mathbf{rp};t) \equiv \sum_i \delta(\mathbf{r}-\mathbf{r}_i(t))\delta(\mathbf{p}-\mathbf{p}_i(t))$$

$$= \sum_i f_{s,i}(\mathbf{rp};t)$$

(4.10)

where

$$\langle f(\mathbf{rp};t)\rangle = \langle f(\mathbf{rp};0)\rangle = nf_0(p).$$

(4.11)

Since now the equilibrium value is finite even in the thermodynamic limit, it is convenient to introduce a phase-space density fluctuation

$$\hat{f}(\mathbf{rp};t) \equiv f(\mathbf{rp};t) - nf_0(p)$$

(4.12)

along with the corresponding time correlation function

$$C(\mathbf{rp},\mathbf{r}'\mathbf{p}';t) \equiv \langle \hat{f}(\mathbf{r}'\mathbf{p}';0)\hat{f}(\mathbf{rp};t)\rangle$$

(4.13)

which is again a function of $\mathbf{r}-\mathbf{r}'$. After the definition (4.10), $C(\mathbf{rp};\mathbf{r}'\mathbf{p}';t)$ comprises a self part $NC_s(\mathbf{rp};\mathbf{r}'\mathbf{p}';t)$ as well as a contribution associated with particle pairs. In particular:

$$C(\mathbf{rp},\mathbf{r}'\mathbf{p}';0) = nf_0(p)\delta(\mathbf{r}-\mathbf{r}')\delta(\mathbf{p}-\mathbf{p}')$$

$$+ n^2[g(|\mathbf{r}-\mathbf{r}'|)-1]f_0(p)f_0(p')$$

(4.14)

where the appearance of the pair distribution function follows from

$$\sum_{i,j\neq i}\langle \delta(\mathbf{r}'-\mathbf{r}_i)\delta(\mathbf{r}-\mathbf{r}_j)\rangle = \sum_{i,j\neq i}\langle \delta(\mathbf{r}'-\mathbf{r}_i)\delta(\mathbf{r}'-\mathbf{r}-\mathbf{r}_{ij})\rangle$$

$$= (1/V)Nng(|\mathbf{r}-\mathbf{r}'|) = n^2g(|\mathbf{r}-\mathbf{r}'|).$$

(4.15)

In analogy with the single-particle case, we may define even here the corresponding quantities in **k**-space, namely

$$\hat{f}(\mathbf{k},\mathbf{p};t) \equiv \int d\mathbf{r}\,\hat{f}(\mathbf{rp};t)\exp(i\mathbf{k}\cdot\mathbf{r})$$

$$= \sum_i \exp[i\mathbf{k}\cdot\mathbf{r}_i(t)]\delta(\mathbf{p}-\mathbf{p}_i(t)) - (2\pi)^3 nf_0(p)f_0(p'),$$

(4.16)

$$C(\mathbf{k},\mathbf{pp}';t) \equiv \int d(\mathbf{r}-\mathbf{r}')C(\mathbf{rp},\mathbf{r}'\mathbf{p}';t)\exp[i\mathbf{k}\cdot(\mathbf{r}-\mathbf{r}')]$$

$$= (1/V)\langle \hat{f}^*(\mathbf{k},\mathbf{p}';0)\hat{f}(\mathbf{k},\mathbf{p};t)\rangle.$$

(4.17)

In particular,

$$C(\mathbf{k},\mathbf{pp}';0) = nf_0(p)\delta(\mathbf{p}-\mathbf{p}') + n[S(k)-1]f_0(p)f_0(p')$$

(4.18)

where we have used the definition (1.14) of the static structure factor. The quantities $C_s(\mathbf{k},\mathbf{pp}';t)$ and $C(\mathbf{k},\mathbf{pp}';t)$ can formally be viewed as matrix elements in the continuum space of the field variables $\mathbf{p}$ and $\mathbf{p}'$. The elements of the corresponding inverse matrices are defined by

$$\int d\mathbf{p}''\,C(\mathbf{k},\mathbf{pp}'';t)C^{-1}(\mathbf{k},\mathbf{p}''\mathbf{p}';t) = \int d\mathbf{p}''\,C^{-1}(\mathbf{k},\mathbf{pp}'';t)C(\mathbf{k},\mathbf{p}''\mathbf{p}';t)$$

$$= \delta(\mathbf{p}-\mathbf{p}')$$

(4.19)

and by a similar equation for C_s. In the following, we shall make use of the quantities $C_s^{-1}(\mathbf{k},\mathbf{pp}';0)$ and $C^{-1}(\mathbf{k},\mathbf{pp}';0)$. In view of (4.19) and of the results (4.9), (4.18), it is readily found that

$$C_s^{-1}(\mathbf{k},\mathbf{pp}';0) = [nf_0(p)]^{-1}\delta(\mathbf{p}-\mathbf{p}')$$

(4.20)

$$C^{-1}(\mathbf{k},\mathbf{pp}';0) = [nf_0(p)]^{-1}\delta(\mathbf{p}-\mathbf{p}') - c(k)$$

(4.21)

where in the structural theories of fluids the quantity $c(k) \equiv (1/n) \times [1-(S(k))^{-1}]$ is referred to as the *direct correlation function* in k-space (Hansen and McDonald 1986).

After this flood of definitions, it is worthwhile to make a short pause to discuss the relevance of these dynamical variables and of the corresponding correlation functions. Although rather heavy in the notations, the phase-space description is a necessity if we wish to understand the basic dynamics of collisional processes without having every time to deal with the different 'details' proper of a particular dynamical variable. At the end, a gratifying consequence of this comprehensive character will be that the time correlations of practical interest can simply be expressed by integrals involving the 'fundamental' correlation functions of the appropriate phase-space densities. For example, the velocity autocorrelation function can be written as

$$\langle \mathbf{v}_i(0) \cdot \mathbf{v}_i(t) \rangle = (1/m^2) \langle \mathbf{p}_i(0) \cdot \mathbf{p}_i(t) \rangle$$

$$= (1/m^2) \int d\mathbf{r} \, d\mathbf{r}' \int d\mathbf{p} \, d\mathbf{p}' \, (\mathbf{p}' \cdot \mathbf{p}) C_s(\mathbf{r}\mathbf{p}, \mathbf{r}'\mathbf{p}'; t)$$

$$= (V/m^2) \int d\mathbf{p} \, d\mathbf{p}' \, (\mathbf{p}' \cdot \mathbf{p}) C_s(\mathbf{k} = 0, \mathbf{p}\mathbf{p}'; t). \qquad (4.22)$$

Similarly, in the collective case the intermediate scattering function and the transverse current correlation function can respectively be expressed as

$$F(k, t) = (1/N) \int d\mathbf{p} \, d\mathbf{p}' \, \langle \hat{f}^*(\mathbf{k}, \mathbf{p}'; 0) \hat{f}(\mathbf{k}, \mathbf{p}; t) \rangle$$

$$= (1/n) \int d\mathbf{p} \, d\mathbf{p}' \, C(\mathbf{k}, \mathbf{p}\mathbf{p}'; t) \qquad (4.23)$$

$$C_T(k, t) = (1/Nm^2) \int d\mathbf{p} \, d\mathbf{p}' \, (p')_x p_x \langle \hat{f}^*(\mathbf{k}, \mathbf{p}'; 0) \hat{f}(\mathbf{k}, \mathbf{p}; t) \rangle$$

$$= (1/nm^2) \int d\mathbf{p} \, d\mathbf{p}' \, (p')_x p_x C(\mathbf{k}, \mathbf{p}\mathbf{p}'; t) \qquad (4.24)$$

where in writing (4.24) we have chosen $\mathbf{k}$ along the z-axis and exploited the result $\int d\mathbf{p} \, p_x f_0(p) = 0$.

The first step to be made in order to understand the events ruling the dynamics of the basic quantities $C_s(\mathbf{k}, \mathbf{p}'; t)$ and $C(\mathbf{k}, \mathbf{p}'; t)$ is clearly to write down their exact equations of motion. As remarked at the beginning of this section, we are particularly interested in exploring physical situations where the uncorrelated-collision approximation becomes suspect. The memory-function framework appears to be the natural approach to assess from the very start the presence and the relevance of non-Markovian effects, as well as to possibly suggest better approximation schemes. The next subsections are consequently devoted to the establishment of such a framework for phase-space variables ('generalized kinetic theory'), as well as to the discussion of important limiting situations which emerge in the course of the analysis.

4.1.2   Generalized kinetic theory: the exact equations of motion

Like any other dynamical variable, both the self-phase-space density $f_{s,i}(\mathbf{k}, \mathbf{p}; t)$ and its collective counterpart $\hat{f}(\mathbf{k}, \mathbf{p}; t)$ satisfy equations of motion of the general form $\dot{f}(t) = \mathrm{i}Lf(t)$, where the Liouvillian (3.2) of the system comprises both a 'free-streaming' part $\sum_i (\mathbf{p}_i/m) \cdot (\partial/\partial \mathbf{r}_i)$ and an 'interaction' contribution which depends on the interatomic potential $\phi(r_{ij})$. For a given wavevector $\mathbf{k}$, we shall now introduce suitable

projection operators over the sets $\{f_{s,i}(\mathbf{k}, \mathbf{p})\} \equiv \{f_{s,i}(\mathbf{k}, \mathbf{p}; t = 0)\}$ and $\{\hat{f}(\mathbf{k}, \mathbf{p})\} \equiv \{\hat{f}(\mathbf{k}, \mathbf{p}; t = 0)\}$ where $\mathbf{p}$ is now a continuous variable. The appropriate generalizations of eqn (3.7) read

$$\mathcal{P}_s \equiv (1/V) \int d\mathbf{p}' \, d\mathbf{p}'' f_{s,i}(\mathbf{k}, \mathbf{p}') \langle f_{s,i}(\mathbf{k}, \mathbf{p}'') \cdots \rangle C_s^{-1}(\mathbf{k}, \mathbf{p}''\mathbf{p}'; t = 0) \qquad (4.25)$$

and

$$\mathcal{P} \equiv (1/V) \int d\mathbf{p}' \, d\mathbf{p}'' \hat{f}(\mathbf{k}, \mathbf{p}') \langle \hat{f}(\mathbf{k}, \mathbf{p}'') \cdots \rangle C^{-1}(\mathbf{k}, \mathbf{p}''\mathbf{p}'; t = 0) \qquad (4.26)$$

where it is readily verified that $\mathcal{P}_s f_{s,i}(\mathbf{k}, \mathbf{p}) = f_{s,i}(\mathbf{k}, \mathbf{p})$ and $\mathcal{P}\hat{f}(\mathbf{k}, \mathbf{p}) = \hat{f}(\mathbf{k}, \mathbf{p})$.

After the usual manipulations of the Mori approach, we arrive at the following memory equations for the two phase-space correlations $C_s(\mathbf{k}, \mathbf{p}'; t)$ and $C(\mathbf{k}, \mathbf{p}'; t)$:

$$\dot{C}_s(\mathbf{k}, \mathbf{p}'; t) = \mathrm{i} \int d\mathbf{p}'' \, \Omega_s(\mathbf{k}; \mathbf{p}'') C_s(\mathbf{k}, \mathbf{p}''\mathbf{p}'; t)$$

$$- \int_0^t d\tau \int d\mathbf{p}'' M_s(\mathbf{k}, \mathbf{p}''; \tau) C_s(\mathbf{k}, \mathbf{p}''\mathbf{p}'; t - \tau), \quad (4.27)$$

$$\dot{C}(\mathbf{k}, \mathbf{p}'; t) = \mathrm{i} \int d\mathbf{p}'' \, \Omega(\mathbf{k}; \mathbf{p}'') C(\mathbf{k}, \mathbf{p}''\mathbf{p}'; t)$$

$$- \int_0^t d\tau \int d\mathbf{p}'' M(\mathbf{k}, \mathbf{p}''; \tau) C(\mathbf{k}, \mathbf{p}''\mathbf{p}'; t - \tau). \quad (4.28)$$

Here the elements of the proper frequency matrices read

$$\mathrm{i}\Omega_s(\mathbf{k}, \mathbf{p}') = (1/V) \int d\mathbf{p}'' \langle f_{s,i}^*(\mathbf{k}, \mathbf{p}'') \dot{f}_{s,i}(\mathbf{k}, \mathbf{p}) \rangle C_s^{-1}(\mathbf{k}, \mathbf{p}''\mathbf{p}'; t = 0), \qquad (4.29)$$

$$\mathrm{i}\Omega(\mathbf{k}, \mathbf{p}') = (1/V) \int d\mathbf{p}'' \langle \hat{f}^*(\mathbf{k}, \mathbf{p}'') \dot{\hat{f}}(\mathbf{k}, \mathbf{p}) \rangle C^{-1}(\mathbf{k}, \mathbf{p}''\mathbf{p}'; t = 0), \qquad (4.30)$$

whereas those of the memory matrices are given by

$$M_s(\mathbf{k}, \mathbf{p}'; t) = (1/V) \int d\mathbf{p}'' \langle [(1 - \mathcal{P}_s) \dot{f}_{s,i}(\mathbf{k}, \mathbf{p}'')]^* \exp[\mathrm{i}(1 - \mathcal{P}_s)Lt]$$

$$[(1 - \mathcal{P}_s) \dot{f}_{s,i}(\mathbf{k}, \mathbf{p})] \rangle C_s^{-1}(\mathbf{k}, \mathbf{p}''\mathbf{p}'; t = 0), \qquad (4.31)$$

$$M(\mathbf{k}, \mathbf{p}\mathbf{p}'; t) = (1/V) \int d\mathbf{p}'' \langle [(1 - \mathcal{P})\dot{\hat{f}}(\mathbf{k}, \mathbf{p}'')]^* \exp[i(1 - \mathcal{P})Lt]$$

$$[(1 - \mathcal{P})\dot{\hat{f}}(\mathbf{k}, \mathbf{p})] \rangle C^{-1}(\mathbf{k}, \mathbf{p}''\mathbf{p}'; t = 0). \qquad (4.32)$$

The final step of the memory function formalism is the introduction for all the time-dependent quantities of the corresponding Laplace transforms

$$\tilde{F}(z) = \int_0^\infty dt \exp(-zt) F(t) \qquad (4.33)$$

to eventually write eqns (4.27) and (4.28) in the form

$$z\tilde{C}_s(\mathbf{k}, \mathbf{p}\mathbf{p}'; z) - C_s(\mathbf{k}, \mathbf{p}\mathbf{p}'; t = 0) = i \int d\mathbf{p}'' \, \Omega_s(\mathbf{k}; \mathbf{p}\mathbf{p}'') \tilde{C}_s(\mathbf{k}, \mathbf{p}''\mathbf{p}'; z)$$

$$- \int d\mathbf{p}'' \tilde{M}_s(\mathbf{k}, \mathbf{p}\mathbf{p}''; z) \tilde{C}_s(\mathbf{k}, \mathbf{p}''\mathbf{p}'; z), \qquad (4.34)$$

$$z\tilde{C}(\mathbf{k}, \mathbf{p}\mathbf{p}'; z) - C(\mathbf{k}, \mathbf{p}\mathbf{p}'; t = 0) = i \int d\mathbf{p}'' \, \Omega(\mathbf{k}; \mathbf{p}\mathbf{p}'') \tilde{C}(\mathbf{k}, \mathbf{p}''\mathbf{p}'; z)$$

$$- \int d\mathbf{p}'' \tilde{M}(\mathbf{k}, \mathbf{p}\mathbf{p}''; z) \tilde{C}(\mathbf{k}, \mathbf{p}''\mathbf{p}'; z). \qquad (4.35)$$

By means of these memory equations (first obtained by Akcasu and Duderstadt (1969)) it is relatively straightforward to make contact with all the basic results of previous kinetic treatments. First of all, one needs the proper frequency matrix elements $\Omega_s(\mathbf{k}; \mathbf{p}\mathbf{p}')$ and $\Omega(\mathbf{k}; \mathbf{p}\mathbf{p}')$. These can be calculated exactly, the final result being (see Appendix F):

$$i\Omega_s(\mathbf{k}; \mathbf{p}\mathbf{p}') = \frac{i}{m}(\mathbf{k} \cdot \mathbf{p})\delta(\mathbf{p} - \mathbf{p}'), \qquad (4.36)$$

$$i\Omega(\mathbf{k}; \mathbf{p}\mathbf{p}') = \frac{i}{m}(\mathbf{k} \cdot \mathbf{p})\delta(\mathbf{p} - \mathbf{p}') - \frac{i}{m}(\mathbf{k} \cdot \mathbf{p})nf_0(p)c(k). \qquad (4.37)$$

Here the contributions proportional to $\delta(\mathbf{p} - \mathbf{p}')$ stem from the 'free-streaming' portion of the Liouvillian, a fact which explains their identical form for the self and the collective cases. In the latter, the additional contribution proportional to $c(k)$ accounts for the *static* correlations occurring between different particles because of the interatomic forces. In eqn (4.37), the latter are taken into account in a typical 'mean-field' way, with the relevant particle separations at a given k being determined by the equilibrium structure of the fluid (cf. eqn (F.8)).

By themselves, the results (4.36), (4.37) alone are not expected to provide an acceptable description of the dynamics of the phase-space correlations. This is fairly obvious for the self case, where $\Omega_s(\mathbf{k}, \mathbf{p}\mathbf{p}')$ only accounts for free motion because the average force on a particle vanishes. Even in the collective case, the mean-field result (4.37) ignores completely the intricate time-dependent effects of the interatomic forces (i.e. the dynamics of 'collisional' events). All these features are clearly 'hidden' in the memory functions M_s and M in eqns (4.27) and (4.28).

Before exploring the latter quantities in detail, it is gratifying to realize the progress inherent to a purely mean-field description with respect to another simple scheme known as the 'Vlasov approximation'. This is easily derived from the exact equation of motion for $\hat{f}(\mathbf{k}, \mathbf{p}; t)$, which reads (cf. eqn (F.5)):

$$\dot{\hat{f}}(\mathbf{k}, \mathbf{p}; t) - \frac{i}{m}(\mathbf{k} \cdot \mathbf{p})\hat{f}(\mathbf{k}, \mathbf{p}; t) = \sum_{i,j \neq i} \exp[i\mathbf{k} \cdot \mathbf{r}_i(t)]$$

$$\frac{\partial}{\partial \mathbf{p}}[\delta(\mathbf{p} - \mathbf{p}_i(t))] \cdot \left[\frac{\partial \phi(r_{ij}(t))}{\partial \mathbf{r}_{ij}(t)}\right]. \qquad (4.38)$$

Here the pair force on the right-hand side can formally be expressed as

$$-\frac{\partial \phi(r_{ij}(t))}{\partial \mathbf{r}_{ij}(t)} = -\int d\mathbf{r} \frac{\partial \phi(r)}{\partial \mathbf{r}} \delta(\mathbf{r} - \mathbf{r}_{ij}(t))$$

$$= -(2\pi)^{-3} \int d\mathbf{k}' \exp(-i\mathbf{k}' \cdot \mathbf{r}_{ij}(t)) \int d\mathbf{r} \frac{\partial \phi(r)}{\partial \mathbf{r}} \exp(i\mathbf{k}' \cdot \mathbf{r})$$

$$= (2\pi)^{-3} \int d\mathbf{k}' \exp(-i\mathbf{k}' \cdot \mathbf{r}_{ij}(t)) i\mathbf{k}' \phi(k') \qquad (4.39)$$

where the pair potential $\phi(r)$ is assumed to be sufficiently regular to have a definite Fourier transform $\phi(k')$. Inserting (4.39) into (4.38) we obtain

$$\dot{\hat{f}}(\mathbf{k}, \mathbf{p}; t) - \frac{i}{m}(\mathbf{k} \cdot \mathbf{p})\hat{f}(\mathbf{k}, \mathbf{p}; t) =$$

$$-(2\pi)^{-3} \sum_{i,j \neq i} \int d\mathbf{k}' \frac{\partial}{\partial \mathbf{p}}[f_{s,i}(\mathbf{k} - \mathbf{k}', \mathbf{p}; t)] \cdot i\mathbf{k}' \phi(k') \int d\mathbf{p}'' f_{s,j}(\mathbf{k}', \mathbf{p}''; t)$$

$$\qquad (4.40)$$

where the integral over $\mathbf{p}''$ has been inserted in order to reproduce the structure of a phase-space density. Equation (4.40) is exact, and the appearance on the right-hand side of the product of *two* phase-space densities reflects the typical hierarchical structure of many-body systems.

In order to make the problem tractable, the quantity $\sum_i f_{s,i}(\mathbf{k} - \mathbf{k}', \mathbf{p}; t)$ is replaced by its average value $(2\pi)^3 n f_0(p)\delta(\mathbf{k} - \mathbf{k}')$, the final result being the *Vlasov equation*

$$\dot{\hat{f}}(\mathbf{k}, \mathbf{p}; t) - \frac{i}{m}(\mathbf{k} \cdot \mathbf{p})\hat{f}(\mathbf{k}, \mathbf{p}; t) = -\frac{i}{m}(\mathbf{k} \cdot \mathbf{p})n f_0(p)\,[-\beta\phi(k)]$$

$$\int d\mathbf{p}''\, f(\mathbf{k}, \mathbf{p}''; t) \qquad (4.41)$$

where we have used $[\partial f_0(p)/\partial \mathbf{p}] = -(\beta/m)f_0(p)\mathbf{p}$. The result (4.41) was originally deduced by a suitable factorization of non-equilibrium distribution functions, followed by the assumption that the departures from equilibrium averages are sufficiently small to be treated perturbatively (e.g. Friedman (1985)). The latter hypothesis is equivalent to the linear-response approach adopted in the memory-function framework (Mori 1965). Multiplying (4.41) by $\hat{f}^*(\mathbf{k}, \mathbf{p}'; 0)$ and taking the average we obtain

$$\dot{C}(\mathbf{k}, \mathbf{p}\mathbf{p}'; t) - \frac{i}{m}(\mathbf{k} \cdot \mathbf{p})C(\mathbf{k}, \mathbf{p}\mathbf{p}'; t) = -\frac{i}{m}(\mathbf{k} \cdot \mathbf{p})n f_0(p)\,[-\beta\phi(k)]$$

$$\int d\mathbf{p}''\, C(\mathbf{k}, \mathbf{p}''\mathbf{p}'; t). \qquad (4.42)$$

This result can be compared with the one predicted by eqn (4.28) in the absence of any memory effects. In the latter case, the insertion of (4.37) yields

$$\dot{C}(\mathbf{k}, \mathbf{p}\mathbf{p}'; t) - \frac{i}{m}(\mathbf{k} \cdot \mathbf{p})C(\mathbf{k}, \mathbf{p}\mathbf{p}'; t) = -\frac{i}{m}(\mathbf{k} \cdot \mathbf{p})n f_0(p)c(k)$$

$$\int d\mathbf{p}''\, C(\mathbf{k}, \mathbf{p}''\mathbf{p}'; t), \qquad (4.43)$$

indicating that the quantity $-\beta\phi(k)$ is replaced by the direct correlation function $c(k)$. This represents a substantial improvement, because at small separations the pair potential $\phi(r)$ usually has a strongly repulsive part which makes questionable the definition of the Fourier transform $\phi(k)$. Whereas the Vlasov approximation neglects any correlation effects between the particles, the mean-field result (4.37) incorporates the fact that two atoms cannot be found at arbitrarily small separations. As a result, the effective 'renormalization' of the bare potential $\phi(r)$ with the quantity $-(1/\beta)c(r)$ is physically sound both for small r (where the effects of the repulsion are taken into account) and for large r (where the correlations become very small, and the two results coincide).

In any case, both the results (4.42) and (4.43) are usually referred to as

'collisionless approximations' because they ignore any dynamical effect of the collisional processes. The ultimate goal of kinetic approaches is instead to account for these time-dependent features in some definite approximation scheme. The simplest physical situation occurs at *low densities*, where a Markovian approximation for the memory functions $M_s(\mathbf{k}, \mathbf{p}\mathbf{p}'; t)$ and $M(\mathbf{k}, \mathbf{p}\mathbf{p}'; t)$ becomes rigorous in the low wavevector limit (Mazenko 1972). For example, eqn (4.35) in this limiting case can be written as

$$z\tilde{C}(\mathbf{k}, \mathbf{p}\mathbf{p}'; z) - C(\mathbf{k}, \mathbf{p}\mathbf{p}'; t = 0) = \int d\mathbf{p}''\,[i\Omega(\mathbf{k}, \mathbf{p}\mathbf{p}'')$$

$$- \Gamma(\mathbf{p}\mathbf{p}'')]\,\tilde{C}(\mathbf{k}, \mathbf{p}''\mathbf{p}'; z). \qquad (4.44)$$

Here

$$\Gamma(\mathbf{p}\mathbf{p}'') \equiv \lim_{z \to 0}\lim_{k \to 0}\lim_{n \to 0} \tilde{M}(\mathbf{k}, \mathbf{p}\mathbf{p}''; z). \qquad (4.45)$$

When written in the time domain, eqn (4.44) has the typical 'relaxation' form of the most famous result of conventional kinetic theories, the *Boltzmann equation* for the approach of the phase-space distribution to equilibrium. Within the usual linearization schemes implying small departures from equilibrium, the result (4.44) is actually found to coincide with the Boltzmann equation (Mazenko 1972). The detailed expression of the 'relaxation rate' $\Gamma(\mathbf{p}\mathbf{p}')$ is reported, for example, by Boon and Yip (1980); an immediate consequence of the density expansion implicit in eqn (4.45) is that $\Gamma(\mathbf{p}\mathbf{p}') = n\sigma_0(\mathbf{p}\mathbf{p}')$, where $\sigma_0(\mathbf{p}\mathbf{p}')$ involves the typical quantities relevant for an *isolated binary collision*, such as the momenta before and after the collision and the 'scattering cross section' which depends on the form of the pair potential $\phi(r)$. In the particular case of *hard spheres*, these low-density results form the backbone of the framework conventionally referred to as *Enskog theory*. Implemented by a suitable criterion of choice of the hard sphere diameter d, the Enskog results have been used quite successfully to account for several properties of real gases at moderate densities, including all the transport coefficients (e.g. Reed and Gubbins 1973).

As remarked at the beginning of Section 4.1.1, the troubles arise as soon as we consider *dense fluids*, where the predictions of the Boltzmann equation begin to fail in several respects. The most evident defect is that the larger probability that two particles have to collide at increasing densities cannot be accounted for by the simple proportionality to n of the quantity $\Gamma(\mathbf{p}\mathbf{p}')$. Indeed, as n becomes larger a certain amount of structure begins to build up at the close distances relevant for the binary encounter; the effect becomes more and more marked at increasing densities, as indicated by the progressively higher first peak of the pair distribution

function $g(r)$. The development at small separations of these structural features yields an additional increase with n of the probability of occurrence of a binary collision; as a result, the density-independent quantity $\sigma_0(\mathbf{pp'})$ must be replaced by a new one, $\sigma(\mathbf{pp'})$, which takes into account the onset of structure and increases with n. While these qualitative considerations are valid for any fluid, rigorous results accounting for this effect have only been obtained for a *hard sphere fluid* (Blum and Lebowitz 1969; Mazenko *et al.* 1972; Konijnendijk and van Leeuwen 1973). As far as the structural effects are concerned, the relevant modification with respect to the low-density Enskog result is the appearance as a factor in $\sigma(\mathbf{pp'})$ of the pair distribution function at contact $g(d)$, which provides the expected increase with n (cf. the result (3.76) for the collision rate). From a theoretical point of view, this *generalized Enskog theory* represents an important milestone and its predictions are found to extend substantially the validity domain of the previous Boltzmann–Enskog results. The improved theory still assumes that two subsequent binary collisions are uncorrelated, and therefore retains the original Markovian character. Note, incidentally, that the meaning of attributes like 'subsequent' and 'binary' is really unambiguous only for hard sphere systems where the collisions are instantaneous. Somewhat improperly, these terms are often used in a broad sense even when dealing with fluids having continuous potentials.

Unfortunately, even the predictions of the generalized Enskog theory are found to become increasingly incorrect as the hard sphere packing fraction approaches the values typical of the liquid state. As already remarked in Section 3.3, these shortcomings are anticipated at lower densities by the appearance of a $t^{-3/2}$ tail in the velocity autocorrelation function $\psi(t)$. However, it is mostly in the very dense hard sphere fluids that the theoretical results become really unsatisfactory. In particular, the theory is intrinsically unable to account for the appearance of a negative region in $\psi(t)$, a feature which implies a substantial reduction of the diffusion coefficient with respect to the Enskog value (3.79). Also, computer simulations performed in dense hard sphere fluids indicate the presence of propagating shear waves in the transverse current spectra $C_T(k, \omega)$ at finite wavevectors (Alley *et al.* 1983). This behaviour is quite unexpected on the basis of the generalized Enskog theory, which in the entire k range does not predict any inelastic peak in $C_T(k, \omega)$.

The inescapable consequence of this failure is that for dense hard sphere fluids the collisions cannot be considered any more as uncorrelated, or equivalently that the memory functions M_s and M develop an increasing non-Markovian character. Because of the instantaneous character of the binary collisions, the Enskog framework is expected to be accurate over a short timescale (of the order of γ_E^{-1}, cf. (3.76)), and/or for large enough frequencies. By itself, any correlation effect between the collisions requires

instead some time to develop. As a consequence, we argue that in dense hard sphere fluids a more appropriate form of the Laplace-transformed memory functions can be written as

$$\tilde{M}_s(\mathbf{k}, \mathbf{pp'}; z) = M_{s,E}(\mathbf{k}, \mathbf{pp'}) + \tilde{M}'(\mathbf{k}, \mathbf{pp'}; z), \qquad (4.46)$$

$$\tilde{M}(\mathbf{k}; \mathbf{pp'}; z) = M_E(\mathbf{k}, \mathbf{pp'}) + \tilde{M}'(\mathbf{k}, \mathbf{pp'}; z), \qquad (4.47)$$

where the suffix E refers to the Markovian results of the generalized Enskog theory, and the primed quantities (which account for the effects of correlated collisions) are expected to be relevant for small z. Physically, the simplest sequence of collisional events leading to a non-Markovian behaviour consists in an initial collision between, say, particles 1 and 2, followed by a collision between particle 2 and another particle 3 and by a final 'recollision' again between particles 1 and 2. Similarly, one may envisage more complicated intermediate sequences involving additional particles. In any case, the occurrence of the final recollision is affected by the previous 'history' of collisional events, leading to a situation where memory effects are important. Whereas the occurrence of these sequences of correlated collisions (or *'ring collisions'*) is unlikely in a dilute system, they are expected to be frequent at sufficiently high densities.

As noted before, in a dense fluid described in terms of a continuous interatomic potential no clearcut separation can in principle be traced between the collisional events, which are now characterized by a finite duration. Nevertheless, the collisional times are quite short ($\approx 10^{-13}$ s) on the timescale of several dynamical phenomena of interest in the liquid state. Correlated-collision sequences similar to those previously described are less precisely defined than for hard sphere systems, but can easily be imagined to have an important role even in this case, especially if their dynamical effects are long-lasting with respect to the collisional times. As a result, even in this case the memory functions can conveniently be separated into a 'fast' collisional part (referred to as 'binary' to keep some analogy with the hard sphere case), and in an addditional contribution associated with a considerably longer decay time. More precisely, in the time domain the memory functions M_s and M can be split as follows:

$$M_s(\mathbf{k}, \mathbf{pp'}; t) = M_{s,B}(\mathbf{k}, \mathbf{pp'}; t) + M_s'(\mathbf{k}, \mathbf{pp'}; t), \qquad (4.48)$$

$$M(\mathbf{k}; \mathbf{pp'}; t) = M_B(\mathbf{k}, \mathbf{pp'}; t) + M'(\mathbf{k}, \mathbf{pp'}; t). \qquad (4.49)$$

Here the suffix B stands for 'binary' and the non-instantaneous character of the collision has been accounted for by giving the binary contributions an unspecified time dependence rather than the typical $\delta(t)$ form of the Markovian scheme. Besides the previous qualitative remarks, eqns (4.48) and (4.49) still appear rather formal (note, however, the analogy of this splitting of the phase-space memory functions with the empirical result

(3.80) for a Lennard–Jones fluid). It is now time to discuss in a more quantitative way the actual information conveyed by the memory functions, with the final objective of ascertaining both the physical content and the mathematical form of the splittings (4.48), (4.49).

4.2 THE PHASE-SPACE MEMORY FUNCTIONS

Let us come back to the definitions (4.31) and (4.32) of the elements $M_s(\mathbf{k}, \mathbf{pp}'; t)$ and $M(\mathbf{k}, \mathbf{pp}'; t)$ of the memory matrices. To express these quantities in detail, we need the components at $t = 0$ of the respective 'fluctuating forces'. In the collective case, the latter after eqn (4.38) can be written as

$$(1 - \mathcal{P})\hat{f}(\mathbf{k}, \mathbf{p}) = (1 - \mathcal{P})\left[(\partial/\partial\mathbf{p}) \cdot \sum_{i, j \neq i} \frac{\partial\phi(r_{ij})}{\partial\mathbf{r}_i} \exp(i\mathbf{k} \cdot \mathbf{r}_i)\delta(\mathbf{p} - \mathbf{p}_i)\right]$$

$$= (1 - \mathcal{P})\left[\frac{\partial}{\partial\mathbf{p}} \cdot \int d\mathbf{R}_1 d\mathbf{P}_1 d\mathbf{R}_2 d\mathbf{P}_2 \frac{\partial\phi(R_{12})}{\partial\mathbf{R}_1}\right.$$

$$\left. \exp(i\mathbf{k} \cdot \mathbf{R}_1)\delta(\mathbf{p} - \mathbf{p}_1)f_2(\mathbf{R}_1\mathbf{P}_1, \mathbf{R}_2\mathbf{P}_2)\right] \quad (4.50)$$

where the free-streaming term $(i/m)(\mathbf{k} \cdot \mathbf{p})\hat{f}(\mathbf{k}, \mathbf{p})$ has been omitted since $(1 - \mathcal{P})\hat{f}(\mathbf{k}, \mathbf{p}) = 0$ by definition. In the last step of (4.50) we have introduced the variable

$$f_2(\mathbf{R}_1\mathbf{P}_1, \mathbf{R}_2\mathbf{P}_2) \equiv \sum_{i, j \neq i} \delta(\mathbf{R}_1 - \mathbf{r}_i)\delta(\mathbf{P}_1 - \mathbf{p}_i)\delta(\mathbf{R}_2 - \mathbf{r}_j)\delta(\mathbf{P}_2 - \mathbf{p}_j)$$

$$\quad (4.51)$$

which can be viewed as a higher-order phase-space density. To simplify somewhat the notations, in the following we shall often adopt the convention of writing the combinations of field variables $(\mathbf{R}_1, \mathbf{P}_1)$, $(\mathbf{R}_2, \mathbf{P}_2)$, ... simply as 1, 2, ... Also, when appropriate, the phase-space variables of the ith particle at time t will be denoted as $q_i(t) \equiv (\mathbf{r}_i(t), \mathbf{p}_i(t))$; as always in this book, the absence of any indication for time t in a dynamical variable means that the latter is evaluated at $t = 0$. From the result (4.50) we deduce that the memory function (4.32) can be written as

$$M(\mathbf{k}, \mathbf{pp}'; t) = \frac{1}{V}\int d\mathbf{p}'' \int d1\, d2\, d3\, d4 \exp(-i\mathbf{k} \cdot \mathbf{R}_1)\frac{\partial\phi(R_{12})}{\partial\mathbf{R}_1} \cdot \frac{\partial[\delta(\mathbf{p}'' - \mathbf{P}_1)]}{\partial\mathbf{p}''}$$

$$\times G(12, 34; t)\exp(i\mathbf{k} \cdot \mathbf{R}_3)\frac{\partial\phi(R_{34})}{\partial\mathbf{R}_3}$$

$$\cdot \frac{\partial[\delta(\mathbf{p} - \mathbf{P}_3)]}{\partial\mathbf{p}} C^{-1}(\mathbf{k}, \mathbf{p}''\mathbf{p}'). \quad (4.52)$$

Here we have defined

$$G(12, 34; t) \equiv \langle \hat{f}_2'(1, 2) \exp[(1 - \mathcal{P})Lt]\hat{f}_2'(3, 4)\rangle \quad (4.53)$$

where $\hat{f}_2' = f_2' - \langle f_2'\rangle$ denotes the fluctuation of the variable $f_2' \equiv (1 - \mathcal{P})f_2$. Recalling the result (4.21) for the elements of the inverse correlation matrix, we obtain

$$M(\mathbf{k}, \mathbf{pp}'; t) = \frac{1}{Nf_0(p')}\int d1\, d2\, d3\, d4 \exp(-i\mathbf{k} \cdot \mathbf{R}_1)\frac{\partial\phi(R_{12})}{\partial\mathbf{R}_1} \cdot \frac{\partial[\delta(\mathbf{p}' - \mathbf{P}_1)]}{\partial\mathbf{p}'}$$

$$\times G(12, 34; t)\exp(i\mathbf{k} \cdot \mathbf{R}_3)\frac{\partial\phi(R_{34})}{\partial\mathbf{R}_3} \cdot \frac{\partial[\delta(\mathbf{p} - \mathbf{P}_3)]}{\partial\mathbf{p}} \quad (4.54)$$

since the term $-c(k)$ in (4.21) gives zero contributions to (4.52). As a result, the memory function ultimately depends on the dynamics of $G(12, 34; t)$ weighted by suitable 'interaction vertices' which depend on the pair forces. From (4.51) it is readily seen that the quantity G describes the motions of up to four different particles in phase-space, with all the possible correlation effects included.

A similar calculation can be performed for the self-memory-function $M_s(\mathbf{k}, \mathbf{pp}'; t)$, the final result being identical to eqn (4.54) without the factor $(1/N)$ and with $G(12, 34; t)$ replaced by

$$G_s(12, 34; t) = \langle \hat{f}_{si,2}'(1, 2) \exp[i(1 - \mathcal{P}_s)Lt]\hat{f}_{si,2}'(3, 4)\rangle. \quad (4.55)$$

Here $\hat{f}_{si,2}'$ is the fluctuation of the variable $f_{si,2}' \equiv (1 - \mathcal{P}_s)f_{si,2}$, and

$$f_{si,2}(1, 2) \equiv \delta(1 - q_i) \sum_{j(\neq i)} \delta(2 - q_j). \quad (4.56)$$

The quantity G_s describes the correlated motions of a tagged particle and of the other particles of the fluid. For example, sequences of correlated collisions like those of the previous subsection are included to all orders in the description of the dynamics brought about by G_s.

The variety of dynamical events accounted for by the presence of G and G_s in the memory functions is formally appealing, but by itself does not contribute very much to make the problem more tractable. For example, eqn (4.54) or its self counterpart are not of great help to improve our knowledge of the dependence of M and M_s on the momenta $\mathbf{p}$ and $\mathbf{p}'$, and how this dependence is ultimately reflected on their time decay. The problem can be effectively bypassed assuming that the memory functions depend on the momenta only through their initial values (which can actually be calculated), whereas their time decay can be modelled by some suitable ansatz. This procedure has in fact been adopted with some success in the self case, at the price of introducing further assumptions for the k-dependence of the relaxation time (Akcasu *et al.* 1970; Desai 1971).

An alternative to the phenomenological approaches is to rephrase the problem in such a way that the analysis of the relevant decay mechanisms is easier. In this respect, a possible procedure is to expand the momentum dependence of the phase-space densities in terms of a complete set of three-dimensional polynomials $H_\lambda(\mathbf{p})$:

$$f_{s,i}(\mathbf{k}, \mathbf{p}; t) = f_0(p) \sum_\lambda A_{si,\lambda}(\mathbf{k}, t) H_\lambda(\mathbf{p}) \qquad (4.57)$$

$$f(\mathbf{k}, \mathbf{p}; t) = f_0(p) \sum_\lambda A_\lambda(\mathbf{k}, t) H_\lambda(\mathbf{p}) \qquad (4.58)$$

where the polynomials are assumed to satisfy the following orthonormality relations

$$\int \mathrm{d}\mathbf{p} f_0(p) H_\lambda(\mathbf{p}) H_{\lambda'}(\mathbf{p}) = \delta_{\lambda,\lambda'} \qquad (4.59)$$

with the equilibrium distribution $f_0(p)$ playing the role of a weight factor. A convenient choice for the H_λ is provided by the three-dimensional Hermite polynomials (Mazenko *et al.* 1972); the first ones read

$$H_0(\mathbf{p}) = 1$$

$$H_1(\mathbf{p}) = \left(\frac{\beta}{m}\right)^{1/2} p_z \qquad H_2(\mathbf{p}) = \left(\frac{\beta}{m}\right)^{1/2} p_x \qquad H_3(\mathbf{p}) = \left(\frac{\beta}{m}\right)^{1/2} p_y$$

$$H_4(\mathbf{p}) = \frac{1}{\sqrt{6}}\left(\frac{\beta}{m} p^2 - 3\right) \qquad H_5(\mathbf{p}) = \frac{\sqrt{3}}{2}\frac{\beta}{m}\left(p_z^2 - \frac{p^2}{3}\right)$$

$$H_6(\mathbf{p}) = \frac{\beta}{m} p_z p_x \qquad H_7(\mathbf{p}) = \frac{\beta}{m} p_x p_y \qquad H_8(\mathbf{p}) = \frac{\beta}{m} p_y p_z \qquad (4.60)$$

From eqns (4.57), (4.58) and the relation (4.59) with $\lambda' = 0$ we deduce that

$$A_{si,\lambda}(\mathbf{k}, t) = \int \mathrm{d}\mathbf{p} f_{s,i}(\mathbf{k}, \mathbf{p}; t) H_\lambda(\mathbf{p}), \qquad (4.61)$$

$$A_\lambda(\mathbf{k}, t) = \int \mathrm{d}\mathbf{p} \hat{f}(\mathbf{k}, \mathbf{p}; t) H_\lambda(\mathbf{p}). \qquad (4.62)$$

As a result, the first few As are readily seen to have a familiar form. In particular, the variables

$$A_{si,0}(\mathbf{k}, t) = \exp[\mathrm{i}\mathbf{k} \cdot \mathbf{r}_i(t)], \qquad (4.63)$$

$$A_0(\mathbf{k}, t) = \sum_i \exp[\mathrm{i}\mathbf{k} \cdot \mathbf{r}_i(t)] - (2\pi)^3 n\delta(\mathbf{k}) \qquad (4.64)$$

can respectively be recognized as the self-density $n_{s,i}(\mathbf{k}, t)$ introduced in Section 1.4.1 and the density fluctuations $\hat{n}(\mathbf{k}, t)$ defined in eqn (1.113). Also, choosing the wavevector $\mathbf{k}$ along the z-axis, the collective variable

$$A_1(\mathbf{k}, t) = (\beta/m)^{1/2} \sum_i p_{i,z}(t) \exp[\mathrm{i}\mathbf{k} \cdot \mathbf{r}_i(t)] \qquad (4.65)$$

is seen to be proportional to the longitudinal current $j_L(\mathbf{k}, t)$, where as $A_2(\mathbf{k}, t)$ and $A_3(\mathbf{k}, t)$ are similarly related to the components of the transverse current $j_T(\mathbf{k}, t)$. Note that all these particular As as $k \to 0$ become *quasi-conserved variables* for any system. Moreover, in the special case of a hard sphere system, an additional quasi-conserved collective variable is provided by

$$A_4(\mathbf{k}, t) = (1/\sqrt{6}) \sum_i [(\beta/m)p_i^2(t) - 3] \exp[\mathrm{i}\mathbf{k} \cdot \mathbf{r}_i(t)] \qquad (4.66)$$

which accounts for k-dependent fluctuations in the kinetic energy (or in the 'temperature') of the system. On the other hand, in general the variables $A_{si,\lambda}(\mathbf{k}, t)$ for $\lambda \geq 1$ and $A_\lambda(\mathbf{k}, t)$ for $\lambda \geq 5$ are not conserved.

The expansions (4.57), (4.58) for the phase-space densities imply a similar decomposition for the corresponding time correlation functions

$$C_s(\mathbf{k}, \mathbf{pp}'; t) = \sum_{\lambda\lambda'} f_0(p) f_0(p') H_\lambda(\mathbf{p}) H_{\lambda'}(\mathbf{p}') C_{s,\lambda\lambda'}(\mathbf{k}, t), \qquad (4.67)$$

$$C(\mathbf{k}, \mathbf{pp}'; t) = \sum_{\lambda\lambda'} f_0(p) f_0(p') H_\lambda(\mathbf{p}) H_{\lambda'}(\mathbf{p}') C_{\lambda\lambda'}(\mathbf{k}, t), \qquad (4.68)$$

where the quantities

$$C_{s,\lambda\lambda'}(\mathbf{k}, t) = (1/V)\langle A_{si,\lambda'}^*(\mathbf{k}, 0) A_{si,\lambda}(\mathbf{k}, t)\rangle, \qquad (4.69)$$

$$C_{\lambda\lambda'}(\mathbf{k}, t) = (1/V)\langle A_{\lambda'}^*(\mathbf{k}, 0) A_\lambda(\mathbf{k}, t)\rangle, \qquad (4.70)$$

may formally be regarded as matrix elements in the discrete space of the indexes λ, λ'. On the basis of the previous remarks, it is immediate to relate some of these quantities with the time correlation functions discussed in Chapter 1. In particular:

$$C_{s,00}(\mathbf{k}, t) = (1/V)F_s(k, t), \qquad (4.71)$$

$$C_{s,11}(\mathbf{k} \to 0, t) = (1/V)\psi(t), \qquad (4.72)$$

$$C_{00}(\mathbf{k}, t) = nF(k, t), \qquad (4.73)$$

$$C_{11}(\mathbf{k}, t) = nm\beta C_L(k, t), \qquad (4.74)$$

$$C_{22}(\mathbf{k}, t) = C_{33}(\mathbf{k}, t) = nm\beta C_T(k, t). \qquad (4.75)$$

Exploiting the results and (4.9) and (4.18), in the new representation the 'matrices' $C_s(\mathbf{k}, t = 0)$ and $C(\mathbf{k}, t = 0)$ are found to be diagonal

$$C_{s,\lambda\lambda'}(\mathbf{k}, t = 0) = (1/V)\delta_{\lambda,\lambda'}, \tag{4.76}$$

$$C_{\lambda\lambda'}(\mathbf{k}, t = 0) = n\{1 + [S(k) - 1]\delta_{\lambda,0}\}\delta_{\lambda,\lambda'}. \tag{4.77}$$

As a result

$$C_{s,\lambda\lambda'}^{-1}(\mathbf{k}, t = 0) = V\delta_{\lambda,\lambda'}, \tag{4.78}$$

$$C_{\lambda\lambda'}^{-1}(\mathbf{k}, t = 0) = \{(1/n) - c(k)\delta_{\lambda,0}\}\delta_{\lambda,\lambda'}. \tag{4.79}$$

Finally, in the discrete space the equivalents of the memory eqns (4.34) and (4.35) read

$$z\tilde{C}_{s,\lambda\nu}(\mathbf{k}, z) - C_{s,\lambda\nu}(\mathbf{k}, t = 0) = \sum_{\lambda'} [i\Omega_{s,\lambda\lambda'}(\mathbf{k}) - \tilde{M}_{s,\lambda\lambda'}(\mathbf{k}, z)]\tilde{C}_{s,\lambda'\nu}(\mathbf{k}, z), \tag{4.80}$$

$$z\tilde{C}_{\lambda\nu}(\mathbf{k}, z) - C_{\lambda\nu}(\mathbf{k}, t = 0) = \sum_{\lambda'} [i\Omega_{\lambda\lambda'}(\mathbf{k}) - \tilde{M}_{\lambda\lambda'}(\mathbf{k}, z)]\tilde{C}_{\lambda'\nu}(\mathbf{k}, z), \tag{4.81}$$

where the elements of the proper frequency matrices read (cf. Appendix F)

$$i\Omega_{s,\lambda\lambda'}(\mathbf{k}) = (i/m)\int d\mathbf{p}\, H_\lambda(\mathbf{p})(\mathbf{k} \cdot \mathbf{p})H_{\lambda'}(\mathbf{p})f_0(p), \tag{4.82}$$

$$i\Omega_{\lambda\lambda'}(\mathbf{k}) = (i/m)\int d\mathbf{p}\, H_\lambda(\mathbf{p})(\mathbf{k} \cdot \mathbf{p})H_{\lambda'}(\mathbf{p})f_0(p)$$
$$- [ik/(m\beta)^{1/2}]nc(k)\delta_{\lambda,1}\delta_{\lambda',0}. \tag{4.83}$$

In turn, the elements of the memory matrices turn out to be

$$\tilde{M}_{s,\lambda\lambda'}(\mathbf{k}, z) = \int d\mathbf{p}\, d\mathbf{p}'\, H_\lambda(\mathbf{p})\tilde{M}_s(\mathbf{k}, \mathbf{pp}'; z)H_{\lambda'}(\mathbf{p}')f_0(p'), \tag{4.84}$$

$$\tilde{M}_{\lambda\lambda'}(\mathbf{k}, z) = \int d\mathbf{p}\, d\mathbf{p}'\, H_\lambda(\mathbf{p})\tilde{M}(\mathbf{k}, \mathbf{pp}'; z)H_{\lambda'}(\mathbf{p}')f_0(p'). \tag{4.85}$$

Inserting here the Laplace transforms of eqn (4.54) and its self counterpart, we end up with

$$\tilde{M}_{s,\lambda\lambda'}(\mathbf{k}, z) = \int d1\, d2\, d3\, d4 \exp(-i\mathbf{k} \cdot \mathbf{R}_1)\nabla_{\mathbf{R}_1}\phi(R_{12}) \cdot \nabla_{\mathbf{P}_1}H_{\lambda'}(\mathbf{P}_1)$$
$$\tilde{G}_s(12, 34; z)\exp(i\mathbf{k} \cdot \mathbf{R}_3)\nabla_{\mathbf{R}_3}\phi(R_{34}) \cdot \nabla_{\mathbf{P}_3}H_\lambda(\mathbf{P}_3), \tag{4.86}$$

$$\tilde{M}_{\lambda\lambda'}(\mathbf{k}, z) = (1/N)\int d1\, d2\, d3\, d4 \exp(-i\mathbf{k} \cdot \mathbf{R}_1)\nabla_{\mathbf{R}_1}\phi(R_{12}) \cdot \nabla_{\mathbf{P}_1}H_{\lambda'}(\mathbf{P}_1)$$
$$\tilde{G}(12, 34; z)\exp(i\mathbf{k} \cdot \mathbf{R}_3)\nabla_{\mathbf{R}_3}\phi(R_{34}) \cdot \nabla_{\mathbf{P}_3}H_\lambda(\mathbf{P}_3). \tag{4.87}$$

Equations (4.86) and (4.87) are the starting point of the analysis of the different collisional decay channels which are relevant for the time correlation functions of physical interest. In particular, we shall now discuss how it is possible to perform in $\tilde{G}_s$ and $\tilde{G}$ an approximate separation between a 'binary' portion and a contribution which stems from correlated collisions. For the latter, the new representation in terms of the variables $A_{si,\lambda}(\mathbf{k}, t)$ and $A_\lambda(\mathbf{k}, t)$ (usually referred to as the *modes*) will be considerably useful to simplify the analysis.

4.3 BINARY COLLISIONS VERSUS CORRELATED COLLISIONS

4.3.1 General analysis

Let us now examine more closely the dynamical processes embodied in the many-particle quantities $\tilde{G}_s$ and $\tilde{G}$ for dense fluids. Our discussion will basically follow the analyses by Sjögren and Sjölander (1979) and by Sjögren (1980b), dealing respectively with the self and the collective cases. These works were anticipated by several approaches developed during the 1970s by different authors, notably by Mazenko and co-workers in the so-called *renormalized kinetic theories* (for a review, see Mazenko and Yip 1977). Although all these contributions often differ in several technical aspects, they share the same basic framework; more important, the physical conclusions which can eventually be drawn turn out to be remarkably similar. As already noticed, an important 'technical' distinction is connected to the assumed pair potential. Hard sphere systems have often been privileged because of the clearcut dynamical separation existing between binary (Enskog) and correlated collisions. For these fluids, additional important contributions have been provided by deSchepper and Cohen (1980, 1982), Leutheusser (1982), and Kirkpatrick (1985). The previously quoted works by Sjögren and Sjölander deal instead with 'realistic' fluids with continuous pair potentials, for which the binary contributions are less precisely defined than for hard spheres. Needless to say, hard spheres or not, all these approaches are formally rather complicated, and in the following we shall limit ourselves to the essential steps of the analysis.

To obtain some insight to the dynamics behind $\tilde{G}_s$ and $\tilde{G}$, we write down for $\tilde{G}_s$ a memory equation of the form

$$z\tilde{G}_{s}(12, 34; z) - G_{s}(12, 34; t = 0) = \int d1' \, d2' \, [i\Omega_{s}(12, 1'2')$$
$$- \tilde{\Gamma}_{s}(12, 1'2'; z)] \tilde{G}_{s}(1'2', 34; z)$$
$$(4.88)$$

and for $\tilde{G}$ a similar equation involving the corresponding quantities Ω and $\tilde{\Gamma}$. Using a short-hand notation, these two equations can be simply written as

$$\tilde{G}_{s}(z) = [zI - i\Omega_{s} + \tilde{\Gamma}_{s}(z)]^{-1} G_{s}(t = 0) \equiv \tilde{R}_{s}(z) G_{s}(t = 0), \quad (4.89)$$

$$\tilde{G}(z) = [zI - i\Omega + \tilde{\Gamma}(z)]^{-1} G(t = 0) \equiv \tilde{R}(z) G(t = 0). \quad (4.90)$$

These formal results can qualitatively be interpreted as follows. For very short times, the quantities $\tilde{\Gamma}_{s}(t)$ and $\tilde{\Gamma}(t)$ which account for the memory effects of the collisions may approximately be neglected and the evolution of G_{s} and G is largely determined by the proper frequency contributions. This instantaneous response corresponds to a 'binary collision' event, where the density effects are taken into account only as an average mean-field background. However, the occurrence of this event causes fast rearrangements among the neighbouring particles, accounted for by rapidly varying parts of the memory functions $\tilde{\Gamma}_{s}$ and $\tilde{\Gamma}$. As a result, a more comprehensive physical picture of the collision is obtained by arguing that the latter is ruled by an effectively time-dependent short-range interaction, whose short lifetime is determined by the duration of the immediate structural rearrangements. In more formal terms, the overall dynamics of these fast events is conveniently described by the quantities

$$\tilde{R}_{s, B}(z) = [zI - i\Omega_{s} + \tilde{\Gamma}_{s, B}(z)]^{-1}, \quad (4.91)$$

$$\tilde{R}_{B}(z) = [zI - i\Omega + \tilde{\Gamma}_{B}(z)]^{-1}, \quad (4.92)$$

where the suffix B stands for 'binary', and $\Gamma_{s, B}(t)$ and $\Gamma_{B}(t)$ account for the previous rapidly varying effects. The remaining parts of the memory functions are responsible for the correlation effects between the collisions. Letting

$$\tilde{\Gamma}_{s, C}(z) \equiv \tilde{\Gamma}_{s}(z) - \tilde{\Gamma}_{s, B}(z) = \tilde{R}_{s}^{-1}(z) - \tilde{R}_{s, B}^{-1}(z)$$
$$= -\tilde{R}_{s, B}^{-1}(z) [\tilde{R}_{s}(z) - \tilde{R}_{s, B}(z)] \tilde{R}_{s}^{-1}(z), \quad (4.93)$$

$$\tilde{\Gamma}_{C}(z) \equiv \tilde{\Gamma}(z) - \tilde{\Gamma}_{B}(z) = \tilde{R}^{-1}(z) - \tilde{R}_{B}^{-1}(z),$$
$$= -\tilde{R}_{B}^{-1}(z) [\tilde{R}(z) - \tilde{R}_{B}(z)] \tilde{R}^{-1}(z), \quad (4.94)$$

we have that $\tilde{R}_{s}(z)$ and $\tilde{R}(z)$ can formally be decomposed into 'binary' portions plus an infinite sequence of correlated binary events:

$$\tilde{R}_{s}(z) = \tilde{R}_{s, B}(z) - \tilde{R}_{s, B}(z) \tilde{\Gamma}_{s, C}(z) \tilde{R}_{s}(z)$$
$$= \tilde{R}_{s B}(z) - \tilde{R}_{s, B}(z) \tilde{\Gamma}_{s, C}(z) \tilde{R}_{s, B}(z)$$
$$+ \tilde{R}_{s, B}(z) \tilde{\Gamma}_{s, C}(z) \tilde{R}_{s, B}(z) \tilde{\Gamma}_{s, C}(z) \tilde{R}_{s, B}(z) + \cdots, \quad (4.95)$$

$$\tilde{R}(z) = \tilde{R}_{B}(z) - \tilde{R}_{B}(z) \tilde{\Gamma}_{C}(z) \tilde{R}(z)$$
$$= \tilde{R}_{B}(z) - \tilde{R}_{B}(z) \tilde{\Gamma}_{C}(z) \tilde{R}_{B}(z)$$
$$+ \tilde{R}_{B}(z) \tilde{\Gamma}_{C}(z) \tilde{R}_{B}(z) \tilde{\Gamma}_{C}(z) \tilde{R}_{B}(z) + \cdots. \quad (4.96)$$

Although the last step of these equations is very pictorial, no real step forward has been made since $\tilde{\Gamma}_{s, C}$ and $\tilde{\Gamma}_{C}$ still contain the exact quantities $\tilde{R}_{s}$ and $\tilde{R}$, namely the full dynamics of the system. However, during the short duration of the binary collision R_{s} and R can be approximated by their binary counterparts $R_{s, B}$ and R_{B}. On the other hand, in the time between the collisions the effects of $\Gamma_{s, C}$ and Γ_{C} may be approximately evaluated by assuming that the 'disturbances' created by the collision proceed independently. This implies that in eqns (4.93) and (4.94) all the quantities R_{s}, $R_{s, B}$, R and R_{B} may be replaced by their 'disconnected' portions in which the many-body dynamics is factorized into two separate contributions. To see what this approximation actually means, consider for example $\tilde{G}_{s}(12, 34; z)$ $= \tilde{R}_{s}(12, 34; z) G_{s}^{-1}(12, 34; t = 0)$. In the time domain its disconnected portion can be written as (Sjögren and Sjölander 1979)

$$G_{s}^{D}(12, 34; t) = C_{s}(13; t) C(24; t) \quad (4.97)$$

where C_{s} and C are the phase-space correlation functions defined in eqns (4.4) and (4.13). Recalling the definition of G_{s} (eqns (4.55) and (4.56)), it is readily seen that the approximation $G_{s} \approx G_{s}^{D}$ is equivalent to consider the tagged particle and the surrounding fluid as moving independently. In more technical terms, this amounts to factorize the full time-dependent average into the product of a self and a collective correlation function, at the same time ignoring any effect due to the presence of the projection operator $\mathcal{P}_{s}$. In eqn (4.93) a 'disentangling approximation' similar to (4.97) is performed even for the binary contribution $R_{s, B}(t) = G_{s, B}(t) [G_{s}(t = 0)]^{-1}$. In this case

$$G_{s, B}^{D}(12, 34; t) = C_{s, B}(13; t) C_{B}(24; t). \quad (4.98)$$

Here, one may proceed even further by noting that at this binary level the decoupling of the tagged particle from the surrounding fluid simply means that $C_{s, B}(13; t)$ describes the free motion of the particle. On the other hand, the collective dynamics of the fluid is virtually unaffected by the removal of a single particle: as far as eqn (4.98) is concerned, we may approximately replace $C_{B}(24; t)$ with the full $C(24; t)$.

Similar approximations can be made for the collective case (Sjögren 1980b). Here $\tilde{R}(z) = \tilde{G}(z)[G(t = 0)]^{-1}$ in eqn (4.94) is replaced by its disconnected portion, which follows from

$$G^D(12, 34; t) = C(13; t)C(24; t) + C(14; t)C(23; t). \qquad (4.99)$$

Note that, in contrast with (4.97), the symmetric character of G allows the possibility of two distinct decouplings. A similar approximation is eventually performed even for G_B^D, thus introducing binary correlation functions like $C_B(13; t)$, etc.

When expressed in terms of disconnected quantities, the results (4.93) and (4.94) may finally be inserted into eqns (4.95) and (4.96). After some simplifications, for $\tilde{G}_s(z)$ and $\tilde{G}(z)$ we find

$$\tilde{G}_s(z) = \tilde{G}_{s,B}(z) + \tilde{V}_{s,B}^\dagger(z)\,[G_s^D(t = 0)]^{-1}$$

$$\{\tilde{G}_s^D(z) - \tilde{G}_{s,B}^D(z)\}\,[G_s^D(t = 0)]^{-1}\,\tilde{V}_s(z), \qquad (4.100)$$

$$\tilde{G}(z) = \tilde{G}_B(z) + \tilde{V}_B^\dagger(z)\,[G^D(t = 0)]^{-1}$$

$$\{\tilde{G}^D(z) - \tilde{G}_B^D(z)\}\,[G^D(t = 0)]^{-1}\,\tilde{V}(z), \qquad (4.101)$$

where the quantities

$$\tilde{V}_s(z) \equiv [\tilde{R}_s^D(z)]^{-1}\tilde{R}_s(z)G_s(t = 0), \qquad (4.102)$$

$$\tilde{V}(z) \equiv [\tilde{R}^D(z)]^{-1}\tilde{R}(z)G(t = 0), \qquad (4.103)$$

(along with similar definitions for $\tilde{V}_{s,B}(z)$ and $\tilde{V}_B(z)$) may formally be interpreted as z-dependent coupling 'vertices'. Although the z-dependence of all these quantities has approximately been worked out (Sjögren 1980b), in the liquid range the dominant role turns out to be provided by the lowest order results

$$\tilde{V}_s(z) \approx \tilde{V}_{s,B}(z) \approx G_s(t = 0), \qquad (4.104)$$

$$\tilde{V}(z) \approx \tilde{V}_B(z) \approx G(t = 0). \qquad (4.105)$$

These *static vertex* approximations simplify considerably the subsequent treatment of the non-binary contributions. Substituting (4.104) and (4.105) respectively in eqns (4.100) and (4.101), we obtain approximate expressions for the quantities $\tilde{G}_s(z)$ and $\tilde{G}(z)$. Restoring a more explicit notation, we find that

$$\tilde{G}_s(12, 34; z) = \tilde{G}_{s,B}(12, 34; z) + \int d1'\,d1''\,d2'\,d2''\,d3'\,d3''\,d4'\,d4''$$

$$G_s(12, 1'2'; t = 0)\,[G_s^D(t = 0)]_{1'2',1''2''}^{-1}$$

$$\times \int_0^\infty dt \exp(-zt)$$

$$[G_s^D(1''2'', 3''4''; t) - G_{s,B}^D(1''2'', 3''4''; t)]$$

$$[G_s^D(t = 0)]_{3''4'',3'4'}^{-1}\,G_s(3'4', 34; t = 0). \qquad (4.106)$$

An entirely analogous result is valid for $\tilde{G}(12, 34; z)$, with the various G_s on the right-hand side replaced by their collective counterparts G. The inverse matrix elements appearing in these equations are evaluated by means of (4.97) and (4.99), with the result that

$$[G_s^D(t = 0)]_{12,34}^{-1} = C_s^{-1}(13; 0)C^{-1}(24; 0), \qquad (4.107)$$

$$[G^D(t = 0)]_{12,34}^{-1} = \tfrac{1}{4}[C^{-1}(13; 0)C^{-1}(24; 0) + C^{-1}(14; 0)C^{-1}(23; 0)]. \qquad (4.108)$$

The final step is to substitute the approximate expressions obtained for $\tilde{G}_s(12, 34; z)$ and $\tilde{G}(12, 34; z)$ into the memory functions (4.86) and (4.87). As a result, we see that the latter naturally split into two separate contributions. In the time domain we obtain

$$M_{s,\lambda\lambda'}(\mathbf{k}, t) = M_{sB,\lambda\lambda'}(\mathbf{k}, t) + M'_{s,\lambda\lambda'}(\mathbf{k}, t), \qquad (4.109)$$

$$M_{\lambda\lambda'}(\mathbf{k}, t) = M_{B,\lambda\lambda'}(\mathbf{k}, t) + M'_{\lambda\lambda'}(\mathbf{k}, t), \qquad (4.110)$$

where the quantities $M_{sB}(\mathbf{k}, t)$ and $M_B(\mathbf{k}, t)$ describe the fast dynamics associated with single binary collisions. These contributions are expected to decay as $\delta(t)$ in the limiting case of a hard-sphere system. On the other hand, the contributions $M'_s(\mathbf{k}, t)$ and $M'(\mathbf{k}, t)$ account approximately for the presence of correlation effects among the collisions. Equations (4.109) and (4.110) have a form identical to the one envisaged at the end of Section 4.1.2 for the phase-space memory functions. While the expressions for the binary contributions still remain somewhat formal, the establishment of explicit results for M'_s and M' shows a substantial progress. Exploiting (4.107) and (4.108), the detailed expressions for these two quantities can be written as

$$M'_{s,\lambda\lambda'}(\mathbf{k}, t) = \int d1\,d2\,d1'\,d2'\,v_{s,\lambda'}^\dagger(\mathbf{k}; 12, 1'2')\int d3'\,d4'\,\Delta_s(1'2', 3'4'; t)$$

$$\int d3\,d4\,v_{s,\lambda}(\mathbf{k}; 3'4', 34), \qquad (4.111)$$

$$M'_{\lambda\lambda'}(\mathbf{k}, t) = (1/2N)\int d1\,d2\,d1'\,d2'\,v_\lambda^\dagger(\mathbf{k}; 12, 1'2')\int d3'\,d4'$$

$$\Delta(1'2', 3'4'; t)\int d3\,d4\,v_\lambda(\mathbf{k}; 3'4', 34). \qquad (4.112)$$

Here the quantities

$$v_{s,\lambda}(\mathbf{k}; 12, 34) = G_s(12, 34; t = 0)\exp(i\mathbf{k} \cdot \mathbf{R}_3)\nabla_{\mathbf{R}_3}\phi(R_{34}) \cdot \nabla_{\mathbf{P}_3}H_\lambda(\mathbf{P}_3),$$
$$(4.113)$$

$$v_\lambda(\mathbf{k}; 12, 34) = G(12, 34; t = 0)\exp(i\mathbf{k} \cdot \mathbf{R}_3)\nabla_{\mathbf{R}_3}\phi(R_{34}) \cdot \nabla_{\mathbf{P}_3}H_\lambda(\mathbf{P}_3),$$
$$(4.114)$$

represent effective interaction vertices, and we have used the conventions $v_{s,\lambda}^\dagger(\mathbf{k}; 12, 34) = v_{s,\lambda}^*(\mathbf{k}; 34, 12)$ and $v_\lambda^\dagger(\mathbf{k}; 12, 34) = v_\lambda^*(\mathbf{k}; 34, 12)$. Moreover, we have let

$$\Delta_s(12, 34; t) = \int d\bar{1}\, d\bar{2}\, d\bar{3}\, d\bar{4}\, C_s^{-1}(1\bar{1}; 0)C^{-1}(2\bar{2}; 0)\,[C_s(\bar{1}3; t)C(\bar{2}4; t)$$
$$- C_{s,B}(\bar{1}3; t)C_B(\bar{2}4; t)]\,C_s^{-1}(\bar{3}3; 0)C^{-1}(\bar{4}4; 0), \quad (4.115)$$

$$\Delta(12, 34; t) = \int d\bar{1}\, d\bar{2}\, d\bar{3}\, d\bar{4}\, C^{-1}(1\bar{1}; 0)C^{-1}(2\bar{2}; 0)\,[C(\bar{1}3; t)C(\bar{2}4; t)$$
$$- C_B(\bar{1}3; t)C_B(\bar{2}4; t)]\,C^{-1}(\bar{3}3; 0)C^{-1}(\bar{4}4; 0). \quad (4.116)$$

Despite the cumbersome appearance of all these results, an important feature is already evident, namely that the memory functions of the phase-space correlations ultimately depend on the same dynamical quantities which we wish to determine. As a consequence, the overall framework has the typical structure of a *self-consistent approach*.

4.3.2 Mode-expansion of the non-binary contributions

Before discussing any implications of the self-consistent structure of the non-binary memory functions, it is worthwhile simplifying the expressions (4.111) and (4.112) by exploiting the decomposition into 'modes' introduced in Section 4.2. In particular, starting from the expressions

$$C(12; t) = C(\mathbf{R}_1\mathbf{P}_1, \mathbf{R}_2\mathbf{P}_2; t) = \frac{1}{8\pi^3}\sum_{\mu\mu'}f_0(P_1)f_0(P_2)\,H_\mu(\mathbf{P}_1)H_{\mu'}(\mathbf{P}_2)$$

$$\int d\mathbf{q}\, C_{\mu\mu'}(\mathbf{q}, t)\exp(-i\mathbf{q} \cdot \mathbf{R}_{12}), \quad (4.117)$$

$$C^{-1}(12; t) = \frac{1}{8\pi^3}\sum_{\mu\mu'}H_\lambda(\mathbf{P}_1)H_{\lambda'}(\mathbf{P}_2)\int d\mathbf{q}\, C_{\mu\mu'}^{-1}(\mathbf{q}, t)\exp(-i\mathbf{q} \cdot \mathbf{R}_{12}),$$
$$(4.118)$$

and similar ones for $C_s(12; t)$ and $C_s^{-1}(12; t)$, we may repeatedly use the orthogonality of the Hermite polynomials as well as the relations (4.76)–(4.79) at $t = 0$. After some algebra we find

$$M'_{s,\lambda\lambda'}(\mathbf{k}, t) = \frac{1}{8\pi^3}\sum_{\nu\nu',\xi\xi'}\int d\mathbf{q}\, v_{\nu\xi,\lambda}^{(s)*}(\mathbf{k}; \mathbf{k} - \mathbf{q}, \mathbf{q})$$
$$\Delta_{\nu\xi,\nu'\xi'}^{(s)}(\mathbf{k} - \mathbf{q}, \mathbf{q}; t)v_{\nu'\xi',\lambda}^{(s)}(\mathbf{k}; \mathbf{k} - \mathbf{q}, \mathbf{q}), \quad (4.119)$$

$$M'_{\lambda\lambda'}(\mathbf{k}, t) = \frac{1}{2n}\frac{1}{8\pi^3}\sum_{\nu\nu',\xi\xi'}\int d\mathbf{q}\, v_{\nu\xi,\lambda}^{(s)*}(\mathbf{k}; \mathbf{k} - \mathbf{q}, \mathbf{q})$$
$$\Delta_{\nu\xi,\nu'\xi'}^{(s)}(\mathbf{k} - \mathbf{q}, \mathbf{q}; t)v_{\nu'\xi',\lambda}(\mathbf{k}; \mathbf{k} - \mathbf{q}, \mathbf{q}), \quad (4.120)$$

where

$$v_{\nu\xi,\lambda}^{(s)}(\mathbf{k}; \mathbf{k} - \mathbf{q}, \mathbf{q}) = \int d1\, d2\, d3\, d4\, \exp\{-i[(\mathbf{k} - \mathbf{q}) \cdot \mathbf{R}_1 + \mathbf{q} \cdot \mathbf{R}_2 - \mathbf{k} \cdot \mathbf{R}_3]\}$$

$$\sqrt{V}\, G_s(12, 34; t = 0)$$

$$H_\nu(\mathbf{P}_1)H_\xi(\mathbf{P}_2)\nabla_{\mathbf{R}_3}\phi(R_{34}) \cdot \nabla_{\mathbf{P}_3}H_\lambda(\mathbf{P}_3), \quad (4.121)$$

$$v_{\nu\xi,\lambda}(\mathbf{k}; \mathbf{k} - \mathbf{q}, \mathbf{q}) = \frac{1}{V}\int d1\, d2\, d3\, d4\, \exp\{-i[(\mathbf{k} - \mathbf{q}) \cdot \mathbf{R}_1 + \mathbf{q} \cdot \mathbf{R}_2 - \mathbf{k} \cdot \mathbf{R}_3]\}$$

$$G(12, 34; t = 0)H_\nu(\mathbf{P}_1)H_\xi(\mathbf{P}_2)\nabla_{\mathbf{R}_3}\phi(R_{34}) \cdot \nabla_{\mathbf{P}_3}H_\lambda(\mathbf{P}_3),$$
$$(4.122)$$

$$\Delta_{\nu\xi,\nu'\xi'}^{(s)}(\mathbf{k} - \mathbf{q}, \mathbf{q}; t) = [C_{s,\nu\nu'}(\mathbf{k} - \mathbf{q}, t)C_{\xi\xi'}(\mathbf{q}, t) - C_{sB,\lambda\lambda'}(\mathbf{k} - \mathbf{q}, t)$$
$$C_{B,\xi\xi'}(\mathbf{q}, t)]\,C_{\xi\xi}^{-1}(\mathbf{q}, 0)C_{\xi'\xi'}^{-1}(\mathbf{q}, 0), \quad (4.123)$$

$$\Delta_{\nu\xi,\nu'\xi'}(\mathbf{k} - \mathbf{q}, \mathbf{q}; t) = [C_{\nu\nu'}(\mathbf{k} - \mathbf{q}, t)C_{\xi\xi'}(\mathbf{q}, t) - C_{B,\lambda\lambda'}(\mathbf{k} - \mathbf{q}, t)$$
$$C_{B,\xi\xi'}(\mathbf{q}, t)]\,C_{\nu\nu'}^{-1}(\mathbf{k} - \mathbf{q}, 0)C_{\xi\xi}^{-1}(\mathbf{q}, 0)$$
$$C_{\nu'\nu'}^{-1}(\mathbf{k} - \mathbf{q}, 0)C_{\xi'\xi'}^{-1}(\mathbf{q}, 0). \quad (4.124)$$

Inserting all these results into eqns (4.109) and (4.110), we obtain the final expressions for $M_{s,\lambda\lambda'}(\mathbf{k}, t)$ and $M_{\lambda\lambda'}(\mathbf{k}, t)$. As already remarked, the binary parts of these memory functions are characterized by a rapid time decay. On the other hand, through the quantities $\Delta^{(s)}$ and Δ the time dependence of M'_s and M' is determined by the superposition of an infinite number of mode contributions, which comprise a variety of different timescales. It is, however, reasonable to expect that the decay of the memory functions at intermediate and long times is affected only by those mode correlations which have the longest lifetimes. A natural choice for these important contributions is provided by those modes which correspond to quasi-conserved dynamical variables.

As a result, in the notation of Section 4.2 we expect that the summations in eqns (4.119) and (4.120) can be restricted to the mode indexes 0, 1, 2, and 3. In the case of a hard-sphere system, we may even include the mode Δ_4

associated with temperature fluctuations and have a complete identification of the relevant modes with the set of hydrodynamic variables. If we deal instead with a liquid characterized by a continuous potential, the quasi-conserved character of energy fluctuations cannot be accounted for within a mode expansion in terms of Hermite polynomials. Fortunately, for wavevectors beyond the strict hydrodynamic regime the relevance of the couplings to energy fluctuations is found to be small (Sjögren 1980*b*), and it is reasonable to neglect them in the intermediate- and large-*k* range usually probed in neutron-scattering experiments and in computer simulations.

As the wavevector becomes larger, a significant contribution to the collective dynamics stems from single-particle motion. To establish a relation between the two descriptions, we consider eqns (4.80) and (4.81) written in a matrix notation. These equations can formally be solved for the correlation matrices $\tilde{C}_s(\mathbf{k}, z)$ and $\tilde{C}(\mathbf{k}, z)$:

$$\tilde{C}_s(\mathbf{k}, z) = [zI - i\Omega_s(\mathbf{k}) + \tilde{M}_s(\mathbf{k}, z)]^{-1} \cdot C_s(\mathbf{k}, 0), \qquad (4.125)$$

$$\tilde{C}(\mathbf{k}, z) = [zI - i\Omega(\mathbf{k}) + \tilde{M}(\mathbf{k}, z)]^{-1} \cdot C(\mathbf{k}, 0). \qquad (4.126)$$

In the term in square brackets on the right-hand side of (4.126) we may extract a self-contribution by adding and subtracting the quantities $i\Omega_s(\mathbf{k})$ and $\tilde{M}_s(\mathbf{k}, z)$. Exploiting (4.125) and coming back with scalar notation, we obtain

$$\tilde{C}_{\lambda\nu}(\mathbf{k}, z) = \sum_{\lambda'\nu'} C_{s,\lambda\lambda'}(\mathbf{k}, 0)\tilde{C}_{s,\lambda'\lambda'}(\mathbf{k}, z)\left[C_{\nu'\nu}(\mathbf{k}, 0) + \sum_\xi \{i[\Omega_{\nu'\xi}(\mathbf{k}) \right.$$
$$\left. - \Omega_{s,\nu'\xi}(\mathbf{k})] - [\tilde{M}_{\nu'\xi}(\mathbf{k}, z) - \tilde{M}_{s,\nu'\xi}(\mathbf{k}, z)]\}\tilde{C}_{\xi\nu}(\mathbf{k}, z) \right]. \qquad (4.127)$$

After using the results (4.77), (4.78), (4.82), and (4.83) we obtain

$$\tilde{C}_{\lambda\nu}(\mathbf{k}, z) = N\{1 + [S(k) - 1]\delta_{\nu,0}\}\tilde{C}_{s,\lambda\nu}(\mathbf{k}, z)$$
$$+ iVk(m\beta)^{-1/2}nc(k)\tilde{C}_{s,\lambda1}(\mathbf{k}, z)\tilde{C}_{0\nu}(\mathbf{k}, z)$$
$$- V\sum_{\nu'\xi}\tilde{C}_{s,\lambda\nu'}(\mathbf{k}, z)[\tilde{M}_{\nu'\xi}(\mathbf{k}, z) - \tilde{M}_{s,\nu'\xi}(\mathbf{k}, z)]\tilde{C}_{\xi\nu}(\mathbf{k}, z). \qquad (4.128)$$

To illustrate this result with an example of physical interest, let us consider $\tilde{C}_{11}(\mathbf{k}, z)$ which is simply related to the longitudinal current correlation function (cf. eqn (4.74)). In this case, eqn (4.128) reads

$$\tilde{C}_{11}(\mathbf{k}, z) = N\tilde{C}_{s,11}(\mathbf{k}, z) + \frac{k^2}{m\beta z}nc(k)\tilde{C}_{s,11}(\mathbf{k}, z)\tilde{C}_{11}(\mathbf{k}, z)$$
$$- V\sum_{\nu'\xi}\tilde{C}_{s,1\nu'}(\mathbf{k}, z)[\tilde{M}_{\nu'\xi}(\mathbf{k}, z) - \tilde{M}_{s,\nu'\xi}(\mathbf{k}, z)]\tilde{C}_{\xi1}(\mathbf{k}, z) \qquad (4.129)$$

where we have used the result

$$z\tilde{C}_{01}(\mathbf{k}, z) = ik(m\beta)^{-1/2}\tilde{C}_{11}(\mathbf{k}, z) \qquad (4.130)$$

which follows directly from (4.81) noting that $C_{01}(\mathbf{k}, 0) = 0$, $i\Omega_{0\lambda'}(\mathbf{k}) = ik(m\beta)^{-1/2}\delta_{\lambda',1}$ and $\tilde{M}_{0\lambda'}(\mathbf{k}, z) = 0$ (cf. eqns (4.83) and (4.87)). If the last term on the right-hand side of (4.129) were neglected, we would obtain

$$\tilde{C}_{11}(\mathbf{k}, z) = \left\{ [N\tilde{C}_{s,11}(\mathbf{k}, z)]^{-1} - \frac{k^2}{m\beta z}nc(k) \right\}^{-1/2}. \qquad (4.131)$$

This 'mean-field' result is expected to become increasingly accurate at large wavevectors, where the dynamics evolves over a microscopic timescale; eventually, both $\tilde{C}_{11}(\mathbf{k}, z)$ and $\tilde{C}_{s,11}(\mathbf{k}, z)$ approach their common free-particle limit and the 'effective potential' $-nc(k)/\beta$ vanishes. At intermediate wavevectors slower features begin to develop in the collective dynamics, and the last term in eqn (4.129) can no longer be neglected. The leading effects of this contribution, however, are approximately accounted for by restricting the summations over the modes with ν', $\xi = 0, \ldots, 3$. The result can further be simplified by noting that for ν' or $\xi = 0$ all the memory functions vanish, and that the transverse modes with ν', $\xi = 2, 3$ give a zero contribution. As a consequence, eqn (4.129) can be cast in the form

$$\tilde{C}_{11}(\mathbf{k}, z) = \left\{ [N\tilde{C}_{s,11}(\mathbf{k}, z)]^{-1} - \frac{k^2}{m\beta z}nc(k) \right.$$
$$\left. + \frac{1}{n}[\tilde{M}_{11}(\mathbf{k}, z) - \tilde{M}_{s,11}(\mathbf{k}, z)] \right\}^{-1}. \qquad (4.132)$$

The memory functions $\tilde{M}_{s,11}(\mathbf{k}, z)$ and $\tilde{M}_{11}(\mathbf{k}, z)$ can now be split into binary- and correlated-collision contributions, following the results of the previous analysis. In particular, in the static vertex approximation the non-binary parts $\tilde{M}'_{s,11}(\mathbf{k}, z)$ and $\tilde{M}'_{11}(\mathbf{k}, z)$ are given by the Laplace transforms of eqns (4.119) and (4.120). The final step is the evaluation of the vertices $v^{(s)}_{\nu\xi,1}$ and $v_{\nu\xi,1}$, with the result (see Appendix G)

$$v^{(s)}_{\nu\xi,1}(\mathbf{k}; \mathbf{k} - \mathbf{q}, \mathbf{q}) = i(V/\beta m)^{1/2}q_z[S(q) - 1]\delta_{\nu,0}\delta_{\xi,0}, \qquad (4.133)$$

$$v_{v\xi,1}(\mathbf{k};\mathbf{k}-\mathbf{q},\mathbf{q}) \approx -in(\beta m)^{-1/2}\{q_z S(|\mathbf{k}-\mathbf{q}|)[S(q)-1]$$

$$+ (\mathbf{k}-\mathbf{q})_z S(q)[S(|\mathbf{k}-\mathbf{q}|)-1]\}\delta_{v,0}\delta_{\xi,0}. \tag{4.134}$$

Thus, the static vertex approximation automatically selects density modes as the relevant decay channels for the 'slow' portion of the memory functions. As already noted, this is generally true in the liquid range, owing to the sluggishness of the structural rearrangements prevailing at high densities. In less dense fluids, additional decay channels (particularly those involving transverse currents) play an important role; in the present framework, these features can be accounted for by suitable approximations for the first few frequency-dependent vertices (Sjögren and Sjölander 1979, Sjögren 1980a,b). As we shall see in Section 4.5, these dynamical events occurring at intermediate densities can also be studied with much less effort by a slightly different approach.

Coming back to the liquid range, we now insert the vertices (4.133) and (4.134) into eqns (4.119) and (4.120). As a result, in the time domain the final results for the memory functions appearing in eqn (4.132) can be summarized as follows:

$$M_{s,11}(\mathbf{k},t) = M_{sB,11}(\mathbf{k},t) + M'_{s,11}(\mathbf{k},t), \tag{4.135}$$

$$M_{11}(\mathbf{k},t) = M_{B,11}(\mathbf{k},t) + M'_{11}(\mathbf{k},t), \tag{4.136}$$

where, restoring the usual notation for the time-correlation functions (cf. (4.71), (4.73)):

$$M'_{s,11}(\mathbf{k},t) = \frac{n}{8\pi^3\beta m}\int d\mathbf{q}\, q_z^2 c^2(q)[F_s(|\mathbf{k}-\mathbf{q}|,t)F(q,t)$$

$$- F_{s,B}(|\mathbf{k}-\mathbf{q}|,t)F_B(q,t)], \tag{4.137}$$

$$M'_{11}(\mathbf{k},t) = \frac{n}{16\pi^3\beta m}\int d\mathbf{q}\,[q_z c(q) + (\mathbf{k}-\mathbf{q})_z c(|\mathbf{k}-\mathbf{q}|)]^2$$

$$[F(|\mathbf{k}-\mathbf{q}|,t)F(q,t) - F_B(|\mathbf{k}-\mathbf{q}|,t)F_B(q,t)]. \tag{4.138}$$

The appearance in these equations of F and F_s, whose second time derivatives are essentially the quantities C_{11} and $C_{s,11}$, makes clear the complicated self-consistent structure which in principle is behind the result (4.132).

4.3.3 The binary terms

It is now time to discuss in some detail the so far ignored 'binary' contributions in all the previous equations. Although their physical meaning is

rather clear at a qualitative level, a satisfactory treatment of these fast dynamical events in a dense fluid with a continuous potential is far from simple. Fortunately, in most cases it turns out that a very detailed knowledge of the functional forms of $M_{s,B}(t)$ and $M_B(t)$ is not required. Broadly speaking, it is reasonable to expect that the initial decay of the full memory matrices $M_s(t)$ and $M(t)$ is dominated by their binary portions. Indeed, in all cases of practical interest it is possible to show that at sufficiently short times the effects of the non-binary contributions are at least of the order t^4 (Sjögren 1980b). As a result, up to the order t^2 included, the full and the binary memory matrices coincide, and the initial decay of $M_{s,B}(t)$ and $M_B(t)$ can be deduced by analysing the short-time behaviour of $M_s(t)$ and $M(t)$. By construction, the binary contributions decrease 'rapidly' in all the situations where the full memory functions develop long-lasting 'tails'. As a consequence, the knowledge of the initial decay can be exploited by making some simple ansatz about the functional forms of $M_{s,B}(t)$ and $M_B(t)$; ideally, the choice of this 'shape function' should be largely irrelevant, provided that it assures a sufficiently rapid decay with respect to the extent in time of the full memory functions. Besides these obvious reasons of simplicity, there is an additional motivation for introducing some element of 'reasonable phenomenology' into the subject. As previously remarked, the important contributions to the long-lasting features of the memory functions are expected to stem from the couplings to the 'slow' modes, typically those which are quasi-conserved. On the other hand, the mode expansions (4.119) and (4.120) comprise a wealth of couplings with other 'fast' (or 'kinetic') modes. If we focus our attention only on the slow features, these additional couplings effectively 'renormalize' the purely binary contributions. As a result, even assuming that the binary dynamics has been solved beyond the level of the initial decay, this would not be the full story for the details of the fast decay of the memory function. In such a situation, it is clearly wiser to assume a more pragmatic attitude by adopting the previously mentioned 'recipes'.

To illustrate these general remarks in a practical case, let us consider eqns (4.135) and (4.136). The short-time behaviour of the full memory functions can be written in the form (cf. (3.33))

$$M_{s,11}(\mathbf{k},t) = M_{s,11}(\mathbf{k},0)\{1 - [t/\tau_{s,11}(k)]^2 + \cdots\}, \tag{4.139}$$

$$M_{11}(\mathbf{k},t) = M_{11}(\mathbf{k},0)\{1 - [t/\tau_{11}(k)]^2 + \cdots\}, \tag{4.140}$$

where the initial decay times $\tau_{s,11}(k)$ and $\tau_{11}(k)$ can be evaluated as in eqn (3.34). At this order, the binary memory functions $M_{sB,11}(\mathbf{k},t)$ and $M_{B,11}(\mathbf{k},t)$ have exactly the same short-time behaviour as their 'full' counterparts. This fact is conveniently exploited by assuming that the overall time dependence of the binary portions can be written in the form

$$M_{sB,11}(\mathbf{k}, t) = M_{s,11}(\mathbf{k}, 0)f(t/\tau_{s,11}(k)), \qquad (4.141)$$

$$M_{B,11}(\mathbf{k}, t) = M_{11}(\mathbf{k}, 0)f(t/\tau_{11}(k)), \qquad (4.142)$$

where the shape function $f(x)$ decays rapidly and is such that $f(x) \approx 1 - x^2$ for small x. Convenient choices satisfying these requirements may, for example, be $f(x) = \exp(-x^2)$ or $f(x) = \mathrm{sech}^2(x)$.

The initial values $M_{s,\lambda\lambda'}(\mathbf{k}, t = 0)$ and $M_{\lambda\lambda'}(\mathbf{k}, t = 0)$ are in any case obtained from a large z expansion of eqns (4.86) and (4.87). Noting that $\tilde{G}_s(z) = G_s(t = 0)/z$ and $\tilde{G}(z) = G(t = 0)/z$ at the lowest order in $1/z$, after some lengthy but straightforward calculations we obtain

$$M_{s,\lambda\lambda'}(\mathbf{k}, t = 0) = \frac{m}{\beta}\Omega_0^2 \int d\mathbf{P} f_0(P)\nabla_P H_\lambda(\mathbf{P}) \cdot \nabla_P H_{\lambda'}(\mathbf{P}), \qquad (4.143)$$

$$M_{\lambda\lambda'}(\mathbf{k}, t = 0) = \frac{m}{\beta}\sum_{a,\beta}\left[\Omega_0^2\delta_{a,\beta} - \gamma_{a\beta}(\mathbf{k}) + \frac{1}{\beta m}k_a k_\beta nc(k)\right]$$

$$\int d\mathbf{P} f_0(P)\frac{\partial H_\lambda(\mathbf{P})}{\partial P_a}\int d\mathbf{P}' f_0(P')\frac{\partial H_{\lambda'}(\mathbf{P}')}{\partial P_\beta'}, \qquad (4.144)$$

where Ω_0 is the Einstein frequency, the summations run over cartesian coordinates, and

$$\gamma_{a\beta}(\mathbf{k}) \equiv \frac{n}{m}\int d\mathbf{R}\frac{\partial^2\phi(R)}{\partial R_a \partial R_\beta}\exp(i\mathbf{k}\cdot\mathbf{R})g(R). \qquad (4.145)$$

The results (4.143) and (4.144) are exact. On the other hand, the expressions for the short-time decay of the memory functions involve both pair and triplet distribution functions, where the latter are usually approximated within the simple 'superposition scheme' (1.17). We shall see some examples of these evaluations in Chapters 5 and 6.

The last point which remains to be discussed in the context of binary quantities is how to deal with the 'matrices' $C_{sB}(t)$ and $C_B(t)$ appearing in eqns (4.123) and (4.124). In Section 4.3.1 we have already argued that in the case of the self-memory functions (4.123) the elements of $C_{sB}(t)$ can be identified with those appropriate for free particles, whereas $C_B(t)$ coincides with the full $C(t)$. When applied to eqn (4.137), these arguments lead to the result

$$M'_{s,11}(\mathbf{k}, t) = \frac{n}{8\pi^3\beta m}\int d\mathbf{q}\, q_z^2 c^2(q)\left[F_s(|\mathbf{k} - \mathbf{q}|, t) - F_0(|\mathbf{k} - \mathbf{q}|, t)\right]F(q, t)$$

$$= \frac{n}{8\pi^3\beta m}\int d\mathbf{q}\, q_z^2 c^2(q)\left[1 - \frac{F_0(|\mathbf{k} - \mathbf{q}|, t)}{F_s(|\mathbf{k} - \mathbf{q}|, t)}\right]F_s(|\mathbf{k} - \mathbf{q}|, t)F(q, t)$$

$$\qquad (4.146)$$

where $F_0(q, t) = \exp(-q^2 t^2/2\beta m)$ is the free-particle expression of the intermediate scattering function. Owing to the factors in square brackets, $M'_{s,11}(\mathbf{k}, t) \propto t^4$ at sufficiently short times. In dense fluids F_0 decays much faster than F_s as t increases, and the square-bracketed factor in the last step of (4.146) rapidly approaches unity. The true long-lasting 'tail' of $M_{s,11}$ is consequently ruled by a decay channel involving the product $F_s F$.

On the other hand, the simple identification $C_B(t) = C(t)$ is not applicable to the collective case. In the case of (4.138), a simple recipe to circumvent the problem while still maintaining the requirement of a rapid decay of $F_B(t)$ is to assume that (Sjögren 1980b)

$$F_B(q, t) = [F_0(q, t)/F_s(q, t)]F(q, t). \qquad (4.147)$$

Equation (4.138) can consequently be written as

$$M'_{11}(\mathbf{k}, t) = \frac{n}{16\pi^3\beta m}\int d\mathbf{q}\,[q_z c(q) + (\mathbf{k} - \mathbf{q})_z c(|\mathbf{k} - \mathbf{q}|)]^2$$

$$\left\{1 - \frac{F_0(|\mathbf{k} - \mathbf{q}|, t)F_0(q, t)}{F_s(|\mathbf{k} - \mathbf{q}|, t)F_s(q, t)}\right\}F(|\mathbf{k} - \mathbf{q}|, t)F(q, t).$$

$$\qquad (4.148)$$

Hence, the tail of $M_{11}(\mathbf{k}, t)$ is ultimately ruled by the product FF.

4.4 A GENERALIZED HYDRODYNAMIC DESCRIPTION

The relevant role played by 'slow modes' in the general kinetic framework has been stressed on several occasions in the last subsections. This circumstance has clear analogies with the situation met in ordinary hydrodynamics, where the attention is focused on a small set of dynamical variables whose time evolution becomes very slow as the wavevector $k \to 0$. As the first few modes are in fact identical with the microscopic hydrodynamic variables, we may ask ourselves whether it is possible to establish a connection between the two descriptions. Since the validity of the kinetic framework is not restricted to a particular range of wavevectors, the correspondence will also establish a sort of 'generalized hydrodynamics', which can be compared with the microscopic treatment discussed in Section 3.4.

A convenient starting point for the analysis is the memory equation (4.81) for the Laplace transforms $\tilde{C}_{\lambda\nu}(z)$ of the collective correlations. Rather than dealing with the full set of indexes λ, ν, we wish to rewrite eqn (4.81) in such a way that only a limited number of modes appears explicitly. This restricted set of H elements is chosen to comprise only those modes which have a correspondence with the microscopic expressions of the

hydrodynamic variables; in practice, we may choose the first four or five modes, according to whether we wish to include explicitly temperature fluctuations in the restricted set. Writing eqn (4.81) in the matrix form

$$z\tilde{C}(\mathbf{k}, z) - C(\mathbf{k}, t = 0) = \mathrm{i}[\Omega(\mathbf{k}) - \tilde{M}(\mathbf{k}, z)]\tilde{C}(\mathbf{k}, z)$$

$$\equiv \sigma(\mathbf{k}, z)\tilde{C}(\mathbf{k}, z), \qquad (4.149)$$

the task of making explicit the appearance of only the H 'hydrodynamic' modes of interest can be accomplished by introducing a suitable projection operator $\mathcal{P}_{\mathrm{hyd}}$ which projects over this restricted set. Adopting a bra-ket notation such that $C_{\lambda v} = \langle \lambda | C | v \rangle$, etc., the completeness of the full set of modes can be expressed by the relation $\sum_{v=0}^{\infty} |v\rangle\langle v| = 1$. Then $\mathcal{P}_{\mathrm{hyd}} = \sum_{v=0}^{H-1} |v\rangle\langle v| \equiv \sum_{n=0}^{H-1} |n\rangle\langle n|$, where the H modes of interest have been denoted with Latin indexes $l, n, \ldots$ (n is of course not to be confused with the number density). Conversely, the complementary operator $Q_{\mathrm{hyd}} = 1 - \mathcal{P}_{\mathrm{hyd}} = \sum_{v=H}^{\infty} |v\rangle\langle v|$ projects over the 'non-hydrodynamic' modes, for which we keep the usual Greek-index notation. After a repeated application of these projection operators on eqn (4.149), we obtain the exact result (Forster and Martin 1970; Forster 1974; Mazenko 1974)

$$z\tilde{C}_{ln}(\mathbf{k}, z) - C_{ln}(\mathbf{k}, t = 0) = \sum_{l'=1}^{H-1} [\mathrm{i}\Omega_{ll'}(\mathbf{k}) - \tilde{M}_{ll'}(\mathbf{k}, z)$$

$$- \tilde{m}_{ll'}(\mathbf{k}, z)]\tilde{C}_{l'n}(\mathbf{k}, z) \qquad (4.150)$$

where the quantities $\tilde{m}_{ll'}(\mathbf{k}, z)$ can be expressed as

$$\tilde{m}_{ll'}(\mathbf{k}, z) = -\sum_{\mu=H}^{\infty}\sum_{\mu'=H}^{\infty} \tilde{\sigma}_{l\mu}(\mathbf{k}, z)\{Q_{\mathrm{hyd}}[zI - Q_{\mathrm{hyd}}\tilde{\sigma}(\mathbf{k}, z)Q_{\mathrm{hyd}}]^{-1}Q_{\mathrm{hyd}}\}_{\mu\mu'}$$

$$\times \tilde{\sigma}_{\mu'l'}(\mathbf{k}, z). \qquad (4.151)$$

In other terms, all the couplings between the H variables of interest and the non-hydrodynamic modes are transferred into the new 'memory functions' $\tilde{m}_{ll'}(\mathbf{k}, z)$.

Let us now consider the density correlation $C_{00}(\mathbf{k}, t) = nF(k, t)$. In the full formulation, its Laplace transform $\tilde{C}_{00}(\mathbf{k}, z)$ satisfies the equation

$$z\tilde{C}_{00}(\mathbf{k}, z) - nS(k) = \sum_{\mu=0}^{\infty} [\mathrm{i}\Omega_{0\mu}(\mathbf{k}) - \tilde{M}_{0\mu}(\mathbf{k}, z)]\tilde{C}_{\mu 0}(\mathbf{k}, z)$$

$$= \mathrm{i}k(m\beta)^{-1/2}\tilde{C}_{10}(\mathbf{k}, z) \qquad (4.152)$$

where in the last step we have used $\mathrm{i}\Omega_{0\mu}(\mathbf{k}) = \mathrm{i}k(\beta m)^{-1/2}\delta_{\mu,1}$ and $\tilde{M}_{0\mu}(\mathbf{k}, z) = \tilde{M}_{\mu 0}(\mathbf{k}, z) = 0$. The result (4.152) is simply the Laplace version of the continuity equation for the number of particles. On the other hand, from the opposite time-reversal symmetries of the modes A_0 and

A_1 it follows that $C_{10}(\mathbf{k}, t) = -C_{01}^*(\mathbf{k}, t)$ (cf. Appendix B). Exploiting eqn (4.130) we find that

$$z[z\tilde{C}_{00}(\mathbf{k}, z) - nS(k)] = -(k^2/m\beta)\tilde{C}_{11}(\mathbf{k}, z). \qquad (4.153)$$

Let us now write the memory equation of $\tilde{C}_{11}(\mathbf{k}, z)$ according the new formulation (4.150). If we choose $H = 4$ we simply obtain

$$z\tilde{C}_{11}(\mathbf{k}, z) - n = \mathrm{i}\Omega_{10}(\mathbf{k})\tilde{C}_{01}(\mathbf{k}, z) - [\tilde{M}_{11}(\mathbf{k}, z) + \tilde{m}_{11}^{(4)}(\mathbf{k}, z)]\tilde{C}_{11}(\mathbf{k}, z)$$

$$(4.154)$$

where we have used $\mathrm{i}\Omega_{11}(\mathbf{k}) = 0$, and noted that the transverse modes A_2 and A_3 are effectively uncoupled. The superscript (4) reminds us that we are dealing with a restricted set of four modes. We may now use (4.130) to eliminate $\tilde{C}_{01}(\mathbf{k}, z)$; noting that

$$\mathrm{i}\Omega_{10}(\mathbf{k}) = \mathrm{i}k(\beta m)^{-1/2} + \mathrm{i}k(\beta m)^{-1/2}nc(k) = [\mathrm{i}k/S(k)](\beta m)^{-1/2}$$

$$(4.155)$$

we find that $\tilde{C}_{11}(\mathbf{k}, z)$ can be expressed as

$$\tilde{C}_{11}(\mathbf{k}, z) = n\{z + [k^2/\beta mS(k)z] + [\tilde{M}_{11}(\mathbf{k}, z) + \tilde{m}_{11}^{(4)}(\mathbf{k}, z)]\}^{-1}.$$

$$(4.156)$$

Substituting this result into eqn (4.153), we obtain

$$\tilde{C}_{00}(\mathbf{k}, z) = nS(k)\left\{z + \frac{[k^2/\beta mS(k)]}{z + [\tilde{M}_{11}(\mathbf{k}, z) + \tilde{m}_{11}^{(4)}(\mathbf{k}, z)]}\right\}^{-1}. \quad (4.157)$$

We now compare eqn (4.157) with a more conventional 'continued-fraction' representation of $\tilde{F}(k, z) = \tilde{C}_{00}(\mathbf{k}, z)/n$, as discussed at the end of Section 3.1. Taking density fluctuations as the only Mori variable, in such a case we would get

$$\tilde{F}(k, z) = S(k)\left[z + \frac{\langle \omega_k^2 \rangle}{z + \tilde{K}_{\mathrm{L}}(k, z)}\right]^{-1} \qquad (4.158)$$

where we have denoted by $K_{\mathrm{L}}(k, t)$ the second-order memory function of $F(k, t)$. Since $\langle \omega_k^2 \rangle = [k_{\mathrm{B}}T/mS(k)]k^2$, we immediately find that

$$\tilde{K}_{\mathrm{L}}(k, z) = \tilde{M}_{11}(\mathbf{k}, z) + \tilde{m}_{11}^{(4)}(\mathbf{k}, z). \qquad (4.159)$$

Expanding this result for large values of z, at the lowest order in $(1/z)$ we find a similar relation for the initial values of the corresponding memory functions. From eqns (3.42b), (1.142), and (1.143) we have that

$$K_{\mathrm{L}}(k, t = 0) = \omega_{\mathrm{L}}^2(k) - \langle \omega_k^2 \rangle$$

$$= \frac{3}{\beta m}k^2 + \Omega_0^2 - \Omega_k^2 - \frac{k^2}{\beta mS(k)}. \qquad (4.160)$$

On the other hand (cf. (4.144))

$$M_{11}(\mathbf{k}, t = 0) = \Omega_0^2 - \gamma_{zz}(\mathbf{k}) + \frac{k^2}{\beta m} nc(k)$$

$$= \frac{k^2}{\beta m} + \Omega_0^2 - \Omega_k^2 - \frac{k^2}{\beta m S(k)}. \qquad (4.161)$$

Equations (4.160) and (4.161) differ by a term $(2k^2/\beta m)$, which clearly must come from couplings to variables not included in our original set of four modes. Indeed, from a large z expansion of $\tilde{m}_{11}^{(4)}(\mathbf{k}, z)$ we obtain

$$m_{11}^{(4)}(\mathbf{k}, t = 0) = -\sum_{\mu\mu'} [i\Omega_{1\mu}(\mathbf{k})] \delta_{\mu,\mu'} [i\Omega_{\mu'1}(\mathbf{k})]$$

$$= -\sum_{\mu} [i\Omega_{1\mu}(\mathbf{k})][i\Omega_{\mu1}(\mathbf{k})]. \qquad (4.162)$$

Noting that

$$i\Omega_{1\mu}(\mathbf{k}) = i\Omega_{\mu1}(\mathbf{k}) = ik(\beta m)^{-1/2} [(\sqrt{6}/3)\delta_{\mu,4} + (2/\sqrt{3})\delta_{\mu,5}] \qquad (4.163)$$

we find

$$m_{11}^{(4)}(\mathbf{k}, t = 0) = \frac{k^2}{\beta m}\left(\frac{6}{9} + \frac{4}{3}\right) = 2k^2/\beta m \qquad (4.164)$$

which is just the 'missing term' in eqn (4.161).

Coming back to the results (4.156) and (4.157), we may wish to explore the collective dynamics at a more refined level by even including kinetic energy fluctuations in the set of relevant modes. This amounts to splitting the memory function $\tilde{m}_{11}^{(4)}(\mathbf{k}, z)$ into a term which explicitly takes into account the coupling with the additional mode, plus a 'remainder' $\tilde{m}_{11}^{(5)}((\mathbf{k}, z)$ which deals with all the other variables with $\mu \geqslant 5$. After some straightforward algebraic manipulations, for $H = 5$ it is found that $\tilde{C}_{11}(\mathbf{k}, z)$ can be written as in eqn (4.156) with

$$\tilde{m}_{11}^{(4)}(\mathbf{k}, z) = \frac{|i\Omega_{14}(\mathbf{k}) - [\tilde{M}_{14}(\mathbf{k}, z) + \tilde{m}_{14}^{(5)}(\mathbf{k}, z)]|^2}{z + [\tilde{M}_{44}(\mathbf{k}, z) + \tilde{m}_{44}^{(5)}(\mathbf{k}, z)]} + \tilde{m}_{11}^{(5)}(\mathbf{k}, z). \qquad (4.165)$$

We finally insert this result into eqn (4.157). As $C_{14}^*(\mathbf{k}, t) = -C_{41}(\mathbf{k}, t)$, we use the relation

$$|i\Omega_{14} - [\tilde{M}_{14} + \tilde{m}_{14}^{(5)}]|^2 = -\{i\Omega_{14} - [\tilde{M}_{14} + \tilde{m}_{14}^{(5)}]\}\{i\Omega_{41} - [\tilde{M}_{41} + \tilde{m}_{41}^{(5)}]\} \qquad (4.166)$$

to express $\tilde{F}(k, z) = \tilde{C}_{00}(\mathbf{k}, z)/n$ in the form

$$\frac{\tilde{F}(k, z)}{S(k)} = \left\{ z + \frac{k^2[k_B T/mS(k)]}{z + \tilde{M}_{11}^{(5)}(\mathbf{k}, z) - \dfrac{[i\Omega_{14}(\mathbf{k}) - \tilde{M}_{14}^{(5)}(\mathbf{k}, z)][i\Omega_{41}(\mathbf{k}) - \tilde{M}_{41}^{(5)}(\mathbf{k}, z)]}{z + \tilde{M}_{44}^{(5)}(\mathbf{k}, z)}} \right\}^{-1}$$

$$(4.167)$$

where we have let $\tilde{M}_{1m}^{(5)} = \tilde{M}_{1m} + \tilde{m}_{1m}^{(5)}$. With the appropriate correspondence of indexes, eqn (4.167) closely resembles the previous result (3.135) obtained in a 'conventional' framework. Since the first four modes are also quasi-conserved variables, this similarity is hardly surprising. Note, however, that in the present approach the fifth mode A_4 accounts for the microscopic fluctuations in the kinetic energy rather than in the total energy (the latter being the actual quasi-conserved variable). The dynamical processes ruling the interchange between kinetic and potential energy are dealt with by the quantity $\tilde{C}_{44}(\mathbf{k}, z)$ which enters in the derivation of eqn (4.165). As a result, the memory function $\tilde{M}_{44}^{(5)}(\mathbf{k}, z)$ appearing in (4.167) contains a contribution which for $k \to 0$ can be identified with the ordinary thermal conductivity κ (Forster 1974; Mazenko 1974).

Considerably simpler results are found for the Laplace transforms $\tilde{C}_{22}(\mathbf{k}, z)$ and $\tilde{C}_{33}(\mathbf{k}, z)$ of the transverse current correlation functions. In such a case, for $H \leqslant 6$ we obtain

$$\tilde{C}_{22}(\mathbf{k}, z) = \tilde{C}_{33}(\mathbf{k}, z) = \frac{n}{z + [\tilde{M}_{22}(\mathbf{k}, z) + \tilde{m}_{22}(\mathbf{k}, z)]}. \qquad (4.168)$$

Comparing this with eqn (3.112), we see that the transverse current memory function $\tilde{K}_T(k, z)$ can simply be expressed as

$$\tilde{K}_T(k, z) = \tilde{M}_{22}(\mathbf{k}, z) + \tilde{m}_{22}(\mathbf{k}, z). \qquad (4.169)$$

Again, it is instructive to check this result at the level of the initial values of the memory functions. Equations (3.42a) and (1.51) give

$$K_T(k, t = 0) = \omega_T^2(k) = (k^2/\beta m) + \Omega_0^2 - (\Omega_k')^2 \qquad (4.170)$$

whereas from (4.144) we deduce

$$M_{22}(\mathbf{k}, t = 0) = \Omega_0^2 - \gamma_{xx}(\mathbf{k}) = \Omega_0^2 - (\Omega_k')^2. \qquad (4.171)$$

The 'missing term' $(k^2/\beta m)$ is again provided by the couplings with non-hydrodynamic modes. In particular, a $(1/z)$ expansion of $\tilde{m}_{22}(\mathbf{k}, z)$ yields

$$m_{22}(\mathbf{k}, t = 0) = -\sum_{\mu=6}^{\infty} [i\Omega_{2\mu}(\mathbf{k})] [i\Omega_{\mu 2}(\mathbf{k})] = -\sum_{\mu=6}^{\infty} [i\Omega_{2\mu}(\mathbf{k})]^2$$

$$= -\sum_{\mu} [ik(\beta m)^{-1/2} \delta_{\mu, 6}]^2 = k^2/\beta m. \tag{4.172}$$

The results (4.167) and (4.168) are formally exact, and at finite wave-vectors provide a suitable generalization of ordinary hydrodynamics in the framework of kinetic approaches. It is of course possible to go beyond the level of this direct correspondence by choosing a larger set of 'relevant modes'. In practice, higher-order couplings are dealt with by some simple approximation scheme, and the problem is formally reduced to the solution of a finite system of linear equations. These techniques are usually referred to as 'kinetic modelling' (Mazenko *et al.* 1972).

When considered from the point of view of the conventional memory functions such as K_L or K_T, the utility of the results (4.159) and (4.169) stems from the fact that by a judicious selection of relevant modes any long-lasting tail in these memory functions may be incorporated into the 'direct' terms $M_{lm}(\mathbf{k}, t)$, or more precisely into their *non-binary* portions $M'_{lm}(\mathbf{k}, t)$. The other contributions (comprising both the 'indirect' terms m_{lm} and the binary portions $M_{B, lm}$) are expected to account for the short time features (including the correct initial value) of $K_L(k, t)$ and $K_T(k, t)$. For example, following these arguments, eqns (4.159) and (4.169) can further be split as

$$K_L(k, t) = [M_{B,11}(\mathbf{k}, t) + m_{11}(\mathbf{k}, t)] + M'_{11}(\mathbf{k}, t)$$
$$\equiv [K_L(k, t)]_{\text{fast}} + M'_{11}(\mathbf{k}, t), \tag{4.173}$$

$$K_T(k, t) = [M_{B,22}(\mathbf{k}, t) + m_{22}(\mathbf{k}, t)] + M'_{22}(\mathbf{k}, t)$$
$$\equiv [K_T(k, t)]_{\text{fast}} + M'_{22}(\mathbf{k}, t) \tag{4.174}$$

where the subscript 'fast' indicates that these contributions account for the rapid initial decay of the memory functions K_L and K_T.

As remarked in Section 4.3.2, these considerations can be pushed even further by arguing that in the expansion (4.120) for $M'_{lm}(\mathbf{k}, t)$ the modes responsible for the long-lasting features are just the 'slow' modes of the original set. For the tails, the results bear a close resemblance to those deducible in an entirely different framework, originally introduced to account for unexpected features in the dynamics of systems near the critical point. We shall close this chapter with a brief discussion of these 'mode-coupling' approaches.

4.5   MODE-COUPLING APPROACHES: CONCEPTS AND A SIMPLE APPLICATION

Let us consider a physical system specified by a given Hamiltonian, and assume that we have good reasons to believe that a dynamical variable A (or, possibly, a limited set of variables) can be regarded as 'slow' in the sense that its evolution proceeds over times considerably longer than those associated with some typical microscopic timescale. By construction, the corresponding fluctuating force f_A is orthogonal to A at all times, and evolves in a different dynamical subspace. As already remarked on several occasions, if A is really slow we may expect a definite separation of timescales between the dynamics of $C_A(t) = \langle AA(t) \rangle$ and that of the memory function $K_A(t) = \langle f_A f_A(t) \rangle / \langle AA \rangle$. The effects of the latter can ultimately be accounted for by a Markovian approximation, and we have made a big step in the direction of predicting a reliable $C_A(t)$.

Unfortunately, these beautifully simple pieces of 'conventional wisdom' turn out to give incorrect results in several cases of considerable physical interest. Paradoxically, the failures are found to be more marked just where the slow character of A seems beyond any doubt. For instance, in critical dynamics (where the decay of the relevant fluctuations is certainly characterized by macroscopically long lifetimes) one observes spectral shapes which are typically non-Lorentzian, in contrast with the Markovian predictions. Outside the critical region, ordinary Navier–Stokes hydrodynamics surely deals with slow variables, and its results are accurate to the order k^2. However, the attempts to extend their validity by considering higher-order terms in k^3 or k^4 (the so-called 'Burnett equations') run immediately into difficulties or even divergences, indicating a clear non-analytic behaviour. Finally, the often mentioned presence of long-time tails $\propto t^{-3/2}$ in many correlation functions definitely cannot be accounted for by a simple Markovian scheme.

The answer given by *mode-coupling theories* to these disturbing problems can be summarized in a few remarks. First, the orthogonality of the fluctuating force to the slow variable A does not necessarily mean that f_A is orthogonal even to combinations of the form AA, AAA, etc. Second, these nonlinear contributions should retain some slowly varying features; thus, the assumed 'fast' subspace of the fluctuating forces may possibly comprise a slow portion, whose presence is ultimately reflected in the dynamics of the memory functions. Finally, the leading contributions to these long-lasting features can be determined by extracting from f_A the parts which behave like the bilinear combinations AA. If these terms exist (i.e. if the 'coupling' to this pair of 'modes' does not vanish), they should

account for any tail occurring at sufficiently long times, and the other couplings to $AAA, \ldots$ can be considered as higher-order effects.

In practice, the simplest way to extract the dominant slow contributions is to introduce another projection operator $\mathcal{P}_2$ which projects any variable onto the subspace spanned by the product AA (in the case of a set of slow modes, AA may clearly involve a bilinear combination of different modes). As a result, the long-time behaviour of $K_A(t)$ as predicted by the mode-coupling framework turns out to be

$$[K_A(t)]_{MC} = \langle \{\mathcal{P}_2 f_A(0)\}^* \exp[i(1 - \mathcal{P})Lt] \{\mathcal{P}_2 f_A(0)\} \rangle / \langle AA \rangle$$

$$= |\langle AA f_A(0) \rangle|^2 \langle AA \exp[i(1 - \mathcal{P})Lt] AA \rangle / \langle AA \rangle \langle AAAA \rangle.$$
$$(4.175)$$

The 'vertex' $\langle AA f_A(0) \rangle$ measures the efficiency of the coupling to the pair variable AA. The time-dependent correlation function in (4.175) is approximately decoupled into the product of two simpler dynamic correlations $\langle AA(t) \rangle$, at the same time replacing the anomalous propagator with the ordinary one $\exp(iLt)$. Note that in Section 4.3.1 similar approximations have been made by replacing the full G_s and G with their respective 'disconnected' portions.

Rather than discussing in more detail the general features of mode-coupling approaches (e.g. Keyes 1977), we prefer to illustrate how the framework works in an important case. In this particular example, the final result will be the emergence of the famous $t^{-3/2}$ long-time tail in the velocity autocorrelation function $\psi(t)$.

Let us begin by considering the self-intermediate scattering function $F_s(k, t)$. Its first-order memory function $K_s(k, t)$ has been introduced in Section 3.4.1, where it was shown that for small wavevectors the ratio $K_s(k, t)/k^2$ approaches the velocity autocorrelation function. Since we are dealing with a single-particle problem, a first slow mode is naturally provided by the wavevector-dependent self-density fluctuations $n_{s,i}$. Owing to the symmetry of the fluctuating force $\mathbf{k} \cdot \mathbf{v}_i \exp(i\mathbf{k} \cdot \mathbf{r}_i)$ under time reversal, the other slow mode is associated with the collective current $\mathbf{j}$. When applying the recipe (4.175), translational invariance requires that the product of the two modes is of the form $n_{s,i}(\mathbf{q}) \mathbf{j}(\mathbf{k} - \mathbf{q})$, where eventually we have to sum over all the intermediate wavevectors $\mathbf{q}$. Making the decoupling approximations discussed above, we arrive at

$$[K_s(k, t)]_{MC} = \frac{k^2}{8\pi^3 n} \int d\mathbf{q} \, [\hat{q}_z^2 C_L(q, t) + (1 - \hat{q}_z^2) C_T(q, t)]$$

$$\times F_s(|\mathbf{k} - \mathbf{q}|, t) \qquad (4.176)$$

where the external wavevector $\mathbf{k}$ has been chosen along the z-axis, and $\hat{q}_z = q_z/q$. Therefore, making the limit $k \to 0$ the normalized velocity autocorrelation function $\psi(t)$ is found to read as

$$[\psi(t)]_{MC} = \frac{\beta m}{24\pi^3 n} \int d\mathbf{q} \, [C_L(q, t) + 2C_T(q, t)] F_s(q, t). \quad (4.177)$$

Because of the mode-coupling arguments used in its derivation, this result is expected to account only for the long-lasting tail of $\psi(t)$. In particular, eqn (4.177) breaks down completely in the short-time region, where the decay is known to be determined by fast and localized collisional processes (cf. Section 3.3). A possible way of taking into account the effects of these microscopic mechanisms has been devised by Gaskell and Miller (1978), the final result being of the form (4.177) with a q-dependent 'vertex' $f(q)$ appearing in the integral. This 'velocity field approach' is discussed in detail in Appendix H.

In the appropriate domain of validity of the result (4.177), namely for sufficiently long times, the slow features of $\psi(t)$ are determined by the contribution of the small wavevectors, where all the correlation functions can be expressed in terms of a hydrodynamic description. In practice, the slowest contribution turns out to be provided by the decay channel involving the product $C_T(q, t) F_s(q, t)$. Inserting into (4.177) the hydrodynamic expressions (3.96), and (3.108), and performing the integral, we eventually find that

$$[\psi(t)]_{MC} = \frac{1}{12n} \left\{ \pi \left[D + \frac{\eta}{nm} \right] t \right\}^{-3/2} \qquad (4.178)$$

which is the aforementioned $t^{-3/2}$ long-time tail. In dense fluids, the amplitude factor in eqn (4.178) is usually dominated by the shear viscosity term, which comes from the effect of transverse current correlations. Physically, this implies the development around the tagged particle of 'vortex patterns' which in a sense may support its motion in a given direction. Both the $t^{-3/2}$ decay law and the presence of vortices has indeed been observed in hard-sphere fluids at intermediate densities (Alder and Wainwright 1970). In principle, the same effect is present even at higher densities, namely in the typical liquid range. However, here the substantial growth of the shear viscosity η decreases the amplitude factor in (4.178) so much as to make this tail virtually unobservable. As we shall see in the next chapter, in the liquid range the actual behaviour of $\psi(t)$ at intermediate and long times (including the 'cage effect') is determined by decay channels having an entirely different physical origin.

REFERENCES

Akcasu, A. Z. and Duderstadt, J. J. (1969). *Phys. Rev.*, **188**, 479.
Akcasu, A. Z., Corngold, N., and Duderstadt, J. J. (1970). *Phys. Fluids*, **13**, 2213.
Alder, B. J. and Wainwright, T. E. (1970). *Phys. Rev. A*, **1**, 18.
Alley, W. B., Alder, B. J., and Yip, S. (1983). *Phys. Rev. A*, **27**, 3174.
Blum, L. and Lebowitz, J. L. (1969). *Phys. Rev.*, **185**, 273.
Boon, J. P. and Yip, S. (1980). *Molecular hydrodynamics*, McGraw-Hill, New York.
Desai, R. C. (1971). *Phys. Rev. A*, **3**, 320.
deSchepper, I. and Cohen, E. G. D. (1980). *Phys. Rev. A*, **22**, 287.
deSchepper, I. and Cohen, E. G. D. (1982). *J. Stat. Phys.*, **27**, 223.
Forster, D. (1974). *Phys. Rev. A*, **9**, 943.
Forster, D. and Martin, P. C. (1970). *Phys. Rev. A*, **2**, 1575.
Friedman, H. L. (1985). *A course in statistical mechanics*, Prentice-Hall, Englewood Cliffs, NJ.
Gaskell, T. and Miller, S. (1978). *J. Phys. C*, **11**, 3749.
Hansen, J.-P. and McDonald, I. R. (1986). *Theory of simple liquids*, 2nd ed, Academic Press, London.
Keyes, T. (1977). In *Statistical mechanics, Part B: Time-dependent processes* (ed. B. J. Berne), p. 259. Plenum Press, New York.
Kirkpatrick, T. R. (1985). *Phys. Rev. A*, **32**, 3130.
Konijnendijk, H. H. U. and van Leeuwen, J. M. J. (1973). *Physica*, **64**, 342.
Leutheusser, E. (1982). *J. Phys. C*, **15**, 2801 and 2827.
Mazenko, G. F. (1972). *Phys. Rev. A*, **5**, 2545.
Mazenko, G. F. (1974). *Phys. Rev. A*, **9**, 360.
Mazenko, G. F. and Yip, S. (1977). In *Statistical mechanics. Part B: Time-dependent processes* (ed. B. J. Berne), p. 181. Plenum Press, New York.
Mazenko, G. F., Wei, T. Y. C., and Yip, S. (1972). *Phys. Rev. A*, **6**, 1981.
Mori, H. (1965). *Progr. Theor. Phys.*, **33**, 423.
Reed, T. M. and Gubbins, K. E. (1973). *Applied statistical mechanics*. McGraw-Hill Kogakusha, Tokyo.
Sjögren, L. and Sjölander, A. (1979). *J. Phys. C*, **12**, 4369.
Sjögren, L. (1980a). *J. Phys. C*, **13**, 705.
Sjögren, L. (1980b). *Phys. Rev. A*, **22**, 2866.

5

Single-particle properties

5.1 THE VELOCITY AUTOCORRELATION FUNCTION REVISITED

In Section 3.3 we have seen that the dynamical processes underlying the velocity autocorrelation function in the liquid range cannot be accounted for by a simplified memory-function analysis. In particular, the assumption that the decay of the memory function is ruled by a single relaxation time must be significantly revised in view of the results of the kinetic framework developed in the last chapter.

In this context, the relevant equations can be summarized as follows. The normalized velocity autocorrelation function $\psi(t)$ satisfies the memory equation (3.66):

$$\dot{\psi}(t) = -\int_0^t dt' \, K(t') \psi(t - t').$$ (5.1)

In terms of Laplace transforms, eqn (5.1) can be written as

$$\tilde{\psi}(z) = [z + \tilde{K}(z)]^{-1}.$$ (5.2)

On the other hand, $\psi(t)$ is readily expressed in terms of the phase-space correlations of Section 4.2:

$$\psi(t) = V C_{s,11}(\mathbf{k} \to 0, t)$$ (5.3)

(cf. (4.72)). In turn, the Laplace transform $\tilde{C}_{s,11}(\mathbf{k}, z)$ satisfies a memory equation of the form (4.80). Since we are presently concerned with the $k \to 0$ limit of $C_{s,11}$, we may ignore the proper frequency terms in eqn (4.80) which all vanish as $k \to 0$ (cf. (4.82)). Noting that $C_{s,11}(\mathbf{k}, t = 0) = 1/V$, eqn (4.80) becomes

$$z\tilde{C}_{s,11}(\mathbf{k} \to 0, z) - (1/V) = -\sum_\mu \tilde{M}_{s,1\mu}(\mathbf{k} \to 0, z)\tilde{C}_{s,\mu 1}(\mathbf{k} \to 0, z).$$ (5.4)

This is still an infinite matrix equation, with the summation running over all the 'modes'. Following the general approach of Chapter 4, the memory function $M_{s,1\mu}(\mathbf{k}, t)$ is split into two contributions

$$M_{s,1\mu}(\mathbf{k}, t) = M_{sB,1\mu}(\mathbf{k}, t) + M'_{s,1\mu}(\mathbf{k}, t). \qquad (5.5)$$

Here $M_{sB,1\mu}(\mathbf{k}, t)$ is a rapidly decaying function of time which describes the effects of essentially uncorrelated binary collisions, whereas $M'_{s,1\mu}(\mathbf{k}, t)$ accounts for the coupling of self motion to long-lasting decay channels. In view of the discussion made in Section 4.3.3, the binary contribution is expected to be dominant at sufficiently short times, where $M'_{s,1\mu}(\mathbf{k}, t) \propto t^4$. As a result, both the initial value and the initial decay of $M_{s,1\mu}(\mathbf{k}, t)$ are entirely determined by the binary contribution. In particular, from eqn (4.143) we deduce that the initial value $M_{s,1\mu}(\mathbf{k}, t = 0) = M_{sB,1\mu}(\mathbf{k}, t = 0)$ is given by (Ω_0 is the Einstein frequency):

$$M_{s,1\mu}(\mathbf{k}, t = 0) = (m/\beta)\Omega_0^2 \int d\mathbf{P} f_0(P)\nabla_{\mathbf{P}}H_1(\mathbf{P}) \cdot \nabla_{\mathbf{P}}H_\mu(\mathbf{P})$$

$$= (m/\beta)^{1/2}\Omega_0^2 \int d\mathbf{P} f_0(P)[\partial H_\mu(P)/\partial P_z]$$

$$= \Omega_0^2 \delta_{\mu, 1} \qquad (5.6)$$

where we have performed a partial integration involving $[\partial f_0(P)/\partial P_z] = -(\beta/m)f_0(P)P_z$, and finally exploited the orthonormality of Hermite polynomials. Owing to the fast character of the binary contribution, it is reasonable to assume that $M_{sB,1\mu}(\mathbf{k}, t)$ retains the diagonal structure (5.6) even at later times (Wahnström and Sjögren 1982). Following the same arguments leading to eqn (4.141), we may approximately write that

$$M_{sB,1\mu}(\mathbf{k}, t) \approx \Omega_0^2 f(t/\tau_{sB}(k))\delta_{\mu,1}. \qquad (5.7)$$

In fluids with continuous potentials the exact details of the 'binary' dynamics are largely unknown, and the shape function $f(x)$ in (5.7) is chosen in such a way to ensure a fast decay of M_{sB} and to satisfy the requirement $f(x \to 0) = 1 - x^2$. In turn, the time $\tau_{sB}(k)$ is determined by expanding the memory function up to the order t^2.

Turning now the attention on the 'long-lasting' contribution $M'_{s,1\mu}(\mathbf{k}, t)$, from eqn (4.119) we have that $M'_{s,10}(\mathbf{k}, t) = 0$ because of the vanishing of the vertex; moreover, any direct coupling to the transverse motions vanishes for symmetry reasons, and $M'_{s,12}(\mathbf{k}, t) = M'_{s,13}(\mathbf{k}, t) = 0$. Since the other direct couplings involving $\mu \geq 4$ are not expected to provide slow decay channels, they are usually neglected, and we are simply left with $M'_{s,11}(\mathbf{k}, t)$. Adopting these approximations and using the relation (5.3), eqn (5.4) reduces to

$$z\tilde{\psi}(z) - 1 = -[\tilde{M}_{sB,11}(\mathbf{k} \to 0, z) + \tilde{M}'_{s,11}(\mathbf{k} \to 0, z)]\tilde{\psi}(z). \qquad (5.8)$$

Comparing with (5.2), we find that in the time domain the memory function of $\psi(t)$ can be expressed as

$$K(t) = M_{sB,11}(\mathbf{k} \to 0, t) + M'_{s,11}(\mathbf{k} \to 0, t)$$

$$\equiv K_B(t) + K'(t). \qquad (5.9)$$

Letting $\tau_{sB}(k \to 0) = \tau$ for notational simplicity, the binary contribution after eqn (5.7) reads

$$K_B(t) = \Omega_0^2 f(t/\tau). \qquad (5.10)$$

The binary time τ has been evaluated in Appendix E by a short time expansion of $K(t)$ (see eqn (E.20)). Physically, $\tau = [-\ddot{K}(0)/2\Omega_0^2]^{-1/2}$ can be interpreted as the duration of a binary collision.

On the other hand, in the static vertex scheme the non-binary part $K'(t) = M'_{s,11}(\mathbf{k} \to 0, t)$ follows directly from eqn (4.145). Thus

$$K'(t) = (nk_BT/8\pi^3m) \int d\mathbf{q}\, q_z^2 c^2(q)\{1 - [F_0(q, t)/F_s(q, t)]\}$$

$$F_s(q, t)F(q, t). \qquad (5.11)$$

Performing the angular integrations, eqn (5.11) can be written as

$$K'(t) = \frac{nk_BT}{6\pi^2m} \int_0^\infty dq\, q^4 c^2(q)S(q) \left\{1 - \frac{F_0(q, t)}{F_s(q, t)}\right\} F_s(q, t)\frac{F(q, t)}{S(q)}. \qquad (5.12)$$

Equations (5.9), (5.10) and (5.12) are the central results of the microscopic kinetic theory of Chapter 4 for the memory function of $\psi(t)$. We shall now proceed to discuss the physical relevance of the separate contributions $K_B(t)$ and $K'(t)$ in different time ranges, having in mind typical liquid-state conditions.

5.1.1 The binary memory function

As already remarked in Chapter 4, the binary contributions are physically associated with collisional mechanisms with a strongly local character both in space and in time. Consequently, $K_B(t)$ should account for the fast initial decrease of the full memory function. The quantity τ provides a convenient measure of the time extent of these processes, which typically last for some 10^{-13} s. The fact that in the liquid range the initial decay time of the velocity autocorrelation function ($\approx \Omega_0^{-1}$) becomes comparable with τ is a clear evidence that at high densities a tagged particle appears to 'collide' all the time. However, the unsatisfactory results obtained in Section 3.3 indicate that the fast collisional processes are unable to account for the subsequent dynamical features of $\psi(t)$. At these intermediate times the binary memory function has already decayed to negligibly small values; in view of this rapid decrease, the uncertainties due to our poor knowledge
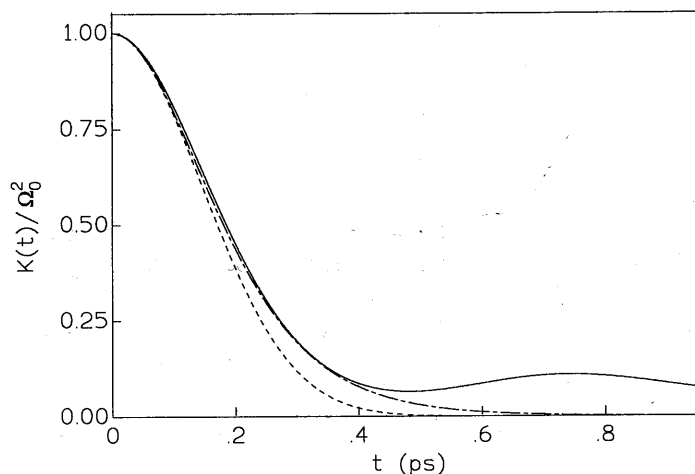
Fig. 5.1 Short-time decay of the normalized memory function of $\psi(t)$ in liquid Rb at 318 K. The dashed and the dot-dashed lines are respectively the results of the approximations (5.13) and (5.14) for the binary memory functions with the theoretical $\tau = 0.205$ ps. The full line denotes the simulation data for the full memory function (Balucani *et al.* 1992).

of the binary dynamics are not so crucial, making reasonable the 'scaled' form assumed for $K_B(t)$ in eqn (5.10). A judicious choice of the shape function $f(x)$ must be guided by the requirements of a correct initial behaviour and of a sufficiently rapid decay. When compared with the simulation data for $K(t)$ in Lennard–Jones liquids and in liquid alkali metals, the Gaussian ansatz

$$K_B(t) = \Omega_0^2 \exp(-t^2/\tau^2) \tag{5.13}$$

is found to reproduce the initial decrease of the memory function found in computer simulation studies fairly well (see Fig. 5.1), even if for an improved agreement one has to adjust τ somewhat by increasing its value by 10–15% (Sjögren 1980a). The theoretical expression of τ comprises a dominant pair contribution and a comparatively smaller term involving the triplet distribution function (see Appendix E). In turn, the triplet distribution function is evaluated by a superposition approximation, which may well introduce some small error in the predicted value of τ. However, the main source of the discrepancy is likely to be due to the Gaussian shape function; in practice, Fig. 5.1 shows that the alternative choice

$$K_B(t) = \Omega_0^2 \operatorname{sech}^2(t/\tau) \tag{5.14}$$

leads to a satisfactory reproduction of the short-time features of the memory function without any need of adjusting the value of τ.

By itself, the finite decay time of the memory function may lead to oscillations in $\psi(t)$. In particular, the simple analysis of Section 3.3 shows that such a behaviour is indeed predicted at liquid densities, where the values of Ω_0^{-1} and τ are comparable and the condition $2\Omega_0 > (1/\tau)$ is satisfied. However, the results in Figs 3.2 and 3.3 indicate that the finiteness of τ alone is insufficient to account for both the period and the phase of these oscillations. As a matter of fact, Fig. 5.1 shows that already at intermediate times there is a substantial portion of $K(t)$ which cannot be described by any simple 'binary-collision' approximation.

5.1.2 General remarks on the non-binary memory function

The dynamical features of the memory function $K(t)$ at intermediate and long times stem from processes which have both a slower and a more collective character than the previous binary-collision mechanism. Generally speaking, the physical nature and the relevance of these long-lasting decay channels are expected to depend on the thermodynamic state of the fluid. In dilute gases, binary collisions provide the overwhelming decay channel, and $K(t) \approx K_B(t)$ at all times. In the opposite extreme, that is in the liquid range, non-binary contributions are instead found to be important. At these high densities structural relaxation processes are slow, and any coupling involving wavevector-dependent density fluctuations is likely to provide a sizable 'tail' of the memory function $K(t)$. One of the advantages of the framework developed in Chapter 4 is to yield this important decay channel automatically in the simplest coupling scheme, the so-called *static vertex approximation*. The rationale for this simplicity is the specific symmetry under time reversal of the dynamical variables appearing in the memory function. If these 'fluctuating forces' transform in the same way as the space coordinates, as in the present case, the leading relaxation channels involving density modes can be found by considering the coupling in the lowest-order 'static' approximation. For $K(t)$, the final outcome of this procedure is expressed by eqn (5.11); other examples will be found in Chapter 6 in connection with the collective quantities.

This rather simple framework is expected to be convenient in all the cases where density modes rule the long-time behaviour of the memory functions, namely for ordinary and supercooled liquids. As the density decreases, the situation is more complicated because of the intervening effects of other decay channels involving collective flows of particles (i.e. the current variables). In particular, in dense gases the dominant non-binary contributions stem from couplings involving slow transverse current modes, which are ultimately responsible for the appearance of $t^{-3/2}$ tails in $\psi(t)$ (cf.

Section 4.5). In view of the previous remarks, these couplings can be accounted for by the general kinetic framework by considering *dynamical* contributions to the interaction vertices (4.102), (4.103). This can actually be done, with some additional approximations (Sjögren and Sjölander 1979; Sjögren 1980*b*). In general, the overall quantitative relevance of these channels is small in the liquid range, and we shall not discuss in detail these more complicated couplings. In principle, the inclusion of several kinds of decay channels paves the way for a microscopic description of a fluid over a quite extended range of states.

A noteworthy consequence of the kinetic approach of Chpter 4 is that non-binary contributions initially increase from a vanishing value at $t = 0$, and only at finite times exhibit the genuine long-lasting decay. In other terms, the buildup of correlation effects among the collisions requires a finite time. In the specific case of interest in this section, the initial increase stems from the factor in curly brackets in eqn (5.11) which leads to a $K'(t) \propto t^4$ as $t \to 0$. As shown in Fig. 5.1, in a still microscopic time range a broad peak appears in the simulation data as a result of the competition between the initial increase and the subsequent decay of $K'(t)$. On the other hand, at liquid densities the free-particle contribution F_0 is expected to decay quite rapidly with respect to the full self-correlation F_s, which is basically ruled by slow diffusive processes. As a result, beyond a comparatively short time interval $K'(t)$ may be approximated by its genuine long-lasting portion

$$[K'(t)]_{\text{tail}} = \frac{nk_B T}{8\pi^3 m} \int d\mathbf{q}\, q_z^2 c^2(q) F_s(q, t) F(q, t). \qquad (5.15)$$

As it stands, the result (5.15) should account for the main dynamical features of the memory function $K(t)$ at intermediate and long times; very long times—the realm of $t^{-3/2}$ tails—are not accounted for, but as noted previously their relevance is negligible in the liquid range.

Equation (5.15) can also be obtained by a direct *mode-coupling analysis*, assuming that the relevant decay channels are provided by a bilinear mode combination of the form $n_{s,i}(\mathbf{q})\hat{n}^*(\mathbf{q})$. Denoting by $\mathcal{P}$ the projection operator over the ath cartesian component of $\mathbf{v}_i$, the full memory function of $\psi(t)$ can be written as

$$K(t) = \frac{m}{k_B T} \langle \dot{v}_{i,a} \exp[i(1 - \mathcal{P})Lt]\, \dot{v}_{i,a} \rangle. \qquad (5.16)$$

According to the prescriptions of Section 4.5, the decay channel involving the modes under consideration is simply obtained by replacing $K(t)$ with

$$K_{\text{MC}}(t) = \frac{m}{k_B T} \langle (\mathcal{P}_2 \dot{v}_{i,a})^* \exp[i(1 - \mathcal{P})Lt]\, (\mathcal{P}_2 \dot{v}_{i,a}) \rangle \qquad (5.17)$$

where $\mathcal{P}_2$ is the projection operator over the product variable $n_{s,i}(\mathbf{q})\hat{n}^*(\mathbf{q})$. In eqn (5.17)

$$\mathcal{P}_2 v_{i,a} = \frac{k_B T}{Nm} \sum_q iq_a \left\{ 1 - \frac{1}{S(q)} \right\} n_{s,i}(\mathbf{q})\hat{n}^*(\mathbf{q}). \qquad (5.18)$$

Performing the usual mode-coupling approximations and exploiting the translational invariance of the averages (cf. (B.21)), it is readily seen that

$$K_{\text{MC}}(t) = \frac{k_B T}{Nm} \sum_q q_a^2 \left\{ 1 - \frac{1}{S(q)} \right\}^2 F_s(q, t) F(q, t)$$

$$= \frac{n^2 k_B T}{Nm} \sum_q q_a^2 c^2(q) F_s(q, t) F(q, t) \qquad (5.19)$$

which is identical to eqn (5.15). Since mode-coupling approaches were originally introduced just to account for long-lasting features, the equivalence $K_{\text{MC}}(t) = [K'(t)]_{\text{tail}}$ is hardly surprising, and indeed is an example of a general property valid for all the memory functions of interest in our analysis. In view of this, we shall often refer to the long-time portion of a memory function as its 'mode-coupling' contribution. Besides accounting for the latter, the kinetic framework of Chapter 4 has the practical advantage of dealing even with the short-time features of the memory functions (both in their 'binary' portions and in the initial increase of the 'correlated-collision' contributions).

Coming back to the mode-coupling techniques, the selection of the product modes relevant for providing a slow decay channel is essentially guided by physical considerations. Again, an important role in this respect is played by the specific symmetry properties of the variables appearing in the memory function. For example, in eqn (5.16) the relevant dynamical variable $\dot{v}_{i,a}$ refers to a tagged particle and transforms in the same way as the space coordinates, so that the choice of the product $n_{s,i}(\mathbf{q})\hat{n}^*(\mathbf{q})$ appears to be the simplest one. In such a way, the role of density fluctuations is naturally emphasized from the very start, and the procedure has a clear analogy with the one adopted previously within the static vertex scheme.

Alternative starting points for the mode-coupling framework may be convenient in specific situations. For example, it is perfectly legitimate to apply the analysis, rather than to $K(t)$, to the velocity autocorrelation function $\psi(t)$ (itself basically a memory function, cf. (3.93)). In such a case the starting variable is the velocity of the tagged particle, with the result that the simplest product modes which one may envisage are of the form $n_{s,i}(\mathbf{q})\mathbf{j}^*(\mathbf{q})$. The consequent involvement of the currents in the decay channel makes easier the deduction of long-lasting features explicitly

associated with $\mathbf{j}(\mathbf{q})$, as indeed shown in Section 4.5 for the $t^{-3/2}$ tails. The analysis can be refined by considering the *second-order* memory function of $\psi(t)$, which involves $\tilde{v}_{i,a}$ (Bosse *et al.* 1978). Since this variable has the same time-reversal symmetry as $v_{i,a}$, the leading product modes are again provided by the combination $n_{s,i}(\mathbf{q})\mathbf{j}^*(\mathbf{q})$. The advantage with respect to the simpler calculation of Section 4.5 is that now even some short-time properties of $\psi(t)$ can be accounted for, leading to a much better description of the overall features of single-particle dynamics.

5.1.3 An approximate treatment of the non-binary contribution

Strictly speaking, the presence of $F_s(q, t)$ and $F(q, t)$ in the result (5.11) indicates that a rigorous account of the features of $K'(t)$ is possible only after a preliminary solution for the self and collective density correlations. As we shall see later on, this fully self-consistent approach is in principle feasible, although at the price of quite heavy numerical computations. On the practical side, the self-consistent aspects turn out to be crucial only in rather special situations, for example when a deeply supercooled liquid approaches an amorphous phase characterized by an extremely long duration of all structural relaxation processes. The physics behind this 'ideal glass transition' will be discussed in some detail in Section 6.3; for the time being, we focus our attention on the ordinary liquid range, where the main long-lasting features can be accounted for by suitable approximations for F_s and F.

In this more manageable context, the quantity $K'(t)$ has been evaluated numerically by Sjögren (1980a) for both liquid rubidium and liquid argon. In an effort to perform a stringent test of all the theoretical results obtained by Sjögren and Sjölander (1979), in both systems the analysis was not limited to the simple decay channel (5.11) associated with density modes, but even included additional couplings, in particular those involving the longitudinal and the transverse currents. As a result of these numerical calculations, the leading role of the density fluctuations channel appears to be confirmed. In particular, for both liquids the coupling term involving the transverse currents is found to be negligibly small for all the times of interest, while the other contributions, although somewhat larger, cancel each other to a significant degree.

Focusing our attention only on the decay channel involving the densities, eqn (5.11) has been evaluated by Sjögren (1980a) adopting the Gaussian approximation (1.72) for $F_s(q, t)$ and a refined version of the viscoelastic model for $F(q, t)$ (cf. Section 6.2), which is suitably parametrized in order to reproduce the experimental data for $S(q, \omega)$ in the two liquids. A clear advantage of this semiempirical procedure is to provide a test of eqn (5.11) free from any uncertainties due to inaccurate input data. The final results
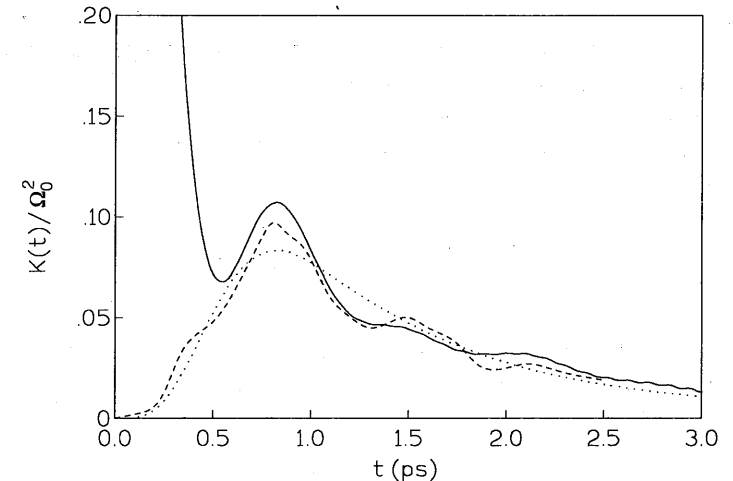
Fig. 5.2 Intermediate and long-time portion of the normalized memory function of $\psi(t)$ in liquid Rb at 318 K. The full line denotes the data obtained by the same simulation of Fig. 5.1 in a much larger time interval. The dashed line is the result of eqn (5.11) as evaluated by Sjögren (1980a). The dotted line denotes the result of a simplified approach (see text), in which the dominant role is provided by slow density fluctuations with a wavevector $q \approx q_m$.

obtained for $K'(t)$ in liquid rubidium are compared in Fig. 5.2 with the simulation data for the full memory function at intermediate and long times (namely in a range where the contribution of $K_B(t)$ has virtually disappeared). It is apparent that all the main features of $K(t)$ in this time interval are quite well reproduced. In particular, both the position and the amplitude of the peak at $t \approx 0.8$ ps are correctly accounted for, as well as the subsequent long-lasting decay of $K(t)$. In Fig. 5.2, the latter appears to be 'modulated' by weak oscillations, present both in the simulation data and in the theoretical results. The presence of this oscillatory behaviour can be traced back to the existence in liquid alkali metals of well-defined inelastic peaks in $S(q, \omega)$ up to relatively high wavevectors (cf. Fig. 1.13). In liquid argon, where these excitations are severely overdamped outside the strict hydrodynamic regime, the modulation effects are instead found to be virtually absent (Sjögren 1980a).

The success achieved by eqn (5.11) at a quantitative level definitely establishes wavevector-dependent density fluctuations as the modes responsible for the long-lasting portion of $K(t)$ in the liquid range. In this respect, the largest contribution is expected to be provided by those density modes having the slowest decay rate. A detailed analysis of the result (5.12) shows

that hydrodynamic wavevectors $q \to 0$ have some quantitative relevance only for very long times, where $K(t)$ has decayed to negligibly small values. On the other hand, beyond the strict hydrodynamic regime $F(q, t)$ is known to exhibit a marked 'de Gennes' slowing down only as q approaches the position q_m of the main peak of the static structure factor (cf. Section 1.6.2). Introducing the quantity $h(q) \equiv S(q) - 1$, eqn (5.12) becomes

$$K'(t) = \frac{k_B T}{6\pi^2 m} \int_0^\infty dq\, q^4 c(q) h(q) \left[1 - \frac{F_0(q, t)}{F_s(q, t)}\right] F_s(q, t) \frac{F(q, t)}{S(q)}.$$

$$(5.20)$$

Owing to the sharpness of the peak of $S(q)$ for $q \approx q_m$, eqn (5.20) can be rewritten in terms of the simplifying approximation $h(q) \approx A\delta(q - q_m)$, which implies $nc(q_m) = 1$. Letting $c = (k_B T/6\pi^2 nm)Aq_m^4$, we obtain

$$K'(t) = c[F_s(q_m, t) - F_0(q_m, t)] \frac{F(q_m, t)}{S(q_m)}. \qquad (5.21)$$

In practice, the amplitude factor c can be determined from the state parameters of the liquid supplemented by a limited knowledge of its structural data, such as the area under the main peak of $S(q)$.

A test of the simple result (5.21) can again be made by accepting the Gaussian approximation (1.72) for $F_s(q_m, t)$, which is found to be fairly good even at these relatively high wavevectors (cf. Fig. 1.7). As far as $F(q_m, t)$ is concerned, its long-lasting decay naturally suggests the validity of a Markovian scheme (cf. Section 3.1). In terms of a memory function representation, the Laplace transform $\tilde{F}(q, z)$ can be written as

$$\frac{\tilde{F}(q, z)}{S(q)} = [z + \tilde{M}(q, z)]^{-1}. \qquad (5.22)$$

For $q \approx q_m$ any residual oscillatory behaviour of $F(q, t)$ has virtually disappeared, and the slow decrease of density fluctuations can approximately be accounted for by letting $\tilde{M}(q, z) \approx \tilde{M}(q, z = 0) \equiv \gamma(q)$. As a result, in the time domain we obtain

$$\frac{F(q, t)}{S(q)} \approx \exp[-\gamma(q)|t|]. \qquad (5.23)$$

In this scheme, the leading slowing down effects as $q \to q_m$ stem from the proportionality of the decay rate $\gamma(q)$ to the quantity

$$M(q, t = 0) = \langle \omega_q^2 \rangle = \frac{k_B T}{mS(q)} q^2 \qquad (5.24)$$

which shows a pronounced decrease in the narrow q range where $S(q)$ attains its main peak. As we shall see in Section 6.2, at these wavevectors

a satisfactory representation of the quantity $\gamma(q)$ is provided by a simplified version of the viscoelastic model, with the result that

$$\gamma(q) = \frac{2\langle \omega_q^2 \rangle}{\{\pi[\omega_L^2(q) - \langle \omega_q^2 \rangle]\}^{1/2}} \qquad (5.25)$$

where $\omega_L^2(q)$ is defined in eqn (1.143).

The simple form of the intermediate scattering function obtained by the approximations (5.23) and (5.25) is eventually to be inserted into eqn (5.21). The outcome of this procedure for $K'(t)$ is illustrated in Fig. 5.2 (dotted line). The comparison with the previous results (which include all q-dependent density channels) and with the simulation data is seen to be still quite favourable. In particular, although the simple result (5.21) is intrinsically unable to account for the aforementioned 'modulation' effects, the underlying long-lasting decrease of $K'(t)$ appears to be satisfactorily reproduced. As a matter of fact, a detailed numerical calculation of the relevance of the different wavevectors in the integral (5.20) confirms the leading role of the density modes with $q \approx q_m$ for the overall decay rate. However, it turns out that a non-negligible contribution to the actual height of the initial 'bump' of $K'(t)$ is provided even by modes with $q < q_m$, indicating that in this short-time range the approximation (5.21) is probably too naïve.

In its simplified version, the theory has been successfully applied to several monatomic liquids near their melting point (Balucani *et al.* 1990*a*, *b* and 1992; Gonzáles *et al.* 1994). In the case of liquid rubidium the analysis has even been extended to moderately supercooled states, for which detailed simulation data for $K(t)$ are available (Kinell and Lovesey 1986). Broadly speaking, in these 'quenched' systems the binary part of the memory function is found to be virtually unchanged, while the amplitude and the lifetime of the long-lasting tail are considerably increased with respect to the ordinary liquid phase (see Fig. 5.3).

Summing up, it appears that a comprehensive account of all the features of $K(t)$ can be achieved in simple terms by a suitable combination of short- and long-time arguments. In principle, the approach can be made more rigorous by incorporating the results obtained for F_s and F by an analysis based on analogous arguments (cf. Section 5.3 and 6.3). For illustrative purposes, however, such a fully self-consistent framework is hardly necessary and the use of few phenomenological assumptions can be tolerated. Moreover, even this limited recourse to phenomenology can be minimized if, rather than trying to account for all the details of $K(t)$, we focus our attention on the corresponding transport property, namely the diffusion coefficient. This will be the subject of the next section.

5.2 THE DYNAMICS BEHIND DIFFUSIVE PROCESSES IN THE LIQUID RANGE

Beyond a microscopic time interval Δt of the order of 1 ps, the motion of a tagged particle in a simple liquid is known to be governed by diffusive processes. As illustrated by the typical results reported in Fig. 1.4, in this 'long-time' regime the mean square displacement $\delta r^2(t)$ of the particle appears to be described by a simple linear law

$$\delta r^2(t) = 6Dt + I \qquad (5.26)$$

where the small intercept I accounts empirically for residual finite-time effects. Proceeding as in Section 1.4.2, it is readily seen that

$$D = \frac{k_B T}{m} \int_0^\infty dt\, \psi(t) = \frac{k_B T}{m} \left[\int_0^\infty dt\, K(t) \right]^{-1}, \qquad (5.27)$$

$$I = -\frac{6k_B T}{m} \int_0^\infty dt\, t\, \psi(t) = \frac{6mD^2}{k_B T} \left[\int_0^\infty dt\, t K(t) - 1 \right]. \qquad (5.28)$$

The 'empirical' character of the law (5.26) becomes apparent noting that the asymptotic $t^{-3/2}$ tail of $\psi(t)$, albeit virtually not observable in the liquid range, leads to a non-analytic behaviour of $\tilde{\psi}(z)$ for small z, and ultimately to a divergent value of I. As a consequence, while the diffusion coefficient D is perfectly defined in any case, the intercept I is only to be viewed as a parameter which is conveniently introduced to describe the available experimental or simulation data.

The results discussed in the previous section indicate that a microscopic theory of the diffusion coefficient (5.27) requires the consideration of dynamical processes occurring over different timescales. To begin with, as a zero-order approximation we may assume that $K(t) \approx K_B(t)$, implying that the diffusive motion arises from the occurrence of essentially uncorrelated collisions. In such a case, eqns (5.14) and (5.27) yield for D the 'binary' result

$$D_B = \frac{k_B T}{m\Omega_0^2 \tau}. \qquad (5.29)$$

When compared with the values of the diffusion coefficient actually observed in several simple liquids, the predictions of eqn (5.29) are found in any case to overestimate considerably the real findings (see Table 5.1). Even worse results are obtained for the parameter I, whose binary estimates are more than one order of magnitude smaller than the values deduced from the computer simulation data (Balucani *et al.*, 1990b).

Table 5.1 Comparison between the theoretical predictions for the diffusion coefficient (D_B binary result, D value from full theory) with the actual findings from molecular-dynamics simulations (D_{MD}) and from experiment (D_{exp}) in several simple liquids near the melting point (except Rb 270, which refers to a supercooled state). The state parameters for the systems under consideration are: (Na) $n = 0.024$ Å^{-3}, $T \approx 380$ K; (Rb 318) $n = 0.010$ Å^{-3}, $T \approx 318$ K; (Rb 270) $n = 0.011$ Å^{-3}, $T \approx 270$ K; (Cs) $n = 0.0083$ Å^{-3}, $T \approx 309$ K; (Ar) $n = 0.021$ Å^{-3}, $T \approx 86.5$ K.

	D_B 10^{-5} cm^2 s^{-1}	D 10^{-5} cm^2 s^{-1}	D_{MD} 10^{-5} cm^2 s^{-1}	D_{exp} 10^{-5} cm^2 s^{-1}
Sodium	6.30	4.11	4.06[a]	4.06–4.35[b]
Rubidium 318	3.89	2.46	2.40[a]	2.60[b]
Rubidium 270	3.26	1.57	1.61[c]	
Caesium	3.33	2.13	2.11[a]	2.16[b]
Argon	2.47	1.50	1.75[d]	1.60[e]

[a] Balucani *et al.* (1992)
[b] Ohse (1985)
[c] Kinell and Lovesey (1986)
[d] Levesque and Verlet (1970)
[e] Naghizadeh and Rice (1963)

These discrepancies are clearly too large to be attributed to our limited knowledge of the binary dynamics. The inescapable conclusion is that the diffusive motions in a liquid are also noticeably affected by the slow processes embodied in the non-binary portion of the memory function. In other words, rather than being given by eqn (5.29), the appropriate expression of the diffusion coefficient reads

$$D = \left[D_B^{-1} + \frac{m}{k_B T} \int_0^\infty dt\, K'(t) \right]^{-1}. \qquad (5.30)$$

Since, in the liquid range, $K'(t)$ is essentially a positive quantity (cf. Figs 5.2, 5.3), the net effect of the inclusion of this contribution is in the correct direction of decreasing the theoretical value of D with respect to the binary prediction (5.29). A quantitative deduction of the magnitude of the effect can be made along lines similar to those discussed in the preceding section. As the integral in eqn (5.30) is expected to be largely insensitive to the minor details of the dynamics, we may use for $K'(t)$ the simplified expression (5.21) and adopt the previous approximations for $F(q_m, t)$ and $F_S(q_m, t)$. In particular, the appearance of $\delta r^2(t)$ in the Gaussian expression of F_S indicates that the additional contribution in eqn (5.30) ultimately contains D, namely just the quantity which we wish to calculate. In other words, in this scheme eqn (5.30) has the structure
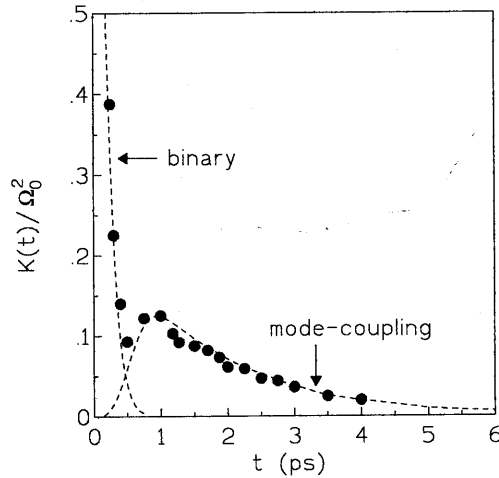
Fig. 5.3 Normalized memory function $K(t)/\Omega_0^2$ of supercooled liquid Rb at $T \approx 273$ K (the melting point is at 312 K). The dots are the computer simulation data of Kinell and Lovesey (1986). The dashed lines denote the separate contributions $K_B(t)/\Omega_0^2$ and $K'(t)/\Omega_0^2$ as obtained from eqns (5.13) and (5.21) (Balucani *et al.* 1990a).

$$D = [D_B^{-1} + \xi(D)]^{-1}, \qquad (5.31)$$

where the function $\xi(D)$ is basically inversely proportional to D. The argument can be cast in more precise terms, both taking into account the short-time interval where $\delta r^2(t)$ has not yet reached the diffusive limit (5.26) and including the effects of the intercept (Balucani *et al.* 1990b). The values of the diffusion coefficient obtained for several monatomic liquids by such a procedure are reported in Table 5.1. It is apparent that the theoretical results are now in quite good agreement with both the simulation and the experimental findings. The improvement with respect to the binary predictions, important in all systems, is particularly striking in the case of the supercooled liquid, as could be expected from the results reported in Fig. 5.3. As a by-product of the calculation, one may also deduce new theoretical values for the intercept I. Despite the ill-defined character of this parameter, the results compare rather well with the values deduced from the simulation data (for example, in ordinary liquid rubidium at 318 K one finds $I = 0.873$ Å^2, to be compared with $I_{MD} = 0.912$ Å^2 and with the binary prediction $I_B = 0.058$ Å^2).

In a more general context, it is interesting to enquire whether a self-consistent equation of the form (5.31) may imply a sort of 'phase transition' toward a physical situation characterized by a vanishing diffusion coeffi-

cient (Sjölander and Turski 1978). For this purpose, it is convenient to extract from the integral in eqn (5.30) the true long-lasting portion of $K'(t)$:

$$D^{-1} = D_B^{-1} + \lambda(t_0) + \frac{m}{k_B T} \int_{t_0}^{\infty} dt\, K'(t)$$

$$\equiv D_0^{-1} + \frac{m}{k_B T} \int_{t_0}^{\infty} dt\, K'(t). \qquad (5.32)$$

Here the quantity $\lambda(t_0)$ refers to the initial time interval $t \leqslant t_0$ where $K'(t)$ increases; in practice, the time t_0, is of the same order as Δt, the duration of the initial transient of $\delta r^2(t)$. In eqn (5.32), all these short-time events already yield a first renormalization of the diffusion coefficient from D_B to a lower value D_0. However, the really important change is provided by the contribution from the interval $t \geqslant t_0$, where $K'(t)$ can be approximated by its mode-coupling expression (5.19). Adopting all the previous approximation schemes we eventually obtain

$$D^{-1} = D_0^{-1} + c\frac{m}{k_B T} \frac{\exp(-q_m^2 I/6)\exp[-b(D)t_0]}{b(D)} \qquad (5.33)$$

where $b(D) \equiv q_m^2 D + \gamma(q_m)$. Equation (5.33) has the typical self-consistent structure sketched in (5.31).

Let us now assume that the temperature is lowered rapidly enough to prevent any crystallization process. In such a case, the liquid enters a metastable supercooled region characterized by a further slowing down of structural relaxation and by smaller and smaller values of D. As these two features are expected to be closely related, we may tentatively set $\gamma(q_m) \propto D$. Then the result (5.33) assumes the typical form of a 'mean field' equation, with a diffusion coefficient which is predicted to vanish at some finite temperature. Broadly speaking, this is just what occurs in several real liquids as they are rapidly 'quenched' from their ordinary state above the melting point. In these systems, the supercooled liquid may eventually approach a metastable condition characterized by a structural arrest. In many cases of practical interest, the lifetime of this non-equilibrium situation may be long enough to exceed (often by several orders of magnitude) the experimental times of observation. As a result, we effectively deal with a new disordered (non-crystalline) 'phase', which can be conveniently referred as an *amorphous solid*, or a *glass*. In the monatomic systems we are concerned with, the quenching rates required to prevent crystallization still exceed by two or three orders of magnitude the highest ones available in practice, and the behaviour of the liquid in the supercooled region can be explored only by computer simulation techniques (and even so, with obvious difficulties related to the competing requirements of long
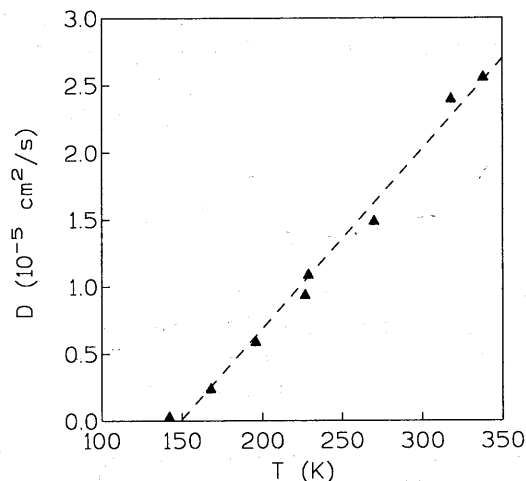
Fig. 5.4 Temperature dependence of the diffusion coefficient in supercooled liquid Rb (R. Vallauri, unpublished computer simulation results). In all cases, the density was kept constant at $n = 0.01 \text{ Å}^{-3}$. The dashed line is a linear fit to the data.

runs and of no intervening nucleation events). Figure 5.4 illustrates typical results obtained for the temperature variation of D in a system which simulates supercooled liquid rubidium. In this case, the data appear to indicate a 'transition temperature' slightly less than 150 K (well below the melting temperature, 312 K).

In this context, the simple approach of eqn (5.33) has the important merit of emphasizing the role of long-lasting dynamical events as those ultimately responsible for the transition. At a quantitative level, even the behaviour of the diffusion coefficient in a moderately supercooled liquid appears to be satisfactorily reproduced (cf. Fig. 5.3 and Table 5.1). However, both the Gaussian approximation (1.72) and the exponential ansatz (5.23) turn out to be increasingly inaccurate as one considers deeply supercooled states. As we shall see in Section 6.3, eqn (5.33) is too oversimplified to be able to describe many important aspects of the approach of a system toward a glassy phase.

Coming back to the diffusive processes occurring in ordinary simple liquids, the data reported in Table 5.1 indicate that the framework behind eqn (5.33) is reliable at a quantitative level. As already remarked, in these more conventional thermodynamic states the self-consistent aspects are not essential. In fact, a satisfactory prediction of the diffusion coefficient can already be obtained by a simple perturbative procedure which involves two successive 'renormalizations' of the binary result D_B. The first one has

been met in connection with eqn (5.32): D_B is effectively replaced by $D_0 = [D_B^{-1} + \lambda(t_0)]^{-1}$. The magnitude of the quantity $\lambda(t_0)$ can be determined by adopting a simple analytical form for the initial rise of $K'(t)$ and arguing that $t_0 \approx 2\pi/\Omega_0$ (Balucani *et al.* 1990*b*). Recalling that $c(m/k_B T) = A q_m^4/6\pi^2 n$, it is eventually found that

$$D_0^{-1} \approx D_B^{-1} + \frac{A q_m^4}{6\pi n \Omega_0} \exp\frac{-2\pi b(D_B)}{\Omega_0}. \tag{5.34}$$

The second renormalization concerns the genuine mode-coupling contributions; neglecting the small effects of the intercept I, from eqn (5.33) we simply obtain

$$D^{-1} \equiv D_0^{-1} + \frac{A q_m^4}{6\pi^2 n} \frac{\exp[-2\pi b(D_0)/\Omega_0]}{b(D_0)}. \tag{5.35}$$

The circumstance that only a few structural quantities are required as input data makes eqns (5.34) and (5.35) particularly convenient in the applications, even if the results for D are expected to be less accurate than those reported previously. To give an example, in the same state of liquid caesium considered in Table 5.1, the successive renormalizations of the diffusion coefficient (in units of $10^{-5}\text{ cm}^2\text{ s}^{-1}$) are found to be: (i) $D_B = 3.33 \rightarrow D_0 = 2.84$ and (ii) $D_0 \rightarrow D = 2.21$. The final value is about 4% higher than both the previous theoretical result and the actual findings (cf. Table 5.1).

5.3 SINGLE-PARTICLE MOTION PROBED OVER DIFFERENT LENGTH SCALES

Despite its importance, the velocity autocorrelation function gives only a partial description of the motion of a tagged particle in a liquid. A full account in this respect is instead provided by the *self-intermediate scattering function*

$$F_s(k, t) = \langle \exp[i\mathbf{k} \cdot (\mathbf{r}_i(t) - \mathbf{r}_i(0))] \rangle. \tag{5.36}$$

As discussed in Section 1.4, this comprehensive character stems from the possibility of exploring the dynamical features of self motion over distinctly different spatial ranges simply by changing the external wavevector k. Given a fluid at some specified state point, a physically relevant scaling unit for k is provided by the inverse of the effective mean free path l of the particle, where l is given approximately by eqn (1.53). In this respect, the extreme situations are $kl \ll 1$, where the self-motion is explored over a quasi-macroscopic length scale, and $kl \gg 1$, where the tagged particle

appears to behave as it were non-interacting. Between these opposite regimes (respectively characterized by a diffusive random walk and by a free streaming) we expect a full variety of situations which need to be interpreted. Pushing the argument somewhat, we may even state that these 'intermediate' features are just those which characterize the actual dynamical behaviour of the liquid state.

In this respect, a typical example is provided by the non-monotonic wavevector dependence of $\Gamma_s(k)$, the halfwidth of the spectrum of $F_s(k, t)$ (see Figure 1.6, which refers to liquid argon). Similar behaviour of $\Gamma_s(k)$ is present in many other simple liquids near the melting point. It is immediately apparent that these data provide a rather severe benchmark to test our theoretical models. Consider, for example, the simplest scheme which we may adopt for $F_s(k, t)$ (cf. (1.72), (1.57)):

$$F_s(k, t) \approx \exp\left[-\tfrac{1}{6} k^2 \delta r^2(t)\right]$$

$$= \exp\left[-\frac{k_B T}{m} k^2 \int_0^t d\tau \,(t - \tau)\psi(\tau)\right]. \qquad (5.37)$$

This 'Gaussian approximation' is clearly exact both for small and for large wavevectors, where it correctly describes the two physical regimes previously mentioned. Some discrepancies are instead apparent at intermediate wavevectors; in particular, in the situation illustrated in Figure 1.7 (where k is near the position k_m of the main peak of $S(k)$), the Gaussian result is seen to overestimate the actual decay rate of $F_s(k, t)$. Even so, on the basis of these direct comparisons the overall results predicted by the Gaussian ansatz are quite acceptable, justifiying the frequent recourse to eqn (5.37) as a simplifying a approximation in several problems in liquid-state dynamics (cf., for example, its use in Section 5.1.3).

In spite of these merits, the Gaussian result is intrinsically unable to account for several features present in the actual data for $\Gamma_s(k)$ in the liquid range. As expected, the main shortcomings are found to occur at the intermediate wavevectors, where the deviations may even reach about 20%. The typical situation is illustrated in Figure 5.5, which reports the simulation data obtained in a Lennard–Jones liquid near melting (Levesque and Verlet 1970). A feature even more important than the precise magnitude of the discrepancies is that the Gaussian approximation predicts an initial increase of the ratio $\Gamma_s(k)/Dk^2$, while the observed behaviour is just the opposite. In this wavevector range it is customary to write the quantity $\Gamma_s(k)$ in the form $D(k)k^2$, where $D(k)$ is a k-dependent effective diffusion coefficient. Then the initial trend of the data of Figure 5.5 implies that the tagged particle has a lower probability to diffuse as its motion is explored over shorter spatial ranges. This tendency is particularly evident as k
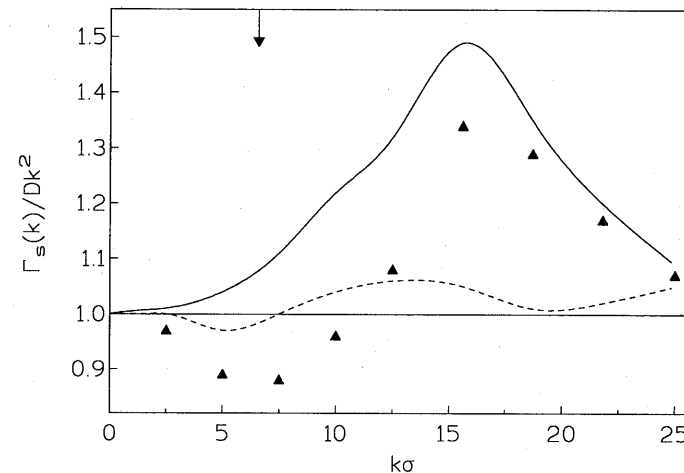
Fig. 5.5 Normalized halfwidth of the spectrum of $F_s(k, t)$ versus wavevector in a Lennard–Jones liquid with $n\sigma^3 = 0.844$ and $k_B T/\varepsilon = 0.722$ (Levesque and Verlet 1970); triangles, actual simulation data; full line, results deduced from the Gaussian approximation (5.37) using for $\delta r^2(t)$ the data generated in the simulation; dashed line, results deduced from eqn (5.45) with fitted values of $\tau_{s,k}$. The arrow denotes the position of the main peak of $S(k)$.

approaches k_m; that is, as the length scale effectively probed becomes comparable with the nearest-neighbour distance.

The incorrect predictions of eqn (5.37) in this wavevector range clearly imply that the presence of *non-Gaussian corrections*. These can be systematically accounted for by the following 'cumulant expansion' (Nijboer and Rahman 1966)

$$F_s(k, t) = \exp\left[-k^2 \delta r^2(t)/6\right]\left\{1 + \tfrac{1}{2}a_2(t)\left[k^2\delta r^2(t)/6\right]^2 + \cdots\right\}.$$
$$(5.38)$$

Here the first non-Gaussian coefficient reads

$$a_2(t) = \frac{3\delta r^4(t)}{5[\delta r^2(t)]^2} - 1 \qquad (5.39)$$

where $\delta r^4(t) \equiv \langle [r_i(t) - r_i(0)]^4 \rangle$. Although even higher order coefficients (involving $\delta r^6(t)$, etc.) have been evaluated, the dominant corrections to the Gaussian result are provided by the term with $a_2(t)$ (Rahman 1964). As eqn (5.37) is essentially correct both at short and long times for all wavevectors, the typical time evolution of $a_2(t)$ deduced from the stimulation findings consists of an initial increase up to a broad maximum, followed by a relatively slow decay at long times. These results are

supported by a similar analysis on the 'real' experimental data obtained by inelastic neutron scattering (Sköld *et al.* 1972). In every case, the coefficient $a_2(t)$ is found to be positive at all times, implying a decay for F_s somewhat slower than the one predicted by (5.37). This feature (previously mentioned in connection with Figure 1.7) is clearly consistent with the overall situation illustrated in Figure 5.5 (larger values of the 'Gaussian' widths with respect to the actual $\Gamma_s(k)$).

Athough instructive and widely used in early treatments, the analysis based on the expansion (5.38) is not enlightening enough to clarify the origin of the initial decrease of $\Gamma_s(k)$ below the diffusion result Dk^2. Our physical understanding is instead much better in the opposite limit of large wavevectors, where the Gaussian result is virtually exact. Starting from a situation with $kl \gg 1$, where

$$\frac{\Gamma_s(k)}{Dk^2} \to \frac{(\Gamma_s(k))_{\text{free}}}{Dk^2} = \left(\frac{2\ln 2}{\beta m}\right)^{1/2}\frac{1}{Dk}, \qquad (5.40)$$

the rise of the ratio at decreasing wavevectors is found to become progressively slower than the $(1/k)$ law predicted by (5.40). This feature clearly marks the breakdown of a free-particle description. As the latter implies that the velocity autocorrelation function is a constant at all times, even a modest improvement of this limiting result is expected to be sufficient to account for the observed effect. Indeed, a better description of the data in this k range is obtained by taking into account the term $-\frac{1}{2}\Omega_0^2 t^2$ in the short time expansion of $\psi(t)$ (Nijboer and Rahman 1966; Levesque and Verlet 1970).

5.3.1 A simple memory function approach

As in the case of the velocity autocorrelation function (Section 3.3), a first insight into k-dependent self-motion can be obtained by a simple application of the memory function framework. We start from the continued fraction representation

$$\tilde{F}_s(k, z) = [z + \tilde{K}_s(k, z)]^{-1} = \left[z + \frac{\langle\omega_k^2\rangle_s}{z + \tilde{M}_s(k, z)}\right]^{-1}. \qquad (5.41)$$

Here $\langle\omega_k^2\rangle = (k_B T/m)k^2$, whereas $\tilde{K}_s(k, z)$ and $\tilde{M}_s(k, z)$ are respectively the Laplace transforms of the first- and second-order memory functions of $F_s(k, t)$. As shown in Section 3.4.1, for sufficiently small wavevectors the quantity $K_s(k, t)/k^2$ tends to the velocity autocorrelation function (cf. (3.93)). Correspondingly, in the same limit $M_s(k, t)$ approaches the memory function $K(t)$, whose properties have been discussed in detail in Sections 3.3 and 5.1. In view of this, for a preliminary analysis at finite

wavevectors it is natural to start with a model which is a simple generalization of the result (3.67) for $K(t)$. In other terms, it is assumed that

$$M_s(k, t) = M_s(k, 0) \exp(-t/\tau_{s,k}). \qquad (5.42)$$

Here the initial value of the memory function follows from eqn (3.42b):

$$M_s(k, 0) = [\langle\omega_k^4\rangle_s/\langle\omega_k^2\rangle_s] - \langle\omega_k^2\rangle_s$$
$$= \Omega_0^2 + 2(k_B T/m)k^2 \equiv \Delta_{s,k} \qquad (5.43)$$

where we have used the result (1.46) for $\langle\omega_k^4\rangle_s$. Inserting the Laplace transform of (5.42) into (5.41) we obtain

$$\tilde{F}_s(k, z) = \left[z + \frac{\langle\omega_k^2\rangle_s}{z + \Delta_{s,k}/(z + 1/\tau_{s,k})}\right]^{-1}. \qquad (5.44)$$

The corresponding frequency spectrum of $F_s(k, t)$ is obtained from the relation $S_s(k, \omega) = (1/\pi) \operatorname{Re}\tilde{F}_s(k, z = i\omega)$. After a few calculations we find

$$S_s(k, \omega) = (1/\pi)\frac{\langle\omega_k^2\rangle_s\Delta_{s,k}\tau_{s,k}}{[\omega\tau_{s,k}(\omega^2 - \langle\omega_k^2\rangle_s - \Delta_{s,k})]^2 + [\omega^2 - \langle\omega_k^2\rangle_s]^2}. \qquad (5.45)$$

The decay time $\tau_{s,k}$ can be either fitted to the data, or estimated by the following approximate procedure (Lovesey 1973). Noting that eqn (5.41) implies $\tilde{K}_s(k, z = 0) = \langle\omega_k^2\rangle_s/\tilde{M}_s(k, z = 0)$, from the ansatz (5.42) we deduce that

$$\int_0^\infty dt\, K_s(k, t) = \langle\omega_k^2\rangle_s(\Delta_{s,k}\tau_{s,k})^{-1}. \qquad (5.46)$$

On the premise that the integral on the left-hand side is likely to be insensitive to the detailed shape of $K_s(k, t)$, this memory function is approximated by a form which fulfils the known short-time properties. Letting $K_s(k, t) \approx \langle\omega_k^2\rangle_s f(\sqrt{\Delta_{s,k}} \cdot t)$, it follows that

$$1/\tau_{s,k} \approx \xi\sqrt{\Delta_{s,k}}. \qquad (5.47)$$

In this scheme, the dimensionless parameter $\xi = \int_0^\infty dx f(x)$ is independent of the wavevector. Its value can be determined by requiring that at zero frequency the prediction of the model

$$\pi S_s(k, \omega = 0) = \frac{\Delta_{s,k}\tau_{s,k}}{\langle\omega_k^2\rangle_s} = \frac{1}{\xi}\frac{\sqrt{\Delta_{s,k}}}{\langle\omega_k^2\rangle_s} \qquad (5.48)$$

coincides with the exact result in the diffusive regime ($=1/Dk^2$) or in the free particle limit ($=(\pi m\beta/2k^2)^{1/2}$). In both cases, it is found that $\xi \approx 1$ (Lovesey 1973).

The results predicted by eqn (5.45) with the above recipes are found to be in fair agreement with the experimental spectra over a rather large wavevector range. However, under more severe tests the oversimplified character of the model becomes apparent. By construction, as $k \to 0$ the model predicts an expression for the velocity autocorrelation function identical with eqns (3.70) or (3.73). Even allowing for some uncertainty for the value of ξ, this result for $\psi(t)$ is known to be rather unsatisfactory in the liquid range (see Figure 3.2). Another stringent test of the validity of the model is the wavevector dependence predicted for the quantity $\Gamma_s(k)/Dk^2$. For sufficiently small k, eqn (5.45) predicts a narrow quasi-Lorentzian spectrum with a halfwidth approximately given by

$$\Gamma_s(k) = \xi\beta mk^2/\sqrt{\Delta_{s,k}}. \tag{5.49}$$

Choosing for ξ the value $m\beta\Omega_0 D$ which reproduces the correct diffusive limit, we find that

$$\Gamma_s(k)/Dk^2 = [1 + (2k_B T/m\Omega_0^2)k^2]^{-1/2}. \tag{5.50}$$

In contrast with the predictions of the Gaussian approximation (5.37), the result accounts for the initial decrease of the width with respect to the hydrodynamic value Dk^2. The coefficient of the term in k^2 on the right-hand side is seen to be proportional to the square of the 'mean free path' l (cf. eqn (1.53)). Within the model, we may consequently interpret the decrease of the ratio $\Gamma_s(k)/Dk^2$ at small wavevectors as being due to an increasing value of kl, or in more physical terms to the fact that the number of collisional events appears to be effectively decreased when detected on a shrinking length scale. Although this picture seems plausible, a numerical calculation of the widths from eqn (5.45) shows clear quantitative discrepancies with respect to the actual findings at all wavevectors (see Figure 5.5, where the values of $\tau_{s,k}$ were obtained by a best fit to (5.45) to the observed spectra). Equally unsatisfactory results are obtained for the k-dependence of the quantity $\pi Dk^2 S_s(k, \omega = 0)$, which is the ratio between the actual intensity at zero frequency and the corresponding hydrodynamic prediction. This failure is not due to a defect of the exponential decay law (5.42); alternative functional forms with a *single* relaxation time have been found to yield no substantial improvement (Levesque and Verlet 1970). As a result, we are forced to conclude that a much deeper analysis of the memory function $M_s(k, t)$ is required to account for the quantitative features of k-dependent self-motion. The situation clearly parallels the one already met for the memory function $K(t)$, with the additional complications brought about by the need of understanding the relevance of the various decay channels over considerably different length scales.

5.3.2   Analysis of $M_s(k, t)$ at different wavevectors

The successful results obtained in the case of the velocity autocorrelation function indicate that the framework of Chapter 4 may account for the dynamics of $M_s(k, t)$ at different wavevectors in a more realistic way than the simple approach discussed so far. The relation between the Laplace transforms of the self-intermediate scattering function $F_s(k, t)$ and of the matrix elements $C_{s,\lambda\lambda'}(\mathbf{k}, t)$ is readily obtained by noting that

$$\tilde{F}_s(k, z) = V\tilde{C}_{s,00}(\mathbf{k}, z) \tag{5.51}$$

(cf. (4.71)). In turn, exploiting the 'self' version of eqn (4.153) $\tilde{C}_{s,00}(\mathbf{k}, z)$ can be expressed as

$$z[z\tilde{C}_{s,00}(\mathbf{k}, z) - (1/V)] = - (k^2/\beta m)\tilde{C}_{s,11}(\mathbf{k}, z). \tag{5.52}$$

The result (5.52) is a direct consequence of the validity of a continuity equation for the motion of the tagged particle.

Equations (5.51) and (5.52) indicate that the features of k-dependent self-motion are ultimately determined by the quantity $\tilde{C}_{s,11}(\mathbf{k}, z)$. The corresponding time correlation function reads (cf. Section 4.2)

$$C_{s,11}(\mathbf{k}, t) = (\beta/mV)\langle p_{i,z}(0)p_{i,z}(t) \exp[i\mathbf{k} \cdot (\mathbf{r}_i(t) - \mathbf{r}_i(0))]\rangle. \tag{5.53}$$

Since $\mathbf{k}$ is along the z-axis, $C_{s,11}(\mathbf{k}, t)$ describes the dynamics of the longitudinal part of the self-current $\mathbf{j}_{s,i}(\mathbf{k}, t)$ (cf. (3.88)). Equations (5.41), (5.51), and (5.52) imply that $\tilde{C}_{s,11}(\mathbf{k}, z)$ can be expressed as

$$\tilde{C}_{s,11}(\mathbf{k}, z) = (1/V) [z + (k^2/\beta mz) + \tilde{M}_s(k, z)]^{-1}. \tag{5.54}$$

The results previously obtained for the velocity autocorrelation function (i.e. essentially for $C_{s,11}(\mathbf{k} = 0, t)$) indicate that the memory function $M_s(k, t)$ should include both rapid 'collisional' processes and slower 'mode-coupling' decay channels. Within a kinetic framework, there have been several attepts of increasing sophistication to account for these dynamical features (Lebowitz *et al.* 1969; Akcasu *et al.* 1970; Desai 1971; Jhon and Forster 1975; Götze and Zippelius 1976). In the following we shall discuss the basic points of the approach by Wahnström and Sjögren (1982), which incorporates many aspects of the general framework of Chapter 4.

The starting point of the analysis is the set (4.80) of memory equations for $\tilde{C}_{s,\lambda\nu}(\mathbf{k}, z)$. In a matrix notation, these equations can be written as

$$[z\mathbf{I} - i\mathbf{\Omega}_s(k) + \tilde{\mathbf{M}}_s(\mathbf{k}, z)] \cdot \tilde{\mathbf{C}}_s(\mathbf{k}, z) = \mathbf{C}_s(\mathbf{k}, t = 0). \tag{5.55}$$

It is convenient to introduce a formally similar equation which involves only the 'binary' part $\tilde{M}_{sB}(\mathbf{k}, z)$ of the full memory matrix $\tilde{M}_s(\mathbf{k}, z)$. Denoting by $\tilde{\mathbf{C}}_{sB}(\mathbf{k}, z)$ the solution of this equation, we have

$$[z\mathbf{1} - i\mathbf{\Omega}_s(\mathbf{k}) + \tilde{\mathbf{M}}_{sB}(\mathbf{k}, z)] \cdot \tilde{\mathbf{C}}_{sB}(\mathbf{k}, z) = \mathbf{C}_s(\mathbf{k}, t = 0). \qquad (5.56)$$

As a result of eqns (5.55) and (5.56) we may formally write that

$$\tilde{\mathbf{C}}_s(\mathbf{k}, z) = \tilde{\mathbf{C}}_{sB}(\mathbf{k}, z) - \tilde{\mathbf{C}}_s(\mathbf{k}, z)\,[\mathbf{C}_s(\mathbf{k}, t = 0)]^{-1}\tilde{\mathbf{M}}_s'(\mathbf{k}, z)\tilde{\mathbf{C}}_{sB}(\mathbf{k}, z)$$

$$(5.57)$$

where $\tilde{\mathbf{M}}_s'(\mathbf{k}, z) \equiv \tilde{\mathbf{M}}_s(\mathbf{k}, z) - \tilde{\mathbf{M}}_{sB}(\mathbf{k}, z)$. In particular, exploiting eqn (4.78) we obtain

$$\tilde{C}_{s,11}(\mathbf{k}, z) = \tilde{C}_{sB,11}(\mathbf{k}, z) - V\sum_{\mu\mu'}\tilde{C}_{s,1\mu}(\mathbf{k}, z)\tilde{M}_{s,\mu\mu'}'(\mathbf{k}, z)\tilde{C}_{sB,\mu'1}(\mathbf{k}, z).$$

$$(5.58)$$

Physically, the second term on the right-hand side accounts for the disturbances induced by the tagged particle in the surrounding medium. As discussed in Chapter 4, we are particularly interested in the long-lasting effects of these disturbances, which give rise to sizeable correlations among the collisions suffered by the particle. Wahnström and Sjögren argue that the leading contribution to these slow features is provided by the couplings to quasi-conserved modes. Exploiting the longitudinal character of the problem and assuming that energy fluctuations have a negligigle role, in (5.58) $\tilde{M}_{s,\mu\mu'}'(\mathbf{k}, z)$ is effectively replaced $\tilde{M}_{s,11}'(\mathbf{k}, z)\delta_{\mu,1}\delta_{\mu',1}$, with the result that

$$\tilde{C}_{s,11}(\mathbf{k}, z) = \frac{\tilde{C}_{sB,11}(\mathbf{k}, z)}{1 + V\tilde{M}_{s,11}'(\mathbf{k}, z)\tilde{C}_{sB,11}(\mathbf{k}, z)}. \qquad (5.59)$$

The first problem to be faced is an adequate representation of the binary contribution $\tilde{C}_{sB,11}(\mathbf{k}, z)$. This is possible by adopting some simple approximation scheme for the matrix elements $\tilde{M}_{sB,\mu\mu'}(\mathbf{k}, z)$ appearing in eqn (5.56). In close analogy with the approach followed in Section 5.1, one makes the ansatz

$$\tilde{M}_{sB,\mu\mu'}(\mathbf{k}, z) = M_{sB,\mu\mu'}(\mathbf{k}, t = 0)\tilde{f}(\mathbf{k}, z). \qquad (5.60)$$

Here $M_{sB,\mu\mu'}(\mathbf{k}, t = 0) = M_{s,\mu\mu'}(\mathbf{k}, t = 0)$ is given in eqn (4.143), and the frequency dependence of all the matrix elements is assumed to be ruled by a common factor $\tilde{f}(\mathbf{k}, z)$. Since the binary part concerns rapidly varying events, it is reasonable to characterize $\tilde{f}(\mathbf{k}, z)$ by the first few terms in a large-z expansion, or equivalently $f(\mathbf{k}, t)$ by its short-time behaviour. In other words, in the time domain we write eqn (5.60) as

$$M_{sB,\mu\mu'}(\mathbf{k}, t) = M_{s,\mu\mu'}(\mathbf{k}, t = 0)\,f(\mathbf{k}, t)$$

$$\approx M_{s,\mu\mu'}(\mathbf{k}, t = 0)\,f(t/\tau_s(k)) \qquad (5.61)$$

where the shape function $f(x)$ is such that

$$f(t/\tau_s(k)) = 1 - (t/\tau_s(k))^2 + \cdots. \qquad (5.62)$$

As a result, the fast decay of all the binary memory functions is ruled by a wavevector-dependent time constant $\tau_s(k)$. Since the buildup of the correlation effects not accounted for by M_{sB} is expected to require a finite time, $\tau_s(k)$ can in practice be deduced from the initial decay of a suitable selected element of the *full* memory matrix $M_s(k, t)$. Again, this procedure leaves unspecified the form of the shape function, which is usually chosen by some simple ansatz which satisfies eqn (5.62) and provides a sufficiently fast decay (e.g. a Gaussian, or $\text{sech}^2 x$ form).

With the approximation (5.60), the solution of eqn (5.56) for $\tilde{\mathbf{C}}_{sB}(\mathbf{k}, z)$ can be expressed analytically (Lebowitz *et al.* 1969; Jhon and Forster 1975). In particular, the matrix element $\tilde{C}_{sB,00}(\mathbf{k}, z)$ reads (Wahnström and Sjögren 1982)

$$\tilde{C}_{sB,00}(\mathbf{k}, z) = [V\Omega_0^2\tilde{f}(\mathbf{k}, z)]^{-1}\sum_{n=0}^{\infty}\frac{[\tilde{\kappa}^2(z)]^n}{\tilde{p}_n(z)} \qquad (5.63)$$

where

$$\tilde{\kappa}^2(z) \equiv (k^2/\beta m)\,[\Omega_0^2\tilde{f}(k, z)]^{-2} \qquad (5.64a)$$

$$\tilde{p}_n(z) \equiv \tilde{p}(z)\,[\tilde{p}(z) + 1]\cdots[\tilde{p}(z) + n] \qquad (5.64b)$$

$$\tilde{p}(z) \equiv \tilde{\kappa}^2(z) + [z/\Omega_0^2 f(k, z)]. \qquad (5.64c)$$

Using the result (5.63) in eqn (5.52), we eventually obtain the quantity $\tilde{C}_{sB,11}(\mathbf{k}, z)$ to be inserted into (5.59).

The next task is to derive an explicit expression for the non-binary memory function which appears in eqn (5.59). From Section 5.1 we already know that in the limit of small k, $M_{s,11}'(\mathbf{k}, t)$ approaches the corresponding non-binary portion of $K(t)$. As in that case, several decay channels may in principle affect the intermediate- and long-time features of $M_{s,11}'$ at finite wavevectors. Nevertheless, in the liquid range the dominant contribution is again provided by those couplings involving the density modes, which yield (cf. eqn (4.146))

$$M_{s,11}'(\mathbf{k}, t) = \frac{nk_BT}{8\pi^3 m}\int d\mathbf{q}\, q_z^2 c^2(q)\left[1 - \frac{F_0(|\mathbf{k}-\mathbf{q}|, t)}{F_s(|\mathbf{k}-\mathbf{q}|, t)}\right]$$

$$\times F_s(|\mathbf{k}-\mathbf{q}|, t)F(q, t). \qquad (5.65)$$

We refer to Wahnström and Sjögren for the explicit expression of the other decay channels, which involve couplings to the longitudinal and transverse currents. As in the case of $K'(t)$, the factor in square brackets in eqn (5.65) yields an initial increase of $M_{s,11}'(\mathbf{k}, t)$ as t^4. The subsequent time dependence is obtained by a numerical evaluation of (5.65), using as input
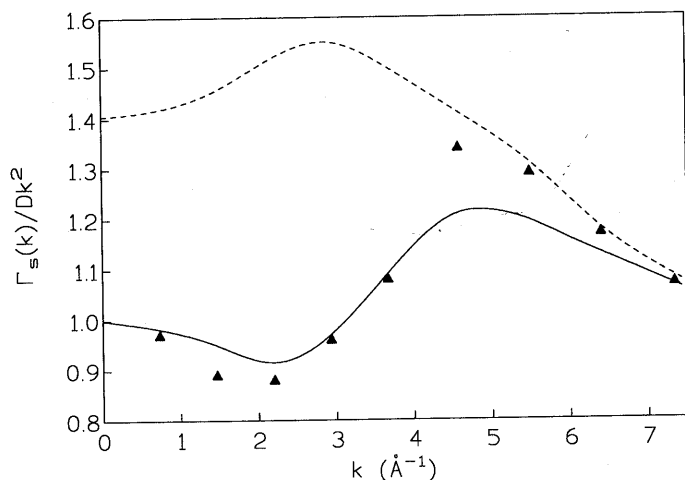
Fig. 5.6 Wavevector dependence of the normalized halfwidth of $S_s(k, \omega)$ in a Lennard–Jones system which simulates liquid argon. The triangles are the same simulation data reported in Fig. 5.5 (Levesque and Verlet 1970). The full line is the result of the theory by Wahnström and Sjögren (1982). The dashed line represents the predictions of a purely 'binary' approach (eqn 5.63).

quantities structural data (needed for the weight factor $c^2(q)$), as well as simple analytical representations for the intermediate scattering functions F_s and F (entirely analogous to those adopted for the evaluation of $K'(t)$). The outcome of these calculations is qualitatively similar to the one discussed in Section 5.1.3: after the initial increase, $M'_{s,11}(\mathbf{k}, t)$ exhibits a broad maximum, followed by a slow decay (ruled by the factor F_sF in eqn (5.65)). The important point to be stressed in the present case is clearly the wavevector dependence of all these dynamical feacutres. Broadly speaking, it is found that the overall relevance of the non-binary contributions decreases at increasing wavevector. In particular, at larger k the broad peak becomes progressively less defined and the amplitude of the tail is gradually reduced with respect to the $k = 0$ case. Eventually, as the wavevector increases beyond a certain range (typically, as $k \geqslant 2.5 \, k_m$), the effects of $M'_{s,11}(\mathbf{k}, t)$ can virtually be neglected and the features of self-motion appear to be entirely ruled by the binary portion of the memory function.

The overall results obtained by Wahnström and Sjögren for the normalized halfwidth $\Gamma_s(k)/Dk^2$ in the case of liquid argon are reported in Fig. 5.6. As a preliminary step, only the effects of binary collisions were taken into account. In this case the spectral features are evaluated by eqns (5.63)–(5.64c), adopting for the quantity $\tilde{f}(k, z)$ the approximation

$$\tilde{f}(k, z) \equiv \int_0^\infty dt \exp(-zt) f(k, t)$$

$$\approx \int_0^\infty dt \exp(-zt) \exp[-t^2/\bar{\tau}_s^2(k)]. \qquad (5.66)$$

Even if this Gaussian ansatz for $f(k, t)$ is likely to be an oversimplification of the true binary dynamics, the previous discussion indicates that the gross features of the collisional decay channel can indeed be accounted for by a single time constant $\bar{\tau}_s(k)$. An important difference with respect to the approximate treatment of Section 5.3.1 is that now the quantity $\bar{\tau}_s(k)$ can be evaluated from 'first principles' by means of a short-time expansion of $F_s(k, t)$ up to terms in t^6 (see Appendix I).

As is apparent from Fig. 5.6, the comparison of the results deduced from the binary theory with the actual findings is unsatisfactory under several respects. First of all, there is an obvious discrepancy as $k \to 0$, where the predicted halfwidth approaches D_Bk^2 rather than the correct result Dk^2. Since the binary diffusion coefficient D_B is considerably larger than D (cf. Section 5.2), the result is that $\Gamma_s(k)/Dk^2$ starts from a value $D_B/D > 1$. Aside from this trivial source of error, the binary approach predicts an initial *increase* of the normalized halfwidth with the wavevector, in clear disagreement with the trend observed in the simulation data. The theoretical results become acceptable only at relatively large values of k, indicating that only in this range binary collisions yield the leading decay mechanism for the self-memory function. The obvious implication is that any serious attempt to account for the 'oscillations' of $\Gamma_s(k)/Dk^2$ at intermediate wavevectors cannot neglect the presence of non-binary contributions. The latter have been taken into account by Wahnström and Sjögren including all the possible decay channels for $M'_{s,11}(\mathbf{k}, t)$ (the most relevant being represented by eqn (5.65)), and inserting the results in (5.59). The final outcome for the normalized halfwidth is reported in Fig. 5.6 (full line). Apart from some minor discrepancies in the amplitudes, this complete calculation is seen to reproduce all the essential features of the simulation data (in particular, the positions of the minimum and maximum of $\Gamma_s(k)/Dk^2$).

The physical picture of k-dependent self-motion which emerges from all this theoretical framework can be summarized as follows. At small wavevectors the tagged particle undergoes an essentially diffusive motion, in which both collisional events and less localized processes play an important role. The precise nature of the second class of phenomena is largely determined by the thermodynamic state of the system. In the case of monatomic liquids near the melting point, the dominant processes (the 'couplings to the density modes') stem from the close-packed structure, which ultimately causes the tagged particle to be 'trapped' to some extent

by the surrounding atoms. The relevance of this effect is clearly enchanced by the low temperature of the liquid, which prevents a rapid thermal disruption of the atomic 'cages'. The trapping appears to be particularly effective for $k \approx k_\mathrm{m}$, where the wavelength approaches the linear size of the cage (typically, of the order of the nearest-neighbour distance) and the apparent diffusion coefficient $\Gamma_\mathrm{s}(k)/k^2$ is a minimum. At even larger wavevectors, the situation changes drastically because the spatial range which is explored is so short that the presence of the cage is not detected. As a consequence, the dynamics of the particle is ruled by essentially uncorrelated collisions, and the halfwidth rapidly increases to approach its binary value (see Fig. 4.6). Eventually, for $kl \gg 1$, even the collisional events are not revealed and the tagged particle is seen as though it were non-interacting.

This picture is to be contrasted with the situation occurring in a dense gas, or in a 'hot' liquid. In this case, the 'cages' are so loose that the motion of the particle gives rise to a backflow of the surrounding atoms, and eventually to the development of vortex patterns of considerable spatial extent and stability. In turn, this modified environment reacts on the particle, whose motion is in a sense 'supported' by the backflow. As anticipated in Section 3.3, the final result of this dynamic process is a slower decay of the velocity autocorrelation function (the positive $t^{-3/2}$ tail) and an *increase* of the diffusion coefficient with respect to the binary prediction. In the less pictorial language of Section 4.5, the effect is ultimately due to the 'coupling' of the particle motion with shear modes of long wavelength.

In such a situation, the first effect observed in dense gases or hot liquids when the self motion is explored at finite wavevectors is a reduction of the effective diffusion coefficient $\Gamma_\mathrm{s}(k)/k^2$ (Verkerk *et al.* 1985, 1989; Montfrooy *et al.* 1986; Morkel and Gläser 1986). Even if this behaviour is apparently similar to the one found for liquids near melting, it arises in a quite different physical context. Broadly speaking, we may argue that at increasing k the gradual shrinking of the length scale decreases the efficiency of the backflow processes on the tagged particle; as a result, the effective diffusion coefficient approaches the binary value, which is now somewhat *lower* than D. The initial evolution of this process is accounted for by a mode-coupling calculation similar to the one discussed in Section 4.5. In particular, for small k the normalized width can be expressed as (de Schepper and Ernst 1979, Verkerk *et al.* 1985)

$$\frac{\Gamma_\mathrm{s}(k)}{Dk^2} = 1 - \frac{H(\delta)}{k^*} k + O(k^{3/2}). \tag{5.67}$$

Here $k^* = 16\pi nmD^2/k_\mathrm{B}T$ and $\delta = D/[D + (\eta/nm)]$, η being the shear viscosity coefficient. Usually δ is a rather small parameter ($\delta \ll 1$), particularly near the melting point where $D \ll (\eta/nm)$. Finally,

$$H(\delta) = 1.4351\, \delta^{3/2} + O(\delta^{5/2}). \tag{5.68}$$

The prediction of eqn (5.67) have been tested against the neutron-scattering data obtained in liquid sodium at different temperatures (Montfrooy *et al.* 1986). Owing to the small magnitude of the effect, this test is particularly meaningful at the highest temperature explored ($T = 803$ K; the melting point is ≈ 371 K). Consistently with the above arguments, in this 'hot' liquid the effective diffusion coefficient $\Gamma_\mathrm{s}(k)/k^2$ never exceeds D; the initial reduction is found to be well accounted for by eqn (5.67). The unambiguous appearance of this linear decrease with k is a signature of the relevance of the same mode-coupling effects leading to the $t^{-3/2}$ tail in the velocity autocorrelation function $\psi(t)$, or equivalently to the presence of a cusp $\propto \omega^{1/2}$ in the corresponding spectrum $Z(\omega)$ for sufficiently small frequencies. Clearly, the experimental detection of this square-root dependence requires a non-trivial extrapolation of $S_\mathrm{s}(k, \omega)$ both at low frequencies and at small wavevectors. Nevertheless, some successful attempts in this sense have been reported (Morkel *et al.* 1987; Verkerk *et al.* 1989).

In all the preceding pages we have mostly confined our discussion to the k-dependence of the normalized halfwidth $\Gamma_\mathrm{s}(k)/Dk^2$, which has been shown to provide a considerable amount of information despite the apparently 'uninteresting' evolution of the full spectrum. A similar analysis can be performed for another quantity of experimental interest, namely the peak amplitude of $S_\mathrm{s}(k, \omega)$ for $\omega = 0$. Even in this case it is convenient to 'normalize' the results with respect to the diffusive limit by introducing the quantity

$$\sum (k) \equiv \pi Dk^2 S_\mathrm{s}(k, \omega = 0). \tag{5.69}$$

Besides the obvious result $\sum(k = 0) = 1$, the definition (5.69) implies that in the free particle limit $\sum(k \to \infty) = (\pi m/2k_\mathrm{B}T)^{1/2}Dk$ (cf. eqn (1.51)). The typical evolution of $\sum(k)$ at finite wavevectors is illustrated in Fig. 5.7, where for convenience we also report the corresponding behaviour of the quantity $\Gamma_\mathrm{s}(k)/Dk^2$. The results obtained for $\sum(k)$ in a liquid near melting (Fig. 5.7a) show a close correspondence with those previously seen for the normalized halfwidth, even if the various features are some what less evident. Similar remarks can be made for the case of a less dense fluid (or of a fluid at high temperature), which shows a considerably larger range of validity of the free-particle regime (see Fig. 5.7b).

It is worthwhile noticing that the behaviour of $\sum(k)$ would be straightforward if we had some indication that the product $\Gamma_\mathrm{s}(k) \cdot S_\mathrm{s}(k, \omega = 0)$ is nearly constant over the entire wavevector range. In such a circumstance, we might for example argue that for a liquid near the melting point the 'oscillations' of $\sum(k)$ and $\Gamma_\mathrm{s}(k)/Dk^2$ should be in a definite phase ratio, with the maxima of one quantity being approximately coincident with the minima of the other quantity and vice versa. As a matter of fact, Fig. 5.7a indicates that this expectation is not verified at a quantitative level. Rather
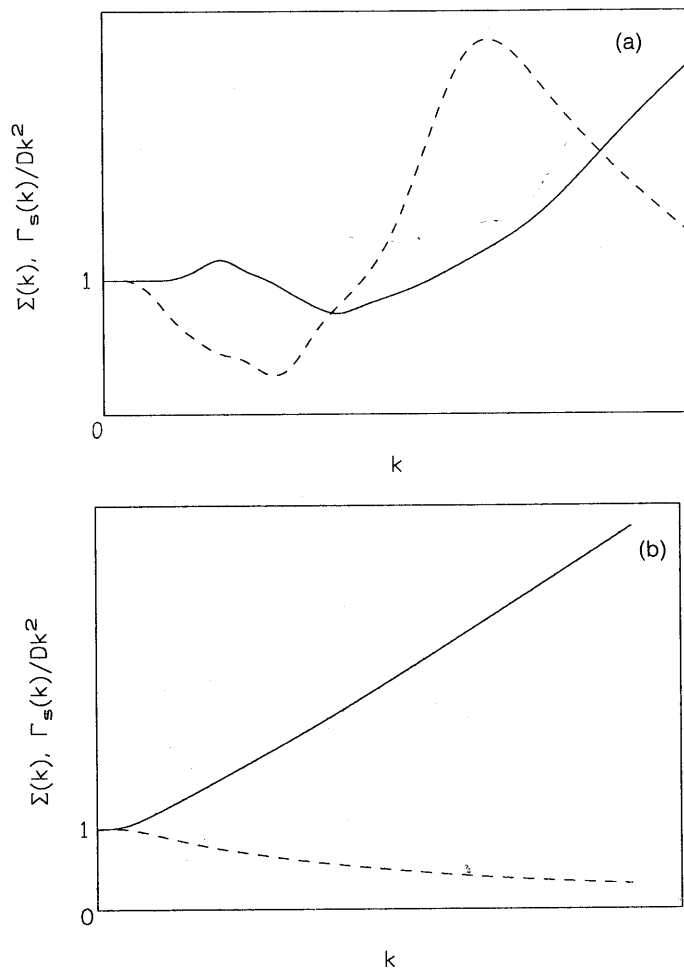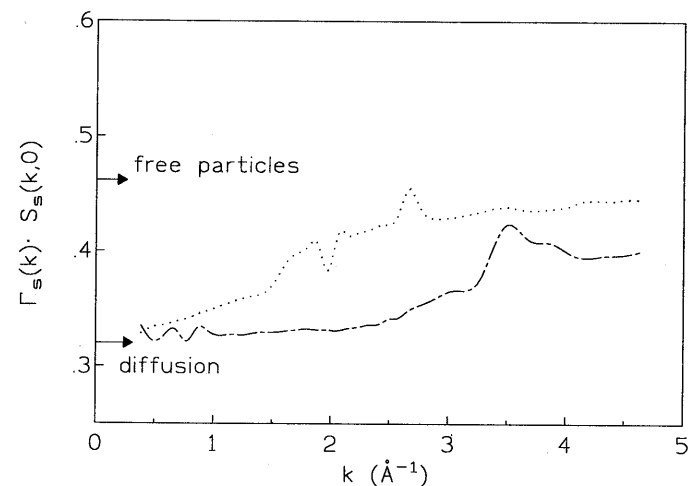
Fig. 5.8 Wavevector dependence of the product $S_s(k, \omega = 0) \cdot \Gamma_s(k)$ in liquid sodium at $T = 403\,\mathrm{K}$ (chain line) and at $T = 803\,\mathrm{K}$ (dotted line). From the incoherent neutron-scattering data of Morkel and Gläser (1986).

and the larger mean free path makes easier the fulfilment of the condition $kl \geqslant 1$.

5.3.3 More recent studies of self-motion

When viewed in perspective, the success achieved in the interpretation of single-particle dynamics by an essentially non-phenomenological framework appears to be considerable. The basic ingredient for this accomplishment is the recognition of the existence of processes evolving over a timescale distinctly longer than the collisional one. As we have seen, different kinds of slow processes are relevant depending on the thermodynamic state of the system. In particular, in a liquid near the melting temperature the motion of the test particle is considerably affected by the sluggishness of the atomic rearrangements. This kind of 'coupling' can readily be accounted for by the theory, with quite satisfactory results at a quantitative level.

It is natural to wonder if any obscure corners are still left in this bright scenario. The answer may be partly subjective depending on which requirements should ultimately be met by a satisfactory physical theory, as well as on the actual accuracy of the experimental or simulation data available. Even so, a thorough analysis of the theoretical framework indicates that in the present stage of development the approach is able to

Fig. 5.7 Schematic wavevector dependence of the two quantities $\Sigma(k)$ (full line) and $\Gamma_s(k)/Dk^2$ (dashed line) in a typical simple fluid: the situation occurring (a) near the melting point and (b) in a dense gas (or 'hot' liquid).

than being constant, the above mentioned product shows instead a systematic increase with the wavevector (Fig. 5.8). This effect is a consequence of the gradual change of $S_s(k, \omega)$ from a Lorentzian shape at small k ($\Gamma_s(k) \cdot S_s(k, 0) = 1/\pi = 0.3183$) to a Gaussian one for $k \to \infty$ ($\Gamma_s(k) \cdot S_s(k, 0) = \sqrt{(\ln 2/\pi)} = 0.4697$). Such a crossover is found to proceed at a slower pace near the melting point than at high temperatures. As a matter of fact, in the latter case a 'binary' picture becomes rapidly appropriate,

Fig. 5.9 Comparison between the features of the effective pair potential in liquid lead (full line) and those of a Lennard–Jones potential (dashed line). The separations are measured in units of the position R_0 of the first peak of $g(r)$ in the two systems. Redrawn from Gudowski *et al.* (1993).

account rather well for the above mentioned long-lasting features; in contrast, our understanding of the fast collisional ('binary') dynamics in real liquids is not so satisfactory. As stressed several times, this limited knowledge can in practice be circumvented by adopting some simple ansatz for the rapid time evolution of the binary memory functions, essentially based on their initial decay rate. As a matter of fact, this rather *ad hoc* procedure is found to yield satisfactory results both for liquid argon and for liquid alkali metals, namely for the traditional archetypes of simple liquids. However, the fast events giving rise to the 'collisional dynamics' are expected to be considerably affected by the detailed shape of the effective interatomic potential. Further tests in other systems may provide additional information, or at least simply justify on a practical basis the status of the theory in its present formulation.

In this context, it is interesting to discuss the results recently obtained in an extensive simulation study of self-motion in liquid lead (Gudowski *et al.* 1993). The effective pair potential $\phi(r)$ in this system is determined by starting with a trial function with several parameters and adopting an iterative fitting procedure such that the static structure factor obtained in the simulations reproduces the available neutron-scattering data as accurately as possible (Dzugutov *et al.* 1988). The potential eventually deduced in this way is considered realistic enough to be employed in a com-

prehensive molecular-dynamics investigation of the properties of liquid lead, aimed to explore their features in a wavevector range uncovered by the neutrons, as well as to obtain information on quantities which are not accessible experimentally (Larsson *et al.* 1990). A noteworthy feature of the adopted potential is that it looks considerably different from, say, the familiar Lennard–Jones potential (see Fig. 5.9). In particular, whereas in the LJ case the position of the minimum of $\phi(r)$ nearly coincides with the 'nearest-neighbour distance' (approximately measured by the location of the first peak of $g(r)$), the effective pair potential in liquid lead appears to be strongly repulsive at that distance. A similar situation is found in another molten semimetal, namely liquid bismuth (Dzugutov and Dahlborg 1989). As a result, in these systems the repulsive portion of $\phi(r)$ appears to have a much longer range than in inert gas liquids or in molten alkali metals.

Coming back to the specific case of liquid lead near the melting point, the simulation was performed with a large system (16 384 particles), thus making possible a study of the dynamics at quite small wavevectors (down to 0.07 Å^{-1}). Although both self- and collective quantities have been investigated (Larsson *et al.* 1990), in the present context we are particularly concerned with the data obtained for single-particle motion by Gudowski *et al.* (1993), which have been used as a benchmark for a stringent test of the predictions of Sjögren and Sjölander (1979) and of Wahnström and Sjögren (1982) for the relevant memory functions. All the input quantities needed in the theoretical expressions (such as the binary decay times, the intermediate scattering functions F_s and F and the currents) were taken from the simulation data, rather than deduced by some approximation scheme.

The most interesting test concerns the memory function $K(t)$ of the velocity autocorrelation function. Recalling that $K(t) = \lim_{k\to 0} M_s(k, t)$, in this case the self-motion is effectively probed over a large spatial range, and yet over an arbitrary timescale comprising even phenomena having a microscopically short duration. As already discussed in Section 5.1, in such a situation the dynamics of $K(t)$ reflects the presence both of rapid collisional events and of slower 'mode-coupling' processes. The results obtained by Gudowski *et al.* (1993) for the theoretical memory function $K(t) = K_s(t) + K'(t)$ in liquid lead are reported in Fig. 5.10. In close correspondence with the original analysis by Sjögren and Sjölander (1979) and by Sjögren (1980b), the long-lasting portion $K'(t)$ was evaluated by including both the dominant density contribution (eqn (5.12)) and the other smaller terms involving the currents. A comparison of this theoretical $K(t)$ with the corresponding simulation findings indicates clear quantitative discrepancies (see Fig. 5.10). In particular, at relatively short times the molecular-dynamics data for $K(t)$ present a deep minimum which is not reproduced by the theory. Moreover, in the majority of the intermediate
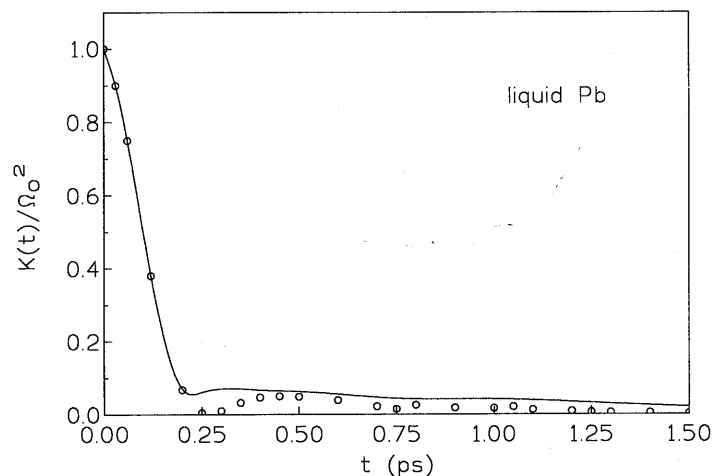
Fig. 5.10 Normalized memory function $K(t)/\Omega_0^2$ of the velocity autocorrelation function in liquid lead at 623 K. The full line denotes the result of the theory by Sjögren and Sjölander (1979) with all the mode-coupling decay channels included. The open circles are the actual computer simulation data. Redrawn from Gudowski *et al.* (1993).

time region the mode-coupling results are found to overestimate the actual amplitude of the tail by about a factor two. Even if these discrepancies may not appear dramatic on the full scale of $K(t)$, their combined effect on eqn (5.27) is such that the theoretical diffusion coefficient underestimates the actual one by as much as 30%. This situation is to be contrasted with the satisfactory results previously seen both for liquid argon and for molten alkali metals.

The reason for these shortcomings in liquid lead is still unclear. The unusual shape of $\phi(r)$ in this system may certainly have some consequences for the binary part of $K(t)$, particularly in the last portion of its decay (i.e. just where the deep minimum occurs). On the other hand, the presence of discrepancies even in the tail (where presumably the potential shape plays a smaller role) poses some problems about the validity of the mode-coupling expressions in their present form.

Summing up, although the theoretical framework certainly provides the keys for a correct interpretation of the different processes relevant for self-motion, both additional tests in other systems and further quantitative improvements are necessary before we can claim the 'universal' character of the present formulation. In this respect, despite their deceivingly simple appearance, single-particle properties are a very sensitive benchmark. In contrast, we shall see in the next chapter that several features of collective dynamics turn out to be ruled by rather trivial structural effects, making

a very detailed knowledge of the relevant memory functions comparatively less important.

REFERENCES

Akcasu, A. Z., Corngold, N., and Duderstadt, J. J. (1970). *Phys. Fluids*, **13**, 2213.
Balucani, U., Vallauri, R., and Gaskell, T. (1990*a*). *Nuovo Cimento D*, **12**, 1511.
Balucani, U., Vallauri, R., and Gaskell, T., and Duffy, S. F. (1990*b*). *J. Phys. Cond. Matter*, **2**, 5015.
Balucani, U., Torcini, A., and Vallauri, R. (1992). *Phys. Rev. A*, **46**, 2159.
Bosse, J., Götze, W., and Zippelius, A. (1978). *Phys. Rev. A*, **18**, 1214.
Desai, R. C. (1971). *Phys. Rev. A*, **3**, 320.
de Schepper, I. M. and Ernst, M. H. (1979). *Physica A*, **98**, 189.
Dzugutov, M. and Dahlborg, U. (1989). *Phys. Rev. A*, **40**, 4103.
Dzugutov, M., Larsson, K.-E., and Ebbsjö, I. (1988). *Phys. Rev. A*, **38**, 3609.
Gonzáles, L. E., Gonzáles, D. J., and Canales, M. (1994). to be published.
Götze, W. and Zippelius, A. (1976). *Phys. Rev. A*, **14**, 1842.
Gudowski, W., Dzugutov, M., and Larsson, K.-E. (1993). *Phys. Rev. E*, **47**, 1693.
Jhon, M. S. and Forster, D. (1975). *Phys. Rev. A*, **12**, 254.
Kinell, T. and Lovesey, S. W. (1986). *J. Phys. C*, **19**, L791.
Larsson, K.-E., Dzugutov, M., and Gudowski, W. (1990). *Nuovo Cimento D*, **12**, 559.
Lebowitz, J. L., Percus, J. K., and Sykes, J. (1969). *Phys. Rev.*, **188**, 487.
Levesque, D. and Verlet, L. (1970). *Phys. Rev. A*, **2**, 2514.
Lovesey, S. W. (1973). *J. Phys. C*, **6**, 1856.
Montfrooy, W., de Schepper, I., Bosse, J., Gläser, W., and Morkel, C. (1986). *Phys. Rev. A*, **33**, 1405.
Morkel, C. and Gläser, W. (1986). *Phys. Rev. A*, **33**, 3383.
Morkel, C., Gronemeyer, C., Gläser, W., and Bosse, J. (1987). *Phys. Rev. Lett.*, **58**, 1873.
Naghizadeh, J. and Rice, S. A. (1963). *J. Chem. Phys.*, **36**, 2710.
Nijboer, B. R. A. and Rahman, A. (1966). *Physica*, **32**, 415.
Ohse, R. W. (ed.) (1985). *Handbook of thermodynamic and transport properties of alkali metals*, Chapter 7.5. Blackwell Scientific, Oxford.
Rahman, A. (1964). *Phys. Rev.*, **136**, A405.
Sjögren, L. (1980*a*). *J. Phys. C*, **13**, 705.
Sjögren, L. (1980*b*). *Phys. Rev. A*, **22**, 2866.
Sjögren, L. and Sjölander, A. (1979). *J. Phys. C*, **12**, 4369.
Sjölander, A. and Turski, L. A. (1978). *J. Phys. C*, **11**, 1973.
Slöld, K., Rowe, J. M., Ostrowski, G. and Randolph, P. D. (1972). *Phys. Rev. A*, **6**, 1107.
Verkerk, P., Builtjes, J. H., and de Schepper, I. M. (1985). *Phys. Rev. A*, **31**, 1731.
Verkerk, P., Westerweel, J., Bafile, U., de Schepper, I. M., and de Graaf, L. A. (1989). In *Static and dynamic properties of liquids* (ed. M. Davidovic and A. K. Soper). Springer, Heidelberg.
Wahnström, G. and Sjögren, L. (1982). *J. Phys. C*, **15**, 401.

6

Collective properties

6.1 GENERALIZED HYDRODYNAMICS

In Section 3.4 we saw that all the results of ordinary Navier–Stokes hydrodynamics can formally be deduced by a microscopic memory function approach. In perspective, this success stems from the slow character of the hydrodynamic variables in the limit of small wavevectors, which in turn implies the validity of a Markovian ansatz for the corresponding memory functions. As a by-product of the approach, it was moreover possible to establish 'Green–Kubo relations' for the macroscopic transport coefficients, which can be expressed as time integrals of ordinary correlation functions.

Starting from this successful picture, let us now explore the dynamics of the same variables at increasing wavevectors; that is, up to values of $2\pi/k$ comparable with atomic sizes. Arguing by common sense, we may expect that in this case the hydrodynamic results are no longer valid. To begin with, the continuum description inherent in the Navier–Stokes equations becomes suspect as we approach microscopic distances. Although deduced by a framework entirely different from hydrodynamics, even a result like eqn (3.136) should ultimately have similar limitations. Also, as k increases the time evolution of the variables, originally classified as 'quasi-conserved', gradually loses any slow character, calling for a critical revision of the basic arguments exploited in Section 3.4.

In practice, the situation actually occurring in the liquid range is somewhat different. To be more specific, we shall see that with some suitable changes the hydrodynamic framework can be extended up to wave vectors considerably larger than anticipated from our intuitive considerations. The basic physical reason for this unexpected success is that in k space the actual domain of validity of hydrodynamics is determined, rather than by the particle size σ, by the requirement that the explored length scale must comprise a sufficiently large number of collisional events. In other words, rather than dealing with the restrictive condition $k\sigma \ll 1$, we simply need that $kl \ll 1$, where the quantity l is of the order of a mean free path. Since at liquid densities l is considerably less than the typical atomic separations (the latter being of the order of $r_0 \approx \sigma$, cf. Section 1.4.2), the effective validity of the hydrodynamic description is extended well beyond the limits inherent to a 'continuum approximation'.

Nevertheless, beyond a certain wavevector the results of ordinary hydrodynamics are bound to break down. The simplest recipe to face this situation is to retain the formal structure of the hydrodynamic equations and to allow for the finiteness of k by replacing both equilibrium properties and transport coefficients with suitable wavevector dependent generalizations. In practice, such a *generalized hydrodynamics* can be derived in several ways. The most straightforward procedure is simply to assume that some or all of the relevant quantities become k-dependent, and to look for physical criteria which may help to establish such a dependence. For example, let us consider the hydrodynamic expression (1.161) of the intermediate scattering function. To illustrate the procedure in a simple situation, let us assume that the effects of the thermal fluctuations can be neglected (i.e. that $\gamma \approx 1$). In such a case eqn (1.161) reads

$$[F(k,t)]_{\mathrm{hyd}} = [F(k,0)]_{\mathrm{hyd}} \exp\left(-\Gamma_{\mathrm{L}} k^2 t\right) [\cos\left(v_{\mathrm{T}} kt\right)$$
$$+ (\Gamma_{\mathrm{L}} k/v_{\mathrm{T}}) \sin\left(v_{\mathrm{T}} kt\right)] \tag{6.1}$$

where $v_{\mathrm{T}} = (nm\chi_{\mathrm{T}})^{-1/2}$ is the isothermal sound velocity and $\Gamma_{\mathrm{L}} = \frac{1}{2}(\eta_{\mathrm{L}}/nm)$. Since the initial value $[F(k,0)]_{\mathrm{hyd}} = nk_{\mathrm{B}} T\chi_{\mathrm{T}}$ can be written as $S(k=0)$ (cf. eqn (1.15)), at finite wavevectors it appears natural to replace it with $S(k)$. As we already know from eqn (1.121), this is in fact the correct result at any k. Similarly, it is reasonable to replace $v_{\mathrm{T}} = [k_{\mathrm{B}} T/mS(k=0)]^{1/2}$ with the wavevector dependent velocity $v_{\mathrm{T}}(k) = [k_{\mathrm{B}} T/mS(k)]^{1/2}$. As a consequence, in this special case with $\gamma = 1$ the quantity $v_{\mathrm{T}} k$ appearing in eqn (6.1) is simply 'generalized' as $v_{\mathrm{T}}(k) \cdot k = \langle \omega_k^2 \rangle^{1/2}$ (cf. eqn (1.128)). In contrast with the rather straightforward treatment of these equilibrium properties, the generalization of the damping rate $\Gamma_{\mathrm{L}} k^2$ at finite wavevectors requires a careful discussion. As a first step in this direction, it is convenient to consider the Laplace transform of eqn (6.1) which for sufficiently small k can be written as

$$[\tilde{F}(k,z)]_{\mathrm{hyd}} \approx [F(k,0)]_{\mathrm{hyd}} \left[z + \frac{(v_{\mathrm{T}} k)^2}{z + 2\Gamma_{\mathrm{L}} k^2}\right]^{-1}. \tag{6.2}$$

This expression is now compared with the formally exact Mori representation of $\tilde{F}(k,z)$ in terms of a continued fraction expansion (cf. eqn (3.42)). At the second level we obtain

$$\tilde{F}(k,z) = S(k) \left[z + \frac{\langle \omega_k^2 \rangle}{z + \tilde{K}_{\mathrm{L}}(k,z)}\right]^{-1}, \tag{6.3}$$

where $\tilde{K}_{\mathrm{L}}(k,z)$ is the Laplace transform of the second-order memory function $K_{\mathrm{L}}(k,t)$. Whereas the exact initial value of $K_{\mathrm{L}}(k,t)$ has already been determined (cf. eqn (4.160)), not very much is known a priori about its time

evolution at arbitrary wavevectors. However, in the hydrodynamic regime we know that, on the timescale of $F(k, t)$, the decay of $K_L(k, t)$ should be fast enough to guarantee the validity of the Markovian approximation

$$K_L(k \to 0, t) = A_k \delta(t) \tag{6.4}$$

or, equivalently, $\tilde{K}_L(k, z) = \frac{1}{2}A_k$. To be consistent with eqn (6.2), the proportionality constant in (6.4) should read

$$A_k = 4\Gamma_L k^2 = 2(\eta_L/nm)k^2. \tag{6.5}$$

Starting from this $k \to 0$ limit, we may now try to extend the framework at finite wavevectors by making the ansatz

$$K_L(k, t) = K_L(k, 0) \exp(-t/\tau_k)$$
$$= [\omega_L^2(k) - \langle \omega_k^2 \rangle] \exp(-t/\tau_k) \tag{6.6}$$

where in the last step we have exploited eqn (4.160). The assumption that the decay of the memory function is ruled by a single k-dependent time constant parallels a similar approximation adopted in Section 5.3.1 for self-motion, and is in fact the simplest one which we may envisage at a preliminary stage. The consequences of the ansatz (6.6) (often referred to as the *viscoelastic model*) will be discussed in detail in the next section; for the time being, it is interesting to see its implications in the strict hydrodynamic regime (i.e. for small wavevectors and small frequencies). In this case, from eqns (6.6) and (1.144) we obtain

$$\tilde{K}_L(k \to 0, z \to 0) = \lim_{z \to 0} (c_L^2 - v_T^2)k^2 [z + (1/\tau_{k \to 0})]^{-1}$$
$$= (c_L^2 - v_T^2)k^2 \tau_{k \to 0}. \tag{6.7}$$

Inserting this limiting expression into eqn (6.3) and comparing the result with eqn (6.2) we deduce that

$$\tau_{k \to 0} = \frac{(\eta_L/nm)}{c_L^2 - v_T^2}. \tag{6.8}$$

Since the velocity c_L turns out to be always larger than v_T, the decay time τ_k entering eqn (6.6) is perfectly defined and finite as $k \to 0$. In practice, the values of $\tau_{k \to 0}$ evaluated from (6.8) are still 'microscopic' (typically, in the picosecond range for simple liquids), while at decreasing wavevectors the decay times associated with $F(k, t)$ become very long owing to the progressive fulfilment of the conservation laws. Eventually we approach an ideal Markovian situation, as in fact expected from the analysis in Section 3.4.

Up to now, for simplicity we have dealt with a sort of 'isothermal hydrodynamics' in which the specific heat ratio $\gamma \approx 1$. Although this

situation is rather well verified in all liquid alkali metals ($\gamma \approx 1.1$), it is not realistic in many other systems, including liquid argon where $\gamma \approx 2.2$. Let us therefore consider the more complicated case in which the presence of thermal fluctuations cannot be neglected. Rather than dealing with eqn (6.2), for $k \to 0$ we now have the complete hydrodynamic expression

$$[\tilde{F}(k, z)]_{hyd} = [F(k, t = 0)]_{hyd} \left[z + \frac{(v_T k)^2}{z + 2\Gamma_L k^2 + \frac{(\gamma - 1)(v_T k)^2}{z + (\kappa/nc_V)k^2}} \right]^{-1} \tag{6.9}$$

(cf. eqn (3.137) and subsequent results). Even in this case, a preliminary 'generalization' of (6.9) is achieved by replacing the quantities $[F(k, t = 0)]_{hyd}$ and $(v_T k)^2$ with their respective equivalents at finite k, that is $S(k)$ and $\langle \omega_k^2 \rangle$. As a second step, eqn (6.9) can be interpreted in terms of the formally exact representation (6.3); this implies that in the hydrodynamic regime the memory function $\tilde{K}_L$ has the form

$$\tilde{K}_L(k \to 0, z) = 2\Gamma_L k^2 + \frac{(\gamma - 1)\langle \omega_{k \to 0}^2 \rangle}{z + (\kappa/nc_V)k^2}. \tag{6.10}$$

Making the identification $2\Gamma_L = \eta_L/nm$, in the time domain eqn (6.10) corresponds to

$$K_L(k \to 0, t) = 2(\eta_L/nm)k^2 \delta(t) + (\gamma - 1)\langle \omega_{k \to 0}^2 \rangle$$
$$\times \exp[-(\kappa/nc_V)k^2 t]. \tag{6.11}$$

In contrast with the first term on the right-hand side, the additional contribution due to thermal fluctuations is seen to have a finite decay time even in the hydrodynamic region. In our attempts to generalize eqn (6.11) at finite wavevectors, it is consequently more sensible to modify the $\delta(t)$ decay of the viscous term than to speculate about possible deviations of the thermal contribution from a purely exponential decay. In analogy with the previous case $\gamma = 1$, we tentatively describe the viscous relaxation processes by a simple viscoelastic model. As a result:

$$K_L(k, t) = [\omega_L^2(k) - \gamma\langle \omega_k^2 \rangle] \exp(-t/\tau_k)$$
$$+ (\gamma - 1)\langle \omega_k^2 \rangle \exp[-(\kappa/nc_V)k^2 t] \tag{6.12}$$

where the amplitude of the first term on the right-hand side is chosen in such a way that the memory function has the correct initial value $K_L(k, 0) = \omega_L^2(k) - \langle \omega_k^2 \rangle$. Turning again to a description in terms of Laplace transforms, the generalized hydrodynamics approach discussed so far for $\tilde{F}(k, z)$ can be summarized as follows:

$$\frac{\tilde{F}(k,z)}{S(k)} = \left[z + \frac{\langle \omega_k^2 \rangle}{z + \tilde{K}_L(k,z)} \right]^{-1} \qquad (6.13)$$

with

$$\tilde{K}_L(k,z) = \frac{\omega_L^2(k) - \gamma \langle \omega_k^2 \rangle}{z + (1/\tau_k)} + \frac{(\gamma - 1)\langle \omega_k^2 \rangle}{z + (\kappa/nc_V)k^2}. \qquad (6.14)$$

The rather intuitive procedure, which has led to eqns (6.13)–(6.14), is the simplest example of the typical arguments used in generalized hydrodynamics. Rather than trying to extend the Navier–Stokes results by a perturbative treatment (e.g. by a step-by-step expansion in the wavevector k), these approaches are based on reasonable 'extrapolations' in which an important criterion is the fulfilment of a limited number of exact short-time properties such as $S(k)$, $\langle \omega_k^2 \rangle$ and $\omega_L^2(k)$. As we shall see in the following, the inclusion of these properties (which are in principle known at *any* wavevector) may indeed extend the validity of the results to a range of (k, ω) considerably larger than the one typical of hydrodynamics.

In any case, the ultimate test for these approaches is the comparison of the theoretical predictions for the spectra $S(k, \omega) = (1/\pi) \, \text{Re} \, \tilde{F}(k, z = i\omega)$ with the experimental or simulation data at increasing wavevectors. Beyond the hydrodynamic regime the observed spectra show a more or less rapid transition from the Rayleigh–Brillouin triplet structure to a lineshape characterized by a single peak at $\omega = 0$. The actual rate of this crossover turns out to be much faster in argon-like liquids than in molten alkali metals (cf. Figs 1.12, 1.13). Generally speaking, in these systems the evolution of the theoretical line shape at increasing k compares rather well with the observations (Ailawadi *et al.* 1971; Levesque *et al.* 1973; Copley and Lovesey 1975). This is particularly true if one proceeds to a further k-dependent generalization of eqn (6.14) by writing

$$\tilde{K}_L(k,z) = \frac{\omega_L^2(k) - \gamma_k \langle \omega_k^2 \rangle}{z + (1/\tau_k)} + \frac{(\gamma_k - 1)\langle \omega_k^2 \rangle}{z + a_k k^2}. \qquad (6.15)$$

In particular, the form (6.15) has been adopted by Levesque *et al.* (1973) in their pioneering work on the collective dynamics on Lennard–Jones liquids. In this simulation study the quantities τ_k, γ_k and a_k were considered as fitting parameters at every wavevector. Despite this rather phenomenological aspect, the results of such an analysis are quite interesting. At sufficiently small wavevectors the parameters τ_k and a_k are indeed found to approach their correct hydrodynamic values $\tau_{k \to 0}$ (eqn (6.8)) and κ/nc_V. On the other hand, the behaviour of γ_k is more subtle. For $k\sigma > 2$ the best-fitted value of γ_k is essentially unity, indicating that the coupling to thermal fluctuations can safely be neglected even for

relatively small wavevectors (note that in the usual Lennard–Jones units the main peak of $S(k)$ occurs approximately for $k\sigma \approx 6.8$). However, for $k \to 0$ the optimum values of γ_k are found to exceed considerably the exact result $\gamma = c_P/c_V$. Since in this limit the second term in eqn (6.15) is characterized by a rather small damping, the presence of the discrepancy indicates that in the low wavevector range $K_L(k, t)$ is affected by *additional* long-lasting processes, which the fit reveals by an effective increase of the amplitude factor $(\gamma_k - 1)$. To test the correctness of this interpretation, Levesque *et al.* included an additional term in $K_L(k, t)$ which should account for the presence of slow features in the *viscous* relaxation. Modelling the time-dependence of this contribution by another exponential decay law, one eventually arrives at the following expression of $\tilde{K}_L(k, z)$:

$$\tilde{K}_L(k,z) = [\omega_L^2(k) - \gamma_k \langle \omega_k^2 \rangle] \left[\frac{1 - a_k}{z + (1/\tau_k)} + \frac{a_k}{z + (1/\tau')} \right]$$
$$+ \frac{(\gamma_k - 1)\langle \omega_k^2 \rangle}{z + a_k k^2} \qquad (6.16)$$

where the additional parameter a_k measures the effective weight of the 'slow' contribution (described for simplicity by a k-independent time constant τ'). Given the larger number of parameters, it is not surprising to find an even better agreement with the simulation data for $S(k, \omega)$. The important result is, however, the fact that for small wavevectors γ_k now smoothly approaches the correct value γ. Moreover, the weight factor a_k (roughly ≈ 0.1 at small k) is found to decrease considerably at larger wavevectors, confirming the approximate validity of the ansatz (6.6) beyond a rather limited range of k.

In the simpler context of the memory function (6.6), several prescriptions were originally proposed for the wavevector dependence of the relaxation time τ_k (Chung and Yip 1969; Akcasu and Daniels 1970). Rather than attempting a microscopic derivation, these approaches provide for τ_k empirical expressions which interpolate between the $k = 0$ result (6.8) and the limiting behaviour expected for a non-interacting system at large k. Since the generalized hydrodynamics framework is intrinsically unable to reproduce the Gaussian line shape (1.1) appropriate for free particles, one may only require that some spectral feature is correctly accounted for. To give an example, we may ask that for large wavevectors the theory reproduces the free particle result $S(k, \omega = 0) = (m/2\pi k_B T k^2)^{1/2}$. This procedure closely parallels the one discussed in Section 5.3.1 for self-motion. Noting that $S(k \to \infty) = 1$, $\langle \omega_{k \to \infty}^2 \rangle = (k_B T/m)k^2$, and $\omega_L^2(k \to \infty) = (3k_B T/m)k^2$, from eqn (6.3) we readily obtain that for large k the predicted value of $S(k, \omega = 0)$ is $(2/\pi)\tau_{k \to \infty}$. To be consistent, we should then require that
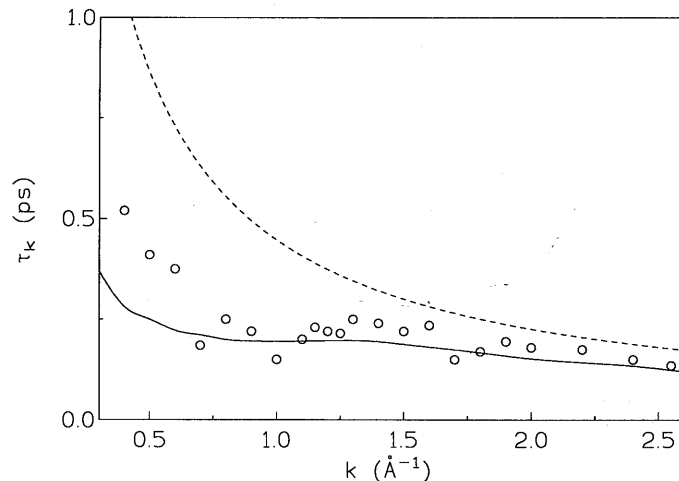
Fig. 6.1 Test of two theoretical schemes for the wavevector dependence of the time τ_k at intermediate k. The open circles are the best-fitted values deduced from the neutron-scattering spectra in liquid Cs at 308 K (Bodensteiner 1990). The dashed line refers to the results from eqn (6.18) and the full line to the expression (6.34) proposed by Lovesey (1971). The position of the main peak of $S(k)$ is at
$$k_\mathrm{m} = 1.4 \ \text{Å}^{-1}.$$

$$\left(\frac{1}{\tau_{k\to\infty}}\right)^2 = \frac{8k_\mathrm{B}T}{\pi m}k^2. \tag{6.17}$$

Then the simplest interpolation scheme which we may envisage can be written as (Chung and Yip 1969)

$$\left(\frac{1}{\tau_k}\right)^2 = \left(\frac{1}{\tau_{k\to 0}}\right)^2 + \frac{8k_\mathrm{B}T}{\pi m}k^2. \tag{6.18}$$

While eqn (6.18) is clearly consistent for both small and large wavevectors, the values of τ_k predicted at intermediate k are generally in rather poor agreement with the simulation data obtained by best-fitting procedures (see Fig. 6.1). The results are not significantly improved with alternative choices for the spectral feature to be reproduced for $k \to \infty$ (for example, the position of the peak of $\omega^2 S(k, \omega)$). A somewhat better agreement is instead obtained by adopting more complicated interpolation formulas, albeit at the price of introducing an additional parameter (Akcasu and Daniels 1970). In the absence of more refined calculations (see, however, the next section), it is nowadays customary to treat the time τ_k as a quantity to be deduced from the observed spectra.

Summing up, the hydrodynamic framework can indeed be extended successfully well beyond its strict range of application — provided that we are ready to accept a certain amount of intuitive and phenomenological arguments in this generalization. If not, an alternative is to resort to the more rigorous approach developed in Section 3.4. In particular, a result like eqn (3.135) still represents a valuable starting point, even if in practice not much progress can be made without further assumptions. A possible solution is to consider an enlarged set of Mori variables, also including the non-conserved ones such as the different components of the microscopic stress tensor (1.178) and of the microscopic energy current (1.182). The main points of this theory (originally developed by Akcasu and Daniels (1970)) are discussed in detail by Boon and Yip (1980); although undoubtedly comprehensive, the approach has, however, not led to a significant improvement of the previous results.

Even with these problems, the main concepts behind the generalized hydrodynamics framework are quite appealing. We have seen that it is in fact possible to retain the basic structure of the hydrodynamic equations, provided that the usual transport coefficients are effectively replaced by wavevector- *and* frequency-dependent quantities. Rather than being purely formal, this replacement has far-reaching physical consequences on the dynamic response of the system. Some of these implications are already apparent in the simplest 'generalization' scheme, the aforementioned viscoelastic model (see Section 6.2); others are more subtle and require a careful consideration of those long-lasting events which have been seen to pervade several features of the dynamics of the liquid state.

Besides an extensive use in the interpretation of the data from real fluids (the works by Bodensteiner *et al.* (1992) and by Youden *et al.* (1992) are only recent examples of a long series), the concepts of generalized hydrodynamics have had a substantial impact even on the studies dealing with *hard-sphere fluids*. In particular, the appropriate generalized forms of the various thermodynamic and transport coefficients have been investigated both theoretically (Leutheusser 1982) and by molecular dynamics simulations (Alley and Alder 1983). Moreover, in the hard-sphere case it proves possible to establish an approximate kinetic framework in which the evolution of the main 'eigenmodes' (cf. Section 1.3) can be followed in a wide range of wavevectors (de Schepper and Cohen 1982; Cohen *et al.* 1984, 1986; Bruin *et al.* 1985). In particular, at finite wavevectors the dynamic structure factor is found to be governed by three eigenmodes reminiscent of the hydrodynamic ones: two symmetrical 'extended sound modes' (generalized Brillouin doublet) and one 'extended heat mode' (generalized Rayleigh component). As a consequence, $S(k, \omega)$ can be represented even for non-hydrodynamic wavevectors as a sum of three Lorentzians with appropriate amplitudes (cf. Section 2.4.1). As k increases toward the

position k_m of the main peak of $S(k)$, the damping of the 'heat' mode is found to be always smaller than that of the others, especially at high densities where the most important features of $S(k, \omega)$ are almost completely determined by this eigenmode. On the other hand, as $k \to k_m$ the framework gives a rather curious result for the dispersion of the sound modes, namely the occurrence of a region with zero frequency (de Schepper *et al.* 1983). These findings aroused a debate about the actual existence of these 'propagation gaps' in real fluids (Lovesey 1984). Since the gaps themselves are found to disappear at sufficiently high density (van Rijs *et al.* 1985), the subject has probably been overemphasized with respect to other more important results of the framework. In a more general context, the predicted three-Lorentzian line shape has been successfully adopted to analyse the neutron-scattering data for $S(k, \omega)$ in a variety of situations. As already mentioned in Section 2.4.2, particularly interesting in this respect are some recent neutron measurements made in argon gas at moderate density (Bafile *et al.* 1990), where the initial deviation from Navier–Stokes hydrodynamics have been detected. In this transition region, the three-Lorentzian analysis and the generalized hydrodynamics framework are found to give an equally good account of the experimental spectra (Youden *et al.* 1992).

6.2 THE VISCOELASTIC MODEL

6.2.1 Density fluctuations

The results discussed in the previous section have made clear the relevance of the memory function $K_L(k, t)$ in determining the features of the intermediate scattering function $F(k, t)$ and of its frequency spectrum $S(k, \omega)$. Before embarking on the detailed analysis of a particularly simple model for $K_L(k, t)$, it is convenient to collect together the basic reference equations. According to the memory function framework, the dynamic structure factor $S(k, \omega)$ can be exactly expressed as

$$\frac{S(k, \omega)}{S(k)} = \frac{1}{\pi} Re \frac{\tilde{F}(k, z = i\omega)}{S(k)}$$

$$= \frac{1}{\pi} Re \left[i\omega + \frac{\langle \omega_k^2 \rangle}{i\omega + \tilde{K}_L(k, z = i\omega)} \right]^{-1}. \tag{6.19}$$

Since

$$\tilde{K}_L(k, z = i\omega) = \int_0^\infty dt \cos \omega t \, K_L(k, t) - i \int_0^\infty dt \sin \omega t \, K_L(k, t)$$

$$\equiv K_L'(k, \omega) - i K_L''(k, \omega) \tag{6.20}$$

we may eventually write that

$$\frac{S(k, \omega)}{S(k)} = \frac{1}{\pi} \frac{\langle \omega_k^2 \rangle K_L'(k, \omega)}{[\omega^2 - \langle \omega_k^2 \rangle - \omega K_L'(k, \omega)]^2 + [\omega K_L''(k, \omega)]^2}. \tag{6.21}$$

A priori, the only exact result which we know about the memory function $K_L(k, t)$ is the initial value

$$K_L(k, t = 0) = \omega_L^2(k) - \langle \omega_k^2 \rangle \equiv \Delta_k. \tag{6.22}$$

The simplest assumption that we may make about the time dependence of $K_L(k, t)$ is the exponential decay law

$$K_L(k, t) = \Delta_k \exp(-t/\tau_k). \tag{6.23}$$

Translated into the frequency domain, this amounts to saying that

$$K_L'(k, \omega) = \Delta_k \frac{(1/\tau_k)}{\omega^2 + (1/\tau_k)^2}, \tag{6.24a}$$

$$K_L''(k, \omega) = \Delta_k \frac{\omega}{\omega^2 + (1/\tau_k)^2}. \tag{6.24b}$$

In the preceding section we have seen that the ansatz (6.23) implies that the effects of the thermal fluctuations are negligible. Consequently, by adopting eqn (6.23) we cannot hope to account for the correct hydrodynamic behaviour of a system characterized by a specific heat ratio noticeably different from one. Also, the assumption that the decay of $K_L(k, t)$ is ruled by a single time constant is a clear oversimplication, particularly in those cases where long-lasting phenomena play a role in the dynamics of the memory function. Nevertheless, there are several good reasons to discuss in detail the consequences of the approximation (6.23) (referred to as the *viscoelastic model*):

(i) The dynamics of density fluctuations at finite wavevectors is controlled to a large extent by structural effects, embodied in the two quantities $\langle \omega_k^2 \rangle$ and $\omega_L^2(k)$. In particular, in the liquid range the normalized second moment $\langle \omega_k^2 \rangle = [k_B T/mS(k)]k^2$ is considerably affected by the sharp variations of the static structure factor $S(k)$ at increasing wavevectors. These features are automatically incorporated into eqns (6.21) and (6.24). This situation is to be contrasted with the case of self-motion, where $\langle \omega_k^2 \rangle_s$ is simply $(k_B T/m)k^2$ and the structural features only appear at a subsequent stage of the continued fraction.

(ii) As already noticed, the relevance of both thermal fluctuations and slow 'tails' appears to be considerably decreased as k approaches k_m; in the

notation of eqn (6.16), $\gamma_k \to 1$ and $a_k \to 0$. Beyond a certain wavevector range we therefore expect that the viscoelastic ansatz (6.23) gives a quite reasonable description of the dynamical features of $K_L(k, t)$.

(iii) The time constant τ_k controls the specific collective behaviour of the system. We shall in fact see that for $t \ll \tau_k$ the fluid responds as it were a 'frozen' solid-like system, whereas for times $t \gg \tau_k$ the viscous mechanisms set in and reveal the inherent dynamic disorder.

Inserting (6.24a) and (6.24b) into eqn (6.21) we obtain

$$\frac{S(k, \omega)}{S(k)} = \frac{1}{\pi} \frac{\Delta_k \langle \omega_k^2 \rangle (1/\tau_k)}{\omega^2 [\omega^2 - \langle \omega_k^2 \rangle - \Delta_k]^2 + (1/\tau_k)^2 [\omega^2 - \langle \omega_k^2 \rangle]^2} . \tag{6.25}$$

The corresponding result for the intermediate scattering function reads (Lovesey 1971):

$$\begin{aligned}
\frac{F(k, t)}{S(k)} = \frac{\langle \omega_k^2 \rangle \Delta_k}{\eta_k^2 + (\xi_k - \theta_k)^2} & \left\{ \frac{1}{\theta_k^2 + \langle \omega_k^2 \rangle} \exp(-\theta_k t) \right. \\
& + \frac{\exp(-\xi_k t)}{[\eta_k^2 - \xi_k^2 - \langle \omega_k^2 \rangle]^2 + 4\xi_k^2 \eta_k^2} \{ (\eta_k^2 - 3\xi_k^2 - \langle \omega_k^2 \rangle + 2\xi_k \theta_k) \cos \eta_k t \\
& \left. + [(\xi_k - \theta_k)(\eta_k^2 - \xi_k^2 - \langle \omega_k^2 \rangle) + 2\xi_k \eta_k^2] (1/\eta_k) \sin \eta_k t \} \right\} .
\end{aligned} \tag{6.26}$$

Here

$$\begin{aligned}
\eta_k &= (1/2\sqrt{3})(r_k + s_k), \\
\xi_k &= (1/6)[r_k - s_k + (2/\tau_k)], \\
\theta_k &= (1/3)[s_k - r_k + (1/\tau_k)],
\end{aligned} \tag{6.27a}$$

with

$$\left.\begin{matrix} r_k \\ s_k \end{matrix}\right\} = \pm [Q_k + \sqrt{Q_k^2 + P_k^3}]^{1/3}, \tag{6.27b}$$

$$Q_k = (1/2\tau_k)[9\omega_L^2(k) - 27\langle \omega_k^2 \rangle + 2(1/\tau_k)^2], \tag{6.27c}$$

$$P_k = 3\omega_L^2(k) - (1/\tau_k)^2. \tag{6.27d}$$

The rather awkward appearance of eqn (6.26) is a direct consequence of the expression for $\tilde{F}(k, z)$ in the viscoelastic model:

$$\frac{\tilde{F}(k, z)}{S(k)} = \left[z + \frac{\langle \omega_k^2 \rangle}{z + \dfrac{\Delta_k}{z + (1/\tau_k)}} \right]^{-1} \tag{6.28}$$

which has a typical three-pole structure (the alternative name of the 'three-pole approximation' is sometimes given to this version of the viscoelastic model). The specific form of $F(k, t)$ is then ultimately determined by the solutions of a cubic equation. If the quantities θ_k, ξ_k, and η_k are real, it is readily seen from eqn (6.26) that $F(k, t)$ comprises both a portion which decays exponentially and two damped oscillatory components with a period $2\pi/\eta_k$.

Coming back to the frequency domain, eqn (6.25) shows that the peaks of $S(k, \omega)$ are located at the minima of the denominator. After some simple algebra it is found that the spectrum has a *central peak* at $\omega = 0$ provided that

$$\omega_L^2(k) > [2\langle \omega_k^2 \rangle]^{1/2}(1/\tau_k). \tag{6.29}$$

Moreover, $S(k, \omega)$ may even have two symmetrical *inelastic peaks* at $\omega = \pm \omega_{\text{peak}}(k)$, where

$$\begin{aligned}
3\omega_{\text{peak}}^2(k) = [2\omega_L^2(k) - (1/\tau_k^2)] + \{ \omega_L^4(k) & \\
- (2/\tau_k^2)[2\omega_L^2(k) - 3\langle \omega_k^2 \rangle] & + (1/\tau_k^4) \}^{1/2}.
\end{aligned} \tag{6.30}$$

This happens provided that

$$\omega_L^2(k) > \sqrt{2} [2\omega_L^2(k) - 3\langle \omega_k^2 \rangle - (1/\tau_k)^2]^{1/2}(1/\tau_k). \tag{6.31}$$

A simpler criterion for the existence of these inelastic peaks is obtained by rearranging the argument of the square root in eqn (6.30) so that

$$\{ \cdots \}^{1/2} = \{ [\omega_L^2(k) - (1/\tau_k)^2]^2 + (2/\tau_k^2)[3\langle \omega_k^2 \rangle - \omega_L^2(k)] \}^{1/2}. \tag{6.32}$$

The argument is certainly non-negative if

$$3\langle \omega_k^2 \rangle \geqslant \omega_L^2(k). \tag{6.33}$$

Equation (6.33) provides a sufficient (although not necessary) condition for the existence of inelastic peaks, irrespectively of the values of $(1/\tau_k)$. In any case, to proceed further in the analysis we must have some approximate scheme to evaluate the relaxation rate $(1/\tau_k)$. The simplest procedure is to adapt to the collective case the arguments set forward in Section 5.3.1 for the corresponding 'self' quantity $1/\tau_{s,k}$. The analogue of eqn (5.47) now reads $(1/\tau_k) \propto \sqrt{\Delta_k}$, where the proportionality constant can again be determined by requiring that the predicted value of $S(k, \omega = 0)$ coincides for $k \to \infty$ with the exact free-particle result. This implies that (Lovesey 1971)

$$1/\tau_k = 2(\Delta_k/\pi)^{1/2}. \tag{6.34}$$

Since for small wavevectors $\Delta_k \to (c_L^2 - v_T^2)k^2$, the approximation (6.34) is seen to be inconsistent with the hydrodynamic result (6.8) which implies a

finite value of $1/\tau_k$ for $k \to 0$. On the other hand, from the discussion at the beginning of this section it is clear that the viscoelastic model is only expected to be particularly reliable for wavevectors outside the strict hydrodynamic regime. Hence, the practical consequences of the above inconsistency are likely to be not so serious. This expectation is supported by the comparison of the values of τ_k from eqn (6.34) with those obtained by a best fit of the line shape (6.25) to the observed spectra (see Fig. 6.1). It is seen that within the experimental uncertainties the scheme (6.34) provides a fair quantitative account of the data both at intermediate and large values of k.

Some spectral shapes obtained from eqn (6.25) for liquid caesium near melting are reported in Fig. 6.2 for two physically different wavevector ranges. In the first case (part a), $k \approx k_m$ and the agreement of the theoretical spectra with the neutron data of Bodensteiner (1990) is seen to be quite good. In this situation the width of $S(k, \omega)$ is controlled by $\langle \omega_k^2 \rangle \propto [S(k)]^{-1}$ which attains very small values; as a result, the dominant feature is a marked de Gennes narrowing of the spectrum (cf. Section 1.6.2). The smallness of the relevant frequency range implies that in eqn (6.28) we may effectively neglect $z = i\omega$ with respect to the quantities $1/\tau_k$ and $\Delta_k \tau_k$. Thus, letting $\gamma(k) \equiv \langle \omega_k^2 \rangle / \Delta_k \tau_k$ we obtain

$$\tilde{F}(k, z) \approx S(k)[z + \gamma(k)]^{-1} \qquad (6.35)$$

which corresponds to a Lorentzian spectrum with halfwidth $\gamma(k)$, or equivalently to an intermediate scattering function

$$F(k, t) \approx S(k) \exp[-\gamma(k)t]. \qquad (6.36)$$

The Markovian result (6.36) has already been used in Section 5.1, and could even be obtained from eqn (6.26) by a perturbative expansion in the small parameters $\langle \omega_k^2 \rangle^{1/2} \tau_k$ and $\langle \omega_k^2 \rangle / \omega_L^2(k)$. Since, in this k range, even the approximation (6.34) yields rather good results (see Fig. 6.1), we may safely conclude that for $k \approx k_m$ the viscoelastic model works remarkably well.

The situation is not as satisfactory for smaller wavevectors (Fig. 6.2b). In the case of liquid alkali metals, $S(k, \omega)$ exhibits for $k < 0.7 k_m$ inelastic peaks which become more and more defined as k is decreased. The criterion (6.33) for the existence of these peaks yields a maximum wavevector of about 1.1 Å^{-1} in liquid caesium (see Fig. 6.3), in rather good agreement with the experimental findings of Bodensteiner *et al.* (1992) as well as with recent simulation data (Balucani *et al.* 1992, 1993*a*; Kambayashi and Kahl 1992). On the whole, even the wavevector dependence of $\omega_{peak}(k)$ is rather well accounted for, particularly in the case where the time τ_k is left as an adjustable parameter. However, in this k range the line shapes predicted by the viscoelastic model show clear deviations from both the experimental and the simulation spectra. In particular, in the case $k = 0.6$ Å^{-1}
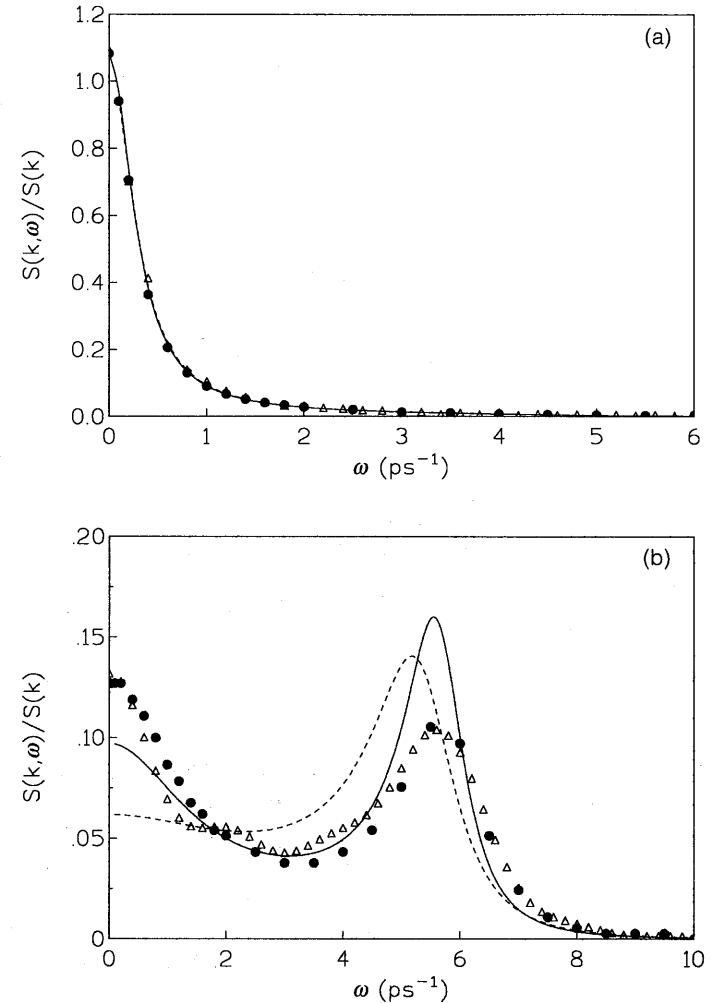
Fig. 6.2 Dynamic structure factor $S(k, \omega)$ in liquid Cs ($T = 308$ K) at the wavevectors (a) $k = 1.4$ Å^{-1} and (b) $k = 0.6$ Å^{-1}. The curves are the viscoelastic spectra evaluated from eqn (6.25), with the only difference being that the value of τ_k is either deduced by eqn (6.34) (dashed line) or treated as an adjustable parameter (full line). The dots are the neutron-scattering data of Bodensteiner *et al.* (1990) and the triangles the computer simulation findings of Balucani *et al.* (1993*a*).
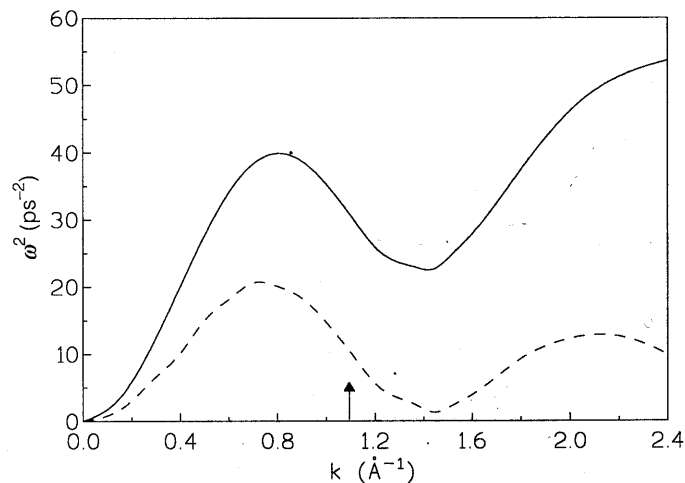
Fig. 6.3 The quantities $\langle \omega_k^2 \rangle$ (dashed line) and $\omega_L^2(k)$ (full line) in liquid Cs at 308 K. The results were obtained from the definitions (1.128) and (1.143), using the data from the computer simulation experiment by Balucani *et al.* (1993*a*) for $\phi(r)$, $g(r)$, and $S(k)$. The largest wavevector for which $3\langle \omega_k^2 \rangle \geqslant \omega_L^2(k)$ is indicated by an arrow.

illustrated in Fig. 6.2b the model appears to exaggerate the sharpness of the inelastic peaks and to underestimate the intensity of the low-frequency features. Since the specific heat ratio γ of liquid alkali metals ≈ 1 even for very small wavevectors, these failures of the viscoelastic model cannot be attributed to the neglect of the effects of thermal fluctuations. Consequently, we are again forced to conclude that the ansatz (6.23) does not take into proper account the existence of additional slow processes in the 'viscous' part of the memory function, which should increase the relative contribution of low frequencies to $S(k, \omega)$. In view of the good results provided by the viscoelastic model for $k \approx k_m$, these slow decay mechanisms are expected to yield a significant contribution only for relatively small wavevectors. These conclusions are in qualitative agreement with those discussed for Lennard–Jones liquids in the previous section, and demand a more rigorous consideration of long-lasting effects in $K_L(k, t)$. Before attempting to do this, we shall however explore the consequences of the viscoelastic approximation on other aspects of the collective dynamics which are not directly accessible to experimental investigation.

6.2.2 Transverse currents

In our attempts to build up a generalized hydrodynamic framework for the collective framework, the attention has so far been focused exclusively on density fluctuations. Although this emphasis is partly justified by the experimental relevance of the dynamic structure factor $S(k, \omega)$, the discussion of Section 3.4.2 has shown that even transverse currents may provide useful information about possible extensions of the framework to microscopic length and timescales. As we shall see later in this section, a preliminary generalization of the hydrodynamic result for $C_T(k, t)$ can be made in a much simpler way than the one followed for $F(k, t)$.

Beyond the strict hydrodynamic regime, the most important feature to be accounted for is the appearance of inelastic peaks in the transverse current spectrum (cf. Fig. 1.14). It is convenient to start our analysis from the exact Mori representation of the Laplace transform of $C_T(k, t)$:

$$\tilde{C}_T(k, z) = (k_B T/m) [z + \tilde{K}_T(k, z)]^{-1} \tag{6.37}$$

(cf. eqn (3.113)). As already noticed in Section 3.4.2, with the formal position

$$\tilde{K}_T(k, z) \equiv (k^2/nm)\tilde{\eta}(k, z) \tag{6.38}$$

eqn (6.37) is seen to have the typical aspect of a generalized-hydrodynamics result. In particular, the quantity $\tilde{\eta}(k, z = i\omega)$ can be interpreted as a *wavevector- and frequency-dependent shear viscosity coefficient*, which is such that

$$\lim_{z \to 0, k \to 0} \tilde{\eta}(k, z) = \eta. \tag{6.39}$$

Although interesting, this point of view does not, however, shed much light on the dynamical features expected for $C_T(k, t)$ outside the hydrodynamic range. Again, the first step which we can make in this direction is to assume that the temporal decay of the memory function $K_T(k, t)$, rather than being $\propto \delta(t)$ as in hydrodynamics, proceeds with a finite decay time $\tau_{T,k}$. As in the case of density fluctuations, the simplest approximation is to assume that the time dependence of K_T is exponential:

$$K_T(k, t) = K_T(k, 0) \exp(-t/\tau_{T,k}) \tag{6.40}$$

Exploiting eqn (3.43a), it is readily seen that the initial value of $K_T(k, t)$ can be written as (cf. eqn (1.151))

$$K_T(k, 0) = (k_B T/m)k^2 + \Omega_0^2 - (\Omega_k')^2$$

$$= \omega_T^2(k). \tag{6.41}$$

Then the Laplace-transformed version of eqn (6.40) reads

$$\tilde{K}_\mathrm{T}(k, z) = \omega_\mathrm{T}^2(k)\, [z + (1/\tau_{\mathrm{T},k})]^{-1}. \tag{6.42}$$

When expressed in terms of generalized shear viscosity, eqn (6.42) implies that

$$\tilde{\eta}(k, \mathrm{i}\omega) = G(k)\, [\mathrm{i}\omega + (1/\tau_{\mathrm{T},k})]^{-1} \tag{6.43}$$

where the quantity $G(k) \equiv (nm/k^2)\omega_\mathrm{T}^2(k)$ is referred to as the (*k*-dependent) *rigidity modulus*. Equation (6.43) is the archetype of all the viscoelastic approximations in liquid-state dynamics. The basic physical concepts behind these models were laid down in a somewhat different context by J. C. Maxwell in the nineteenth century, and can be summarized as follows. If the dynamics is observed over times sufficiently long with respect to those appropriate to the relaxation process, the system is able to 'adjust' itself to the probe; in the particular case under consideration, the ordinary hydrodynamic behaviour stems from the condition $\omega\tau_{\mathrm{T},k\to0} \ll 1$, which is equivalent to

$$\tilde{\eta}(k \to 0, z \to 0) = G(k \to 0)\tau_{\mathrm{T},k\to0} = \eta. \tag{6.44}$$

In other terms, the response of the liquid to a shear perturbation of long wavelength and small frequency has a purely viscous character:

$$C_\mathrm{T}(k, \omega) = (k_\mathrm{B}T/m\pi)\, \frac{(\eta/nm)k^2}{\omega^2 + [(\eta/nm)k^2]^2}. \tag{6.45}$$

As we shall see in Section 6.5, at finite wavevectors (but still in a long-time limit) this sort of behaviour can formally be described in terms of a '*k*-dependent viscosity coefficient', which according to the result (6.43) is simply given by $\eta(k) = G(k)\tau_{\mathrm{T},k}$. For our present purposes, it is however convenient to see the predictions of the model in the opposite physical situation where $\omega \gg 1/\tau_{\mathrm{T},k}$. In this case the liquid cannot follow the rapid variation of the external probe, and reacts with an instantaneous response which is dominated by the interatomic forces. In this short-time regime the memory function $K_\mathrm{T}(k, t)$ can be taken as approximately equal to its initial value (6.41), and $\tilde{K}_\mathrm{T}(k, z) \approx \omega_\mathrm{T}^2(k)/z$. The consequence of all this is that the spectrum $C_\mathrm{T}(k, \omega) = (1/\pi)\tilde{C}_\mathrm{T}(k, z = \mathrm{i}\omega + 0^+)$ now exhibits sharp peaks at the frequency $\omega_\mathrm{T}(k)$, much as if we were probing the transverse-phonon dispersion relation of an elastic solid. In the approximation described by eqns (6.40)–(6.43), one tries to 'interpolate' in the simplest way between the above-mentioned limiting cases; this mixed character is clearly the origin of the attribute 'viscoelastic' traditionally used for this sort of models in liquid-state dynamics.

The general consequences of the approximation (6.40) on the features of $C_\mathrm{T}(k, t)$ are readily seen. In fact, the mathematical structure of the memory equation

$$\dot{C}_\mathrm{T}(k, t) = -\omega_\mathrm{T}^2(k) \int_0^t \mathrm{d}t'\, \exp(-t'/\tau_{\mathrm{T},k})C_\mathrm{T}(k, t - t') \tag{6.46}$$

is formally identical to the one met in Section 3.3 for an approximate theory of the velocity autocorrelation function. In the present case we obtain

$$C_\mathrm{T}(k, t) = (k_\mathrm{B}T/m) \exp(-t/2\tau_{\mathrm{T},k})\{\cosh[A(k)t/2\tau_{\mathrm{T},k}]$$
$$+ [A(k)]^{-1} \sinh[A(k)t/2\tau_{\mathrm{T},k}]\} \tag{6.47}$$

where we have let

$$A^2(k) \equiv 1 - 4\omega_\mathrm{T}^2(k)\tau_{\mathrm{T},k}^2 = 1 - 4(k^2/nm)G(k)\tau_{\mathrm{T},k}^2. \tag{6.48}$$

The corresponding spectrum reads

$$C_\mathrm{T}(k, \omega) = (k_\mathrm{B}T/m\pi)\mathrm{Re}\left[\mathrm{i}\omega + \frac{\omega_\mathrm{T}^2(k)}{\mathrm{i}\omega + (1/\tau_{\mathrm{T},k})}\right]^{-1}$$
$$= (k_\mathrm{B}T/m\pi)\, \frac{(1/\tau_{\mathrm{T},k})\omega_\mathrm{T}^2(k)}{[\omega^2 - \omega_\mathrm{T}^2(k)]^2 + (\omega/\tau_{\mathrm{T},k})^2}. \tag{6.49}$$

Inelastic peaks are found at the frequencies

$$\omega_\mathrm{peak} = \pm[\omega_\mathrm{T}^2(k) - \tfrac{1}{2}(1/\tau_{\mathrm{T},k})^2]^{1/2} \tag{6.50}$$

provided that

$$2\omega_\mathrm{T}^2(k)\tau_{\mathrm{T},k}^2 > 1. \tag{6.51}$$

The fulfilment of the condition (6.51) at a given wavevector depends both on the quantity $\omega_\mathrm{T}^2(k) = (k^2/nm)G(k)$—which is readily evaluable from eqn (1.151) in terms of $\phi(r)$ and $g(r)$—and on the time $\tau_{\mathrm{T},k}$.

As in other similar cases discussed previously, the model (6.40) does not provide any definite criterion for the determination of $\tau_{\mathrm{T},k}$. Some preliminary insight is obtained by considering the small-*k* case where $\omega_\mathrm{T}^2(k \to 0) = c_\mathrm{T}^2k^2$, with the velocity c_T being given by (1.159). Then from eqn (6.44) we deduce that the time $\tau_{\mathrm{T},k}$ remains finite for $k \to 0$:

$$\tau_{\mathrm{T},k\to0} = \eta/G(k = 0) = \eta/nmc_\mathrm{T}^2. \tag{6.52}$$

In this limit the quantity $A(k)$ in eqn (6.47) is real and ≈ 1:

$$A(k \to 0) = 1 - 2(k^2/nm)G(k = 0)\tau_{\mathrm{T},k\to0}^2$$
$$= 1 - 2(k^2/nm)\eta\tau_{\mathrm{T},k\to0}. \tag{6.53}$$

As a result, $C_\mathrm{T}(k \to 0, t)$ decays monotonically to zero. Inserting (6.53) into eqn (6.47), it is easily verified that outside a microscopic time interval $C_\mathrm{T}(k, t)$ indeed approaches the correct hydrodynamic result (3.109). Consequently, eqn (6.49) is a valuable starting point for the construction of

phenomenological expressions for the k-dependence of $\tau_{T,k}$. As in the case of the time τ_k discussed in the previous section, the basic ingredients of these approximate recipes are (i) the choice of an appropriate quantity to be matched for $k \to \infty$ with the exact free particle result (in the present case with the result from eqn (1.156)), and (ii) the formulation of a simple interpolation scheme between the results obtained for $\tau_{T,k}$ in the opposite limits of small and large wavevectors. In this respect, the most successful recipe has been proposed several years ago by Akcasu and Daniels (1970), who demanded that for $k \to \infty$ the peak frequency (6.50) of $C_T(k, \omega)$ should vanish in order to satisfy eqn (1.156). This implies that

$$(1/\tau_{T,k \to \infty})^2 = 2\omega_T^2(k \to \infty). \tag{6.54}$$

On the basis of this result, at finite wavevectors Akcasu and Daniels suggested the following interpolation formula

$$(1/\tau_{T,k})^2 = 2\omega_T^2(k) + [1 + (k/k_0)^2]^{-1}$$

$$\times \{(1/\tau_{T,k \to 0})^2 - 2\omega_T^2(k) + 2(k_B T/m)k^2\} \tag{6.55}$$

where the parameter k_0 is typically chosen of the order of $0.7\,k_m$.

Since no inelastic peaks are present in $C_T(k, \omega)$, both for very small and very large wavevectors, a liquid is able to support the propagation of *transverse waves* only inside a finite k interval. In the framework of the viscoelastic model, the criterion (6.51) for the appearance of these peaks can be written as

$$k^2 > \frac{nm}{2G(k)} \left(\frac{1}{\tau_{T,k}}\right)^2 \tag{6.56}$$

where (cf. eqns (1.151)–(1.152))

$$G(k) \approx nk_B T + \frac{nm\Omega_0^2}{k^2}[1 - j_0(kr_0) - j_2(kr_0)]. \tag{6.57}$$

In practice, it is found that both $G(k)$ and $\tau_{T,k}$ decrease considerably as k increases. Although the details of this wavevector dependence vary with the specific liquid under consideration, the decrease of the rigidity modulus is always found to be more marked than that of $\tau_{T,k}$. Consequently, the *threshold wavevector* k_T above which shear-wave peaks appear is system dependent, and largely affected by the actual magnitude of the second term on the right-hand side of eqn (6.57). Broadly speaking, k_T is found to range from $\approx 0.45/r_0$ in liquid alkali metals near the melting point to $\approx 0.9/r_0$ in Lennard–Jones liquids (the position of the main peak of $S(k)$ being $k_m \approx 7/r_0$ in both cases).

When compared with the only 'experimental' data available (namely those obtained by computer simulation techniques), the predictions of the
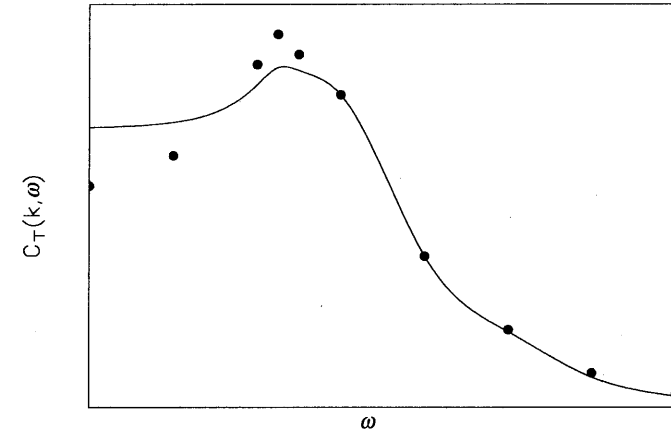
Fig. 6.4 Schematic comparison between the spectrum (6.49) predicted by the viscoelastic approximation (full line) and the one typically observed in the simulations of simple liquids near the melting point (dots). The results refer to a wavevector k of the order of $3k_T$.

viscoelastic model for $C_T(k, t)$ or $C_T(k, \omega)$ are found to be fairly good. In particular, the 'sudden' appearance of the inelastic peaks in $C_T(k, \omega)$ is accounted for, even if the model predicts values of k_T somewhat higher than the actual findings. Moreover, the position and the wavevector dependence of ω_{peak} appear to be reasonably well reproduced. However, even in this case a more detailed comparison between the theoretical results and the simulation data indicates clear discrepancies. Again, these defects of the viscoelastic model are not the consequence of the (somewhat arbitrary) recipe adopted for the estimate of the time $\tau_{T,k}$; as a matter of fact, the improvement achieved by letting $\tau_{T,k}$ to be an adjustable parameter at every wavevector appears to be rather modest. The first indication of this failure of the approximation (6.40) for $K_T(k, t)$ came again from the comprehensive simulation study of Levesque *et al.* (1973) in Lennard–Jones liquids. In particular, it was found that the inelastic peaks predicted by the viscoelastic model were less sharp than those observed in the simulations. This situation is typical for several other simple liquids, and is schematically illustrated in Fig. 6.4. The flatter appearance of the peaks predicted by the model is seen to be mostly due to the excess intensity of the theoretical spectrum in the low frequency region. Since, for small ω, $C_T(k, \omega)$ is roughly inversely proportional to the spectrum $K_T(k, \omega)$ of the memory function, the origin of the discrepancy can be traced back to the neglect of a low-frequency contribution in $K_T(k, \omega)$. In other words, we are again faced with a situation in which a single
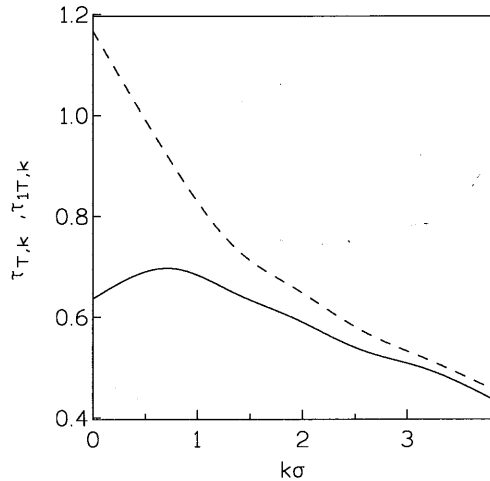
Fig. 6.5 Wavevector dependence of the times $\tau_{T,k}$ (eqn (6.40); dashed line) and $\tau_{1T,k}$ (eqn (6.58); full line) as obtained by a fitting procedure to the simulation data in Lennard–Jones liquids (Levesque *et al.* 1973). The times are reported in the Lennard–Jones unit $\tau_{LJ} = (m\sigma^2/48\varepsilon)^{1/2}(\tau_{LJ} \approx 0.311$ ps for a choice of parameters appropriate to liquid argon). In the same units, the 'long' time τ_{2T} appearing in eqn (6.58) is found to be 4.72. The position of the main peak of $S(k)$ is $k_m\sigma \approx 6.8$.

relaxation-time approximation fails because of the presence of additional decay mechanisms with a considerably slower time dependence. The first empirical remedy parallels the one already seen in the case of density fluctuations (cf. Section 6.1), and consists in allowing the presence of *two* suitably weighted relaxation mechanisms in $K_T(k,t)$:

$$K_T(k,t) = \omega_T^2(k)\left[(1 - a_{T,k})\exp(-t/\tau_{1T,k}) + a_{T,k}\exp(-t/\tau_{2T})\right]$$

$$(6.58)$$

where for simplicity the longer relaxation time τ_{2T} is assumed to be independent of the wavevector (Levesque *et al.* 1973). The presence of the second term in square brackets leads to a substantial improvement of the 'theoretical' results, particularly in the wavevector range where the inelastic peaks are more evident. In Lennard–Jones liquids the weight factor $a_{T,k}$ is found to decrease rapidly at increasing k, and in practice as $k \to k_m$ one recovers the results of the simple viscoelastic model (see Fig. 6.5). A similar trend is observed even in molten alkali metals (Balucani *et al.* 1987; Kambayashi and Kahl 1992). At wavevectors $k \geqslant k_m$ any residual deviation between the predictions of the viscoelastic model and the simulation results is due to 'trivial' effects, such as the inability of a purely exponential

---

model to reproduce the correct short-time decay of the true memory function.

Although eqn (6.68) is useful both for its heuristic value and for the analysis of simulation data, a genuine theoretical approach for transverse collective dynamics must rely on less phenomenological assumptions. Even in this case, the general framework discussed in Chapter 4 provides a rationale for the existence of two distinct mechanisms affecting the decay of the memory function. In particular, in Section 4.5 it has been argued that $K_T(k,t)$ can be split as follows (cf. eqn (4.174)):

$$K_T(k,t) = [K_T(k,t)]_{\text{fast}} + M'_{22}(\mathbf{k},t)$$

$$(6.59)$$

where the first term on the right-hand side accounts for both the initial value $K_T(k,t=0) = \omega_T^2(k)$ and the rapid decay of $K_T(k,t)$ at short times. On the other hand, the second contribution to eqn (6.59), initially almost negligible, should account for all the long-lasting features present in $K_T(k,t)$. Recalling the expression (4.120) for $M'_{\lambda\lambda'}(\mathbf{k},t)$ and exploiting the result (G.18) for the static vertex, it is easily found that

$$M'_{22}(\mathbf{k},t) = \frac{1}{16\pi^3 n}\int d\mathbf{q}\,|v_{00,2}(\mathbf{k};k-q,q)|^2 \Delta_{00,00}(\mathbf{k}-\mathbf{q},\mathbf{q};t)$$

$$= \frac{nk_BT}{16\pi^3 m}\int d\mathbf{q}\,q_x^2\,[c(|\mathbf{k}-\mathbf{q}|) - c(q)]^2\,[F(|\mathbf{k}-\mathbf{q}|,t)F(q,t)$$

$$- F_B(|\mathbf{k}-\mathbf{q}|,t)F_B(q,t)]$$

$$(6.60)$$

where the external wave vector $\mathbf{k}$ has been chosen along the z-axis. A comprehensive study of eqns (6.59)–(6.60) for arbitrary k has not yet been attempted. The particular case $k \to 0$ has, however, been analysed in some detail because of its relevance for the study of the shear stress autocorrelation function and of the associated transport property, the shear viscosity coefficient (see Section 6.4).

6.2.3 Longitudinal modes

In the previous subsection we have seen that a liquid is able to propagate transverse waves only if the wavevector exceeds a certain critical value. This situation is to be contrasted with the one occurring for longitudinal modes, which are easily supported even in the hydrodymamic region. This difference stems from the fact that density fluctuations and longitudinal current modes are intimately connected by the relation (1.114):

$$\dot{n}(\mathbf{k},t) = ikj_L(\mathbf{k},t)$$

$$(6.61)$$

and that for $k \to 0$ both these variables become quasi-conserved (see Section 1.6.1). In this limit, the presence of the Rayleigh-Brillouin triplet structure

in $S(k, \omega)$ has an immediate correspondence in the longitudinal current spectrum $C_L(k, \omega) = (\omega^2/k^2) S(k, \omega)$, which is characterized by well defined inelastic peaks at the frequencies $\omega = \pm v_s k$.

As a result of the mathematical form of $C_L(k, \omega)$, in the longitudinal spectrum these finite-frequency peaks are in fact present at any wavevector, namely even in situations where the damping processes make hardly discernible (or invisible) any structure in the spectrum $S(k, \omega)$. Even if no new physics is really involved, a separate analysis of $C_L(k, \omega)$ consequently appears to be particularly profitable to explore the evolution of longitudinal modes in a wide wavevector range. Again, it is convenient to start from the formally exact memory function result

$$C_L(k, \omega) = \frac{1}{\pi} \frac{(k_B T/m)\omega^2 K_L'(k, \omega)}{[\omega^2 - \langle \omega_T^2 \rangle - \omega K_L'(k, \omega)]^2 + [\omega K_L''(k, \omega)]^2}$$

(6.62)

which is easily deduced from eqns (1.148) and (6.21). For the memory function $\tilde{K}_L(k, z = i\omega)$ we may select one of the various models discussed in Section 6.1; to begin with, let us consider the simplest one, namely the *viscoelastic model*. The quantities $K_L'(k, \omega)$ and $K_L''(k, \omega)$ are then given by eqns (6.24a,b), and after some simple algebra we obtain

$$C_L(k, \omega) = \frac{k_B T}{m\pi} \frac{\omega^2 \Delta_k (1/\tau_k)}{\omega^2 [\omega^2 - \langle \omega_k^2 \rangle - \Delta_k]^2 + (1/\tau_k)^2 [\omega^2 - \langle \omega_k^2 \rangle]^2}.$$

(6.63)

The result (6.63) could of course have been written down immediately by exploiting eqns (1.148) and (6.25). A study of eqn (6.63) shows that, apart from the trivial minimum at $\omega = 0$, the extrema of $C_L(k, \omega)$ are determined by the roots of a cubic equation in ω^2:

$$2(\omega^2)^2 [\omega^2 - \omega_L^2(k)] + (1/\tau_k)^2 [(\omega^2)^2 - \langle \omega_k^2 \rangle^2] = 0 \quad (6.64)$$

where we recall that $\omega_L^2(k) = \langle \omega_k^2 \rangle + \Delta_k$. It is particularly interesting to consider the following limiting cases.

(i) For sufficiently small wavevectors, the quantities $\langle \omega_k^2 \rangle$ and $\omega_L^2(k)$ vanish as k^2, while the time τ_k remains finite at the value (6.8). Consequently, to the lowest order in k^2, the dominant contribution to eqn (6.64) is provided by the second term on the left-hand side which gives a peak frequency for $C_L(k, \omega)$ at $\pm \langle \omega_k^2 \rangle^{1/2}$. This is the correct hydrodynamic result in the 'isothermal' conditions which we are implicitly dealing with. In this range, a slightly better approximation for the peak frequency of $C_L(k, \omega)$ is

$$\omega_{peak}^2 \approx \langle \omega_k^2 \rangle [1 + \Delta_k \tau_k^2].$$

(6.65)

Since Δ_k is always found to be non-negative, eqn (6.65) shows that for small k the dispersion relation of the longitudinal modes 'bends up' with respect to the limiting behaviour for $k \to 0$. In other words, the phase velocity of the longitudinal sound waves increases with k (*positive dispersion*).

(ii) For larger wavevectors (but still smaller than the position k_m of the main peak of $S(k)$) the value of ω_{peak} increases substantially, until it becomes larger than the relaxation rate $1/\tau_k$. Owing to the increase of $S(k)$ in this k range, $\langle \omega_k^2 \rangle$ is often found to be considerably smaller than $\omega_L^2(k)$. In such a case, eqn (6.64) has the approximate solution

$$\omega_{peak}^2 \approx \omega_L^2(k) - \tfrac{1}{2}(1/\tau_k)^2.$$

(6.66)

Slightly better analytic approximations can be worked out, but in any case the result shows a tendency of the effective velocity ω_{peak}/k to approach the limiting value $c_L(k) \equiv \omega_L(k)/k$. The extent to which this velocity crossover is completed depends on the actual rate of the relaxation mechanisms; in the model we are dealing with, these processes control the transition from a low-frequency 'viscous' behaviour to a high-frequency 'elastic' response. Conventionally, the increase of the effective longitudinal velocity from $v_T(k) = \langle \omega_k^2 \rangle^{1/2}/k$ to $c_L(k)$ is referred to as being due to 'viscosity relaxation'.

(iii) At even larger wavevectors, the longitudinal response of the system is initially dominated by structural features. In particular, as k approaches k_m the pronounced de Gennes narrowing of $S(k, \omega)$ leads to a considerable decrease of the peak frequency of $C_L(k, \omega)$, down to a minimum for $k \approx k_m$. At wavevectors $k > k_m$ free-particle aspects begin gradually to prevail and eventually for $k \gg k_m$, $C_L(k, \omega)$ should approach the limiting form (1.155) — although this cannot exactly be reproduced by the simple model (6.63).

All these features of the dispersion relation $\omega_{peak}(k)$ are illustrated in Fig. 6.6a, which refers to liquid caesium near the melting point. These results were obtained by a numerical solution of eqn (6.64), with the quantities $\langle \omega_k^2 \rangle$ and $\omega_L^2(k)$ evaluated as in Fig. 6.3 and the rate $1/\tau_k$ deduced by a best fit of eqn (6.25) to the spectra $S(k, \omega)$ obtained by computer simulation (Balucani *et al.* 1993a,b). Since in all molten alkali metals the effect of thermal fluctuations is quite small even at small wavevectors ($\gamma \approx 1.1$), the restriction to a sort of 'isothermal hydrodynamics' inherent to the model (6.23) is expected to be not too serious. Indeed, Fig. 6.6b shows that the values predicted for the k-dependent longitudinal velocity are in rather good agreement with the experimental data reported by Bodensteiner *et al.* (1992). It appears that the maximum increase of the velocity with respect to the hydrodynamic value occurs at relatively small wavevectors, and is of the order of 20%.
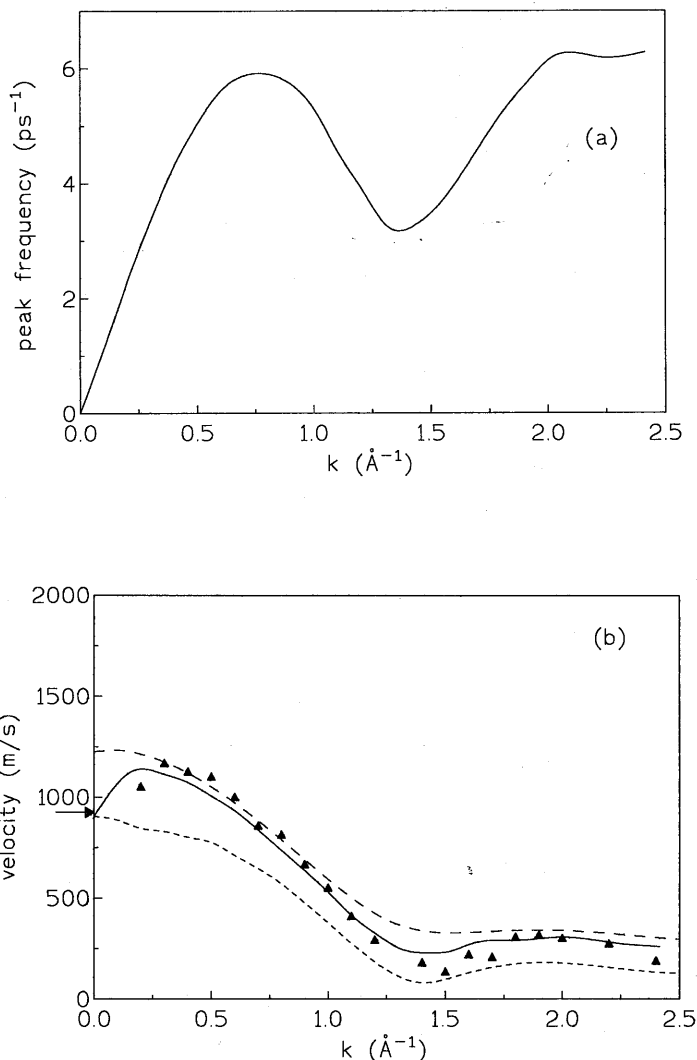
Fig. 6.6   (a) Wavevector dependence of the peak frequency ω_{peak} of $C_L(k, \omega)$ in liquid Cs at 308 K (obtained from eqn (6.64)). (b) Effective velocity ω_{peak}/k of the longitudinal waves in the same system: theoretical results (full line) and experimental data (triangles; Bodensteiner *et al.* 1992). The dashed and the long-dashed curves denote the velocities $v_T(k)$ and $c_L(k)$, respectively (see text). The experimental value of the hydrodynamic sound velocity ($\approx 960\ \mathrm{m\ s^{-1}}$) is indicated by an arrow.

The actual magnitude of this positive dispersion is strongly system dependent. An estimate of the maximum size of the effect can, however, be made as follows. In any system, the peak frequency of $C_L(k, \omega)$ tends to approach $\omega_L(k) = c_L(k)k$, and this crossover usually begins at small k. Then, a convenient 'measure' of the maximum positive dispersion to be expected is provided by the ratio

$$\left(\frac{c_L}{v_T}\right)^2 = \frac{\omega_L^2(k \to 0)}{\langle \omega_{k \to 0}^2 \rangle} \approx \frac{3[(k_B T/m) + (\Omega_0^2 r_0^2/10)]}{k_B T/mS(0)} \tag{6.67}$$

where we have exploited the approximation (1.143) for $\omega_L^2(k)$ and performed a small-k expansion. In the liquid range the numerator of (6.67) turns out to be dominated by the second term in the square brackets; consequently, letting $\Gamma \equiv m\Omega_0^2 r_0^2/k_B T$ we may approximately write

$$\left(\frac{c_L}{v_T}\right)^2 \approx \frac{3}{10} S(0)\Gamma. \tag{6.68}$$

Thus, high values of the product $S(0)\Gamma$ are expected to give rise to a potentially large positive dispersion (the actual magnitude of the latter being ultimately controlled by the relaxation rate $1/\tau_k$). Other things being equal, this situation is likely to occur in all simple liquids characterized by harsh repulsive potentials (and consequently by high Einstein frequencies; cf. Section 1.4.2). For example, owing to their relatively 'soft' potential all molten alkali metals are expected to have values of the ratio c_L/v_T considerably smaller than those found, say, in the typical Lennard–Jones liquids. Indeed, near the melting point this ratio is found to be 'only' 1.28 in liquid caesium, to be compared with the value $c_L/v_T \approx 2.16$ in liquid argon (note, however, that in the latter system, owing to a specific heat ratio $\gamma \approx 2.2$, the hydrodynamic sound velocity is far from being isothermal).

It is interesting to observe that the occurrence of high values of c_L/v_T is somewhat contradictory with the possibility of observing well-defined inelastic peaks in $S(k, \omega)$ for wavevectors beyond the strict hydrodynamic regime. To show this in the simplest way, consider the sufficient criterion (6.33). Adopting the same approximations used in eqn (6.67), for small wavevectors the condition (6.33) implies that

$$\frac{1}{10} S(0)\Gamma \leqslant 1. \tag{6.69}$$

Comparing eqns (6.69) and (6.67), it is readily seen that a liquid which easily supports oscillatory density modes at finite wavevectors is unlikely to exhibit a large positive dispersion of the longitudinal sound waves. Liquid alkali metals are the typical paradigm of such a behaviour. A striking example of the opposite situation is provided by liquid water, where at finite

k Teixeira *et al.* (1985) have observed values of the longitudinal velocity $\approx 3300 \, \text{m s}^{-1}$, more than twice as high as the ordinary sound speed v_s $\approx 1450 \, \text{m s}^{-1}$. In this system, no inelastic peak in the dynamic structure factors is in fact discernible even at the smallest wavevectors explored outside the hydrodynamic range. Despite the rather complex nature of this hydrogen-bonded liquid, all these findings can be interpreted successfully by a simple application of the previous concepts (Balucani *et al.* 1993b).

The majority of the preceding discussion has considered cases in which thermal fluctuations have a negligible role. In principle, it is straightforward to extend the analysis to encompass situations in which γ is substantially different from unity, at the price of some additional complications in the algebra. For the longitudinal current spectrum we may again start from eqn (6.62), and adopt a generalized hydrodynamics framework in which

$$K_L(k, t) = [\omega_L^2(k) - \gamma_k \langle \omega_k^2 \rangle] \exp(-t/\tau_k) + (\gamma_k - 1) \langle \omega_k^2 \rangle \exp(-a_k k^2 t)$$

$$\equiv \Delta_{1k} \exp(-\Gamma_{1k} t) + \Delta_{2k} \exp(-\Gamma_{2k} t). \qquad (6.70)$$

The model (6.70) is the time-domain counterpart of eqn (6.15), and permits a straightforward evaluation of the quantities $K_L'(k, \omega)$ and $K_L''(k, \omega)$ to be inserted into (6.62). After some algebraic manipulations we obtain

$$C_L(k, \omega) = \frac{k_B T}{m\pi} \frac{f_1 \omega^2 + f_2 (\omega^2)^2}{h_0 + h_1 \omega^2 + h_2 (\omega^2)^2 + h_3 (\omega^2)^3 + h_4 (\omega^2)^4} \qquad (6.71)$$

where

$$f_1 = \Gamma_{1k} \Gamma_{2k} (\Delta_{1k} \Gamma_{2k} + \Delta_{2k} \Gamma_{1k})$$

$$f_2 = \Delta_{1k} \Gamma_{1k} + \Delta_{2k} \Gamma_{2k}$$

$$h_0 = \langle \omega_k^2 \rangle^2 \Gamma_{1k}^2 \Gamma_{2k}^2$$

$$h_1 = (\Delta_{1k} \Gamma_{2k} + \Delta_{2k} \Gamma_{1k})^2 + 2 \langle \omega_k^2 \rangle (\Delta_{1k} \Gamma_{2k}^2 + \Delta_{2k} \Gamma_{1k}^2)$$

$$\qquad + \langle \omega_k^2 \rangle^2 (\Gamma_{1k}^2 + \Gamma_{2k}^2) - 2 \langle \omega_k^2 \rangle \Gamma_{1k}^2 \Gamma_{2k}^2$$

$$h_2 = \omega_L^2(k) - 2 (\Delta_{1k} \Gamma_{2k}^2 + \Delta_{2k} \Gamma_{1k}^2) - 2 \langle \omega_k^2 \rangle (\Gamma_{1k}^2 + \Gamma_{2k}^2) + \Gamma_{1k}^2 \Gamma_{2k}^2$$

$$h_3 = -2\omega_L^2(k) + (\Gamma_{1k}^2 + \Gamma_{2k}^2)$$

$$h_4 = 1$$

$$(6.72)$$

A trivial minimum of eqn (6.71) is always found at $\omega = 0$, where $C_L(k, \omega)$ vanishes. The other extrema are the roots of a fifth-order equation in ω^2:

$$2 f_2 h_4 (\omega^2)^5 + (3 f_1 h_4 + f_2 h_3)(\omega^2)^4 + 2 f_1 h_3 (\omega^2)^3$$

$$\qquad + (f_1 h_2 - f_2 h_1)(\omega^2)^2 - 2 f_2 h_0 \omega^2 - f_1 h_0 = 0. \qquad (6.73)$$

Equation (6.73) can approximately be solved by noting that, in the *k* range where the effects of positive dispersion are more evident, the main peak of $C_L(k, \omega)$ is expected to be only marginally affected by the thermal damping Γ_{2k}. This is indeed true for small wavevectors where $\omega_{\text{peak}} \approx k$ and $\Gamma_{2k} \approx k^2$, and approximately correct even at larger *k* because of the decreasing role of the thermal fluctuation term (cf. Section 6.1). The neglect of Γ_{2k} reduces eqn (6.73) to the cubic equation $2 h_4 (\omega^2)^3 + h_3 (\omega^2)^2 - h_1 = 0$, which can be rearranged to give

$$2(\omega^2)^2 [\omega^2 - \omega_L^2(k)] + \Gamma_{1k}^2 [(\omega^2)^2 - \gamma_k^2 \langle \omega_k^2 \rangle^2] = 0 \qquad (6.74)$$

where $\Gamma_{1k} = (1/\tau_k)$. Comparing with eqn (6.64), it is seen that the only difference is the replacement of $\langle \omega_k^2 \rangle$ with $\gamma_k \langle \omega_k^2 \rangle$. We may therefore repeat all the considerations seen in the isothermal case, with the advantage of reproducing the correct 'adiabatic' sound velocity as $k \to 0$. In this amended version, the theory accounts remarkably well for most of the dispersion curve of the longitudinal mode in liquid argon (Boon and Yip 1980).

To close this section, it is worthwhile mentioning that the onset of viscoelastic behaviour is not the only mechanism capable of yielding a positive sound dispersion. A mode-coupling analysis similar to that employed in Section 4.5 for the $t^{-3/2}$ tails in $\psi(t)$ yields for the sound mode a *non-analytic dispersion relation* of the form $v_s k + a k^{5/2}$ at low k (Ernst and Dorfman 1972, 1975). As a is very small in liquids near the melting temperature, the non analyticity is most likely to be detected at lower densities or higher temperatures. Nevertheless, there are indications that the effect has been observed in liquid argon at 120 K (de Schepper *et al.* 1984).

6.3 MODE-COUPLING THEORY AT WORK

In Section 6.2 the viscoelastic model was shown to provide a rather satisfactory account of the main features of microscopic collective motion in simple liquids, both in its longitudinal and transverse versions. To be sure, occasionally the model had to be modified (as in systems where thermal fluctuations play a non-negligible role); yet, these 'extensions' were in most cases relatively straightforward, and did not require a substantial modification of the overall picture. It is worthwhile recalling that in the context of a memory function framework similar single-relaxation-time approximations were previously discussed for self-motion, with much less satisfactory results (cf. Sections 3.3 and 5.3.1). At first sight this difference may appear surprising, because ultimately single-particle and collective properties reflect just two aspects of the same many-body dynamics. At a given thermodynamic state of the system, the two sets of properties are in fact

affected by similar structural quantities (such as $g(r)$, $S(k)$, Ω_0^2, etc.) which are assumed to be known. However, whereas structural effects have an immediate impact on collective dynamics, their influence on self-motion is felt only at subsequent times (cf. eqns (1.128) and (1.38)). Consider, for example, the sharp peak occurring in the static structure factor at $k = k_m$: while this feature is directly responsible of the marked de Gennes narrowing of $S(k, \omega)$ as $k \rightarrow k_m$, its effect on the width of $S_s(k, \omega)$, although non-negligible, is certainly both less striking and more subtle (see Section 5.3). Moreover, features such as the peak frequencies of $S(k, \omega)$ or of $C_L(k, \omega)$ are immediately apparent from the spectra, and it is natural to argue that their evolution with k can be accounted for by a simple memory function ansatz in an easier way than that of a more elusive quantity as the width $\Gamma_s(k)$ of a featureless spectrum.

Even so, we have already seen that several aspects of collective dynamics can fully be understood only by abandoning single-relaxation-time approximations in favour of alternative approaches which take into explicit account the existence of additional decay channels for the memory functions. Typically, these processes are associated with timescales considerably longer than those pertinent to the various viscoelastic approximations; also, their influence appears to be particularly relevant only at rather small wavevectors. In the previous sections we have noticed on several occasions that most of the defects of the single-relaxation-time models can in fact be removed by assuming a *two-exponential* form for the decay of the memory function of interest. In this respect, an empirical evidence for the role played by slow processes at small wavevectors is provided by Fig. 6.5, which is based on best-fit estimates of the time constants occurring in eqns (6.40) and (6-58). It is clearly seen that at small k the optimized viscoelastic model (6.40) 'does its best' to account for the presence of a long-lasting tail in $K_T(k, t)$ by artificially increasing the value of $\tau_{T,k}$ with respect to the 'short' decay time $\tau_{1T,k}$ occurring in the two-exponential ansatz (6.58).

In order to achieve a comprehensive physical picture of collective dynamics, these evidences for the presence of two distinct contributions to the memory functions must be given a less phenomenological interpretation. Again, the general framework developed in Chapter 4 appears to be particularly suited to this purpose. To be more specific, the splitting of the memory functions into rapidly decaying 'binary' contributions (associated with fast collisional events) and slow 'tails' (accounted for by a 'mode-coupling' framework) is just what is needed to give a sounder basis to the previous findings. Again, the sluggishness of the structural relaxation processes typical of the liquid range suggests that the slow decay of the collective memory functions at long times is basically due to couplings to k-dependent density modes. Aside from a possibly different quantitative

relevance of the two contributions, this situation closely parallels the one seen in Chapter 5 for the self case.

It is now time to discuss several cases of physical interest (and of increasing complexity) in which the role of slowly varying features is particularly important. To begin with, we shall consider the density and longitudinal current correlations.

6.3.1 The tail of the longitudinal memory function

As in Section 6.2, it is convenient to start our analysis by reporting the Mori representations of the Laplace transforms of $F(k, t)$ and $C_L(k, t)$:

$$\tilde{F}(k, z) = S(k) \left[z + \frac{\langle \omega_k^2 \rangle}{z + \tilde{K}_L(k, z)} \right]^{-1}, \qquad (6.75)$$

$$\tilde{C}_L(k, z) = (k_B T/m) [z + (\langle \omega_k^2 \rangle/z) + \tilde{K}_L(k, z)]^{-1}. \qquad (6.76)$$

The result (6.76) is a direct consequence of eqn (6.75) and of

$$\beta m \tilde{C}_L(k, z) = -\frac{z}{\langle \omega_k^2 \rangle} \left[z \frac{\tilde{F}(k, z)}{S(k)} - 1 \right] \qquad (6.77)$$

which is a Laplace-transformed version of the 'continuity equation' (1.147).

The central quantity in both the representations (6.75) and (6.76) is the memory function $K_L(k, t)$. To specify its time dependence (and, in particular, the possible presence of slow features), up to now we have made use of simple empirical recipes; henceforth, we wish instead to perform a more rigorous analysis following the framework developed in Chapter 4. For the present purposes it is convenient to adopt a simplified version of the generalized hydrodynamic description of Section 4.4, and to write

$$K_L(k, t) = [K_L(k, t)]_{\text{fast}} + M'_{11}(k, t) \qquad (6.78)$$

(cf. eqn (4.173)). The first term on the right-hand side includes a strictly 'binary' part $M_{B,11}(\mathbf{k}, t)$ as well as an additional quantity $m_{11}(\mathbf{k}, t)$ which involves couplings to non-hydrodynamic modes; taken together, these contributions are responsible of the rapid short-time decay of the memory function from the initial value $K_L(k, t = 0) = \Delta_k = \omega_L^2(k) - \langle \omega_k^2 \rangle$. On the other hand, the second term on the right-hand side of (6.78) is expected to be nearly negligible initially; however, owing to its slower decay, it plays a dominant role at intermediate and long times, where $[K_L(k, t)]_{\text{fast}} \approx 0$. Note that in adopting the description of Section 4.4 we have implicitly chosen a number $H = 4$ of relevant modes: for the present purposes thermal fluctuations are in fact not particularly important, and in a first approximation can be included in the non-hydrodynamic modes.

The manifold events accounted for by $[K_L(k,t)]_{fast}$ makes difficult an accurate description of the rapid decay of this contribution. Following the same procedure adopted in Chapter 5 for the self case, we must content ourselves with a less detailed analysis which relies on the *initial* decay of the full memory function:

$$K_L(k,t) = \Delta_k\{1 - [t/\tau(k)]^2 + \cdots\} \qquad (6.79)$$

where the initial decay time $\tau(k)$ can be approximately evaluated in terms of the sixth frequency moment of $S(k,\omega)$ (see Appendix I). Broadly speaking, the values of $\tau(k)$ are expected to be of the same order as those obtained in a two-exponential model for the 'short' time τ_k. A numerical calculation performed in liquid rubidium (Sjögren 1980) appears indeed to support this expectation. Since for sufficiently short times $K_L(k,t)$ and $[K_L(k,t)]_{fast}$ nearly coincide, for the latter we may adopt a 'scaled' expression similar to the one seen in the self case:

$$[K_L(k,t)]_{fast} \approx \Delta_k f(t/\tau(k)) \qquad (6.80)$$

where the shape function $f(x)$ should be such to ensure a sufficiently fast decay.

From the above it is clear that at sufficiently short times a certain degree of uncertainty is still difficult to avoid. We are instead in a better position for the long-lasting features of $K_L(k,t)$, accounted for by the second term in eqn (6.78). According to the results obtained in Section 4.3.2 we have:

$$M'_{11}(\mathbf{k},t) = \frac{nk_BT}{16\pi^3 m}\int d\mathbf{q}\,[q_z c(q) + (\mathbf{k}-\mathbf{q})_z c(|\mathbf{k}-\mathbf{q}|)]^2$$

$$[F(q,t)F(|\mathbf{k}-\mathbf{q}|,t) - F_B(q,t)F_B(|\mathbf{k}-\mathbf{q}|,t)] \qquad (6.81)$$

where we recall that the direct correlation function $c(q)$ is defined by the relation $nc(q) = 1 - [1/S(q)]$. In the result (6.81), the term involving the 'binary' intermediate scattering functions F_B has the effect of making $M'_{11}(\mathbf{k},t)$ very small at short times (in particular, $M'_{11}(\mathbf{k},t=0) = 0$). This reflects the intuitive concept that any coupling to the collective modes of the medium—here, the density modes—requires a finite time to build up (in the jargon of kinetic theory, we equivalently speak of 'correlated-collisions' effects). In the explicit calculations, this feature can for example be accounted for by approximating $F_B(q,t)$ as in (4.147). In any case, whichever the precise form adopted for the 'binary' correlation F_B, its intrinsically rapid decay has the effect of making the last product term in eqn (6.81) virtually negligible beyond a microscopically short time interval. In other words, the genuine long-lasting features of the memory function $K_L(k,t)$ only stem from a typical 'mode-coupling' contribution:

$$\frac{nk_BT}{16\pi^3 m}\int d\mathbf{q}\,[q_z c(q) + (\mathbf{k}-\mathbf{q})_z c(|\mathbf{k}-\mathbf{q}|)]^2 F(q,t)F(|\mathbf{k}-\mathbf{q}|,t)$$

$$\equiv [K_L(k,t)]_{MC}. \qquad (6.82)$$

The notation used on the right-hand side of eqn (6.82) is in fact justified by noting that the same result can be obtained by a direct mode-coupling approach (see Section 4.5), in which the product $\hat{n}(\mathbf{q})\cdot\hat{n}(\mathbf{k}-\mathbf{q})$ plays the role of the relevant pair variable.

For the numerical evaluation of eqns (6.81)–(6.82), it is convenient to expand the squared vertex $[\cdots]^2$ and to choose the external wavevector $\mathbf{k}$ along the z-axis. Of the two angular integrations over the direction of $\mathbf{q}$, one can now be directly performed, with the result that, for example, eqn (6.82) can be written as

$$[K_L(k,t)]_{MC} = \frac{k_BT}{32\pi^2 mk^3}\int_0^\infty dq\,q\int_{|k-q|}^{k+q} dp\,p\{(k^2+q^2-p^2)^2 c(q)$$

$$\times [S(q)-1]S(p) + (k^2-q^2+p^2)^2 c(p)[S(p)-1]S(q)$$

$$+ [k^4 + (q^2-p^2)^2][S(q)-1][S(p)-1]\}$$

$$\times \frac{F(q,t)}{S(q)}\frac{F(p,t)}{S(p)}. \qquad (6.83)$$

We may now insert in (6.83) some simple phenomenological model for $F(q,t)$, and finally arrive at a quantitative assessment for the tail of $K_L(k,t)$ at the various wavevectors. Proceeding along similar lines in eqn (6.81), we may go even further and determine the quantity $M'_{11}(\mathbf{k},t)$ to be inserted into the expression (6.78) of the full memory function $K_L(k,t)$. After a numerical Laplace transform, one may finally exploit eqn (6.75) to obtain $S(k,\omega) = (1/\pi)\,\mathrm{Re}\,\tilde{F}(k,z=i\omega)$. A typical result of this procedure is illustrated in Fig. 6.7, which refers to liquid rubidium at a wavevector where $S(k,\omega)$ shows a well-defined inelastic peak (Sjögren 1980). The improvement with respect to the results obtained by letting $M'_{11}(\mathbf{k},t) \equiv 0$ is particularly evident at small frequencies, where the full theory yields a larger intensity in agreement with the simulation data. This tendency (which is even more marked at lower wavevectors) is clearly a consequence of the inclusion of slow contributions in the memory function. On the other hand, the position of the inelastic peak is seen to be rather well reproduced, even by taking into account only the fast portion of the memory function. At larger wavevectors, the contribution of $M'_{11}(\mathbf{k},t)$ rapidly decreases, indicating that the dynamics is more and more determined by short-duration events. Eventually, for $k \geqslant k_m$ the spectra obtained by using $K_L(k,t)$ or $[K_L(k,t)]_{fast}$ nearly coincide. All these
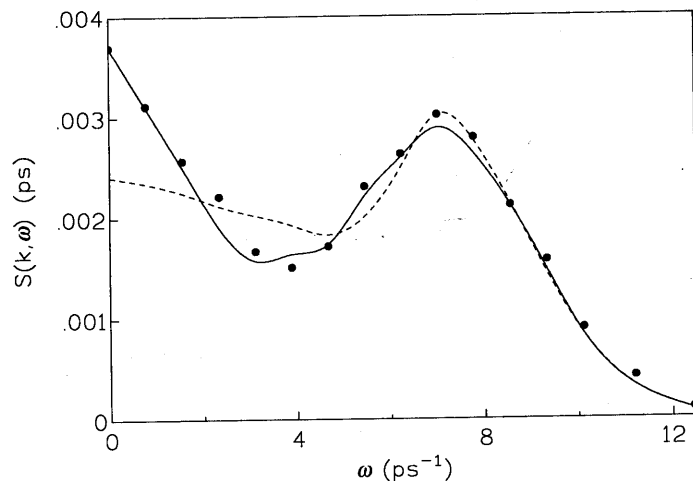
Fig. 6.7 Dynamic structure factor in liquid Rb at 318 K at a wavevector $k = 0.797$ Å^{-1}: dashed line, spectrum deduced by letting $K_L(k, t) = [K_L(k, t)]_{fast}$; full line, spectrum obtained by including $M'_{11}(k, t)$ (eqn (6.81)); the dots are the computer simulation data of Rahman (1974). In this system, the wavevector $k_m \approx 1.54$ Å^{-1}. Redrawn from Sjögren (1980).

features are consistent with the results found in Section 6.2.1 by the 'empirical' two-exponential model. As expected in the liquid range, no substantial changes are instead found in the theoretical spectral shapes by including additional decay channels involving the currents (Sjögren 1980).

6.3.2 Toward a fully self-consistent framework

A noteworthy feature of the expressions seen in the previous subsection is the possibility of building up a self-consistent approach for the dynamical property under consideration (here $F(k, t)$ or $S(k, \omega)$). This is typical of all mode-coupling theories, and often it is just the combination of this self-consistent aspect with the nonlinearity of the equations which leads to an unusual dynamical behaviour. In this respect, the best example is still provided by the very first application of the mode-coupling framework, namely the study of critical dynamics (Kawasaki 1970). Although in this field the occurrence of slowly varying phenomena is qualitatively predicted even by the traditional Markovian theories, it is only by turning to a mode-coupling description that one is able to account for several unexpected features, such as line shapes which are markedly non-Lorentzian, or critical exponents which deviate considerably from the conventional predictions. As we shall see in some detail in the next subsection, in recent years

an equally important application of mode-coupling concepts has emerged. The problem is even more intriguing than critical dynamics, and concerns the dynamical transition from a stable liquid toward a metastable glassy phase.

Coming back to the ordinary liquid range, the self-consistent nature of the mode-coupling results was recognized from the very start (Götze and Lücke 1975). Exploiting this aspect, one may in fact be able to establish a comprehensive approach for the main dynamical quantities of interest, with the only knowledge of a limited number of structural data. In this respect, the first bases were set by a number of papers in which the self-consistency was explicitly taken into account (Munakata and Igarashi 1977, 1978; Bosse *et al.* 1978*a,b*). In all these works, the main emphasis was placed on the various mode-coupling decay channels. The results were encouraging, even if at the price of several approximations. In his detailed analysis of density fluctuations, Sjögren (1980) treated both short-time ('kinetic') and long-time ('mode-coupling') features on an equal footing, and established a connection between single-particle and collective aspects of the dynamics. However, a fully self-consistent calculation of the mode-coupling integrals was not attempted. The current status of the theoretical studies in the collective dynamics of liquids is summarized in a number of review articles (e.g. Sjölander 1987; Yoshida and Takeno 1989). From these one draws the conclusion that, although in principle possible and interesting, a comprehensive self-consistent analysis of collective motion is not particularly necessary *in the ordinary liquid range*. To be more specific, the satisfactory results reported in the preceding pages (as well as in several other works where the 'loop' structure was ignored) indicate that the self-consistent aspects are not so crucial as to make a further 'escalation' in the numerical computations worthwhile. Physically, this reflects the fact that in the collective dynamics of liquids near the melting point the effects conventionally referred to as 'mode-coupling features', although certainly present and non-negligible, are usually not large enough to trigger some 'unexpected' behaviour.

This situation changes as soon as the liquid is 'quenched' to enter a supercooled phase. Here the structural relaxation may become so sluggish to increase considerably both the magnitude and the duration of all the long-lasting features in the time correlations. This leads to a further slowing down of the dynamics via the mode-coupling decay channels, and so on. Eventually the process attains the typical features of a positive-feedback mechanism in which self-consistency plays a major role. We shall now see which sort of qualitatively new phenomena can actually occur in such a physical situation.

6.3.3 The ideal glass transition

Glasses are conventionally defined as 'extremely viscous liquids' in which the shear viscosity coefficient η may attain values of the order of 10^{13}

poise, to be compared with those $\approx 10^{-2}$ poise typical of most ordinary liquids near the melting point. An equivalent definition of a glass is that of a liquid with virtually no diffusive motions: the diffusion coefficient $D \approx 10^{-15} \, \text{cm}^2 \, \text{s}^{-1}$, at least *ten orders of magnitude* lower than in an ordinary liquid. Both these figures make a glass resemble a crystalline solid, were it not for its structure which is intrinsically disordered or 'amorphous'. In practice, a glassy phase may be obtained from the ordinary liquid ('the melt') by a suitable quenching of its temperature.

Although the previous definitions vividly illustrate some extremely peculiar features, they encompass only a limited portion of the complex physical behaviour of glassy systems. To begin with, in contrast with gases, liquids and solids, glasses are not a stable phase of matter. As a matter of fact, when observed over a sufficiently long time interval, glasses manifest the tendency to 'nucleate' toward the really stable phase, which is usually a crystalline solid. In the monatomic systems we are concerned with, this crystallization process occurs quite rapidly (even in a few picoseconds), making the experimental observation of a real glassy behaviour extremely difficult or impossible. In these simple systems computer simulations have, however, provided useful pieces of information about the gradual disappearing of diffusive motions and/or the onset of nucleation phenomena. In other systems of more practical interest (window glass being the typical example) the crystallization process may require years, or even centuries. This circumstance justifies the characterization of glasses as systems in *metastable* (rather than thermodynamic) equilibrium. Another important aspect concerns the details of the experimental technique by which a glass is actually 'produced'. Depending on the system, the actual observability of the transition toward a glassy phase is found to be strongly related to the quenching rate. In particular, while certain 'easy glass formers' such as SiO_2 and B_2O_3 can be made amorphous by a rather slow cooling (of the order of 0.1–$1 \, \text{K} \, \text{s}^{-1}$), some metallic substances can be 'glassified' only by quite high quenching rates ($\approx 10^6$–$10^8 \, \text{K} \, \text{s}^{-1}$). Again, an extreme case is provided by monatomic systems, which even in the liquid phase are characterized by a close-packed arrangement of particles. In such a situation, it is difficult to overcome the tendency of these systems to crystallize upon cooling, and indeed the quenching rate required to 'freeze' the disordered structure is found to exceed the highest that can be achieved by present experimental techniques. Fortunately, even in this case one may resort to computer simulations, where it is relatively easy to 'produce' cooling rates as high as 10^{12}–$10^{13} \, \text{K} \, \text{s}^{-1}$. Finally, even assuming that in some way or another an amorphous system has been obtained, one has to face the fact that the details of the transition *ordinary liquid → supercooled liquid → glass* (including the very existence of a well-defined 'critical temperature') depend both on the nature of the system and on its experimental

'history' (memory effects, hysteresis loops, and so on are common features). Clearly, we are rather far away from the 'universal features' typical, for example, of an ordinary second-order phase transition.

Even from the previous schematic remarks it is clear that a comprehensive study of glassy systems should encompass vastly different areas, ranging from intriguing statistical-mechanics problems to subjects typical of material physics. Here we can only refer the interested reader to a limited number of books and rewiew articles which make a suitable selection between the various ingredients of such a rich menu (Angell *et al.* 1981; Zallen 1983; Elliott 1984; Jäckle 1986). Even the more restricted field of the liquid-glass transition has seen rapidly growing activity in several directions in recent years (e.g. Fredrickson 1988). In the following we shall limit ourselves to a very short account of the mode-coupling approach to this particular field, referring to a recent review by Götze and Sjögren (1992) for a more thorough discussion of the entire subject.

The first point to appreciate is that something 'unusual' has to occur in the time correlation functions of the system as it approaches a glassy phase. Since one of the main features of a glass is the freezing of all the motional degrees of freedom, it is natural to expect that correlation functions such as $F(k, t)$ or $F_s(k, t)$, rather than showing a more or less monotonic decay to zero, should ultimately be 'blocked' to some finite value. For example, in the case of the intermediate scattering function, in a situation of structural arrest one should have that

$$\lim_{t \to \infty} \frac{F(k, t)}{F(k, t = 0)} = \lim_{t \to \infty} \frac{F(k, t)}{S(k)} = f_k \qquad (6.84)$$

where $f_k \neq 0$. This behaviour is in marked contrast with the one found in the liquid phase, and is in fact the ultimate consequence of the occurrence of slower and slower relaxation processes. In other terms, the 'transition' under investigation has a purely dynamic origin.

Given this picture, it is natural to argue that, owing to their intrinsic slow character, mode-coupling decay channels are likely to play a major role in triggering the transition. To actually see how this comes out, it is again convenient to refer to the representation (6.75) for the Laplace transform of $F(k, t)$. As in Section 6.3.1, we shall make use of the expression (6.78) for the memory function $K_L(k, t)$. However, now our main interest is to ascertain the effects of the genuine long-lasting features of $K_L(k, t)$, and it is worthwhile to split eqn (6.78) in a slightly different way. More precisely, we write

$$K_L(k, t) = K_0(k, t) + [K_L(k, t)]_{MC} \qquad (6.85)$$

where $[K_L(k, t)]_{MC}$ is given by (6.82), and the quantity $K_0(k, t)$ accounts for all the short-time features of the memory function. As the latter are

not expected to be particularly relevant in the present problem, we may content ourselves of a simple representation of these rapidly decaying contributions. Specifically, we adopt a Markovian approximation of the form

$$K_0(k, t) = 2a_k \cdot \delta(t) \tag{6.86}$$

(a similar scheme was previously used in eqn (6.4) to describe the full memory function in the hydrodynamic region; now the representation is extended to finite wavevectors, but only to describe the short-time portion of $K_L(k, t)$). As we shall see, a specification of the constant a_k is not necessary for our present purposes. Rearranging eqn (6.75) we obtain

$$\frac{[\tilde{F}(k, z)/S(k)]}{1 - z[\tilde{F}(k, z)/S(k)]} = \frac{1}{\langle \omega_k^2 \rangle} [z + \tilde{K}_L(k, z)]$$

$$\approx \frac{1}{\langle \omega_k^2 \rangle} \{z + a_k + [\tilde{K}_L(k, z)]_{MC}\}. \tag{6.87}$$

Equation (6.84) implies that for $z \to 0$ the quantity $[\tilde{F}(k, z)/S(k)]$ has a singular behaviour of the form

$$\frac{\tilde{F}(k, z)}{S(k)} \approx \frac{f_k}{z}. \tag{6.88}$$

Inserting this limiting result into (6.87), consistency demands that an equally singular behaviour must be present even in the memory function $\tilde{K}_L(k, z \to 0)$. Now, the Laplace transform of the rapidly decaying part $K_0(k, t)$ is perfectly regular for $z \to 0$, with a contribution given by the constant a_k. Consequently, the singularity of K_L is entirely due to the mode-coupling contribution. Thus, letting

$$[\tilde{K}_L(k, z \to 0)]_{MC} = [K_L(k, t \to \infty)]_{MC}/z \tag{6.89}$$

in order to be consistent we should require that

$$\frac{f_k}{1 - f_k} = \frac{1}{\langle \omega_k^2 \rangle} [K_L(k, t \to \infty)]_{MC}. \tag{6.90}$$

The next important step is now to see whether eqn (6.90) is actually capable of predicting a non-vanishing value of f_k, namely a real asymptotic plateau for $F(k, t)$. Starting from the expression (6.83) of $K_L(k, t)$ and using eqn (6.84), Bengtzelius *et al.* (1984) gave a positive answer to this question in the case of a hard-sphere system. In this particular case where the only relevant thermodynamic variable is the number density, the numerical solution of eqn (6.90) in fact yields $f_k \neq 0$ as the packing fraction exceeds a certain critical value. At even higher densities, f_k is found to increase considerably for all wavevectors; this trend is particularly

evident for $k = k_m$, where eventually f_k approaches unity. All these findings confirmed the results obtained previously by a simpler mathematical approach (Leutheusser 1984).

In their numerical calculations Bengtzelius *et al.* noticed that the dominant contribution to eqn (6.83) comes from wavevectors near the main peak of the static structure factor. This circumstance can be exploited to construct an approximate model which has a simple analytical solution. Specifically, Bengtzelius *et al.* assumed that the structure factors in eqn (6.83) can be approximated as

$$S(q) = 1 + A\delta(q - k_m) \tag{6.91}$$

where the only parameter is the area A under the main peak of the quantity $h(q) \equiv S(q) - 1$. An approximation identical to (6.91) can be performed even for the mode-coupling integrals relevant for self-motion (cf. Section 5.1.3). The ansatz (6.91) implies that $nc(k_m) = 1$, and leads to a considerable simplification of the result (6.83) for $[K_L(k, t)]_{MC}$. In particular, after some algebra it is found that eqn (6.90) reduces to

$$\frac{f_k}{1 - f_k} = \lambda f_k^2 \tag{6.92}$$

where

$$\lambda \equiv \frac{k_m S(k_m) A^2}{8\pi^2 n}. \tag{6.93}$$

It is readily verified that for $\lambda < 4$ eqn (6.92) admits only one real solution, namely $f_k = 0$. This corresponds to the situation which one has in the liquid range. On the other hand, if $\lambda > 4$ one also finds two additional real solutions. Only one of these turns out to be physical, and reads

$$f_k = \tfrac{1}{2} + \tfrac{1}{2}[1 - (4/\lambda)]^{1/2}. \tag{6.94}$$

The result (6.94) is clearly the one appropriate for a phase characterized by a structural arrest. As argued by Bengtzelius *et al.*, this phase can only be a 'glass': any nucleation process toward an ordered crystal would in fact require an explicit account of higher order structural correlations, and these were effectively neglected in the factorization approximations of mode-coupling theory. Consequently, the critical value $\lambda = 4$ can be interpreted as marking the transition toward an amorphous solid. Finally, the fact that $f_k \to 1$ as λ increases well above the critical value is in qualitative agreement with the previous numerical findings.

In connection with the non-trivial result (6.94), it is worthwhile remarking the crucial role played by the self-consistent and nonlinear character of the entire mode-coupling framework. Although this was our main purpose in this section, the analysis of the requirement (6.90) is only the first step

of a full body of theoretical developments, collectively referred to as the *mode-coupling theories of the glass transition*. In these treatments, an important subject of investigation is the actual dynamic evolution of the various time- or frequency-dependent quantities on both sides of the transition point. Even in this respect, the pioneering works by Leutheusser (1984) and by Bengtzelius *et al.* (1984) were rapidly followed by several more sophisticated approaches. Again, for a detailed account we refer the reader to the aforementioned review by Götze and Sjögren (1992) as well as to recent work by Lai and Chen (1993). In turn, the unconventional dynamical response has been shown to affect the behaviour of several thermodynamic quantities, which exhibit discontinuous changes in the neighbourhood of the transition (Bengtzelius and Sjögren 1986).

Whereas the most part of these theoretical approaches deal with relatively simple model systems, the materials which actually exhibit a transition toward a glassy phase are always rather 'complex', both from the chemical and the structural point of view. In such a situation it is probably too pretentious to look for a direct quantitative test of the mode-coupling predictions. Broadly speaking, the various theories are however found to account remarkably well for several dynamical features observed in the supercooled region (for instance, the occurrence of markedly non-exponential time decays). Evidence in this sense were provided by several computer simulation studies (e.g. Brakkee 1990), as well as by real experiments both with neutrons (Mezei *et al.* 1987; Richter *et al.* 1988) and with light (Tao *et al.* 1991, 1992). On the other hand, in the close neighbourhood of the transition point the theoretical predictions are not so satisfactory (and are sometimes referred to as describing an 'ideal' glass transition). An important source of these discrepancies with real life is believed to be the neglect of thermally activated processes, at least in the less sophisticated versions of the theoretical framework. Even with these limitations, the introduction of mode-coupling concepts in the theories of the glass transition represented a real breakthrough, and the near future will certainly see further important developments in this complex physical problem.

6.4 STRESS AUTOCORRELATION FUNCTION, AND ORDINARY AND GENERALIZED SHEAR VISCOSITY

6.4.1 The dynamics of the shear stress autocorrelation function

In the hydrodynamic region, the transverse current correlation function $C_T(k, t)$ is known to exhibit a slow exponential decay with a lifetime inversely proportional to k^2:

$$C_T(k, t) = (k_B T/m) \exp\left[-(\eta/nm)k^2 |t|\right]. \tag{6.95}$$

The actual magnitude of the decay rate is controlled by the shear viscosity coefficient η. In Section 3.4.2 we have seen that η can be expressed in term of a simple Green–Kubo integral

$$\eta = (k_B T V)^{-1} \int_0^\infty dt \, \langle \sigma^{zx}(0) \, \sigma^{zx}(t) \rangle$$

$$\equiv \int_0^\infty dt \, \eta(t). \tag{6.96}$$

The result (6.96) involves the time autocorrelation function of the non-diagonal components of the stress tensor σ (cf. (3.10)). In the last step of (6.96) we have explicitly introduced the quantity $\eta(t)$, often referred to as the *(shear) stress autocorrelation function* (SACF).

Clearly, the study of the dynamical features of $\eta(t)$ at various thermodynamic points is expected to provide useful information over the state dependence of the shear viscosity coefficient. According to the definition (3.10), the variable σ^{zx} comprises both kinetic and potential terms:

$$\sigma^{zx} = \sum_i m v_{i,z} v_{i,x} - \tfrac{1}{2} \sum_{i,j \neq i} (z_{ij} x_{ij}/r_{ij}) \phi'(r_{ij})$$

$$\equiv (\sigma^{zx})_K + (\sigma^{zx})_P. \tag{6.97}$$

As a result, the SACF can be split into four different contributions:

$$\eta(t) = \eta_{KK}(t) + \eta_{KP}(t) + \eta_{PK}(t) + \eta_{PP}(t) \tag{6.98}$$

where

$$\eta_{KK}(t) = (k_B T V)^{-1} \langle (\sigma^{zx}(0))_K (\sigma^{zx}(t))_K \rangle$$

$$= \frac{nm^2}{N k_B T} \sum_{i,1} \langle v_{i,z}(0) v_{i,x}(0) v_{1,z}(t) v_{1,x}(t) \rangle \tag{6.99a}$$

$$\eta_{KP}(t) = (k_B T V)^{-1} \langle (\sigma^{zx}(0))_K (\sigma^{zx}(t))_P \rangle \tag{6.99b}$$

$$\eta_{PK}(t) = (k_B T V)^{-1} \langle (\sigma^{zx}(0))_P (\sigma^{zx}(t))_K \rangle \tag{6.99c}$$

$$\eta_{PP}(t) = (k_B T V)^{-1} \langle (\sigma^{zx}(0))_P (\sigma^{zx}(t))_P \rangle$$

$$= \frac{nm^2}{4 N k_B T} \sum_{i,j \neq i} \sum_{l,m \neq l} \left\langle \frac{z_{ij}(0) x_{ij}(0)}{r_{ij}(0)} \phi'(r_{ij}(0)) \right.$$

$$\left. \frac{z_{lm}(t) x_{lm}(t)}{r_{lm}(t)} \phi'(r_{lm}(t)) \right\rangle. \tag{6.99d}$$

Since the variables $(\sigma^{zx})_K$ and $(\sigma^{zx})_P$ are both real and invariant under time reversal, the cross-correlation functions $\eta_{KP}(t)$ and $\eta_{PK}(t)$ are in fact equal

(cf. Appendix B). Also, $\eta_{KP}(t = 0) = \eta_{PK}(t = 0) = 0$. As a result, the initial value of the SACF can simply be written as

$$\eta(0) = \eta_{KK}(0) + \eta_{PP}(0) \equiv G \qquad (6.100)$$

where the quantity G is the $k \to 0$ limit of the rigidity modulus $G(k)$. More precisely, from the results of Section 6.2.2 it is easy to verify that

$$G = G(k \to 0) = \frac{nm}{k^2} K_T(k \to 0, t = 0)$$

$$= nk_B T + \tfrac{1}{2}n^2 \int d\mathbf{r} \, \frac{\partial^2 \phi(r)}{\partial x^2} z^2 g(r)$$

$$= nk_B T + \frac{4\pi n^2}{30} \int_0^\infty dr \, r^4 \left[\phi''(r) + \frac{4\phi'(r)}{r} \right] g(r). \qquad (6.101)$$

In the same approximation scheme adopted in (6.57), eqn (6.101) reduces to

$$G = nk_B T + \frac{1}{10} nm\Omega_0^2 r_0^2. \qquad (6.102)$$

Even these preliminary results offer the possibility of making several important remarks over the dynamics of the SACF. First of all, from eqn (6.101) it is readily seen that in a dilute fluid with $n \to 0$ the value of $\eta(0) = G$ is essentially determined by the kinetic ('ideal gas') contribution $nk_B T$. Vice versa, at the high densities typical in the liquid range the potential term is found to be the dominant one. Similar remarks apply even to the different time-dependent contributions to $\eta(t)$. In particular, at sufficiently low densities (and/or sufficiently high temperatures) $\eta(t)$ is expected to be $\approx \eta_{KK}(t)$, and indeed by this approximation it is possible to deduce for η all the well-known results of the kinetic theory of gases (e.g. McQuarrie 1976). On the other hand, in very dense fluids the kinetic and the cross contributions in eqn (6.98) are likely to be considerably smaller than $\eta_{PP}(t)$ at all the times of practical interest. This expectation has indeed been verified in a number of computer simulation experiments, ranging from hard-sphere systems (Alder *et al.* 1970) to more realistic model fluids (Schoen and Hoheisel 1985; Balucani *et al.* 1988). Thus in the liquid range we may conclude that $\eta(t) \approx \eta_{PP}(t)$.

Another noteworthy feature follows from the specific form (6.99d) of $\eta_{PP}(t)$. Recalling the definition (2.60) of the time-dependent distribution function $\mathcal{G}(\mathbf{r}0; \mathbf{r}'t)$ we may equivalently write that

$$\eta_{PP}(t) = \int d\mathbf{r} \int d\mathbf{r}' \, A_\eta(\mathbf{r}) A_\eta(\mathbf{r}') \, \mathcal{G}(\mathbf{r}0; \mathbf{r}'t) \qquad (6.103)$$

where we have let

$$A_\eta(\mathbf{r}) \equiv \tfrac{1}{2}(nm^2/k_B T)^{1/2} (zx/r) \phi'(r). \qquad (6.104)$$

When expressed in this way, the quantity $\eta_{PP}(t)$ is seen to have the typical form of the time correlation functions usually met in interaction-induced phenomena (cf. Section 2.6). This analogy has in fact been exploited (Balucani *et al.* 1988; Montrose *et al.* 1991). Even so, between the two cases there is an important difference which is worth mentioning. In the same way as for the general correlation function (1.108), eqn (6.99d) can indeed be split into two-, three-, and four-particle contributions; however, for $t = 0$ the particular form (6.104) of the 'weight factor' $A_\eta(\mathbf{r})$ is such that $\eta_{PP}(0)$ can exactly be written in terms of only pair contributions, as in eqn (6.101). This result can also be obtained from (6.99d) by exploiting the hierarchy of the *n*-particle static distribution functions (Balucani *et al.* 1988). In contrast, in the case of interaction-induced phenomena the many-particle aspects cannot be bypassed, and the initial value of the relevant correlation (namerly, the integrated intensity of the spectrum) can only be evaluated by resorting to some approximation scheme (see Appendix J).

In the liquid range, the actual evaluation of $\eta(t)$ makes use of the relation

$$\eta(t) = (k_B TV)^{-1} \langle \sigma^{zx}(0)\sigma^{zx}(t) \rangle = nm \lim_{k \to 0} [K_T(k, t)/k^2] \qquad (6.105)$$

and of the results (6.59)–(6.60) for the memory function $K_T(k, t)$. As a consequence, the SACF is naturally split into two contributions associated with distinctly different timescales:

$$\eta(t) = \eta_0(t) + \eta_1(t). \qquad (6.106)$$

In particular, $\eta_0(t) \equiv nm \lim_{k \to 0} \{[K_T(k, t)]_{fast}/k^2\}$ is essentially determined by short-lived collisional events of the 'binary' type, which account for the fast decay of $\eta(t)$ at short times. On the other hand, performing the $k \to 0$ limit of eqn (6.60) and inserting the result into eqn (6.105) it is readily seen that

$$\eta_1(t) \equiv nm \lim_{k \to 0} [M_{22}'(\mathbf{k}, t)/k^2]$$

$$= \frac{n^2 k_B T}{16\pi^3} \int d\mathbf{q} \left(\frac{q_x q_z}{q} \right)^2 [c'(q)]^2 [F^2(q, t) - F_B^2(q, t)] \qquad (6.107)$$

where $c'(q) = dc(q)/dq = (1/n)S'(q)/S^2(q)$. Performing the angular integrations we obtain

$$\eta_1(t) = \frac{n^2 k_B T}{60\pi^2} \int_0^\infty dq \, q^4 [c'(q)]^2 [F^2(q, t) - F_B^2(q, t)]. \qquad (6.108)$$

Finally, adopting the model (4.147) for $F_B(q, t)$ we end up with

$$\eta_1(t) = \frac{k_B T}{60\pi^2} \int_0^\infty dq\, q^4 \left[\frac{S'(q)}{S(q)}\right]^2 \left\{1 - \left[\frac{F_0(q,t)}{F_s(q,t)}\right]^2\right\} \left[\frac{F(q,t)}{S(q)}\right]^2.$$

$$(6.109)$$

Aside from the factor in curly brackets, eqn (6.109) can be derived even by a simple mode-coupling calculation (Geszti 1983). Specifically, one has to extract from σ^{xx} all the contributions involving the most relevant pair variables. In the liquid range the dominant couplings involve the product $\hat{n}(\mathbf{q}) \cdot \hat{n}(-\mathbf{q})$ of two density modes, and the result is eventually to be summed over all the intermediate wavevectors $\mathbf{q}$. This procedure automatically selects the potential part of the SACF as the one which gives a non-zero contribution, thus confirming the practical relevance of $\eta_{PP}(t)$ even beyond the short-time domain. Needless to say, this mode-coupling result is expected to be strictly valid only *beyond* a microscopic time interval. On a purely practical basis, its validity range can however be increased by restricting the integration up to a cutoff wavevector:

$$\eta_{MC}(t) = \frac{k_B T}{60\pi^2} \int_0^{q_c} dq\, q^4 \left[\frac{S'(q)}{S(q)}\right]^2 \left[\frac{F(q,t)}{S(q)}\right]^2 \qquad (6.110)$$

where q_c can be determined in such a way that $\eta_{MC}(t = 0)$ reproduces the correct initial value of $\eta_{PP}(t)$. This *ad hoc* procedure has in fact been adopted with some success (Geszti 1983; Balucani *et al.* 1988). To achieve a satisfactory description of the tail of the SACF, the integration interval $(0, q_c)$ must in any case include the wavevector range where $S(q)$ has its main peak.

Turning now the attention on the more 'rigorous' approach of eqns (6.106), (6.109), it remains to specify the rapidly decaying term $\eta_0(t)$. Even in this case, the fact that $\eta_0(t)$ and $\eta(t)$ coincide up to the order t^2 included suggests the ansatz

$$\eta_0(t) = Gf(t/\tau_\eta) \qquad (6.111)$$

where the shape function $f(x)$ is chosen in such a way that (i) $f(x \to 0) \approx 1 - x^2$ and (ii) $f(x) \approx 0$ for large x. In turn, the time constant τ_η can be determined by a short-time expansion of the full $\eta(t)$; this implies that

$$\tau_\eta = [|\ddot{\eta}(0)|/2G]^{-1/2}. \qquad (6.112)$$

A detailed calculation (Balucani *et al.* 1988) shows that the quantity $\ddot{\eta}(0)$ can be expressed as a sum of two contributions, which respectively involve the pair and triplet distribution functions. Adopting for the latter a superposition approximation, the time τ_η is readily evaluable. In practice, the values of τ_η obtained in such a way in several simple liquids lie in the typical 'collision-time' range (some tenths of a picosecond) and are more
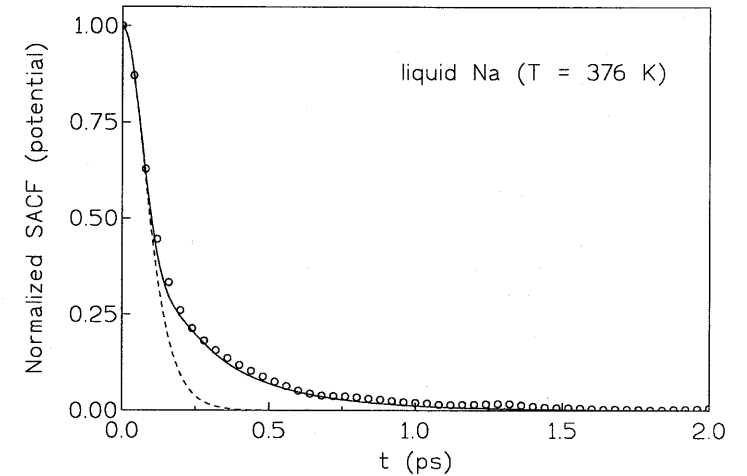
Fig. 6.8 Normalized potential part of the stress autocorrelation function in liquid Na at 376 K (Balucani *et al.* 1993a). The dashed line represents the rapidly decaying portion $\eta_0(t)/G = f(t/\tau_\eta)$, with $f(x) = \mathrm{sech}^2 x$ and $\tau_\eta = 0.110$ ps. The full line denotes the complete result of eqn (6.106), with $\eta_1(t)$ evaluated from (6.109). The open circles are computer simulation data. On the scale of the graph, the contributions of the cross and kinetic terms in eqn (6.98) are quite small, with an overall maximum magnitude ≈ 0.04 at very short times.

or less similar to those found in Section 5.1 for the initial decay time τ of the memory function $K(t)$.

The ultimate test of the approach is obtained by comparing the predictions of eqns (6.106), (6.109), and (6.111) with the data of $\eta(t)$ obtained by computer simulation. As in the case of the memory function $K(t)$, the comparison can be made at various levels, depending on which approximation is used in eqn (6.109) for $F_s(q, t)$ and $F(q, t)$. In any case, it is found that the leading contribution to the tail of $\eta(t)$ is provided by those density modes with wavevectors q close (but not exactly at) the position q_m of the main peak of $S(q)$. On the basis of (6.109), this feature can be attributed to a sort of 'compromise' between the amplitude of the tail (which decreases as $q \to q_m$) and its actual long-lasting character (which is more pronounced for wavevectors $q \approx q_m$).

As in Section 5.1.3, the dominance of a relatively narrow range of wavevectors in the integral (6.109) can be exploited to simplify considerably the expression of $\eta_1(t)$. Whichever the level of approximation adopted for the evaluation of eqn (6.109), the overall results obtained for $\eta_{pp}(t)$ are found to compare rather well with the corresponding simulation data in various monatomic liquids (Balucani 1990; Balucani *et al.* 1993a). Figure 6.8

illustrates such a comparison in the case of liquid sodium near the melting point: despite a systematic tendency of the theoretical curve to lie slightly below the simulation results, the overall agreement appears to be satisfactory.

6.4.2 Ordinary and generalized shear viscosity

The successful description of the main dynamical features of the SACF achieved in the previous subsection suggests the possibility of using eqn (6.96) to obtain reliable predictions for the shear viscosity coefficient η. The first step is the evaluation of the quantity

$$\eta_0 \equiv \int_0^\infty dt\, \eta_0(t) = G\tau_\eta \int_0^\infty dx\, f(x) \qquad (6.113)$$

which represents the contibution of the rapidly decaying portion of the SACF. The shape function in eqn (6.113) can be approximated by a convenient mathematical expression. Choosing $f(x) = \text{sech}^2 x$ (cf. Fig. 6.8), we simply obtain that

$$\eta_0 = G\tau_\eta. \qquad (6.114)$$

The predictions of eqn (6.114) are always found to underestimate considerably the actual values of η, confirming that the contribution of the long-lasting portion of the SACF is far from being negligible. As a consequence, we have to deal with

$$\eta = \eta_0 + \int_0^\infty dt\, \eta_1(t) \qquad (6.115)$$

where $\eta_1(t)$ is given by eqn (6.109). Equation (6.115) has been evaluated numerically for several simple liquids, focusing the attention on the dominant potential contributions (Balucani 1990; Balucani *et al.* 1993a). Some results of these calculations are reported in Table 6.1. Comparing these theoretical values with the corresponding computer simulation data, a substantial improvement with respect to the results of eqn (6.114) is apparent. In the case of liquid alkali metals, however, one notes a persisting underestimate of the order of 10%. This discrepancy stems from the aforementioned feature that the amplitude of the tail of $\eta_{PP}(t)$ predicted by the theory turns out to be slightly lower than the actual data (cf. Fig. 6.8), and these systematic deviations clearly sum up in the integral (6.115). In this context, a more accurate evaluation of eqn (6.109) (possibly with the use of extensive simulation data for both $F(q, t)$ and $F_s(q, t)$) is needed to ascertain the actual origin of these residual discrepancies.

Owing to its intrinsic hydrodynamic nature, the shear viscosity coefficient

Table 6.1 Comparison between the theoretical predictions for the potential contribution to the shear viscosity coefficient and the corresponding molecular-dynamics data η_{MD} (Balucani 1990; Balucani *et al.* 1993a). The results refer to the same simple liquids considered in Table 5.1. For completeness, the MD results for the full η are also reported (bracketed entries).

	η_0 10^{-3} poise	η 10^{-3} poise	η_{MD} 10^{-3} poise
Sodium	3.02	4.89	5.22 (6.30)
Rubidium 318	3.10	5.33	5.84 (5.95)
Rubidium 270	3.29	6.71	(7.26)
Caesium	3.23	5.40	6.07 (6.16)
Argon	1.80	2.80	(2.72)

η is the only quantity needed in a fluid to specify transverse collective motions on a macroscopic scale. However, this simple picture begins to change as soon as we move toward a more microscopic description. In Section 6.2.2 we have in fact seen that over short distances a liquid is able to support high-frequency transverse sound waves. At intermediate and high wave vectors considerable changes do occur even in the low-frequency response. A formal way to describe these non-hydrodynamic features is to introduce a wavevector- and frequency-dependent shear viscosity coefficient $\tilde{\eta}(k, z = i\omega)$, defined as in eqn (6.38). At finite frequencies $\tilde{\eta}(k, i\omega)$ is in general a complex quantity, with an imaginary part which gives rise to shear-wave propagation and a real part which accounts for damping effects. As $\omega \to 0$, $\tilde{\eta}(k, i\omega)$ becomes purely real, and it is reasonable to describe the microscopic low-frequency response of the system by a *generalized shear viscosity coefficient*

$$\eta(k) \equiv \frac{nm}{k^2} \tilde{K}_T(k, z = 0)$$

$$= \frac{nk_B T}{k^2} [\tilde{C}_T(k, z = 0)]^{-1} \qquad (6.116)$$

where we have exploited eqn (6.37). Clearly, for sufficiently small wavevectors, $\eta(k)$ approaches the ordinary shear viscosity coefficient η. On the other hand, at large k, $C_T(k, t)$ is known to approach the free-particle result (1.154); thus in this limit

$$\eta(k) \to \left(\frac{2n^2 mk_B T}{\pi}\right)^{1/2} \frac{1}{k}. \qquad (6.117)$$
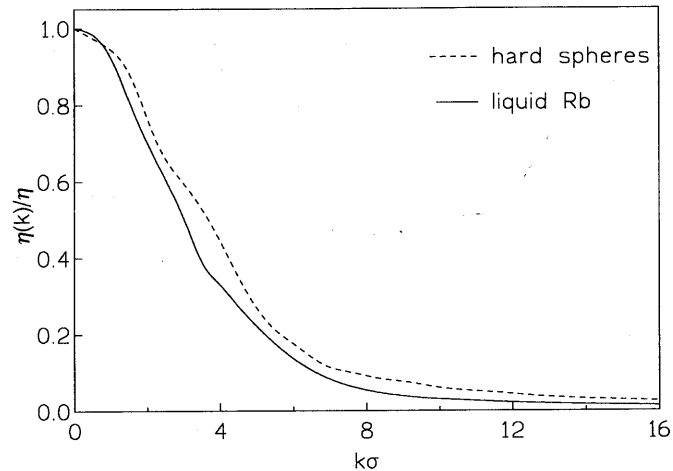
Fig. 6.9 Computer simulation data for the wavevector dependence of the generalized shear viscosity $\eta(k)/\eta$ in two systems at densities typical of the liquid range: dashed line, fluid of hard spheres at a reduced density $n\sigma^3 = 0.884$ (Alley and Alder 1983); full line, liquid Rb at $T = 332\,K$ and a reduced density $n\sigma^3 = 0.905$ (Balucani *et al.* 1987). The length parameter σ denotes either the particle diameter (hard-sphere system) or the position of the first zero of the effective pair potential (liquid metal).

At finite wavevectors, computer simulation data have been obtained for $\eta(k)$ in several model systems at densities typical of the liquid range (Alley and Alder 1983; Balucani *et al.* 1987; Gaskell *et al.* 1987; Vogelsang and Hoheisel 1987; Larsson *et al.* 1990). Some of these data are reported in Fig. 6.9 using properly scaled units. In all the systems which have been investigated, it is apparent a quite substantial decrease of $\eta(k)$ as the wavevector moves from the strict hydrodynamic regime toward the position k_m of the main peak of $S(k)$ (in the reduced units of the figure, $k_m\sigma \approx 6.7$–6.8).

The gross features of the decay of $\eta(k)$ from its hydrodynamic value can be understood on the basis of a simple viscoelastic model. As a matter of fact, from eqn (6.43) we deduce that

$$\eta(k) = G(k)\tau_{T,k}. \tag{6.118}$$

In this picture, the observed wavevector dependence of $\eta(k)$ stems from the marked decrease with k of both $G(k)$ and $\tau_{T,k}$ (cf. eqns (6.57) and (6.55)). As might be expected, a somewhat better agreement with the simulation data can be obtained by allowing the presence in $K_T(k, t)$ of a second decay mechanism with a longer relaxation time, as in eqn (6.58). However,

even in this case some discrepancies persist at intermediate wavevectors, where a sort of 'shoulder' in the data cannot be reproduced by either one of these phenomenological models (Balucani *et al.* 1987).

6.4.3 The Stokes–Einstein relation

An important consequence of the introduction of $\eta(k)$ is a microscopic generalization of the so-called 'Stokes–Einstein relation' between the diffusion and shear viscosity coefficients. This was originally introduced to describe the diffusive motion of a large 'Brownian' particle of radius R in a continuous fluid with shear viscosity η. More precisely, the relation can be written as (Landau and Lifshitz 1963)

$$D = \frac{k_B T}{c\pi\eta R} \tag{6.119}$$

where c is a numerical constant which depends on the specific form assumed for the velocity field of the fluid at the 'surface' of the particle. To be specific, at the surface we may match either the full fluid velocity with that of the particle, or simply the two normal components (with no tangential frictional force acting on the particle). These two possibilities are usually referred to as 'stick' and 'slip' boundary conditions, and imply for the constant in eqn (6.119) the values $c = 6$ and $c = 4$, respectively.

Owing to the large size of the particle, the description of the fluid by a continuum implicit in eqn (6.119) seems quite reasonable. Surprisingly enough, the Stokes–Einstein relation is, however, found to work fairly well even in genuine one-component systems, where any distinction between the diffusing particle and those of the surrounding fluid disappears. Actually, it is not uncommon to find quantitative discrepancies up to $\sim 20\%$, but these are often dealt with empirically by some suitable change in the constant c and/or in the 'effective' radius R of the particle (which certainly cannot be accurately defined).

In the simple liquids we are concerned with, it proves possible to give a sounder physical justification for the approximate validity of eqn (6.119). By itself, the Stokes–Einstein relation implies the existence of some connection between single-particle motion (D) and the dynamics of transverse currents (η), with both aspects being probed over an essentially macroscopic space scale and timescale. Such a mutual relationship can, however, be established at any level by introducing a *microscopic velocity field* (see Appendix H). The key result in this respect is a simplified version of eqn (H.10):

$$\langle \mathbf{v}_i(0) \cdot \mathbf{v}_i(t) \rangle = \frac{1}{8\pi^3} \int d\mathbf{q}\, f(q)\, [C_L(q, t) + 2C_T(q, t)] \tag{6.120}$$

where, owing to the slowness of the diffusive processes in the liquid range, the self-intermediate scattering function has effectively been replaced by its initial value $F_s(q, 0) = 1$. Integrating both sides of (6.120) over time and exploiting the result (1.67) for the diffusion coefficient, we find

$$3D = \frac{1}{8\pi^3} \int dq f(q) \int_0^\infty dt \left[C_L(q, t) + 2C_T(q, t) \right]$$

$$= \frac{1}{4\pi^3} \int dq f(q) \tilde{C}_T(q, z = 0) \tag{6.121}$$

since the longitudinal contribution involves $\tilde{C}_L(q, z = 0) = 0$. Introducing the definition (6.116) and performing the angular integrations it is easily shown that

$$D = \frac{n k_B T}{3\pi^2} \int_0^\infty dq \frac{f(q)}{\eta(q)}. \tag{6.122}$$

The result (6.122) is a sort of *generalized Stokes–Einstein relation* in which the microscopic aspects are properly taken into account by the presence of a wavevector dependent shear viscosity coefficient (Gaskell 1984; Gaskell *et al.* 1989). If the q-dependence of $\eta(q)$ were ignored by letting $\eta(q) \approx \eta$, we would simply obtain

$$D = \frac{n k_B T}{3\pi^2 \eta} \int dq f(q) = \frac{k_B T}{4\pi \eta a} \tag{6.123}$$

where we have made use of eqn (H.6) for the Fourier-transformed form factor of the velocity field. The result (6.123) is seen to be identical to eqn (6.119) in which $c = 4$ and the effective particle radius R is naturally replaced by the length $a = (3/4\pi n)^{1/3}$.

In practice, the values of D predicted by eqn (6.123) are always found to underestimate the actual diffusion coefficients. For example, in a Lennard–Jones system simulating liquid argon at $T = 95\,\mathrm{K}$ and $n = 0.021\,\text{Å}^{-3}$, it is found that eqn (6.123) predicts $D = 1.84 \times 10^{-5}\,\mathrm{cm^2\,s^{-1}}$ whereas the real value is $2.39 \times 10^{-5}\,\mathrm{cm^2\,s^{-1}}$. Clearly, the decrease of $f(q)$ with the wavevector is not fast enough to ensure the validity of the approximation $\eta(q) \approx \eta$ in (6.122). In the particular case under consideration, a simple viscoelastic model for $\eta(q)$ is sufficient to increase the value of D to $2.47 \times 10^{-5}\,\mathrm{cm^2\,s^{-1}}$, in close agreement with the actual data. In other systems the integral in eqn (6.122) is found to be more sensitive to the minor details of $\eta(q)$, such as the 'shoulder' mentioned at the end of section 6.4.2. Whichever the situation actually met, it is clear that in one-component fluids the simplicity of eqn (6.119) is to some extent deceiving, and the 'relation' must in fact be supplemented by some

additional information about the microscopic behaviour of the liquid under consideration.

REFERENCES

Ailawadi, N. K., Rahman, A., and Zwanzig, R. (1971). *Phys. Rev. A*, **4**, 1616.

Akcasu, A. Z. and Daniels, E. (1970). *Phys. Rev. A*, **2**, 962.

Alder, B. J., Gass, D. M., and Wainwright, T. E. (1970). *J. Chem. Phys.*, **53**, 3813.

Alley, W. E. and Alder, B. J. (1983). *Phys. Rev. A*, **27**, 3158.

Amar, J. G. and Mountain, R. (1987). *J. Chem. Phys.*, **86**, 2236.

Angell, C. A., Clarke, J. R. H., and Woodcock, L. V. (1981). *Adv. Chem. Phys.*, **48**, 397.

Bafile, U., Verkerk, P., Barocchi, F., de Graaf, L. A., Suck J.-B., and Mutka, H. (1990). *Phys. Rev. Lett.*, **65**, 2394.

Balucani, U. (1990). *Mol. Phys.*, **71**, 123.

Balucani, U., Vallauri, R., and Gaskell, T. (1987). *Phys. Rev. A*, **35**, 4263.

Balucani, U., Vallauri, R., and Gaskell, T. (1988). *Phys. Rev. A*, **37**, 3386.

Balucani, U., Torcini, A., and Vallauri, R. (1992). *Phys. Rev. A*, **46**, 2159.

Balucani, U., Torcini, A., and Vallauri, R. (1993a). *Phys. Rev. B*, **47**, 3011.

Balucani, U., Ruocco, G., Torcini, A., and Vallauri, R. (1993b). *Phys. Rev. E*, **47**, 1677.

Bengtzelius, U. and Sjögren, L. (1986). *J. Chem. Phys.*, **84**, 1744.

Bengtzelius, U., Götze, W., and Sjölander, A. (1984). *J. Phys. C*, **17**, 5915.

Bodensteiner, T. (1990). Ph.D. Thesis, Technische Universität München, Germany.

Bodensteiner, T., Morkel, C., Gläser, W., and Dorner, B. (1992). *Phys. Rev. A*, **45**, 5709.

Boon, J. P. and Yip, S. (1980). *Molecular hydrodynamics*. McGraw-Hill, New York.

Bosse, J., Götze, W., and Lücke, M. (1978a). *Phys. Rev. A*, **17**, 434.

Bosse, J., Götze, W., and Lücke, M. (1978b). *Phys. Rev. A*, **17**, 447.

Brakkee, M. J. D. (1990). Ph.D. Thesis, University of Amsterdam (Netherlands).

Bruin, C., Michels, J. P. J., van Rijs, J. C., de Graaf, L. A., and de Schepper, I. M., (1985). *Phys. Lett.*, **110 A**, 40.

Chung, C.-H. and Yip, S. (1969). *Phys. Rev.*, **182**, 323.

Cohen, E. G. D., de Schepper, I. M., and Zuilhof, M. J. (1984). *Physica B + C*, **127**, 282.

Cohen, E. G. D., Kamgar-Parsi, B., and de Schepper, I. M. (1986). *Phys. Lett.*, **114 A**, 241.

Copley, J. R. D. and Lovesey, S. W. (1975). *Rep. Progr. Phys.*, **38**, 461.

de Schepper, I. M. and Cohen, E. G. D. (1982). *J. Stat. Phys.*, **27**, 223.

de Schepper, I. M., Verkerk, P., van Well, A. A., and de Graaf, L. A. (1983). *Phys. Rev. Lett.*, **50**, 974.

de Schepper, I. M., Verkerk P., van Well, A. A., and de Graaf, L. A. (1984). *Phys. Lett.*, **104A**, 29.

Elliott, S. R. (1983). *Physics of Amorphous Materials*. Longman, London.

Ernst, H. and Dorfman, J. R. (1972). *Physica*, **61**, 157.
Ernst, H. and Dorfman, J. R. (1975). *J. Stat. Phys.*, **12**, 311.
Fredrikson, G. H. (1988). *Ann. Rev. Phys. Chem.*, **39**, 149.
Gaskell, T. (1984). *J. Non-Cryst. Solids*, **61-2**, 913.
Gaskell, T., Balucani, U., Gori, M., and Vallauri, R. (1987). *Phys. Scripta*, **35**, 37.
Gaskell, T., Balucani, U., and Vallauri, R. (1989). *Phys. Chem. Liq.*, **19**, 193.
Geszti, T. (1983). *J. Phys. C*, **16**, 5805.
Götze, W. and Lücke, M. (1975). *Phys. Rev. A*, **11**, 2173.
Götze, W. and Sjögren, L. (1992). *Rep. Progr. Phys.*, **55**, 241.
Jäckle, J. (1986). *Rep. Progr. Phys.*, **49**, 171.
Kambayashi, S. and Kahl, G. (1992). *Phys. Rev. A*, **46**, 3255.
Kawasaki, K. (1970). *Ann. Phys.*, **61**, 1.
Lai, S. K. and Chen, H. C. (1993). *J. Phys. Cond. Matter*, **5**, 4325.
Landau, L. D. and Lifshitz, E. M. (1963). *Fluid Mechanics*. Pergamon Press, London.
Larsson, K.-E., Dzugutov, M., and Gudowski, W. (1990). *Nuovo Cimento*, **12 D**, 559.
Leutheusser, E. (1982). *J. Phys. C*, **15**, 2801 and 2827.
Leutheusser, E. (1984). *Phys. Rev. A*, **29**, 2765.
Levesque, D., Verlet, L., and Kürkijarvi, J. (1973). *Phys. Rev. A*, **7**, 1690.
Lovesey, S. W. (1971). *J. Phys. C*, **4**, 3057.
Lovesey, S. W. (1984). *Phys. Rev. Lett.*, **53**, 401.
Mc Quarrie, D. A. (1976). *Statistical Mechanics*, Harper & Row, New York.
Mezei, F., Knaak, W., and Farago, B. (1987). *Phys. Rev. Lett.*, **58**, 571.
Montrose, C. J., Litovitz, T. A., Birnbaum, G., and Mennella, R. (1991). *J. Non-Cryst. Solids*, **131-133**, 177.
Munakata, T. and Igarashi, A. (1977). *Progr. Theor. Phys.*, **58**, 1345.
Munakata, T. and Igarashi, A. (1978). *Progr. Theor. Phys.*, **60**, 45.
Rahman, A. (1974). *Phys. Rev. A*, **9**, 1656.
Richter, D., Frick, B., and Farago, B. (1988). *Phys. Rev. Lett.*, **61**, 2465.
Schoen M. and Hoheisel, C. (1985). *Mol. Phys.*, **56**, 653.
Sjögren, L. (1980). *Phys. Rev. A*, **22**, 2883.
Sjölander, A. (1987). In *Amorphous and Liquid Materials* (ed. E. Lüscher, G. Fritsch, and G. Jacucci). Martinus Nijhoff Publishers, Dordrecht.
Tao, N. J., Li, G., Chen, X., Du, W. M., and Cummins, H. Z. (1991). *Phys. Rev. A*, **44**, 6665.
Tao, N. J., Li, G., and Cummins, H. Z. (1992). *Phys. Rev. B*, **45**, 686.
Teixeira, J., Bellissent-Funel, M. C., Chen, S. H., and Dorner, B. (1985). *Phys. Rev. Lett.*, **54**, 2681.
van Rijs, J. C., de Schepper, I. M., Bruin, C., van Delft, D. A., and Bakker, A. F. (1985). *Phys. Lett.*, **111A**, 58.
Vogelsang, R. and Hoheisel, C. (1987). *Phys. Rev. A*, **35**, 1786.
Yoshida, F. and Takeno, S. (1989). *Phys. Reports*, **173**, 301.
Youden, J., Egelstaff, P. A., Mutka, J., and Suck, J.-B. (1992). *J. Phys. Condens. Matter*, **4**, 8945.
Zallen, R. (1983). *The Physics of Amorphous Solids*. Wiley & Sons, New York.

Appendix A

The Hermitian character of the classical Liouville operator

Let us consider the scalar product (A, B) between two arbitrary phase-space variables of the functional space introduced in Section 1.3. The Hermitian-conjugate $L^\dagger$ of the Liouville operator (1.22) is then defined by the relation

$$(A, LB) = (B, L^\dagger A)^*. \tag{A.1}$$

The purpose of this appendix is to prove that $L^\dagger = L$, that is that L is a Hermitian operator. Choosing the classical statistical average $\langle A^* B \rangle$ as a convenient physical representation of the scalar product (A, B), we have that

$$(A, LB) = \langle A^* LB \rangle = \frac{1}{Z_N} \int dr^N dp^N A^* LB \exp(-\beta \mathcal{H})$$

$$= \frac{i}{Z_N} \sum_{i,a} \int dr^N dp^N A^* \left[\frac{\partial \mathcal{H}}{\partial r_{i,a}} \frac{\partial B}{\partial p_{i,a}} - \frac{\partial \mathcal{H}}{\partial p_{i,a}} \frac{\partial B}{\partial r_{i,a}} \right] \exp(-\beta \mathcal{H}). \tag{A.2}$$

Here, we have exploited the definitions (1.5) and (1.22), and the summation over a runs over the cartesian components. Equation (A.2) can be integrated by parts taking $(\partial B/\partial p_{i,a})$ and $(\partial B/\partial r_{i,a})$ as integrating factors. We obtain

$$(A, LB) = -\frac{i}{Z_N} \sum_{i,a} \int dr^N dp^N B \left[\frac{\partial}{\partial p_{i,a}} \left(A^* \frac{\partial \mathcal{H}}{\partial r_{i,a}} e^{-\beta \mathcal{H}} \right) \right.$$

$$\left. - \frac{\partial}{\partial r_{i,a}} \left(A^* \frac{\partial H}{\partial p_{i,a}} e^{-\beta \mathcal{H}} \right) \right]. \tag{A.3}$$

Performing the derivatives of the bracketed products, it is readily found the contributions involving the derivatives of $\mathcal{H}$ or the factor $\exp(-\beta \mathcal{H})$ cancel each other. As a result

$$(A, LB) = \frac{-i}{Z_N} \sum_{i,a} \int dr^N dp^N B \left[\frac{\partial \mathcal{H}}{\partial r_{i,a}} \frac{\partial A^*}{\partial p_{i,a}} - \frac{\partial \mathcal{H}}{\partial p_{i,a}} \frac{\partial A^*}{\partial r_{i,a}} \right] e^{-\beta \mathcal{H}}$$

$$= \langle B^* LA \rangle^* = (B, LA)^*. \tag{A.4}$$

Comparing (A.4) with (A.3) and noting that the phase-space variables are arbitrary, we immediately deduce that $L^\dagger = L$.

Appendix B

Classical time correlation functions and their spectra

In this appendix we shall discuss some general properties of the time correlation functions

$$C_{AB}(t) = (B(0), A(t)) = \langle B^*(0)A(t) \rangle$$

$$= \langle B^*(0) \exp(iLt)A(0) \rangle \tag{B.1}$$

where $A(0) = A$ and $B(0) = B$ are two dynamical variables (not necessarily real) of a classical system ruled by the Hamiltonian (1.1). The properties which we shall establish for $C_{AB}(t)$ will also provide useful relations for the corresponding frequency spectra

$$C_{AB}(\omega) = \frac{1}{2\pi} \int_{-\infty}^{\infty} dt \exp(-i\omega t) C_{AB}(t). \tag{B.2}$$

Together with (B.2), in the following we shall make use of the inverse Fourier transform

$$C_{AB}(t) = \int_{-\infty}^{\infty} d\omega \exp(i\omega t) C_{AB}(\omega). \tag{B.3}$$

The first property is a direct consequence of the Hermitian character of the Liouvillian (cf. Appendix A). Since $L^\dagger = L$, the time propagator $\exp(iLt)$ is unitary; that is, $[\exp(iLt)]^\dagger = \exp(-iLt)$. On the other hand, from the definition of Hermitian-conjugate operator one has that

$$C_{AB}(t) = \langle B^* \exp(iLt)A \rangle = \langle A^*[\exp(iLt)]^\dagger B \rangle^*. \tag{B.4}$$

Thus, as a result of the unitarity of $\exp(iLt)$ we find that

$$C_{AB}(t) = C_{BA}^*(-t). \tag{B.5}$$

Equation (B.5) is a particular case of the *stationarity property*

$$\langle B^*(0)A(t) \rangle = \langle B^*(\tau)A(t + \tau) \rangle \tag{B.6}$$

which is easily demonstrated by writing $\exp(iLt)$ as $\exp(-iL\tau)$. $\exp[iL(t + \tau)]$ and exploiting again the unitarity of the time propagator. Equation (8.6) states that the statistical averages are not affected by a shift

τ of the time origin. In particular, for $\tau = -t$ eqn (8.6) reduces to (8.5). Also, letting $t = 0$ eqn (B.6) gives $\langle B^* A \rangle = \langle B^*(\tau)A(\tau) \rangle$. In the special case that the variable B is simply a constant, we deduce that as a consequence of stationarity $\langle A(\tau) \rangle = \langle A(0) \rangle$; that is, the averages of a single dynamical variable at time τ and time zero are identical.

Suppose now that in the phase space $\{\mathbf{r}^N, \mathbf{p}^N\}$ we perform a transformation which changes the sign of all the momenta and leaves the positions unchanged. While the Hamiltonian $\mathcal{3C}$ is clearly invariant under this transformation, eqn (1.22) shows that the Liouvillian L changes sign, so that the time propagator $\exp(\mathrm{i}Lt)$ becomes $\exp(-\mathrm{i}Lt)$. In other words, the result of the transformation is an effective *time reversal* in the propagator. The dynamical variables of main interest in classical statistical mechanics usually have a definite 'parity' (or 'symmetry') under the change $\{\mathbf{r}^N, \mathbf{p}^N\} \to \{\mathbf{r}^N, -\mathbf{p}^N\}$, namely they are either invariant ('even') or change sign ('odd'). On the other hand, the statistical averages and the correlation functions are unchanged by the transformation. Thus, denoting with γ_A and γ_B the respective signatures of the variables A, B under this time reversal $(\gamma_A, \gamma_B = \pm 1)$, we have that $\langle B^* \exp(\mathrm{i}Lt)A \rangle = \gamma_A\gamma_B \langle B^* \exp(-\mathrm{i}Lt)A \rangle$, or

$$C_{AB}(t) = \gamma_A\gamma_B C_{AB}(-t). \tag{B.7}$$

In the case when A and B have the same time-reversal symmetry, $\gamma_A\gamma_B = 1$ and eqn (B.7) states that the correlation function $C_{AB}(t)$ is even in time. Vice versa, if $\gamma_A\gamma_B = -1$, $C_{AB}(t)$ is an odd function of time; in particular, the initial value of the correlation function of two variables with opposite time-reversal symmetry vanishes.

In view of its frequent occurrence, the special case of *time auto-correlation functions* $(B \equiv A)$ deserves a detailed discussion. Combining eqns (B.5) and (B.7) we find $(\gamma_A^2 = 1)$:

$$C_{AA}(t) = C_{AA}^*(-t) = C_{AA}(-t), \tag{B.8}$$

that is, $C_{AA}(t)$ is real and even in time. As a result, the spectrum $C_{AA}(\omega)$ is also a real and even function of the frequency ω

$$C_{AA}(\omega) = \frac{1}{\pi} \int_0^\infty \mathrm{d}t \cos(\omega t) C_{AA}(t) = C_{AA}(-\omega). \tag{B.9}$$

In terms of the Laplace transform

$$\tilde{C}_{AA}(z) = \int_0^\infty \mathrm{d}t \exp(-zt) C_{AA}(t) \tag{B.10}$$

the spectrum can be expressed by an analytic continuation in the complex plane near the imaginary axis:

$$C_{AA}(\omega) = \frac{1}{\pi} \operatorname{Re} \tilde{C}_{AA}(z = \mathrm{i}\omega + \varepsilon) \tag{B.11}$$

where $\varepsilon > 0$ is an infinitesimal quantity ensuring the convergence of (B.10). In practice, the term in ε is only needed when we deal with spectra with δ-like features. Because of the even character of the autocorrelation functions, the short time expansion of $C_{AA}(t)$

$$C_{AA}(t) = \sum_{n=0}^\infty \left[\frac{\mathrm{d}^n C_{AA}(t)}{\mathrm{d}t^n} \right]_{t=0} \frac{t^n}{n!} \equiv \sum_{n=0}^\infty (a_n/n!)t^n \tag{B.12}$$

is such that the coefficients a_n with odd n vanish. Exploiting eqn (B.3) we obtain

$$C_{AA}(t) = \sum_{n=0}^\infty \frac{1}{n!} \mathrm{i}^n (\overline{\omega^n})_{AA} t^n \tag{B.13}$$

where the quantity $(\overline{\omega^n})_{AA}$ (referred to as the nth *frequency moment* of the spectrum $C_{AA}(\omega)$) is defined by

$$(\overline{\omega^n})_{AA} \equiv \int_{-\infty}^\infty \mathrm{d}\omega\, \omega^n C_{AA}(\omega). \tag{B.14}$$

In the expansion (B.13) only even frequency moments yield a non-zero contribution. Letting $n = 2p$ we have

$$
\begin{aligned}
C_{AA}(t) &= \sum_{p=0}^\infty (-1)^p (\overline{\omega^{2p}})_{AA} [t^{2p}/(2p)!] \\
&= C_{AA}(0) - (1/2!)(\overline{\omega^2})_{AA} t^2 + (1/4!)(\overline{\omega^4})_{AA} t^4 - \cdots \\
&= C_{AA}(0)[1 - (1/2!)\langle \omega^2 \rangle_{AA} t^2 + (1/4!)\langle \omega^4 \rangle_{AA} t^4 - \cdots]
\end{aligned}
\tag{B.15}
$$

where in the last step we have introduced the 'normalized frequency moments' $\langle \omega^n \rangle_{AA} \equiv (\overline{\omega^n})_{AA}/(\overline{\omega^0})_{AA} = (\overline{\omega^n})_{AA}/C_{AA}(0)$.

Coming back to the general case, we may similarly introduce frequency moments $(\overline{\omega^n})_{AB}$ defined either in terms of a short-time expansion of $C_{AB}(t)$ (cf. (B.13)) or through frequency integrals involving the spectrum $C_{AB}(\omega)$ (cf. (B.14)). In any case

$$(\overline{\omega^n})_{AB} = (-\mathrm{i})^n \left[\frac{\mathrm{d}^n C_{AB}(t)}{\mathrm{d}t^n} \right]_{t=0} = (-\mathrm{i})^n \left\langle B^*(0) \left[\frac{\mathrm{d}^n A(t)}{\mathrm{d}t^n} \right]_{t=0} \right\rangle. \tag{B.16}$$

Noting that, for $n \geq 1$, $[\mathrm{d}^n A(t)/\mathrm{d}t^n] = \mathrm{i}L[\mathrm{d}^{n-1}A(t)/\mathrm{d}t^{n-1}]$, we may exploit the property (A.4) to write

$$\left\langle B^*(0)\left(\frac{\mathrm{d}^n A(t)}{\mathrm{d}t^n}\right)_{t=0}\right\rangle = -\left\langle \left(\frac{\mathrm{d}B^*(t)}{\mathrm{d}t}\right)_{t=0}\left(\frac{\mathrm{d}^{n-1}A(t)}{\mathrm{d}t^{n-1}}\right)_{t=0}\right\rangle.$$

$$\text{(B.17)}$$

The result (B.17) can obviously be iterated, and turns out to be very useful for the practical evaluation of the frequency moments. For example, if we deal with an autocorrelation function $C_{AA}(t)$, a repeated use of (B.17) leads to the following expressions for the second and fourth frequency moments:

$$(\overline{\omega^2})_{AA} = -\langle A^*(0)\ddot{A}(0)\rangle = \langle \dot{A}^*(0)\dot{A}(0)\rangle \qquad \text{(B.18)}$$

$$(\overline{\omega^4})_{AA} = \langle A^*(0)\ddddot{A}(0)\rangle = \langle \ddot{A}^*(0)\ddot{A}(0)\rangle \qquad \text{(B.19)}$$

where the dots indicate time derivatives.

Although the behaviour of correlation functions under a time-reversal transformation is clearly important in all dynamical properties, there are several other symmetry properties of the system which can be conveniently exploited to simplify the calculations. An example of such properties is the invariant character of the Hamiltonian $\mathcal{H}$ and of the Liouvillian L under an *inversion* transformation which changes the sign of all the coordinates and momenta of the particles of the system. Assuming that we deal with dynamical variables A, B which have a definite symmetry under the change $\{\mathbf{r}^N, \mathbf{p}^N\} \to \{-\mathbf{r}^N, -\mathbf{p}^N\}$, the correlation function $C_{AB}(t)$ vanishes unless A and B have the same parity (even or odd) under this inversion transformation. Another useful property is associated with the invariance of $\mathcal{H}$ and L under a *reflection* transformation, such as $\{(x^N, y^N, z^N), (p_x^N, p_y^N, p_z^N)\} \to \{(-x^N, y^N, z^N), (-p_x^N, p_y^N, p_z^N)\}$. The consequences of this reflection symmetry through the yz plane (or of the analogous reflections through the zx and xy planes) are that the correlation functions which change sign under these transformations are bound to vanish. While these symmetry operations are present even in a cubic crystal with the edges of the cell parallel to the (xyz) axes, in a *isotropic system* like a fluid additional simplifications are brought about by the *full rotational symmetry* (cf., for instance, the discussion in Section 3.4.3 about the various correlation functions of the microscopic stress tensor).

Finally, in a fluid another powerful symmetry operation is related to the invariance of $\mathcal{H}$ and L with respect to a shift of the origin of the reference frame by an arbitrary constant vector $\boldsymbol{\rho}$. The consequences of this *translational symmetry* under the transformation $(\mathbf{r}_i, \mathbf{p}_i) \to (\mathbf{r}_i + \boldsymbol{\rho}, \mathbf{p}_i)$ for $i = 1, \ldots, N$ are readily found in the case of dynamical variables of the form

$$A(\mathbf{k}) = \sum_i a(\mathbf{r}_i, \mathbf{p}_i)\exp(i\mathbf{k}\cdot\mathbf{r}_i) \qquad \text{(B.20)}$$

where the quantity a is not affected by the shift of the origin. Typical examples of this class are the quasi-conserved collective variables, namely the particle, current and energy densities (cf. (1.112), (1.115), and (1.173)). As a result of the above transformation, the correlation function $\langle A_2^*(\mathbf{k}, 0)A_1(\mathbf{k}', t)\rangle$ appears to change to $\exp[i(\mathbf{k}' - \mathbf{k})\cdot\boldsymbol{\rho}] < A_2^*(\mathbf{k}, 0) A_1(\mathbf{k}', t)\rangle$. Since the shift $\boldsymbol{\rho}$ is arbitrary, translational invariance requires that $\mathbf{k}' = \mathbf{k}$ in order to have a non-zero correlation. In other words,

$$\langle A_2^*(\mathbf{k}, 0)A_1(\mathbf{k}', t)\rangle = \langle A_2^*(\mathbf{k}, 0)A_1(\mathbf{k}, t)\rangle\delta_{\mathbf{k}',\mathbf{k}}. \qquad \text{(B.21)}$$

In a continuum representation of the wavevectors, the Kronecker δ is replaced by a Dirac δ according to the usual recipe

$$\delta_{\mathbf{k}',\mathbf{k}} \to [(2\pi)^3/V]\delta(\mathbf{k}' - \mathbf{k}). \qquad \text{(B.22)}$$

As is well known, a result similar to (B.21) holds even in crystalline solids, where the invariance is restricted to the discrete set of lattice vectors. In such a case, the equality $\mathbf{k}' = \mathbf{k}$ is valid only if the wavevectors $\mathbf{k}'$ and $\mathbf{k}$ lie in the same Brillouin zone of the reciprocal lattice space.

Appendix C

The light-scattering cross section for a system of interacting atoms

Although not conceptually difficult, the derivation of the result (2.43) for the correlation function involved in light scattering from an interacting system is much more involved than that for the corresponding result (2.23) for neutron scattering. Also, a comprehensive discussion of this subject is not easily found in the general literature (a notable exception being a review article by Gelbart (1974)). Hence, in this appendix we shall report the basic steps of this derivation, along with a more detailed discussion of several physical points which emerge in the course of the calculation.

C.1 THE PROBLEM

Let us consider an unperturbed system of N interacting atoms, and denote by $|\psi\rangle$ a stationary quantum state of the system. If the atoms are all identical and Z is their common atomic number, the properties of the system can in principle be deduced by solving a many-body Schrödinger equation for the N nuclei and the NZ electrons. This is clearly an impossible task if N or Z exceed a few units. In order to make the problem more manageable, one exploits the large difference between the masses of the electrons and of the nuclei, and resorts to the well-known 'Born–Oppenheimer approximation', which represents the eigenstates of the system as a product of nuclear eigenstates $|n\rangle$ and electronic eigenstates $|e^{(n)}\rangle$:

$$|\psi\rangle = |\psi(n, e)\rangle \approx |n\rangle |e^{(n)}\rangle. \tag{C.1}$$

Whereas the state $|n\rangle$ describes the distribution and the motion of the nuclei, the total electronic eigenstate $|e^{(n)}\rangle$ depends parametrically on the position of the nuclei, and is supposed to follow any nuclear motion instantaneously. As a result of the Born–Oppenheimer approximation, the two Hilbert spaces of the nuclei and of the electrons can be separated, and the eigenstates satisfy two distinct completeness relations of the form $\sum |..\rangle\langle..| = I$.

Let us now consider an *electromagnetic field* in a spatial region where

no field source is present ('radiation field'). It is well known that in such a case the properties of the field are completely specified by the 'vector potential' $\mathbf{A}(\mathbf{r})$, which is such that $\nabla \cdot \mathbf{A} \equiv 0$. In the formalism of second quantization, $\mathbf{A}(\mathbf{r})$ can be expressed in terms of photon annihilation and creation operators a and $a^\dagger$ as follows (Louisell 1973):

$$\mathbf{A}(\mathbf{r}) = \sum_{\mathbf{k},a} (2\pi\hbar c^2/\omega_k V)^{1/2} [a_{\mathbf{k}a} \exp(i\mathbf{k}\cdot\mathbf{r}) + a^\dagger_{\mathbf{k}a} \exp(-i\mathbf{k}\cdot\mathbf{r})]\mathbf{e}_{\mathbf{k}a} \tag{C.2}$$

where c is the velocity of the electromagnetic waves and $\omega_k = ck$. In other terms, the field has been decomposed into transverse plane-wave modes $(\mathbf{k}, a)$, each of which is specified by a wavevector $\mathbf{k}$, a polarization index a and a polarization vector $\mathbf{e}_{\mathbf{k}a}$ such that $\mathbf{k} \cdot \mathbf{e}_{\mathbf{k}a} = 0$. Strictly speaking, in eqn (C.2) V is simply the volume in which the field has been quantized; later on, for all practical purposes V can be identified with the volume of the system which scatters the photons. In the same formalism, the Hamiltonian of the field is known to be

$$\mathcal{H}_{\text{field}} = \sum_{\mathbf{k},a} \hbar\omega_k (a^\dagger_{\mathbf{k}a} a_{\mathbf{k}a} + \tfrac{1}{2}) \tag{C.3}$$

where $\hbar\omega_k$ is the energy of a photon with momentum $\hbar\mathbf{k}$.

At a given time (which we shall choose as $t = 0$) the atomic system and the radiation field are supposed to interact. The Hamiltonian describing this interaction can be written as (Louisell 1973)

$$\mathcal{H}_{\text{int}} = \sum_i \left[\frac{e}{m_e c} \mathbf{p}_i \cdot \mathbf{A}(\mathbf{r}_i) + \frac{e^2}{2m_e c^2} A^2(\mathbf{r}_i) \right]$$
$$+ \sum_a \left[-\frac{Z_a e}{M_a c} \mathbf{P}_a \cdot \mathbf{A}(\mathbf{R}_a) + \frac{Z_a^2 e^2}{2M_a c^2} A^2(\mathbf{R}_a) \right] \tag{C.4}$$

where $\mathbf{r}_i$ and $\mathbf{p}_i$ are the position and momentum operators of the ith electron with mass m_e and charge $-e$, and the index i runs over all the electrons of the system. Similarly, $\mathbf{R}_a$ and $\mathbf{P}_a$ are the position and momentum operators of the ath nucleus ($a = 1, \ldots, N$) with mass M_a and atomic number Z_a. Since $m_e \ll M_a$, the terms in the second summation on the right-hand side of eqn (C.4) can safely be neglected, and we are left with

$$\mathcal{H}_{\text{int}} = \sum_i \left[\frac{e}{m_e c} \mathbf{p}_i \cdot \mathbf{A}(\mathbf{r}_i) + \frac{e^2}{2m_e c^2} A^2(\mathbf{r}_i) \right]. \tag{C.5}$$

As a result of the interaction, the global system S made of the N interacting atoms plus the quantized radiation field performs a 'transition' from an initial state $|i\rangle$ to a final state $|f\rangle$. In particular, the atomic system we are

interested in evolves from an initial state $|a\rangle$ to a final one $|b\rangle$. In turn, the initial state of the field can be characterized by the presence of n_0 photons in the mode $(\mathbf{k}_0, a_0)$ and of n_1 photons in the mode $(\mathbf{k}_1, a_1)$; using a shorthand notation, this state will be denoted by $|n_0, n_1\rangle$. Then a typical *scattering process* can schematically be represented by the transition from $|i\rangle = |a\rangle |n_0, n_1\rangle$ to $|f\rangle = |b\rangle |(n_0 - 1), (n_1 + 1)\rangle$. In other terms, as far as the field is concerned, one photon has been 'transferred' from the mode $(\mathbf{k}_0, a_0)$ to the mode $(\mathbf{k}_1, a_1)$. We wish now to evaluate the transition probability of this overall process.

C.2   TIME-DEPENDENT PERTURBATION THEORY

The initial and final states of the global system S can be assumed to be eigenstates of the full unperturbed Hamiltonian $\mathcal{H}_S = \mathcal{H}_{syst} + \mathcal{H}_{field}$, where $\mathcal{H}_{syst}$ denotes the Hamiltonian of the atomic system. As a consequence, the transition occurs between initial and final stationary eigenstates which satisfy the time-independent Schrödinger equations $\mathcal{H}_S |i\rangle = E_i |i\rangle$ and $\mathcal{H}_S |f\rangle = E_f |f\rangle$, where E_i and E_f are the initial and final energy eigenvalues.

Assuming that the perturbation introduced by the interaction Hamiltonian $\mathcal{H}_{int}$ is small, at any time the state of S can be conveniently expressed as a linear combination of unperturbed eigenstates:

$$|\psi(t)\rangle = \sum_S c_S(t) \exp(-iE_S t/\hbar) |S\rangle \qquad (C.6)$$

where the possible occurrence of the transition $|i\rangle \to |f\rangle$ has been accounted for by allowing the coefficients $c_S(t)$ to be time dependent. In eqn (C.6), $|c_S(t)|^2$ is known to give the probability that the global system is found at time t in the eigenstate $|S\rangle$ with energy E_S. In the following, we are consequently interested in the evaluation of the quantity $|c_f(t)|^2$, with the condition that initially all the coefficients c_S vanish except $c_i = 1$.

A formal solution for $c_f(t)$ is readily obtained by inserting eqn (C.6) into the time-dependent Schrödinger equation $i\hbar |\dot{\psi}(t)\rangle = (\mathcal{H}_S + \mathcal{H}_{int}) |\psi(t)\rangle$. This reads:

$$c_f(t) = \delta_{f,i} - (i/\hbar) \sum_S \int_0^t d\tau \exp[-i(E_S - E_f)\tau/\hbar] \langle f|\mathcal{H}_{int}|S\rangle c_S(\tau). \qquad (C.7)$$

Equation (C.7) can be solved iteratively, provided that the effects of the perturbation are sufficiently small that the coefficients $c_S(t)$ are slowly

varying. At the zeroth order, we clearly obtain $c_f^{(0)}(t) = \delta_{f,i}$ (i.e. no transition at all). The first-order solution reads:

$$c_f^{(1)}(t) = \delta_{f,i} - (i/\hbar) \int_0^t d\tau \exp[-i\Omega_{if}\tau/\hbar] \langle f|\mathcal{H}_{int}|i\rangle \qquad (C.8)$$

where we have let $\Omega_{if} = (E_i - E_f)/\hbar$. Equation (C.8) involves the matrix element of the interaction Hamiltonian between the initial and the final states. At this order, only the second term on the right-hand side of eqn (C.5) turns out to be effective in giving rise to a scattering process. In fact, in view of the expansion (C.2), the term of $\mathcal{H}_{int}$ linear in $\mathbf{A}$ can just annihilate or create a single photon, thereby leading to absorption or emission of radiation, rather than to scattering. However, it is readily seen that the linear term does give rise to scattering processes if the iteration is carried out up to the second order. At this level it is found that

$$c_f^{(2)}(t) = c_f^{(1)}(t) - (1/\hbar^2) \sum_S \int_0^t d\tau \int_0^\tau d\tau' \exp(i\Omega_{fs}\tau) \exp(i\Omega_{si}\tau')$$

$$\langle f|\mathcal{H}_{int}|S\rangle \langle S|\mathcal{H}_{int}|i\rangle. \qquad (C.9)$$

The term in eqn (C.5) linear in $\mathbf{A}$ can now connect the initial and final states of the scattering process through the 'intermediate' states $|S\rangle$.

The matrix elements of $\mathcal{H}_{int}$ which appear in the expressions of $c_f^{(1)}(t)$ and $c_f^{(2)}(t)$ can be evaluated by making use of the following well known results for the photon creation and annihilation operators

$$a^\dagger |n\rangle = (n + 1)^{1/2} |(n + 1)\rangle \qquad a|n\rangle = n^{1/2} |(n - 1)\rangle \qquad (C.10)$$

along with $a^\dagger a|n\rangle = n|n\rangle$. In the present case, these relations refer to a specific field mode, whose indexes $(\mathbf{k}, a)$ have not been explicitly written out in eqn (C.10) for notational simplicity. Exploiting the orthonormal character of the photon states, from eqns (C.5), (C.2), and (C.10) we eventually obtain

$$\langle f|\mathcal{H}_{int}|i\rangle = \frac{2\pi\hbar e^2}{m_e V} \left[\frac{n_0(n_1 + 1)}{\omega_0 \omega_1}\right]^{1/2} (\mathbf{e}_0 \cdot \mathbf{e}_1) \left\langle b \left| \sum_i \exp[i(\mathbf{k}_0 - \mathbf{k}_1) \cdot \mathbf{r}_i] \right| a \right\rangle \qquad (C.11)$$

where ω_0, $\mathbf{e}_0$, ... are short-hand notations for ω_{k_0}, $\mathbf{e}_{k_0, \alpha_0}$, ... The calculation of the product of matrix elements appearing in eqn (C.9) is more cumbersome, and the result depends on the specific photon intermediate state $|I_{ph}\rangle$. After some algebra it is found that

$$\langle f| \mathcal{H}_{\mathrm{int}} |S\rangle \langle S| \mathcal{H}_{\mathrm{int}} |i\rangle = \frac{2\pi\hbar e^2}{m_e^2 V} \left[\frac{n_0(n_1 + 1)}{\omega_0 \omega_1} \right]^{1/2}$$

$$\times \begin{cases} \left\langle b \left| \sum_i \mathbf{p}_i \cdot \mathbf{e}_0 \exp(i\mathbf{k}_0 \cdot \mathbf{r}_i) \right| I \right\rangle \left\langle I \left| \sum_j \mathbf{p}_j \cdot \mathbf{e}_1 \exp(-i\mathbf{k}_1 \cdot \mathbf{r}_j) \right| a \right\rangle \\ \qquad\qquad\qquad \text{if } |I_{\mathrm{ph}}\rangle = |n_0, (n_1 + 1)\rangle \\[1em] \left\langle b \left| \sum_i \mathbf{p}_i \cdot \mathbf{e}_1 \exp(-i\mathbf{k}_1 \cdot \mathbf{r}_i) \right| I \right\rangle \left\langle I \left| \sum_j \mathbf{p}_j \cdot \mathbf{e}_0 \exp(+i\mathbf{k}_0 \cdot \mathbf{r}_j) \right| a \right\rangle \\ \qquad\qquad\qquad \text{if } |I_{\mathrm{ph}}\rangle = |(n_0 - 1), n_1\rangle \end{cases}$$

(C.12)

where $|I\rangle$ denotes an intermediate eigenstate of the atomic system.

C.3   THE SCATTERING TRANSITION PROBABILITY

The results (C.11) and (C.12) can now be inserted into the expression (C.9) of the coefficient $c_f(t)$. Before doing that, let us recall that usually the quantity of experimental interest is the probability of occurrence of the scattering transition (namely, $|c_f(t)|^2$) in a situation where any transient effect due to the 'switching on' of $\mathcal{H}_{\mathrm{int}}$ at $t = 0$ has disappeared. Formally, this can be achieved by letting $t \to \infty$ in the final result. We are ultimately interested in the scattering cross section, which depends on the probability of the scattering event *per unit time* (the so-called 'transition probability'). As a consequence, we have to evaluate the quantity $|c_f(t)|^2/t$ in a situation where $t \to \infty$.

The first step is to perform the time integrals in eqns (C.8) and (C.9). This is easily done for eqn (C.8), with the result that

$$c_f^{(1)}(t) = \delta_{f,i} - \langle f| \mathcal{H}_{\mathrm{int}} |i\rangle \frac{\exp(i\Omega_{fi}t) - 1}{\hbar\Omega_{fi}}.$$

(C.13)

Here

$$\hbar\Omega_{fi} \equiv E_f - E_i = E_b - E_a + \hbar(\omega_1 - \omega_0)$$

(C.14)

where E_a and E_b denote the initial and final energies of the atomic system. The evaluation of the double integral in eqn (C.9) is slightly more involved. Performing the integration over τ', we obtain

$$\int_0^t d\tau \int_0^\tau d\tau' \exp(i\Omega_{fS}\tau)\exp(i\Omega_{Si}\tau') = (1/i\Omega_{Si})\int_0^t d\tau [\exp(i\Omega_{fi}\tau) - \exp(i\Omega_{fS}\tau)].$$

(C.15)

As we shall see later on in this section, the important scattering events are such that the total energy of the global system is conserved. Consequently, in eqn (C.15) the quantity Ω_{fi} is very small. On the other hand, no such restriction exists for $\Omega_{fS} = (E_f - E_S)/\hbar \approx (E_i - E_S)/\hbar$, which remains finite. As a result, the phase of the second exponential is never close to zero, yielding rapid oscillations (and eventually a vanishing time integral) as $t \to \infty$. Hence, collecting all the previous results eqn (C.9) can be written as

$$c_f^{(2)}(t) = \delta_{f,i} - \frac{2\pi\hbar e^2}{m_e V} \left[\frac{n_0(n_1 + 1)}{\omega_0\omega_1} \right]^{1/2} \frac{\exp(i\Omega_{fi}t) - 1}{\Omega_{fi}} M_{ba}$$ (C.16)

where $M_{ba} = \langle b|M|a\rangle = M_{ab}^*$ is the matrix element of the operator

$$M \equiv (\mathbf{e}_0 \cdot \mathbf{e}_1) \sum_i \exp[i(\mathbf{k}_0 - \mathbf{k}_1) \cdot \mathbf{r}_i]$$

$$- \frac{1}{m_e} \sum_I \left\{ \frac{\sum_i \mathbf{p}_i \cdot \mathbf{e}_0 \exp(i\mathbf{k}_0 \cdot \mathbf{r}_i) \left| I \right\rangle \left\langle I \right| \sum_j \mathbf{p}_j \cdot \mathbf{e}_1 \exp(-i\mathbf{k}_1 \cdot \mathbf{r}_j)}{E_I - E_a + \hbar\omega_1} \right.$$

$$\left. + \frac{\sum_i \mathbf{p}_i \cdot \mathbf{e}_1 \exp(-i\mathbf{k}_1 \cdot \mathbf{r}_i) \left| I \right\rangle \left\langle I \right| \sum_j \mathbf{p}_j \cdot \mathbf{e}_0 \exp(i\mathbf{k}_0 \cdot \mathbf{r}_j)}{E_I - E_a - \hbar\omega_0} \right\}.$$

(C.17)

In obtaining eqns (C.16)–(C.17), we have made use of the following results for the quantity Ω_{Si}:

$$\hbar\Omega_{Si} = E_S - E_i = (E_I + E_{I_{\mathrm{ph}}}) - (E_a + n_0\hbar\omega_0 + n_1\hbar\omega_1)$$
$$= \begin{cases} E_I - E_a + \hbar\omega_1 & \text{if } |I_{\mathrm{ph}}\rangle = |n_0, (n_1 + 1)\rangle \\ E_I - E_a - \hbar\omega_0 & \text{if } |I_{\mathrm{ph}}\rangle = |(n_0 - 1), n_1\rangle \end{cases}$$ (C.18)

according to the two cases seen in eqn (C.12). Noting that in a real scattering event the initial and the final states are necessarily different and $\delta_{f,i} = 0$, for the quantity $|c_f(t)|^2$ we obtain

$$|c_f(t)|^2 = \left(\frac{2\pi\hbar e^2}{m_e V} \right)^2 \frac{n_0(n_1 + 1)}{\omega_0\omega_1} \frac{4\sin^2(\Omega_{fi}t/2)}{\Omega_{fi}^2} |M_{ba}|^2$$ (C.19)

Performing the limit $t \to \infty$ and exploiting the result $\lim_{t\to\infty} \sin^2(at)/a^2 t = \pi\delta(a)$, the scattering transition probability $W_{\mathrm{scatt}} = |c_f(t)|^2/t$ can eventually be written as

$$W_{\text{scatt}} = \left(\frac{2\pi e^2}{m_e V}\right)^2 \cdot \frac{n_0(n_1+1)}{\omega_0 \omega_1} |M_{ba}|^2 2\pi\delta\left(\frac{E_b - E_a}{\hbar} + \omega_1 - \omega_0\right)$$

(C.20)

where clearly the δ-function reflects the conservation of energy in the scattering process.

C.4   THE ELECTRIC DIPOLE APPROXIMATION

In a tight-bonding model of the N-atom system, the electrons can be considered as 'belonging' to their respective nuclei. This implies that in eqn (C.17) each of the two summations over i, j (which run over all the electrons of the system) can be replaced by a double sum over the nuclei and over their respective bound electrons. Also, in this appendix we are primarily interested in light scattering and we can exploit the fact that the atomic sizes are much smaller than the optical wavelengths (the so-called 'electric dipole approximation'). Therefore, in the quantity M the terms involving $\exp(\pm i k_{0,1} \cdot r_i)$ can be approximated as

$$\sum_i \exp(\pm i k_{0,1} \cdot r_i) = \sum_\alpha Z_\alpha \exp(\pm i k_{0,1} \cdot R_\alpha)$$

(C.21)

$$\sum_i p_i \cdot e_{0,1} \exp(\pm i k_{0,1} \cdot r_i) = \sum_\alpha \exp(\pm i k_{0,1} \cdot R_\alpha) \sum_{i_\alpha} p_{i_\alpha} \cdot e_{0,1}.$$

(C.22)

As a result, the scattering transition probability can be written in the form (C.20), where

$$M_{ba} = A_{ba} + (B_{ba} + C_{ba})$$

(C.23)

and

$$A_{ba} = (e_0 \cdot e_1)\left\langle b \left| \sum_\alpha Z_\alpha \exp[i(k_0 - k_1) \cdot R_\alpha] \right| a \right\rangle,$$

(C.24)

$$B_{ba} = \frac{-1}{m_e} \sum_I \frac{\left\langle b \left| \sum_\alpha \exp(ik_0 \cdot R_\alpha) \sum_{i_\alpha} p_{i_\alpha} \cdot e_0 \right| I \right\rangle \left\langle I \left| \sum_\beta \exp(-ik_1 \cdot R_\beta) \sum_{j_\beta} p_{j_\beta} \cdot e_1 \right| a \right\rangle}{E_I - E_a + \hbar\omega_1},$$

(C.25)

$$C_{ba} = \frac{-1}{m_e} \sum_I \frac{\left\langle b \left| \sum_\alpha \exp(-ik_1 \cdot R_\alpha) \sum_{i_\alpha} p_{i_\alpha} \cdot e_1 \right| I \right\rangle \left\langle I \left| \sum_\beta \exp(ik_0 \cdot R_\beta) \sum_{j_\beta} p_{j_\beta} \cdot e_0 \right| a \right\rangle}{E_I - E_a - \hbar\omega_0}.$$

(C.26)

C.5   A CLASSIFICATION OF THE ENERGY LEVELS

As a result of the Born–Oppenheimer approximation, the total energy of the N-atom system can be split into nuclear and electronic contributions. The nuclear component is given by the sum of the kinetic and potential energy of the nuclei, and in the present context can be referred to as the *translational energy*, with a magnitude $\approx Nk_B T$. For a specific eigenstate $|m\rangle$ of the N-atom system with energy E_m, the above mentioned separation can be expressed by the relations

$$|m\rangle = |t_m\rangle \cdot |e_m(t_m)\rangle$$

(C.27)

$$E_m = E_m^{(t)} + E_m^{(e)}$$

(C.28)

where the labels t and e stand respectively for translational and electronic.

Before proceeding, it is important to realize the relative order of magnitude of the different energies which are involved in W_{scatt}. A convenient reference point is provided by the energy of the electronic ground state. When referred to this level, the electronic energies are distinctly larger than both the translational ones and the photon energies typical of the optical range. More precisely, at room temperature, thermal energies are found to be two orders of magnitude smaller than those of optical photons; in turn, the latter are smaller than those typical of the electronic transitions. For example, Table 2.2 shows that even in the unfavourable case of xenon, the first excited electronic level of rare-gas atoms has an energy definitely greater than that of optical photons.

In view of all this, assuming that initially the N-atom system is in its ground electronic state, we argue that even the final electronic level is the ground state. Therefore the matrix elements (C.24)–(C.26) can be written as

$$A_{ba} = (e_0 \cdot e_1)\left\langle t_b \left| \sum_\alpha Z_\alpha \exp[i(k_0 - k_1) \cdot R_\alpha] \right| t_a \right\rangle,$$

(C.29)

$$B_{ba} = \frac{-1}{m_e} \sum_{t_I, e_I} \frac{\left\langle t_b \left| \sum_\alpha \exp(ik_0 \cdot R_\alpha) p_{\alpha, bI} \cdot e_0 \right| t_I \right\rangle \left\langle t_I \left| \sum_\beta \exp(-ik_1 \cdot R_\beta) p_{\beta, Ia} \cdot e_1 \right| t_a \right\rangle}{E_I^{(e)} - E_a^{(e)} + E_I^{(t)} - E_a^{(t)} + \hbar\omega_1},$$

(C.30)

$$C_{ba} = \frac{-1}{m_e} \sum_{t_I, e_I} \frac{\left\langle t_b \left| \sum_\alpha \exp(-ik_1 \cdot R_\alpha) p_{\alpha, bI} \cdot e_1 \right| t_I \right\rangle \left\langle t_I \left| \sum_\beta \exp(ik_0 \cdot R_\beta) p_{\beta, Ia} \cdot e_0 \right| t_a \right\rangle}{E_I^{(e)} - E_a^{(e)} + E_I^{(t)} - E_a^{(t)} + \hbar\omega_0},$$

(C.31)

where we have let

$$\mathbf{p}_{\alpha, bI} \equiv \left\langle e_b(t_b) \middle| \sum_{i_\alpha} \mathbf{p}_{i_\alpha} \middle| e_I(t_I) \right\rangle, \tag{C.32}$$

$$\mathbf{p}_{\beta, Ia} \equiv \left\langle e_I(t_I) \middle| \sum_{j_\beta} \mathbf{p}_{j_\beta} \middle| e_a(t_a) \right\rangle. \tag{C.33}$$

Assuming that both $|e_a\rangle$ and $|e_b\rangle$ coincide with the electronic ground state, $E_a^{(e)} = E_b^{(e)}$ and the energy conservation relation becomes simply

$$E_a^{(t)} + \hbar\omega_0 = E_b^{(t)} + \hbar\omega_1 \tag{C.34}$$

As a result, the energy denominator in eqn (C.30) can be written as $E_I^{(e)} - E_a^{(e)} + E_I^{(t)} - E_b^{(t)} + \hbar\omega_0$. We shall now exploit the above-mentioned fact that the energy difference between the electronic levels is distinctly larger than the other energy terms in the denominators of eqns (C.30) and (C.31). In particular, the translational energy differences are the smallest ones, and can safely be neglected.

A first consequence of this approximation is that in the expressions of B_{ba} and C_{ba} we may now make use of the completeness relation for the intermediate translational states, obtaining

$$B_{ba} = \frac{-1}{m_e} \sum_{e_I} \frac{\left\langle t_b \middle| \sum_\alpha \exp(i\mathbf{k}_0 \cdot \mathbf{R}_\alpha) \mathbf{p}_{\alpha, bI} \cdot \mathbf{e}_0 \sum_\beta \exp(-i\mathbf{k}_1 \cdot \mathbf{R}_\beta) \mathbf{p}_{\beta, Ia} \cdot \mathbf{e}_1 \middle| t_a \right\rangle}{E_I^{(e)} - E_a^{(e)} + \hbar\omega_0}, \tag{C.35}$$

$$C_{ba} = \frac{-1}{m_e} \sum_{e_I} \frac{\left\langle t_b \middle| \sum_\alpha \exp(-i\mathbf{k}_1 \cdot \mathbf{R}_\alpha) \mathbf{p}_{\alpha, bI} \cdot \mathbf{e}_1 \sum_\beta \exp(i\mathbf{k}_0 \cdot \mathbf{R}_\beta) \mathbf{p}_{\beta, Ia} \cdot \mathbf{e}_0 \middle| t_a \right\rangle}{E_I^{(e)} - E_a^{(e)} + \hbar\omega_0}, \tag{C.36}$$

Next, we may expand the energy denominators in the photon energy $\hbar\omega_0$. In the *zeroth-order* result ($\hbar\omega_0 = 0$) we exploit the Heisenberg equation of motion $\mathbf{p}_{i_\alpha} = (m/i\hbar)\,[\mathbf{r}_{i_\alpha}, \mathcal{H}^{(e)}]$, where $\mathcal{H}^{(e)}$ is the electronic Hamiltonian. By definition, the eigenstates of $\mathcal{H}^{(e)}$ are the states $|e_m(t_m)\rangle$ introduced in eqn (C.27). Using this property and the completeness relation for the electronic eigenstates, at the zeroth order in $\hbar\omega_0$ eqns (C.35) and (C.36) can be written as

$$B_{ba}^{(0)} = \frac{-i}{\hbar} \left\langle t_b \middle| \sum_\alpha \exp(i\mathbf{k}_0 \cdot \mathbf{R}_\alpha) \left\langle e_a \middle| \sum_{i_\alpha, j_\beta} \mathbf{p}_{i_\alpha} \cdot \mathbf{e}_0 \, \mathbf{r}_{j_\beta} \cdot \mathbf{e}_1 \middle| e_a \right\rangle \sum_\beta \exp(-i\mathbf{k}_1 \cdot \mathbf{R}_\beta) \middle| t_a \right\rangle, \tag{C.37}$$

$$C_{ba}^{(0)} = \frac{i}{\hbar} \left\langle t_b \middle| \sum_\beta \exp(-i\mathbf{k}_1 \cdot \mathbf{R}_\beta) \left\langle e_a \middle| \sum_{i_\alpha, j_\beta} \mathbf{r}_{j_\beta} \cdot \mathbf{e}_1 \, \mathbf{p}_{i_\alpha} \cdot \mathbf{e}_0 \middle| e_a \right\rangle \sum_\alpha \exp(i\mathbf{k}_0 \cdot \mathbf{R}_\alpha) \middle| t_a \right\rangle. \tag{C.38}$$

In eqns (C.37)–(C.38) the inner average over the electronic states depends on the nuclear positions only parametrically. Hence the exponentials containing $\mathbf{R}_\alpha$ and $\mathbf{R}_\beta$ can safely be interchanged. Summing the two results we arrive at

$$B_{ba}^{(0)} + C_{ba}^{(0)} = \frac{-i}{\hbar} \left\langle t_b \middle| \sum_{\alpha, \beta} \exp[i(\mathbf{k}_0 \cdot \mathbf{R}_\alpha - \mathbf{k}_1 \cdot \mathbf{R}_\beta)] \mathbf{e}_0 \cdot \left\langle e_a \middle| \sum_{i_\alpha, j_\beta} [\mathbf{p}_{i_\alpha}, \mathbf{r}_{j_\beta}] \middle| e_a \right\rangle \cdot \mathbf{e}_1 \middle| t_a \right\rangle$$

$$= -\left\langle t_b \middle| \sum_\alpha Z_\alpha \exp[i(\mathbf{k}_0 - \mathbf{k}_1) \cdot \mathbf{R}_\alpha] \middle| t_a \right\rangle (\mathbf{e}_0 \cdot \mathbf{e}_1) \tag{C.39}$$

where in the last step we have used the commutation relation between the electronic position and momentum. It is easily seen that the result (C.39) cancels exactly the contribution (C.29) from A_{ba}. Therefore, at the zeroth order in $\hbar\omega_0$ the contribution to the cross section vanishes identically.

Similar manipulations can be made in the *first-order* terms of the expansion in $\hbar\omega_0$. Again, one exploits the expression of the momentum operator $\mathbf{p}_{i_\alpha}$ in terms of $[\mathbf{r}_{i_\alpha}, \mathcal{H}^{(e)}]$. The final result of this first order calculation is that $B_{ba}^{(1)} + C_{ba}^{(1)} \equiv 0$.

Turning eventually to the *second-order* contributions, we may again make use of the above-mentioned expression of $\mathbf{p}_{i_\alpha}$ in both $B_{ba}^{(2)}$ and $C_{ba}^{(2)}$. The final result for these two quantities is

$$B_{ba}^{(2)} = -m_e \omega_0^2 \left\langle t_b \middle| \sum_{\alpha, \beta} \exp[i(\mathbf{k}_0 \cdot \mathbf{R}_\alpha - \mathbf{k}_1 \cdot \mathbf{R}_\beta)] \right.$$

$$\sum_{e_I} \frac{\left\langle e_a \middle| \sum_{i_\alpha} \mathbf{r}_{i_\alpha} \cdot \mathbf{e}_0 \middle| e_I \right\rangle \left\langle e_I \middle| \sum_{j_\beta} \mathbf{r}_{j_\beta} \cdot \mathbf{e}_1 \middle| e_a \right\rangle}{E_I^{(e)} - E_a^{(e)}} \left| t_a \right\rangle \tag{C.40}$$

$$C_{ba}^{(2)} = -m_e \omega_0^2 \left\langle t_b \middle| \sum_{\alpha, \beta} \exp[i(\mathbf{k}_0 \cdot \mathbf{R}_\alpha - \mathbf{k}_1 \cdot \mathbf{R}_\beta)] \right.$$

$$\sum_{e_I} \frac{\left\langle e_a \middle| \sum_{j_\beta} \mathbf{r}_{j_\beta} \cdot \mathbf{e}_1 \middle| e_I \right\rangle \left\langle e_I \middle| \sum_{i_\alpha} \mathbf{r}_{i_\alpha} \cdot \mathbf{e}_0 \middle| e_a \right\rangle}{E_I^{(e)} - E_a^{(e)}} \left| t_a \right\rangle \tag{C.41}$$

Strictly speaking, the many-body character of these expressions prevents any separation of single-atom contributions. Indeed, $B_{ba}^{(2)}$ and $C_{ba}^{(2)}$ are seen to involve operators associated with different atoms, correlated by a

common many-atom electronic term. In the general case, a rigorous quantum-mechanical solution of this problem is clearly impossible. In order to proceed, we have then to resort to some approximate physical arguments.

Let us tentatively assume that for different atoms the electronic eigenstates could be factorized. In such a limiting case, the intermediate state $|e_I\rangle$ would become a product of single-atom states in which only one atom moves to an excited level while all the others remain in their ground state. Consequently, in this scheme the indexes α and β in the electronic averages inside $B_{ba}^{(2)}$ and $C_{ba}^{(2)}$ should refer to the same atom. We shall suppose that a factor $\delta_{\alpha,\beta}$ is present even in the general case. If we now introduce the *polarizability of the α-th atom* defined as (Gelbart 1974)

$$\mathbf{A}_\alpha = 2e^2 \sum_{e_I} \frac{\left\langle e_a \left| \sum_{i_\alpha} \mathbf{r}_{i_\alpha} \right| e_I \right\rangle \left\langle e_I \left| \sum_{j_\alpha} \mathbf{r}_{j_\alpha} \right| e_a \right\rangle}{E_I^{(e)} - E_a^{(e)}} \qquad (C.42)$$

it turns out that $\mathbf{A}_\alpha$ depends on the position of all the atoms of the system only in a parametric way, and the expressions of $B_{ba}^{(2)}$ and $C_{ba}^{(2)}$ become much simpler. Adding these two terms, we end up with the result

$$M_{ba} = B_{ba}^{(2)} + C_{ba}^{(2)}$$
$$= \frac{-m_e \omega_0^2}{e^2} \left\langle t_b \left| \sum_\alpha \exp(i\mathbf{k} \cdot \mathbf{R}_\alpha) \, \mathbf{e}_0 \cdot \mathbf{A}_\alpha \cdot \mathbf{e}_1 \right| t_a \right\rangle \qquad (C.43)$$

where we have let $\mathbf{k} = \mathbf{k}_0 - \mathbf{k}_1$. The result (C.43) is valid for 'quasi-elastic' scattering of photons in the optical region, and is eventually to be inserted into eqn (C.20).

Equation (C.43) relies on the assumption of an absence of any dynamic interaction among the different atoms during the scattering event. In other words, the latter is assumed to occur on a single atom, involving transitions between the electronic states determined by the instantaneous local configuration of the neighbouring atoms. In this context, it should be stressed that the 'atomic' polarizability as defined in eqn (C.42), rather than being a strict single-atom quantity, depends on the positions of all the particles of the system. As a consequence, the spatial distribution of neighbouring atoms does affect the properties of each scattering centre; in a dense fluid, this yields an effective dependence of the atomic polarizability on the density of the system.

C.5 THE SCATTERING CROSS SECTION

In the derivation of eqn (C.20) for W_{scatt} we have tacitly assumed we are dealing with a well-defined final photon state. In practice, the scattered photons are instead detected within a certain solid angle around the scattering direction in a laboratory frame, and only an analysis of their energy is performed. In order to evaluate the transition probability appropriate for this situation, we have to take into account all the accessible final photon states.

The number of modes of the electromagnetic field within the solid angle $d\Omega$ and having a fixed polarization and a frequency in the interval $(\omega_1, \omega_1 + d\omega_1)$ is known to be (Louisell 1973)

$$dn_1 = \frac{V}{(2\pi c)^3} \omega_1^2 \, d\omega_1 \, d\Omega. \qquad (C.44)$$

Therefore, the transition probability from the translational state $|t_a\rangle$ to the state $|t_b\rangle$, with a simultaneous scattering in the solid angle $d\Omega$ of a photon with energy in the range $d(\hbar\omega_1)$ around $\hbar\omega_1$ is given by the product of eqn (C.20) and (C.44):

$$dW_{a,b} = r_e^2 \frac{n_0(n_1+1)c}{V} \frac{\omega_1}{\omega_0} |M_{ab}|^2 \delta\left(\frac{E_b^{(t)} - E_a^{(t)}}{\hbar} + \omega_1 - \omega_0\right) d\omega_1 \, d\Omega \qquad (C.45)$$

where $r_e \equiv e^2/m_e c^2 \approx 2.8 \times 10^{-13}$ cm is the so-called 'classical radius' of the electron, and $M_{ab} = M_{ba}^*$ is given by eqn (C.43). In order to obtain the actual scattering cross section, eqn (C.45) must firstly be divided by the flux $n_0 c/V$ of the incident photons. The result must then be summed over the final translational states $|t_b\rangle$, and averaged over the initial states $|t_a\rangle$ according to their statistical weight p_a. Hence the differential scattering cross section can be expressed as

$$\frac{d^2\sigma}{d\Omega \, d\omega_1} = r_e^2 (n_1+1) \frac{\omega_1}{\omega_0} \left(\frac{m_e \omega_0^2}{e^2}\right)^2 \sum_{t_a} p_a \sum_{t_b} \left\langle t_a \left| \sum_\alpha \exp(-i\mathbf{k} \cdot \mathbf{R}_\alpha)(\mathbf{e}_0 \cdot \mathbf{A}_\alpha \cdot \mathbf{e}_1)^\dagger \right| t_b \right\rangle$$
$$\left\langle t_b \left| \sum_\beta \exp(i\mathbf{k} \cdot \mathbf{R}_\beta)(\mathbf{e}_0 \cdot \mathbf{A}_\beta \cdot \mathbf{e}_1) \right| t_a \right\rangle \delta\left(\frac{E_b^{(t)} - E_a^{(t)}}{\hbar} + \omega_1 - \omega_0\right). \qquad (C.46)$$

It is now convenient to exploit in eqn (C.46) the well-known integral representation the δ-function, $\delta(x) = (1/2\pi)\int_{-\infty}^{\infty} dt \exp(ixt)$. Letting $\omega = \omega_0 - \omega_1$ (cf. eqn (2.2); positive ω refer to the 'Stokes' side of the spectrum) and recalling that $|t_a\rangle$ and $|t_b\rangle$ are eigenstates of the translational Hamiltonian $\mathcal{H}$, eqn (C.46) can be written as

$$\frac{d^2\sigma}{d\Omega d\omega_1} = r_e^2(n_1 + 1)\frac{\omega_1}{\omega_0}\left(\frac{m_e^2\omega_0^4}{2\pi e^4}\right)\sum_{t_a}p_a\sum_{t_b}\left\langle t_a\left|\sum_\alpha \exp(-i\mathbf{k}\cdot\mathbf{R}_\alpha)(\mathbf{e}_0\cdot\mathbf{A}_\alpha\cdot\mathbf{e}_1)^\dagger\right|t_b\right\rangle$$

$$\int_{-\infty}^{\infty}dt\exp(-i\omega t)\left\langle t_b\left|\exp(i\mathcal{H}t/\hbar)\sum_\beta \exp(i\mathbf{k}\cdot\mathbf{R}_\beta)(\mathbf{e}_0\cdot\mathbf{A}_\beta\cdot\mathbf{e}_1)\right.\right.$$

$$\left.\left.\exp(-i\mathcal{H}t/\hbar)\right|t_a\right\rangle. \tag{C.47}$$

Finally, introducing time-dependent operators in the Heisenberg picture and exploiting the completeness relation for the translational states $|t_b\rangle$, the differential cross section becomes

$$\frac{d^2\sigma}{d\Omega\, d\omega} = \frac{N}{2\pi}(n_1 + 1)(\omega_0 - \omega)\omega_0^3\left(\frac{m_e r_e}{e^2}\right)^2\int_{-\infty}^{\infty}dt\exp(-i\omega t)I_L(\mathbf{k}, t) \tag{C.48}$$

where the quantity

$$I_L(\mathbf{k}, t) \equiv \frac{1}{N}\sum_{t_a}p_a\left\langle t_a\left|\sum_\alpha \exp[-i\mathbf{k}\cdot\mathbf{R}_\alpha(0)](\mathbf{e}_0\cdot\mathbf{A}_\alpha(0)\cdot\mathbf{e}_1)^\dagger\right.\right.$$

$$\left.\left.\sum_\beta \exp[i\mathbf{k}\cdot\mathbf{R}_\beta(t)](\mathbf{e}_0\cdot\mathbf{A}_\beta(t)\cdot\mathbf{e}_1)\right|t_a\right\rangle$$

$$= \frac{1}{N}\sum_{\alpha,\beta}\left\langle\exp[-i\mathbf{k}\cdot\mathbf{R}_\alpha(0)](\mathbf{e}_0\cdot\mathbf{A}_\alpha(0)\cdot\mathbf{e}_1)^\dagger\right.$$

$$\left.(\mathbf{e}_0\cdot\mathbf{A}_\beta(t)\cdot\mathbf{e}_1)\exp[i\mathbf{k}\cdot\mathbf{R}_\beta(t)]\right\rangle \tag{C.49}$$

can be interpreted as the time correlation function which is probed in light-scattering experiments. The quantity (C.49) is just the 'intermediate scattering function for light scattering' introduced in Section 2.3.6 (cf. eqn (2.43)).

The total cross section is obtained integrating (C.48) in $d\omega$. If we neglect the small difference between $(\omega_0 - \omega)$ and ω_0 (quasi-elastic scattering) the integration is immediate and gives:

$$\frac{d\sigma}{d\Omega} = (n_1 + 1)N\omega_0^4\left(\frac{m_e r_e}{e^2}\right)^2 I_L(\mathbf{k}, t = 0) \tag{C.50}$$

which shows the characteristic ω_0^4 dependence typical of Rayleigh scattering. For the quantity $I_L(\mathbf{k}, t = 0)$ appearing in eqn (C.50) we may

exploit the fact that, although $\mathbf{R}_\alpha(0)$ and $\mathbf{R}_\beta(t)$ in general do not commute, they do when $t = 0$. Therefore, even in the quantum case we may write

$$I_L(\mathbf{k}, t = 0) = \frac{1}{N}\left\langle\sum_{\alpha,\beta}\exp[-i\mathbf{k}\cdot(\mathbf{R}_\alpha - \mathbf{R}_\beta)](\mathbf{e}_0\cdot\mathbf{A}_\alpha\cdot\mathbf{e}_1)^\dagger(\mathbf{e}_0\cdot\mathbf{A}_\beta\cdot\mathbf{e}_1)\right\rangle. \tag{C.51}$$

REFERENCES

Gelbart, W. (1974). *Adv. Chem. Phys.*, **24**, 1.

Louisell, W. H. (1973). *Quantum-statistical properties of radiation*. Wiley, New York.

Appendix D

Symmetry properties of the memory functions

Given an orthogonal set $\{A_\nu\}$ of dynamical variables, the basic results of Section 3.1 for the correlation functions $C_{\lambda\nu}(t) = (A_\nu, A_\lambda(t))$ can be summarized by the memory equation

$$\dot{C}_{\lambda\nu}(t) = \sum_{\lambda'} \left[i\Omega_{\lambda\lambda'} C_{\lambda'\nu}(t) - \int_0^t d\tau\, K_{\lambda\lambda'}(\tau) C_{\lambda'\nu}(t-\tau) \right]. \qquad (D.1)$$

Here the elements of the proper frequency matrix and of the memory matrix are respectively defined as

$$i\Omega_{\lambda\lambda'} = (A_{\lambda'}, iLA_\lambda)/(A_\lambda, A_\lambda) \qquad (D.2)$$

$$K_{\lambda\lambda'}(t) = (f_{\lambda'}, \exp[i(1-\mathcal{P})Lt]f_\lambda)/(A_\lambda, A_\lambda) \qquad (D.3)$$

where $\mathcal{P}$ is the projection operator (3.8) over the set $\{A_\nu\}$ and $f_\lambda = i(1-\mathcal{P})LA_\lambda$ are the components of the fluctuating force.

We wish to discuss the consequences of the time-reversal symmetry on the quantities $\Omega_{\lambda\lambda'}$ and $K_{\lambda\lambda'}(t)$. This is straightforward for the proper frequency matrix elements (D.2), which are ordinary static correlation functions. Since under the transformation $\{\mathbf{r}^N, \mathbf{p}^N\} \to \{\mathbf{r}^N, -\mathbf{p}^N\}$ the Liouvillian L changes sign, the result (B.7) can now be written as $(A_{\lambda'}, LA_\lambda) = -\gamma_\lambda \gamma_{\lambda'} (A_{\lambda'}, LA_\lambda)$, where γ_λ and $\gamma_{\lambda'}$ and the signatures of A_λ and $A_{\lambda'}$. Noting that the quantity (A_λ, A_λ) is unchanged by the transformation, we obtain

$$\Omega_{\lambda\lambda'} = -\gamma_\lambda \gamma_{\lambda'} \Omega_{\lambda\lambda'}. \qquad (D.4)$$

This result tells us that the element $\Omega_{\lambda\lambda'}$ is different from zero only if the variables A_λ and $A_{\lambda'}$ have opposite time-reversal symmetries. Consequently, all the diagonal elements of the proper frequency matrix identically vanish.

On the other hand, the analysis of the symmetry properties of $K_{\lambda\lambda'}(t)$ is less immediate because of the presence of the anomalous propagator $\exp[i(1-\mathcal{P})Lt]$. Denoting again by γ_λ the signature of the variable A_λ, under time-reversal the projection operator $\mathcal{P} = \sum_\lambda (A_\lambda, \ldots)$ $(A_\lambda, A_\lambda)^{-1} A_\lambda$ changes according to $\mathcal{P} \to \gamma_\lambda \gamma_\lambda^2 \gamma_\lambda \mathcal{P}$. Since $\gamma_\lambda^2 = 1$, both

$\mathcal{P}$ and $(1-\mathcal{P})$ are unchanged by the transformation, whereas the fluctuating forces f_λ and the anomalous propagator become respectively $-\gamma_\lambda f_\lambda$ and $\exp[-i(1-\mathcal{P})Lt]$. As a result, the overall time-reversal symmetry requires that

$$K_{\lambda\lambda'}(t) = \gamma_\lambda \gamma_{\lambda'} K_{\lambda\lambda'}(-t). \qquad (D.5)$$

Comparing with (B.7), we see that memory functions behave as ordinary time correlations as far as time-reversal symmetry is concerned. Moreover, exploiting the idempotent character of projection operators we may write that

$$\exp[i(1-\mathcal{P})Lt]f_\lambda = \exp[i(1-\mathcal{P})L(1-\mathcal{P})t]f_\lambda. \qquad (D.6)$$

Repeating the same passages seen in Appendix A, it is readily shown that the operators $\mathcal{P}L\mathcal{P}$ and $(1-\mathcal{P})L(1-\mathcal{P})$ are Hermitian and that the anomalous time propagator is unitary, as is the ordinary one. As a result, the analogous of eqn (B.5) now reads

$$K_{\lambda\lambda'}(t) = K^*_{\lambda'\lambda}(t). \qquad (D.7)$$

Combining eqn (D.5) and (D.7), we deduce that the diagonal elements of the memory matrix are real and even in time. Also, the memory function of two variables with opposite time-reversal signatures is odd in time.

Similar arguments can be repeated for the other symmetries (inversion, reflection, etc.) present in the system. Summing up, the memory functions share the same symmetry requirements of the corresponding time correlation functions.

Appendix E

Short-time dynamics of the velocity autocorrelation function

In a classical system characterized by a continuous pair potential, the normalized velocity autocorrelation function $\psi(t) = \beta m \langle v_{i,x}(0) v_{i,x}(t) \rangle$ at short times can be expanded as

$$\psi(t) = 1 + \beta m \langle v_{i,x} \dot{v}_{i,x} \rangle (t^2/2) + \beta m \langle v_{i,x} \dddot{v}_{i,x} \rangle (t^4/4!) + \cdots$$
$$= 1 - \beta m \langle \dot{v}_{i,x}^2 \rangle (t^2/2) + \beta m \langle \ddot{v}_{i,x}^2 \rangle (t^4/4!) - \cdots . \tag{E.1}$$

As already discussed in Section 1.4.2, the coefficient of the quadratic term in (E.1) is simply the square of the Einstein frequency

$$\Omega_0^2 = \beta m \langle \dot{v}_{i,x}^2 \rangle = \frac{n}{m} \int d\mathbf{r} \, \frac{\partial^2 \phi(r)}{\partial x^2} g(r)$$

$$= \frac{4\pi n}{3m} \int_0^\infty dr \, r^2 \left\{ \phi''(r) + \frac{2\phi'(r)}{r} \right\} g(r). \tag{E.2}$$

Similarly, we may perform an analogous short-time expansion for the memory function $K(t)$ of the velocity autocorrelation function. Introducing a projection operator $\mathcal{P}$ over the variable $v_{i,x}$,

$$\mathcal{P} = \beta m \langle v_{i,x} \ldots \rangle v_{i,x}, \tag{E.3}$$

the memory function reads

$$K(t) = \beta m \langle (1 - \mathcal{P}) \dot{v}_{i,x} \exp[i(1 - \mathcal{P}) L t] (1 - \mathcal{P}) \dot{v}_{i,x} \rangle$$
$$= \beta m \langle \dot{v}_{i,x} \exp[i(1 - \mathcal{P}) L t] \dot{v}_{i,x} \rangle \tag{E.4}$$

since $\mathcal{P} \dot{v}_{i,x} = 0$. Then, in the short-time expansion

$$K(t) = K(0) + \ddot{K}(0)(t^2/2) + \cdots \tag{E.5}$$

we have

$$K(0) = \beta m \langle \dot{v}_{i,x}^2 \rangle = \Omega_0^2, \tag{E.6}$$

$$\ddot{K}(0) = \beta m \langle \dot{v}_{i,x}[i(1 - \mathcal{P})L][i(1 - \mathcal{P})L] \dot{v}_{i,x} \rangle. \tag{E.7}$$

Since $i(1 - \mathcal{P})L\dot{v}_{i,x} = \ddot{v}_{i,x} + \Omega_0^2 v_{i,x}$ and $\langle v_{i,x} \ddot{v}_{i,x} \rangle = \langle v_{i,x} \dot{v}_{i,x} \rangle = 0$, we may write eqn (E.7) in the form

$$\ddot{K}(0) = \beta m \{ \langle \ddot{v}_{i,x} \ddot{v}_{i,x} \rangle + \Omega_0^2 \langle \dot{v}_{i,x} \dot{v}_{i,x} \rangle \}$$
$$= -\beta m \langle \ddot{v}_{i,x}^2 \rangle + \Omega_0^4. \tag{E.8}$$

Noting that $(a = x, y, z)$

$$\ddot{v}_{i,x} = -\frac{1}{m} \sum_{j(\neq i)} \sum_a \frac{\partial^2 \phi(r_{ij})}{\partial x_{ij} \partial r_{ij,a}} v_{ij,a} \tag{E.9}$$

we have

$$\langle \ddot{v}_{i,x}^2 \rangle = \frac{1}{m^2} \sum_{j,l(\neq i)} \sum_{a,\beta} \left\langle \frac{\partial^2 \phi(r_{ij})}{\partial x_{ij} \partial r_{ij,a}} \frac{\partial^2 \phi(r_{il})}{\partial x_{il} \partial r_{il,\beta}} v_{ij,a} v_{il,\beta} \right\rangle$$

$$= \frac{1}{\beta m^3} \sum_{j,l(\neq i)} \sum_a \left\langle \frac{\partial^2 \phi(r_{ij})}{\partial x_{ij} \partial r_{ij,a}} \frac{\partial^2 \phi(r_{il})}{\partial x_{il} \partial r_{il,a}} \right\rangle (1 + \delta_{l,j})$$

$$= \frac{2}{\beta m^3} \sum_{j(\neq i)} \sum_a \left\langle \left(\frac{\partial^2 \phi(r_{ij})}{\partial x_{ij} \partial r_{ij,a}} \right)^2 \right\rangle$$

$$+ \frac{1}{\beta m^3} \sum_{j(\neq i)} \sum_{l(\neq i,j)} \sum_a \left\langle \frac{\partial^2 \phi(r_{ij})}{\partial x_{ij} \partial r_{ij,a}} \frac{\partial^2 \phi(r_{il})}{\partial x_{il} \partial r_{il,a}} \right\rangle. \tag{E.10}$$

Introducing the pair and triplet distributions functions

$$ng(r) = \sum_{j(\neq i)} \langle \delta(\mathbf{r} - \mathbf{r}_{ij}) \rangle, \tag{E.11}$$

$$n^2 g^{(3)}(\mathbf{r}, \mathbf{r}') = \sum_{j(\neq i)} \sum_{l(\neq i,j)} \langle \delta(\mathbf{r} - \mathbf{r}_{ij}) \delta(\mathbf{r}' - \mathbf{r}_{il}) \rangle, \tag{E.12}$$

we may write that

$$\langle \ddot{v}_{i,x}^2 \rangle = \frac{2n}{\beta m^3} \sum_a \int d\mathbf{r} \left(\frac{\partial^2 \phi(r)}{\partial x \partial r_a} \right)^2 g(r)$$

$$+ \frac{n^2}{\beta m^3} \sum_a \iint d\mathbf{r} \, d\mathbf{r}' \, \frac{\partial^2 \phi(r)}{\partial x \partial r_a} \frac{\partial^2 \phi(r')}{\partial x' \partial r_a'} g^{(3)}(\mathbf{r}, \mathbf{r}'). \tag{E.13}$$

In the absence of a precise knowledge of the triplet distribution function, the second term on the right-hand side of (E.13) is evaluated within the *superposition approximation*

$$g^{(3)}(\mathbf{r}, \mathbf{r}') \approx g(r)g(r')g(|\mathbf{r} - \mathbf{r}'|)$$

$$= g(r)g(r')\{1 + (8\pi^3 n)^{-1} \int d\mathbf{q} \, [S(q) - 1] \exp[-i\mathbf{q} \cdot (\mathbf{r} - \mathbf{r}')]\}$$
$$\tag{E.14}$$

where we have expressed $g(|\mathbf{r} - \mathbf{r}'|)$ through the inverse Fourier transform of eqn (1.14). Inserting (E.14) into (E.13) and exploiting isotropy, we obtain

$$\langle \ddot{v}_{i,x}^2 \rangle \approx \frac{2n}{3\beta m^3} \sum_{\alpha,\beta} \int \mathrm{d}\mathbf{r} \left(\frac{\partial^2 \phi(r)}{\partial r_\alpha \partial r_\beta} \right)^2 g(r) + \frac{1}{\beta m} \Omega_0^4$$

$$+ \frac{1}{\beta m} \frac{1}{24\pi^3 n} \sum_{\alpha,\beta} \int \mathrm{d}\mathbf{q} \, [S(q) - 1] \gamma_{\alpha\beta}^2(\mathbf{q}) \qquad (E.15)$$

where (cf. (3.317)):

$$\gamma_{\alpha\beta}(\mathbf{q}) \equiv \frac{n}{m} \int \mathrm{d}\mathbf{r} \, \frac{\partial^2 \phi(r)}{\partial r_\alpha \partial r_\beta} \exp(\mathrm{i}\mathbf{q} \cdot \mathbf{r}) g(r). \qquad (E.16)$$

Finally, we perform the angular integrations on the right-hand side of (E.15). After some tedious calculations we obtain

$$\langle \ddot{v}_{i,x}^2 \rangle \approx \frac{8\pi n}{3\beta m^3} \int_0^\infty \mathrm{d}r \, r^2 \left\{ [\phi''(r)]^2 + 2 \left[\frac{\phi'(r)}{r} \right]^2 \right\} g(r) + \frac{1}{\beta m} \Omega_0^4$$

$$+ \frac{1}{6\pi^2 n\beta m} \int_0^\infty \mathrm{d}q \, q^2 [S(q) - 1] [\gamma_L^2(q) + 2\gamma_T^2(q)] \qquad (E.17)$$

where

$$\gamma_L(q) = \frac{4\pi n}{3m} \int_0^\infty \mathrm{d}r \, r^2 \left\{ [j_0(qr) - 2j_2(qr)] \phi''(r) \right.$$

$$\left. + 2[j_0(qr) + j_2(qr)] \left[\frac{\phi'(r)}{r} \right] \right\} g(r), \qquad (E.18)$$

$$\gamma_T(q) = \frac{4\pi n}{3m} \int_0^\infty \mathrm{d}r \, r^2 \left\{ [j_0(qr) + j_2(qr)] \phi''(r) \right.$$

$$\left. + 2[j_0(qr) + j_2(qr)] \left[\frac{\phi'(r)}{r} \right] \right\} g(r). \qquad (E.19)$$

In the above calculation, the rather involved algebra illustrates the increasing difficulty of dealing with short-time expansions beyond the first coefficients. The appearance of many-body distribution functions (which are largely unknown) introduces additional complications. Fortunately, for the correlation functions of practical interest a detailed knowledge of the short-time behaviour beyond the first few terms is hardly necessary (and ultimately useless because of the slow convergence of the expansion). In the case under consideration, the interest in the evaluation of $\langle \ddot{v}_{i,x}^2 \rangle$ is not due to the rather modest improvement expected in the description (E.1) of the

short-time dynamics of $\psi(t)$, but rather to the fact that this quantity establishes the initial decay time τ of the memory function $K(t)$; that is, an approximate value of the 'duration of a collision' (see Section 3.3). Writing (E.5) as $K(t) = \Omega_0^2 [1 - (t/\tau)^2 + \ldots]$, from (E.16) we obtain

$$\frac{\Omega_0^2}{\tau^2} = -\tfrac{1}{2} \ddot{K}(0) = \frac{4\pi n}{3m^2} \int_0^\infty \mathrm{d}r \, r^2 \left\{ [\phi''(r)]^2 + 2 \left[\frac{\phi'(r)}{r} \right]^2 \right\} g(r)$$

$$+ \frac{1}{12\pi^2 n} \int_0^\infty \mathrm{d}q \, q^2 [S(q) - 1] [\gamma_L^2(q) + 2\gamma_T^2(q)]. \qquad (E.20)$$

Numerical calculations indicate that the dominant contribution to Ω_0^2/τ^2 is provided by the first term on the right-hand side of (E.20), and in particular by the part proportional to $[\phi''(r)]^2$.

Appendix F

The elements of the proper frequency matrix for phase-space densities

In this appendix we shall report the detailed evaluation of the proper frequency matrix elements $\Omega_s(\mathbf{k}, \mathbf{pp}')$ and $\Omega(\mathbf{k}, \mathbf{pp}')$, respectively associated with the self and the collective phase-space densities. From the result (4.29) for $\Omega_s(\mathbf{k}, \mathbf{pp}')$ it is seen that we need the $t = 0$ value of the quantity

$$\dot{f}_{s,i}(\mathbf{k}, \mathbf{p}; t) = \frac{d}{dt} [\exp(i\mathbf{k} \cdot \mathbf{r}_i(t))\delta(\mathbf{p} - \mathbf{p}_i(t))]$$

$$= \frac{i}{m} \mathbf{k} \cdot \mathbf{p}_i(t)\exp(i\mathbf{k} \cdot \mathbf{r}_i(t))\delta(\mathbf{p} - \mathbf{p}_i(t))$$

$$+ \exp(i\mathbf{k} \cdot \mathbf{r}_i(t))\dot{\delta}(\mathbf{p} - \mathbf{p}_i(t))$$

$$= \frac{i}{m}(\mathbf{k} \cdot \mathbf{p})f_{s,i}(\mathbf{k}, \mathbf{p}; t)$$

$$- \exp(i\mathbf{k} \cdot \mathbf{r}_i(t))(\partial/\partial\mathbf{p})[\delta(\mathbf{p} - \mathbf{p}_i(t))] \cdot \dot{\mathbf{p}}_i(t). \quad \text{(F.1)}$$

As a result

$$\langle f_{s,i}(\mathbf{k}, \mathbf{p}'')\dot{f}_{s,i}(\mathbf{k}, \mathbf{p})\rangle = \frac{i}{m}(\mathbf{k} \cdot \mathbf{p})\langle f_{s,i}(\mathbf{k}, \mathbf{p}'')f_{s,i}(\mathbf{k}, \mathbf{p})\rangle$$

$$- \left\langle \delta(\mathbf{p}'' - \mathbf{p}_i)\frac{\partial}{\partial\mathbf{p}}[\delta(\mathbf{p} - \mathbf{p}_i)] \cdot \dot{\mathbf{p}}_i\right\rangle. \quad \text{(F.2)}$$

Since $\dot{\mathbf{p}}_i = -\partial V_N/\partial\mathbf{r}_i$ depends only on the coordinates, the average in the second term on the right-hand side can be factorized, eventually yielding a vanishing result because $\langle\dot{\mathbf{p}}_i\rangle = 0$. Therefore

$$\langle f_{s,i}(\mathbf{k}, \mathbf{p}'')\dot{f}_{s,i}(\mathbf{k}, \mathbf{p})\rangle = \frac{i}{m}(\mathbf{k} \cdot \mathbf{p})VC_s(\mathbf{k}, \mathbf{pp}''; t = 0). \quad \text{(F.3)}$$

Inserting this result into (4.29) and exploiting (4.19) it is readily found that

$$i\Omega_s(\mathbf{k}, \mathbf{pp}') = \frac{i}{m}(\mathbf{k} \cdot \mathbf{p})\delta(\mathbf{p} - \mathbf{p}'). \quad \text{(F.4)}$$

As a consequence, in the case of the self-phase-space density the proper frequency matrix reflects only a 'free-streaming' dynamics, basically because the total force acting on a given particle averages out to zero.

This is not the case for the collective proper frequency matrix (4.30). The counterpart of (F.1) now reads

$$\dot{\hat{f}}(\mathbf{k}, \mathbf{p}; t) = \frac{d}{dt}\left[\sum_i f_{s,i}(\mathbf{k}, \mathbf{p}; t) - (2\pi)^3 n f_0(p)\delta(\mathbf{k})\right]$$

$$= \frac{i}{m}(\mathbf{k} \cdot \mathbf{p})\hat{f}(\mathbf{k}, \mathbf{p}; t) - \sum_i \exp(i\mathbf{k} \cdot \mathbf{r}_i(t))\frac{\partial}{\partial\mathbf{p}}[\delta(\mathbf{p} - \mathbf{p}_i(t))] \cdot \dot{\mathbf{p}}_i(t)$$

$$\text{(F.5)}$$

where in the first term we have reinstalled $(2\pi)^3 n f_0(p)\delta(\mathbf{k})$, which yields a zero contribution because of the factor $(\mathbf{k} \cdot \mathbf{p})$. When performing the average $\langle\hat{f}^*(\mathbf{k}, \mathbf{p}'')\hat{f}(\mathbf{k}, \mathbf{p})\rangle$ needed in eqn (4.30), the first term in eqn (F.5) ultimately yields for $\Omega(\mathbf{k}, \mathbf{pp}')$ a free-streaming contribution identical to the one found for $\Omega_s(\mathbf{k}, \mathbf{pp}')$. On the other hand, the second term of (F.5) causes the presence in the average of a double summation $\sum_{i,j}$, which can be split into self ($j = i$) and distinct ($j \neq i$) contributions. The self part reproduces the same structure seen for Ω_s, and vanishes for the same reasons. As a consequence

$$\langle\hat{f}^*(\mathbf{k}, \mathbf{p}'')\dot{\hat{f}}(\mathbf{k}, \mathbf{p})\rangle = \frac{i}{m}(\mathbf{k} \cdot \mathbf{p})\langle\hat{f}^*(\mathbf{k}, \mathbf{p}'')\hat{f}(\mathbf{k}, \mathbf{p})\rangle$$

$$- \sum_{i,j \neq i}\left\langle\delta(\mathbf{p}'' - \mathbf{p}_j)\frac{\partial}{\partial\mathbf{p}}[\delta(\mathbf{p} - \mathbf{p}_i)] \cdot \dot{\mathbf{p}}_i \exp(i\mathbf{k} \cdot \mathbf{r}_{ij})\right\rangle. \quad \text{(F.6)}$$

In the second term on the right-hand side the average over the coordinates can be factorized from that over the momenta, and the latter can further be split into separate contributions involving the ith and jth particles. Noting that $\langle\delta(\mathbf{p}'' - \mathbf{p}_j)\rangle = f_0(p'')$, we find that the second term can be rewritten as

$$- \sum_{i,j \neq i}\langle\delta(\mathbf{p}'' - \mathbf{p}_j)\rangle\left\langle\frac{\partial}{\partial\mathbf{p}}[\delta(\mathbf{p} - \mathbf{p}_i)]\right\rangle \cdot \langle\dot{\mathbf{p}}_i \exp(i\mathbf{k} \cdot \mathbf{r}_{ij})\rangle$$

$$= \frac{\beta}{m}f_0(p)f_0(p'')\mathbf{p} \cdot \sum_{i,j \neq i}\langle\dot{\mathbf{p}}_i \exp(i\mathbf{k} \cdot \mathbf{r}_{ij})\rangle \quad \text{(F.7)}$$

where in the last step we used the result $df_0(p)/d\mathbf{p} = -(\beta/m)f_0(p)\mathbf{p}$. Using (1.133) and (1.120), we may write

$$\sum_{i,j \neq i} \langle \exp(\mathrm{i}\mathbf{k} \cdot \mathbf{r}_{ij}) \dot{\mathbf{p}}_i \rangle = -\sum_{i,j \neq i} \left\langle \exp(\mathrm{i}\mathbf{k} \cdot \mathbf{r}_{ij}) \left[\frac{\partial V_N}{\partial \mathbf{r}_i} \right] \right\rangle$$

$$= -k_\mathrm{B}T \sum_{i,j \neq i} \left\langle \frac{\partial}{\partial \mathbf{r}_i} \exp(\mathrm{i}\mathbf{k} \cdot \mathbf{r}_{ij}) \right\rangle$$

$$= -k_\mathrm{B}T\mathrm{i}\mathbf{k} \sum_{i,j \neq i} \langle \exp(\mathrm{i}\mathbf{k} \cdot \mathbf{r}_{ij}) \rangle$$

$$= -Nk_\mathrm{B}T\mathrm{i}\mathbf{k}[S(k) - 1 + (2\pi)^3 n\delta(\mathbf{k})]$$

$$= -Nk_\mathrm{B}T\mathrm{i}\mathbf{k}[S(k) - 1]. \qquad (\mathrm{F}.8)$$

Therefore

$$\langle \hat{f}^*(\mathbf{k}, \mathbf{p}'') \dot{\hat{f}}(\mathbf{k}, \mathbf{p}) \rangle = \frac{\mathrm{i}}{m}(\mathbf{k} \cdot \mathbf{p}) \langle \hat{f}^*(\mathbf{k}, \mathbf{p}'') \hat{f}(\mathbf{k}, \mathbf{p}) \rangle$$

$$- \frac{\mathrm{i}}{m}(\mathbf{k} \cdot \mathbf{p}) f_0(p) f_0(p'') N[S(k) - 1]. \quad (\mathrm{F}.9)$$

Inserting this result into (4.30) and using (4.21) we find

$$\mathrm{i}\Omega(\mathbf{k}, \mathbf{pp}') = \frac{\mathrm{i}}{m}(\mathbf{k} \cdot \mathbf{p}) \left[\delta(\mathbf{p} - \mathbf{p}') + nf_0(p)[S(k) - 1] \right.$$

$$\left. \int \mathrm{d}\mathbf{p}'' f_0(p'') \{ [nf_0(p'')]^{-1}\delta(\mathbf{p}'' - \mathbf{p}) - c(k) \} \right]$$

$$= \frac{\mathrm{i}}{m}(\mathbf{k} \cdot \mathbf{p}) \{ \delta(\mathbf{p} - \mathbf{p}') - f_0(p)[S(k) - 1][1 - nc(k)] \}$$

$$= \frac{\mathrm{i}}{m}(\mathbf{k} \cdot \mathbf{p})[\delta(\mathbf{p} - \mathbf{p}') - nf_0(p)c(k)] \qquad (\mathrm{F}.10)$$

since $1 - nc(k) = [S(k)]^{-1}$. Equations (F.4) and (F.10) are the results (4.36) and (4.37) of the main text.

Finally, in the representation in terms of three-dimensional Hermite polynomials $H_\lambda(\mathbf{p})$ of Section 4.2, the elements of the proper frequency matrices read

$$\mathrm{i}\Omega_{s,\lambda\lambda'}(\mathbf{k}) = \mathrm{i}\iint \mathrm{d}\mathbf{p}\,\mathrm{d}\mathbf{p}'\, H_\lambda(\mathbf{p})\Omega_s(\mathbf{k}, \mathbf{pp}')H_{\lambda'}(\mathbf{p}')f_0(p')$$

$$= \frac{\mathrm{i}}{m}\int \mathrm{d}\mathbf{p}\, H_\lambda(\mathbf{p})(\mathbf{k} \cdot \mathbf{p})H_{\lambda'}(\mathbf{p})f_0(p) \qquad (\mathrm{F}.11)$$

$$\mathrm{i}\Omega_{\lambda\lambda'}(\mathbf{k}) = \mathrm{i}\iint \mathrm{d}\mathbf{p}\,\mathrm{d}\mathbf{p}'\, H_\lambda(\mathbf{p})\Omega(\mathbf{k}, \mathbf{pp}')H_{\lambda'}(\mathbf{p}')f_0(p')$$

$$= \frac{\mathrm{i}}{m}\int \mathrm{d}\mathbf{p}\, H_\lambda(\mathbf{p})(\mathbf{k} \cdot \mathbf{p})H_{\lambda'}(\mathbf{p})f_0(p) - \left(\frac{m}{\beta} \right)^{1/2} nc(k)\delta_{\lambda,1}\delta_{\lambda',0}$$

$$(\mathrm{F}.12)$$

where in the last step of (F.12) we have exploited the orthonormality relations (4.59).

Appendix G

The static interaction vertices $v^{(s)}$ and v

In this appendix we shall express in a more manageable form the vertices $v^{(s)}_{\nu\xi,1}(\mathbf{k};\mathbf{k}-\mathbf{q},\mathbf{q})$ and $v_{\nu\xi,1}(\mathbf{k};\mathbf{k}-\mathbf{q},\mathbf{q})$ introduced in Section 4.3.2. To simplify the calculations, we shall set the 'external' wavevector $\mathbf{k}$ directed along the z-axis.

In the self case, we start from eqn (4.121) and note that $\nabla_{\mathbf{P}_3}H_1(\mathbf{P}_3) = (\beta/m)^{1/2}\hat{\imath}_z$, where $\hat{\imath}_z$ is the z-axis unit vector. Then, using eqns (4.55) and (4.56) we obtain

$$v^{(s)}_{\nu\xi,1}(\mathbf{k};\mathbf{k}-\mathbf{q},\mathbf{q}) = \left(\frac{V\beta}{m}\right)^{1/2}\int d1\,d2\,d3\,d4\,\exp\{-i[(\mathbf{k}-\mathbf{q})\cdot\mathbf{R}_1+\mathbf{q}\cdot\mathbf{R}_2-\mathbf{k}\cdot\mathbf{R}_3]\}$$

$$\langle\{(1-\mathscr{P}_s)f_{si,2}(1,2)\}^*(1-\mathscr{P}_s)f_{si,2}(3,4)\rangle$$

$$H_\nu(\mathbf{P}_1)H_\xi(\mathbf{P}_2)\frac{\partial\phi(R_{34})}{\partial Z_3}. \tag{G.1}$$

Here in the statistical average we have omitted terms of the form

$$\langle(1-\mathscr{P}_s)f_{si,2}(1,2)\rangle = (n/V)f_0(P_1)f_0(P_2)[g(R_{12})-1] \tag{G.2}$$

as they give rise to 'disconnected' contributions $\propto\delta(\mathbf{k})$, which eventually vanish for the anisotropy inherent to $\partial\phi(R_{34})/\partial Z_3$. Since

$$\langle\{(1-\mathscr{P}_s)f_{si,2}(1,2)\}^*(1-\mathscr{P}_s)f_{si,2}(3,4)\rangle = \langle\{(1-\mathscr{P}_s)[f_{si,2}(1,2)]\}^*$$

$$f_{si,2}(3,4)\rangle$$

$$= \sum_{j(\neq i)}\sum_{l(\neq i)}\langle\{(1-\mathscr{P}_s)[\delta(\mathbf{R}_1-\mathbf{r}_i)\delta(\mathbf{P}_1-\mathbf{p}_i)\delta(\mathbf{R}_2-\mathbf{r}_j)\delta(\mathbf{P}_2-\mathbf{p}_j)]\}^*$$

$$\delta(\mathbf{R}_4-\mathbf{r}_l)\delta(\mathbf{P}_4-\mathbf{p}_l)\rangle\delta(\mathbf{R}_3-\mathbf{R}_1)\delta(\mathbf{P}_3-\mathbf{P}_1), \tag{G.3}$$

the integrals over $\mathbf{R}_3$, $\mathbf{P}_3$, $\mathbf{R}_4$, and $\mathbf{P}_4$ can be performed immediately, whereas the averages over $\mathbf{P}_1$ and $\mathbf{P}_2$ yield a factor $f_0(P_1)f_0(P_2)$. Thus

$$v^{(s)}_{\nu\xi,1}(\mathbf{k};\mathbf{k}-\mathbf{q},\mathbf{q}) = \left(\frac{V\beta}{m}\right)^{1/2}\int d\mathbf{P}_1\,d\mathbf{P}_2 f_0(P_1)f_0(P_2)H_\nu(\mathbf{P}_1)H_\xi(\mathbf{P}_2)$$

$$\int d\mathbf{R}_1\,d\mathbf{R}_2\sum_{j,l(\neq i)}\left\langle\{(1-\mathscr{P}_s)[\delta(\mathbf{R}_1-\mathbf{r}_i)\delta(\mathbf{R}_2-\mathbf{r}_j)]\}^*\right.$$

$$\left.\frac{\partial\phi(r_{il})}{\partial z_i}\right\rangle\exp[i\mathbf{q}\cdot(\mathbf{R}_1-\mathbf{R}_2)]. \tag{G.4}$$

Because of the orthogonality of the Hermite polynomials, the integrals over $\mathbf{P}_1$ and $\mathbf{P}_2$ give simply $\delta_{\nu,0}\delta_{\xi,0}$. Noting that $m\dot{v}_{i,z} = -\sum_{l(\neq i)}[\partial\phi(r_{il})/\partial z_i]$, we obtain

$$v^{(s)}_{\nu\xi,1}(\mathbf{k};\mathbf{k}-\mathbf{q},\mathbf{q}) = -(V\beta m)^{1/2}\left\langle\{(1-\mathscr{P}_s)\Big[\sum_{j(\neq i)}\exp(i\mathbf{q}\cdot\mathbf{r}_{ij})\Big]\}^*\dot{v}_{i,z}\right\rangle$$

$$\delta_{\nu,0}\delta_{\xi,0}. \tag{G.5}$$

In the thermodynamic limit the effect of $\mathscr{P}_s$ can be neglected, and exploiting the stationarity of the averages we may write that

$$\left\langle\sum_{j(\neq i)}\exp(i\mathbf{q}\cdot\mathbf{r}_{ij})\dot{v}_{i,z}\right\rangle = -\left\langle\sum_{j(\neq i)}(i\mathbf{q}\cdot\mathbf{v}_{ij})\exp(i\mathbf{q}\cdot\mathbf{r}_{ij})v_{i,z}\right\rangle$$

$$= -iq_z\sum_{j(\neq i)}\langle v_{i,z}^2\rangle\langle\exp(i\mathbf{q}\cdot\mathbf{r}_{ij})\rangle$$

$$= -iq_z(\beta m)^{-1}\sum_{j(\neq i)}\int d\mathbf{r}\exp(i\mathbf{q}\cdot\mathbf{r})\langle\delta(\mathbf{r}-\mathbf{r}_{ij})\rangle$$

$$= -iq_z(\beta m)^{-1}\int d\mathbf{r}\exp(i\mathbf{q}\cdot\mathbf{r})ng(r)$$

$$= -iq_z(\beta m)^{-1}[S(q)-1] \tag{G.6}$$

where in the last step we have introduced the definition (1.14) of the static structure factor and used the relation $q_z\delta(\mathbf{q}) = 0$. As a consequence, we eventually find that

$$v^{(s)}_{\nu\xi,1}(\mathbf{k};\mathbf{k}-\mathbf{q},\mathbf{q}) = i\left(\frac{V}{\beta m}\right)^{1/2}q_z[S(q)-1]\delta_{\nu,0}\delta_{\xi,0}, \tag{G.7}$$

namely the result (4.133) of the main text.

The evaluation of the collective vertex $v_{\nu\xi,1}(\mathbf{k};\mathbf{k}-\mathbf{q},\mathbf{q})$ proceeds by

similar steps. Starting from eqn (4.122) in this case, the counterpart of eqns (G.4) and (G.5) reads

$$v_{\nu\xi,1}(\mathbf{k};\mathbf{k}-\mathbf{q},\mathbf{q}) = \frac{1}{V}\left(\frac{\beta}{m}\right)^{1/2}\int d\mathbf{P}_1\,d\mathbf{P}_2 f_0(P_1) f_0(P_2) H_\nu(\mathbf{P}_1) H_\xi(\mathbf{P}_2)$$

$$\int d\mathbf{R}_1\,d\mathbf{R}_2\,d\mathbf{R}_3\,d\mathbf{R}_4 \exp\{-i[(\mathbf{k}-\mathbf{q})\cdot\mathbf{R}_1 + \mathbf{q}\cdot\mathbf{R}_2 - \mathbf{k}\cdot\mathbf{R}_3]\}$$

$$\frac{\partial\phi(R_{34})}{\partial Z_3}\left\langle\left\{(1-\mathcal{P})\left[\sum_{i,j\neq i}\delta(\mathbf{R}_1-\mathbf{r}_i)\delta(\mathbf{R}_2-\mathbf{r}_j)\right]\right\}^*\right.$$

$$\left.\sum_{l,m\neq l}\delta(\mathbf{R}_3-\mathbf{r}_l)\delta(\mathbf{R}_4-\mathbf{r}_m)\right\rangle$$

$$= -\frac{(\beta m)^{1/2}}{V}\int d\mathbf{R}_1\,d\mathbf{R}_2 \exp\{-i[(\mathbf{k}-\mathbf{q})\cdot\mathbf{R}_1 + \mathbf{q}\cdot\mathbf{R}_2]\}$$

$$\left\langle\left\{(1-\mathcal{P})\sum_{i,j\neq i}\delta(\mathbf{R}_1-\mathbf{r}_i)\delta(\mathbf{R}_2-\mathbf{r}_j)\right\}^*\right.$$

$$\left.\sum_l \exp(i\mathbf{k}\cdot\mathbf{r}_l)\dot{v}_{l,z}\right\rangle\delta_{\nu,0}\delta_{\xi,0}. \tag{G.8}$$

Using the definition (4.26), it is readily seen that for a variable $F(\mathbf{r}^N)$ which depends only on the coordinates one has

$$\mathcal{P}F(\mathbf{r}^N) = (1/N)[1 - nc(k)]\langle\hat{n}^*(\mathbf{k})F(\mathbf{r}^N)\rangle\hat{n}(\mathbf{k})$$

$$= [NS(k)]^{-1}\langle\hat{n}^*(\mathbf{k})F(\mathbf{r}^N)\rangle\hat{n}(\mathbf{k})$$

$$= \langle\hat{n}^*(\mathbf{k})\hat{n}(\mathbf{k})\rangle^{-1}\langle\hat{n}^*(\mathbf{k})F(\mathbf{r}^N)\rangle\hat{n}(\mathbf{k}) \tag{G.9}$$

where $\hat{n}(\mathbf{k}) = \sum_i \exp(i\mathbf{k}\cdot\mathbf{r}_i) - (2\pi)^3 n\delta(\mathbf{k})$ are the wavevector-dependent density fluctuations. In other words, the effect of the phase-space projection operator $\mathcal{P}$ is simply to project $F(\mathbf{r}^N)$ onto the density variable $\hat{n}(\mathbf{k})$. Then

$$\left\langle\left\{\mathcal{P}\left[\sum_{i,j\neq i}\delta(\mathbf{R}_1-\mathbf{r}_i)\delta(\mathbf{R}_2-\mathbf{r}_j)\right]\right\}^*\sum_l\exp(i\mathbf{k}\cdot\mathbf{r}_l)\dot{v}_{l,z}\right\rangle$$

$$= [NS(k)]^{-1}\left\langle\hat{n}^*(\mathbf{k})\sum_{i,j\neq i}\delta(\mathbf{R}_1-\mathbf{r}_i)\delta(\mathbf{R}_2-\mathbf{r}_j)\right\rangle^*\left\langle\hat{n}^*(\mathbf{k})\sum_l\exp(i\mathbf{k}\cdot\mathbf{r}_l)\dot{v}_{l,z}\right\rangle$$

$$= -i\mathbf{k}(\beta m)^{-1}nc(k)\left\langle\sum_{i,j\neq i}\delta(\mathbf{R}_1-\mathbf{r}_i)\delta(\mathbf{R}_2-\mathbf{r}_j)\sum_l\exp(i\mathbf{k}\cdot\mathbf{r}_l)\right\rangle \tag{G.10}$$

where we have exploited the result (G.6) and repeatedly used the relations $k\delta(\mathbf{k}) = 0$ and $\sum_l \dot{v}_{l,z} = 0$. Inserting (G.10) into (G.8) and integrating over $\mathbf{R}_1$ and $\mathbf{R}_2$ we obtain

$$v_{\nu\xi,1}(\mathbf{k};\mathbf{k}-\mathbf{q},\mathbf{q}) = -\frac{(\beta m)^{1/2}}{V}\delta_{\nu,0}\delta_{\xi,0}$$

$$\left\{\left\langle\sum_{i,j\neq i}\exp\{-i[(\mathbf{k}-\mathbf{q})\cdot\mathbf{r}_i + \mathbf{q}\cdot\mathbf{r}_j]\}\right.\right.$$

$$\left.\sum_l\exp(i\mathbf{k}\cdot\mathbf{r}_l)\dot{v}_{l,z}\right\rangle + ik(\beta m)^{-1}nc(k)$$

$$\left.\left\langle\sum_{i,j\neq i}\exp\{-i[(\mathbf{k}-\mathbf{q})\cdot\mathbf{r}_i + \mathbf{q}\cdot\mathbf{r}_j]\}\sum_l\exp(i\mathbf{k}\cdot\mathbf{r}_l)\right\rangle\right\}. \tag{G.11}$$

Exploiting stationarity, the first average in curly brackets can be written as

$$\left\langle\sum_{i,j\neq i}\exp\{-i[(\mathbf{k}-\mathbf{q})\cdot\mathbf{r}_i + \mathbf{q}\cdot\mathbf{r}_j]\}\sum_l\exp(i\mathbf{k}\cdot\mathbf{r}_l)\dot{v}_{l,z}\right\rangle$$

$$= \frac{i}{\beta m}\left\{(k-q_z)\sum_{i,j\neq i}\langle\exp(i\mathbf{q}\cdot\mathbf{r}_{ij})\rangle + q_z\sum_{i,j\neq i}\langle\exp[-i(\mathbf{k}-\mathbf{q})\cdot\mathbf{r}_{ij}]\rangle\right.$$

$$\left.-k\left\langle\sum_{i,j\neq i}\exp\{-i[(\mathbf{k}-\mathbf{q})\cdot\mathbf{r}_i + \mathbf{q}\cdot\mathbf{r}_j]\}\sum_l\exp(i\mathbf{k}\cdot\mathbf{r}_l)\right\rangle\right\}. \tag{G.12}$$

Thus

$$v_{\nu\xi,1}(\mathbf{k};\mathbf{k}-\mathbf{q},\mathbf{q}) = -i\frac{n}{(\beta m)^{1/2}}\delta_{\nu,0}\delta_{\xi,0}\frac{1}{N}\left\{\sum_{i,j\neq i}[(k-q_z)\langle\exp(i\mathbf{q}\cdot\mathbf{r}_{ij})\rangle\right.$$

$$+ q_z\langle\exp[-i(\mathbf{k}-\mathbf{q})\cdot\mathbf{r}_{ij}]\rangle] - (k/S(k))$$

$$\left.\left\langle\sum_{i,j\neq i}\exp\{-i[(\mathbf{k}-\mathbf{q})\cdot\mathbf{r}_i + \mathbf{q}\cdot\mathbf{r}_j]\}\sum_l\exp(i\mathbf{k}\cdot\mathbf{r}_l)\right\rangle\right\}. \tag{G.13}$$

Splitting the summation in the last term of eqn (G.13) according to the formal decomposition $\sum_l = [\sum_{l\neq i,j} + (l = i) + (l = j)]$, it is readily seen that the collective vertex depends both on pair and triplet distribution functions. The latter can approximately be treated by the superposition scheme (1.17), with the result that

$$v_{\nu\xi,1}(\mathbf{k}; \mathbf{k} - \mathbf{q}, \mathbf{q}) \approx -\mathrm{i}\,\frac{n}{(\beta m)^{1/2}}\,\{(k - q_z)S(q) + q_z S(|\mathbf{k} - \mathbf{q}|)$$

$$- kS(q)S(|\mathbf{k} - \mathbf{q}|)\}\delta_{\nu,0}\delta_{\xi,0}$$

$$= \mathrm{i}\,\frac{n}{(\beta m)^{1/2}}\,\{q_z S(|\mathbf{k} - \mathbf{q}|)[S(q) - 1]$$

$$+ (k - q_z)S(q)[S(|\mathbf{k} - \mathbf{q}|) - 1]\}\delta_{\nu,0}\delta_{\xi,0} \tag{G.14}$$

which is eqn (4.134). An equivalent form of the result (G.14) is

$$v_{\nu\xi,1}(\mathbf{k}; \mathbf{k} - \mathbf{q}, \mathbf{q}) \approx \mathrm{i}\,\frac{n^2}{(\beta m)^{1/2}}\,S(q)S(|\mathbf{k} - \mathbf{q}|)$$

$$[q_z c(q) + (k - q_z)c(|\mathbf{k} - \mathbf{q}|)]\delta_{\nu,0}\delta_{\xi,0}. \tag{G.15}$$

It is also convenient to report the expressions of the 'transverse' vertices $v^{(s)}_{\nu\xi,2}(\mathbf{k}; \mathbf{k} - \mathbf{q}, \mathbf{q})$ and $v_{\nu\xi,2}(\mathbf{k}; \mathbf{k} - \mathbf{q}, \mathbf{q})$. In the self case, every-thing proceeds as for $v^{(s)}_{\nu\xi,1}$ except that the z-component is replaced by the one along x. Thus

$$v^{(s)}_{\nu\xi,2}(\mathbf{k}; \mathbf{k} - \mathbf{q}, \mathbf{q}) = \mathrm{i}\left(\frac{V}{\beta m}\right)^{1/2} q_x [S(q) - 1]\delta_{\nu,0}\delta_{\xi,0}. \tag{G.16}$$

In the collective case, the replacement $z \to x$ in the result (G.8) has the effect that the contribution (G.10) coming from the projection operator $\mathcal{P}$ vanishes. Moreover, in eqn (G.12) any contribution proportional to k vanishes since $k_x = 0$. Therefore:

$$v_{\nu\xi,2}(\mathbf{k}; \mathbf{k} - \mathbf{q}, \mathbf{q}) = -\mathrm{i}\,\frac{n}{(\beta m)^{1/2}}\,\delta_{\nu,0}\delta_{\xi,0}q_x$$

$$\frac{1}{N}\sum_{i,j \neq i}\{\langle\exp[-\mathrm{i}(\mathbf{k} - \mathbf{q})\cdot\mathbf{r}_{ij}]\rangle - \langle\exp(\mathrm{i}\mathbf{q}\cdot\mathbf{r}_{ij})\rangle\}. \tag{G.17}$$

Noting that $(1/N)\sum_{i,j \neq i}\langle\exp(\mathrm{i}\mathbf{q}\cdot\mathbf{r}_{ij})\rangle = S(q) - 1 + (2\pi)^3 n\delta(\mathbf{q})$ we obtain

$$v_{\nu\xi,2}(\mathbf{k}; \mathbf{k} - \mathbf{q}, \mathbf{q}) = -\mathrm{i}\,\frac{n}{(\beta m)^{1/2}}\,q_x[S(|\mathbf{k} - \mathbf{q}|) - S(q)]\delta_{\nu,0}\delta_{\xi,0}. \tag{G.18}$$

The result (G.18) is used in Section 6.2.

Appendix H

The velocity field approach

Suppose that we wish to evaluate the velocity autocorrelation function of a tagged particle in a dense fluid, and that we are interested in dynamical features occurring over length and time ranges considerably larger than the typical microscopic scales. A possible procedure is to resort to a hydrodynamic description of the fluid, with the microscopic variables effectively replaced by suitable 'coarse-grained' averages. In the case under consideration, we would deal with a *velocity field* $\mathbf{v}(\mathbf{r}, t)$ defined in a continuum version of the fluid. Typically, this hydrodynamic framework has been adopted to account for the $t^{-3/2}$ long-time tail of the velocity autocorrelation function (Zwanzig and Bixon 1970; Schofield 1975).

A possible way to generalize these approaches and include even microscopic features was proposed by Gaskell and Miller (1978a). These authors introduced a *microscopic velocity field*

$$\mathbf{v}(\mathbf{r}, t) \equiv \sum_j f(|\mathbf{r} - \mathbf{r}_j(t)|)\mathbf{v}_j(t) \tag{H.1}$$

where the 'form factor' f is determined by a number of physical requirements. First of all, if $\mathbf{r}$ is sufficiently close to a position of a particular atom, the velocity field should essentially coincide with the actual velocity of the atom. In particular, for $\mathbf{r} = \mathbf{r}_i(t)$ it is required that

$$\mathbf{v}(\mathbf{r}_i(t), t) = \mathbf{v}_i(t). \tag{H.2}$$

For $\mathbf{r} = \mathbf{r}_i(t) + \boldsymbol{\rho}$, it is expected that $\mathbf{v}(\mathbf{r}, t)$ is still $\sim \mathbf{v}_i(t)$ for separations ρ smaller than a suitable 'atomic radius' a. In such a way, the microscopic velocity field near a particle is essentially constant across an atomic diameter. For example, these requirements are met by choosing for the form factor the step function

$$f(r) = \theta(a - r). \tag{H.3}$$

Alternative choices for $f(r)$ with the same behaviour and which are continuous (e.g. $f(r) = \exp[-(r/a)^{12}]$) have been tested by Gaskell and Miller, with no basic changes in the final results. In physical situations characterized by a rather close-packed arrangement of particles, eqns (H.1) and (H.3) provide a convenient definition of a velocity field at a

microscopic level. In addition, Gaskell and Miller required that the field satisfies the macroscopic condition

$$n \int d\mathbf{r}\, \mathbf{v}(\mathbf{r}, t) = \sum_i \mathbf{v}_i(t). \tag{H.4}$$

Introducing a space Fourier transform of the form factor

$$f(q) = \int d\mathbf{r} \exp(i\mathbf{q} \cdot \mathbf{r}) f(r), \tag{H.5}$$

the condition (H.4) is equivalent to the requirement that $f(q = 0) = \int d\mathbf{r} f(r) = (1/n)$. Choosing for $f(r)$ the simple form (H.3), this implies that $(4/3)\pi na^3 = 1$, so that the length a plays the role of an effective 'particle radius'. In this case

$$f(q) = \frac{4\pi a^2 j_1(qa)}{q} = \frac{3}{n}\frac{j_1(qa)}{qa} \tag{H.6}$$

where $j_1(x) = \sin(x)/x^2 - \cos(x)/x$ is the spherical Bessel function of order one.

According to these prescriptions, the velocity autocorrelation function of a tagged particle can be written as

$$\langle \mathbf{v}_i(0) \cdot \mathbf{v}_i(t) \rangle = \langle \mathbf{v}_i(0) \cdot \mathbf{v}(\mathbf{r}_i(t), t) \rangle$$

$$= \int d\mathbf{r} \langle \mathbf{v}_i(0) \cdot \mathbf{v}(\mathbf{r}_i(0) + \mathbf{r}, t) \delta(\mathbf{r} + \mathbf{r}_i(0) - \mathbf{r}_i(t)) \rangle$$

$$= (2\pi)^{-3} \int d\mathbf{r} \int d\mathbf{q} \exp(-i\mathbf{q} \cdot \mathbf{r}) \langle \mathbf{v}_i(0) \exp[-i\mathbf{q} \cdot \mathbf{r}_i(0)]$$

$$\mathbf{v}(\mathbf{q}, t) \delta(\mathbf{r} + \mathbf{r}_i(0) - \mathbf{r}_i(t)) \rangle \tag{H.7}$$

where $\mathbf{v}(\mathbf{q}, t)$ is the Fourier transform of the velocity field. To make contact with the hydrodynamic approach, Gaskell and Miller replaced $\mathbf{v}(\mathbf{q})$ by its projection over the current density $\mathbf{j}(\mathbf{q}) = \sum_j \mathbf{v}_j \exp(i\mathbf{q} \cdot \mathbf{r}_j)$; in other terms,

$$\mathbf{v}(\mathbf{q}) \approx \frac{\langle \mathbf{j}^*(\mathbf{q}) \cdot \mathbf{v}(\mathbf{q}) \rangle}{\langle \mathbf{j}^*(\mathbf{q}) \cdot \mathbf{j}(\mathbf{q}) \rangle} \mathbf{j}(\mathbf{q}) = f(q)\mathbf{j}(\mathbf{q}). \tag{H.8}$$

Substituting into (H.7), it is apparent that the statistical average in this equation accounts for two different time-dependent processes, respectively associated with the currents and with the space coordinates. At liquid densities, the slowness of diffusive motions makes the timescales of the two processes considerably different. Thus the average can approximately be factorized into two separate contributions, yielding

$$\langle \mathbf{v}_i(0) \cdot \mathbf{v}_i(t) \rangle = \frac{1}{8\pi^3} \int d\mathbf{q}\, f(q) \langle \mathbf{v}_i(0) \exp[-i\mathbf{q} \cdot \mathbf{r}_i(0)] \cdot \mathbf{j}(\mathbf{q}, t) \rangle$$

$$\int d\mathbf{r} \exp(-i\mathbf{q} \cdot \mathbf{r}) \langle \delta(\mathbf{r} + \mathbf{r}_i(0) - \mathbf{r}_i(t)) \rangle$$

$$= \frac{1}{8\pi^3 N} \int d\mathbf{q}\, f(q) \langle \mathbf{j}^*(\mathbf{q}, 0) \cdot \mathbf{j}(\mathbf{q}, t) \rangle F_s(q, t) \tag{H.9}$$

where in the last step we have introduced the self-intermediate scattering function. Choosing $\mathbf{q}$ in the z-direction, the current correlation function in eqn (H.9) can be split into longitudinal and transverse contributions, with the result that

$$\langle \mathbf{v}_i(0) \cdot \mathbf{v}_i(t) \rangle = \frac{1}{8\pi^3} \int d\mathbf{q}\, f(q) [C_L(q, t) + 2C_T(q, t)] F_s(q, t). \tag{H.10}$$

Equation (H.10) is the main outcome of the microscopic velocity field approach. Comparing with the mode coupling result (4.177), we note an essentially identical structure, the only difference being the presence in (H.10) of the quantity $f(q)$ which replaces a constant factor $(1/n)$. Since $f(q = 0) = (1/n)$, the two approaches give identical results in all the cases where the dominant role in the integral (H.10) is played by sufficiently small wavevectors. As discussed in Section 4.5, this circumstance typically occurs for the slowly decaying $t^{-3/2}$ tail of $\langle \mathbf{v}_i(0) \cdot \mathbf{v}_i(t) \rangle$, which is essentially determined by the hydrodynamic forms of the correlation functions in eqn (H.10). Thus, the asymptotic behaviour of the velocity autocorrelation function is correctly accounted for, even by the velocity field approach.

However, it is at short and intermediate times that the framework reveals its practical usefulness. In contrast with the mode-coupling result (4.177), eqn (H.10) reproduces the exact short-time behaviour of $\langle \mathbf{v}_i(0) \cdot \mathbf{v}_i(t) \rangle$. Noting that $C_L(q, 0) = C_T(q, 0) = k_B T/m$ and $F_s(q, 0) = 1$, for the initial value we correctly obtain

$$\langle \mathbf{v}_i^2(0) \rangle = \frac{3k_B T}{m} \frac{1}{8\pi^3} \int d\mathbf{q}\, f(q) = \frac{3k_B T}{m} f(r = 0)$$

$$= \frac{3k_B T}{m}. \tag{H.11}$$

Moreover, the initial time decay of $\langle \mathbf{v}_i(0) \cdot \mathbf{v}_i(t) \rangle$ predicted by eqn (H.10) is ruled by

$$\langle \mathbf{v}_i(0) \cdot \ddot{\mathbf{v}}_i(0) \rangle = \frac{1}{8\pi^3} \int d\mathbf{q}\, f(q) \left\{ [\ddot{C}_L(q, 0) + 2\ddot{C}_T(q, 0)] + \frac{3k_B T}{m} \ddot{F}_s(q, 0) \right\}. \tag{H.12}$$

Here (cf. eqns (1.149), (1.150), and (1.38)):

$$\ddot{C}_L(q,0) + 2\ddot{C}_T(q,0) = -\frac{k_B T}{m}\left[\omega_L^2(q) + 2\omega_T^2(q)\right]$$

$$= -k_B T/m\left[\frac{5k_B T}{m}q^2 + 3\Omega_0^2 - (\Omega_q^2 + 2\Omega_q'^2)\right],$$

$$\text{(H.13)}$$

$$\ddot{F}_s(q,0) = -\frac{k_B T}{m}q^2. \qquad \text{(H.14)}$$

Inserting these results into eqn (H.12), the kinetic terms are found to give a contribution proportional to $[\nabla^2 f(r)]_{r=0}$, which vanishes if the form factor $f(r)$ is sufficiently flat as $r \to 0$. On the other hand, the contribution of $(\Omega_q^2 + 2\Omega_q'^2)$ eventually involves an integral of the form $\int d\mathbf{r}\,\nabla^2\phi(r)f(r)g(r)$. Since at liquid density the range a of $f(r)$ is typically of the order of a particle 'radius' (i.e. $a \approx \sigma/2$), the product $f(r)g(r)$ is effectively zero. Consequently we are left with

$$\langle \mathbf{v}_i(0)\cdot\ddot{\mathbf{v}}_i(0)\rangle = -\frac{3k_B T}{m}\Omega_0^2 \frac{1}{8\pi^3}\int d\mathbf{q}\,f(q)$$

$$= -\frac{3k_B T}{m}\Omega_0^2 f(r=0)$$

$$= -\frac{3k_B T}{m}\Omega_0^2 \qquad \text{(H.15)}$$

which is the correct result for the initial decay rate of the velocity autocorrelation function. In perspective, it is seen that the ability of the approach to account for the short-time behaviour of $\langle \mathbf{v}_i(0)\cdot\mathbf{v}_i(t)\rangle$ is a consequence of the reasonable assumptions made for the velocity field at microscopic distances.

Owing to the presence in eqn (H.10) of the unknown correlations C_L, C_T, and F_s, the framework does not provide a genuine 'theory' for the velocity autocorrelation function at arbitrary times. However, the previous tests in different regimes indicate that the structure of eqn (H.10) is essentially correct, with the result that relatively simple approximations for C_L, C_T, and F_s are expected to yield satisfactory results for $\langle \mathbf{v}_i(0)\cdot\mathbf{v}_i(t)\rangle$. In particular, in the liquid range the separation of timescales between the current correlations and the slow diffusive motions is so sharp that, in eqn (H.10), $F_s(q,t)$ may be replaced by its initial value 1 with no substantial influence on the results. As far as C_L and C_T are concerned, Gaskell and Miller (1978a, b) basically adopted the simple results provided by viscoelastic theory (cf. Section 6.2). The predictions obtained for the velocity autocorrelation function were tested against computer simulation
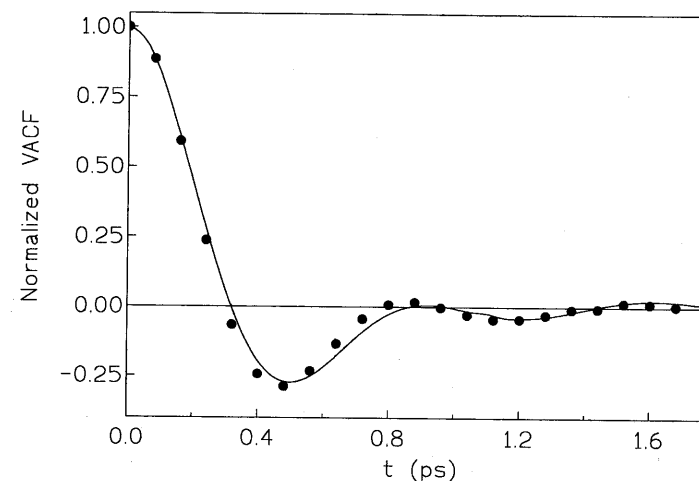
Fig. H.1 Normalized velocity autocorrelation obtained by the velocity field approach in liquid Rb at 332 K. The dots are the corresponding simulation data. Redrawn from Balucani *et al.* (1984).

data in several simple liquids (such as liquid rubidium, sodium, and argon), obtaining in any case a quite satisfactory agreement (see Fig. H.1).

The velocity field framework has subsequently been extended to treat several other dynamical quantities, such as the memory function of the self intermediate scattering function (Gaskell and Miller 1979) and the cross-velocity correlations of Section 1.5.2 ruling the momentum transfer to the surrounding atoms (Gaskell and Woolfson 1982; Balucani *et al.* 1983, 1984). Another interesting application concerns a microscopic generalization of the Stokes–Einstein relation between the diffusion and the shear viscosity coefficients; this subject is discussed in detail in Section 6.4.3.

REFERENCES

Balucani, U., Vallauri, R., Murthy, C. S., Gaskell, T., and Woolfson, M. S. (1983). *J. Phys. C*, **16**, 5605.

Balucani, U., Vallauri, R., Gaskell, T., and Gori, M. (1984). *Phys. Lett.*, **102A**, 109.

Gaskell, T. and Miller, S. (1978a). *J. Phys. C*, **11**, 3749.

Gaskell, T. and Miller, S. (1978b). *J. Phys. C*, **11**, 4839.

Gaskell, T. and Miller, S. (1979). *J. Phys. C*, **12**, 2705.

Gaskell, T. and Woolfson, M. S. (1982). *J. Phys. C*, **15**, 6339.

Schofield, P. (1975). Specialist reports: statistical mechanics II. The Chemical Society, London.

Zwanzig, R. and Bixon, M. (1970). *Phys. Rev. A*, **2**, 2005.

Appendix I

Short-time dynamics of the intermediate scattering functions (self and collective)

A better understanding of the relevance of fast collisional events in the dynamics probed by $F_s(k, t)$ and $F(k, t)$ requires a rather detailed knowledge of the short-time properties of these correlation functions. Some information in this respect was provided in Chapter 1 with the deduction of the expansion coefficients up to the order t^4. On the other hand, the approaches discussed in Chapters 5 and 6, rather than being explicitly concerned with F_s and F, deal with the corresponding *second-order* memory functions. The collisional events of the 'binary' type are directly associated with the initial decay of these memory functions (i.e. with the coefficients in t^6 of the short time expansions of F_s and F). Although rather cumbersome, the evaluation of these 'sixth moments' is still manageable. In this appendix, we shall limit ourselves to report the essential steps of the calculation for both correlation functions.

Starting with the self case, the short-time expansion of $F_s(k, t) = \langle n_{s,i}^*(\mathbf{k}, 0) n_{s,i}(\mathbf{k}, t) \rangle$ can be written as

$$F_s(k, t) = 1 - \langle \omega_k^2 \rangle_s \frac{t^2}{2!} + \langle \omega_k^4 \rangle_s \frac{t^4}{4!} - \langle \omega_k^6 \rangle_s \frac{t^6}{6!} + \cdots \qquad (I.1)$$

where we already know that

$$\langle \omega_k^2 \rangle_s = \frac{k_B T}{m} k^2 \qquad (I.2)$$

$$\langle \omega_k^4 \rangle_s = \frac{k_B T}{m} k^2 \left[\frac{3k_B T}{m} k^2 + \Omega_0^2 \right] \qquad (I.3)$$

(cf. Section 1.4.1). Exploiting stationarity, the sixth moment $\langle \omega_k^6 \rangle_s$ can be expressed in the form

$$\langle \omega_k^6 \rangle_s = -\left\langle n_{s,i}^*(\mathbf{k}, 0) \left[\frac{d^6 n_{s,i}(\mathbf{k}, t)}{dt^6} \right]_{t=0} \right\rangle$$

$$= \langle \ddot{n}_{s,i}^*(\mathbf{k}, 0) \ddot{n}_{s,i}(\mathbf{k}, 0) \rangle \qquad (I.4)$$

where

$$\ddot{n}_{s,i}(\mathbf{k}, 0) = \{ i\mathbf{k} \cdot \dot{\mathbf{v}}_i(0) + 3[i\mathbf{k} \cdot \mathbf{v}_i(0)][i\mathbf{k} \cdot \dot{\mathbf{v}}_i(0)]$$

$$+ [i\mathbf{k} \cdot \mathbf{v}_i(0)]^3 \} \exp[i\mathbf{k} \cdot \mathbf{r}_i(0)]. \qquad (I.5)$$

Choosing $\mathbf{k}$ along the z-axis, after some algebra we find

$$\langle \omega_k^6 \rangle_s = k^2 [\langle \dot{v}_{i,z}^2 \rangle + 15k^2 \langle v_{i,z}^2 \dot{v}_{i,z}^2 \rangle + k^4 \langle v_{i,z}^6 \rangle]$$

$$= k^2 \left[\langle \dot{v}_{i,z}^2 \rangle + 15k^2 \frac{k_B T}{m} \langle \dot{v}_{i,z}^2 \rangle + 15k^4 \left(\frac{k_B T}{m} \right)^3 \right]$$

$$= k^2 \frac{k_B T}{m} \left\{ [\Omega_0^4 - \ddot{K}(0)] + 15k^2 \frac{k_B T}{m} \Omega_0^2 + 15k^4 \left(\frac{k_B T}{m} \right)^2 \right\} \qquad (I.6)$$

where in the last step we have exploited the results (E.6) and (E.8) for the memory function $K(t)$ of the velocity autocorrelation function. At sufficiently short times $K(t)$ can be expanded as (cf. eqn (E.20)):

$$K(t) = K(0) + \frac{1}{2} \ddot{K}(0) t^2 + \cdots \equiv \Omega_0^2 \left[1 - \left(\frac{t}{\tau} \right)^2 + \cdots \right]. \qquad (I.7)$$

As a result

$$\langle \omega_k^6 \rangle_s = k^2 \frac{k_B T}{m} \left\{ \Omega_0^2 \left[\Omega_0^2 + \left(\frac{2}{\tau^2} \right) \right] + 15k^2 \frac{k_B T}{m} \left[\Omega_0^2 + k^2 \frac{k_B T}{m} \right] \right\}. \qquad (I.8)$$

From eqn (I.8) it is straightforward to deduce the short-time features of the second-order memory function $M_s(k, t)$ appearing in eqn (5.41). Starting from the expression

$$M_s(k, t) = M_s(k, 0) + \frac{1}{2} \ddot{M}_s(k, 0) t^2 + \cdots$$

$$\equiv M_s(k, 0) \left[1 - \left(\frac{t}{\tau_s(k)} \right)^2 + \cdots \right] \qquad (I.9)$$

and using eqns (3.43b) and (3.43c), we deduce that

$$M_s(k, 0) = \frac{\langle \omega_k^4 \rangle_s}{\langle \omega_k^2 \rangle_s} - \langle \omega_k^2 \rangle_s = \frac{2k_B T}{m} k^2 + \Omega_0^2 \qquad (I.10)$$

$$-\ddot{M}_s(k, 0) = \frac{\langle \omega_k^6 \rangle_s}{\langle \omega_k^4 \rangle_s} - \left[\frac{\langle \omega_k^4 \rangle_s}{\langle \omega_k^2 \rangle_s} \right]^2$$

$$= \frac{2\Omega_0^2}{\tau^2} + \frac{3k_B T}{m} k^2 \left[3\Omega_0^2 + \frac{2k_B T}{m} k^2 \right]. \qquad (I.11)$$

Therefore the initial decrease of the memory function $M_s(k, t)$ is ruled by the decay rate
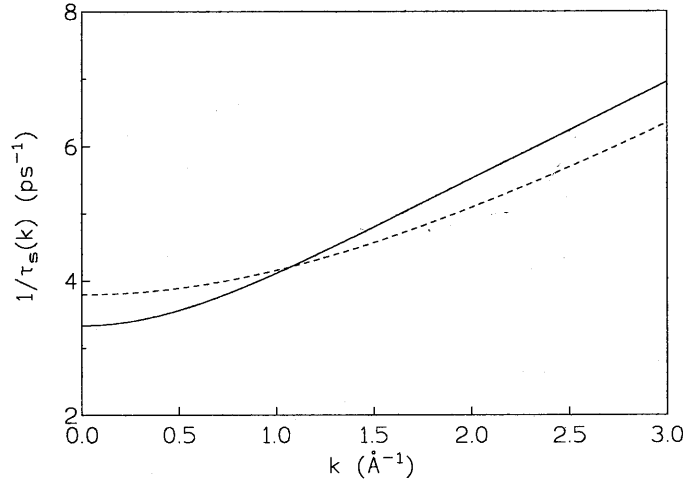
Fig. I.1 Wavevector dependence of the rate $[\tau_s(k)]^{-1}$ in liquid Cs at 308 K according to eqn (I.12) (full line). In this system, $\tau \approx 0.30$ ps and $\Omega_0^2 \approx 19.22$ ps^{-2}. The dashed line denotes the results of the approximation (5.47), with the parameter $\zeta = \sqrt{3}/2$ chosen in such a way to reproduce the asymptotic form (I.13) for $k \to \infty$.

$$\frac{1}{\tau_s(k)} = \left[\frac{-\ddot{M}_s(k,0)}{2M_s(k,0)}\right]^{1/2}$$

$$= \left\{\frac{2(\Omega_0^2/\tau^2) + 3(k_B T/m)k^2[3\Omega_0^2 + 2(k_B T/m)k^2]}{2\Omega_0^2 + 4(k_B T/m)k^2}\right\}^{1/2}.$$

$$(I.12)$$

The wavevector dependence of $\tau_s(k)$ is entirely due to terms having a kinetic origin. Starting from $\tau_s(k \to 0) = \tau$, $\tau_s(k)$ is found to decay monotonically with k (see Fig. I.1, where the results are compared with those obtained by the simple approximation (5.47)). Eventually, for $k \to \infty$ one has

$$\frac{1}{\tau_s(k)} \to \left(\frac{3k_B T}{2m}\right)^{1/2} k.$$

$$(I.13)$$

This result corresponds to free-particle behaviour, and can be obtained directly from the Gaussian form of the spectrum $S_s(k, \omega)$ appropriate for this case (cf. eqn (1.51)). Indeed, for a Gaussian all the quantities $\langle\omega_k^{2n}\rangle_s$ can be expressed exactly in terms of the second frequency moment:

$$\langle\omega_k^{2n}\rangle_s = (2n-1)!![\langle\omega_k^2\rangle_s]^n = (2n-1)!!\left(\frac{k_B T}{m}\right)^n k^{2n}.$$

$$(I.14)$$

Consequently, for free particles $M_s(k,0) = 2\langle\omega_k^2\rangle_s$ and $\ddot{M}_s(k,0) = -6[\langle\omega_k^2\rangle_s]^2$, that is $[1/\tau_s(k)]^2 = \frac{1}{2}[-\ddot{M}_s(k,0)/M_s(k,0)] = \frac{3}{2}\langle\omega_k^2\rangle_s$.

Turning now the attention to the collective case, we already know that the second and fourth frequency moments of $S(k, \omega)$ read

$$\langle\omega_k^2\rangle = \frac{k_B T}{mS(k)} k^2$$

$$(I.15)$$

$$\langle\omega_k^4\rangle = \langle\omega_k^2\rangle\left\{\frac{3k_B T}{m}k^2 + \frac{n}{m}\int d\mathbf{r}\,\frac{\partial^2\phi(r)}{\partial z^2}(1 - \cos kz)g(r)\right\}$$

$$(I.16)$$

(cf. Section 1.6.1). In eqn (I.16), $\mathbf{k}$ has been chosen along the z-axis. The evaluation of the sixth frequency moment

$$\langle\omega_k^6\rangle = \langle\ddot{\tilde{n}}^*(\mathbf{k})\ddot{\tilde{n}}(\mathbf{k})\rangle/S(k)$$

$$(I.17)$$

is also straightforward, although quite tedious. Here we shall simply report the final result; choosing again $\mathbf{k}\,/\!/\,z$-axis, it is found that (e.g. Kim and Nelkin 1971; Yoshida and Takeno 1975)

$$\langle\omega_k^6\rangle = \langle\omega_k^2\rangle\left\{15\left(\frac{k_B T}{m}\right)^2 k^4 + 15\left(\frac{nk_B T}{m^2}\right)k^2\int d\mathbf{r}\,\frac{\partial^2\phi(r)}{\partial z^2}g(r)\right.$$

$$+ \frac{6nk_B T}{m^2}k\int d\mathbf{r}\,\frac{\partial^3\phi(r)}{\partial z^3}\sin kz\, g(r)$$

$$+ \frac{2n}{m}\int d\mathbf{r}\left[\nabla\left(\frac{\partial\phi(r)}{\partial z}\right)\right]^2(1 - \cos kz)g(r)$$

$$+ \left(\frac{n}{m}\right)^2\int d\mathbf{r}\,d\mathbf{r}'\left[\nabla\left(\frac{\partial\phi(r)}{\partial z}\right)\right]\cdot\left[\nabla'\left(\frac{\partial\phi(r')}{\partial z'}\right)\right]$$

$$\left.[1 + \cos k(z - z') - 2\cos kz]g^{(3)}(\mathbf{r}, \mathbf{r}')\right\}$$

$$(I.18)$$

where $\nabla' \equiv \partial/\partial\mathbf{r}'$. The occurrence of the triplet distribution function in the last term of (I.18) clearly prevents an accurate numerical evaluation of $\langle\omega_k^6\rangle$. A similar problem was present even in the expression (I.6) of $\langle\omega_k^6\rangle_s$ (cf. the results (E.8) and (E.13) for $\ddot{K}(0)$). As in that case, the usual remedy is a recourse to the superposition approximation (1.17) for $g^{(3)}$. It is a fortunate circumstance that in eqn (I.18) the errors inherent to such a scheme appear to compensate, so that the final result for $\langle\omega_k^6\rangle$ is found to be remarkably accurate (Bansal and Bruns 1978).

Having determined $\langle\omega_k^6\rangle$, it is possible to proceed as in the self case to establish the initial decay time $\tau(k)$ of $K_L(k, t)$, the second-order memory function of $F(k, t)$. As before, one has

$$\frac{1}{\tau(k)} = \left[\frac{-\ddot{K}_{L}(0)}{2K_{L}(0)}\right]^{1/2} \qquad (I.19)$$

where

$$K_{L}(k,0) = \frac{\langle\omega_{k}^{4}\rangle}{\langle\omega_{k}^{2}\rangle} - \langle\omega_{k}^{2}\rangle \qquad (I.20a)$$

$$-\ddot{K}_{L}(k,0) = \frac{\langle\omega_{k}^{6}\rangle}{\langle\omega_{k}^{2}\rangle} - \left[\frac{\langle\omega_{k}^{4}\rangle}{\langle\omega_{k}^{2}\rangle}\right]^{2}. \qquad (I.20b)$$

Broadly speaking, the values of $\tau_{s}(k)$ and $\tau(k)$ are found to be rather similar. As might be expected, the largest differences occur at relatively small wavevectors, where the presence of structural effects in the frequency moments gives rise to an oscillatory behaviour of $\tau(k)$. Such features are obviously absent in $\tau_{s}(k)$. In any case, at increasing k the oscillations of $\tau(k)$ are rapidly damped; the two times approach each other, and ultimately coincide for large wavevectors.

REFERENCES

Bansal, R. and Bruns, W. (1978). *Phys. Rev. A*, **18**, 1637.
Kim, K. and Nelkin, M. (1971). *Phys. Rev. A*, **4**, 2065.
Yoshida, F. and Takeno, S. (1975). *Progr. Theor. Phys.*, **53**, 293.

Appendix J

Many-particle correlation functions as probed by depolarized light scattering

As remarked in Section 1.5.3, several time correlation functions of interest in liquid dynamics can be written as

$$C(t) = \left\langle \sum_{i,j\neq i} A(\mathbf{r}_{ij}(0)) \sum_{l,m\neq l} A(\mathbf{r}_{lm}(t)) \right\rangle \qquad (J.1)$$

where the dynamical variable A depends on the vector separation between two particles. For example, correlation functions of the form (J.1) are met in the context of depolarized light scattering (DLS) from simple fluids (see eqn (2.54)). In this case

$$A(\mathbf{r}_{ij}) = \frac{1}{\sqrt{N}} a_{zx}^{(2)}(\mathbf{r}_{ij}) \qquad (J.2)$$

where $a_{zx}^{(2)}(\mathbf{r}_{ij})$ is a non-diagonal component of the 'interaction-induced' polarizability tensor of the pair (i,j). Moreover, the potential–potential contribution to the shear stress autocorrelation function can also be written in the form (J.1), with

$$A(\mathbf{r}_{ij}) = \tfrac{1}{2}\left(\frac{nm^{2}}{Nk_{B}T}\right)^{1/2} \frac{z_{ij}x_{ij}}{r_{ij}} \varphi'(r_{ij}) \qquad (J.3)$$

(cf. Section 6.4.1).

Irrespective of the specific meaning of the variable A, eqn (J.1) can formally be written as

$$C(t) = N \iint d\mathbf{r}\, d\mathbf{r}'\, A(\mathbf{r}) A(\mathbf{r}') \mathcal{G}(\mathbf{r}\, 0; \mathbf{r}'t) \qquad (J.4)$$

where

$$\mathcal{G}(\mathbf{r}\, 0;, \mathbf{r}'t) \equiv \frac{1}{N} \sum_{i,j\neq i} \sum_{l,m\neq l} \langle \delta(\mathbf{r} - \mathbf{r}_{ij}(0))\delta(\mathbf{r}' - \mathbf{r}_{lm}(t))\rangle. \qquad (J.5)$$

In other terms, the dynamical features of all the correlation functions (J.1) are ultimately ruled by the quantity $\mathcal{G}(\mathbf{r}\, 0; \mathbf{r}'t)$, which can be interpreted as the joint probability density that two particles are separated by $\mathbf{r}$ at $t = 0$

and two particles (either the same pair, or a different one) are separated by $\mathbf{r}'$ at a later time t. If the pair at time t is the same as the initial one, $\mathcal{G}(\mathbf{r}\,0; \mathbf{r}'t)$ reduces simply to $2G_2(\mathbf{r}\,0; \mathbf{r}'t)$, where G_2 is the time-dependent pair distribution function introduced in Section 1.5.1, and the factor 2 stems from the two possible choices of the labels of the particles (either $l = i$, $m = j$ or $l = j$, $m = i$).

However, in general $\mathcal{G}(\mathbf{r}\,0; \mathbf{r}'t)$, is a complicated many-particle correlation function comprising pair, triplet, and quadruplet contributions (cf. eqn (1.108)). In view of its importance in liquid-state dynamics, it is worthwhile looking for possible connections with other simpler fundamental quantities, such as the van Hove correlation function

$$G(r, t) = \frac{1}{N}\sum_{i,j}\langle\delta(\mathbf{r} + \mathbf{r}_i(0) - \mathbf{r}_j(t))\rangle - n \qquad (J.6)$$

(cf. Section 1.6.2). Whereas $G(r, t)$ refers at most to two particles, $\mathcal{G}(\mathbf{r}\,0; \mathbf{r}'t)$ can involve up to four different atoms. As a consequence, any relationship between $\mathcal{G}$ and G (and, ultimately, any expression of $C(t)$ in terms of simpler pair correlation functions) is likely to be the result of some approximation scheme. A noteworthy exception is the *initial value* of $\eta_{pp}(t)$, which can be expressed exactly in terms of the pair distribution function $g(r)$ (cf. Section 6.4.1). No such simple result exists for the quantity $I_{L,DEP}(t = 0)$, which is proportional to the integrated intensity of the DLS spectrum. In both examples, some sort of approximate treatment is instead required at *finite times*, where the many-particle character of $C(t)$ cannot be circumvented. Even here, however, the analysis turns out to be simpler for $\eta_{pp}(t)$ than for $I_{L,DEP}(t)$. Indeed, as shown in Section 6.4.1, a theory combining kinetic and mode-coupling concepts is found to provide a quite satisfactory account of the dynamical features of $\eta_{pp}(t)$ both at short and at long times. Because of the aforementioned uncertainties, such a comprehensive approach cannot be attempted in the more complicated case of $I_{L,DEP}(t)$. In the following we shall therefore discuss a number of alternative approximation schemes, specifically developed to deal with the DLS correlation functions. Some further insight into the problem is finally provided by the data obtained by computer simulation techniques.

J.1   DIRECT FACTORIZATION OF $\mathcal{G}(\mathbf{r}\,0; \mathbf{r}'t)$

The simplest approximation which one can attempt to connect $\mathcal{G}$ and G is found on the basis of intuitive physical arguments. First, we note that in eqn (J.5) for $\mathcal{G}(\mathbf{r}\,0; \mathbf{r}'t)$ the particles i and j should be a distance $\mathbf{r}$ apart at the same time $t = 0$. It is therefore reasonable to infer that this situation
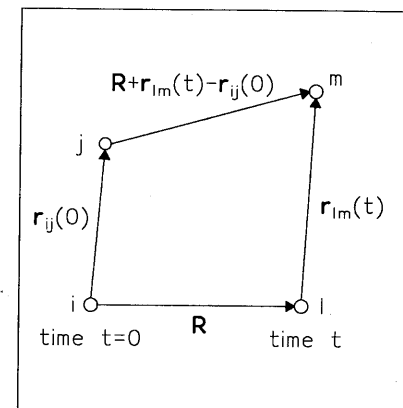
Fig. J.1 Derivation of the approximate expression (J.7) for the quantity $\mathcal{G}(\mathbf{r}\,0; \mathbf{r}'t)$. Particles i and j are considered at time $t = 0$, while particles l and m are considered at a later time t.

should give rise to a term involving the equal-time pair distribution function $g(r)$. For the same reason, the fact that the particles l and m are found at a distance $\mathbf{r}'$ at time t should bring in a term proportional to $g(r')$. Secondly, these two 'static' contributions to $\mathcal{G}$ must be connected by appropriate terms accounting for the 'propagation' of the particles. Assuming that one atom of the second pair (at time t) is at a distance $\mathbf{R}$ from one of the atoms of the first pair, the separation between the other two particles is seen to be $\mathbf{R} - \mathbf{r} + \mathbf{r}'$ (Fig. J.1). The required propagators are then given by the van Hove correlation functions $G(R, t)$ and $G(|\mathbf{R} + \mathbf{r}' - \mathbf{r}|, t)$. Finally, we should integrate over all the separations $\mathbf{R}$ to obtain

$$\mathcal{G}(\mathbf{r}\,0, \mathbf{r}'t) \approx 2ng(r)g(r')\int d\mathbf{R}\, G(R, t)G(|\mathbf{R} + \mathbf{r}' - \mathbf{r}|, t) \qquad (J.7)$$

where the factor 2 accounts for the two possible choices of linking the two pairs. In more formal terms, the many-particle correlation function $\mathcal{G}$ has approximately been factorized into all possible (both static and dynamic) pair contributions by neglecting any effect of higher-order fluctuations.

Rather than in terms of the van Hove correlation functions, it is convenient to express the result (J.7) in terms of the space Fourier transforms of the Gs, namely of the intermediate scattering functions $F(k, t)$. A straightforward calculation then gives:

$$\mathcal{G}(\mathbf{r}, 0; \mathbf{r}', t) \approx 2ng(r)g(r')\left(\frac{1}{2\pi}\right)^3\int d\mathbf{k}\, F^2(k, t)\exp[i\mathbf{k}\cdot(\mathbf{r} - \mathbf{r}')]$$

$$(J.8)$$

We may now insert this approximate result into the expression of $I_{L,DEP}(t)$. Writing the latter in the form (2.59) we find

$$I_{L,DEP}(t) \approx \frac{2n}{15}\left(\frac{1}{2\pi}\right)^3 \int dk\, F^2(k, t) \int dr\, \beta(r)g(r)$$

$$\int dr'\beta(r')g(r')P_2\left[\frac{\mathbf{r}\cdot\mathbf{r}'}{rr'}\right]\exp[i\mathbf{k}\cdot(\mathbf{r}-\mathbf{r}')] \qquad (J.9)$$

where $\beta(r)$ is the anisotropic part of the pair polarizability and $P_2(x)$ denotes the second-order Legendre polynomial. In order to write eqn (J.9) in a more manageable form, it is convenient to exploit the well-known expansions of $P_2(x)$ and of the exponential in terms of spherical harmonics $Y_{LM}(\Omega)$:

$$P_2\left(\frac{\mathbf{r}\cdot\mathbf{r}'}{rr'}\right) = \frac{4\pi}{5}\sum_{M=-2}^{2}[Y_{2M}(\Omega_r)]^* Y_{2M}(\Omega_{r'}) \qquad (J.10)$$

$$\exp(i\mathbf{k}\cdot\boldsymbol{\rho}) = 4\pi\sum_{L=0}^{\infty}\sum_{M=-L}^{L} i^L j_L(k\rho)[Y_{LM}(\Omega_k)]^* Y_{LM}(\Omega_\rho) \qquad (J.11)$$

where the orientation of the vector $\mathbf{r}$ is specified by $\Omega_r \equiv (\theta_r, \phi_r)$, and $j_L(x)$ is the spherical Bessel function of order L. Inserting eqns (J.10) and (J.11) into (J.9) and making use of the orthonormality of the spherical harmonics we readily arrive at

$$I_{L,DEP}(t) \approx \frac{4n}{15}\int_0^\infty dk\, k^2 m^2(k)F^2(k, t). \qquad (J.12)$$

Here the function $m(k)$ is defined as

$$m(k) \equiv \int_0^\infty dr\, r^2 \beta(r)g(r)j_2(kr) \qquad (J.13)$$

with $j_2(x) = [(3/x^2) - 1][\sin(x)/x] - 3[\cos(x)/x^2]$. The result (J.12) suggests a rather simple physical interpretation of the DLS correlation function. In this picture, $I_{L,DEP}(t)$ can be viewed as a weighted sum of double-scattering events, represented by the *squared* terms $F^2(k, t)$, with a k-dependent weight factor which involves the specific scattering mechanism modulated by structural effects.

To have an explicit representation of the function $m(k)$, we adopt the simple *dipole-induced-dipole* (DID) model for the pair polarizability anisotropy (e.g. Gelbart 1974):

$$\beta(r) = 6a_0^2/r^3 \qquad (J.14)$$

where a_0 is the single-atom polarizability. The integral (J.13) can now be evaluated numerically by inserting for $g(r)$ either simulation results or data deduced from diffraction measurements. In Fig. J.2 we have reported $m^2(k)$ as obtained in liquid argon near the triple point, together with the experimental data for the static structure factor $S(k)$ (Yarnell *et al.* 1973). It is apparent that the function $m^2(k)$ is essentially localized at low wavevectors, where the structure factor $S(k) \approx S(0)$ has a small value determined by the isothermal compressibility (cf. eqn (1.15)). The relevance of k-dependent structural effects in eqn (J.12) can be fully appreciated by introducing the normalized intermediate scattering function $f(k, t) \equiv F(k, t)/S(k)$, so that

$$I_{L,DEP}(t) \approx \frac{4n}{15}\int_0^\infty dk\, w(k)f^2(k, t) \qquad (J.15)$$

where $w(k) \equiv k^2 S^2(k)m^2(k)$. The combined effect of the three factors occurring in $w(k)$ is now such that this weight function has a very sharp maximum in the region of the main peak of the static structure factor, and only some minor wiggles in correspondence with the secondary oscillations of $S(k)$ (see Fig. J.2).

A more detailed understanding of the approximate result (J.15) is obtained by adopting simple models for $f(k, t)$. Specifically, we may assume the following.

(i) A *free particle model*, in which $f(k, t) = \exp(-k_B Tk^2 t^2/2m)$ is a Gaussian. This is likely to be appropriate only at very short times, and in a physical situation where the dominant contribution to the integral (J.15) comes from sufficiently large wavevectors.

(ii) A *diffusive model* in the framework of the Vineyard approximation, for which $f(k, t) = \exp(-Dk^2|t|)$ (cf. Section 2.4.1). Although this form is only appropriate for the self portion of $F(k, t)$ in the hydrodynamic region, it is instructive to see the consequences of such a simple scheme on the dynamics predicted for $I_{L,DEP}(t)$.

(iii) A more refined *viscoelastic model*, which incorporates the correct short-time dynamics of $f(k, t)$ up to t^4 included ((Copley and Lovesey 1975) see Section 6.2.1). Besides this, an important feature of this model is its ability to account rather well for the slowing down of $f(k, t)$ for $k \approx k_m$, namely in the wavevector region which provides the largest contribution to the integral (J.15).

The time correlation functions evaluated by inserting these three models into eqn (J.15) can readily be Fourier transformed to obtain the spectral shapes $I_{L,DEP}(\omega)$ shown in Fig. J.3. For illustrative purposes, the three spectra have been reported in a semi-logarithmic scale, so that only the
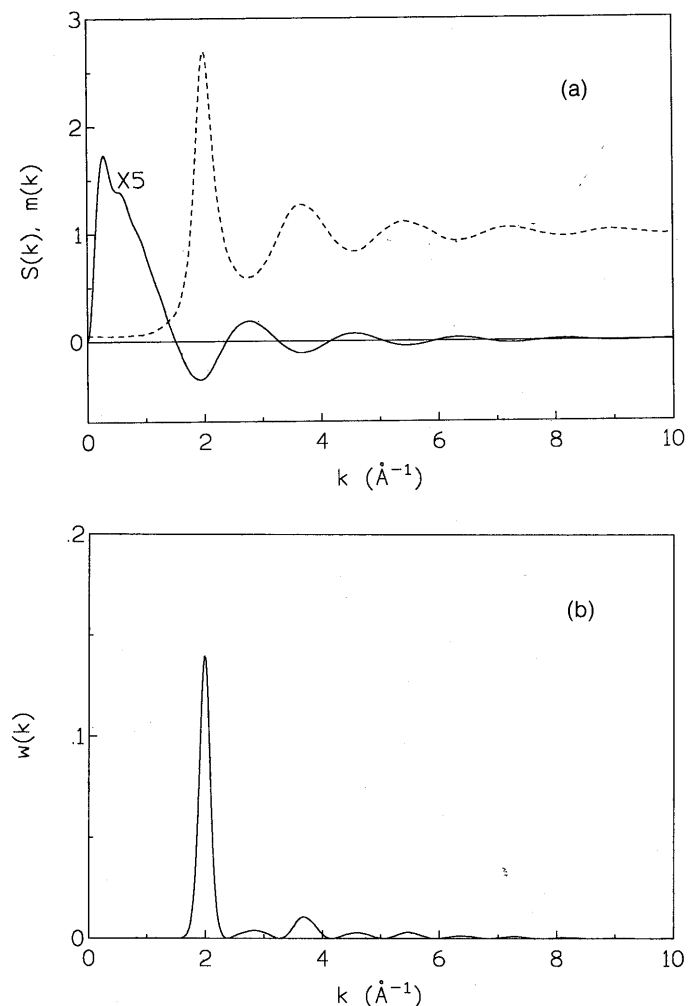
Fig. J.2 Weight functions for depolarized light scattering in the direct factorization approximation for $\mathcal{G}$ and the DID model for $\beta(r)$. (a) The dashed line is the experimental data of $S(k)$ in liquid argon (Yarnell *et al.* 1973), and the full line the function $m^2(k)/(36\,a_0^4)$; (b) The product $w(k) = k^2 S^2(k) m^2(k)$, that is the full weight which appears in eqn (J.15).
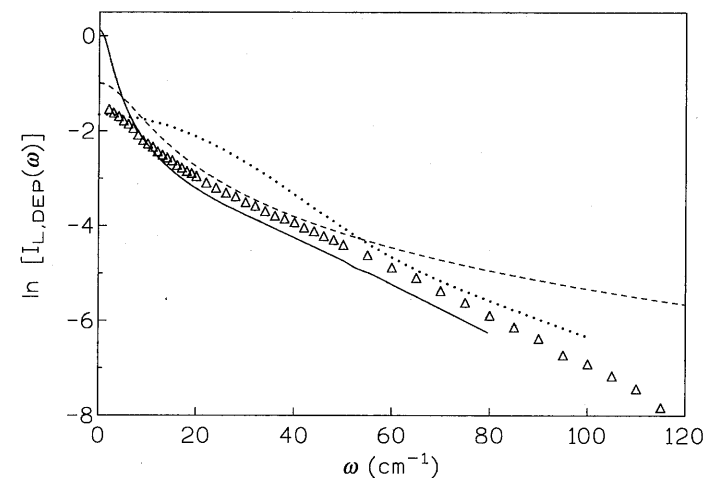
Fig. J.3 Depolarized-light-scattering spectrum of liquid Ar at the melting point. The dotted line denotes the results of the free-particle model, the dashed line those of the diffusive model, and the full line those of the viscoelastic theory (respectively, models (i), (ii), and (iii) in the text). The experimental spectra of An *et al.* (1976) and of Varshneya *et al.* (1981) are represented by the triangles (the differences between the two sets of data being within the size of the symbols). In this semi-logarithmic plot, the experimental spectrum has been shifted by an arbitrary amount with respect to the theoretical curves (which are normalized to a common integrated intensity = 1).

relative comparison of the shapes is meaningful. It is apparent that there are substantial differences among the three theoretical curves, especially between the predictions obtained by the models (i) and (ii) . In this respect, the spectral shape deduced from the viscoelastic model (iii) has an 'intermediate' character, being qualitatively similar to the one obtained from the diffusive model at intermediate frequencies and to the one corresponding to free particles for large frequencies.

A definitive answer about the validity of these theoretical results can only be obtained from a comparison with the available experimental data. For liquid argon near the melting point, DLS spectra have been reported by An *et al.* (1976) and by Varshneya *et al.* (1981), with only minor differences between the two sets of data. As illustrated in Fig. J.3, the experimental spectrum is found in any case to be markedly different from the one obtained by the free-particle model (i). On the other hand, the diffusive model predictions are seen to be acceptable only at low frequencies, $\omega < 50\,\mathrm{cm}^{-1}$. In contrast, the theoretical spectra deduced from the viscoelastic model appear to be in reasonable agreement with the data for

all frequencies $\omega > 10\,\mathrm{cm}^{-1}$. Apart from possible shortcomings due to the use of the DID model for $\beta(r)$, the ultimate origin of the remaining discrepancies between the theoretical and the experimental spectra can be traced back to the approximation (J.7) for $\mathcal{G}(r\,0;\,r'\,t)$.

Before discussing alternative approximation schemes for the many-particle dynamics, it is interesting to compare the previous theoretical spectra with those predicted by a naïve model in which only *pair motion* is taken into account. In other words, any contribution to $\mathcal{G}$ coming from triplets and quadruplets of particles is ignored. In such a case, rather than dealing with eqn (2.58), we would simply have

$$[I_{\mathrm{L,DEP}}(t)]_{\mathrm{pairs}} = \frac{2}{15N}\sum_{i,j\neq i}\langle \beta(r_{ij}(0))\beta(r_{ij}(t))P_2(\cos\theta(ij,0;ij,t))\rangle$$

$$= \frac{2}{15}\int d\mathbf{r}\int d\mathbf{r}'\,\beta(r)\beta(r')P_2\left[\frac{(\mathbf{r}\cdot\mathbf{r}')}{rr'}\right]G_2(r\,0;\,r'\,t) \quad (\mathrm{J.16})$$

where we have exploited the definition (1.84) of the time-dependent pair distribution function G_2. The result (J.16) is clearly equivalent to eqn (2.59) with $\mathcal{G}(r\,0;\,r'\,t)$ replaced by its pair contribution $2G_2(r\,0;\,r'\,t)$. A priori, this replacement is expected to be justified only at low densities.

Rather than attempting an accurate treatment of the pair dynamics (such as that obtained on the basis of eqn (1.101)), we shall content ourselves with a simpler treatment which is based on the same approximations previously adopted for $\mathcal{G}$. Pursuing the same arguments as before, the final result for $G_2(r\,0;\,r'\,t)$ turns out to be formally analogous to eqn (J.7), with the van Hove correlation functions G replaced by their self counterparts G_s:

$$G_2(r\,0,\,r'\,t) \approx ng(r)g(r')\int d\mathbf{R}\,G_s(R,t)G_s(|\mathbf{R}+\mathbf{r}'-\mathbf{r}|,t) \quad (\mathrm{J.17})$$

(note that in the present case there is only one possible way to connect the particles; as a consequence, the factor 2 in eqn (J.7) is now absent). The result (J.17) is seen to be quite similar to the 'convolution approximation' (1.90), the only difference being the presence of $g(r')$ as an additional factor. As it stands, eqn (J.17) does not reproduce the correct initial value (1.85), in contrast with eqn (1.90). However, the inclusion of $g(r')$ has the merit of taking approximately into account the dynamical features illustrated in Fig. 1.10, thus providing a more appropriate description of the evolution of G_2 at finite times.

Inserting the approximate result (J.17) into eqn (J.16) and turning to a k-space representation in terms of the self-intermediate scattering function F_s, we may perform the angular integrations over $\mathbf{r}$ and $\mathbf{r}'$ by the same procedure previously adopted for the total correlation $I_{\mathrm{L,DEP}}(t)$. Eventually we end up with
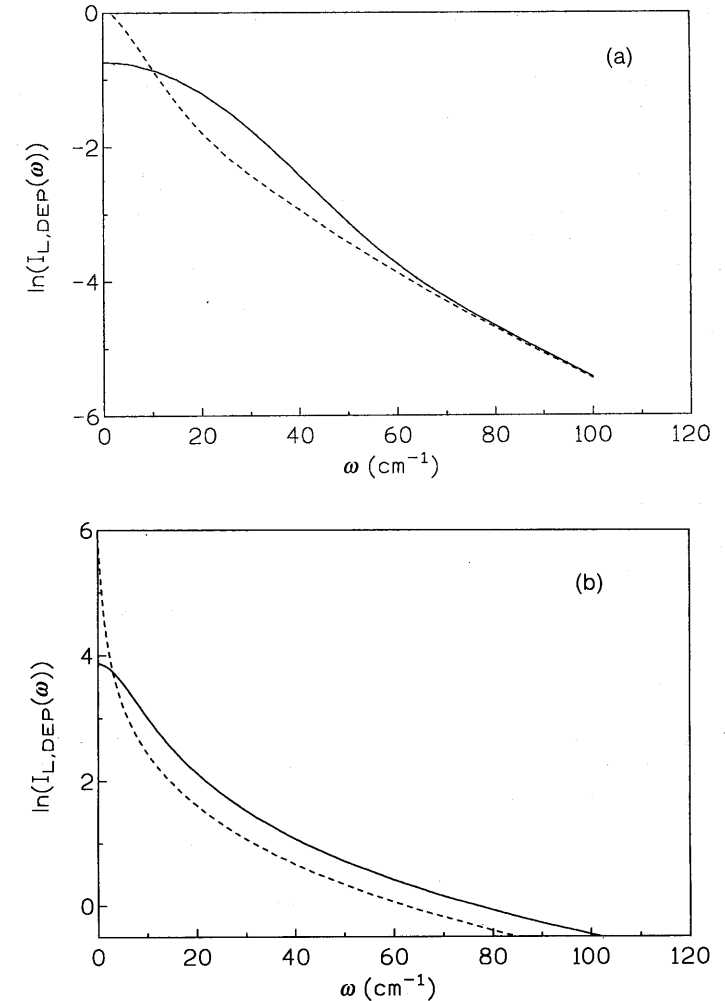
Fig. J.4 Contribution of the pair dynamics (dashed line) to the total depolarized spectrum (full line) of liquid Ar at the melting point: (a) results obtained in the free-particle model; (b) results obtained in the diffusive model.

$$[I_{\mathrm{L,DEP}}(t)]_{\mathrm{pairs}} \approx \frac{4n}{15}\int_0^\infty dk\,k^2 m^2(k)F_s^2(k,t) \quad (\mathrm{J.18})$$

which is seen to differ from the result (J.12) only for the substitution $F \rightarrow F_s$. Since $F_s(k,t=0)=1$, no normalization is now needed; comparing with eqn (J.15), one notices a substantial change of the full

k-dependent weight factor in the integral, where the factor $S^2(k)$ is now lacking.

Although eqn (J.18) is not expected to provide a reliable description of the DLS correlation in dense fluids, there are some interesting features which are worth mentioning. In particular, one may insert into eqn (J.18) for F_s the two limiting expressions previously referred to as models (i) and (ii), evaluate the spectra and compare the results with those obtained in the same approximations from eqn (J.15). Such a comparison is reported in Fig. J.4, which again refers to liquid argon. It is apparent that the total and the pair spectra evaluated by the free-particle model merge for frequencies ω above 70–80 cm^{-1}. In contrast, the use of the diffusive model yields remarkably similar spectral shapes even at much lower frequencies; on the semi-logarithmic plot of the figure, the difference between the two results does not change up to very high frequencies, implying that the two spectra differ by a constant factor. In both cases, one may conclude that at large ω the total spectral shape appears to be determined by pair dynamics.

J.2 BEYOND THE DIRECT FACTORIZATION APPROXIMATION

An alternative approach for $\mathcal{G}(\mathbf{r}\,0;\mathbf{r}'t)$ can be developed by turning to a k-space representation of the δ-functions in eqn (J.5) (Madden 1978). This makes it possible to extract the terms in $\mathbf{r}$ and $\mathbf{r}'$ from the statistical average, and to perform the integration over the angular parts of these vectors. Consequently, eqn (2.59) becomes

$$I_{L,DEP}(t) = \frac{16\pi^2}{15}\left(\frac{1}{2\pi}\right)^6 \int d\mathbf{k} \int d\mathbf{k}' \int_0^\infty dr\, r^2 \beta(r) j_2(kr)$$

$$\int_0^\infty dr'\, r'^2 \beta(r') j_2(k'r') P_2\left[\frac{(\mathbf{k}\cdot\mathbf{k}')}{kk'}\right] \mathcal{F}(\mathbf{k}\,0;\mathbf{k}'t) \quad (J.19)$$

where the quantity

$$\mathcal{F}(\mathbf{k}\,0;\mathbf{k}'t) \equiv \frac{1}{N}\sum_{i,j\neq i}\sum_{l,m\neq l}\langle\exp\{i\mathbf{k}\cdot[\mathbf{r}_i(0)-\mathbf{r}_j(0)]\}$$

$$\exp\{-i\mathbf{k}'\cdot[\mathbf{r}_l(t)-\mathbf{r}_m(t)]\}\rangle \quad (J.20)$$

can be interpreted as a sort of *bilinear* density correlation function. Rather than proceeding to a direct 'decoupling' of eqn (J.20), Madden (1978) has worked out an approximate theory for the Laplace transform of $\mathcal{F}(\mathbf{k}\,0;\mathbf{k}'t)$ based on the Mori projection operator framework. Since the many-particle

character of eqn (J.20) is retained, the approach is superior to the direct factorization approximation, even if in practice it is necessary to resort to several simplifying assumptions (such as the restriction to the case $\mathbf{k}' = \mathbf{k}$ and the use of the superposition approximation for the evaluation of the frequency moments). For the DLS spectrum, the final result of this approach can be cast in the form

$$I_{L,DEP}(\omega) \propto \int_0^\infty dk\, k^2 [m'(k)]^2 \mathcal{F}(k,\omega). \quad (J.21)$$

Here $\mathcal{F}(k,\omega)$ is the spectrum of $\mathcal{F}(\mathbf{k}\,0;\mathbf{k}\,t)$, and

$$m'(k) \equiv \int_d^\infty dr\, r^2 \beta(r) j_2(kr) \quad (J.22)$$

where the cutoff separation d (necessary to prevent self-polarization) is chosen of the order of the distance of closest approach. Inserting for $\mathcal{F}(k,\omega)$ the results obtained from the above-mentioned Mori approach and performing the wavevector integration, Madden was able to obtain a DLS spectrum whose shape closely resembles the one observed experimentally in liquid argon. Specific results were obtained by adopting for $\beta(r)$ both the usual DID model (J.14) and a suitably modified form proposed by Oxtoby and Gelbart (1975), with no substantial changes in the predicted spectral shapes.

A closer examination of the weight of the different wavevectors in the integral (J.21) reveals that the dominant low-frequency portion of the DLS spectrum is ruled by the contributions of the wavevectors near the position k_m of the main peak of $S(k)$. On the other hand, the high-frequency tail of the spectrum is largely determined by the wavevectors $k \gg k_m$. Both these findings are consistent with the results discussed in the previous section.

The success of the approach in accounting for the interaction-induced spectral shapes has subsequently been confirmed by a detailed experimental analysis of the DLS spectra of liquid krypton (An *et al.* 1979). As noted by Madden himself, a delicate point of his theory is the choice of the cutoff distance d in eqn (J.22). Although when interpreted as a distance of closest approach the value of d eventually chosen appears to be quite reasonable, minor changes in this quantity are found to alter the quality of the theoretical predictions substantially. Also, the choice of d as a parameter to be adapted for a successful account of the line shape is found to yield rather poor results for the integrated intensity of the DLS spectrum. These shortcomings are partly due to our poor knowledge of the quantity $\beta(r)$ at very small separations, a range where the DID model is surely no longer appropriate. Similar defects are in principle present even in the simple

approximation scheme discussed in Section J.1, and are effectively only circumvented by the presence of the pair distribution function in eqn (J.13).

J.3 ALTERNATIVE APPROACHES FOR THE DLS SPECTRUM: A BRIEF SURVEY

The shapes of the experimental DLS spectra of rare-gas fluids are found to be remarkably similar: when appropriately scaled, they can indeed be made to nearly coincide, thus providing an evidence for the existence of a 'corresponding states law' at a dynamical level (e.g. Rouch *et al.* 1977). In all these fluids, the frequency dependence of the spectra is characterized by a fast monotonic decrease, which can approximately be described by an exponential law, $I_{L,DEP}(\omega) \propto \exp(-\omega/\Delta)$. Adopting this simple represen-tation, Fleury *et al.* (1971) reported that in a wide range of thermodynamic states of neon, argon, and krypton the observed slope Δ is found to increase both with temperature (as $\sqrt{T}$) and with density (according a parabolic law). Although a closer examination of the spectra reveals deviations from a single-exponential decay (e.g. Fig. J.3 for liquid argon), the simplicity of all these empirical results is undoubtedly attractive. An interpretation of these findings has in fact been attempted in a number of theoretical works, ranging from simple *ad hoc* treatments (e.g. Balucani and Vallauri 1979*b*) to more sophisticated kinetic approaches (Madden and Evans 1988).

Another important quantity of physical interest in the DLS spectra is the integrated intensity $I_{L,DEP} = \int_{-\infty}^{\infty} d\omega\, I_{L,DEP}(\omega)$. Although this will be discussed in some detail in Section J.5, it is worthwhile reporting here a few qualitative remarks about the dependence of $I_{L,DEP}$ on the thermo-dynamic state of the fluid. As shown in Appendix C, the intensive quantity $I_{L,DEP}$ is basically the scattering cross section per particle (cf. eqn (C.48)). As a result, the depolarized cross section $(d\sigma/d\Omega)_{DEP} \propto nI_{L,DEP}$ should be very small in dilute gases, where the phenomenon is basically ruled by the dynamics of atomic pairs. As in this limit $I_{L,DEP} \approx [I_{L,DEP}(t=0)]_{pairs} \propto n$ (cf. eqns (J.16) and (1.85)), for small n the depolarized cross section is predicted to be proportional to the *square* of the density. This law is indeed confirmed by the experiments performed in dilute gases, giving a clear indication of the role played by binary collisions (hence the attribute 'collision induced', frequently given to this kind of light scattering), or in other terms of the dominant contribution of atomic pairs. As the density increases, however, $(d\sigma/d\Omega)_{DEP}$ is gradually found to increase less than implied by the n^2 law, indicating that three-particle clusters begin to play an important role. Qualitatively, the smaller values of the cross section $(d\sigma/d\Omega)_{DEP}$ with respect to the n^2 prediction (or equivalently of $I_{L,DEP}$ with respect to a linear increase with n) can be understood arguing that

the presence of three neighbouring particles tends to increase the local symmetry seen by the incident photons, and thereby to decrease any depolarized component in the scattered light. At even higher densities, the effect becomes so marked that the overall intensity $I_{L,DEP}$ reaches a plateau, and subsequently rapidly decreases with n. As a result, in the liquid range the integrated intensity is again very small, indicating that the increased close packing has given rise to nearly symmetrical arrangements of particles. Eventually, in a crystalline solid any residual depolarizing effect can only be due to the displacement of the atoms from their equilib-rium positions in the lattice, and the many-particle correlations probed by DLS spectra can be viewed as steming from a 'two-phonon correlation function' (Fleury *et al.* 1973; Alder *et al.* 1976). The growing importance of nearly symmetrical clusters of particles in dense fluids naturally suggests an interpretation of the DLS spectra in terms of *lattice-gas models*, in which an important parameter is the ratio between the actual number density n and the one in an ideal system in which all the lattice sites are occupied. Such concepts have in fact been adopted both in an early attempt to account for the density dependence of the integrated intensity (Thibeau *et al.* 1968) as well in a more comprehensive study of the spectral features of $I_{L,DEP}(\omega)$ (Guillot *et al.* 1980, 1982).

We close this section by mentioning a few recent studies and develop-ments of DLS spectroscopy. The close similarity between the DLS correla-tions and those ruling the dynamics of shear stresses has been noted and explicitly analysed by Montrose *et al.* (1991). As already noted at the beginning of this appendix, further studies in this direction will certainly provide a better understanding of many-particle correlations in dense fluids. This will possibly pave the way for a rigorous theory of the dynamical features of DLS spectra, based on a combined kinetic and mode-coupling approach similar to those described in Chapters 5 and 6. The achievement of such an objective is not likely to be far off, as indicated by the successful use of mode-coupling concepts in two recent applications of DLS spectroscopy to the study of the liquid–glass transition (Tao *et al.* 1991, 1992).

J.4 SEPARATION INTO PAIR, TRIPLET, AND QUADRUPLET CONTRIBUTIONS

It is readily seen that eqn (J.20) can be decomposed into pair, triplet, and quadruplet contributions according to

$$\mathfrak{F}(k\,0;\,k't) = 2NF_2(k\,0;\,k't) + 4N^2F_3(k\,0;\,k't) + N^3F_4(k\,0;\,k't)$$

$$(J.23)$$

where $N \gg 1$, and

$$F_2(\mathbf{k}\,0;\mathbf{k}'t) \equiv \langle \exp\{-i\mathbf{k}\cdot[\mathbf{r}_1(0) - \mathbf{r}_2(0)]\}\exp\{i\mathbf{k}'\cdot[\mathbf{r}_1(t) - \mathbf{r}_2(t)]\}\rangle,$$
$$(J.24)$$

$$F_3(\mathbf{k}\,0;\mathbf{k}'t) \equiv \langle \exp\{-i\mathbf{k}\cdot[\mathbf{r}_1(0) - \mathbf{r}_2(0)]\}\exp\{i\mathbf{k}'\cdot[\mathbf{r}_1(t) - \mathbf{r}_3(t)]\}\rangle,$$
$$(J.25)$$

$$F_4(\mathbf{k}\,0;\mathbf{k}'t) \equiv \langle \exp\{-i\mathbf{k}\cdot[\mathbf{r}_1(0) - \mathbf{r}_2(0)]\}\exp\{i\mathbf{k}'\cdot[\mathbf{r}_3(t) - \mathbf{r}_4(t)]\}\rangle.$$
$$(J.26)$$

Although interesting, the decomposition (J.23) is of limited use in the liquid range because of our poor knowledge of the triplet and quadruplet terms (J.25) and (J.26). To throw some light on the role of the different contributions in the DLS correlation function $I_{L,DEP}(t)$, Ladd *et al.* (1979) made recourse to computer simulations, performed in Lennard–Jones argon at different densities. In all cases, the authors assumed a DID model for the pair polarizability anisotropy $\beta(r)$. More specifically, Ladd *et al.* inserted (J.23) into eqn (J.19), obtaining a result which can be written in the form

$$I_{L,DEP}(t) = I_2(t) + I_3(t) + I_4(t) \qquad (J.27)$$

where $I_2(t)$, $I_3(t)$, and $I_4(t)$ denote the time-dependent contributions due to pairs, triplet, and quadruplets, respectively.

The simulation data obtained in the liquid range for all these time correlation functions are reported in Fig. J.5. The most striking feature is an almost complete cancellation among $I_2(t)$, $I_3(t)$, and $I_4(t)$ in the long-time region. As a result, the time extent of the total correlation function $I_{L,DEP}(t)$ is much shorter than those of the partial contributions. As both $I_2(t)$ and $I_4(t)$ are always found to be positive, the origin of the effect is due to the rather large negative values of the triplet contribution $I_3(t)$. Although the cancellation is complete only for sufficiently long times (where the ratios among the three components $I_2(t)$, $I_3(t)$, and $I_4(t)$ are found to be $1:-2:1$), it is apparent from Fig. J.5 that the effect is present even at much shorter times. In particular, at $t = 0$ the quantities $I_2(0)$, $|I_3(0)|$, and $I_4(0)$ are found to be noticeably larger than the initial value of the total correlation function. Since $I_{L,DEP}(t = 0)$ is essentially the integrated intensity of the DLS spectrum, the simulation data provide a first insight into the origin of the small values of $I_{L,DEP}$ experimentally observed in the liquid region. A noteworthy point stressed by Ladd *et al.* is that the ratios of the pair : triplet : quadruplet terms would be exactly $1:-2:1$ *at all times* if the environment of a particle were perfectly isotropic (as in a static cubic lattice). Consequently, the fact that in the liquid one only observes these values at long times and the fact that even the $t = 0$ ratios are not very different (being $1:-1.8:0.8$) indicates that in a dense fluid the deviations from isotropic environments are quite small.
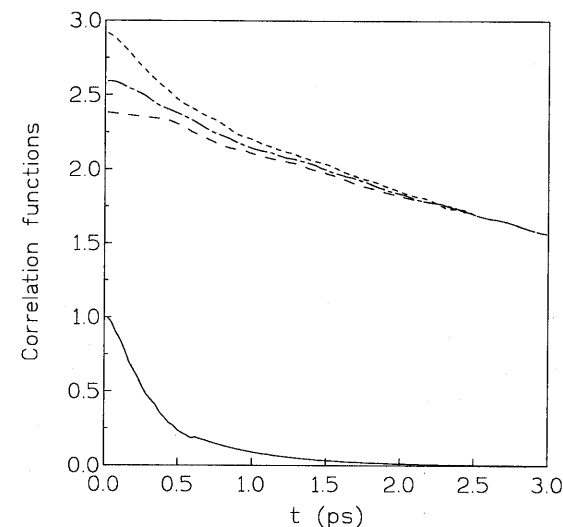
Fig. J.5 Simulation data for Lennard–Jones Ar near the triple point showing the pair (short-dashed line), triplet (dot-dashed line) and quadruplet (long-dashed line) contributions to the full DLS time correlation function $I_{L,DEP}(t)/I_{L,DEP}(t = 0)$ (full line). For clarity, the pair and quadruplet terms have been divided by a factor 10, and the triplet term by a factor -20. In these units, the approach of the three partial contributions to a common value indicates the presence of a strong cancellation effect. All the data refer to a DID model for the polarizability anisotropy. Redrawn from Ladd *et al.* (1979).

To interpret all these simulation results, Ladd *et al.* made the assumption that beyond a short-time interval the quantity $\mathcal{F}(\mathbf{k}\,0;\mathbf{k}'t)$ defined by eqn (J.20) may be factorized as

$$\mathcal{F}(\mathbf{k}\,0;\mathbf{k}'t) \approx \frac{1}{N}\sum_{i,j \neq i}\sum_{l,m \neq l}\langle \exp[-i\mathbf{k}\cdot\mathbf{r}_{ij}(0)]\exp[i\mathbf{k}'\cdot\mathbf{r}_{lm}(0)]\rangle$$
$$\langle \exp\{-i\mathbf{k}'\cdot[\mathbf{r}_{lm}(t) - \mathbf{r}_{lm}(0)]\}\rangle \qquad (J.28)$$

where the second average in eqn (J.28) can be regarded as a self-intermediate scattering function for the pair (l, m). Such a quantity is basically the space Fourier transform of the time-dependent pair distribution function $G_2(\mathbf{r}\,0;\mathbf{r}'t)$ introduced in eqn (1.87). Adopting for the latter the convolution approximation (1.90), it is readily seen that in the diffusive regime

$$\langle \exp\{-i\mathbf{k}'\cdot[\mathbf{r}_{lm}(t) - \mathbf{r}_{lm}(0)]\}\rangle \approx \exp(-2Dk'^2t) \qquad (J.29)$$

(cf. eqn (1.93)). To arrive at a manageable expression of eqn (J.28), Ladd *et al.* assumed that the dominant contribution to the DLS is provided by

the terms with $\mathbf{k}' = \mathbf{k}$ (cf. a similar assumption in Section J.2), and finally evaluated the first static average in eqn (J.28) by a superposition scheme. In such a way they arrived at the approximate result

$$\mathfrak{F}(\mathbf{k}\,0;\mathbf{k}'\,t) \approx N[S(k)]^2 \exp(-2Dk^2t)\delta_{\mathbf{k}',\mathbf{k}}$$

$$= (2\pi)^3 n[S(k)]^2 \exp(-2Dk^2t)\delta(\mathbf{k}' - \mathbf{k}). \qquad (J.30)$$

Inserting (J.30) into eqn (J.19), one eventually obtains

$$I_{L,DEP}(t) \approx \frac{4n}{15} \int_0^\infty dk\, k^2 [m'(k)]^2 [S(k)]^2 \exp(-2Dk^2t) \qquad (J.31)$$

where $m'(k)$ is defined by eqn (J.22). Equation (J.31) closely resembles the result (J.15) in which a diffusive model has been adopted for $f(k, t)$. As a consequence, the spectrum deduced from eqn (J.31) does not provide an accurate representation of the DLS lineshape at high frequencies, and moreover suffers from the same defects noted in Section J.2 in connection with the artificial cutoff separation d. The important point is, however, that approximations similar to those made for $I_{L,DEP}(t)$ can easily be extended even to the separate contributions $I_2(t)$, $I_3(t)$, and $I_4(t)$ with the result that

$$I_2(t) \approx \frac{4n}{15} \int_0^\infty dk\, k^2 [m'(k)]^2 \exp(-2Dk^2t), \qquad (J.32)$$

$$I_3(t) \approx \frac{4n}{15} \int_0^\infty dk\, k^2 [m'(k)]^2 2[S(k) - 1] \exp(-2Dk^2t), \qquad (J.33)$$

$$I_4(t) \approx \frac{4n}{15} \int_0^\infty dk\, k^2 [m'(k)]^2 [S(k) - 1]^2 \exp(-2Dk^2t), \qquad (J.34)$$

where clearly

$$1 + 2[S(k) - 1] + [S(k) - 1]^2 = [S(k)]^2. \qquad (J.35)$$

Ladd *et al.* show that at sufficiently long times the dominant contribution to eqns (J.32)–(J.34) comes from the low wavevector region, where $S(k) \ll 1$. As a result, at long times the ratios of the pair : triplet : quadruplet terms approach the values $1 : -2 : 1$, as is indeed observed in the simulation data. By the same arguments, the total correlation function $I_{L,DEP}(t)$ (which involves $S^2(k)$) is found to be negligible for long times. On a shorter timescale, the dominant contribution to eqn (J.31) does indeed come from the wavevectors $k \approx k_m$ (cf. Section J.1).

J.5 THE INTEGRATED INTENSITY AND THE SECOND FREQUENCY MOMENT OF THE DLS SPECTRUM

In the previous sections we have seen that the *shape* of the DLS spectrum in dense fluids can be accounted for reasonably well by a number of approximation schemes for the dynamic correlation function $I_{L,DEP}(t)$. In contrast, the situation for the integrated intensity $I_{L,DEP} \equiv I_{L,DEP}(t = 0)$ is less satisfactory, even leaving aside any problem connected with the precise form of the pair polarizability anisotropy $\beta(r)$. The origin of this unfortunate circumstance lies in the fact that the small magnitude of $I_{L,DEP}$ is ultimately determined by a delicate balance among the various partial contributions due to pairs, triplets, and quadruplets. As a result of the large amount of cancellation among these terms at high density, any small error introduced by an approximate treatment of these partial static averages is likely to be considerably magnified in the evaluation of the total intensity $I_{L,DEP}$.

As already mentioned in Section J.3, the first attempt to account for the density dependence of the DLS integrated intensity in dense fluids and liquids made use of a lattice-gas model (Thibeau *et al.* 1968). Within a DID model for $\beta(r)$, it is found that

$$I_{L,DEP} = A_2 n[1 - (n/n_0)^2] \qquad (J.36)$$

where the quantity A_2 can be determined by the low-density data (or evaluated in terms of the pair contribution), and the ratio n/n_0 is a measure of the relative 'filling' of the lattice with respect to a situation in which all sites are occupied and the number density is n_0. Rather than comparing the predictions of eqn (J.36) with the absolute integrated intensities, Thibeau *et al.* tested their approach in rare-gas fluids by looking at an easily measurable quantity, the so-called 'depolarization ratio' $I_{L,DEP}/I_L^{zz}$. While the agreement between theory and experiment is rather good at moderate densities, the comparison is found to be less satisfactory in dense fluids, particularly if one notes that the model does not provide a well-defined recipe to establish the value of n_0.

An alternative approach is to rely on the results found for the n dependence of $I_{L,DEP}$ in moderately dense fluids (which can be obtained rather accurately) and to adopt some extrapolation scheme to infer the behaviour at high densities. This procedure has been followed with some success in a number of cases (e.g. Balucani and Vallauri 1979a), but has a clear empirical character.

A systematic theoretical analysis of both the integrated intensity and the second frequency moment of the DLS spectrum has subsequently been worked out by Briganti *et al.* (1986). Besides making further tests on the
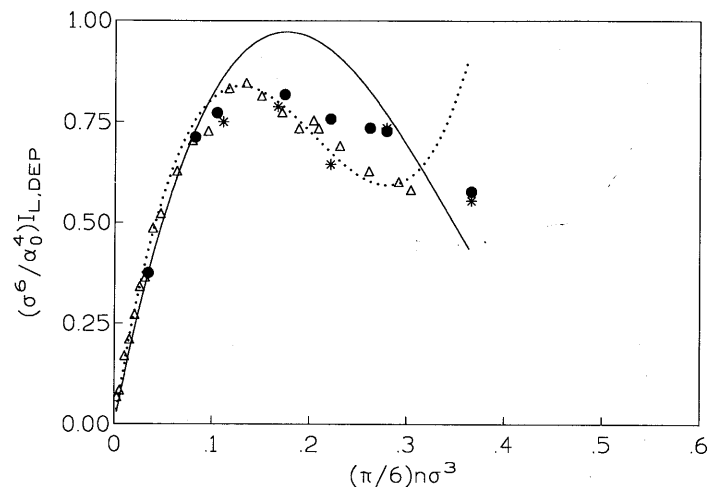
Fig. J.6 Density dependence of $(\sigma^6/a_0^4)I_{\mathrm{L,DEP}}$ in gaseous Ar at room temperature. This dimensionless quantity is proportional to the actual integrated intensity divided by the number density of the system. The triangles denote the experimental data (Zoppi *et al.* 1981), along with a 'virial-expansion' fit of the form $A_2 n + A_3 n^2 + A_4 n^3$ (dotted line). The dots are the simulation data obtained for a Lennard–Jones system within the DID model (Balucani and Vallauri 1979*b*); the asterisks are the corresponding theoretical results evaluated within a superposition scheme (Briganti *et al.* 1986). The full line denotes the prediction of the lattice-gas model (eqn (J.36)) with the quantity $\pi n_0 \sigma^3/6$ chosen as 0.527.

Table J.1 Comparison between the dimensionless DLS integrated intensities for liquid Ar as obtained in the experiment and in various computer simulations. The first experimental value reported for this quantity was 0.03 (Fleury and McTague 1969).

T (K)	$\pi n \sigma^3/6$	$[\sigma^6 I_{\mathrm{L,DEP}}/a_0^4]_{\mathrm{exp}}$	$[\sigma^6 I_{\mathrm{L,DEP}}/a_0^4]_{\mathrm{simul}}$
90.8	0.428	0.11 ± 0.01[a]	
89.0	0.433		0.195[a]
89.0	0.433		0.135[b]
88.8	0.428		0.120[c]

[a] Varshneya *et al.* (1981). The simulation value refers to Lennard–Jones liquid argon with a DID model for $\beta(r)$.
[b] Zoppi *et al.* (1981). Again, Lennard–Jones liquid argon, but with $\beta(r)$ empirically determined from low-density data.
[c] Zoppi and Spinelli (1986). Liquid argon with the pair interaction potential of Barker *et al.* (1971); $\beta(r)$ has the same form as in [b].

results of the previous approaches, these authors investigated in some detail the consequences of a superposition approximation scheme on the triplet and quadruplet contributions to $I_{\mathrm{L,DEP}}$ at different densities. Specific results were obtained for a Lennard–Jones fluid and within a DID model for the pair polarizability anisotropy. In order to assess the validity of the approximations without any ambiguity, the theoretical results were tested against the computer simulation data obtained by Alder *et al.* (1973*b*) for the same model system and the same DID mechanism for $\beta(r)$. The overall agreement between the two sets of data is found to be fairly good, as shown in Fig. J.6. For completeness, in the figure we have also reported the lattice-gas predictions by Thibeau *et al.* (1968) and the experimental findings for compressed gaseous argon at room temperature (Zoppi *et al.* 1981). Aside from any defect of the theoretical approaches, from Fig. J.6 it is apparent that there is some discrepancy between the simulation data for $I_{\mathrm{L,DEP}}$ (which in principle should be 'exact') and the experimental ones.

A much larger discrepancy was initially found in the liquid range, where the simulations of Alder *et al.* (1973*b*) gave a value of $I_{\mathrm{L,DEP}}$ which was

more than five times larger than the first experimental determination of this quantity reported by Fleury and McTague (1969). In contrast, the DLS spectrum obtained by Alder *et al.* (1973*a*) from computer simulations performed in the same conditions (namely, Lennard–Jones fluids and DID model for $\beta(r)$) was found to reproduce the experimental lineshape rather well.

This contradictory situation stimulated more accurate experimental measurements of $I_{\mathrm{L,DEP}}$, as well as a careful analysis of any possible source of 'cutoff errors' of the simulation result for $I_{\mathrm{L,DEP}}$ at high density. Indeed, for fixed $N \approx 10^2 – 10^3$, the size of the simulation box becomes rather small in the liquid range and any premature truncation in space may considerably affect the relatively long-ranged DID correlations, particularly in the static case (Ladd *et al.* 1980). Moreover, the sensitivity of the value of $I_{\mathrm{L,DEP}}$ to these features stimulated a critical revision of all the basic assumptions, including the models of the interaction potential and of the pair polarizability, as well as possible defects of the pairwise assumption for these two quantities.

The final results of all this activity are quite gratifying (see Table J.1). First of all, new accurate measurements in the liquid range (Varshneya *et al.* 1981) gave a value of $I_{\mathrm{L,DEP}}$ much larger than the original one. As a consequence, the discrepancy from the experimental result of the best-simulated value of $I_{\mathrm{L,DEP}}$ in the Lennard–Jones plus DID model was considerably reduced. This difference is brought to ~20% by using in the simulations an empirical model of $\beta(r)$ deduced from low-density measurements (Zoppi *et al.* 1981). Finally, even this residual discrepancy can be decreased and

brought to lie within the experimental accuracy by using a more realistic model for the argon interaction potential (Zoppi and Spinelli 1986).

To conclude this section, we mention that the splitting (J.27) of $I_{L,DEP}(t)$ into pair, triplet, and quadruplet contributions can be exploited to evaluate the short-time behaviour of this correlation function. A noteworthy result of this analysis is that the quantity $\ddot{I}_{L,DEP}(t=0)$ — namely, the unnormalized *second frequency moment* $\overline{\omega^2}$ of the DLS spectrum — turns out to depend only on pair and triplet terms. Any quadruplet contribution would in fact involve velocity averages of the form $\langle v_{ij}^z v_{lm}^z \rangle$ where $\mathbf{v}_{ij} = \mathbf{v}_i - \mathbf{v}_j$ and with labels $i, j, l,$ and m all different, eventually giving a vanishing result. As a consequence, the evaluation of $\overline{\omega^2}$ is somewhat simpler than that of $I_{L,DEP}$, and can in fact be performed even at rather high density adopting a superposition approximation (Balucani and Vallauri 1979*b*; Briganti *et al.* 1986). The knowledge of $I_{L,DEP}$ and $\overline{\omega^2}$ may in turn be exploited to account for the gross features of the DLS spectrum at different densities (e.g. Zoppi *et al.* 1981).

REFERENCES

Alder, B. J., Strauss, H. L., and Weis, J. J. (1973*a*). *J. Chem. Phys.*, **59**, 1002.

Alder, B. J., Weis, J. J., and Strauss, H. L. (1973*b*). *Phys. Rev. A*, **7**, 281.

Alder, B. J., Strauss, H. L., Weis, J. J., Hansen, J. P., and Klein, M. L. (1976). *Physica*, **88A**, 347.

An, S. C., Montrose, C. J., and Litovitz, T. A. (1976). *J. Chem. Phys.*, **64**, 3717.

An, S. C., Fishman, L., Litovitz, T. A., Montrose, J. C., and Posch, H. A. (1979). *J. Chem. Phys.*, **70**, 4626.

Balucani, U. and Vallauri, R. (1979*a*). *Mol. Phys.*, **38**, 1099.

Balucani, U. and Vallauri, R. (1979*b*). *Mol. Phys.*, **38**, 1115.

Barker, J. A., Fisher, R. A., and Watts, R. O. (1971). *Mol. Phys.*, **21**, 657.

Briganti, G., Rocca, D., and Nardone, M. (1986). *Mol. Phys.*, **59**, 1259.

Copley, J. R. D. and Lovesey, S. W. (1975). *Rep. Progr. Phys.*, **38**, 461.

Fleury, P. A. and McTague, J. P. (1969). *Opt. Commun.*, **1**, 164.

Fleury, P. A., Daniels, W. B., and Worlock, J. M. (1971). *Phys. Rev. Lett.*, **27**, 1493.

Fleury, P. A., Worlock, J. M., and Carter, H. L. (1973). *Phys. Rev. Lett.*, **30**, 591.

Gelbart, W. M. (1974). *Adv. Chem. Phys.*, **26**, 1.

Guillot, B., Bratos, S., and Birnbaum, G. (1980). *Phys. Rev. A*, **22**, 2230.

Guillot, B., Bratos, S., and Birnbaum, G. (1982). *Phys. Rev. A*, **25**, 773.

Ladd, A. J. C., Litovitz, T. A., and Montrose, C. J. (1979). *J. Chem. Phys.*, **71**, 4242.

Ladd, A. J. C., Litovitz, T. A., Clarke, J. H. R., and Woodcock, L. V. (1980). *J. Chem. Phys.*, **72**, 1759.

Madden, P. (1978). *Mol. Phys.*, **36**, 365.

Madden, P. and Evans, G. T. (1988). *J. Chem. Phys.*, **89**, 685.

Montrose, C. J., Litovitz, T. A., Birnbaum, G., and Mennella, R. (1991). *J. Non-Cryst. Solids*, **131–133**, 177.

Oxtoby, D. W. and Gelbart, W. (1975). *Mol. Phys.*, **30**, 1569.

Rouch, J., Boon, J.-P., and Fleury, P. A. (1977). *Physica*, **88A**, 347.

Tao, N. J., Li, G., Chen, X., Du, W. M., and Cummins, H. Z. (1991). *Phys. Rev. A*, **44**, 6665.

Tao, N. J., Li, G., and Cummins, H. Z. (1992). *Phys. Rev.*, **45**, 686.

Thibeau, M. M., Oksengorn, B., and Vodar, B. (1968). *J. Physique*, **29**, 287.

Varshneya, D., Shirron, S. F., Litovitz, T. A., Zoppi, M., and Barocchi, F. (1981). *Phys. Rev. A*, **23**, 77.

Yarnell, J. L., Katz, M. J., Wenzel, R. G., and Koenig, S. H. (1973). *Phys. Rev. A*, **7**, 2130.

Zoppi, M., Barocchi, F., Varshneya, D., Neumann, M., and Litovitz, T. A. (1981). *Canad. J. Phys.*, **59**, 1475.

Zoppi, M. and Spinelli, G. (1986). *Phys. Rev. A*, **33**, 939.

Index